Architectures moléculaire et supramoléculaires à base de Lanthanides Luminescents

Gulay Bozoklu

UNIVERSITÉ DE GRENOBLE

THÈSE

Pour obtenir le grade de

DOCTEUR DE L'UNIVERSITÉ DE GRENOBLE

Spécialité : **Chimie Inorganique et Bio-inorganique**

Arrêté ministériel : 7 août 2006

Présentée par

Gülay BOZOKLU

Thèse dirigée par **Marinella MAZZANTI** et
codirigée par **Daniel IMBERT**

préparée au sein du **Laboratoire de Reconnaissance Ionique et Chimie de Coordination du Service de Chimie Inorganique et Biologique, INAC, CEA-Grenoble**

Architectures Moléculaires et Supramoléculaires à base de Lanthanides Luminescents

Thèse soutenue publiquement le **29 septembre 2011**,
devant le jury composé de :

Mme Frédérique LOISEAU
Professeur ; Université de Grenoble ; Présidente et Examinatrice
Mr François NIEF
Professeur ; École Polytechnique, CNRS ; Rapporteur
Mr Stéphane PETOUD
Professeur ; CNRS Orléans ; Rapporteur
Mme Anja-Verena MUDRING
Professeur ; Ruhr University Bochum ; Examinatrice
Mr Daniel IMBERT
Docteur ; CEA Grenoble ; Co-directeur de thèse
Mme Marinella MAZZANTI
Docteur ; CEA Grenoble ; Directeur de thèse

UNIVERSITÉ DE GRENOBLE

THESIS

For obtaining the degree of

DOCTOR OF PHILOSOPHY OF UNIVERSITY OF GRENOBLE

Speciality: **Inorganic and Bio-Inorganic Chemistry**

Ministerial order: 7 August 2006

Presented by

Gülay BOZOKLU

Thesis directed by **Marinella MAZZANTI** and
codirected by **Daniel IMBERT**

prepared in the **Laboratoire de Reconnaissance Ionique et Chimie de Coordination du Service de Chimie Inorganique et Biologique, INAC, CEA-Grenoble**

Luminescent Lanthanide-Based Molecular and Supramolecular Architectures

Thesis defended in public on **29 September 2011**,
In front of the jury composed of:

Mrs. Frédérique LOISEAU
Professor; University of Grenoble; President and Examiner
Mr. François NIEF
Professor; École Polytechnique, CNRS; Rapporteur
Mr. Stéphane PETOUD
Professor; CNRS Orléans; Rapporteur
Mrs. Anja-Verena MUDRING
Professor; Ruhr University Bochum; Examiner
Mr. Daniel IMBERT
Doctor; CEA Grenoble; Thesis Co-director
Mrs. Marinella MAZZANTI
Doctor; CEA Grenoble; Thesis director

RÉSUMÉ

La construction de complexes polymétalliques de lanthanides préprogrammés et sophistiqués, de taille nanométrique, pour le développement de matériaux luminescents présentant des propriétés photophysiques nouvelles ou améliorées (double émission, transfert d'énergie intermétallique, etc.) est un des sujets de la chimie supramoléculaire des lanthanides suscitant énormément d'intérêt. La compréhension, le contrôle et la programmation de l'auto-assemblage de complexes de lanthanides est un défi majeur en raison de la difficulté à contrôler l'environnement de coordination de ces ions qui se caractérise par des nombres de coordinations importants et variables et peu de préférences stéréochimiques. Ainsi, la plupart des complexes polynucléaires de lanthanides décrits dans la littérature sont formés de façon fortuite plutôt que par conception rationnelle.

Afin d'inclure les ions lanthanides dans des architectures polymétalliques de haute nucléarité tout en améliorant leurs propriétés photophysiques, nous nous sommes concentrés sur des études de complexation de ligands dissymétriques (tridentates anioniques, tétradentates chiraux) permettant de promouvoir la formation des assemblages. Nous avons par ailleurs commencé à explorer le potentiel d'une méthode synthétique originale de clusters oxo par réactivité redox de complexes divalents de lanthanides. Nous présentons ici la synthèse et les propriétés photophysiques de complexes stables émettant dans le proche infrarouge basés sur des ligands anioniques hydroxyquinoléine fonctionnalisé par des groupes carboxylates ou tétrazolates. En outre, nous pouvons montrer que l'utilisation de ligands chiraux possédant un groupement oxazoline favorise l'auto-assemblage diastéréosélectif de complexes de lanthanides homo- et hétéro-polymétalliques énantiopures émettant dans le visible et le proche infrarouge. Un complexe trinucléaire d'europium énantiopure a été caractérisé par cristallographie, celui-ci présentant une forte activité en polarisation circulaire de luminescence (CPL). Le ligand chiral oxazoline a permis d'obtenir une roue heptanucléaire d'europiums, le plus important assemblage polymétallique énantiopure. Enfin, nous avons pu préparer et caractériser des complexes de lanthanides divalents hautement réactifs basés sur un ligand tripode neutre possédant des groupements pyridine (tpa). Des résultats préliminaires montrent que ces complexes peuvent être des précurseurs très utiles pour isoler des clusters oxo polymétalliques. En particulier, la réaction d'un complexe de néodyme hautement réactif a conduit à isoler un cluster oxo volumineux et très intéressant par clivage de THF en présence de tpa.

Mots-clés
Lanthanides divalents et trivalents, auto-assemblage, polymétallique, cluster, diastéréosélectif, chiralité, CPL, luminescence, 8-hydroxyquinoléine, oxazoline, pyridine

Discipline
Chimie Inorganique

Laboratoire
Laboratoire de Reconnaissance Ionique et Chimie de Coordination
Service de Chimie Inorganique et Biologique, UMR-E3 CEA-UJF
Institut Nanosciences et Cryogénie, CEA Grenoble
17 Rue des Martyrs, 38054 Grenoble Cedex, France

ABSTRACT

The construction of preprogrammed, sophisticated and nanoscopic polymetallic lanthanide complexes for the development of luminescent materials that possess new or improved photophysical properties (dual emission, intermetallic energy transfer, etc.) is one of the hot topics in the lanthanide supramolecular chemistry. Understanding, controlling and programming self assembly of lanthanide complexes is a key challenge due to the difficulty in controlling the coordination environment of these ions which display high and variable coordination numbers with little stereochemical preferences. As a result of this, most of the polynuclear lanthanide complexes reported in literature are formed by serendipity rather than rational design.

In order to include lanthanide ions in discrete high nuclearity polymetallic architectures with improved photophysical properties we have concentrated on complexation studies with dissymmetric chelating ligands (tridentate anionic ligands, tetradentate chiral ligand) with possibility of promoting assembly formation, and we started to investigate the potential of an original synthetic method using the redox reactivity of divalent lanthanides complexes for the synthesis of oxo clusters. Here we present the synthesis and photophysical properties of NIR emissive stable complexes obtained with hydroxyquinoline based tridentate dianionic ligands functionalised with carboxylic acid and tetrazole groups. Moreover we show that the use of a chiral tetradentate ligand possessing oxazoline ring promotes the diastereoselective self assembly of enantiopure homo- and hetero-polymetallic lanthanide complexes emitting in the visible and NIR range. An original enantiopure trinuclear europium complex was crystallographically characterised and we found that it displays a high circularly polarized luminescence (CPL) activity. The chiral oxazoline based ligand also led to the synthesis of the largest enantiopure polynuclear assembly of europium, a heptanuclear wheel. Finally we were able to prepare and characterize highly reactive complexes of divalent lanthanides with a neutral tripodal pyridine based ligand and very preliminary results show that these complexes can be useful precursors for the isolation of polymetallic oxoclusters. Notably, the reaction of the highly reactive neodymium complex led to the isolation of a very interesting large neodymium oxo cluster by cleavage of THF in the presence of the ligand tpa.

Keywords
Trivalent and divalent lanthanides, self-assembly, polymetallic, cluster, diastereoselective, chiral, CPL, luminescence, 8-hydroxyquinoline, oxazoline, pyridine

Specialty
Inorganic Chemistry

Laboratory
Laboratoire de Reconnaissance Ionique et Chimie de Coordination
Service de Chimie Inorganique et Biologique, UMR-E3 CEA-UJF
Institut Nanosciences et Cryogénie, CEA Grenoble
17 Rue des Martyrs, 38054 Grenoble Cedex, France

ACKNOWLEDGEMENTS

First of all, I would like to express my deep gratitude to Professor François Nief, Professor Stéphane Petoud, Professor Anja-Verena Mudring and Professor Frédérique Loiseau for accepting to judge the quality of this thesis work.

I would like to express my special thanks to my thesis director Dr. Marinella Mazzanti for giving me the opportunity to work in her group, for her advises and support in this thesis. I am very grateful to my co-director Dr. Daniel Imbert who has shared his knowledge and experience in luminescence measurements with me during this thesis. I would also like to thank them for their support and patience during the preparation of the present manuscript.

I would also like to thank Dr. Pascale Maldivi, who welcomed me in the SCIB for the thesis. I am also very thankful to all the members of SCIB and I specially thank Zohra Termache, the best secretary ever, for helping me with all the administrative issues.

I would like to give sincere gratitude to Dr. Jacques Pécaut for X-Ray diffraction measurements and resolution of the structures and for his positivity and patience against my questions. I would like to thank Colette Lebrun for ES-MS analysis of the compounds, for the good coffee in the mornings and her kindness. I would like to thank Christelle Gateau for the help with the organic synthesis of the ligands and Pierre-Alain Bayle for the help with the NMR measurements. Finally I would like to thank Lydia Plassais for the help in organic synthesis and for her friendship. I will keep good memories from our ski trips on Saturdays.

I am also very thankful to Prof. Dr. Gilles Muller and his group for their kindness and help on CPL measurements. I kindly thank Dr. Yaroslav Filinchuk for the challenging resolution of our unsymmetrical wheel structure and for the discussions on crystallography.

Many thanks go in particular to Victor Mougel, Gaylord Tallec and Clément Camp for their friendship, for the great discussions on chemistry and materials, for helping me with French language, for the great dinners they prepared and for making it so pleasant to work with them in the lab. I would like to thank specially Nicolas Gauthier for his support in the last months and for his help and advises in the preparation of the manuscript and defense. I would like to acknowledge Claire Marchal for her support and availability during the preparation of the articles and Marco Giardiello for his great personality and making my first year in Grenoble so fun. I am very grateful to Eugen Andreiadis for his friendship and his support during the last months of my thesis. It is a pleasure to express my gratitude to Pawel Horeglad and his wife for their kind hospitality during my stay in Varsaw. Thanks to Yves Chenavier for helping me with computers and providing me with nice plants to decorate our office. It is a pleasure to mention my colleagues Marion, Gregory, Biplap, Lucile, Graeme, Viviana, Simon, Anais, Laetitia, Agnieszka, Mikhael, Nicolas, Maud and Anne Solène and thank them for creating a nice working ambiance.

Finally, I would like to thank my parents and my brother for their endless love, understanding and support. Last but not least, I would like to thank a very special person, without whose love, patience, encouragement and editing assistance, I would not have finished this thesis. I would also like to thank his family for their support and love.

RÉSUMÉ ÉTENDU EN FRANÇAIS

I) Introduction

Les ions lanthanides (Ln) comprennent 15 éléments de la première période du bloc f, allant du Lanthane (Z=57) au Lutécium (Z=71). Le lanthane, de configuration électronique $[Xe]5d^16s^24f^0$ est inclus par extension, les autres lanthanides adoptent majoritairement la configuration $[Xe]6s^24f^{n+1}$, les sept orbitales 4*f* étant remplies de f^0 à f^{14}. Les orbitales 4f sont blindées par les couches externes $5s^25p^6$ et ont une faible extension radiale. Ainsi, les propriétés spectroscopiques et magnétiques des lanthanides dans les complexes sont très peu affectées par leur environnement et sont similaires à celles de l'ion libre. De plus, les électrons de valence 4f ne sont pas disponibles pour former des interactions covalentes avec des ligands coordinants. De ce fait, les interactions lanthanide-ligand sont purement ioniques et conduisent à de faibles préférences stéréochimiques et une sphère de coordination labile conduisant à des nombres de coordination variables (de 3 à 14) ainsi que de multiples géométries. Les tailles importantes des ions lanthanides conduisent à la formation de complexes ayant communément des nombres de coordination entre 8 et 9. Si ce nombre de coordination n'est pas complété par le ligand coordinant, la sphère de coordination est complétée par des molécules de solvant. Ceci rend difficile la prédiction du nombre de coordination en solution, la préférence entre les nombres de coordination et les géométries ayant tendance à être contrôlée par des effets stériques (minimisation des répulsions) provenant de la géométrie du ligand et de la contraction des lanthanides tout au long de la série.

La luminescence des lanthanides présente des caractéristiques importantes, de fines bandes d'émission, de longs temps de décroissance de luminescence, ainsi que d'importants déplacements de Stoke. A l'exception des ions La(III) et Lu(III) ($4f^0$ et $4f^{14}$ respectivement) chaque lanthanide trivalent est luminescent, sur une gamme couvrant la totalité du spectre, de l'UV (Gd) au visible (Eu, Tb) jusqu'au proche infrarouge (Nd, Er, Yb, Ho). Quelques ions (Sm, Dy, Tm, and Pr) émettent tant dans les gammes visibles qu'infrarouge. Les coefficients d'extinctions molaires des ions lanthanides sont faibles (ε = <10 $M^{-1}cm^{-1}$) et de ce fait ne permettent pas d'obtenir des complexes de lanthanides hautement luminescent par excitation directe des transitions f-f en dehors des sources d'excitations à haute énergie comme les lasers à argon ou à colorants. Une excitation indirecte (appelée sensibilisation ou effet d'antenne) par transfert d'énergie entre un chromophore organique agissant comme antenne est une stratégie efficace pour la sensibilisation de la luminescence des lanthanides. La conception des ligands est ainsi une donnée importante de la chimie des ions lanthanides. Une haute

denticité des ligands permettra une forte protection des centres lanthanides aux oscillateurs O-H et aux molécules de solvant coordinantes qui sont des « quencheurs » efficaces de la luminescence des lanthanides. Une conception rationnelle et des stratégies synthétiques originales sont nécessaires afin de diminuer voir supprimer d'une part les processus de désactivation non radiatifs provenant des oscillateurs O-H et, d'autre part, afin d'obtenir des complexes de lanthanides de haute nucléarité pour le développement de nouveaux matériaux luminescents.

II) Objectifs du projet

Les matériaux basés sur les lanthanides sont devenus très attractifs ces dernières années du fait de leurs propriétés spectroscopiques et magnétiques uniques. Ceci à conduit à la découverte d'une large gamme d'applications allant de la science des matériaux (diodes organiques électroluminescentes (OLED) pour les écrans plats, amplificateurs pour fibres optiques) aux applications biomédicales (marqueurs luminescents pour molécules biologiques, senseurs, agents de contraste pour l'imagerie par résonance magnétique (IRM)). L'assemblage de complexes de coordination sophistiqués et de haute nucléarité à partir de ligands relativement simples conduit à la combinaison d'une taille nanoscopique et de propriétés optiques et magnétiques permettant d'obtenir d'intéressants nouveaux matériaux. Néanmoins, le nombre d'études dans ce domaine est limité du fait de la difficulté à contrôler l'environnement de coordination des éléments f qui montrent des nombres de coordination variables avec de faibles préférences stéréochimiques. De nombreuses stratégies synthétiques ont été adaptées afin de préparer des complexes de lanthanides polymétalliques mais la plupart de ces complexes ont été obtenus par hasard plutôt que par conception rationnelle. En l'absence d'études en solution, il est difficile de comprendre et prédire leur formation.

L'objectif de ce travail de thèse est le développement de stratégies synthétiques permettant d'inclure des ions lanthanides dans des architectures polymétalliques de haute nucléarité par l'utilisation de ligands organiques et l'étude des propriétés photophysiques des assemblages finaux afin d'améliorer les propriétés optiques pour de nouveaux matériaux. A cette fin, nous avons concentré nos efforts sur des études de complexation avec des ligands dissymétriques et prédisposés (ligands anioniques tridentés et chiraux tétradentés) avec la possibilité de promouvoir la formation d'assemblages. De plus, nous avons débuté l'investigation d'une méthode synthétique originale utilisant le potentiel rédox de lanthanides divalents afin de synthétiser des clusters oxo pour matériaux luminescents.

III) Complexes trianioniques nonacoordinnés à base de 8-hydroxyquinoléine

Dans la première partie de ce travail qui sera présenté dans le chapitre 2, des études de complexation ont été entreprises avec des ligands hydroxyquinoléine tridentes et dianioniques substitués par des groupes carboxyles (H_2hqa) et tétrazoles (H_2hqt), avec pour objectif d'obtenir des complexes polynucléaires. Le chromophore 8-hydroxyquinoléine est bien connu pour la sensibilisation des ions lanthanides Nd(III), Yb(III) et Er(III) émettant dans le proche infrarouge. Des études de complexation avec le ligand H_2hqa et l'ion Nd(III) ont déjà été conduites dans notre groupe ; Ici nous allons étendre cette étude aux ions Er(III) et Yb(III) et à un nouveau ligand tetrazole basé sur la 8-hydroxyquinoléine. Nous avons choisi des ligands dianioniques et tridentes afin d'étudier l'effet de charge et de géométrie du ligand sur la formation des assemblages finaux. Les structures en solution et à l'état solide des complexes résultants ont été caractérisées par spectroscopie RMN et difffraction de rayons X. De plus, les propriétés photophysiques ont été investiguées en détail, tant en solution qu'à l'état solide.

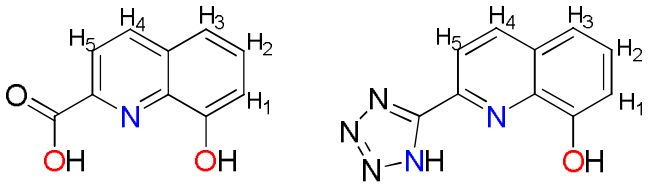

Schéma 1 : Ligands H_2hqa et H_2hqt

La combinaison du chromophore 8-hydroxyquinoléine avec des groupements anioniques aditionnels (carboxyles, tetrazoles) permet d'obtenir des complexes trianioniques luminescents. Ces ligands forment des complexes $[Ln(hqa)_3]K_3$ et $[Ln(hqt)_3]K_3$ tris-chélates et tris-anioniques dans l'eau à pH 12. A plus bas pH, des espèces partiellement protonnées sont formées. Les complexes à base de hqa et hqt avec les ions Nd(III), Yb(III) et Er(III), ainsi que le complexe partiellement protonné $[Nd\ (H_{1/2}hqa)_3]_2(Et_3NH)_3.Et_3NHOtf$ ont été cristallisés à partir de solutions méthanoliques. La complexation des ligands avec les sels de lanthanides ne conduit pas à la formation d'assemblages polynucléaires discrets ; Seules les espèces dimériques et polymériques peuvent être isolées sur les bases utilisées.

La structure par diffraction de rayons X des cristaux ($[Nd(hqa)_3]K_3.8CH3OH_\infty$, $[Er(hqa)_3]K_3.7CH3OH_\infty$ et $[Nd(hqt)_3]K_3.6CH3OH_\infty$) montrent un arrangement en hélice tant pour les ligands avec une géométrie « *anti* » pour hqa qu'une géométrie « *syn* » pour hqt (Figure 1). Seuls les complexes tris-chélates sont formés dans l'eau ou le méthanol à 0.04 M pour les deux ligands. Une géométrie « *syn* » est trouvée pour les complexes dimériques

partiellement protonnés et est conservée dans le méthanol. Une distribution statistique d'espèces "*anti*" et "*syn*" est trouvée pour les complexes $[Ln(hqa)_3]K_3$ en solution tandis que la géométrie majoritaire des complexes $[Ln(hqt)_3]K_3$ est « *syn* ».

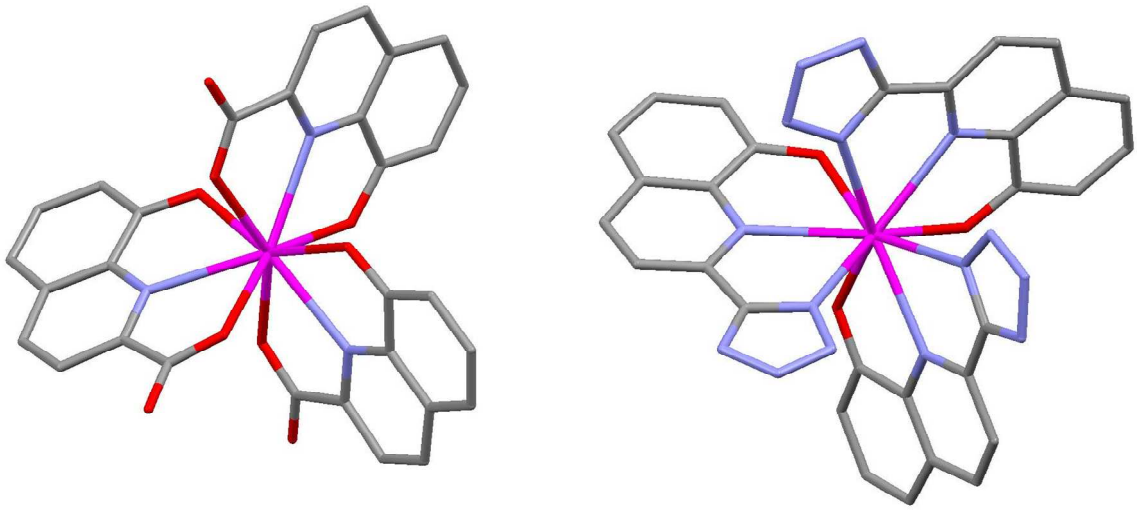

Figure 1 : Diagramme Mercury de $[Nd(hqa)_3]^{3-}$ et $[Nd(hqt)_3]^{3-}$ présentants des arangements hélicoïdaux anti et syn, respectivement

Des études photophysiques ont été menées sur tous les complexes en solution dans le méthanol ou à l'état solide. Les mesures ont été conduites à l'air sans précautions particulières afin de prévenir la présence d'oxygène. Tous les complexes isolés à base de hqt et hqa avec les ions Nd(III), Yb(III) et Er(III), en incluant le complexe partiellement protonné ($[Nd(H_{1/2}Hqa)_3]_2^{3-}$) montrent une importante luminescence infrarouge centrée sur le métal tant à l'état solide que dans le méthanol. De plus, à 295 °K, l'émission centrée sur le ligand contribue très faiblement à la luminescence totale lorsque l'on excite dans l'UV sur les bandes d'absorption du ligand $\pi \rightarrow \pi^*$ et $n \rightarrow \pi^*$ (<5 % de l'émission de fluorescence comparé au ligand libre). Ceci indique clairement un processus de transfert d'énergie efficace du ligand sur les niveaux accepteurs des ions métalliques. La sensibilisation de la luminescence dans l'infrarouge est confirmée par les spectres d'excitation des complexes de Nd(III), Yb(III) et Er(III) qui démontrent clairement le rôle d'antenne des ligands par recouvrement et correspondance avec les bandes d'absorption des spectres électroniques (Figure II-19, gauche). A température ambiante et sous excitation sur les larges bandes d'absorption des ligands à 371, 344 et 483 nm, tous les complexes montrent des spectres de luminescence identiques à l'état solide ou dissous dans le méthanol avec des bandes d'émission dans le proche infrarouge correspondant aux transitions f-f attendues.

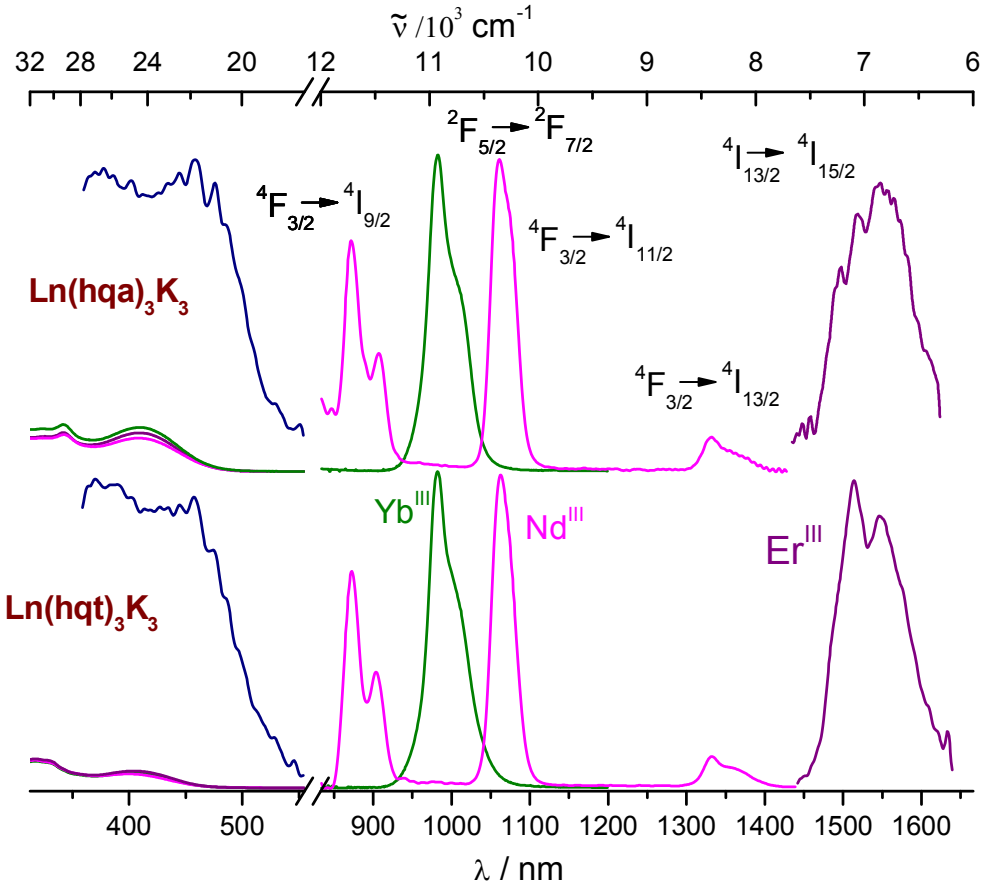

Figure 2 : Gauche : Spectres d'absorption et d'excitation normalisés (λ_{an} = 1540 (Er), 1063 (Nd), et 976 nm (Yb)). Droite : Spectres d'émission dans le proche IR (λ_{ex} =371 nm) des complexes à base de hqa et hqt d'Er^{III}, Nd^{III}, et Yb^{III}

Des rendements quantiques d'émission dans le proche infrarouge ont été mesurés pour les complexes $[Ln(hqa)_3]K_3$ à l'état solide (0.06 %, 0.18 %, 0.0051 % pour Nd(III), Yb(III) et Er(III) respectivement) et dans le méthanol (0.063 %, 0.28 %, 0.0019 % pour Nd(III), Yb(III) et Er(III) respectivement). Toutes les valeurs de rendements quantiques obtenues pour les complexes à base de hqt sont 15 à 20 % plus importantes que celles mesurées pour les complexes à base de hqa. Les complexes trianioniques présentent de fortes solubilités dans des solvants aqueux ou organiques et une bonne résistance à la dissociation des ligands en comparaison des complexes neutres de 8-hydroxyquinoléine.

En résumé, dans ce chapitre, nous avons investigué la capacité de deux ligands tridentes et dianioniques basés sur la 8-hydroxyquinoléine à former des complexes de lanthanides polynucléaires, avec pour résultat des complexes tris avec une forte émission dans le proche infrarouge. Afin d'obtenir des complexes polynucléaires, nous avons décidé d'étudier la complexation d'un ligand chiral tétradente dérivé de la terpya. Dans le prochain chapitre, nous allons discuter de la synthèse diastéréosélective de complexes de lanthanides formés par ce nouveau ligand synthétisé au laboratoire.

IV) Auto-assemblage diastéréosélectif d'architectures chirales polynucléaires de lanthanides

Les composés de coordination chiraux énantiopures basés sur les ions lanthanides ont des applications cruciales comme catalyseurs asymétriques ou senseurs chiraux pour la reconnaissance de substrats biologiques. Néanmoins, le nombre d'études sur la synthèse de complexes de lanthanides énantiopures est très faible en comparaison avec ceux à base de métaux de transition. Les complexes de lanthanides, du fait de leur labilité cinétique, impliquent un échange rapide des diastéréoisomères en solution et, de ce fait, il est très difficile d'isoler un diastéréoisomère. La plupart des complexes chiraux à base de lanthanides de la littérature sont des complexes mononucléaires où la chiralité du ligand est transférée au complexe. Quand le ligand chiral est coordinné au centre métallique, les réactions sont fortement stéréosélectives. L'objectif ici est d'introduire la chiralité dans les complexes de lanthanides et l'utilisation de leurs propriétés spectroscopiques et catalytiques pour permettre la conception de complexes luminescents chiraux. Ceux-ci pourraient être utilisés comme catalyseurs chiraux pour préparer des composés organiques énantiopures ou comme sondes luminescentes pour la reconnaissance chirale et senseurs de molécules biologiques.

Dans la seconde partie de la thèse, nous proposons l'utilisation de simples ligands chiraux dissymétriques et tétradentes laissant certaines positions de coordination vacantes autour de l'ion métallique pour permettre l'assemblage direct de larges complexes de lanthanides. Notre groupe a précédemment montré que l'utilisation d'un ligand dissymétrique tétradente (terpya) conduit à isoler un complexe cyclique hexamérique avec un ion métallique central. Cette stratégie par étapes est utilisée pour obtenir des complexes hétéropolymétalliques possédant deux environnements de coordination. Dans cette thèse, afin de comprendre les effets des caractéristiques des ligands (géométrie, basicité…) sur l'assemblage final et vérifier la formation des assemblages heptanucléaires avec un autre ligand dissymétrique tétradente, nous avons synthétisé un ligand chiral tétradente Phbipox dérivé de la bipyridine et contenant un cycle oxazoline pour l'assemblage de complexes énantiopures de lanthanides.

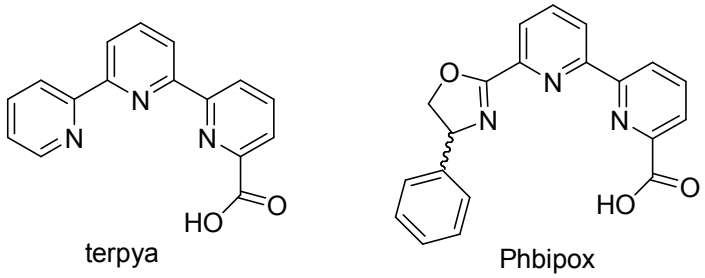

Schéma 2 : Ligands dissymétriques tétradentes pour le développement d'assemblages supramoléculaires

Le travail présenté dans ce chapitre est focalisé sur l'autoassemblage d'architectures polynucléaires chirales et luminescentes à partir de complexes mononucléaires à base de ligand simple dissymétrique tétradente. Le ligand Phbipox ((6-(4-phenyloxazolin-2-yl)-2,2-bipyridine-6-acide carboxylique)) a été utilisé pour promouvoir l'autoassemblage contrôlé par les cations ou contrôlé par la concentration utilisée. Les complexes finaux ont été caractérisés par spectroscopie RMN, diffraction de rayons X, dichroïsme circulaire et luminescence circulaire polarisée. Les propriétés photophysiques ont été comparées à celles des complexes de terpya afin de comprendre les effets des paramètres des ligands sur l'assemblage.

L'assemblage d'un complexe trinucléaire et homochiral a été observé dans l'acétonitrile et dans des solutions méthanoliques fortement concentrées et suivi par des études RMN. La chiralité du ligand est transférée et est fonction de la concentration des solutions sur l'assemblage trinucléaire pour donner des isomères énantiopures d'europium et néodyme ΔΔΔ-S ou ΛΛΛ-R. La formation des assemblages trinucléaires n'est pas observée dans des conditions similaires pour les ions de plus petite taille comme l'ytterbium, du fait de l'augmentation des interactions stériques. La diastéréosélectivité de la formation de l'assemblage provient des interactions stériques du groupe phényle des complexes monomériques à deux ligands durant le processus d'autoassemblage. De plus, de fortes interactions π-π ont été observées dans ces complexes. La stéréosélectivité des complexes mononucléaires a aussi été démontrée dans l'autoassemblage de deux ligands autour du centre europium pour donner les isomères monomériques Λ et Δ et est linéaire à la taille du cation métallique. Les études CPL sur les complexes d'europium ont montré que les espèces trinucléaires ont une forte activité CPL avec un facteur g_{lum} de +0.45. Ces complexes sont prometteurs pour de futures études comme sondes CPL luminescentes et chirales. Les études CPL avec des complexes émettant dans le proche infrarouge devraient être entreprises dans un futur proche.

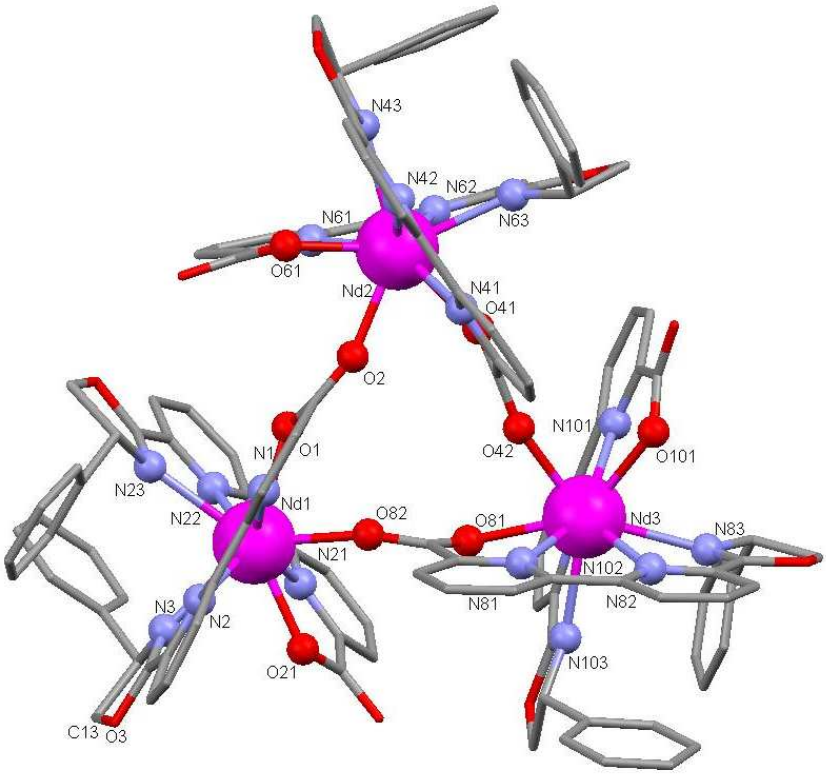

Figure 3 : Diagramme Mercury de la structure $\{(\Lambda\Lambda\Lambda)\text{-}[Nd(R\text{-}Phbipox)_2]_3\}^{+3}$ (**VIII**)

Ce système est particulièrement bien adapté pour l'autoassemblage de composés polynucléaires de lanthanides de taille nanoscopique par l'utilisation de cations « template » comme montré avec le ligand tétradente terpyridine carboxylate (terpya). L'ajout d'un excès de lanthanides à des complexes 2:1 permet la formation de la plus importante architecture chirale à base de néodyme et d'europium décrite à ce jour. La formation des complexes est contrôlée par la taille du cation. Le complexe d'ytterbium ne conduit pas à la formation d'un complexe heptanucléaire. La roue hétérochirale hexamérique est formée à partir de trois diastéréoisomères delta et trois lambda connectés entre eux et au cation central par des ponts carboxylates. Les complexes hétéropolymétalliques ont été formés par une stratégie synthétique rationnelle développée avec le ligand terpya et requièrent des tailles de cations différentes pour les deux sites métalliques présents dans la roue (central et périphérique). De plus, les spectres d'émission de la roue heptanucléaire montrent la présence de deux sites d'émissions différents : l'un provenant du centre, et six de la périphérie. Selon ce résultat, des roues $[(Ln(Phbipox)_2)_6]^{9+}$ (Eu, Nd) abritant des ions lanthanides plus petits (Lu, Yb) au centre ont été préparées en solution. Les études CPL montrent de façon inattendue que la roue (g_{lum}=0.10) ne présente pas d'augmentation d'activité CPL comparé aux complexes mononucléaires, ceci étant probablement dû à son hétérochiralité.

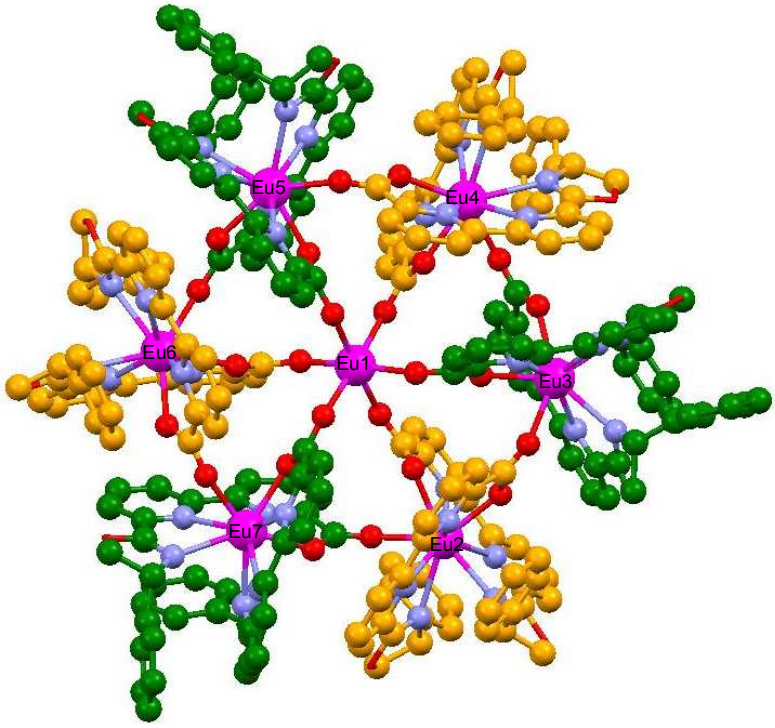

Figure 4 : Structure du cation $[Eu\subset(\Lambda\text{-}Eu(R\text{-}Phbipox)_2\Delta\text{-}Eu(R\text{-}Phbipox)_2)_3]^{9+}$. Oxygène : rouge ; europium : rose ; carbones de $[\Lambda\text{-}Eu(R\text{-}Phbipox)_2]^+$: vert ; carbones de $[\Delta\text{-}Eu(Phbipox)_2]^+$: orange

Le rendement quantique de luminescence centrée sur le métal du complexe heptanucléaire (27 à 37%) est légèrement plus important que celui du complexe mononucléaire (21 à 25%). Ceci suggère que l'arrangement cyclique des six europiums ne conduit pas à des effets intramoléculaires « quencheurs » de luminescence, en dépit de la relative faible distance entre les unités EuL_2 voisines (6.34 Å). De plus, une émission importante dans le proche infrarouge est détectée pour les complexes de Nd et d'Yb à température ambiante.

En résumé nous avons investigué, dans ce chapitre de thèse, un assemblage chiral rare, contrôlé par la géométrie du ligand, la taille du cation utilisé, ainsi que sa concentration en solution. Les complexes ont été complètement caractérisés en solution et à l'état solide. La stéréosélectivité de l'autoassemblage des complexes mononucléaires ainsi que les propriétés photophysiques peuvent être modulés par un changement de conception du ligand. Ceci pourrait nous aider à obtenir de meilleures qualités de cristaux de la roue, par le fait que la symétrie de la molécule devrait augmenter avec la forte stéréosélectivité. De plus, différentes géométries de ligands pourraient donner de plus faibles interactions stériques, et ainsi permettre la formation de plus importants assemblages nucléaires avec une plus large variété de lanthanides. Les espèces heptanucléaires sont idéales pour l'étude des processus de transfert d'énergie mais aussi comme précurseurs potentiels pour le développement de

dispositifs optiques. Les complexes trinucléaires pourraient aussi être intéressants pour des études magnétiques et du dichroïsme magnétochiral.

V) Oxydation de lanthanides divalents

Dans cette dernière partie, nous avons débuté la synthèse et l'étude de précurseurs divalents pour la préparation de clusters de haute nucléarité par oxydation de lanthanides divalents. Les clusters de lanthanides ont montré posséder des propriétés optiques non usuelles comme de fortes efficacités quantiques et des bandes d'émission uniques. Les clusters, de part leur solubilité en solvants organiques, leur relative absence de modes vibrationnels à haute énergie, et leur relativement forte concentration ions lanthanide/unité de volume, sont prometteurs comme source d'ions lanthanides pour la préparation de matériaux émissifs. Les clusters avec des ligands oxo émettent à des longueurs d'ondes que l'on ne trouve pas dans les oxydes conventionnels. Néanmoins, des voies de synthèse doivent être développées afin de synthétiser ces clusters de lanthanides et comprendre totalement leur chimie.

Dans cette thèse, afin de contrôler la formation des clusters, nous nous proposons d'utiliser les réactions rédox sur les précurseurs divalents de lanthanides avec des ligands donneurs oxo. La chimie des lanthanides divalents est un domaine où le challenge est présent pour l'étude des lanthanides. Dans notre laboratoire, nous avons montré que l'utilisation d'un ligand tripode tris(2-pyridylmethyl)amine (tpa) ou de petits ligands comme des iodures, triflates ou encore benzoates, permettaient l'obtention de larges clusters par oxydation de complexes d'uranium(III). Ainsi, nous avons l'objectif de développer des méthodes synthétiques originales pour la préparation de larges clusters oxo. Tout d'abord, nous avons étudié la complexation par le ligand tpa puis les précurseurs obtenus par spectroscopie RMN et diffraction de rayons X.

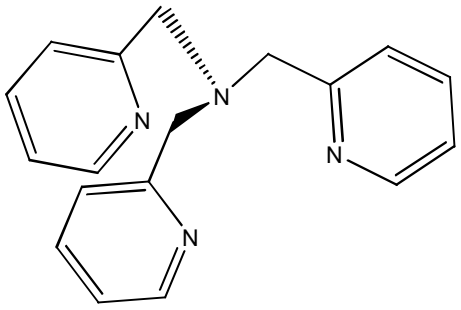

Schéma 3 : Ligand tris (2-pyridylmethyl)amine (tpa)

Les complexes bis tpa à base d'Eu(II), Sm(II) et Yb(II) ont été isolés et caractérisés complètement. Les complexes mono tpa présentent un équilibre en solution et seulement deux cristaux d'Eu et Yb ont pu être analysés. Les complexes divalents de lanthanides non

classiques (Tm(II), Dy(II), Nd(II)) n'ont pas pu être analysés du fait de leur extrême réactivité. Un cluster oxo de néodyme très intéressant a été obtenu par coupure du THF, et analysé par cristallographie. Un autre important cluster oxo de samarium a été obtenu par réaction de SmI_2 avec de la pyridine-N-oxyde dans le THF. Cette thématique en est à ses débuts dans le laboratoire et ces résultats préliminaires prometteurs démontrent que les complexes obtenus peuvent être des précurseurs utiles afin d'isoler des clusters oxo polymétalliques. Les études de luminescence du cluster final n'ont pu être obtenues durant le temps limité de cette thèse mais pourraient fournir une meilleure compréhension de la relation entre structure et propriétés de ce type de clusters de lanthanides.

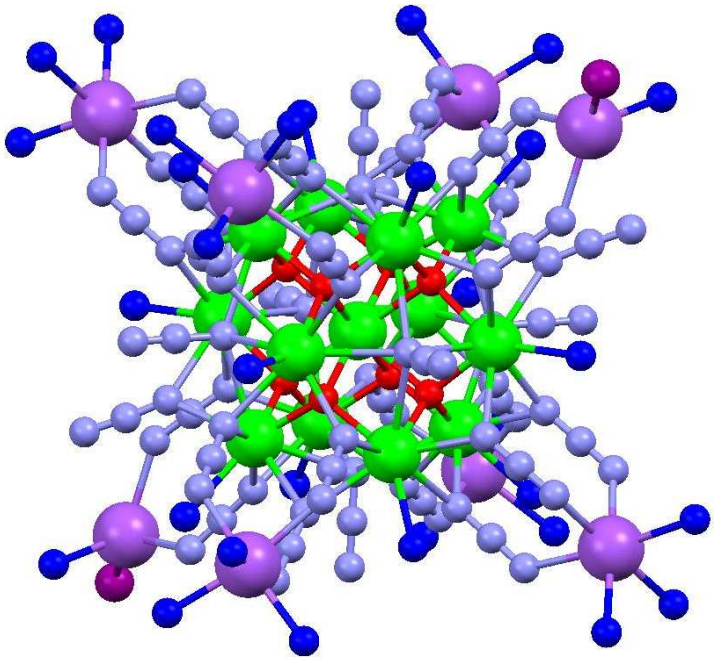

Figure 5 : $[Nd_{13}(\mu_4\text{-}O_8)Na_8(\mu_4\text{-}1,1,1,1\text{-}N_3)_6(\mu_3\text{-}1,1,3\text{-}N_3)_{24}(py)_{28}I]\cdot(py)_7$ Pyridines non coordinées, carbones et hydrogènes supprimés. Nd : vert, oxygène : rouge, azido azotes : bleu clair, azotes pyridine : bleu foncé, sodium : violet, iode : pourpre

LIST OF ABBREVIATIONS

Å	angström
CD	Circular Dichroism
COSY	Correlation spectroscopy
CN	coordination number
Cp	cyclopentadienyl
CPL	Circularly Polarized Luminescence
DIPE	diisopropylether
DME	dimethoxyethane
Ln	lanthanide
Me	methyl
NIR	Near infrared
NHE	normal hydrogen electrode
NOESY	Nuclear Overhauser effect spectroscopy
TPA	Tris(2-pyridylmethyl)amine
LMCT	Ligand to metal charge transfer
MLCT	Metal to ligand charge transfer
Otf	Triflate
ORTEP	Oak Ridge thermal ellipsoid program
PFGSTE	Pulsed-field gradient stimulated echo
Ph	phenyl
Py	pyridine
RT	room temperature
tBu	tert-butyl
THF	tetrahydrofuran
TMS	trimethylsilyl

TABLE OF CONTENTS

CHAPTER I General Introduction

1- Luminescence of Lanthanides and Applications

1.1- The Lanthanides

The interest in lanthanides started first in 1787 when a young Swedish artillery officer, Lieutenant Carl Alex Arrhenius, found a black mineral which he called "ytterbite" at a small town called Ytterby close to Stockholm. Due to limitations in the chemical analysis of 18th century it was not easy to study the chemical composition of this mineral. In the following centuries, with the discovery of X-Ray techniques, these newly discovered elements (lanthanides) were analysed and placed in the periodic table. Finally with the synthesis and characterization of the final lanthanide: promethium, which does not occur naturally (prepared by neutron irradiation of Nd), all the lanthanides series have been completed in 1947 [1].

The lanthanides (Ln) series comprises the 15 elements of the first period of the f-block (Figure I-1) from lanthanum (Z=57) to lutetium (Z=71) with electronic configurations consisting of a xenon core with periodic filling of the seven 4*f* orbitals, from f^0 to f^{14}. With the inclusion of scandium (Sc) and yttrium (Y), this total of 17 elements is referred to as the rare earth elements (RE). Despite the name being "rare" earth, the most abundant lanthanide, cerium (Ce), is present at ~ 66 ppm in the earth's crust; this is therefore the 26th most abundant element on earth. Even the least common naturally occurring lanthanide, thulium (0.5 ppm) is more abundant than mercury or iodine. The main mineral sources of lanthanides are bastnasite $LnFCO_3$; monazite (Ln, Th)PO_4; and xenotime (Y, Ln)PO_4 [2].

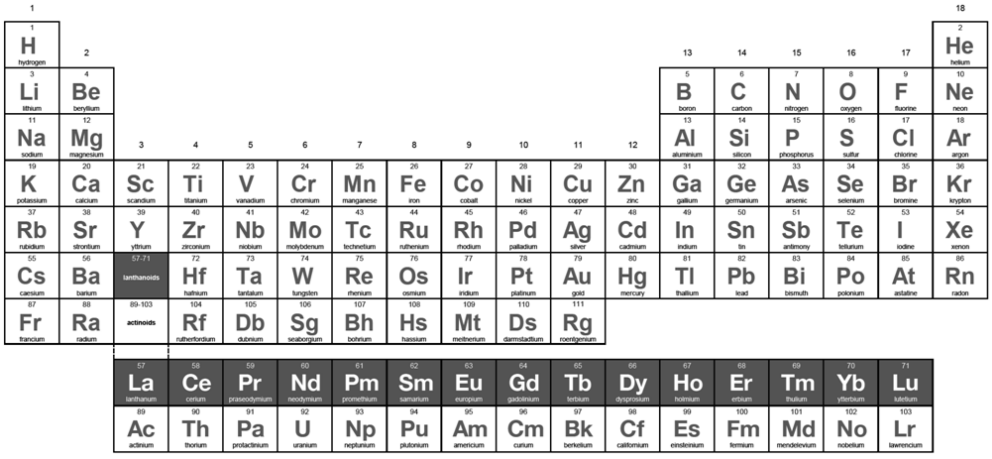

Figure I-1: Position of the lanthanide series in the periodic table

There are two types of electronic configurations for the lanthanide elements: $[Xe]4f^n6s^2$ and $[Xe]4f^{n-1}5d^16s^2$ (Table I-1) [3]. With the exception of La(III) and Lu(III), each of the Ln(III) ions contain one to seven unpaired 4f electrons and they are therefore paramagnetic. Loss of three electrons (one 4f or 5d electron and two 6s electrons) results in the formation of trivalent lanthanide ions. This oxidation state is highly stable throughout the series. However there are exceptional states in accordance with Hund's rule (electron shells are stable when empty $4f^0$, full $4f^{14}$ or half-full $4f^7$). For example, the configurations $4f^0$ (La^{3+}), $4f^7$ (Gd^{3+}), and $4f^{14}$ (Lu^{3+}) are stable. According to this rule the configurations of $4f^7$ of Eu^{2+} , $4f^{14}$ of Yb^{2+} , $4f^0$ of Ce^{4+} and $4f^7$ of Tb^{4+} are stable and these unusual oxidation states (divalent and tetravalent) are accessible for some lanthanides [3].

Table I-1: Electron configurations of the lanthanides and their common ions [4]

Element name	Symbol	Z	Ground state electronic configuration				Radius / pm	
			Ln	Ln^{2+}	Ln^{3+}	Ln^{4+}	Ln	Ln^{3+} ‡
Lanthanum	La	57	$[Xe]6s^25d^1$	$[Xe]5d^1$	$[Xe]4f^0$		188	116
Cerium	Ce	58	$[Xe]4f^16s^25d^1$	$[Xe]4f^2$	$[Xe]4f^1$	$[Xe]4f^0$	183	114
Praseodymium	Pr	59	$[Xe]4f^36s^2$	$[Xe]4f^3$	$[Xe]4f^2$	$[Xe]4f^1$	182	113
Neodymium	Nd	60	$[Xe]4f^46s^2$	$[Xe]4f^4$	$[Xe]4f^3$		181	111
Promethium	Pm	61	$[Xe]4f^56s^2$	$[Xe]4f^5$	$[Xe]4f^4$		181	109
Samarium	Sm	62	$[Xe]4f^66s^2$	$[Xe]4f^6$	$[Xe]4f^5$		180	108
Europium	Eu	63	$[Xe]4f^76s^2$	$[Xe]4f^7$	$[Xe]4f^6$		199	107
Gadolinium	Gd	64	$[Xe]4f^76s^25d^1$	$[Xe]4f^75d^1$	$[Xe]4f^7$		180	105
Terbium	Tb	65	$[Xe]4f^96s^2$	$[Xe]4f^9$	$[Xe]4f^8$	$[Xe]4f^7$	178	104
Dysprosium	Dy	66	$[Xe]4f^{10}6s^2$	$[Xe]4f^{10}$	$[Xe]4f^9$	$[Xe]4f^8$	177	103
Holmium	Ho	67	$[Xe]4f^{11}6s^2$	$[Xe]4f^{11}$	$[Xe]4f^{10}$		176	102
Erbium	Er	68	$[Xe]4f^{12}6s^2$	$[Xe]4f^{12}$	$[Xe]4f^{11}$		175	100
Thulium	Tm	69	$[Xe]4f^{13}6s^2$	$[Xe]4f^{13}$	$[Xe]4f^{12}$		174	99
Ytterbium	Yb	70	$[Xe]4f^{14}6s^2$	$[Xe]4f^{14}$	$[Xe]4f^{13}$		194	99
Lutetium	Lu	71	$[Xe]4f^{14}6s^25d^1$	$[Xe]4f^{14}5d^1$	$[Xe]4f^{14}$		173	98

‡ Ionic radius for an 8 coordinate ion

The 4f orbitals are well shielded by the xenon core by the large expansion of the $5s^25p^6$ subshells (Figure I-2). Thus, as the atomic number increases, an electron is not added to the outermost shell but rather to the inner 4f shell. The increasing effective nuclear charge, Z_{eff}, along the series is partly shielded by the 4f electrons resulting in the large contraction of the ionic radii. The phenomenon is called as "lanthanide contraction" with a decrease in ionic radii across the series (La (III) 1.16 Å and Lu (III) 0.98 Å) [5]. Another consequence of shielding of 4f orbitals is that these orbitals experience negligible interactions with ligand orbitals. Therefore, spectroscopic and magnetic properties of the lanthanides in complexes are essentially unaffected by the environment and are similar to the free ion. Furthermore core like 4f orbitals are not available for covalent interactions with coordinating ligands. Therefore lanthanide-ligand interactions are purely ionic. As a result of ionic character, Ln ions possess weak stereochemical preferences and a labile coordination sphere that leads to variable

coordination numbers (from 3 to 14) and geometries [2]. The large size of the lanthanide ions results in complex formation with coordination numbers of 8 and 9 being the most common. If the coordination number is not satisfied with the ligand, then the lanthanide completes its coordination sphere with solvent molecules. This makes it hard to predict coordination numbers in solution. The most common coordination geometries of the Ln^{3+} complexes in the solid state are square antiprismatic and dodecahedral for CN=8, tricapped trigonal antiprismatic and monocapped square antiprismatic for CN=9. Preferences between different coordination numbers and geometries tend to be controlled by steric effects (minimizing repulsion) due to ligand geometry and lanthanide contraction through the series.

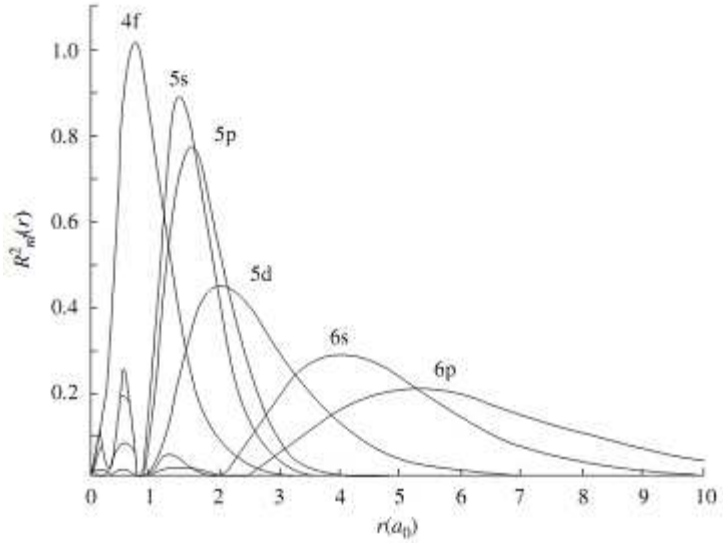

Figure I-2: Radial distribution functions of 4f, 5s, 5p, 5d, 6s, and 6p electrons for cerium [3]

1.2- Lanthanide Luminescence

Luminescence is defined as the emission of light associated to the relaxation of an electron from an excited state to the ground state. Lanthanide luminescence has important characteristics: line like emission, long life times (delayed emission) and large Stokes shift. With the exception of La(III) and Lu(III) ($4f^0$ and $4f^{14}$ respectively), each of the trivalent lanthanide ions are luminescent, with emission covering the entire spectrum from UV (Gd) to visible (Eu, Tb) and to near IR regions (Nd, Er, Yb, Ho). Some ions (Sm, Dy, Tm, and Pr) emit in both visible and NIR ranges.

There are two types of relaxation mechanisms: fluorescence (when there is no change in the spin of the transitions from the excited to the ground states [$\Delta S = 0$]) and phosphorescence (when there is a change in the spin of the transitions from the excited to the ground states [$\Delta S \neq 0$]). Fluorescence has a lifetime in the range of 10^{-12} to 10^{-6} second while the lifetime of phosphorescence is longer (10^{-6} to 10 s). Some ions are fluorescencent without

change in spin ($\Delta S=0$), $S_1 \rightarrow S_0$ i.e. Yb ($^2F_{5/2} \rightarrow {}^2F_{7/2}$) and some are phosphorescent with a change in spin ($\Delta S \neq 0$) $T_1 \rightarrow S_0$ i.e. Eu ($^5D_0 \rightarrow {}^7F_J$) transitions [6]. Luminescence could also be classified according to the excitation process: photoluminescence (excitation by photons), cathodoluminescence (excitation by cathode rays or energetic electrons), electroluminescence (excitation by an electric field), triboluminescence (subject to mechanical forces, i.e. grinding), and chemiluminescence (as a result of a chemical reaction) are types of luminescence processes.

Lanthanides have sharp f-f emission bands and small Stokes shifts as the rearrangement of electrons in 4f orbitals does not lead to a significant change in chemical bond lengths unlike organic compounds and d-transition metals. Figure I-3 compares the displacement of excited state potential energy curve to the ground state curve for an organic molecule and lanthanide ion. In view of Franck Condon principle, the vertical excitation leads to vibrationally excited states resulting in broad band spectra for an organic molecule. In contrast, Ln(III) ions result in narrow emission bands due to small offset of the electronic levels as shown in configurational coordinate diagram (Figure I-3).

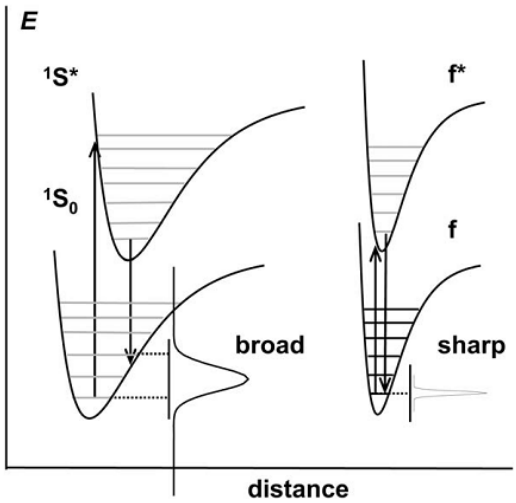

Figure I-3: Configurational coordinate diagram for emission from an organic molecule and a lanthanide ion [7]

1.2.1 Energy Levels

The spectroscopic properties of trivalent lanthanide ions are fascinating in that their [Xe]$4f^n$ electronic configuration generates numerous electronic levels (number of different ways to arrange the electrons in f orbitals), up to 3432 for Gd(III) for instance, as one easily calculates from the combinatorial formula (4l+2)!/n!(4l+2-n)! where l=3 for f-electrons [8]. The energy levels of a given lanthanide ion in a complex can be calculated by considering several interactions within the ion. The interactions that split up the levels belonging to the [Xe] $4f^n$ $5d^0$ configurations are shown in Figure I-4. The Coulombic interaction (electron electron repulsions) yields terms with separation of 10^4 cm^{-1}. Further splitting of these terms into J levels with separation of 10^3 cm^{-1} are provided by the spin orbit coupling. Ligand field further splits these levels slightly (due to shielding of 4f orbital) in to sublevels with 10^2 cm^{-1} separation (5000-30000 cm^{-1} for transition metals) [9]. This last splitting is mostly ignored for lanthanides however it could be used for gaining information on the symmetry of the complex.

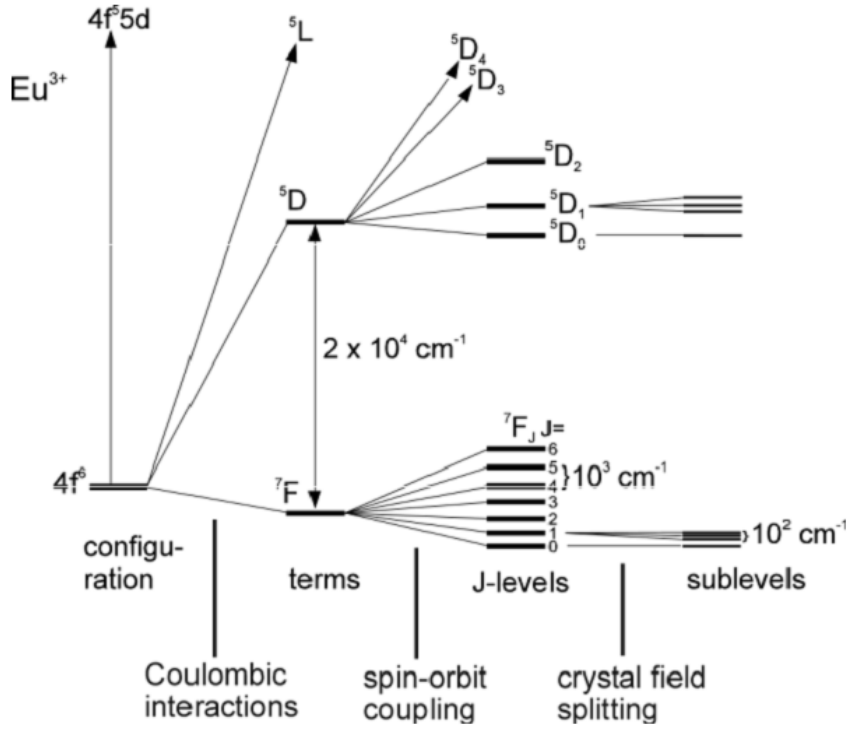

Figure I-4: The interactions leading to the different electronic energy levels for the [Xe] $4f^6$ $5d^0$ configuration of Eu^{3+}[10]

Each 4f electron is characterized by four quantum numbers n=4, l=3, m_l, m_s. The energy levels of lanthanides are represented by the term symbol $^{(2S+1)}L_J$ where S is the total spin quantum number and L is the total orbital angular momentum quantum number. The spin orbit coupling gives quantum number J which is the vector addition of S and L (J= (L+S), (L+S) -1, □ ,(L□S)). The ground state (according to the Hund□s rule) is determined to have the

highest S and L quantum numbers, and the spin orbit coupling quantum number J takes J=L-S for n < 7 (La-Eu) and J = L+S for n ≥ 7 (Gd-Lu). Figure I-5 shows the partial energy diagrams of lanthanides where the transitions from the emissive levels to the ground state of some lanthanides are indicated (i.e. Eu transition from $^5D_0$ to $^7F_0$, Yb from $^2F_{5/2}$ to $^2F_{7/2}$).

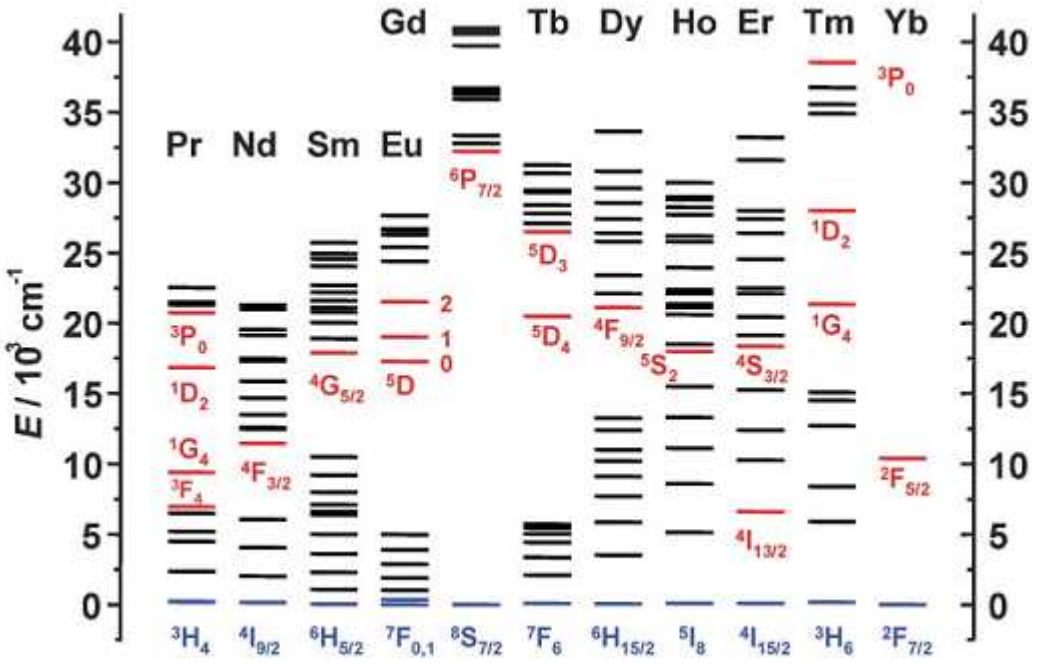

Figure I-5: Partial energy diagrams for the lanthanide aquo ions. The main luminescent levels are drawn in red, while the fundamental level is indicated in blue

1.2.2 Electronic Transitions and Selection Rules

Transitions between the energy levels occur via two operators; the electric dipole operator (ED) and the magnetic dipole operator (MD). Because of selection rule constraints, many transitions between different energy levels are forbidden transitions and the number of visible spectral lines is far less than expected [3]. One of these selection rules is the so-called Laporte□s rule (or parity rule) which requires, for ED transitions, the difference of the sum of the angular momenta of the electrons in the initial and final states to be an odd integer. Accordingly d-p or p-f transitions are allowed, whereas p-p or f-f transitions are forbidden. The other selection rules apply to S, L, and J quantum numbers; $\Delta S = 0$, $\Delta L = 0$ and $\Delta J = 0 \pm 1$ is allowed while $\Delta J = 0 \rightarrow 0$ is forbidden. In addition to these rules there are also symmetry related selection rules in between the sublevels that results from the ligand field effect. Site symmetry of the complex could be determined from the absorption or emission spectra by the splitting of J levels (Table I-2). For example, for Eu^{3+} the $^5D_0 \rightarrow {}^7F_1$ transitions is split in two in C_3 or C_4 symmetry, lower symmetry splits these transitions in three.

Table I-2: Number of ligand-field sub-levels in function of the J quantum number for Eu ion in various point symmetry

		Integer *J*								
Symmetry	Site symmetry	0	1	2	3	4	5	6	7	8
Cubic	T, T_d, T_h, O, O_h	1	1	2	3	4	4	6	6	7
Hexagonal	C_{3h}, D_{3h}, C_6, C_{6h}, C_{6v}, D_6, D_{6h}	1	2	3	5	6	7	9	10	11
Trigonal	C_3, S_6, C_{3v}, D_3, D_{3d}	1	2	3	5	6	7	9	10	11
Tetragonal	C_4, S_4, C_{4h}, C_{4v}, D_4, D_{2d}, D_{4h}	1	2	4	5	7	8	10	11	13
Low	C_1, C_S, C_2, C_{2h}, C_{2v}, D_2, D_{2h}	1	3	5	7	9	11	13	15	17

Lanthanide luminescence arises from three types of electronic transitions: (i) Charge transfer transitions (ligand to metal (LMCT) or metal to ligand (MLCT) charge transfer), (ii) 4f-5d transitions, (iii) f-f transitions. Charge transfer (observed mostly for Eu(III), Yb(III), while it is quite common for transition metals) and 4f-5d transitions (observed commonly for Ce(III), Pr(III), Tb(III)) are allowed by Laporte's selection rule however due to high energies (above 40000 cm^{-1}) of these transitions very few are observed. The most important source of lanthanide luminescence arises from the Laporte forbidden f-f transitions which become partially allowed in a chemical environment, resulting in long lasting emission (in the order of milliseconds).

1.2.3 Sensitization Processes

The intrinsic low extinction coefficients of the lanthanides ($\varepsilon = <10\ M^{-1}cm^{-1}$) prevents obtaining highly luminescent lanthanide complexes by direct excitation of the f-f transitions unless high energy excitation sources are used such as tuneable dye lasers and argon lasers. Indirect excitation (called sensitization or antenna effect) by energy transfer from an organic chromophore acting as an antenna is an efficient strategy for the sensitization of lanthanide luminescence which has been discovered by Weissman in 1942 [11]. He had studied the energy transfer from aromatic carboxylic acids, β-diketonates and alcohols to the metal ion. Sensitization of a lanthanide complex for the light emission is realised in a three-step mechanism: absorption of light by the surrounding chromophores, transfer onto the lanthanide ion, and emission of light at a different wavelength as shown in Figure I-6. The crucial point here is the sufficient absorption of light by the chromophore to yield intense emission at the end. Therefore the chromophores with high extinction coefficients are required for the sensitization of lanthanides.

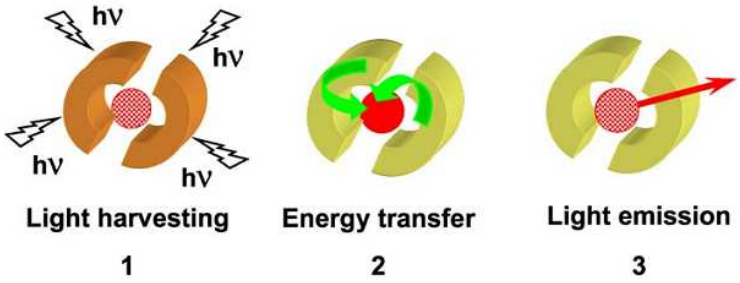

Figure I-6: Schematic representation of the sensitization process of lanthanide luminescence by organic chromophores [7]

Incorporation of organic chromophore not only enhances the population of excited states of lanthanides but also provides large Stokes shifts that leads to luminescence without background fluorescence. Organic molecules fluoresce at the UV region of the electromagnetic spectrum (λ_{ex}=270-300nm, λ_{em}=350-400nm). Except Gd(III) (emitting in the UV region), lanthanides emission is in the visible and near infrared region.

Sensitization of lanthanide ions with organic ligands is extremely complex and includes several mechanism and rate constants. The simplified mechanism of energy transfer from the organic ligand to the metal ion is given by the Jabloński diagram in Figure I-7. Organic chromophore with high extinction coefficients absorb light in the UV region and populate their singlet $^1\pi\pi^*$ excited state. Radiative deactivation to the ground state could occur through molecular fluorescence (F) or the electron can undergo non-radiative intersystem crossing (ISC) from the singlet state to the triplet state of the ligand. Enhanced spin orbit coupling from the presence of heavy atom (Ln) induces the increased rate of intersystem crossing (ISC) from the singlet to the triplet excited state. The triplet state can be deactivated by molecular phosphorescence (P) to the ground state radiatively.

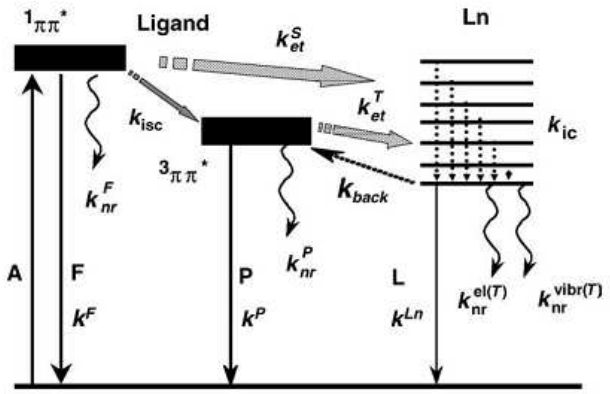

Figure I-7: Simplified diagram showing the energy migration paths in a Ln(III) complex ($^1\pi\pi^*$, singlet state; $^3\pi\pi^*$, triplet state; A, absorption; F, fluorescence; P, phosphorescence; L, luminescence (either fluorescence or phosphorescence); isc, intersystem crossing; nr, nonradiative; ic, internal conversion; et, energy transfer; back, back transfer; T, temperature dependent; el, electronic, vibr, vibrational [12]

The energy transfer from the ligand to the metal can occur from the excited $^1\pi\pi^*$ singlet and $^3\pi\pi^*$ triplet states of the ligand. In most of the cases energy transfer from the singlet state is negligible; therefore the triplet state is highly important for the sensitization process [13]. By the population of lanthanide excited states with this energy transfer from the ligand triplet states, the radiative transition to ground state results in line like photoluminescence of the lanthanide ion. There could be also non-radiative deactivation pathways to the ground state due to electronic deactivation processes and high frequency vibrational modes of the C-H, O-H, and N-H oscillators of the ligand in close proximity of the metal ion and the coordinating solvent molecules resulting in luminescence quenching. The energy transfer from the triplet state of the ligand to the lanthanide can occur through two mechanisms: via an exchange mechanism (Dexter mechanism) or via dipolar interactions (Förster mechanism). The mechanism of Dexter relies on an electronic exchange between ligand and metal. This exchange requires a good orbital overlap of metal and ligand, thus its efficiency depends on the distance between them (e^{-R}). Förster's (dipole dipole) mechanism relies on coupling between the dipole moments of triplet state and 4f orbitals. The efficiency of energy transfer in Förster's mechanism can be estimated by the equation:

$$\eta_{ET} = \frac{1}{1+\left(\frac{R}{R_0}\right)^6} \qquad \text{I-1}$$

where R is the distance between ligand and metal and R_0 is the critical distance for 50% transfer. While energy transfer by the Dexter mechanism is efficient at very small distances, Förster mechanism could be effective at longer distances. Therefore exchange mechanism is the preferred mechanism for energy transfer from the ligands to the metal ion; whereas dipole-dipole transfers are the main operating mechanisms in metal-to-metal energy transfer processes [7].

Luminescence of lanthanide ions is the result of the competition of radiative and non-radiative pathways in the relaxation of an electronically excited species. In the next section, the requirements for obtaining highly luminescent lanthanide complexes with high quantum yields will be discussed.

1.2.4 Efficiency and Quenching of Lanthanide Luminescence

The luminescence properties of a lanthanide ion depend on the efficiency of population of the excited states and the minimization of the nonradiative de-excitation paths. As explained in the previous section, organic chromophores are used for indirectly exciting lanthanide ions because of their low absorption coefficients. The efficiency of lanthanide luminescence is indicated by the overall quantum yield Q_{Ln}^{L} which is defined as the ratio of the number of emitted photons to the number of absorbed photons and also by the lifetime of the excited state $\tau_{obs}=1/k_{obs}$ (k_{obs} is the rate constant in s^{-1} of the de-population of the excited state). The total efficiency of the lanthanide luminescence depends on the efficiency of the energy transfer from the ligand to the metal as given in the equation I-2. Overall efficiency of the ligand to metal charge transfer η_{sens} could be divided into two terms: efficacy of the intersystem crossing process (η_{ISC}) and to the effectiveness of the $^{3}T \rightarrow 4f^{*}$ transfer (η_{ET}). Intrinsic quantum yield Q_{Ln}^{Ln}, the quantum yield obtained upon direct metal ion excitation, is related to the observed τ_{obs} and radiative lifetime τ^{rad} (the lifetime in absence of nonradiative deactivation) of the Ln excited state as given in equation I-3.

$$Q_{Ln}^{L} = \eta_{sens} Q_{Ln}^{Ln} = \eta_{ISC} \eta_{ET} Q_{Ln}^{Ln} \qquad \text{I-2}$$

$$Q_{Ln}^{Ln} = \frac{\tau_{obs}}{\tau^{rad}} = \frac{k^{rad}}{k_{obs}} \qquad \text{I-3}$$

There are several factors affecting the efficiency of lanthanide luminescence according to these equations. First of all the quenching of ligand singlet state by ligand fluorescence should be minimized and the population of triplet states should be enhanced by intersystem crossing (ISC). Afterwards it is critical to transfer energy from ligand triplet states to the lanthanide excited states (η_{ET}) which is enhanced by reduction of the Ln(III)-antenna distance (the rate of energy transfer is r^{-6} distance dependent) [14]. Another important point is the energy difference between the lowest triplet state of the ligand and the emitting level of the lanthanides. If the energy difference is too small, the total quantum yield decreases due to an energy back-transfer. Therefore the energy of the triplet excited state of the ligand should be optimized to be higher than the lanthanide excited states. Latva et al. have shown that highest quantum yields are obtained when the energy gap between the triplet state of the ligand and the emissive level is less than about 1 850 cm^{-1} for Tb($^{5}D_{4}$) level and around 2 500 or 4 800 cm^{-1} for Eu($^{5}D_{0}$) level [15]. Therefore it is crucial to optimize the ligand triplet states to obtain the highest possible quantum yield from lanthanide luminescence.

The intrinsic quantum yield Q_{Ln}^{Ln} essentially depends on the extent of non-radiative deactivation processes. Experimental determination of Q_{Ln}^{Ln} is difficult due to low extinction coefficient of f-f transitions. Therefore Q_{Ln}^{Ln} is derived from the equation I-3 in which radiative lifetime τ^{rad} could be determined from the absorption spectrum by using Einstein's rate of spontaneous emission. Europium radiative lifetime can be determined with a simplified equation I-4.

$$\frac{1}{\tau_{rad}} = A_{MD,0} n^3 \left(\frac{I_{tot}}{I_{MD}} \right) \qquad \text{I-4}$$

with $A_{MD,0}$ being a constant equal to 14.65 s^{-1}, n being the refractive index of the media and (I_{tot}/I_{MD}) the ratio of the total integrated $^5D_0 \rightarrow {}^7F_J$ emission (J = 0–6) to that of the $^5D_0 \rightarrow {}^7F_1$ magnetic dipole transition.

The rate constant k_{obs} is the sum of the rates of various deactivation processes, where k^{rad} and k^{nr} are the radiative and nonradiative constants which are shown in equation I-5. k^{vibr} is the rate of vibration induced processes, k^{pet} photoinduced electron transfer processes (LMCT, MLCT). The rate constant k^{nr} is associated with the remaining deactivation paths.

$$k_{obs} = k^{rad} + \sum_i k_n^{nr} = k^{rad} + \sum_i k_i^{vibr}(T) + \sum_j k_j^{pet}(T) + \sum_k k_k^{nr} \qquad \text{I-5}$$

The vibration induced non-radiative deactivation processes (high energy vibrations O-H, C-H, … etc) are much more effective if the energy gap ΔE between the excited and the ground state of the lanthanide ion is small, which is observed with most of the lanthanides emitting in the NIR region. The highest energy gap (ΔE=32 200cm^{-1} ($^6P_{7/2} \rightarrow {}^8S_{7/2}$)) is observed for the Gd ion, however the emission in UV region is not very useful for the design of luminescent tags as the luminescence of this ion interferes with the organic part of the complex. Eu and Tb also have high energy gaps with ΔE=12 300cm^{-1} ($^5D_0 \rightarrow {}^7F_6$) and ΔE=14 800$cm^{-1}$ ($^5D_4 \rightarrow {}^7F_0$) therefore high quantum yields are obtained with these ions in solution or solid state due to reduced deactivation processes compared to the other Ln ions.

The effect of vibrational non-radiative deactivation can be minimized by a careful ligand design. The coordination numbers of lanthanides are high (6-12), so the ligand should saturate inner coordination sphere possessing sufficient donor atoms. If it is not the case, the

coordination sphere is filled with solvent molecules which are detrimental to lanthanide luminescence through quenching by non radiative deactivation processes.

Electronic deactivation processes (PET photoinduced electron transfer) occur through intermolecular electron transfer from the excited ligand singlet states to the metal (resulting in a reduction of Ln^{3+} to Ln^{2+}), instead of population of triplet states of the ligand. These transitions should be avoided by the modulation of the redox potentials of the ligands (i.e. by attaching electron withdrawing groups to aromatic ring chromophores to increase the oxidation potential) [16].

1.3- Applications of Lanthanide Luminescence

The luminescence of trivalent lanthanide ions has found applications in various fields like lighting, displays, lasers, optical telecommunications, biotechnology, medical diagnostics, solar energy, bio-imaging and material science. A full description of all the applications of lanthanide-based materials is beyond the scope of this thesis. Therefore only a brief overview of some applications will be given in this section to mention the significance of lanthanide complexes in various areas of technology and science.

The first commercial application of lanthanides date back to 1891 when the gas mantle (99% ThO_2 and 1% of CeO_2) of Carl Auer von Welsbach provided the widespread use of incandescent gas lamps both indoors and outdoors [2]. Lanthanide doped phosphors are (i.e. highly emissive Eu doped Y_2O_3 giving the red color) heavily used for fluorescent lamps, flat panel displays and cathode ray tubes of televisions [17-19]. Lanthanide ions are also applied as the light generating and amplifying constituents in lasers (e.g. in the Nd^{3+}: YAG laser with an intense and monochromatic emission 1060 nm) and optical amplifiers (erbium (III) doped optical fibers for telecommunications) [10, 20].

The interest in luminescent coordination complexes started when Eu and Tb complexes with polyaminocarboxylates and β-diketonates ligands have been proposed as bioprobes in time-resolved luminescent (TRL) immunoassays in 70s [21]. Luminescent lanthanide complexes provide very long decay time, large Stokes Shift and sharp emission profiles which are different from organic fluorescence dyes. Therefore they have found various applications in medical diagnostics as lanthanide luminescent bioprobes (LLBs), labeling reagents in time resolved luminescent (TRL) immunoassays, luminescent stains in

tissue and cell imaging, due to their easy and efficient background discrimination in fluorometric analysis. Moreover, NIR emitting complexes have recently shown to be very interesting for cell imaging as they provide a deep investigation (20 mm) of the tissue [22]. Time resolved luminescence spectroscopy (TRLS) finds application in highly sensitive immunoassays and bio-imaging because of the high signal/noise ratio. Notably in TRLs the excitation is followed by a time delay in order to suppress the luminescence from the organic background in biological samples as shown in Figure I-8.

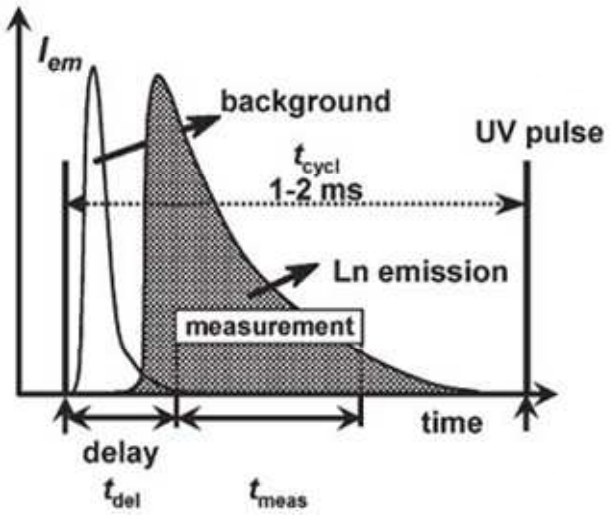

Figure I-8: Principles of time resolved luminescence spectroscopy [6]

Recently, lanthanide complexes were also proposed as luminescent materials for electroluminescent devices i.e. organic light emitting diodes (OLEDs) [23, 24]. OLEDs consist of a number of layers deposited on either solid (glass) or flexible polymer substrates. These layers can be deposited by several techniques like vacuum deposition, spin coating, inkjet printing, etc. The light emission results from formation of excitons by the recombination of holes ejected from an anode and electrons from a cathode in the emissive layer. Incorporation of lanthanide complexes in OLED applications provides quasi monochromatic emission and higher efficiency of the device due to the energy transfer from the triplet state of the host to the lanthanide emissive levels. [$Tb(acac)_3$] (acac= acetylacetonate) was used for the fabrication of the first lanthanide based visible-emitting OLED in 1990 [25]. In the NIR range $Er(hq)_3$ (hq= 8-quinolinate) was proposed as the emitting layer in OLEDs [26]. Since then, significant progresses were achieved in the field, however further improvements in the quantum efficiencies and the stability of the complexes are needed in order to maintain required device properties.

Another potential application of lanthanides is in the solar (SC) or photovoltaic (PV) cells for the transformation of solar light into electricity. Silicon is the most widely used inorganic semiconductor with a bandgap of 1.12 eV collecting about 50% of the sun power as shown in Figure I-9. The limitations in efficiency and main energy losses in silicon based solar cells are related to this spectral mismatch. The lanthanide complexes could be used in photovoltaic cells for improving the efficiency by extending the absorption range of solar cells. They could be adapted to solar cells as down converting or up converting materials in order to recover the solar energy which is not absorbed by silicon. Efficient down conversion can be achieved by using appropriate lanthanide couples. For example Tb^{3+}-Yb^{3+} couple in $(Y,Yb)PO_4:Tb^{3+}$ is the first published study in solar cells [27] that leads to conversion of UV-blue emission into NIR with enhanced quantum efficiencies. On the other side, NIR emission could be transformed into visible light by up converting materials. Er doped compounds have shown to be efficient up converting materials for solar cells. Recently up conversion of 1480-1580 nm excitation into 545, 665, 800 and 900 nm emission has been demonstrated by $Gd_2(MoO_4)_3:Er^{3+}$ nanophosphor [28].

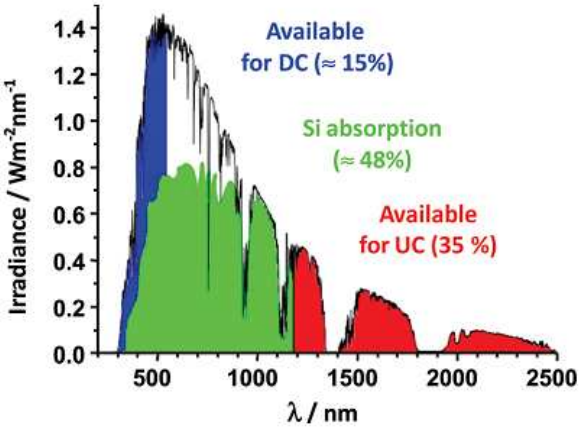

Figure I-9: Air mass (AM) 1.5 solar spectrum together with the fraction absorbed by a thick silicon layer as well as the spectral ranges available for down-conversion (DC) and up-conversion (UC) [29]

Lanthanides have also been used in less common applications like in agriculture. Plastics doped with lanthanides have shown to increase crop yield by 10% through conversion of the UV portion of the solar energy (detrimental to cell growth) to the visible light [30]. The luminescence of lanthanides has found to be useful in a variety of highly sensitive applications such as security inks and bar codes. For example, euro bills were printed with an anticounterfeiting ink yielding under UV light red emission on one side and green emission on the other side of the bill. The red emission is predicted to be tris(β-diketonate) complexes of Eu^{3+} while greenish blue emission could arise from a Eu^{2+} complex [30]. As lanthanides

have sharp and easily recognisable emission bands, they are easily adaptable as bar-coded materials. Recently Petoud et al. have shown a very nice example of a barcoded system based on polymetallic lanthanide complexes that simultaneously emit several independent NIR signals arising from different lanthanide cations resulting in distinguishable emission profiles [31].

1.4- Design of Luminescent Lanthanide Complexes

The lanthanide ions are hard Lewis acids according to Pearson's classification, preferentially binding anionic ligands which have nitrogen and/or oxygen donor groups. Stable lanthanide complexes form with hard anionic Lewis bases such as carboxylates, phosphonates, phospinates and β-diketonates. As mentioned before, to increase the emission intensity of the Ln(III), the ligand should have a strong absorption and a fast inter-system crossing in order to populate triplet states of the ligand, and the triplet state of the ligand should match with the emitting states of the lanthanide to ensure efficient energy transfer. These requirements have been met by organic chromophores characterized by high efficiency of light absorption (high extinction coefficient ε) and high efficiencies of intersystem crossing and energy transfer processes.

Several chromophores have been used in lanthanide coordination chemistry for sensitizing visible and NIR luminescence of lanthanides with the aim of obtaining highly luminescent lanthanide complexes. The chromophores studied the most are N-heterocyclic ligands including pyridine, bipyridine, terpyridine, phenanthroline, benzimidazole, pyrazole, hydroxyquinoline, etc. In order to avoid vibrational non-radiatiative deactivation processes these chromophores are further adapted to polydentate or macrocyclic ligands or associated to β-diketonate ligands in ternary complexes to saturate coordination sphere of the lanthanides. In order to keep this thesis at a reasonable length, only some selected examples of chromophores used in lanthanide coordination chemistry will be given in this section.

1.4.1 Suitable Chromophores and Ligands for Luminescent Lanthanide Complexes

Picolinates are effective antennas for the luminescence sensitization of visible emitting lanthanides. A simple tridentate pyridine containing ligand pyridine-2,6-dicarboxylic acid or dipicolinic acid (H_2dpa) [32-39] is widely used to prepare tris complexes with lanthanides $[Ln(dpa)_3]^{3-}$ (Ln=Eu, Tb) that possess good luminescence properties leading their use as standards for the determination of quantum yields of lanthanide complexes [40]. In our

laboratory tetrapodal decadentate ligands have been prepared with four picolinate building blocks connected with a linear flexible spacer (ethylendiamine: H_4tpaen; butylendiamine: H_4tpabn) that yields high-luminescence emission quantum yields (39 - 45%) for the terbium complexes.[41-43]

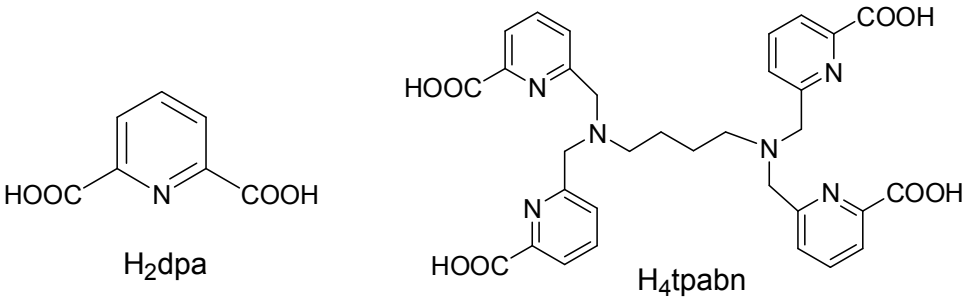

Scheme I-1: Examples of pyridine based ligands

The bidentate bipyridine (bipy) and tridentate terpyridine (terpy) are also efficient chromophores for the luminescence sensitization of visible emitting lanthanides. Several research groups have studied different bidentate bipyridine based ligands with anionic groups (COOH, PO_3H_2) for increased stability [44, 45] or bipy unit has been adapted to podating architectures [46, 47]. Lehn et al. have designed an interesting bipy based cryptate (bipy, bipy, bipy) which provided high stability and good energy transfer to sensitize Eu and Tb ions and has been used as a commercial luminescent probe [48]. Bünzli and coworkers studied the sensitization of lanthanides with tridentate terpyridine (terpy) based ligands where they have shown that the substitution of terpyridine with ethyl and t-butyl groups enhanced the luminescence properties. For example, they measured a quantum yield of 67% for $[Tb(t\text{-}Bu\text{-}terpy)_3]^{3+}$ in anhydrous acetonitrile whereas 5% quantum yield was measured for $[Tb(terpy)_3]^{3+}$ [49]. Similar luminescence properties to terpy complexes have been measured with the complexes prepared by the ligand mbzimpy in which the terminal pyridine units have been replaced by benzimidazole groups [50].

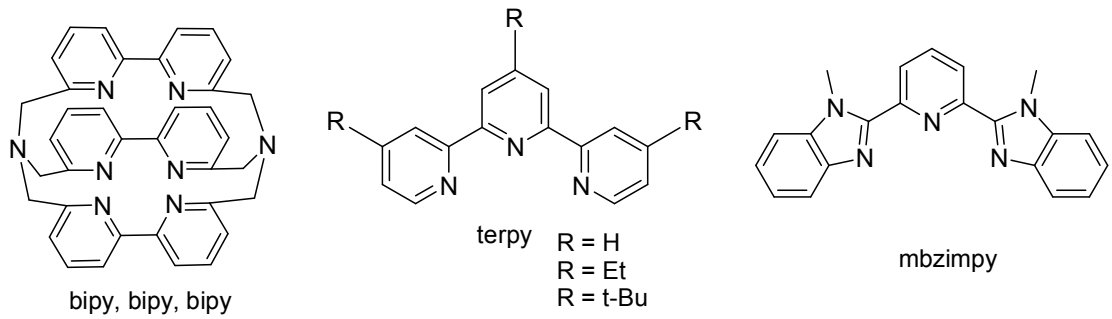

Scheme I-2: Examples of bipy and terpy based ligands

It has recently been shown by our group that tetrazolates can act as efficient sensitizers of lanthanide luminescence. A series of stable, highly luminescent lanthanide complexes based on the terpyridine, bipyridine, and pyridine tetrazolate chromophores have been prepared in comparison to the isostructural carboxylate complexes. Various substituents such as bromo-phenyl, bromo-thiophene, phenyl-pyridine or bis-thiophene have been attached to the ligands in order to modulate the energies of the ligand excited states. The replacement of the carboxylate group with tetrazolate extended the excitation window of the corresponding terpyridine- (~20 nm) and bipyridine-based (25 nm) complexes towards the visible region (up to 350 nm). The tetrazole-based ligands sensitize efficiently the luminescent emission of lanthanide ions in the visible and near-IR regions with quantum yields ranging from 5 to 53% for Eu(III) complexes, 6 to 35% for Tb(III) complexes, and 0.1 to 0.3% for Nd(III) complexes, which is among the highest reported for a neodymium complex [51, 52].

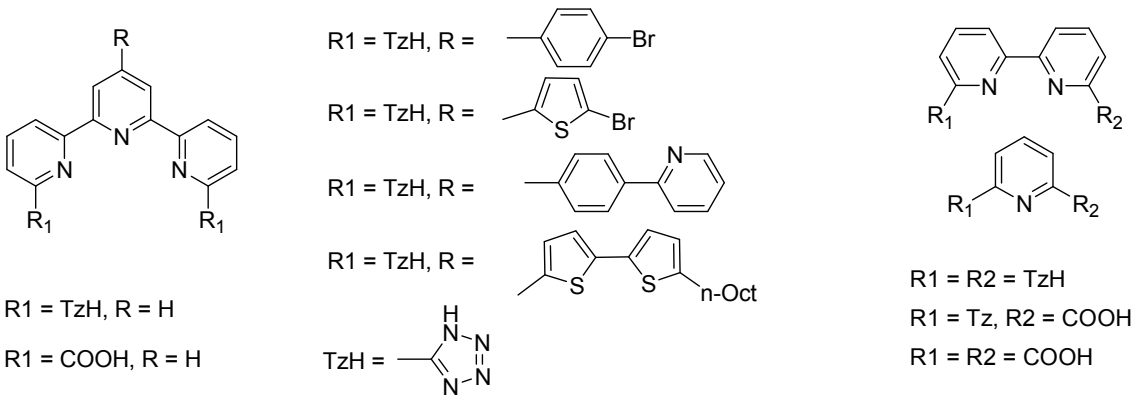

Scheme I-3: Series of tetrazole or carboxylate ligands based on pyridine, bipyridine and terpyridine

The 1,10-Phenantroline (phen) is a well known chromophore that is efficient for the sensitization of lanthanide luminescence. The ternary complexes of phenantrolines with β-diketonate ligands [53] tend to show intense luminescence [54]. Barigelletti and coworkers have reported the water soluble highly luminescent complexes formed by ligands bearing 1,10-phenantroline units attached to a flexibly connected diethylenetriamine tetracarboxylic acid unit (H_4-phen-DTTA) or to tetraazacyclododecane triacetic acid unit, (H_4-phen-DO3A) as shown in Scheme I-4. The quantum yields in water solutions were measured to be 21-24% and 11-45% for the europium and terbium ions respectively [55, 56].

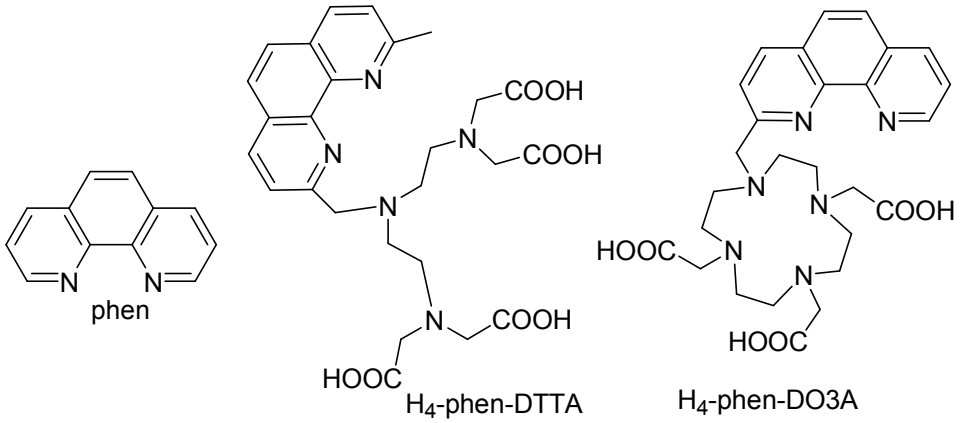

Scheme I-4: Examples of phenantroline based ligands

Tropolonate, azulene and 8-hydroxyquinoline were shown to be effective to sensitize lanthanides emitting in the NIR region (Scheme I-5). Petoud and coworkers have shown that the tropolonate unit is an efficient chromophore to sensitize five different lanthanides (Nd^{3+}, Er^{3+}, Ho^{3+}, Tm^{3+}, Yb^{3+}) in their tetrakis $[Ln(Trop)_4]^-$ complexes in solution with a quantum yield of $1.9x10^{-2}$ % for Yb^{3+} in DMSO [57]. The authors have reported recently the use of a chromophore called azulene which has a lower triplet state (13 600 cm^{-1}) than tropolonate (17 200 cm^{-1}) matching better with the NIR lanthanide emissive levels. The azulene unit sensitize four different lanthanides (Nd^{3+}, Er^{3+}, Tm^{3+}, Yb^{3+}) and the quantum yields recorded for Yb^{3+} (3.8% in acetonitrile) is one of the highest values recorded in literature [58]. 8-hydroxyquinolinate is a common chromophore studied widely to sensitize lanthanide NIR luminescence since $[Er(hq)_3]$ [26] was shown to be compatible with silicon technology. This chromophore has been adapted to several ligand architectures to enhance NIR luminescence of lanthanides.

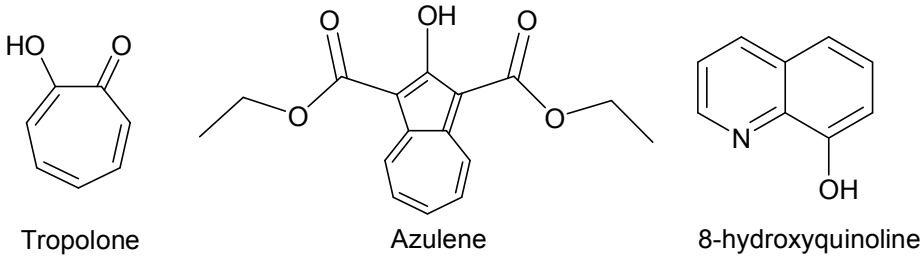

Scheme I-5: Chromophores used for sensitizing NIR emitting lanthanides

Hydroxyquinolate groups have been included into tripodal ligands [59-63] (Scheme I-6) in order to better control the structural properties with a large chelate effect. Sulfonate groups are attached to provide water solubility for biological applications. In our laboratory recently the complexes $[Ln(L_{1b})(H_2O)_2]$ (Ln = Gd, Nd, Yb) have been prepared as potential bimodal MRI/NIR imaging agents [62]. The photophysical studies

showed that the tripodal ligand is an efficient sensitizer of lanthanide luminescence in water. Remarkable quantum yields of 5 x 10^{-4} % for Nd^{3+} and 1.2 x 10^{-3} % for Yb^{3+} have been obtained inspite of the presence of two coordinated water molecules. The replacement of the pivotal amine group by the 1,4,7-triazacyclononane core resulted in the tripodal nonadentate ligand thtqtcn (L_{1c}) which led to the preparation of neutral monomeric [Ln(L_{1c})] complexes. The ligand L_{1c} sensitizes efficiently the NIR emission of Nd and Yb complexes in solid state with 0.10% and 0.60% of quantum yields respectively. The water soluble complexes of the sulfonated L_{1d} ligand show quantum yields of 0.016% for Nd and 0.14% for Yb complexes in water [63]. Imbert et al. have synthesized the tetrapodal Tsox ligand L_{2a} and L_{2b} where water soluble sulfonated ligand gave highly stable complexes suitable to be adapted as probes for bioanalysis [60].

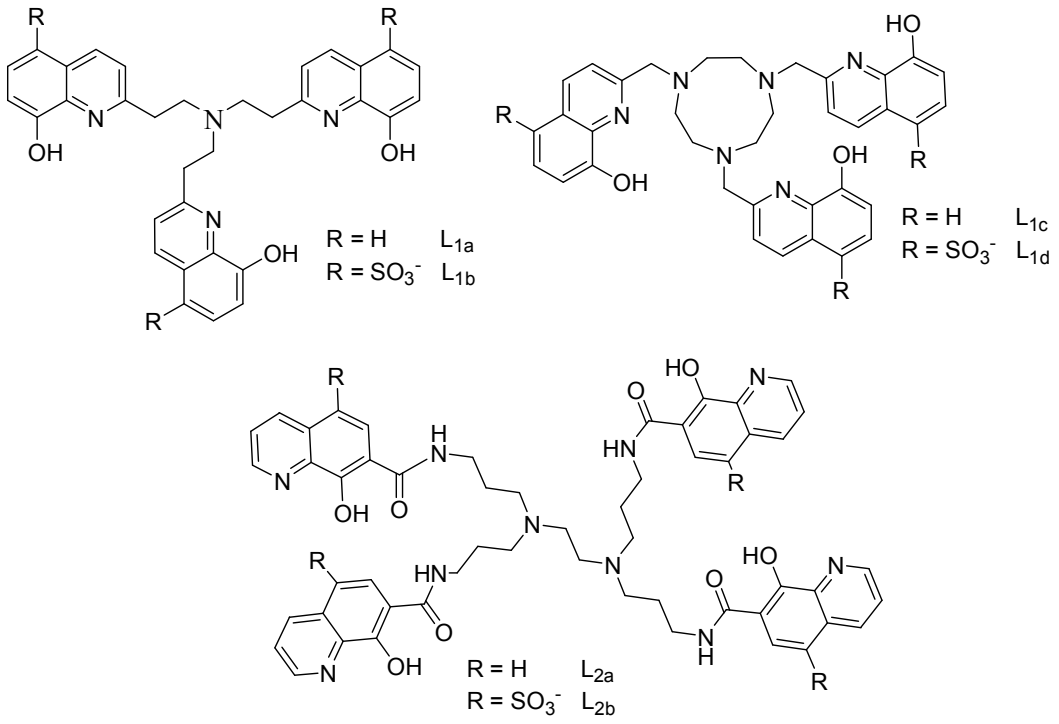

Scheme I-6: Tripodal and tetrapodal ligands incorporating 8-hydroxyquinoline moieties

2- Molecular and Supramolecular Lanthanide Complexes

In view of weak steric requirement of the lanthanide ions, several strategies have been developed over the past decades for the design of mono- and polynuclear assemblies [64-66]. In this section, the synthetic methods with different ligand types allowing the introduction of lanthanides into elaborate monometallic and polymetallic edifices will be examined.

2.1- Strategies towards Mononuclear Lanthanide Complexes

In order to achieve structural control and improved stability in monometallic complexes, in general two different strategies have been investigated. One is the so-called lock and key principle which relies on encapsulation of lanthanides into a preorganised macrocycle. The match between the cavity size and the ionic radii is the key to the recognition process by changing the form, size, number and nature of donor atoms of the macrocyle for a better fit. The ionic radii in lanthanide series vary only slightly (La(III) 1.16 Å and Lu(III) 0.98 Å), therefore it is a great challenge to fine tune the cavity size with the lanthanide radius.

Second approach is called induced fit principle where predisposed macrocycles with pendant arms, podand ligands and flexible multidentate receptors are used for complexing lanthanide ions by forming an induced cavity that matches the lanthanide size. In the latter the non covalent interactions like hydrogen bonding, π-π stacking and metal interactions play an important role in the stabilization of the complexes. The macrocyclic ligands with pendant arms have shown to be good chelating agents for lanthanides, however no significant improvement was observed in size selectivity due to difficulties in tuning the size of the macrocycle for a best fit to lanthanide radius. The complexes with 1,4,7,10-tetrakiscarboxymethyl-1,4,7,10-tetraazacyclododecane (DOTA) have shown high stability (log K in the range 22-26) due to the perfect match between cycle and lanthanide radius but also due to the hard ion-ion interaction between the wrapping carboxylate anions and the lanthanides.

The synthetic difficulties on attaching polydentate arms onto macrocycles lead to the podand type ligands developed by attaching two, three or four ligands to a central atom or an aromatic ring. The number and nature of donor groups of a podand can be easily changed. However, since these types of ligands are not as predisposed as macrocylic analogues, the correct orientation of the arms upon complexation requires more work and mostly several isomers can be found after complexation. The solution to this problem relies on non-covalent interactions such as hydrogen bonding that could be used for organizing the arms. Tetrapodal

polyaminopolycarboxylate systems in which four or more acetic groups are covalently attached to a polyamino skeleton, such as ethylendiaminetetraacetic acid EDTA, form highly stable and water soluble complexes.

2.2- Strategies towards Polynuclear Lanthanide Complexes

In contrast to the large number of the studies in mononuclear complexes, the number of studies in the field of polynuclear lanthanide complexes has been limited due to difficulties in controlling the coordination environment of f elements that show variable coordination numbers with little stereochemical preferences. The development of polynuclear lanthanide complexes could provide novel supramolecular functions that cannot be reached by mononuclear complexes. Moreover, optical properties of lanthanides complexes could be ameliorated by energy transfers between metallic centers in the same structure [67, 68]. The luminescence intensity should be improved as the number of lanthanide cations per unit volume is increased in polynuclear complexes with a good control of the intermetallic distances to avoid concentration quenching. For example, Brennan et al. have observed a correlation between quantum efficiencies and cluster size by measuring the quantum efficiencies of 9% in $(DME)_2Nd(SC_6F_5)_3$, 16% in $(THF)_8Nd_8O_2Se_2(SePh)_{14}$ [69], and 12% in $(py)_{18}Nd_{12}O_6Se_{12}(SePh)_8(SeSePh)_2Hg$ [70], the 35% in $(py)_{16}Nd_{17}NaSe_{18}(SePh)_{16}$ [71]. The great interest on these high nuclearity lanthanide clusters resides in the fact that they can be used as precursors for functional materials in optics, electronics or catalysis, also they can adopt easily to the techniques of deposition (CVD, etc.) [72]. In addition to homo-polymetallic complexes, selective assembly of different Ln emitters in large molecular architectures, although very challenging due to the similar properties of Ln ions, is of high interest for the preparation of precursors of doped materials, for the implementation of energy transfer and for the development of multi colour devices. The presence of several lanthanide ions in the structure also presents a strong fundamental interest for the understanding of energy transfer mechanisms.

Several strategies could be found in the literature focusing on supramolecular assemblies. In the next section, a brief review on these strategies will be given. The control of assembly is still highly challenging. Indeed, mostly mixtures of compounds are obtained and different crystallization conditions result in different compounds. Similar to the mononuclear complexes, some studies present the use of macrocyclic receptors and the lock and key principle, while the others concentrate on predisposed ligands according to the induced fit

concept to lead to self assembled polynuclear lanthanide complexes by noncovalent interactions.

The approaches that have been reported in literature for the preparation of discrete polynuclear lanthanide complexes will be discussed in the following subsections.

2.2.1 Macrocyclic Ligands

In this approach, the size of macrocyclic receptors is adapted in order to include several Ln ions to obtain polymetallic lanthanide complexes (Scheme I-7). Dimetallic complexes $[Eu_2(L_4\text{-}6H)\text{-}(DMF)_5]$ [73], $[Gd_2(L_5\text{-}6H)(H_2O)_2]$ [74], $[Ln_2(L_6\text{-}2H)(NO_3)_4]$ [75], $[Ln_2(L_7\text{-}2H)\text{-}(NO_3)_4]$ [76], and $[La_2(L_8\text{-}2H)(OAc)_4]$ [77] are obtained successfully with these ligands with a good control of lanthanide distance by the ligand architecture. They form rigid structures that the conformation of the complexes does not change in solution and solid state. Even tough it is possible to control intermetallic distance in these macrocyclic ligands by increasing the size of the ligand, inclusion of different lanthanides is not an easy task, where dissymmetrisation of the ligand could be a solution. In this approach the size of the ligand determines the nuclearity of the final complex. The challenging organic synthesis of larger macrocycles prevents the preparation of higher nuclear complexes with this approach.

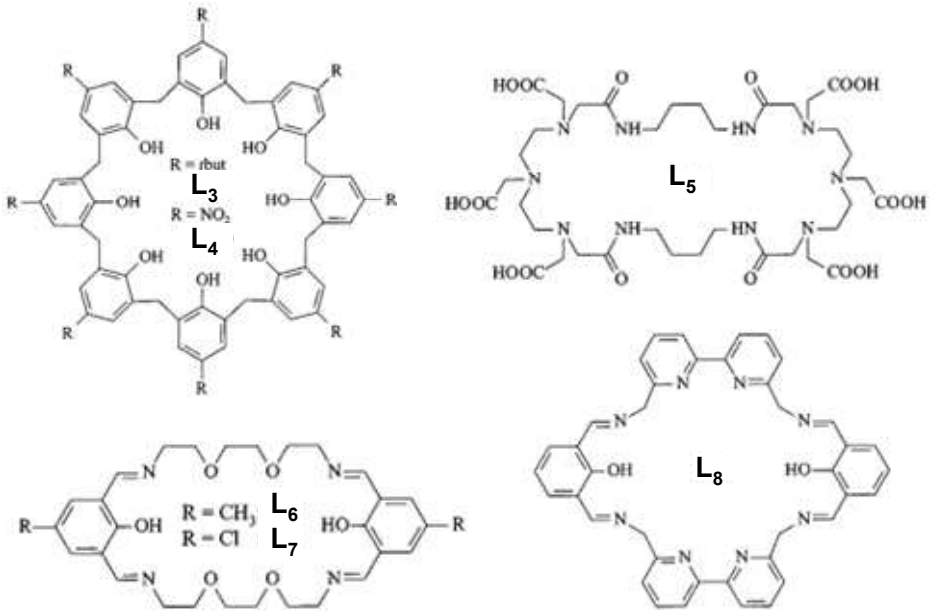

Scheme I-7: Macrocyclic ligands used for preparing dimetallic complexes

One of the strategies to obtain heteropolymetallic complexes is to combine several macrocyclic ligands by suitable linkers. For example, Faulkner et al. have obtained dinuclear complexes Ln_2L where ligand contained DO3A units connected by phenylene spacer [78]. By attaching the two DO3A units with a DTPA arm, they have isolated heterotrinuclear complex

($Ln_2Ln'L_9$) with two Tb and one Yb included (Scheme I-8) [68]. This assembly illustrates the energy transfer in between two metallic cations: where excitation of the complex in the absorption bands of terbium results in ytterbium luminescence.

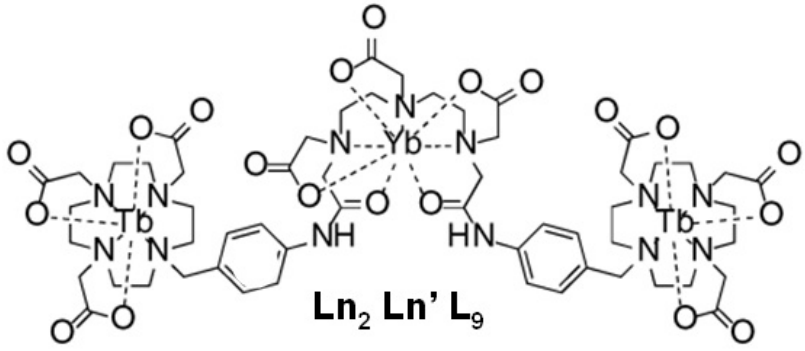

Scheme I-8: Macrocyclic receptor derived from DO3A for the preparation of polymetallic complexes

2.2.2 Dendrimers

Dendrimers are globular, highly branched polymers with internal cavities where ions can be hosted. Suitably designed dendrimers can be used as light harvesting antennas and as ligands for metal ions [79]. Kawa and Frechet reported a luminescent metallodendrimer formed by self assembly of three polybenzyl ether dendrons by carboxylate anion coordination to a central trivalent lanthanide ion (Er, Tb, Eu) (Figure I-10a) [80]. The enhancement of the luminescence properties is related to the increased antenna effect with the increase of the size of the dendrimer and the shielding of encapsulated lanthanide ion from solvent interactions. Dendrimers can also coordinate to several metal ions by the ligand units in their branches leading to polymetallic complexes. Petoud et al. designed a ligand based on PAMAM (polyamidoamine) dendrimer whose branches contain internal amide groups capable of binding hard Lewis acid lanthanide ions through their oxygen atoms, and which have terminal primary amine end branches functionalized with 32 2,3-naphthalimide chromophoric groups [81]. They have followed the formation of well defined species (Figure I-10b) by luminescence titrations. Due to a large number of chromophores (32 2,3-naphthalimide) and 8 lanthanide cations per volume, the species with dendrimer/lanthanide ratio of 1:8 showed an intense Eu^{3+} emission confirming that this strategy is a promising one to obtain luminescent polymetallic lanthanide complexes.

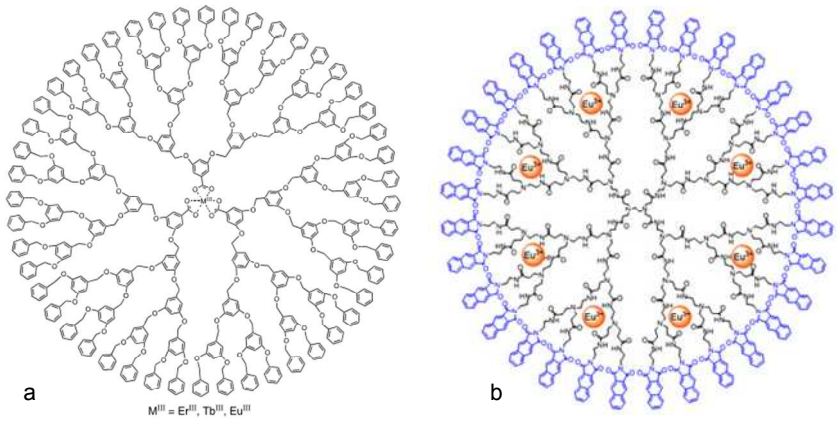

Figure I-10: a) Ln-cored dendrimer complexes [80]
b) Polymetallic complex formed by reaction of a generation-3 PAMAM dendrimer whose branches have been functionalized with 32 2,3-naphthalimide groups with eight Eu^{3+} cations [81]

2.2.3 Self Assembly Processes

Self assembly in coordination chemistry can be defined as the spontaneous association of metal and ligand molecules under thermodynamic equilibrium by means of programmed weak noncovalent interactions such as hydrogen bonds, metal-coordination and π-π interactions. The loss of conformational entropy compared to preorganised systems is overcome by favourable enthalpic contributions originating from these noncovalent interactions. By using self assembly processes, certain predictability of the architecture could be achieved with a good ligand design which works as geometrically pre-determined building blocks. Several flexible predisposed ligands have shown to form stable self assembled complexes in the last two decades. Figure I-11 shows an example of a self assembled tris complex formed by three benzimidazole moieties organized spatially by Ln-N ion dipole bonds and by π-π interactions between almost parallel aromatic rings [82]. Apart from that self assembly could lead to the formation of polynuclear lanthanide complexes with a rational ligand design. Interesting polynuclear assemblies have been obtained by using tripodal ligands, helicates and small predisposed ligands. Some examples will be given in the following subsections.

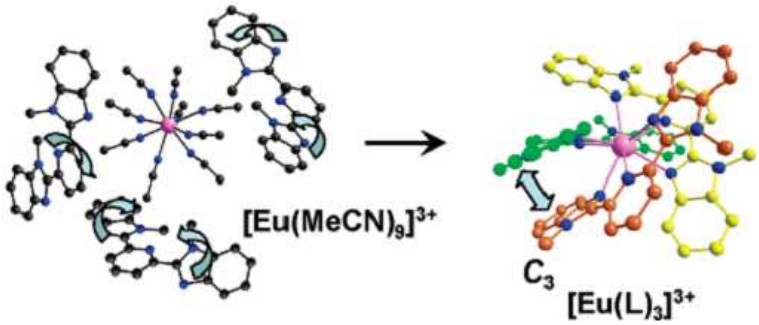

Figure I-11: Formation of a tris benzimidazole complex by self assembly [64]

a) Tripodal Ligands

Tripodal ligands can bridge to two or more metal ions to yield polymetallic lanthanide complexes. A recent example is given by Hamacek et al. where the symmetric tripodal ligand **L_{10}** leads to 3D tetrahedral species $[Ln_4(\mathbf{L_{10}})_4]^{12+}$ [83], whereas the ternary self-assembly of the ligands **L_{10}** and **L_{11}** with lanthanide cations in stoichiometric quantities is thermodynamically driven to the first pentanuclear 3D lanthanide complex $[Ln_5(\mathbf{L_{10}})(\mathbf{L_{11}})_3]^{15+}$ [84] (Figure I-12). Even though no crystal structure of pentametallic complex could be obtained, the formation of these species has been followed by NMR and ES-MS studies. The pentanuclear assemblies could be adapted to prepare heteronuclear complexes by a rational ligand design in the near future.

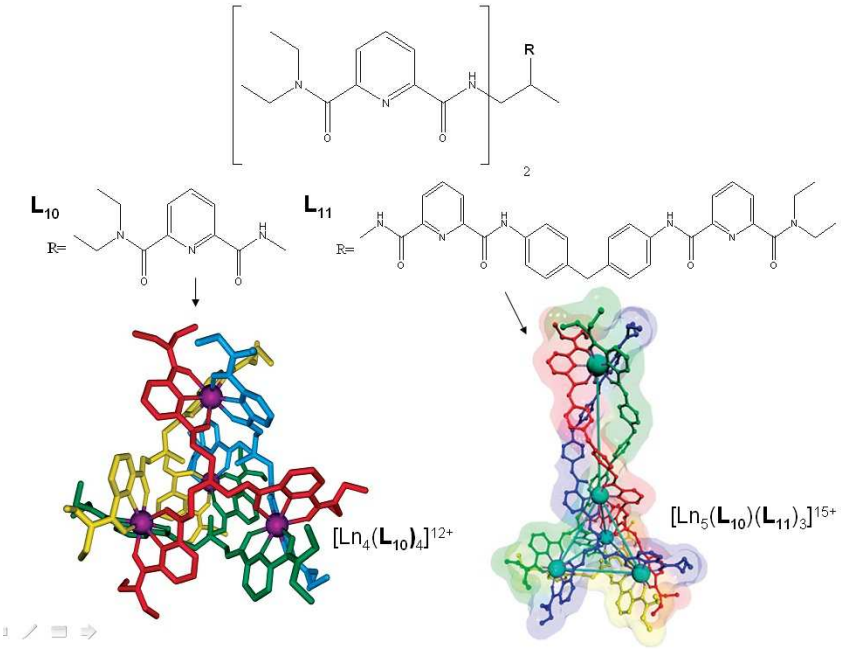

Figure I-12: The tripodal ligands L_{10} and L_{11} and the structure of $[Ln_4(L_{10})_4]^{12+}$ and molecular modelling of pentanuclear complex [83, 84]

Some other podand ligands that lead to sophisticated polynuclear architectures are given in Scheme I-9. In our group, it has been shown that the design of a new dodecadentate tripodal ligand L_{12} leads to the self assembly of a trimetallic complex $[La_3(L_{12})_2(Otf)_4(H_2O)_2](Otf)_5$ [85]. Raymond et al. have obtained the first cyclic octametallic lanthanide complex $[La_8(L_{13})]$ in which nine coordinate lanthanum centers are coordinated by three bidentate pyrazolone chelating units [86]. Tripodal Schiff base ligand L_{14} presented in Scheme I-9 leads to the isolation of first heterometallic complex Yb/La [87]. The optimised stepwise synthetic strategy allowed the isolation of a pure heterodimetallic complex $[\mathbf{L_{14}}LnLn'(NO_3)_3]$ that has been prepared by the addition of less acidic larger second lanthanide into the monometallic complex $[Ln\mathbf{L_{14}}]$ [88].

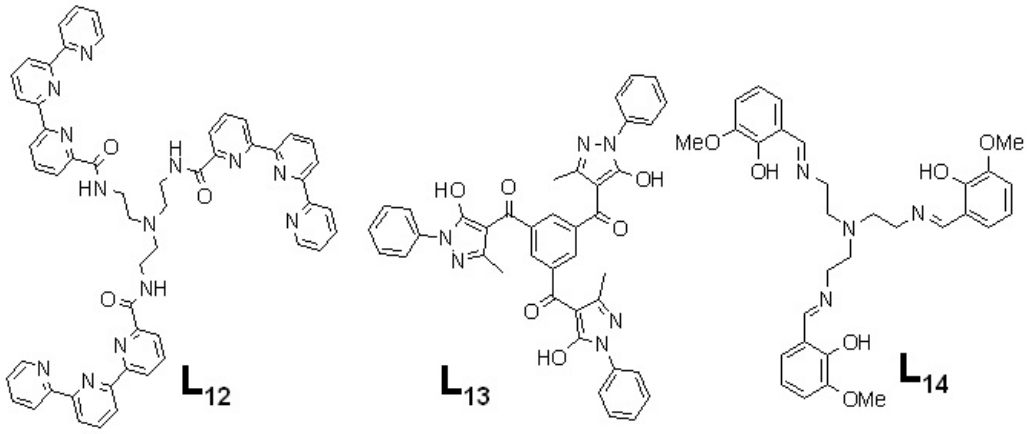

Scheme I-9: Podand ligands used for preparing polynuclear complexes

b) Helicates

The helicates have an important place in the understanding of supramolecular self assembly processes in lanthanide coordination chemistry [89, 90]. Helicates as introduced by Lehn in 1987 refer to discrete poylnuclear structures where at least two ligands wrap around a series of metal ions defining the helical axes [91]. The incorporation of lanthanides in helicate type structures dates back to 1992 [92]. Piguet et al. deeply studied the formation of helicates based on lanthanides. They are the ones who obtained the first dimetallic helicate $[Ln_2(\mathbf{L_{15}})_3]^{6+}$with a polydentate and homotopic ligand where the D_3 pseudo-symmetry of the helicate preserved both in solution and solid state (Figure I-13). Since then, many efforts have been put to design adapted organic ligands and synthetic methods to understand and control the preparation of organised supramolecular helicates which result in a better understanding and predictability of the self assembly of helical complexes.

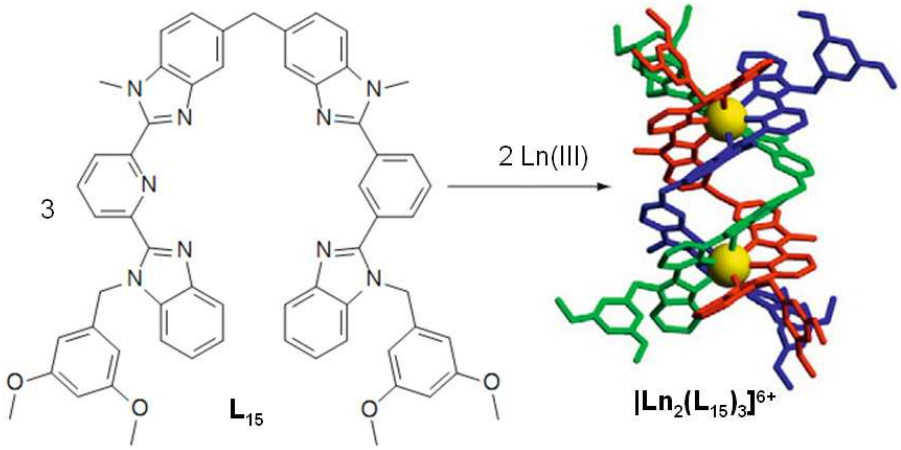

Figure I-13: Formation of the first binuclear triple-stranded helicates with neutral bis-tridentate homotopic C_{2v}-symmetrical ligand L_{15} [92]

The programming of lanthanide helicates relies on the rational design of ligands. In literature, it has been shown that the ligand strands with tridentate chelating units [92] give triple stranded helicates with coordination number of 9 while bidentate chelating units give quadruple stranded helicates with coordination number of 8 [93]. The choice of spacer between the ligand strands is also important. Senegas et al. have observed that with the bis-tridentate pyridine benzimidazole ligand, triple stranded helicates are obtained when diphenylen spacers are used, in constrast the use of para-xylyl spacers gives a bidimensional circular helicates [94]. Ligand design could also affect the nuclearity. The nuclearity of the complex can be increased by increasing the number of coordinating unit that lead to the linear, triple-stranded trinuclear and even tetranuclear 4f helicates. The ligand L_{16}, possessing three tridentate units, promoted self assembly of trinuclear helicates stable $[Ln_3(L_{16})_3]^{9+}$ [95] in solution (Figure I-14). Similarly, extension of the ligand L_{16} to L_{17} by incorporation of a new tridentate segment promoted formation of tetranuclear complexes. $[Ln_4(L_{17})_4]^{12+}$ [96].

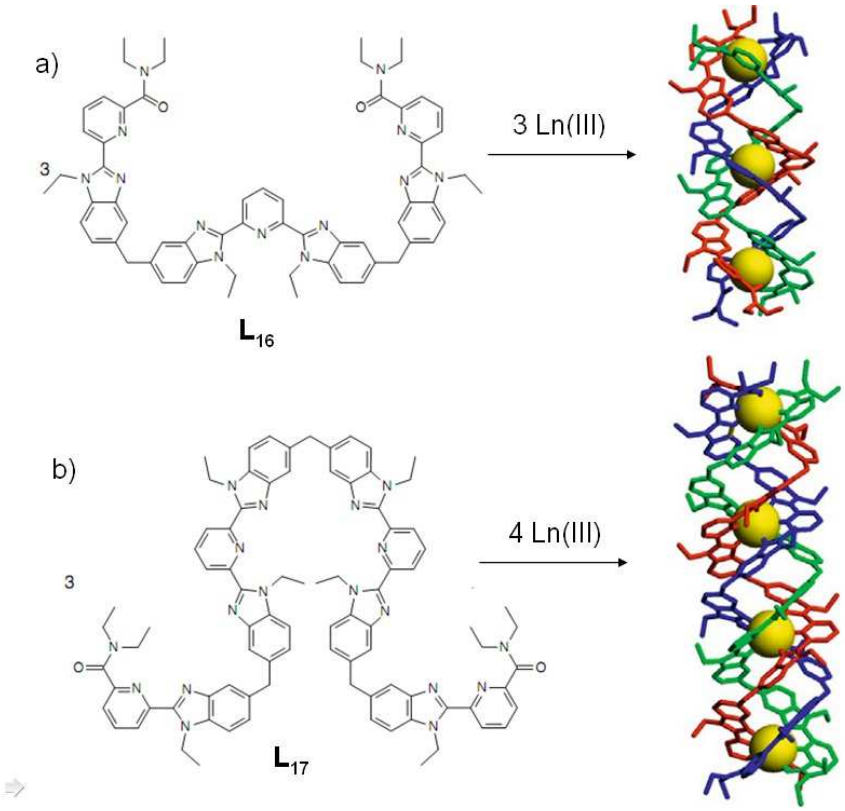

Figure I-14: Formation of a) trinuclear $[Eu_3(L_{16})_3]^{9+}$ [95] and b) tetranuclear $[Eu_4(L_{17})_3]^{12+}$ [96] triple-stranded helicates with neutral heterotopic C_{2v}-symmetrical ligands

In the preparation of heteropolymetallic lanthanide helicates, the possibility of tuning intermetallic properties and dual emission lead to the design of ligand strands for a selective recognition of the lanthanide ions. In order to provide selectivity towards a given metal pair,

small differences in the ligand strands have been envisioned. For example André et al. have designed a dissymmetric ligand with one strand being benzimidazole-pyridine-carboxamide unit to complex preferentially with smaller lanthanides, while pyridine-bis(benzimidazole) unit prefers bigger cations leading to $[EuLa(L)_3]^{6+}$ heterodimetallic triple stranded helicates [97].

The hydroxyquinoline group have also been incorporated into polydentate ditopic ligands that lead to the self assembly of discrete bimetallic [98] or trimetallic [99] helicates (Scheme I-10). Albrecht et al. have isolated $[KLn_2(L_{18})_3]OTf$ and $[KAlLn(L_{19})_3]OTf$ (Ln=Nd, Yb, Gd, Er) where three ligand strands wrap around the two lanthanide centers and binding of a templating potassium in the interior of the complex [100]. The stability of these complexes has been demonstrated by NMR studies. The helicates display sizeable NIR emission with efficient energy transfer from the ligand.

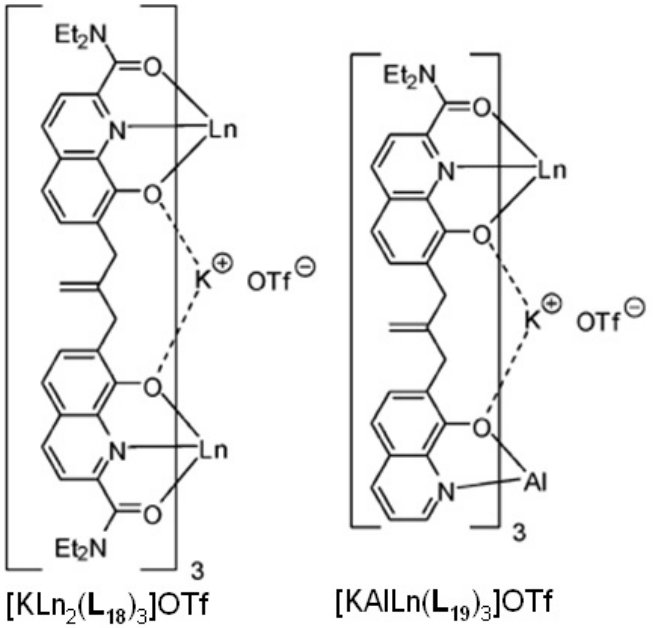

Scheme I-10: Trimetallic helicates with ditopic 8-hydroxyquinoline based ligands [100]

c) Self Assembly with Small Ligands

Another strategy to obtain polymetallic lanthanide complexes is to use dissymmetric and low denticity ligands letting one (or more) vacant coordination site around the metallic center promoting the self assembly processes. Thereby Comby et al. reported assembly of a nonanuclear cluster $Ln\subset Na_6Ln_8(L_{20})_{16}$ (Ln = Eu, Gd, Tb, and Er) with a tridentate ligand derived from a bipyridine and a phosphonic acid [101]. $Eu\subset Na_6Eu_8(L_{20})_{16}$ has a sizeable quantum yield of 32% (Figure I-15). Eight lanthanide and six sodium atoms encircled a central Ln ion which completes its coordination sphere by four molecules of water and four

oxygens from phosphonic acid. The cluster is stabilised by a relatively complex network of bridging phosphonates. In addition to that, a similar heterometallic structure $Na_6Eu_xYb_{9-x}(L_{20})_{16}$ displaying dual luminescence in the visible and NIR ranges, has been obtained.

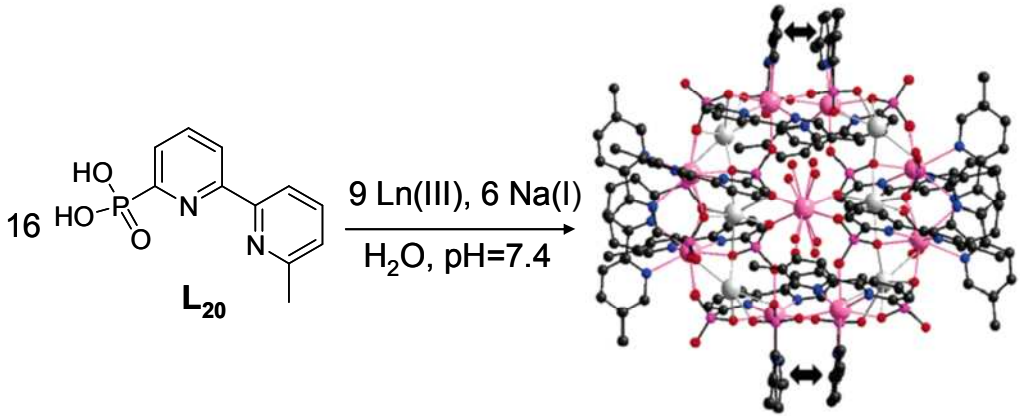

Figure I-15: The self assembly of a nonanuclear cluster $Ln \subset Na_6Ln_8(L_{20})_{16}$ (Ln = Eu, Gd, Tb, and Er) with a dyssmmetric tridentate ligand [101]

An octameric complex $[Ln_8(L_{21})_{12}(H_2O)_{24}]$ (Ln = La, Ce) displaying nonlinear optical properties was recently formed by a tridentate (tbzcapc = 6-[2-N-(1,3,4-thiabiazolyl)carboxamido]-2-pyridylcarboxylate) ligand [102]. In this C_3 symmetric novel ellipsoidal structure, six Ln ions, each coordinated by three ligands, define the quasi-equatorial plane, while the two other ions are in axial positions (Figure I-16). The dianionic tridentate ligand not only triple coordinates to one Ln ion by N-pyridyl, carbonyl, carboxylate groups but also bridges another Ln ion through carboxylates. Even though the important role of central Ln ions could be anticipated in these two systems; the lack of information on the structures in solution prevents a better understanding of assembly process.

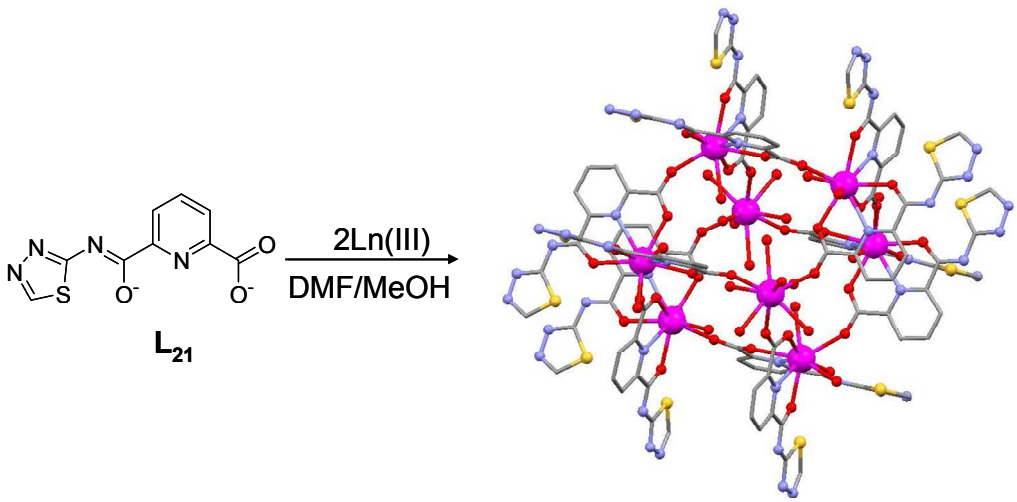

Figure I-16: Formation of octameric ellipsoid lanthanide complex with a tridentate dianionic ligand [102]

Small ligands like alkoxides and aryloxides are commonly used as bridging ligands to obtain polynuclear lanthanide complexes. Recently Caneschi et al. reported a self assembly of decanuclear wheel of dysprosium $Dy_{10}(OC_2H_4OCH_3)_{30}$ by salt metathesis where the metallic cations are bridged by the methanoxyethanolate ligands (Figure I-17) [103].

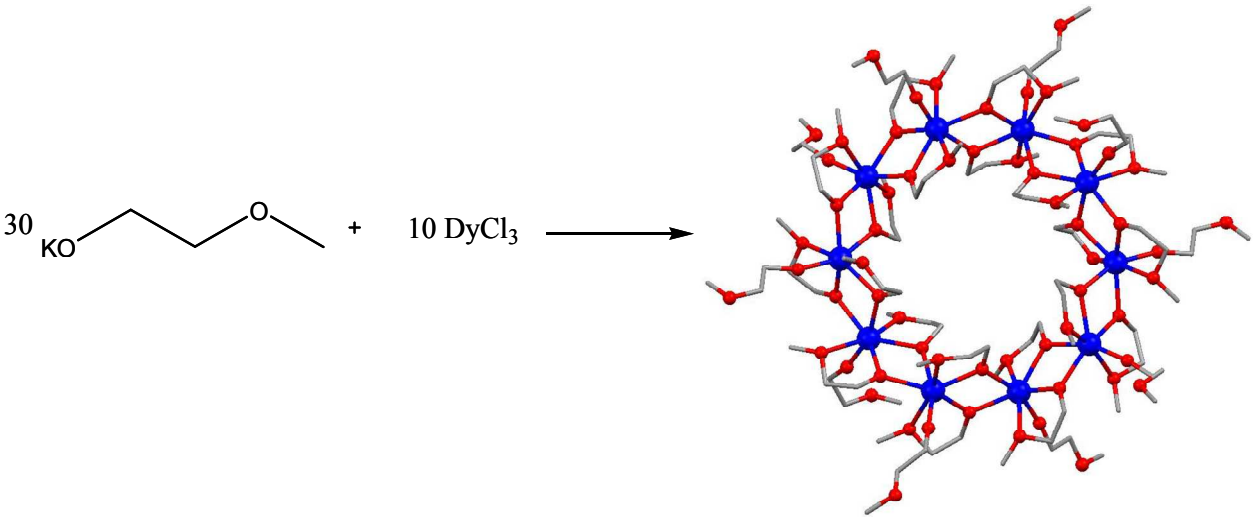

Figure I-17: The synthesis and structure of $Dy_{10}(OC_2H_4OCH_3)_{30}$ [103]

In our laboratory, it has been shown that the use of simple asymmetric tetradentate ligands leaving some coordination vacancies around the metal ion directs the assembly of large lanthanide cluster. Tetradentate terpyridine carboxylate ligand (**terpya**) (6, 2□ 6□, 2□- terpyridine-2-carboxylic acid) is used for the development of homo- and heterometallic assemblies with high nuclearity [104]. The reaction of 2 equivalents of the ligand terpya with 1 equivalent of $Ln(Otf)_3$ (Ln = Eu, Tb, Nd, Gd) in presence of triethylamine resulted in the formation of mononuclear complexes $[Ln(terpya)_2]^+$ where lanthanide ion has a coordination number of 8 (Figure I-18). ^1H NMR spectra of the complexes in methanol confirms the presence of single rigid C_2-symmetric species. The addition of an excess of $Ln(Otf)_3$ to a suspension of the mononuclear $[Ln(terpya)_2](Otf)$ complex in acetonitrile results in complete dissolution of the complex and isolation of heptanuclear complexes $[Ln\subset(Ln(terpya)_2)_6](Otf)_9$. X-Ray diffraction studies show that a central cation is encapsulated by an hexameric assembly including six mononuclear complexes $[Ln(terpya)_2]^+$ (Figure I-18).

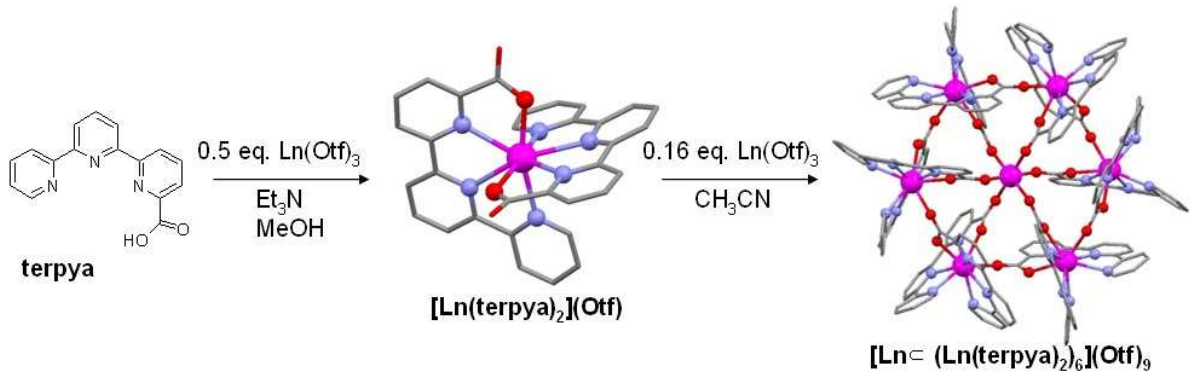

Figure I-18: Two step self assembly of the hexameric lanthanide wheel $[Ln\subset(Ln(terpya)_2)_6](Otf)_9$ with the terpya ligand [104]

The molecular structure of the $[Ln\subset(Ln(terpya)_2)_6](Otf)_9$ complexes presents two very distinct coordination environments. The six nine-coordinated mononuclear complexes are connected by six bridging carboxylates forming a ring. The central cation presents regular octahedral coordination geometry by the coordination of six carboxylate oxygens from six ligands. The proton NMR spectrum of europium complexes in anhydrous acetonitrile presents only one set of 20 signals in agreement with the presence of two terpyridinecarboxylate ligands in two different coordination environments. Dissolution of the complex in methanol leads to the disruption of the cyclic structure to give the corresponding monometallic complexes.

Similar NMR studies with other lanthanide ions have shown that the nuclearity of the assembly is controlled by the size of metallic cation. The intermediate Ln ions Eu-Tb favour the formation of heptanuclear assembly which is observed to be the only specie present in the solution of the complexes. For larger ions such as Nd(III), these species are observed as major solution products. No assembly formation has been observed with the smaller lanthanide (Y, Yb, Lu) ions. In fact, the self assembly of the wheel structure requires the presence of a free coordination site on the mononuclear species to allow the coordination of a bridging carboxylate ligand. The end of the lanthanide series is too small to favour this additional coordination. The larger ions provide a higher coordination number; therefore they probably favour assemblies with different nuclearities.

Selective addition of different lanthanide ions lead to the formation of heterometallic wheel structures. In fact, in anhydrous conditions, the addition of a smaller lanthanide ion Ln1 into the mononuclear complex $Ln2(terpya)_2$ leads to the formation of stable heterometallic $[Ln1\subset(Ln2(terpya)_2)_6](Otf)_9$ complexes in solution [105]. The studies on terpya complexes

have shown that the assembly process depends on the size of the lanthanide ion and the reaction conditions.

2.2.4 Clusters

Clusters are finite polymetallic entities with great interest due to their adaptability to functional materials as precursors, ceramics, catalysts and thin film coatings. A large number of polymetallic lanthanide complexes featuring cluster like, polyhedral core structures have been reported in the last two decades [106, 107]. The saturation of coordination sphere of metal ions by bridging organic ligands or small bridging units such as oxo, hydroxo, hydrido, halo and chalcogenido groups (due to adventitious hydrolysis or degradation of solvent molecules) leads to the formation of polymetallic clusters. Most of these structures are the unexpected reaction products revealing the difficulty in the synthesis of predesigned clusters due to lability of lanthanide ions.

a) Clusters obtained by controlled hydrolysis

Clusters obtained by stoichiometric hydrolysis of the lanthanide ions present the bridging oxo and hydroxo ligands in their core. These oxo/hydroxo clusters are shown to be important in several applications as magnets, optical materials, catalysts for the hydrolytic cleavage of RNA and DNA. Zheng et al. have shown that controlled hydrolysis of lanthanide salts $LnCl_3$ or $LnClO_4$ with aqueous NaOH in presence of an α-aminoacid type ligand resulted in the formation of tetranuclear assemblies $[Ln_4(\mu_3\text{-}OH)_4]^{8+}$ [108]. Other ligands used for the hydrolysis of lanthanides are the β-diketonate ligands. Tetradecanuclear and nonanuclear clusters have been isolated respectively with ligands acetylacetonate [109] and benzoylacetonate [110]. No detailed study of the species in solution has been performed. Apart from clusters obtained with organic ligands, direct hydrolysis of lanthanide iodides has also been reported (Figure I-19). The first basic rare earth iodide with an oxygen-centered M_6X_8-cluster core has been reported by Mudring et al. in 2005 [111]. Hexametallic clusters $[M_6(\mu_3\text{-}OH)_8(\mu_6\text{-}O)\ (H_2O)_{24}]I_8(H_2O)_8$ (M = Nd, Eu, Tb, and Dy) are formed by an usual μ_6-oxo and face-capping μ_3-OH groups and 24 terminal aqua ligands (four on each of the six metal atoms) [112].

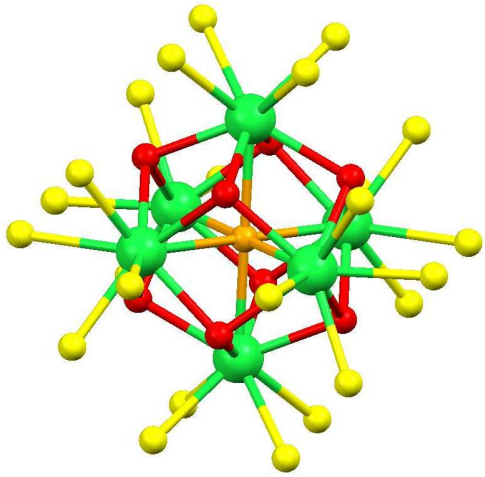

Figure I-19: Crystal structure of $[Nd_6(\mu_3\text{-}OH)_8(\mu_6\text{-}O)(H_2O)_{24}]^{8+}$. Nd: green, central O: orange, -OH: red, H_2O: yellow [111]

b) Chalcogenide Clusters

Most of the research efforts on lanthanide containing clusters focus on their synthetic and structural aspects. However recent studies by Brennan and coworkers show a series of chalcogen derivated $Ln(EPh)_3$ (E = S, Se, Te) clusters with exciting luminescent properties in terms of emission wavelength, emission intensity, and quantum efficiency. For example, $(THF)_{14}Er_{10}S_6(Se_2)_6I_6$ obtained from the reaction of $Er(SePh)_3$ with elemental S/Se emits exceptionally at 1.54μm with 78% quantum efficiency [113]. Recently they have isolated a spherical cluster with 1 nm diameter $(py)_{16}Ln_{17}NaSe_{18}(SePh)_{16}$ (Ln = Ce, Pr, Nd) [71]. The structure consists of a central Ln ion surrounded by a layer of eight Se^{2-} and 16 Ln ion. The outer Ln ions complete their coordination sphere with additional μ_3 and μ_5 Se^{2-}, μ_3 and μ_4 $SePh^-$, and pyridine donors (Figure I-20). The presence of Na has an important role in the cluster formation. Different lower nuclearity clusters have been obtained when Li or K is used in the reaction instead of Na. The NIR photopysical studies of Nd cluster reveal a very high quantum efficiency of 35%.

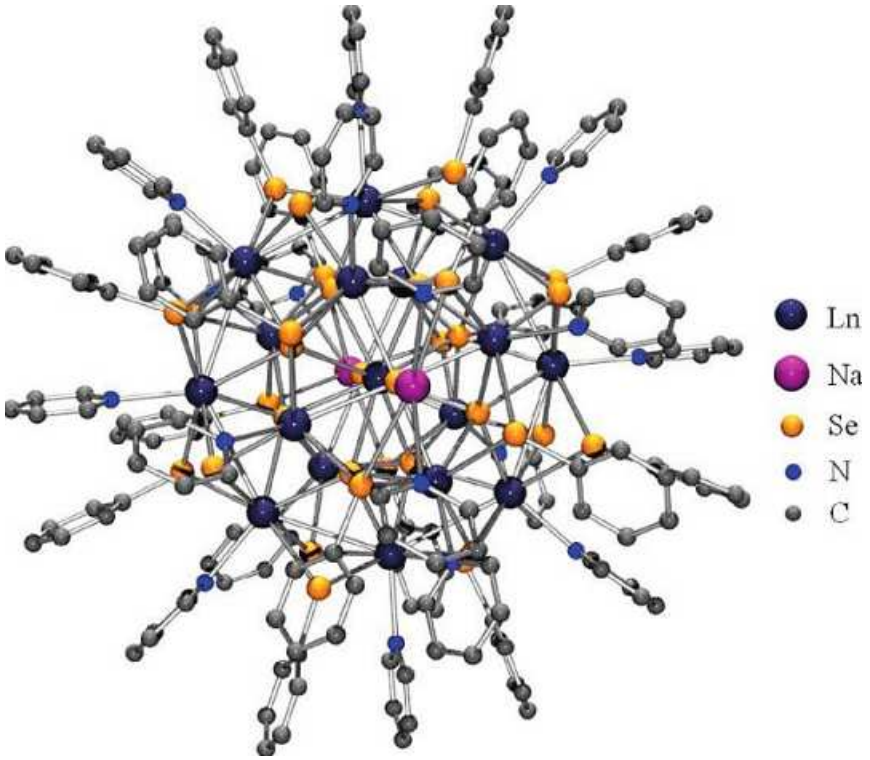

Figure I-20: The structure of $(py)_{16}Ln_{17}NaSe_{18}(SePh)_{16}$ using spheres of arbitrary size [71]

The potential of the chalcogenated clusters in important photonic applications such as low-power lasers, active fibers and waveguides has been summarized in a recent review [114]. These clusters called as « molecular minerals » are monodisperse, have well-defined structures and are highly soluble in organic solvents due to the encapsulation of organic ligands, so that they could be easily used as precursors for the preparation of nanocomposites. They provide luminescent properties that were previously inaccessible, as the rigidity provided by cluster core leads to the protection of the lanthanide ions from vibronic quenching through high energy oscillators such as O-H, C-H, N-H.

c) Oxo clusters

Even though enhanced optical properties can be obtained by chalcogenide clusters, these compounds show air sensitivity which is detrimental for their application to functional devices. In order to improve the stability of the clusters, oxo ligands are integrated into the cluster. For example, oxidation of chalcogeneted $Nd(SePh)_3$ by selenium dioxide resulted in the assembly of cluster $[Nd_8(\mu_3\text{-}O)_2(\mu_5\text{-}Se)_2(SePh)_{16}(THF)_8]$ (Figure I-21a) which emits at 1349 and 1832 nm, not accessible with other Nd compounds [69]. Further they have obtained a dodecanuclear cluster $([(py)_{18}Nd_{12}O_6Se_4(Se_2)_4(SePh)_4(Se_2Ph)_2Hg_2(SePh)_4]$ $[(Hg(SePh)_3]_2)$ (Figure I-21b) by reacting $Nd(SePh)_3$ with SeO_2 and Hg in pyridine [70]. NIR emission properties of this Nd_{12} cluster are less intense compared to the Nd_8 clusters. The decrease in

quantum efficiency from 16% to 12% is related to the increasing number of high phonon energy Nd-O ligands in the Nd_{12} cluster. These quantum efficiencies are the highest values obtained for Nd compounds, while the other molecular Nd compounds listed in literature have quantum efficiencies in the range of 0.001-1.0% [115].

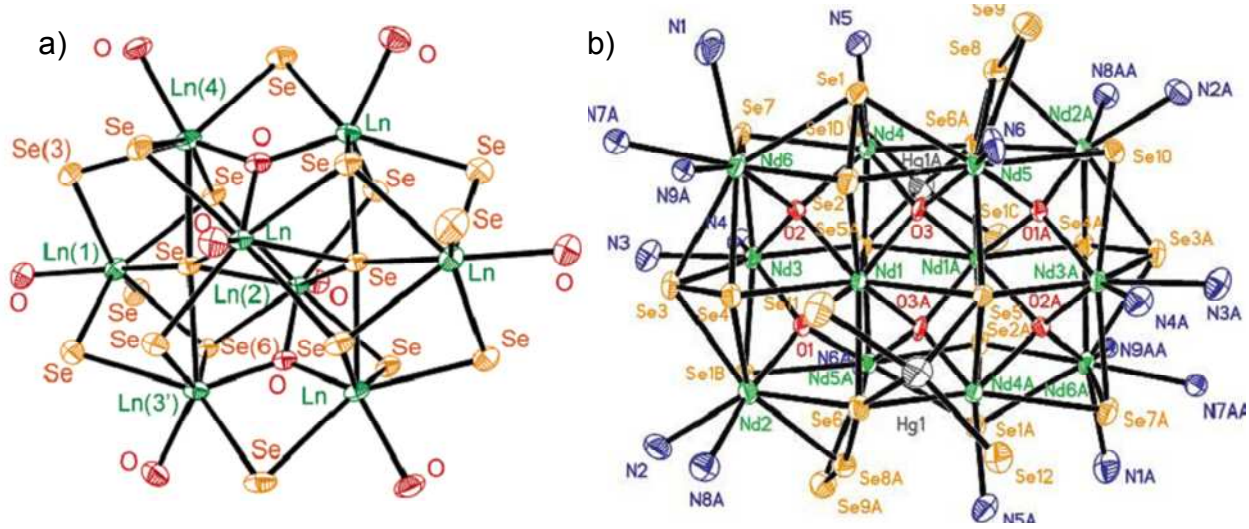

Figure I-21: Structures of a) $[Nd_8(\mu_3\text{-}O)_2(\mu_5\text{-}Se)_2(SePh)_{16}(THF)_8$ [69] and b) $([(py)_{18}Nd_{12}O_6Se_4(Se_2)4(SePh)_4(Se_2Ph)_2Hg_2(SePh)_4]$- $[(Hg(SePh)_3]_2)$ [70]

Oxo clusters are particularly attractive for the development of new functional materials, but they are hard to isolate as they tend to form hydroxides by reacting with water. Most of the attemps conclude in obtaining oxo/hydroxo clusters. It is more interesting to obtain oxo only clusters instead of oxo/hydroxo clusters as OH groups quench the emission of lanthanides. Oxo clusters are assembled by aggregation of mononuclear complexes by organic bridging ligands fulfilling the high-coordination number requirement of lanthanides. Alkoxides and aryloxides [116] are commonly used as bridging ligands for obtaining precursor lanthanide oxides for sol-gel and CVD processing [72, 107].

2.3- Outlook

The aim of this chapter was to give a specific literature review on the supramolecular lanthanide coordination chemistry. Several polymetallic complexes were reported in the last two decades. Nevertheless the absence of solution studies in most of the cases renders difficult the understanding of self assembly processes and therefore its control. The macrocycles and helicates provided a better programming of the final nuclearity and structure of the complexes by tailoring the ligand size and geometry of the ligand. However, the largest complexes obtained with these ligands could not exceed tetrametallic complexes up to now. In contrast dendrimers, podand ligands, or small low denticity flexible ligands provide a better alternative to obtain high nuclearity complexes (up to decanuclear complexes reported

in literature). The controlled preparation of polymetallic complexes is still a great challenge due to similar chemical properties of lanthanides. Even though the prediction of final assembly is difficult, certain control could be maintained by controlling ligand geometry (sterics), non-covalent interactions, and reaction conditions (solvent, pH, temperature, etc.). Furthermore, recently some oxochalcogenido clusters with good yield could be obtained and the high rigidity of the lanthanide environment in these systems led to high luminescence quantum yields. The potential applications of lanthanide clusters due to their unique spectroscopic properties will certainly lead to progress in this field of chemistry in the near future.

3- Context and objectives of the project

As seen in the introduction, several synthetic strategies have been adapted in order to prepare polymetallic lanthanide complexes. However, most of the complexes are obtained by serendipity rather than by rational design, and the absence of solution studies makes it difficult to understand and predict their formation.

The aim of this thesis work is the development of synthetic strategies to include lanthanide ions in discrete high nuclearity polymetallic architectures by using suitable organic ligands and the study of photophysical properties of the final assemblies to improve optical properties for new materials. To do that, we have concentrated on complexation studies with dissymmetric predisposed ligands (tridentate anionic ligands, tetradentate chiral ligands) with possibility of promoting assembly formation, and as a final project we started to investigate an original synthetic method using the redox potential of divalent lanthanides for the synthesis of oxo clusters for luminescent materials.

As shown in the previous section, some polynuclear complexes have been obtained by using tridentate [101] and dianionic [102] ligands. Therefore for the first part of this work, complexation studies have been performed with two tridentate dianionic hydroxyquinoline ligands substituted with carboxylate (H_2hqa) and tetrazolate (H_2hqt) binding groups (Scheme I-11) with the aim of obtaining polynuclear complexes. 8-hydroxyquinoline chromophore is well known for the sensitisation of Near-Infrared luminescence of the Nd(III), Yb(III) and Er(III) ions. Complexation studies with H_2hqa with Nd(III) have already been performed in our group; here we extended this study to Er (III) and Yb (III) and also to a new hydroxyquinoline based tetrazole ligand. We have chosen

the tridentate dianionic ligand in order to study the effect of charge and geometry of the ligand on the final assembly formation. The solution and solid state structures of the resulting complexes have been properly characterized by NMR spectroscopy and X-Ray diffraction. Additionally, the photophysical properties have been investigated in detail, in solution and in the solid states.

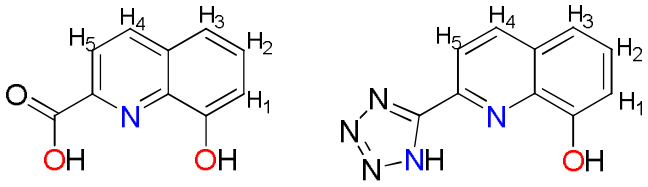

Scheme I-11: H_2hqa and H_2hqt ligands

In the second part, we propose to use simple dissymmetric tetradentate chiral ligand leaving some coordination vacancies around the metal ion to direct the assembly of large lanthanide complexes. Our group has shown that the use of a dissymmetric tetradentate terpyridinecarboxylate (terpya) ligand led to the isolation of hexameric cyclic complexes with a central lanthanide ion. This stepwise strategy is used for obtaining heteropolymetallic complexes as there are two different coordination environments. In this thesis, in order to understand the effects of ligand characteristics (geometry, basicity, etc) on the final assembly and to verify the formation of heptametallic assemblies with another tetradentate dissymmetric ligand, we have synthesized a tetradentate chiral Phbipox ligand derivated from bipyridine unit containing an oxazoline ring for the assembly of enantiopure lanthanide complexes. The aim of introducing chirality into lanthanide complexes is to use their spectroscopic and catalytic properties to design luminescent chiral complexes that could be used either as chiral catalysts for preparing enantiopure organic compounds or as luminescent probes for chiral recognition and sensing of biological molecules. The final complexes have been characterized by NMR spectroscopy, X-Ray diffraction, Circular Dichroism, Circularly Polarized Luminescence. The photophysical properties of the complexes have been compared with the complexes of terpya in order to understand the effect of ligand parameters on assembly.

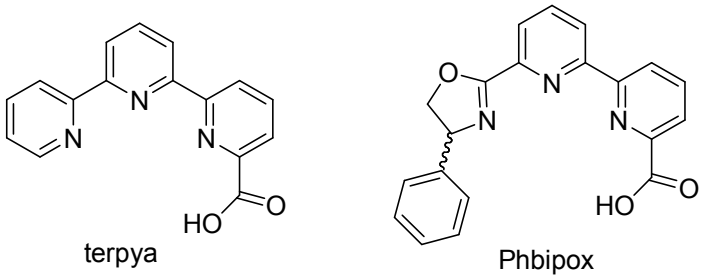

Scheme I-12: Dissymmetric tetradentate ligands for the development of supramoleculer assemblies

In the last part, we started to study the synthesis of divalent precursors for the preparation of high nuclear clusters by the oxidation of divalent lanthanides. The lanthanide clusters have shown to possess unusual optical properties like high quantum efficiencies and unique emission bands. In this thesis, in order to control the formation of clusters, we proposed to use redox reactions of divalent lanthanide precursors with oxo donor ligands. Divalent lanthanide chemistry is a challenging field in lanthanide studies. In our laboratory, it has been shown that the use of tripodal ligand tris(2-pyridylmethyl)amine (tpa) with smaller ligands such as iodides affords larger clusters with oxidation chemistry of uranium complexes [117]. Therefore, with the objective of developing original synthetic methods for the preparation of oxo complexes of Ln(III), we decided to use this tripodal ligand to prepare divalent lanthanide precursor complexes for preparing high nuclearity clusters. At first we have studied the complexation with tpa ligand and the preliminary precursors obtained have been characterized by NMR spectroscopy and X-ray diffractometry.

CHAPTER II Near-IR emitting 8-hydroxyquinoline-based Complexes

1- Introduction

There is high current interest for the design of lanthanide complexes displaying metal-centered emission in the near-infrared (NIR) region because of the wide variety of applications in material science, lighting and telecommunication technology and in bioanalysis [6-8, 20, 23, 64, 115, 118-122]. The emission of Nd(III), Yb(III) or Er(III) ions is particularly attractive because their emission falls in the transparent window of biological tissues and silica [26, 123]. As mentioned in the first chapter the NIR emitting lanthanides have small energy gap between the excited and ground states which matches well the energy of the first and second vibrational overtones of O□H and C□H groups that act as efficient quenchers via vibrational excitation in the first and second coordination of the metal ion. Therefore these ions require careful design of ligands that could coordinate tightly to metal to avoid solvent coordination. The ligand should absorb light efficiently and the triplet state of the ligand should match well to the lanthanide excited states (at lower energy compared to the Ln emitting in the visible region) for an efficient energy transfer and final NIR emission.

In this chapter we will present the complexation studies of two tridentate dianionic ligands with the aim of obtaining polynuclear complexes. Here we report water soluble hydroxyquinoline based tris-anionic tris-ligand complexes prepared using dianionic hydroxyquinoline ligands substituted with carboxylate (H_2hqa) and tetrazolate (H_2hqt) binding groups. Complexation studies with H_2hqa and Nd(III) has already been performed in our group here we extended this study to Er(III) and Yb(III) and also with a new hydroxyquinoline based tetrazole ligand [124]. The dianionic character of the tridendate ligands favors the formation of stable structures with Lewis acid lanthanide cations. Moreover some polynuclear complexes have been obtained by using tridentate [101] and dianionic [102] ligands in the literature. These studies inspired us to conduct the research with hydroxyquinoline based tridentate dianionic ligands in view of their potential as building blocks of supramolecular NIR emitting lanthanide architectures.

2- Hydroxyquinoline unit in lanthanide coordination chemistry

Thanks to its low energy triplet state (17100 cm^{-1}, 585 nm) and its visible absorption (at 370 nm) the 8-hydroxyquinoline unit (8-hq $\mathbf{L_{1a}}$) is a choice chromophore for the sensitization of NIR emitting lanthanides. The first applications of this chromophore were reported in 1987 by Tang and Van Slyke who designed the first organic light-emitting diode with the [Al(8-hq)$_3$] complex [125]. In the last years lanthanide complexes with the 8-hydroxyquinoline ligand (Scheme II-1) and its derivatives have been studied to elucidate the structure of complexes and/or to optimize the photophysical properties [126-129].

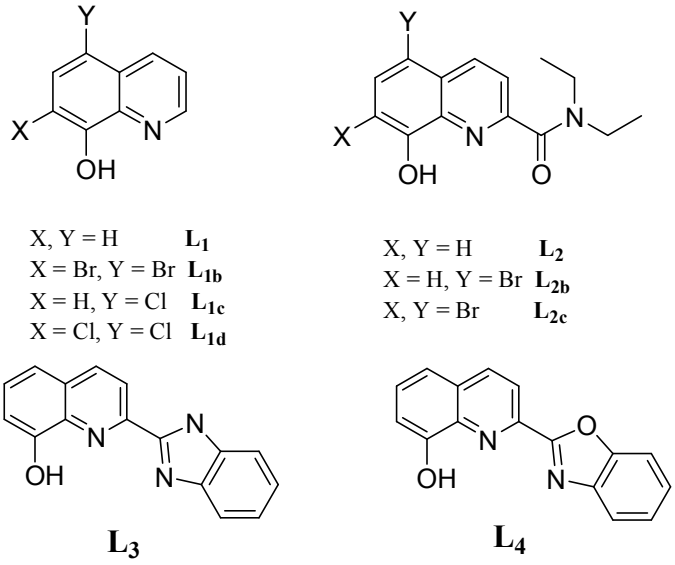

Scheme II-1: Bidentate and tridentate ligands incorporating 8-hydroxyquinoline moieties

The main problem of the lanthanide quinolinate complexes is that obtaining pure tris complexes is difficult due to the ligand geometry and the lability of the lanthanide complexes. Most of the compounds used as components in device preparation might be in reality a mixture of species which makes it difficult to relate structural properties to the luminescence. The bidentate ligand does not satisfy the high coordination requirement of lanthanides therefore either solvated products or higher nuclearity species form by bridging through hydroxo groups of the ligand. The versatility of the coordination chemistry of this bidentate ligand with Ln(III) was only recently demonstrated by Binnemans and co-workers [127]. It was indeed found out that most of the synthetic methods for isolating rare-earth quinolinates yield mixtures of different species. Tris complexes; corresponding to 1:3 metal-to-ligand ratio, tetrakis complexes; corresponding to a 1:4 metal-to-ligand ratio, and trimeric complexes; with a 3:8 metal-to-ligand ratio have been observed depending on the reaction conditions (solvent, base) and ligand used (Figure II-1).

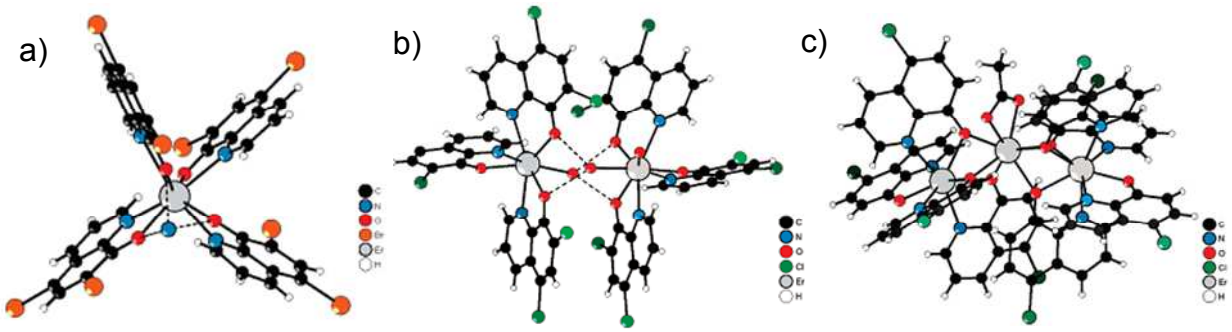

Figure II-1: Three different type of complexes a) tetrakis complex $NH_4[Er(L_{1b})_4]C_4H_8O_2$, b) tris complex $Er(L_{1d})_3 \cdot 6C_4H_8O_2$, c) trinuclear complex $Er_3(L_{1c})_8(CH_3COO) \cdot 6CHCl_3$ isolated from reaction of lanthanides with halogen substitured 8-hydroxyquinoline based ligands [127]

These studies showed that species differing for their nuclearity and stoichiometry form in the reaction of lanthanide ions with bidentate 8-hydroxyquinolines. Some characterized species also present coordinated water molecules which are deleterious for the efficiency of Near-IR emission. Moreover these complexes are sensitive to moisture, which leads to ligand dissociation reducing the devices stability and efficiency.

To get a better control of coordination chemistry of 8- hydroxyquinolinate derivatives to rare-earth (III) ions, Albrecht and co-workers extended the coordination ability of this ligand by attaching further donor functionalities [130]. In particular, it was shown that tridentate 2-carboxamide-8-hydroxyquinoline L_{2a} derivatives form monometallic 3:1 complexes possessing strong NIR emission. Substitution of bromine atoms to minimize C-H vibrators on the ligand core as in L_{2b} and L_{2c} enhanced the luminescence properties with a quantum yield increase of a factor of 2.5-2.9 [131]. In these complexes three ligand strands coordinate to the metal ion in an helical fashion leading in solution to two isomers: syn (up-up-up) and anti (up-up-down) conformation of the ligands in a 1:3 syn/anti statistical ratio. As shown in Figure II-2 the crystal structures obtained show a syn isomer of $Er(L_{2a})_3$ and an anti isomer of $Yb(L_{2a})_3$.

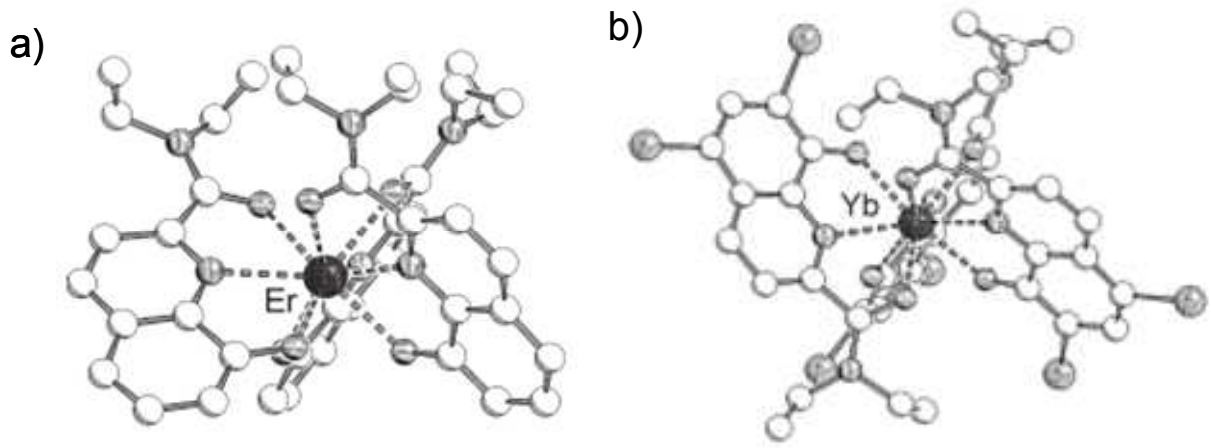

Figure II-2: Molecular structures of $Er(L_{2a})_3$ and $Yb(L_{2a})_3$ showing syn and anti conformation respectively [131]

Recently Bünzli and coworkers have prepared mononuclear neutral tris-ligand complexes of lanthanides using monoanionic tridentate N,N,O ligands obtained by substitution of the hydroxyquinoline group with neutral benzimidazole L_3 and benzoxazole L_4 groups (Scheme II-1) [132, 133]. The crystal structures of the complexes show that the three ligands are arranged in an "up-up-down" fashion in the tris ligand complexes formed. These ligands provide large absorption in the visible region and sensitize Nd luminescence efficiently with quantum yields of 0.33-0.34%. Similarly halogenation of the ligands results in an increase of quantum yields of the tris complexes.

Hydroxyquinoline unit has been adapted to various polydentate ligands. As mentioned in the previous chapter hydroxyquinoline unit has been attached to tripodal ligands [59-63] in order to provide better control of structural properties with a large chelate effect. Moreover the hydroxyquinoline group has been incorporated into polydentate ditopic ligands that lead to the self assembly of discrete bimetallic [98] or trimetallic [99] helicates.

3- The Choice of the Ligands

As seen in the previous section the coordination chemistry of ligands based on 8-hydroxyquinoline is quite rich but not always controllable. Dianionic expanded ligands can be prepared by substitution of 8-hydroxyquinoline with well chosen lanthanide binding groups such as carboxylate and tetrazolate. Carboxylate have been widely used in lanthanide chemistry to yield water stable complexes [134]. Tetrazoles have attracted increasing attention in recent years in coordination chemistry due to the excellent coordination ability of the four nitrogen atoms of the functional group to act as either a multidentate or a bridging

building block in supramolecular assemblies. Moreover tetrazoles and carboxylate groups have similar pKa values (≈4). The incorporation of tetrazole groups as carboxylic acid replacements for the sensitization of lanthanide emission has recently been described for the first time by our group [51, 52].

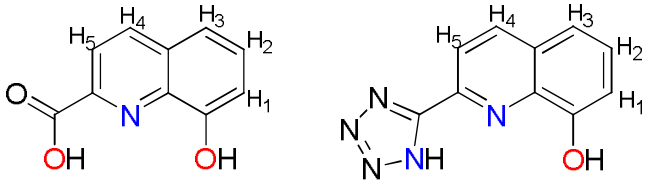

Scheme II-2: H_2hqa and H_2hqt ligands

The H_2hqa ligand is commercialy available. Complexation ability of the ligand H_2hqa was largely studied for transition metals [135, 136] but no lanthanide based complexes have been to date reported. The ligand H_2hqt was conveniently prepared from commercial 8-hydroxyquinoline-2-carbonitrile in a one- step synthesis with 90% yield. The easy access to both ligands renders them very attractive for potential applications. Moreover we indeed thought that the dianionic character of these ligands would favour the formation of stable and original structures with Ln(III) Lewis acids.

4- Complexation studies with hydroxyquinoline based ligands

At first we have tested the possibility of obtaining polynuclear assemblies from complexes where the coordination number is not satisfied by the ligand donor groups. However, no crystals could be isolated from the synthesis of complexes with different ligand to metal ratio (1Ln:2L; 1Ln:2L) and their NMR spectra presented broad signals suggesting the presence of fluxional/exchanging solution species. Addition of an excess $Ln(Otf)_3$ into the insitu prepared reaction mixtures (1Ln:2L; 1Ln:2L) in acetonitrile resulted in the formation of a yellow precipitate. Several trials to crystallize this precipitate did not yield to quality crystals for X-ray diffraction studies. Similarly slow diffusion of the excess metal salt onto the complex in acetonitrile did not lead to any polynuclear assemblies. NMR titrations with different ligand to metal stoichiometries have been performed and only 3:1 ligand to metal ratio gave well defined species in solution. Therefore in order to isolate stable tris complexes emitting in the NIR region we have studied the complexation of these ligands with Nd(III), Er(III) and Yb(III) in presence of two different base (Et_3N, KOH). Here we present the complexes obtained from these studies.

4.1- Partially Deprotonated Dimeric Complexes

4.1.1 $[Nd(H_{1/2}hqa)_3]_2(Et_3NH)_3$ (I)

The reaction of $Nd(Otf)_3$ with three equivalents of H_2hqa in methanol in the presence of 6 equivalent of triethylamine results in C_3 symmetric species in solution (Scheme II-3). The ^1H NMR spectra of the complex shows only the presence of one sets of 5 signals in agreement with the presence of *C3* symmetric species in solution (Figure II-3). Crystallization of the dimeric complex $[Nd(H_{1/2}hqa)_3]_2(Et_3NH)_3{\cdot}Et_3NHOtf$ (**I**), by diffusion of diisopropylether in the methanolic solution showed the presence of partially protonated species. Dimerisation occurs through hydrogen bond formation between two partially protonated *syn* complexes.

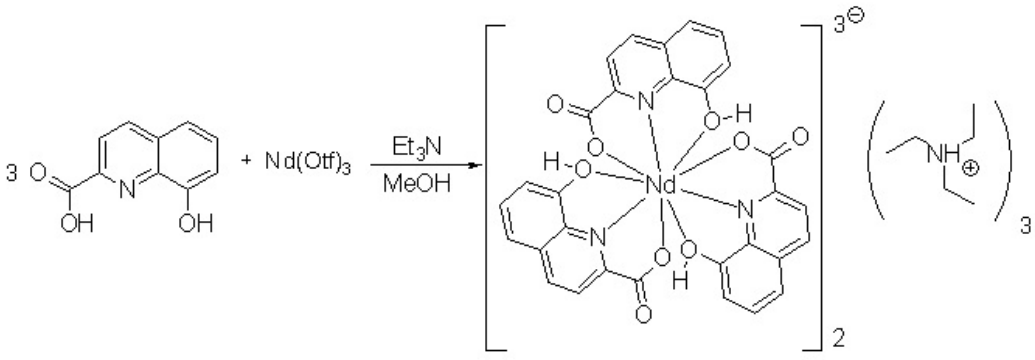

Scheme II-3: Reaction scheme for the synthesis of the $[Nd(H_{1/2}hqa)_3]_2(Et_3NH)_3$ complex

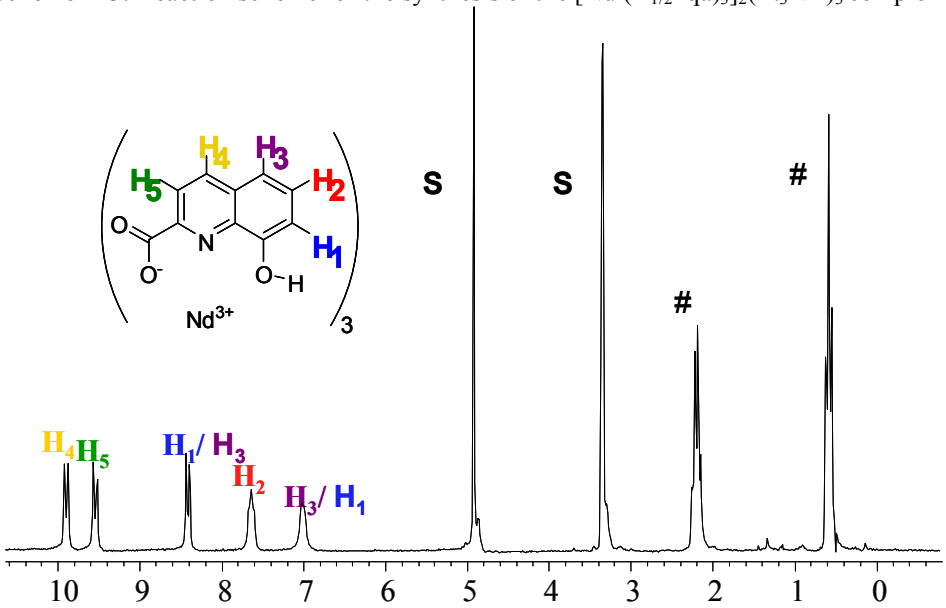

Figure II-3: ^1H NMR spectra of a 1:3 Nd:H_2hqa solution after addition of 6 equiv. of triethylamine. Symbols # and S indicate the signals of triethylammonium and solvents, respectively (0.03 M in ligand CD_3OD, 400 MHz, 298 K).

The X-ray diffraction study of the complex reveals the presence of a centrosymmetric dimer in the *C2/c* space group with the formula [Nd

$(H_{1/2}hqa)_3]_2(Et_3NH)_3{\cdot}Et_3NHOtf$. An ortep view of the $\{[Nd(H_{1/2}hqa)_3]_2\}^{3-}$ anion is presented in Figure II-4 and selected distances are given in Table II-1. The structure consists of nine-coordinated neodymium ions with a slightly distorted tricapped trigonal prism geometry. The metal ion is coordinated by three non-symmetry related hqa ligands which act as tridentate ligands, binding to neodymium through the pyridine nitrogen and the hydroxo and carboxylate oxygens. The three ligand strands bind the metal ion in a helical fashion with a *syn* arrangement. The three hydrogen atoms of the partially deprotonated hqa ligand are shared between the six phenol oxygen atoms. The resulting strong H-bonds connect two neodymium complexes in a dimeric structure with a Nd-Nd separation of 5.793 Å.

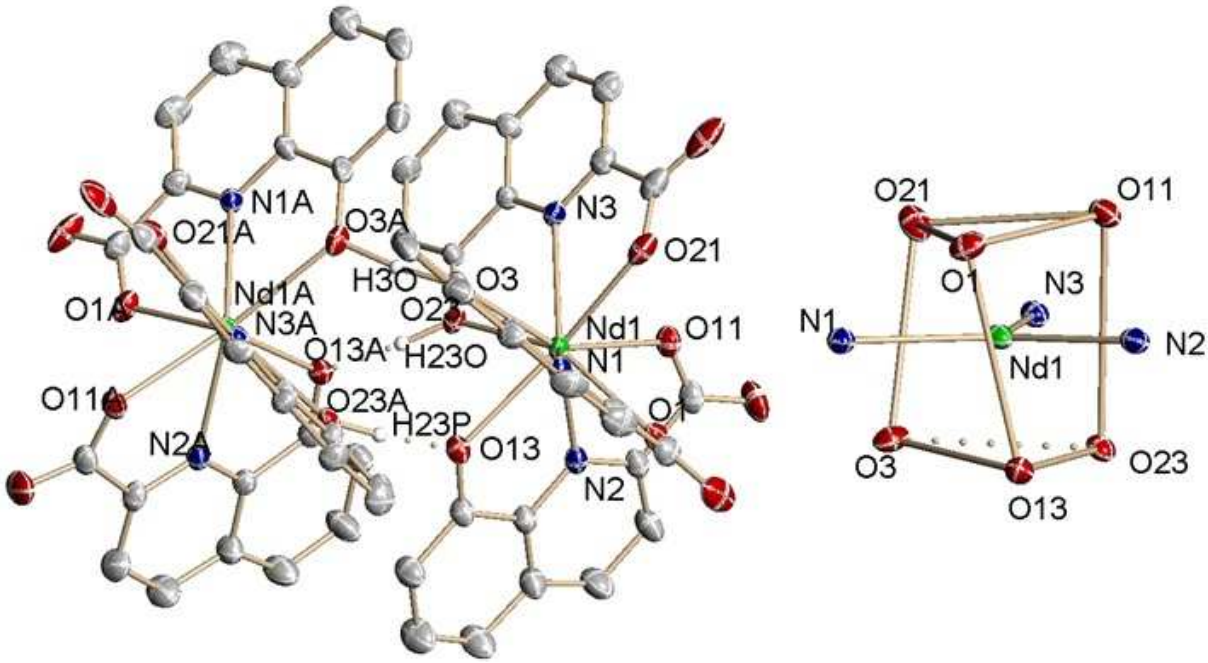

Figure II-4: ORTEP view of the anion $[Nd(H_{1/2}hqa)_3]_2^{3-}$ and coordination polyhedron. Atoms labelled A and P are C_2-symmetry related. The ellipsoids are shown at the 30% probability level

Table II-1: Selected bond lenghts (Å) for the complex $[Nd\ (H_{1/2}hqa)_3]_2(Et_3NH)_3$

$Ln\text{-}O_{carboxyl}$		$Ln\text{-}N_{py}$		$Ln\text{-}O_{phenol}$	
Nd(1)-O(1)	2.489(3)	Nd(1)-N(1)	2.603(3)	Nd(1)-O(3)	2.510(3)
Nd(1)-O(11)	2.481(3)	Nd(1)-N(2)	2.570(3)	Nd(1)-O(13)	2.499(3)
Nd(1)-O(21)	2.459(3)	Nd(1)-N(3)	2.592(3)	Nd(1)-O(23)	2.595(2)
Nd-O av	2.48(2)	**Nd-N av**	2.59(2)	**Nd-O av**	2.53(5)

The geometries of the H-bonds are reported in Table II-2. According to the Jeffrey's classification [137, 138] these hydrogen bonds have energies close to covalent bonds. Because of the strong hydrogen bonds the presence of dimeric structures could also be anticipated in solution and is probably at the origin of the observed high symmetry of

the protonated solution species. The mean value of the distances between the metal center and carboxylate oxygens 2.48(2) Å are shorter than Nd-Ophenol distances 2.53(5) Å, in agreement with the presence of partially protonated phenol oxygen atoms.

Table II-2: Hydrogen bonds (Å) and angles (°) in complex $[Nd(H_{1/2}hqa)_3]_2(Et_3NH)_3$ **(I)**. A (acceptor), D (donor)

D-H...A	d(D-H)	d(H...A)	d(D...A)	<(DHA)
O(3)-H(3O)...O(3A)	1.214(2)	1.214(2)	2.421(2)	171(9)
O(23)-H(23O)...O(13A)	1.00(6)	1.50(6)	2.494(4)	174(6)
O(23A)-H(23P)...O(13)	1.00(6)	1.50(6)	2.494(4)	174(6)

The formation of lanthanide complexes containing partially protonated ligands is observed (presence of *C_3* symmetric species in the proton NMR) in water at pH lower than 12 or in methanol solution in the presence of weak bases and is compatible with the high pKa value of the hydroxyl group of the 8-hydroxyquinoline moiety (pKa = 9.8 in 8-hydroxyquinoline). Similar species have been already observed for 8-hydroxyquinoline based podating ligands [59, 63]. The high solution symmetry of the partially protonated species suggests that the strong hydrogen bonds observed in the solid state structure are maintained in solution.

4.1.2 $[Nd(H_{1/2}hqt)_3]_2(Et_3NH)_3$ (II)

Similarly the reaction of $Nd(Otf)_3$ with three equivalents of H_2hqt in methanol in presence of 6 equivalent of triethylamine results in C_3 symmetric species in solution (Scheme II-4). The ^1H NMR spectra of the complex shows only the presence of one sets of 4 signals integrating for 5 protons in agreement with the presence of *C_3* symmetric species in solution (Figure II-5). X-ray diffraction of crystals isolated in similar conditions for the neodymium complex of hqt^{2-} suggests the presence of a similar species. Although the crystal data are not of good quality, the dimeric structure is observed in the obtained crystal structure revealing the presence of hydrogen bonding in between two mononuclear complexes (Figure II-6).

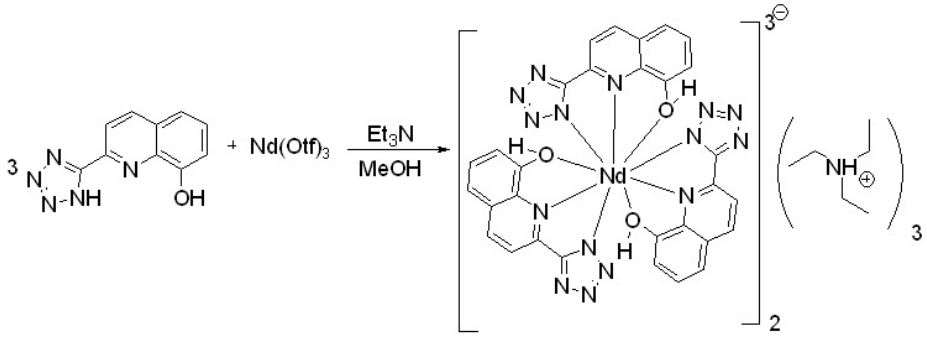

Scheme II-4: Reaction scheme for the synthesis of the $[Nd\ (H_{1/2}hqt)_3]_2(Et_3NH)_3$ complex

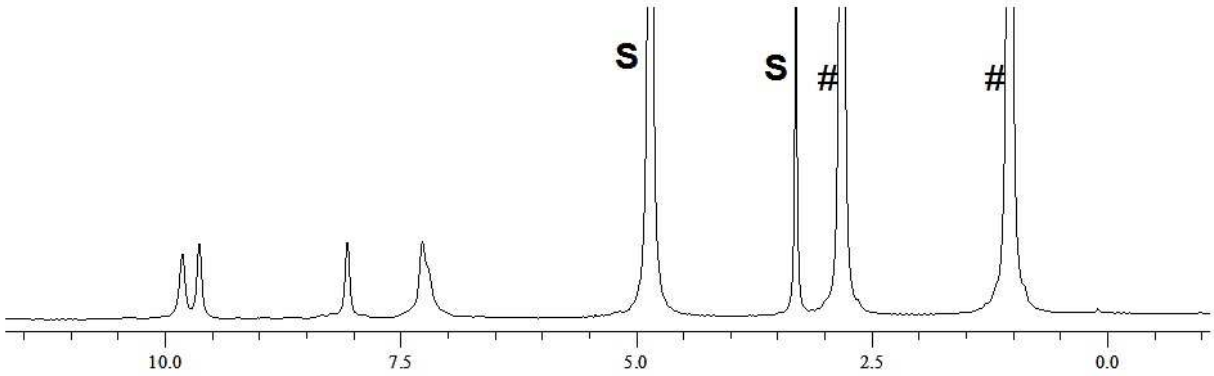

Figure II-5: ^1H NMR spectra of a 1:3 Nd:H_2hqt solution after addition of 6 equiv. of triethylamine. Symbols # and S correspond to the signals of triethylammonium and solvents, respectively (0.03 M in ligand CD_3OD, 400 MHz, 298 K**)**

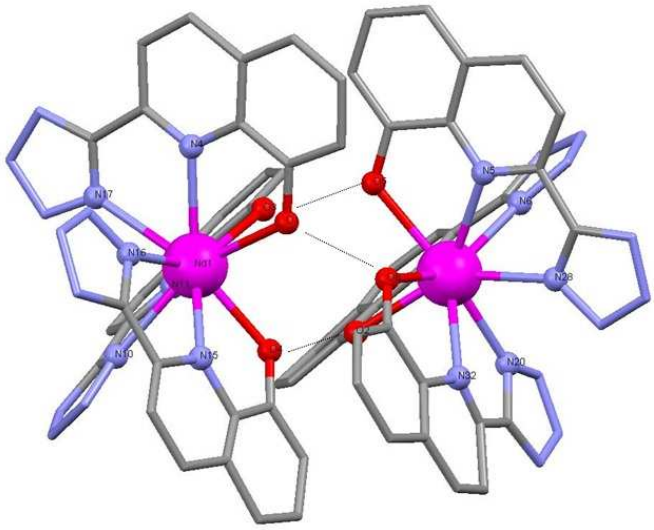

Figure II-6: Mercury diagram of the anion $[Nd(H_{1/2}hqt)_3]_2^{3-}$

4.2- Fully Deprotonated Polymeric Complexes

The homoleptic complexes $[Ln(hqa)_3]K_3$ and $[Ln(hqt)_3]K_3$ were prepared by reacting a solution of $Ln(Otf)_3$ (H_2hqa; Ln = Nd (**III**), Er (**IV**), Yb; H_2hqt; Ln = Nd(**V**), Er, Yb) in water with 3 equivalents of ligand (H_2hqa/H_2hqt) at pH 12 adjusted by addition of aqueous KOH (1M). Crystallization from a mixture of methanol/ diisopropylether

afforded the complexes in ~60 % yield. The analytical results are in agreement with the presence of tris-ligand complexes. In this section the synthesis and full characterization of the complexes will be discussed for both of the ligands.

4.2.1 $[Ln(hqa)_3]K_3$ complexes

The reaction of $Ln(Otf)_3$ (Ln = Nd, Er, Yb) with three equivalents of H_2hqa in water at pH 12 adjusted by 1 M KOH solution resulted in the formation of unsymmetrical complexes as shown in Scheme II-5.

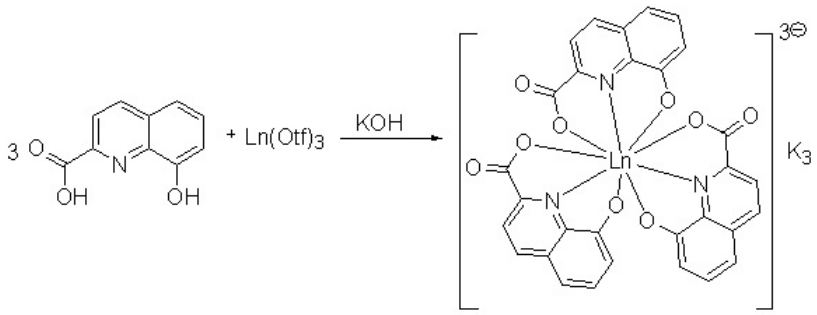

Scheme II-5: Reaction scheme for the synthesis of the $[Ln(hqa)_3]K_3$ complex

a) ^{1}H NMR Solution Studies

The ^{1}H NMR spectrum of $[Nd(hqa)_3]K_3$ in CD_3OD shows two well defined sets of signals which were assigned to the two geometric isomers *syn* (12%) and *anti* present in solution (Figure II-7). The major set of 13 signals was assigned to the 15 protons of an unsymmetrical *anti* species in which the three hqa^{-2} ligands are arranged in a "up-up-down" geometry. The second set of 5 signals was assigned to the 15 protons of the C_3 symmetric *syn* species in which the three hqa^{-2} adopt an "up-up-up" arrangement. The observed *anti/syn* ratio is only slightly higher of the expected statistical 75% ratio found in other tridentate unsymmetrical substituted hydroxyquinoline ligands [131]. A very similar proton NMR spectrum was found for the $[Nd(hqa)_3]K_3$ complex in water at pD 12. At 298 K the ^{1}H NMR signals are relatively large suggesting an exchange between *anti* and *syn* isomers. At 278 K the ^{1}H NMR spectrum of the $[Nd(hqa)_3]K_3$ complex in water at pD 12 is well resolved (Figure II-8). These results show that the $[Nd(hqa)_3]K_3$ complex remains undissociate in basic 0.04 M aqueous solution and confirms the strong resistance of these anionic complexes to hydrolysis. Similar NMR spectra have been obtained for Er and Yb complexes however due to strong paramagnetic broadening and shift of the peaks the complete assignment of the peaks could not be performed. However, the presence of 15 major peaks and 5 minor peaks could be identified by integration for $[Yb(hqa)_3]K_3$

complex (Figure II-9).

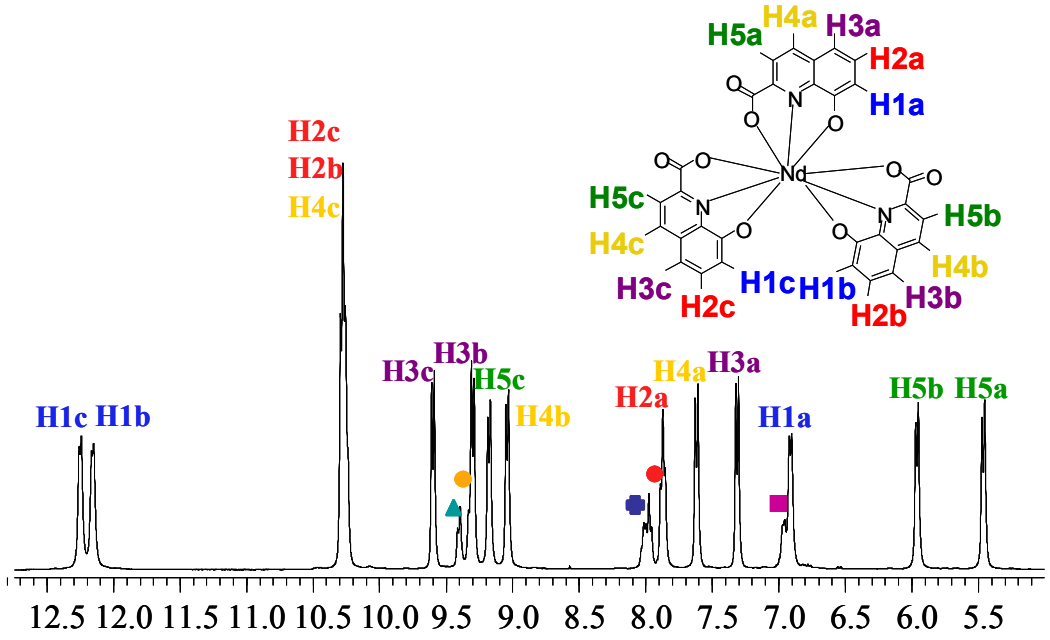

Figure II-7: ^{1}H NMR spectrum of $[Nd(hqa)_3]^{-3}$ (CD_3OD, 400 MHz, 298 K) [0.04 M]

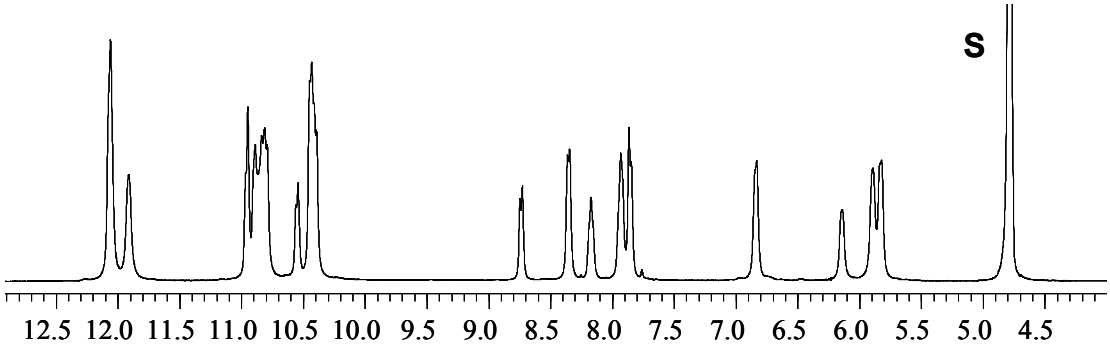

Figure II-8: ^{1}H NMR (400 MHz, 278 K) spectrum of $[Nd(hqa)_3]^{-3}$ in D_2O (0.04 M , pD = 12)

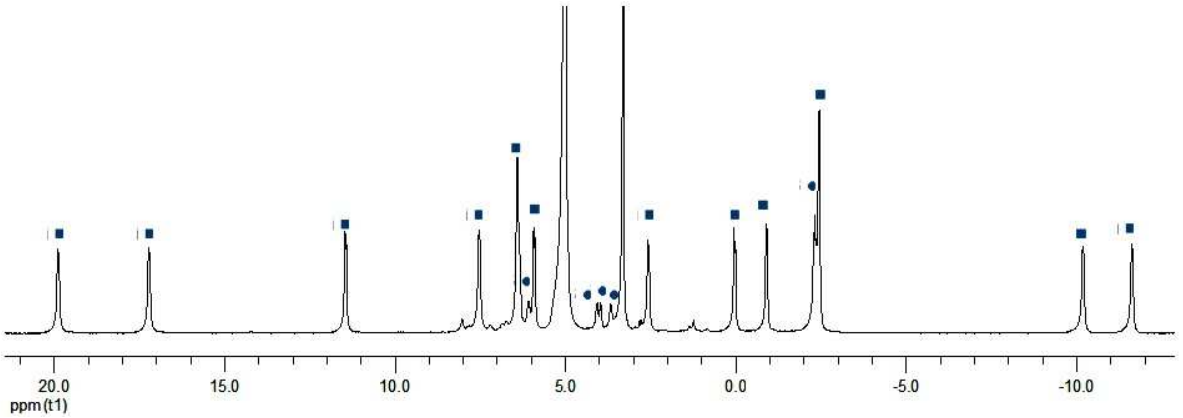

Figure II-9: ^{1}H NMR spectrum of $[Yb(hqa)_3]K_3$, where ● signals corresponds to the syn species and ■ signals corresponds to the anti species. (CD_3OD, 500 MHz, 298 K)

b) Solid State Structure

Crystals suitable for X-ray diffraction have been obtained for the complexes of $[Nd(hqa)_3]K_3$ and of $[Er(hqa)_3]K_3$ by slow diffusion of diisopropylether in methanol solutions. X-ray diffraction studies on crystals of $[Nd(hqa)_3]K_3$ and of $[Er(hqa)_3]K_3$ revealed respectively the formation of a centrosymmetric structure crystallizing in the *P2(1)/n* space group with the formula $[Nd(hqa)_3]K_3 \cdot 8CH_3OH_\infty$**(III)** and of a structure crystallizing in the *C2/c* space group with the formula $[Er(hqa)_3]K_3 \cdot 7CH_3OH \cdot 0.25DIPE_\infty$ **(IV) (**DIPE = diisopropylether). Ortep views of the structure of $[Nd(hqa)_3]K_3 \cdot 8CH_3OH$ are represented in Figure II-10 and selected bond distances of $[Nd(hqa)_3]K_3$ and of $[Er(hqa)_3]K_3$ are given in Table II-3.

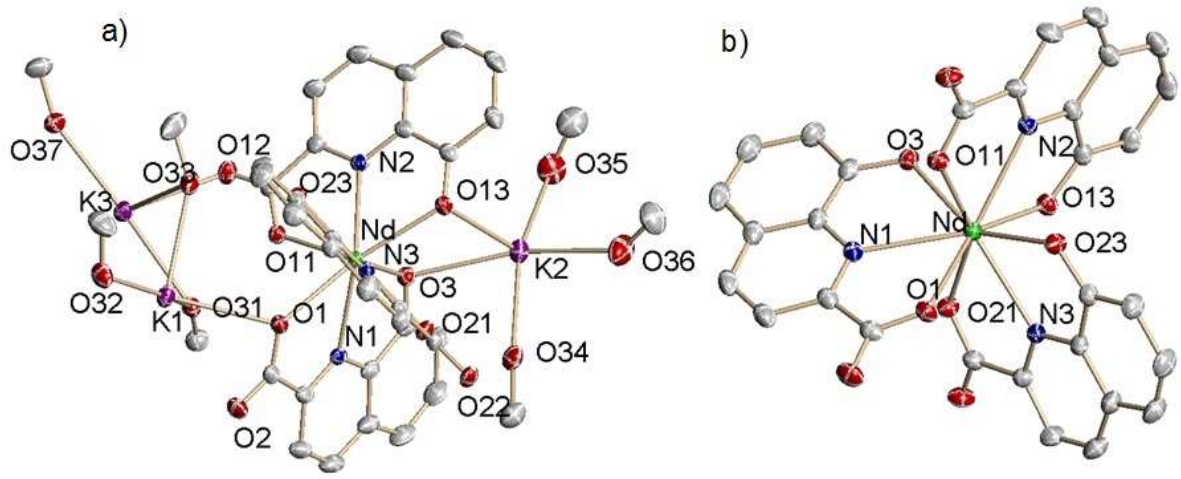

Figure II-10: ORTEP views of a) $[Nd(hqa)_3]K_3 \cdot 8CH_3OH$ (asymmetric unit) and of b) $[Nd(hqa)_3]^{3-}$ anion. The ellipsoids are shown at the 30% probability level

In $[Nd(hqa)_3]K_3$ and $[Er(hqa)_3]K_3$ complexes three deprotonated hqa^{2-} ligands bind the metal ion in a tridentate fashion through the 8-hydroxyquinolato units and the carboxylate oxygens, yielding a nine-coordinated complex with a slightly distorted tricapped trigonal prism geometry (Figure II-11). The three ligands adopt a helical arrangement with an *anti* conformation "up-up-down" ((O(23), O(21) and N(3)) is the "down" ligand). A very similar coordination environment was also found from X-ray studies for the ytterbium complex although the quality of the resulting crystal structure is not sufficient due to the quality of the isolated crystals.

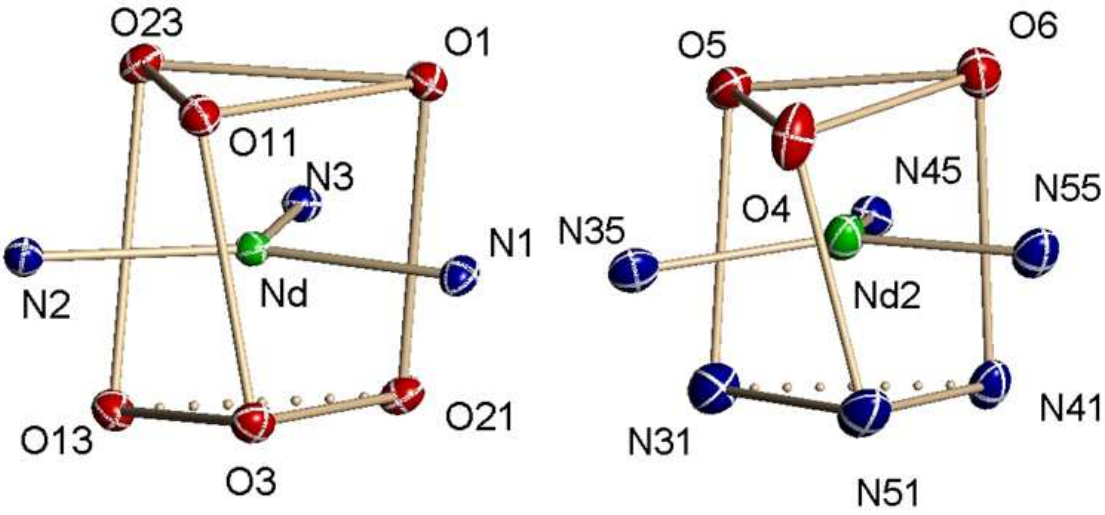

Figure II-11: Coordination Polyhedron in $[Nd(hqa)_3]^{-3}$ (left) and $[Nd(hqt)_3]^{-3}$ (rigth)

Table II-3: Selected bond lenghts (Å) for the $[Nd(hqa)_3]K_3$ and of $[Er(hqa)_3]K_3$ complexes

$[Nd(hqa)_3]K_3$

$Ln\text{-}O_{carboxyl}$		$Ln\text{-}N_{py}$		$Ln\text{-}O_{phenol}$	
Nd-O(1)	2.546(14)	Nd-N(1)	2.609(16)	Nd-O(3)	2.509(13)
Nd-O(11)	2.470(14)	Nd-N(2)	2.563(16)	Nd-O(13)	2.478(14)
Nd-O(21)	2.492(13)	Nd-N(3)	2.574(15)	Nd-O(23)	2.482(14)
Nd-O av	2.50 (4)	Nd-N av	2.58 (2)	Nd-O av	2.49(2)

$[Er(hqa)_3]K_3$

$Ln\text{-}O_{carboxyl}$		$Ln\text{-}N_{py}$		$Ln\text{-}O_{phenol}$	
Er-O(1)	2.431(3)	Er-N(1)	2.466(4)	Er-O(3)	2.417(3)
Er-O(11)	2.411(2)	Er-N(11)	2.458(3)	Er-O(13)	2.426(3)
Er-O(21)	2.447(2)	Er-N(21)	2.435(3)	Er-O(23)	2.368(2)
Er-O av	2.43(2)	Er-N av	2.45(2)	Er-O av	2.40(3)

The mean values of the Nd-O distances (Nd-Ophenol 2.49(2) Å and Nd-Ocarboxyl 2.50(4) Å) in $[Nd(hqa)_3]K_3$ are very similar to those found in the dimeric partially protonated complex (Nd-Ophenol 2.53(5) Å and Nd-Ocarboxyl 2.48(2) Å), indicating that the partial protonation of the ligand is not affecting significantly the Nd-O bond strength. On the other end smaller values of the Er-Ophenol (2.40(3) Å) and Er-Ocarboxyl (2.43(2) Å) distances are found in the $[Er(hqa)_3]K_3$ with respect to the Nd(III) complex ($[Nd(hqa)_3]K_3$) which is in agreement with the decrease of ionic radii along the lanthanide series [5].

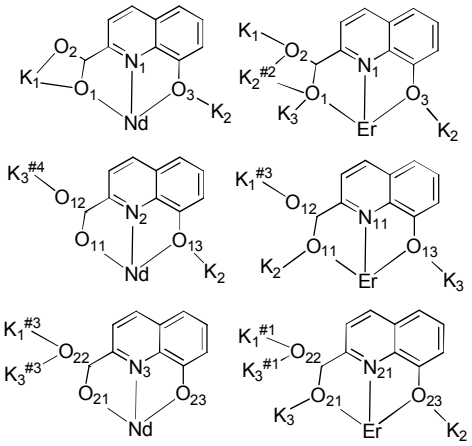

Scheme II-6: Coordination mode of the three hqa^{2-} ligands in $[Nd(hqa)_3]K_3$ and $[Er(hqa)_3]K_3$. Symmetry transformations used for generating equivalent atoms in ($[Nd(hqa)_3]K_3$): #3 x-1/2,-y+3/2,z-1/2; and in ($[Er(hqa)_3]K_3$) #4 -x+2,-y+2,-z+2; #1 -x+1/2,-y+1/2,-z+1; #2 -x+1/2,y-1/2,-z+1/2; #3 -x+1/2,y+1/2,-z+1/2

The complete deprotonation of the three hqa^{2-} ligands in $[Nd(hqa)_3]K_3$ and in $[Er(hqa)_3]K_3$ leads to the presence of three potassium counter-ions in the structures which coordinate the phenol and carboxylate oxygen atoms as shown in Scheme II-6. The potassium ions also bind 8 methanol molecules which act as bridging ligands between adjacent neodymium complexes leading to a 2D polymeric network (Figure II-12). For the erbium complex the methanol molecules do not act as bridging ligands, but the potassium ions bind directly to the carboxylate oxygens of the adjacent complex yielding a 2D network (Figure II-13). Therefore the Er-Er distances are significantly shorter in $[Er(hqa)_3]K_3$ (9.964 Å) than the Nd- Nd distances in $[Nd(hqa)_3]K_3$ (12.728 Å).

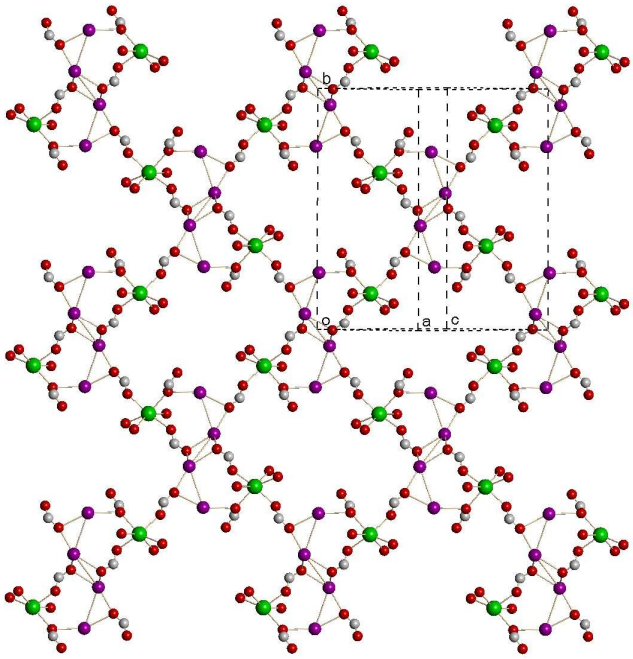

Figure II-12: ORTEP diagram of the polymeric 2D network in $[Nd(hqa)_3]K_3 \cdot 8CH_3OH_\infty$ along c-a axis (a+c, b plane) K:purple, O:red, Ln:green

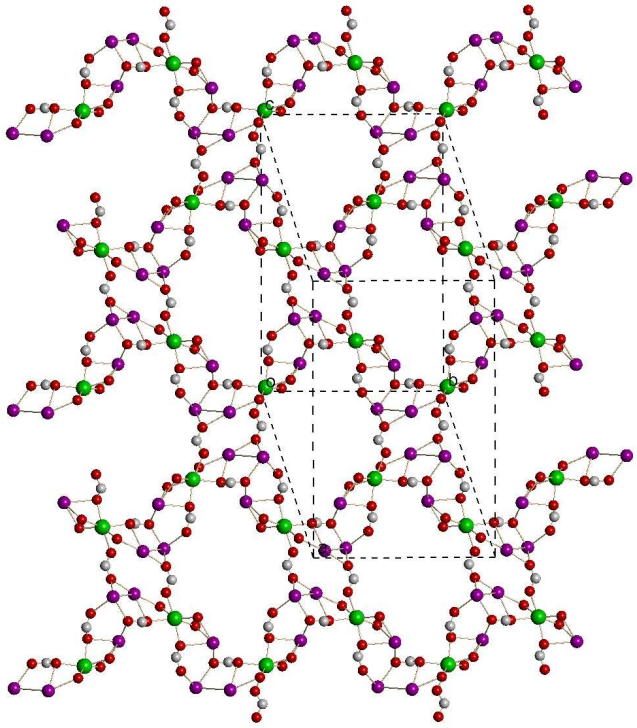

Figure II-13: ORTEP diagram of the polymeric 2D network in $[Er(hqa)_3]K_3 \cdot 7CH_3OH \cdot 0.25DIPE_\infty$ (bc plane). K:purple, O:red, Ln:green

4.2.2 $[Ln(hqt)_3]K_3$ complexes

The reaction of $Ln(Otf)_3$ with three equivalents of H_2hqt in water at pH 12 adjusted by 1M KOH solution resulted in the formation of symmetrical complexes as shown in Scheme II-7.

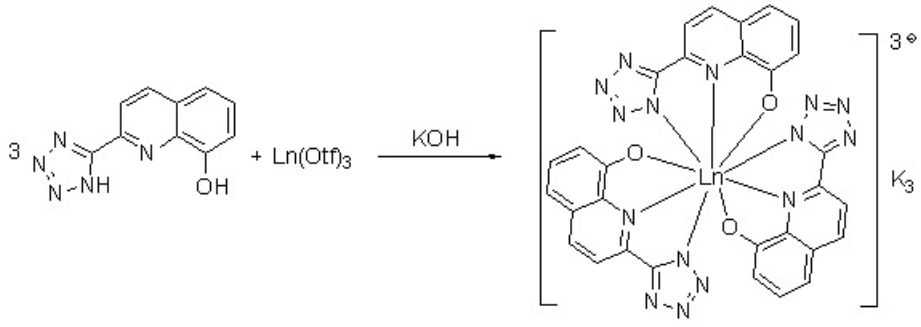

Scheme II-7: Reaction scheme for the synthesis of the $[Nd(hqt)_3]K_3$ complex

a) ^{1}H NMR Solution Studies

The ^{1}H NMR spectrum of $[Nd(hqt)_3]K_3$ (similar to $[Nd(hqa)_3]K_3$) in CD_3OD shows two sets of signals which were assigned to the two geometric isomers *syn* and *anti* (Figure II-14). However in this complex the *syn/anti* ratio is inverted (*syn*: 65%) with respect to the expected statistical distribution. This result suggests that the solid state structure is retained in solution probably due to the coordination of potassium by the tetrazole binding

units. ^{1}H NMR spectrum of $[Ln(hqt)_3]K_3$ complexes in water at pD 12 at 25°C gives similar signals as in methanol revealing the stability of complexes in aqueous media. Similar NMR spectra have been obtained for Er and Yb complexes. Due to strong paramagnetic broadening and shift of the peaks the complete assignment of the peaks could not be performed. However, the presence of 5 major peaks and 15 minor peaks could be assigned by integration for $[Yb(hqt)_3]K_3$ complex (Figure II-15).

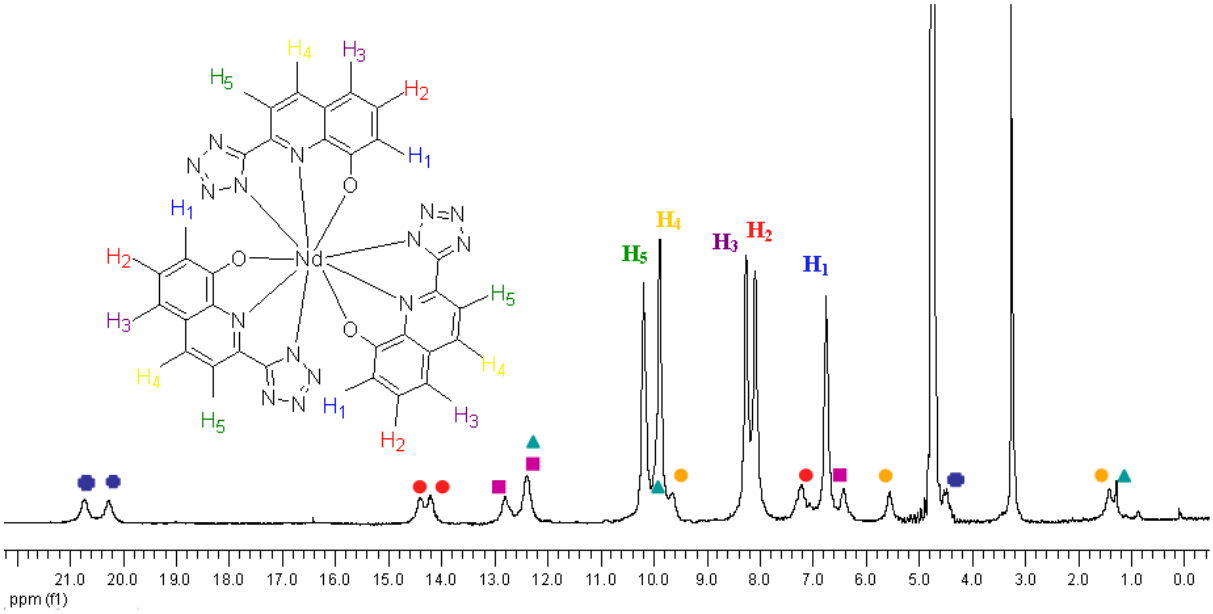

Figure II-14: ^{1}H NMR spectrum of $[Nd(hqt)_3]^{-3}$. (CD_3OD, 400 MHz, 298 K) [0.04 M]

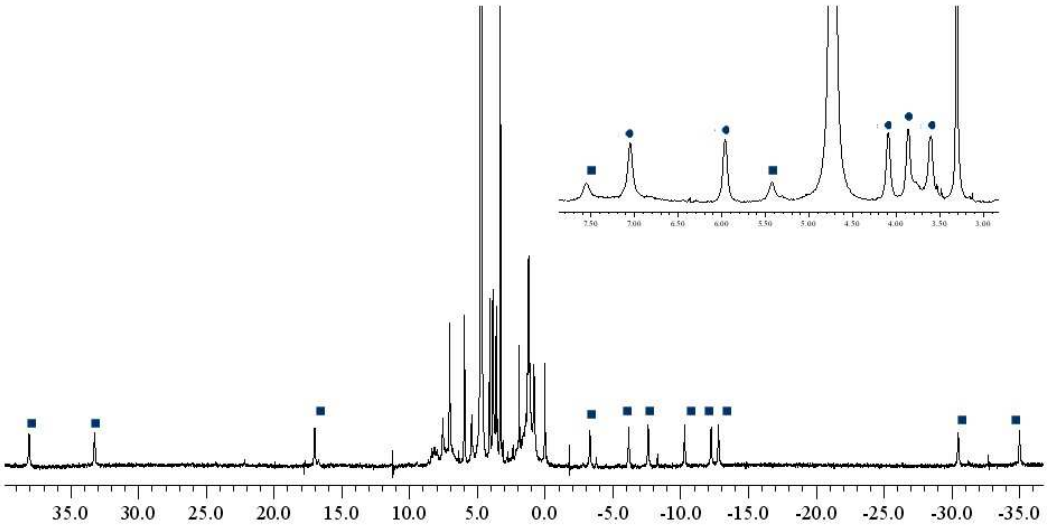

Figure II-15: ^{1}H NMR spectrum of $[Yb(hqt)_3]K_3$, where ● signals corresponds to the syn species and ■ signals corresponds to the anti species (CD_3OD, 400 MHz, 298 K)

b) Solid State Structure

Crystals suitable for X-ray diffraction have been obtained for the $[Nd(hqt)_3]K_3$ complex by slow diffusion of diisopropylether in methanol solutions. X-ray diffraction studies on single crystals of $[Nd(hqt)_3]K_3$ revealed the formation of a centrosymmetric structure crystallising in the P_{-1} space group with the formula $[Nd(hqt)_3]K_3 \cdot 6CH_3OH_\infty$ **(V)**. Ortep views of the structure are represented in Figure II-16.

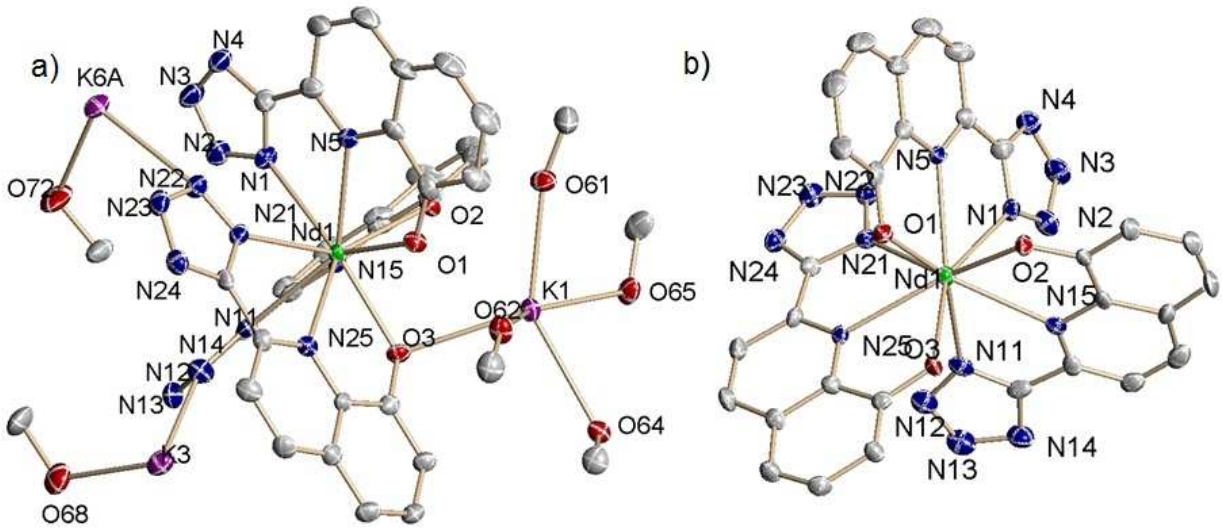

Figure II-16: ORTEP views of a) $[Nd(hqt)_3]K_3$ showing the potassium bridged tetrazoles and of b) the $[Nd(hqt)_3]^{3-}$ anion. The ellipsoids are shown at the 30% probability level

The three deprotonated hqt^{2-} ligands bind in a tridentate O,N,N fashion through the quinolato units and the tetrazole nitrogens, affording a nine-coordinated Nd(III) complex with a slightly distorted tricapped trigonal prism geometry (Figure II-11). As a major feature of the complex the helical arrangement of the three ligands present a *syn* conformation. A similar arrangement is also suggested by X-ray studies for the Er complex $[Er(hqt)_3]K_3$ although the crystal structure is not of good quality.

Table II-4: Selected bond lenghts (Å) for the $[Nd(hqt)_3]K_3$ and complexes

$Ln\text{-}O_{carboxyl}$		$Ln\text{-}N_{py}$		$Ln\text{-}N_{tetrazole}$	
Nd(1)-O(1)	2.396(5)	Nd(1)-N(5)	2.608(6)	Nd(1)-N(1)	2.672(5)
Nd(1)-O(2)	2.436(4)	Nd(1)-N(15)	2.604(6)	Nd(1)-N(11)	2.681(6)
Nd(1)-O(3)	2.425(4)	Nd(1)-N(25)	2.625(5)	Nd(1)-N(21)	2.650(5)
Nd-O av	2.42(2)	Nd-N av	2.61(1)	Nd-N av	2.67(2)

Complete deprotonation of the three hqt^{2-} ligands leads to the presence of three potassium ions as counter-ions. The mean value of the distances between the metal center

and carboxylate oxygens 2.42(2) Å are shorter than Nd-$N_{tetrazole}$ distances 2.67(2) Å. Two crystallographically independent complexes are found in the structure. They differ in their potassium coordination (Scheme II-8). Each complex is bound to six potassium ions connecting different complexes to yield a 2D network which propagates along the a, b plane. The potassium ions bound to the three hydroxyquinoline oxygen atoms are connected through methanol molecules yielding a 3D network (Figure II-17).

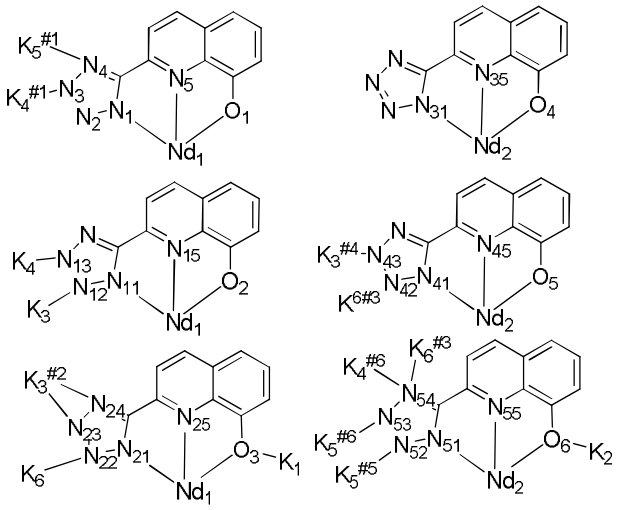

Scheme II-8: Coordination mode of the three hqt^{2-} ligands in complex $[Nd(hqt)_3]K_3$. Symmetry transformations used for generating equivalent atoms:#1 -x,-y,-z+1; #2 -x+1,-y,-z+1; #3 x,y,z-1; #4 -x+1,-y,-z; #5 x,y+1,z-1; #6 -x,-y,-z

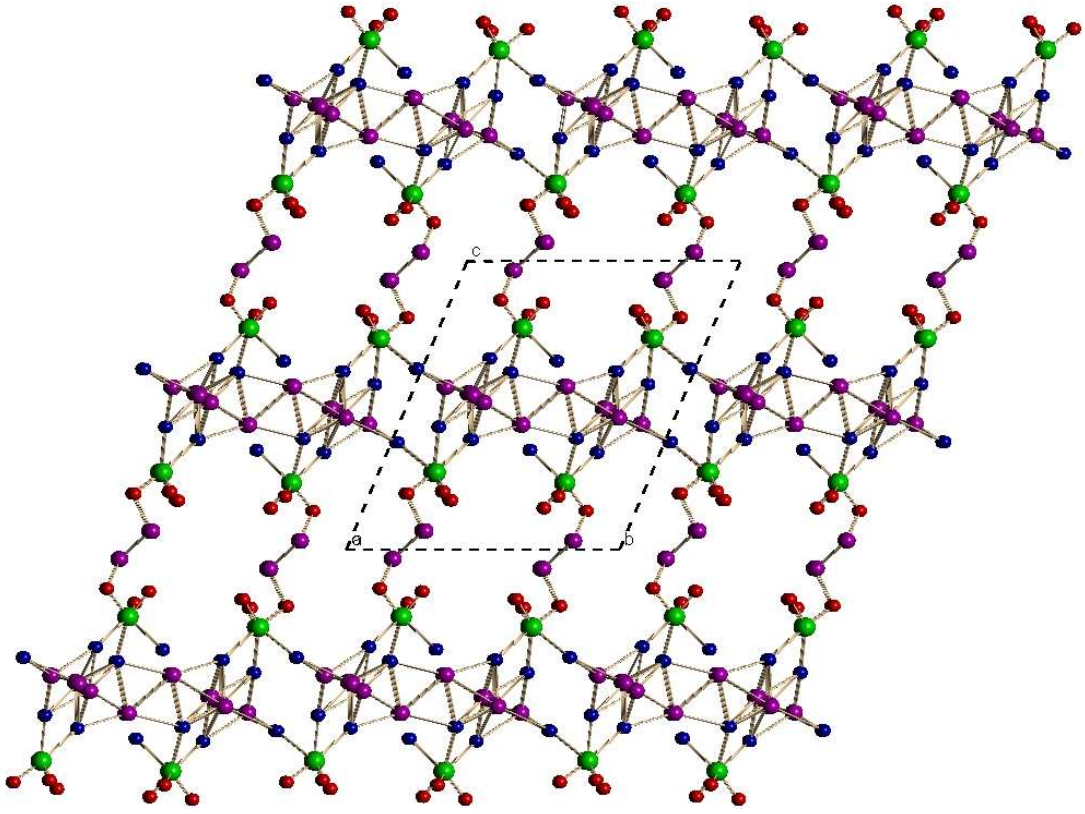

Figure II-17: ORTEP diagram of the polymeric 2D network in $[Nd(hqt)_3]K_3.6CH_3OH_\infty$ along the a axis. K:purple, O:red, Nd:green, N:blue

5- Sensitization of Lanthanide-Centered NIR Emission

In methanol, the absorption spectrum of the hqa and hqt ligands features three main bands located around 250, 305, 344 and 264, 317, 349 nm, respectively (Figure II-18) with absorption extending up to 400 nm. They are assigned to $\pi \rightarrow \pi^*$ and $n \rightarrow \pi^*$ transitions. In the Ln(III) complexes of both ligands, the more energetic bands are blue-shifted and characteristic bands appear at 411 and 402 nm for the hqa and hqt ligands, respectively with absorption extending up to 500 nm.

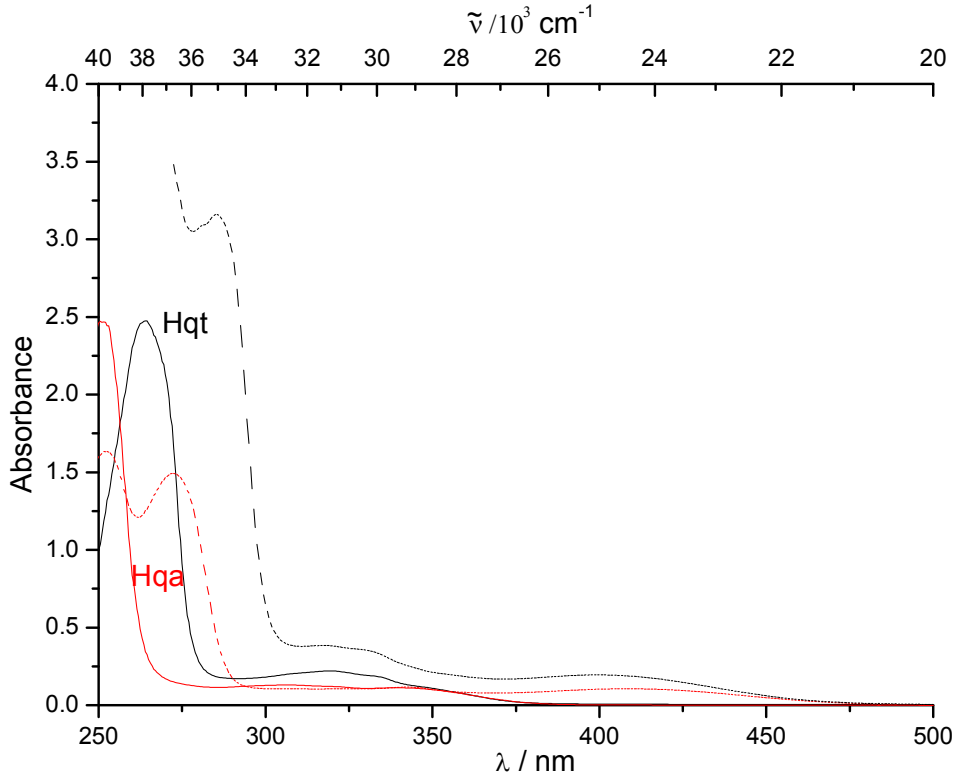

Figure II-18: Absorption spectra of the hqa (red line) and hqt (black line) ligands and their respective Nd(III) complexes (dotted lines) in CH_3OH at 16 µM

Photophysical studies were carried out on all complexes in solid state and in methanol. The measurements were effectuated in air without particular precaution to prevent the presence of oxygen. All the isolated complexes of hqt and hqa with the Nd(III), Yb(III) and Er(III) ions including the dimeric partially protonated complex ($[Nd(H_{1/2}hqa)_3]_2^{3-}$) display sizable metal-centered NIR luminescence in solid state and in methanolic solution. In addition, at 295 K, the ligand-centered emission contributes only faintly to the luminescence with UV excitation in the $\pi \rightarrow \pi^*$ and $n \rightarrow \pi^*$ absorption bands of the ligand resulting in a very faint emission (<5 % compared with the free ligand) through fluorescence from the $^1\pi\pi^*$ state ligand emission spectra. It indicates an efficient energy transfer process to the acceptor

levels of the metal ions. Sensitization of the NIR luminescence by the ligands is ascertained by the excitation spectra of the Nd(III), Yb(III) and Er(III) complexes and clearly demonstrate the antenna effect of the ligand with components matching the absorption bands of the electronic spectra (Figure II-19, left). At room temperature and upon broad band excitation through both ligand levels at 371, 344 and 483 nm all complexes show identical luminescence spectra in solid state or dissolved in methanol and display peaks corresponding to the expected f-f NIR transitions.

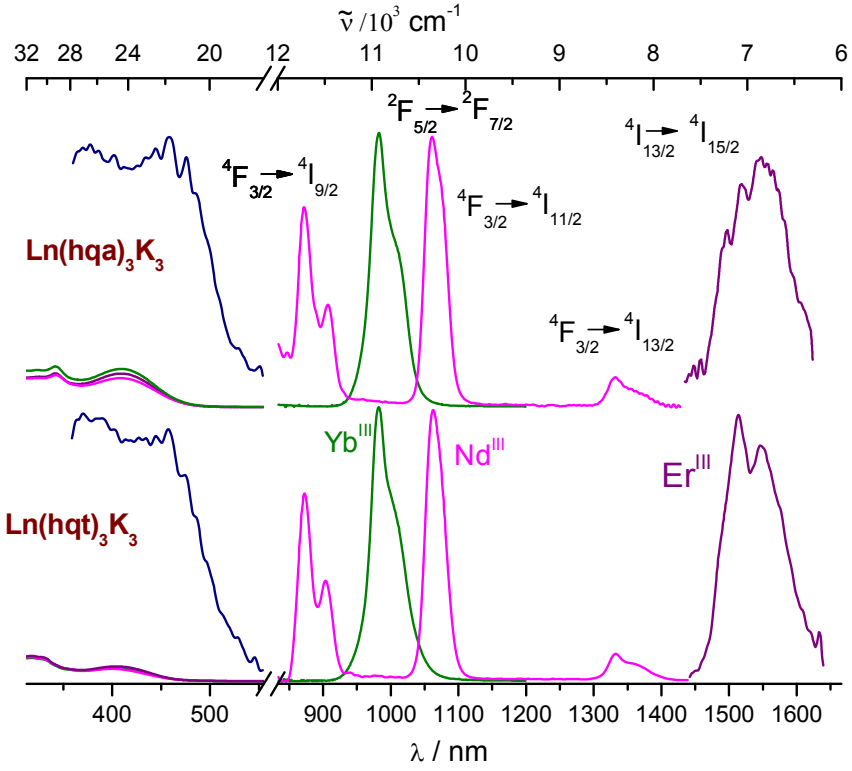

Figure II-19: Left: Normalized absorption and excitation spectra (λ_{an} = 1540 (Er), 1063 (Nd), and 976 nm (Yb)). Right: Emission spectra in the NIR region (λ_{ex} =371 nm) of the hqa and hqt complexes of Er(III), Nd(III), and Yb(III)

The Yb(III) complexes are characterized by a band in the 905-1095 nm range, assigned to the $^2F_{5/2} \rightarrow {}^2F_{7/2}$ transition, with a sharp main component at 981 nm and broader components at longer wavelengths due, in part, to vibronic transitions. The Nd(III) complexes display three bands in the 835-1420 nm range, the main band occurring between 1005 and 1145 nm ($^4F_{3/2} \rightarrow {}^4I_{11/2}$), with a maximum at 1060 nm; two other bands are visible between 835-950 ($^4F_{3/2} \rightarrow {}^4I_{9/2}$) and 1285-1420 nm ($^4F_{3/2} \rightarrow {}^4I_{13/2}$). Finally the Er(III) complexes emit a band centered at 1551 nm, assigned to the $^4I_{13/2} \rightarrow {}^4I_{15/2}$ transition.

The luminescence decays obtained upon excitation through both hqa and hqt ligands electronic levels are single-exponential functions of time, indicating a fast energy transfer from the ligand to the metal ion and also the presence of efficient nonradiative deactivation processes, since they are much shorter than the radiative lifetimes. The corresponding lifetimes of the Nd($^4F_{3/2}$), Yb($^2F_{5/2}$) and Er($^4I_{13/2}$) excited states are reported in Table II-5 and indicate that both ligands provide an adequate protective coordination environment around the metal ion.

In the solid state, the lifetimes are smaller than in methanol solution as often observed for lanthanide complexes. The lifetimes of the monomeric ($Ln(hqa)_3K_3$, $Ln(hqt)_3K_3$) Nd(III) and Yb(III) complexes in the solid state are 0.240, 0.225, 2.99 and 3.15 μs, and compare well to those measured in methanol (0.322, 0.367, 3.89 and 5.15 μs respectively). The situation is different for the Er(III) complexes of both ligands where the luminescence decays increases significantly in the solid state compared to the methanol solutions.

Table II-5: Metal-ion-centered lifetimes and absolute quantum yields for Nd($^4F_{3/2}$), Er ($^4I1_{3/2}$), and Yb($^2F_{5/2}$) in the hqa and hqt Ln(III) complexes (Ln = Nd, Er, Yb) in solution and in solid state

Compound		τ(μs)	Q_{Ln}^{L} (%)
$[Nd(hqa)_3]K_3$	Solid	0.240(1)	0.060(1)
	CH_3OH	0.322(1)	0.063(2)
	H_2O	0.127(1)	$<2\cdot10^{-4}$
$[Nd(H_{1/2}hqa)_3]_2(Et_3NH)_3$	solid	0.356(1)	0.059(4)
	CH_3OH	0.296(1)	0.035(1)
$[Nd(hqt)_3]K_3$	Solid	0.225(1)	0.067(1)
	CH_3OH	0.367(1)	0.068(1)
$[Yb(hqa)_3]K_3$	Solid	2.99(1)	0.18(1)
	CH_3OH	3.89(1)	0.28(1)
$[Yb(hqt)_3]K_3$	Solid	3.15(1)	0.21(1)
	CH_3OH	5.15(1)	0.31(1)
$[Er(hqa)_3]K_3$	Solid	0.479(1)	0.0051(1)
	CH_3OH	0.375(1)	0.0019(1)
$[Er(hqt)_3]K_3$	Solid	0.623(1)	0.0059(2)
	CH_3OH	0.471(1)	0.0020(1)

To quantify the ability of the chromophoric subunits to sensitize the NIR-emitting lanthanides, the absolute quantum yields of the Ln(III) complexes (Ln = Nd, Er, Yb) in solid state and methanol solution have been determined upon ligand excitation. The quantum yields are sizeable for the $[Nd(hqa)_3]K_3$ (0.06%) and $[Yb(hqa)_3]K_3$ (0.18%) complexes in the solid state, and 0.063% and 0.28%, respectively, in methanol solution. The NIR luminescence of the $[Er(hqa)_3]K_3$ chelate is sufficiently intense at room temperature for allowing the calculation of quantum yields which are smaller in methanol (0.0019%) compared to the value (0.0051%) obtained in solid state. Since the $[Nd(hqa)_3]K_3$ complex is stable in NMR concentration in water at pH 12 we could measure the NIR luminescence of this complex but it was not sufficiently intense at room temperature for allowing the calculation of the quantum yield.

However, the luminescence lifetime values measured in methanol (0.367(1) and 0.322(1) µs, for $[Nd(hqt)_3]K_3$ and $[Nd(hqa)_3]K_3$, respectively and the one obtained for complex $[Nd(hqa)_3]K_3$ in water at pH 12 (0.127(1) µs) are very similar to the values found for water stable Nd podates in water (0.13(1) - 0,25(3) µs) [61].This result suggest the fact that these complexes remain associated even in low concentration aqueous solutions. Accordingly to the good values observed for the overall quantum yields, the efficiencies of the sensitizing process are important and the de-activation processes are essentially due to vibrational oscillators located outside the first coordination sphere.

Finally in order to study the influence of the protonation state of the hydroxyquinoline unit on the spectroscopic properties of the Nd(III) ion, luminescence measurements were carried out also on the dimeric ($[Nd(H_{1/2}hqa)_3]_2^{3-}$) complex in the solid state as well as in solution. Excitation and emission spectra of the complexes in solution and in the solid state are almost identical (Figure II-20). The luminescence decay of the Nd($^4F_{3/2}$) excited state measured at room temperature is mono-exponential. Corresponding luminescence lifetimes and absolute quantum yields are listed in Table II-5. They are very similar for both protonated and deprotonated Nd(III) complexes in the solid state and in solution in CH_3OH. The presence of the O-H oscillators close to the metal ion has apparently no influence on the Nd(III) luminescence, probably because of the implication of these O-H groups in very strong H-bonds; deactivation of the Nd(III) luminescence is therefore limited.

All the values of quantum yields obtained for the hqt complexes are 15□20 % higher than those measured for the hqa complexes. This is consistent with the trend observed for the lifetimes. These quantum yields are lower than those found for halogenated expanded 8-hydroxyquinoline ligands (up to 0.4% in the solid state for a neutral Nd(III) tris 8-hydroxyquinoline complex) [131, 133] but comparable to the best photophysical properties reported in the literature for lanthanide complexes of non-halogenated 8-hydroxyquinolines in solutions (between 0.01 and 0.07 % for the Nd(III) and from 0.14 to 0.53% for Yb(III)) [115].

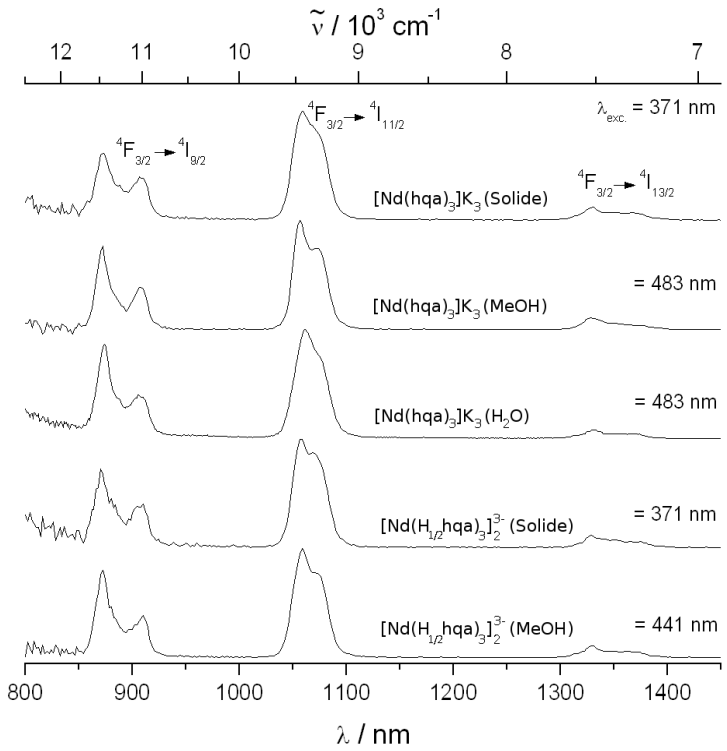

Figure II-20: Normalized emission spectra (λ_{exc}= 371 nm) of the Nd(III) complexes in solution and in the solid state at 295K

6- Conclusions

In this chapter we have shown that two new ligands the 2-(1H-tetrazol-5-yl)quinoline-8-ol (8-hydroxyquinoline-2-tetrazole) (H_2Hqt) and the 8-hydroxyquinoline-2-carboxylic acid (H_2hqa) provide convenient dianionic tridentate O,N,N- and O,N,O- chelating units containing the 8-hydroxyquinoline chromophore. The combination of the 8-hydroxyquinoline chromophore with an additional anionic binding group (carboxylate or tetrazolate) yields luminescent trianionic complexes. These ligands form tris-chelate tris-anionic complexes $[Ln(hqa)_3]K_3$ and $[Ln(hqt)_3]K_3$ in water at pH=12. At lower pH partially protonated species are formed. The Nd(III), Yb(III) and Er(III) complexes of hqa, and hqt and the partially protonated complex $[Nd(H_{1/2}hqa)_3]_2(Et_3NH)_3{\cdot}Et_3NHOtf$ **(I)** have been crystallised from

methanol solution. The X-ray crystal structure ($[Nd(hqa)_3]K_3 \cdot 8CH_3OH_\infty$ **(III)**, $[Er(hqa)_3]K_3 \cdot 7CH_3OH_\infty$ **(IV)** and $[Nd(hqt)_3]K_3 \cdot 6CH_3OH_\infty$ **(V)**) show an helical arrangement of both ligands with an "*anti*" geometry for hqa and a "*syn*" geometry for hqt. Only tris-chelate complexes are formed in water and methanol 0.04M solutions for both ligands. A "*syn*" geometry is found for the partially protonated dimeric complexes which is preserved in methanol solution. A statistical distribution of "*anti*" and "*syn*" species is found for $[Ln(hqa)_3]K_3$ complexes in solution while the major solution geometry of $[Ln(hqt)_3]K_3$ complexes is "*syn*".

Sizable Near-IR emission quantum yields were measured for the $[Ln(hqa)_3]K_3$ complexes in solid state (0.06 %, 0.18%, 0.0051% for Nd(III), Yb(III) and Er(III) respectively) and in methanol (0.063%, 0.28%, 0.0019% for Nd(III), Yb(III) and Er(III) respectively). All the values of quantum yields obtained for the hqt complexes are 15–20 % higher than those measured for the hqa complexes. The trianionic complexes present a high solubility in organic and aqueous solvents and a good resistence to ligand dissociation compared to neutral tris 8-hydroxyquinoline complexes.

The emission quantum yields could be further optimized by halogenation of the quinoline units. These complexes show a significantly increased solubility and stability towards ligand dissociation with respect to neutral compounds providing robust systems for potential applications. Moreover the trianionic nature of these complexes allows the tuning of solubility by suitable choice of counterions and should prove very useful in the development of new lanthanide based materials [139-141].

The complexation of these dianionic hydroxyquinoline based tridentate ligands with lanthanide salts did not lead to formation of high nuclearity discrete assemblies. Only dimeric and polymeric species could be isolated depending on the base used. These ligands could be used in the future studies in developing new luminescent infinite polymetallic complexes (coordination polymers or extended metal organic frameworks), where dual emission could be obtained by the replacement of the potassium in the network with a different lanthanide ion. Morover the isolated ionic complexes could have potential applications in the design of lanthanide based ionogels and ionic liquids [142, 143].

In order to prepare discrete polynuclear assemblies we have decided to study complexation of a dissymmetric chiral tetradentate ligand. In the next chapter we will discuss the diastereoselective synthesis of lanthanide complexes formed by this new ligand synthesized in our laboratory.

CHAPTER III Diastereoselective Self-Assembly of Chiral Polynuclear Lanthanide Architectures

1- Introduction

Enantiopure compounds are not only an interest of scientific curiosity but they also have a high market value. The classical example given to show the difference of biological activity between two enantiomers is the racemic thalidomide, which was widely used in the 60s to treat morning sickness. One of the enantiomers was effective at reducing morning sickness while the other one was causing birth defects. This explains why enantiopure compounds are crucial for human being. Therefore in order to understand and control their chirality and biological effects, reliable tools and effective synthetic methods should be developed.

The aim of introducing chirality to lanthanide complexes is to use their spectroscopic and catalytic properties for designing luminescent chiral complexes that can be used either as chiral catalysts for preparing enantiopure organic compounds or as luminescent probes for chiral recognition and sensing of biological molecules. Chemical separation techniques are well established for separating enantiomers of transition metal compounds. On the other side the kinetic lability and the weak coordination preferences of the Ln(III) centers challenge the synthesis of stable "true" enantiopure lanthanide coordination compounds.

This chapter will first give a short introduction to chirality in coordination compounds and techniques to separate enantiomers. After that a brief summary of the enantiopure lanthanide complexes reported till now will be given. Finally the diastereoselective self-assembly of luminescent polynuclear homochiral lanthanide architectures promoted by the rational design and the use of the chiral carboxylate-derivatized bipyoxazoline ligand **Phbipox** (6-(4-phenyloxazolin-2-yl)-2,2'-bipyridine-6-carboxylic acid) will be described.

1.1- Chirality in Coordination Chemistry

A molecule is considered as chiral if it has no improper symmetry axis and if it exists as a pair of enantiomers, which are non super imposable mirror images of each other. Chirality is explained mostly with tetrahedral carbon, and methods for preparing predetermined chirality at carbon center have been highly developed in organic chemistry. In contrast, chirality in coordination compounds is a much more complex phenomenon due to higher coordination numbers and the multitude of possible central atoms {Knof U., 1999 #262}. The notion of chirality in coordination chemistry started in 1911 with the resolution of a Co(III) complex called hexol by Alfred Werner (Figure III-1) into its optical isomers. This chiral complex having no carbon atom had overthrown the theory of J. H. van't Hoff and J. A. LeBel that chiral molecules should contain at least one tetrahedral carbon in them.

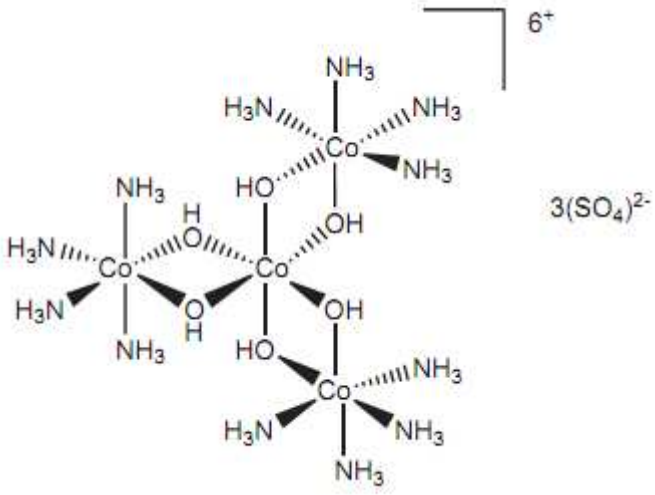

Figure III-1: The hexol: first chiral compound seperated into its isomers

The source of chirality in metal ligand coordination compounds is generated from the coordination of chiral ligands (R/S), the helicity around the metal center (Δ/Λ), the helicity of the molecule through a chiral axis (P/M), or from the helical twist of macrocyclic ligand [144]. One of the most common chiral arrangement around a metal center of a transition metal chelate complexes of the type [M(bidentate)$_3$] is given in Figure III-2 where three bidentate ligands bind to the metal center in a helical fashion. If all the metal centers have the same chirality in a supramolecular compound the structure is homochiral, if different chiralities exist then the compound is called heterochiral.

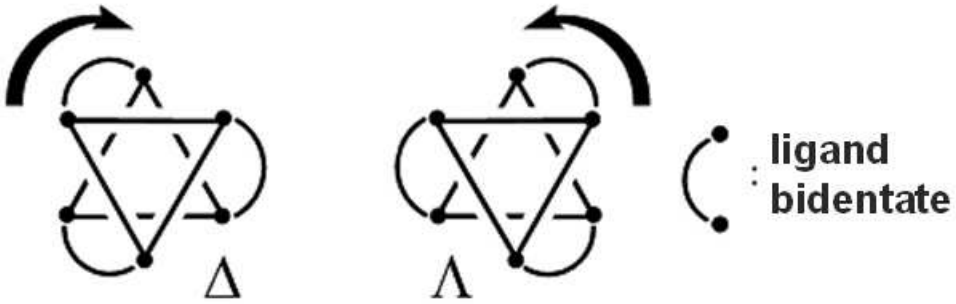

Figure III-2: Representation of Λ and Δ stereoisomers of an octahedral complex

1.2- Resolution of Enantiomers

Chiral structures should have an enantiomeric stability and purity before being used as functional materials. Therefore it is essential to control the chirality of the metallic complexes. The majority of the supramolecular compounds are formed as racemic mixtures. The enantiomers have in general similar thermodynamic stability in absence of strong non-covalent or steric interactions in self assembly processes. Thus isolating an enantiopure complex is a challenge. In coordination chemistry several methods have been reported for the separation of enantiomers, i.e. spontaneaous resolution by crystallization, using a chiral auxiliary and diastereoselective synthesis, however none of these described below have been well developed for lanthanides till now so there are only a few publications on them.

1.2.1 The preferential crystallization of one enantiomer

Spontaneous resolution of enantiomers by crystallization has been observed several times in transition metal chemistry {Seeber, 2006 #263;Knof U., 1999 #262;Crassous, 2009 #264;Aspinall, 2002 #255}. On the other side for the lanthanide complexes this chiral induction is rarely observed because of the lability of complexes favoring racemisation in solution. The conditions for this method are difficult to control so the predictability of the final structure is low. Another limitation is the necessity of high quantity of compound that could be problematic where the multistep ligand synthesis or expensive materials are used.

$[SmI_2\text{-}(dme)_3]$ (dme: dimethoxyethane) is the first reported eight-coordinate complex to undergo spontaneous resolution and crystallize in noncentrosymmetric space group with the structure of $\Lambda(\delta\delta\delta)$-$[SmI_2\text{-}(dme)_3]$ [145]. Recently a chiral metal organic framework structure has been reported where an achiral chelating and bridging dihydroxymalonato (mesoxalato) ligand (L) yields the Δ/Λ-metal configured homochiral MOFs 2D-

$[Ln_2(L)_3(H_2O)_6]$ (Ln = La(III), Gd(III)) through self-resolution during crystal growth (Figure III-3) [146].

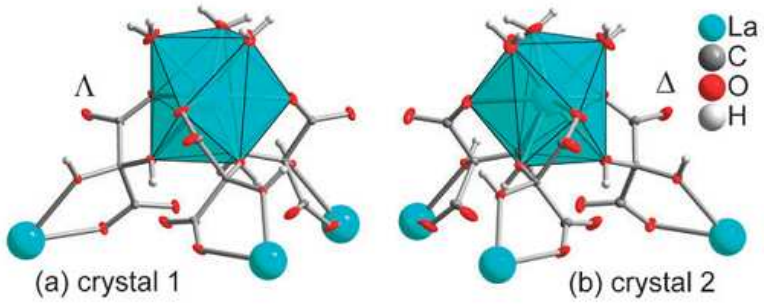

Figure III-3: The coordination sphere in (a) Λ and (b) Δ from two different crystals in a polyhedral presentation to illustrate the tri-capped trigonal prism; also showing the bridging action of the mesoxalato ligand to the next La atoms (50% thermal ellipsoids for C and O) [146]

1.2.2 Resolution by a chiral auxiliary

Chiral recognition of an enantiomer by a chiral auxiliary enables the separation of enantiomers from a racemic mixture. A rare example of supramolecular assemblies where complete enantiomeric resolution can be achieved was given by Raymond and coworkers (Figure III-4). Assembly of $[Ga_4L_6]$ tetrahedron produces a racemic mixture of homochiral ΔΔΔΔ and ΛΛΛΛ structures. A chiral auxiliary (S)□N-methylnicotinium (s-nic) preferentially precipitates the diastereomeric ion-pair of (ΔΔΔΔ)-(s-nic). The chirality is kept at least 8 months and does not change even after replacing the chiral auxiliary by achiral counterions such as NMe_4^+ and NEt_4^+ or heating the solution [147]. A similar effect of a chiral auxiliary has been observed in lanthanide chemistry. For example Sobolev et al. observed that the tris dipicolinate lanthanide complexes $[Ln(dpa)_3]^{3-}$ crystallize in centrosymmetric space groups with both Δ and Λ forms present in the crystal when the counterion is achiral. In contrast a chiral counterion results in the separation of enantiomers [148].

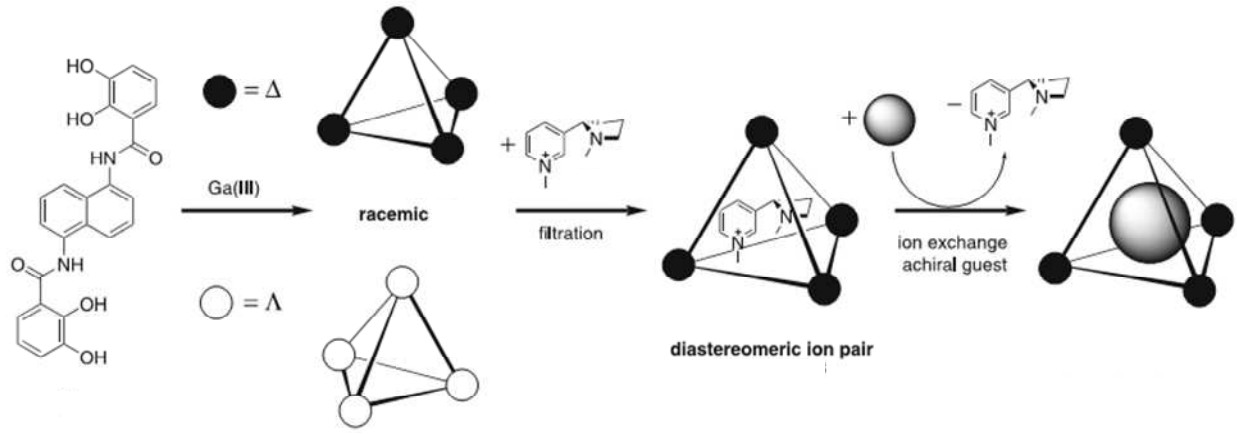

Figure III-4: Overview of the synthesis and resolution of solution stable chiral tetrahedron

1.2.3 Diastereoselective synthesis

In coordination chemistry diastereoselective synthesis is widely used for controlling the supramolecular chirality with enantiopure organic ligands. "Predetermined chirality" (induction of preferential formation of metal complexes displaying one absolute configuration at the metal center) is realised by the transfer of chiral information from ligand to the metal center by coordination. This synthesis method is successful when one of the diastereomers is thermodynamically favored. In order to favour one diastereomer compared to the other one, intelligent chiral ligand design is necessary. There are several examples of diastereoselective synthesis in transition metals {Knof U., 1999 #262;Crassous, 2009 #264;Seeber, 2006 #263;Aspinall, 2002 #255}, but in lanthanides the number of publications on this subject is limited due to difficulties in controlling the coordination environment of Ln ions. Some examples of diastereoselective synthesis of lanthanide complexes will be given in the section 1.4.

1.3- Applications of Chiral Lanthanide Complexes

Chiral lanthanide complexes have found applications as chiral shift reagents for resolving NMR spectra of chiral Lewis bases, as highly enantioselective catalysts and in chiral recognition of molecular substrates.

1.3.1 Chiral NMR Shift Reagents

Chiral lanthanide complexes with β-diketonates or polyaminocarboxylate ligands are known and used as chiral NMR shift reagents since the 70s [149]. In principle they interact with the enantiomers of the substrate to form diastereomers and in addition to the external magnetic field the substrate experiences the magnetic field of the lanthanide ion. The observed chemical shift results from (i) a transfer of electron spin density from the lanthanide center to the associated nuclei, "contact shift", or from (ii) magnetic effects of the unpaired electron magnetic moment "pseudocontact shift". They often give the resolved NMR signal which was a great help before the presence of high field NMR spectrometers. The chiral lanthanide NMR shift reagents are also effective in the determination of enantiomeric excess [150].

1.3.2 Enantioselective Catalysis by Chiral Lanthanide Complexes

Chiral lanthanide complexes are highly effective as enantioselective catalysts in several organic reactions. The first example of chiral lanthanide complex catalyzed reaction was given by Danishefsky et al. in 1983 [151]. They reported promotion of hetero Diels Alder reaction by [Eu(hfc)$_3$] with moderate enantiomeric excess (58% ee) as shown in Scheme III-1. The high coordination number of lanthanide ions enables the rapid association with substrates and rapid dissociation of products which makes them ideal Lewis acid catalysts with high efficiency.

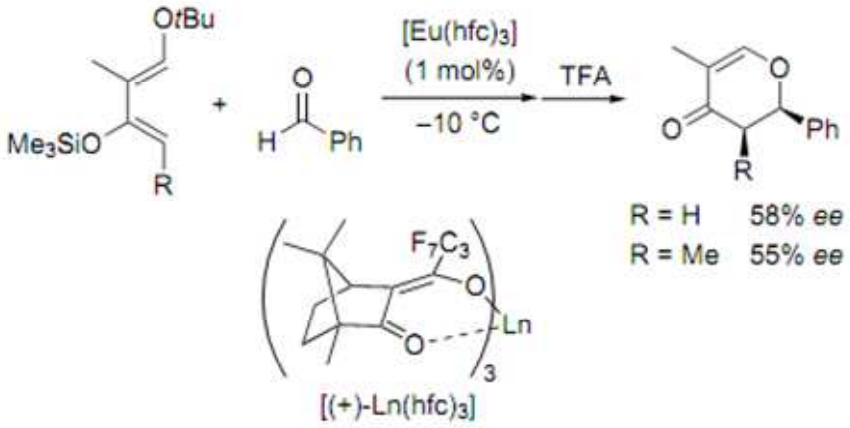

Scheme III-1: Hetero Diels Alder reaction catalyzed by [Eu(hfc)$_3$]

The assymmetric catalysis of organic reactions can be greatly enhanced by the use of lanthanide complexes with chiral ligands. Several lanthanide complexes with chiral ligands have been studied as enantioselective catalysts with high enantiomeric excess and reaction yields [152-154]. Shibasaki reported that the chiral lanthanide complex formed with a chiral Binapthol (binol) ligand is an efficient asymmetric catalyst for direct aldol reactions of aldehydes and unmodified ketones [155]. The chiral heterobimetallic complex LaLi$_3$-tris(binaphthoxide) (LLB) (see Figure III-7a) gives high yield aldol product with high enantioselectivity (94% ee) (Scheme III-2).

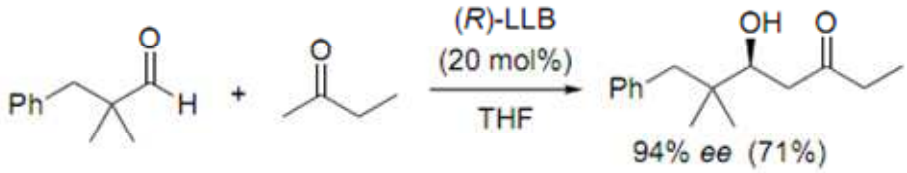

Scheme III-2: Aldol reaction catalyzed by LLB based complex

1.3.3 Chiral Sensing/ Recognition of Biological Substrates

Coordinatively unsaturated chiral Ln(III) systems are effective receptors for the selective sensing/ recognition of many biologically important molecules. By coordination of a given substrate to the lanthanide ion, the structural changes in the complex result in changes in chiroptical properties. These changes can be characterized by NMR, CD or CPL studies. For example Tsukube et al. studied the anion-specific luminescent receptor properties of Eu and Tb complexes with the chiral tri(2-pyridylmethyl)amine ligand. The Eu^{3+} complexes act as a luminescent receptor effective for NO_3^- anion selectivity, while the corresponding Tb^{3+} complex exhibits Cl^- anion selectivity. The addition of 3 equivalent anions enhanced the luminescence intensity at 618 nm by 4.9 times with NO_3^- for Eu complex (Figure III-5a) and at 548 nm by 5.4 time with Cl^- for Tb complex (Figure III-5b) [156].

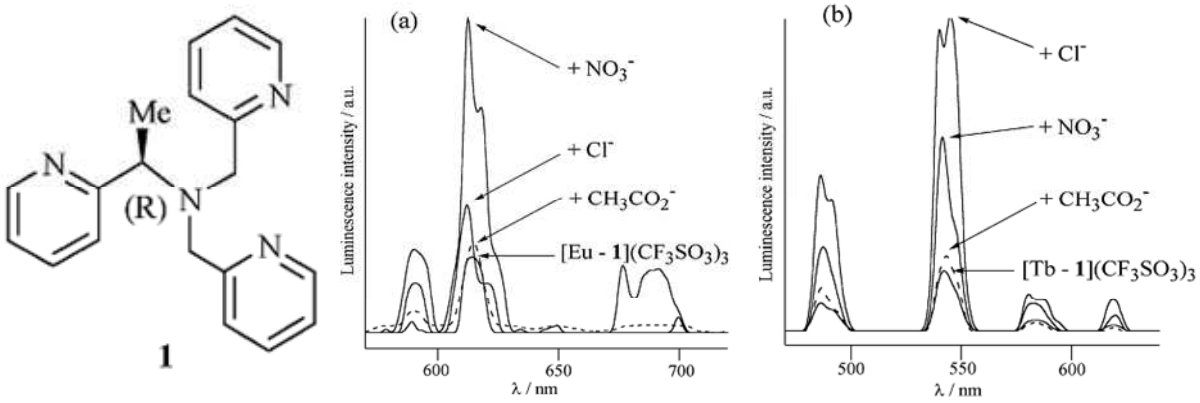

Figure III-5: Luminescence spectral changes of $[Eu\text{-}1](CF_3SO_3)_3$ and $[Tb\text{-}1](CF_3SO_3)_3$ by the addition of NO_3^-, Cl^- and $CH_3CO_2^-$ anions in acetonitrile. Excitation at 260 nm; Normalized based on UV absorbance at 260 nm; $[Ln(CF_3SO_3)_3] = 4.80 – 5.20 \times 10^{-6}$ M; [Anion] = 1.45 – 1.55 $\times 10^{-5}$ M; Slit width was adjusted as 10.0 nm for excitation and 5.0 nm for emission [156]

Parker et al. focused on the design of water soluble Ln(III) systems with chiral DOTA-based macrocyclic ligand derivatives. Recently they have reported a unique chiroptical probe for serum albumin binding. They showed that the (SSS)-Δ enantiomer of a terbium and europium complex (Figure III-6) binds selectively to the "drug site II" in serum albumin. This binding process resulted in an inversion of the complex helicity as signalled by a sign and form change in the CPL spectra. No such behaviour occurs with the (RRR)-Λ complexes [157].

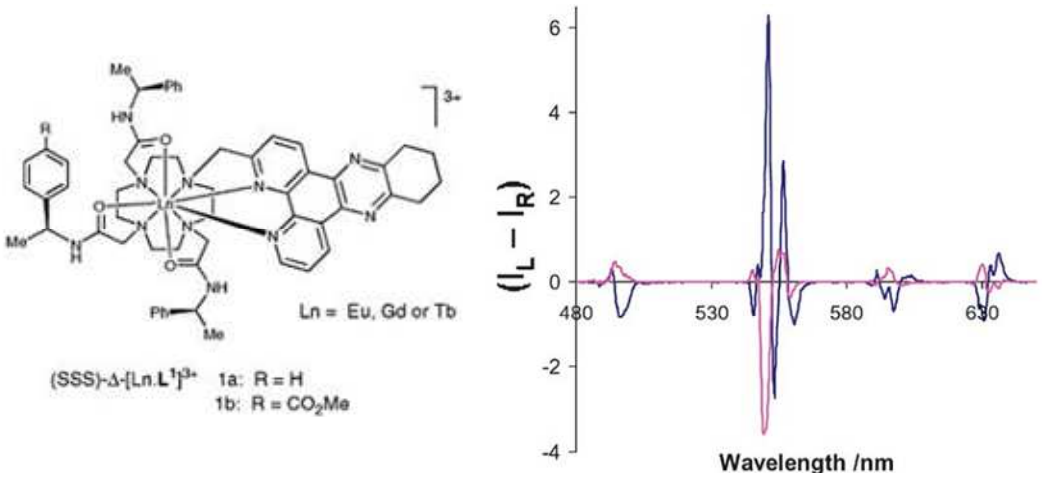

Figure III-6: (SSS)-Δ-[Ln.L^1]$^{3+}$ and CPL spectra for (SSS)-Δ-[Tb.L^{1b}]$^{3+}$ (blue) and in the presence of added BSA (red) (295 K, D_2O, λ_{exc} = 348 nm, 15 μM complex, 30 μM protein; relative (I_L + I_R) = 60 on this scale) [157]

1.4- Chiral Luminescent Lanthanide Complexes

As given in the previous section, enantiopure lanthanide based coordination compounds find crucial application as asymmetric catalysts or as chiral sensors for recognition of biological substrates. However, the number of reports on the synthesis of enantiopure lanthanide complexes is quite small in comparison to the transition metal complexes. Lanthanide complexes due to their kinetic lability undergo rapid exchanges of diastereomers in solution, thus it is a challenge to isolate enantiopure compounds. Most of the enantiopure chiral lanthanide complexes in literature are mononuclear complexes where the chirality of the ligand is transferred to the complex. When chiral ligands are coordinated to a metal center the reactions are highly stereoselective.

1.4.1 Mononuclear Enantiopure Lanthanide Complexes

Some examples of chiral ligands that have been used for preparing Ln(III) complexes with predetermined chirality are given in Figure III-7. Binapthol was one of the first chiral ligands to be investigated for enantioselective catalysis due to the oxophilicity of lanthanides and the highly stable chiral configuration of the ligand. Shibasaki et al. prepared a homochiral La complex by reacting $LaCl_3{\cdot}7H_2O$, Li_2(binol) (2.7 mol equiv), and NaO-t-Bu (0.3 mol equiv) in THF. The general formula of the obtained catalysts is $LaLi_3$-tris(binaphthoxide) (LLB) as given in Figure III-7a [158]. The ligand transfers its chirality to the complex thus only Δ diastereomer is obtained with the R ligand and Λ diastereomer is obtained with the S ligand.

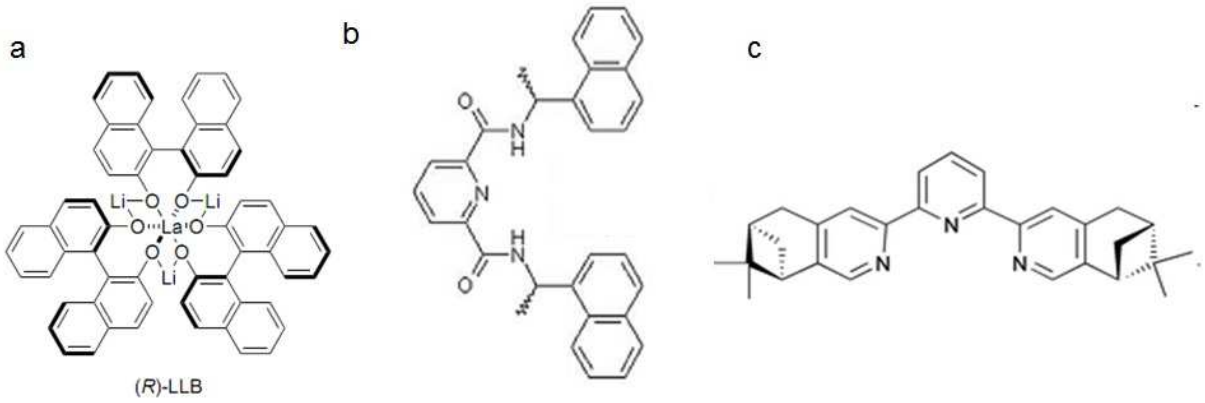

Figure III-7: Some examples of chiral ligands used in diastereoselective Ln complexes formation

Gunnlaugsson et al. have demonstrated the chiral transfer from a simple chiral pyridiylamine ligand (Figure III-7b) during self assembly to give either Δ or Λ metal stereochemistry. Using CPL and X-Ray crystallography they have shown that L (S,S) induces Δ chirality around the metal ions whereas L(R,R) induces Λ chirality [159].

The chiral pinene group has lead to great success in the diastereoselective synthesis of chiral transition metal complexes. For the lanthanides Mürner et al. have obtained the first diastereoselective formation of Ln(III) triple helical complexes with a chiral terpy-pinene ligand (Figure III-7c) [160]. NMR and CPL studies were performed to prove the presence of only one diastereomer in solution.

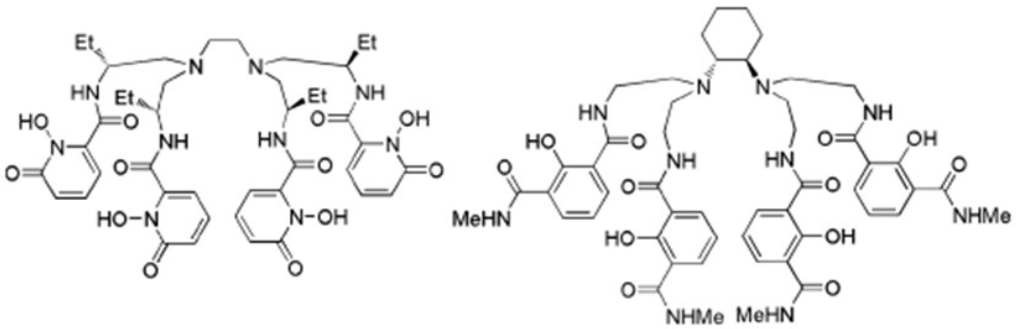

Figure III-8: Tetrapodal polydentate chiral ligands for luminescent lanthanide complexes with CPL activity

Chiral, octadentate, tetrapodal, 2-hydroxyisophthalamide ligands (Figure III-8) are reported to form stable lanthanide complexes with good luminescence properties in solution and strong CPL activity [161]. They obtained relatively high luminescence dissymmetry factors (glum) around 0.40 for Tb and 0.20 for Eu. These complexes are potentially promising to be used as analytical CPL probes.

1.4.2 Complexes with macrocyclic ligands

There are two sources of chirality in macrocyclic ligands: conformational chirality in the chelate rings and helical chirality arising from the orientation of the pendant arms. Macrocylic ligands like DOTA with lanthanides have been widely studied due to their great stability in aqueous solution. DOTA complexes can exist in two diastereomeric forms: Δ(λλλλ)/Λ(δδδδ) and Δ(δδδδ)/Λ(λλλλ). A DOTA ligand with chiral amide arms has been reported to induce stereoselectivity thus Δ(λλλλ) complex obtained by SSSS-ligand and Λ(δδδδ) complex obtained by RRRR-ligand (Figure III-9) [162]. These complexes are stereochemically rigid; there is no Δ/Λ interconversion in the temperature range 220-320 K.

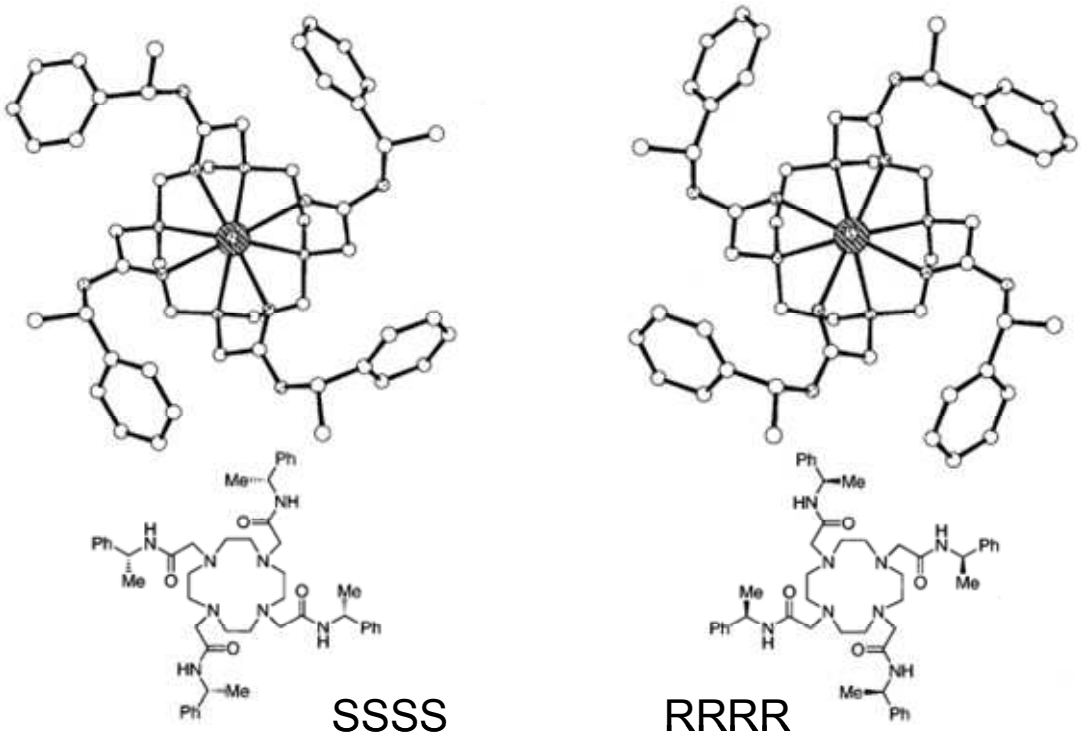

Figure III-9: Structure of the Δ(λλλλ) and Λ(δδδδ) enantiomers of $Eu(L)(H_2O)]^{3+}$

1.4.3 Polynuclear Enantiopure Lanthanide Complexes

Fewer examples of chiral polynuclear assemblies have been described for lanthanides [163-169]. Some original examples of chiral assemblies were obtained from the controlled hydrolysis [163, 166, 167] or CO_2 fixation reactions [164, 165] of lanthanides salts in the presence of chiral ligands. In these synthetic methods the hydroxo and the carbonate groups play an important role in the formation of the heteroleptic assemblies rendering difficult the rational design of the final assembly.

a) Enantiopure polynuclear complexes with a pinene bipyridine based ligand

Mamula et al. reported an enantiopure polynuclear assembly with a pinene bipyridine ligand functionalized with a carboxylate donor group. The reaction of this chiral ligand with lanthanides resulted in an enantiopure trinuclear assembly $[Ln_3((+)\text{-}L)_6(\mu_3\text{-}OH)(H_2O)_3]^{2+}$ in methanol and an enantiopure tetranuclear assembly $[Ln_4L_9(OH)](ClO_4)_2$ in acetonitrile. The six ligands around the metal core coordinate to metal in two different ways as shown in Figure III-10 with green and orange coloring.

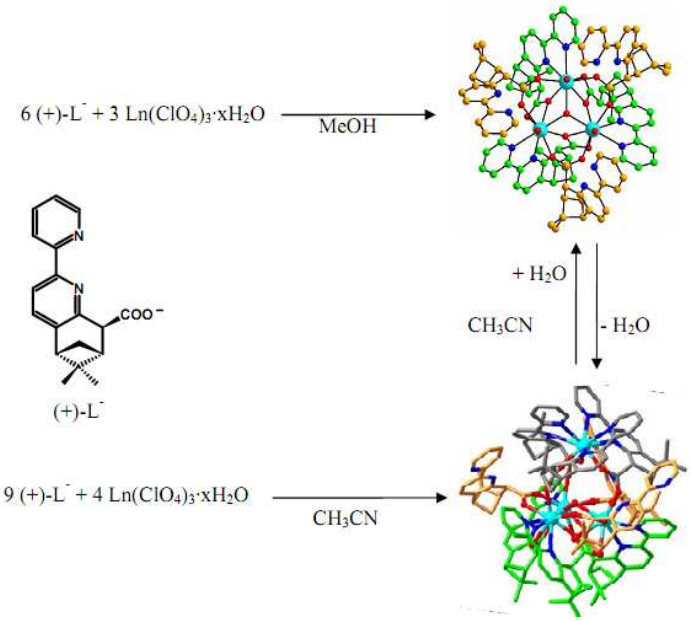

Figure III-10: Reaction conditions leading to the synthesis of trinuclear and tetranuclear Ln(III) complexes with ligand (+)-L

The first set of three ligands coordinates through two pyridine nitrogen and carboxylate group and shows M propeller like arrangement, while the other set of ligands coordinates only through carboxylate group and wraps around the trimetallic core in a P helical fashion. If the (+)-L ligand is used, P and M helical arrangements are obtained (Figure III-11a), in contrast if the (-)-L ligand is used opposite M and P helicitiy are observed (Figure III-11b). These assemblies are particulary important as they are the first examples of true enantiopure polynuclear complexes obtained [163, 170].

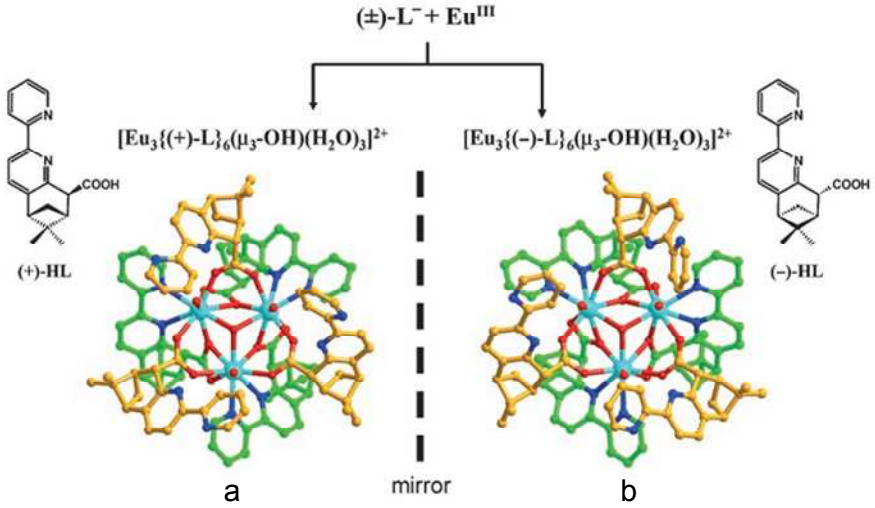

Figure III-11: Representation of homochiral recognition process. Color code: Eu: turquoise, N: blue, O: red. Ligand set 1: green, ligand set 2: orange. a: $[Eu_3((+)\text{-}L)_6(\mu_3\text{-}OH)(H_2O)_3]^{2+}$; b: $[Eu_3((-)\text{-}L)_6(\mu_3\text{-}OH)(H_2O)_3]^{2+}$

b) CO_2 fixation reactions

Two interesting chiral polynuclear lanthanide assembly formation were reported recently by CO_2 fixation reactions [164, 165]. The reaction of a chiral ligand (*S*,*S*)- 4,5-Di(4-carboxyphenyl)-2,2-dimethyl-[1,3]dioxolane (L) with $LnCl_3.H_2O$ resulted in the formation of colorless crystals of $[La_{18}\{(S,S)\text{-}L\}_{24}(CO_3)_2(H_2O)_{32}]^{2+}$ where two carbonate anions each bind to three La^{3+} ions in the core of the structure (Figure III-12). The obtained spherical supramolecule (a diameter of 3.0 nm) shows unique structural resemblance to ferritin. Therefore it is called as lanthanitin. S-lanthanitin forms a right handed double helix whereas R-lanthanitin forms a left handed double helix confirmed by the mirror symmetrical CD spectra with opposite signs.

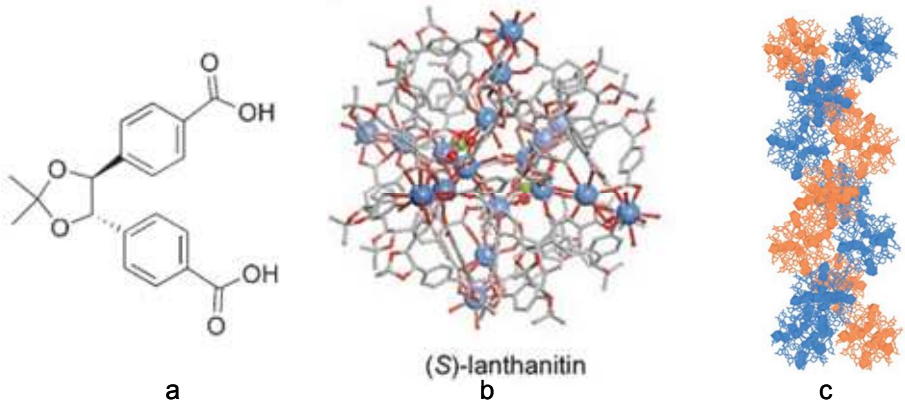

Figure III-12: a) Ligand (*S*,*S*)- 4,5-Di(4-carboxyphenyl)-2,2-dimethyl-[1,3]dioxolane
b) Molecular structure of (S)-Lanthanitin with octahedral arrangement of 18 La ions as large blue balls and the central carbonate carbon atoms as small green balls. Hydrogen atoms are omitted for clarity. Color code: C gray, O red
c) Right handed double helix formed by the (S)-Lanthanitins. The two single helices are distinguished by blue and light brown colors

Another example of CO_2 fixation by a chiral system has recently been reported by Tang et al. where a multidentate chiral aminoacid containing reduced Schiff base ligand transfers its chirality to produce a new homochiral helix. As shown in Figure III-13 the CO_3^{2-} anion plays an important role as a template in the formation of the heptanuclear lanthanum cluster $[La_7\{(S)\text{-}L\}_6(CO_3)(NO_3)_6(OCH_3)(CH_3OH)_7]\cdot 2CH_3OH\cdot 5H_2O$. When S-ligand is used M helicity is observed in the structure. In contrary the R-ligand resulted in a P helical arrangement in the final structure. The authors have also studied the anion recognition properties of this system and showed by optical rotation that this system has an excellent ability to selectively recognize CO_3^{2-} in water [165].

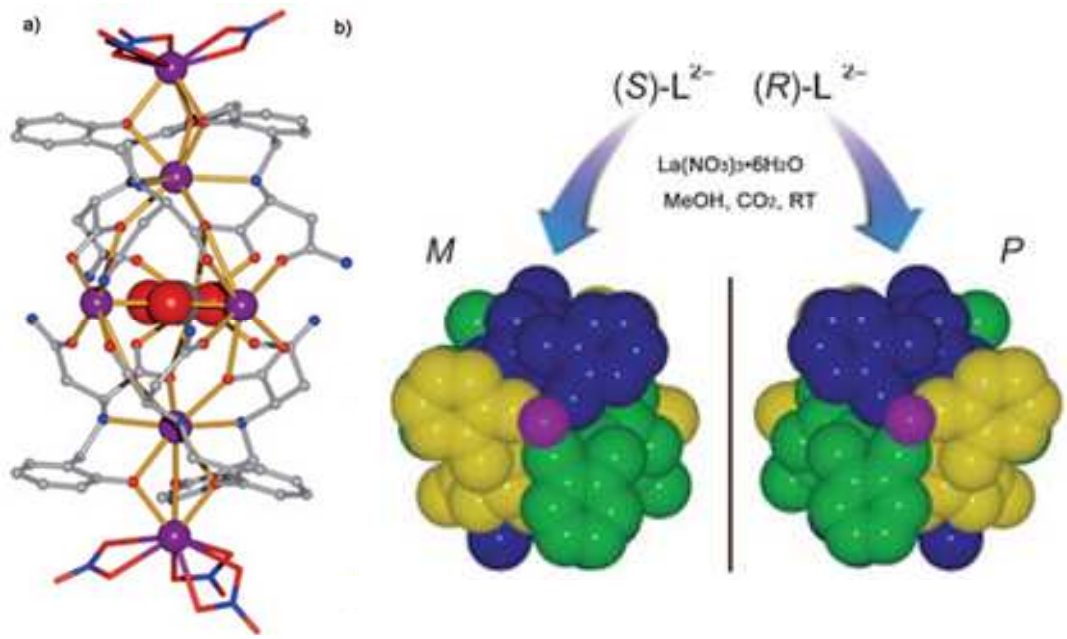

Figure III-13: a) Molecular structure of lanthanide-based cluster containing seven La(III) ions and six (S)-L^{2-} ligands. The CO_3^{2-} ion is encapsulated by La(III) ions and shown in a space-filling representation.
b) Preparation of the two lanthanide-based enantiomeric clusters, which are shown in a space-filling representation. Hydrogen atoms, nitrate groups, and solvent molecules are omitted for clarity. Each (S or R)-L^{2-} ligand is represented in a different color, while the lanthanide ions are shown in violet.

c) Trinuclear complexes with a chiral macrocycle

As shown in the Chapter I, the size of the macrocycle can be adjusted in order to encapsulate several lanthanides. Recently Lisowski et al. have reported synthesis and characterization of new type of enantiopure trinuclear Sm(III), Eu(III) and Tm(III) complexes with a chiral enantiopure macrocycle. The macrocycle is large enough to bind three lanthanide ions. The formation of these trinuclear Ln(III) complexes is accompanied by cooperative formation of a $Ln_3(\mu_3\text{-}OH)_2$ core within the cavity of the macrocycle (Figure III-

14). The large trioxahexaaza chiral macrocyclic amine forms symmetrical trinuclear complexes which are confirmed by ^{1}H NMR [169].

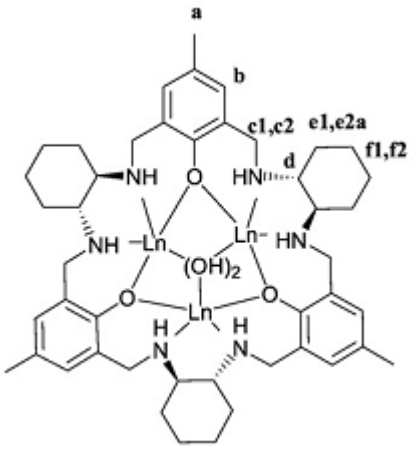

Figure III-14: RRRRRR isomer of a trinuclear complex of a trioxahexaaza chiral macrocyclic amine

d) Helicates

Helicates refer to discrete poylnuclear structures where at least two ligands wrap around a series of metal ions defining the helical axes. In helical polynuclear metal complexes other than chirality at the metal center, the chirality due to the orientation of bridging ligand is important. This chirality comes from whether P right handed or M left handed orientations. Chiral ligands provide predetermination of both chirality of the metal center (Δ/Λ) and the helicity of the molecule (right handed P or left handed M). One of the remarkable features of the helicates is the high degree of stereoselectivity often observed at the metal centers. The helicates are mostly homochiral so that they are found only as ΔΔ or ΛΛ enantiomers, and the meso ΔΛ complexes are not observed (Figure III-15).

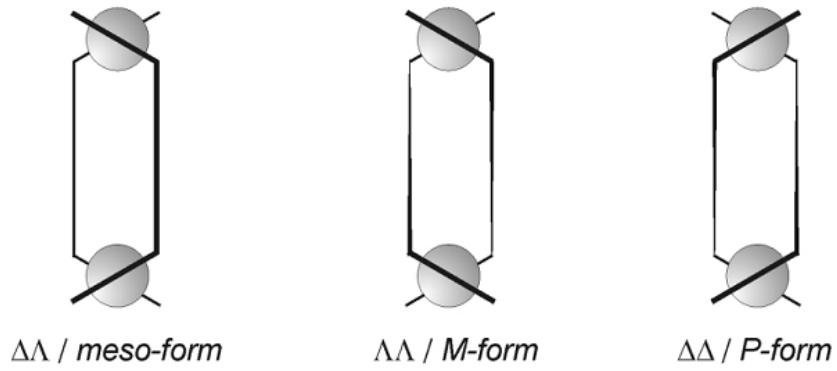

Figure III-15: Represantation of chirality in helicates [171]

Enantiomerically pure helicate complexes have been prepared using a chiral ligand where two dipicolinic acid moieties have been linked by a chiral cyclohexane unit Figure III-

16 [172]. The ligand dpa-chxn-R,R favors assembly of helicates [Ln_2(dpa-chxn-$(R,R)_3$] in which both metal centers present same chirality (ΔΔ or ΛΛ). CD spectrum shows a strong Cotton effect confirming the presence of only one diastereomer ΔΔ or ΛΛ in solution. Dimetallic triple-stranded helicates represent to date the only reported example of pre-programmed enantiomerically pure polynuclear lanthanide assemblies.

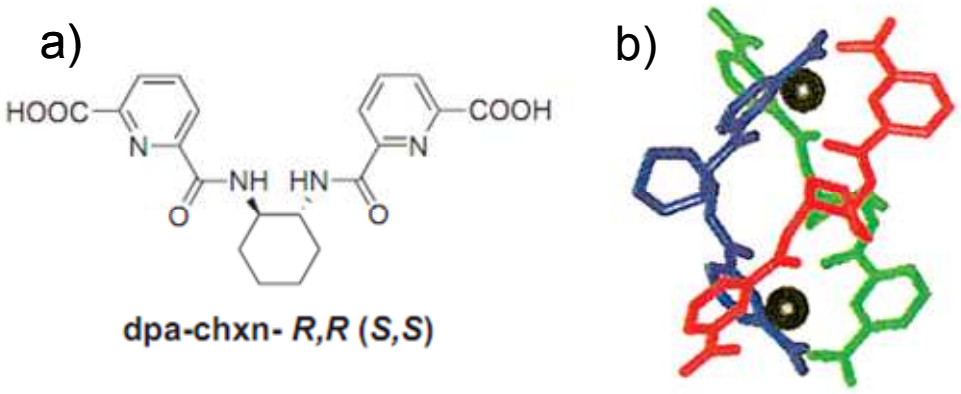

Figure III-16: a) Ligand dpa-chxn-R,R (S,S) used in the formation of b) enantiopure dinuclear triple-stranded helicate (ΔΔ) formation [172]

As seen in the brief introduction the control of chirality of supramolecular lanthanide coordination complexes is a fascinating field of research but still in its infancy. The weak stereochemical preferences of lanthanides render the synthesis of enantiopure lanthanide complexes extremely difficult. Preprogrammed enantiopure complexes are quite rare and there are no examples other than macrocycles and helicates. Therefore in this thesis in order to obtain enantiopure polynuclear complexes we have decided to investigate the diastereoselective self assembly processes of a dissymmetric tetradentate ligand with a chiral oxazoline unit.

2- The Choice of the Ligand

Chiral oxazoline based ligands are one of the most successful, versatile and commonly used classes of ligands in enantioselective catalysis since their first application in 1986 [173]. Heterocyclic oxazoline is easily synthesized by condensation of an amino alcohol on carboxylic acid or nitrile derivatives (Scheme III-3). This straightforward synthesis of ligands from available precursors has lead to a great number of studies with oxazoline unit in asymmetric catalysis [174].

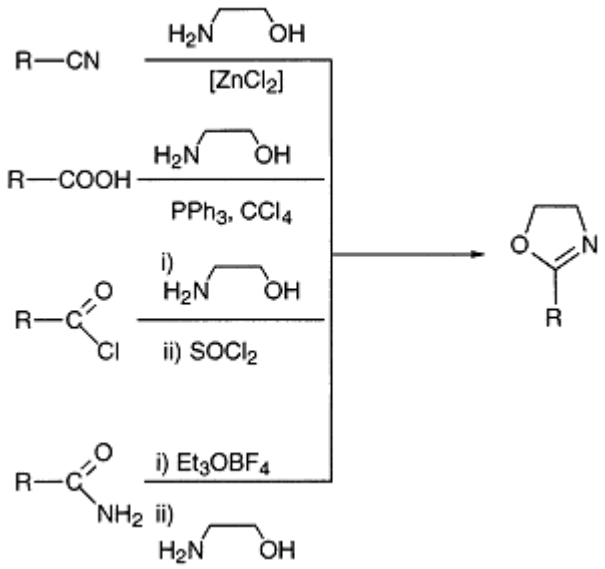

Scheme III-3: Different ways to synthesize oxazoline unit

C_2 symmetric bis oxazoline ligands with high denticity derived from pyridine or bipyridine are better adapted to lanthanide coordination chemistry due to the high coordination number requirement of lanthanide ions (Scheme III-4). Pybox type ligands have been largely used with great success in enantioselective transition-metal catalyzed reactions, while their use with lanthanide dates back to 1997 [175]. However no polynuclear lanthanide complexes have been reported till now. Recently it has been shown that apart from catalytic properties pyridine bis oxazoline (Pybox) type ligands act as sensitizers in lanthanide luminescence [176]. De Bettencourt-Dias et al. used a pyridine bis oxazoline ligand as a sensitizer for the tris complex (3L:1Eu) with ligand 4-thiophen-3-yl-pyridine-2,6-bis(oxazoline) (Scheme III-4) which presents a quantum yield of 76% and a lifetime of 2 ms in acetonitrile [177]. These values are one of the best values obtained from lanthanide complexes in literature.

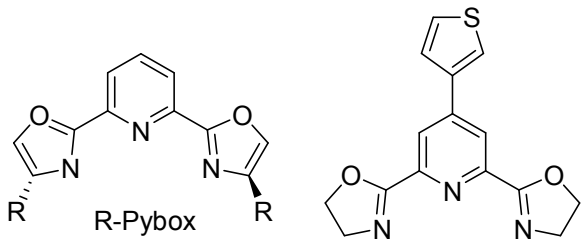

Scheme III-4: Structure of the ligand Pybox and 4-thiophen-3-yl- pyridine-2,6-bis(oxazoline)

The design of the ligand is important for the final properties of the chiral luminescent assembly. The versatility of the oxazoline ligands (chiral induction and sensitization of

lanthanide luminescence) motivated us to study the capacity of this group for the assembly formation with lanthanide ions. In our laboratory, it has been shown that the use of simple dissymmetric tetradentate ligands leaving some coordination vacancies around the metal ion directs the assembly of large lanthanide clusters. Tetradentate terpyridine carboxylate ligand (**terpya**) (6, 2□ 6□, 2□-terpyridine-2-carboxylic acid) (Scheme III-5) is used for the development of homo- and heterometallic assemblies with high nuclearity. In order to understand the effect of ligand geometry and basicity on the self assembly process we have synthesized a new ligand Phbipox where a pyridine group of terpyridine has been replaced by an oxazoline cycle. An oxazoline unit has been chosen due to its chiral properties and good luminescence sensitization of lanthanides.

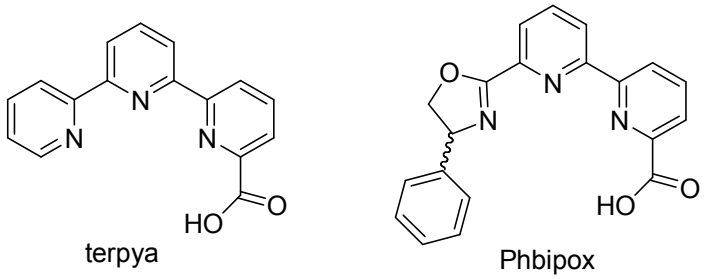

Scheme III-5: Dissymmetric tetradentate ligands terpya and Phbipox

The aim of attaching phenyl group to the asymmetric carbon atom on the oxazoline ring is to favour diastereoselectivity of the final complexes by the steric interactions between ligands. Several examples are given in literature showing the effect of steric hindrance on diastereoselectivity. For example, Provent et al. have shown that Pybox ligand forms preferentially a heterochiral complex [Co((R,R)-Pybox) ((S,S)-Pybox)]$^{2+}$ with Co(II) when R = Ph as a result of interligand repulsion but if R = Me a mixture of diastereomers is observed [178].

The following chapters will present the synthesis and characterization of chiral luminescent complexes obtained with Phbipox ligand.

2.1- Synthesis of the Phbipox Ligand

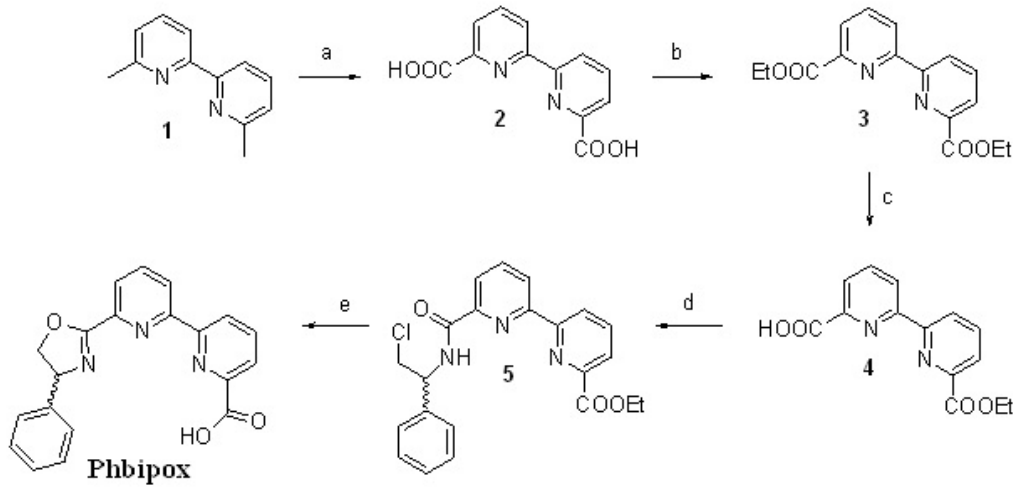

Scheme III-6: Reagents and conditions: a) CrO_3, H_2SO_4, 98 %; b) H_2SO_4, EtOH, 83 %; c) NaOH, $EtOH/CH_2Cl_2$, 38 %; d) i. $SOCl_2$, DMF cat.; ii. (S/R/rac)-2-phenylglycinol, Et_3N, $CHCl_3$; iii. $SOCl_2$, 59 % for S; e) KOH, $EtOH/H_2O$, 73 % for S.

The enantiomerically pure ligand S/R-Phbipox, and rac-Phbipox has been prepared in 7 steps from commercial dimethylbipyridine in 13% total yield (Scheme III-6). The synthetic procedure is outlined in the experimental part has been developed in our laboratory [124]. After the oxidation (Scheme III-6a) and esterification (Scheme III-6b) of bipyridine, the disymmetrisation of the bipyridine is accomplished by incorporating carboxylate on one side and oxazoline cycle on the other side. It has been realised by the monosaponification (Scheme III-6c) step of the diethyl-2,2′-bipyridine-6,6′-dicarboxylate (**3**). The dissymmetric bipyridine 6′-ethoxycarbonyl-2,2′-bipyridine-6-dicarboxylic acid (**4**) possesses a carboxylate and an ethylester group in positions 6 and 6′ respectively. Afterwards the carboxylate group has been converted to acyl chloride by reaction with $SOCl_2$. The condensation of the acyl chloride with (S/R/rac)-phenyglycinol lead to the corresponding hydroxyamide which has been tranformed to amidochloride by one pot treatment with $SOCl_2$ (Scheme III-6d). The cyclisation and the saponification of the ester function was realised in basic media by treating the compound with 3 equivalents of aqueous 1M KOH at room temperature (Scheme III-6e). The desired ligand (S/R/rac)-Phbipox is finally obtained by crystallisation in water at pH 3. The obtained ligand was isolated in its monoprotonated form and characterized by ^{1}H NMR (Figure III-17), 2D-COSY, ES-MS, elemental analysis (details are given in experimental section). The enantiomeric purity of the ligand was analysed by CD studies by comparing S and R enantiomers (see section 5 below). The multistep synthesis and the low yield of the Phbipox

ligand due to mainly monosaponification step were limiting to extend the study to various lanthanide ions. Therefore we have chosen to work only with europium, neodymium and ytterbium in this thesis. These ions provide a mean to check the sensitization properties of the ligand in the visible and NIR ranges.

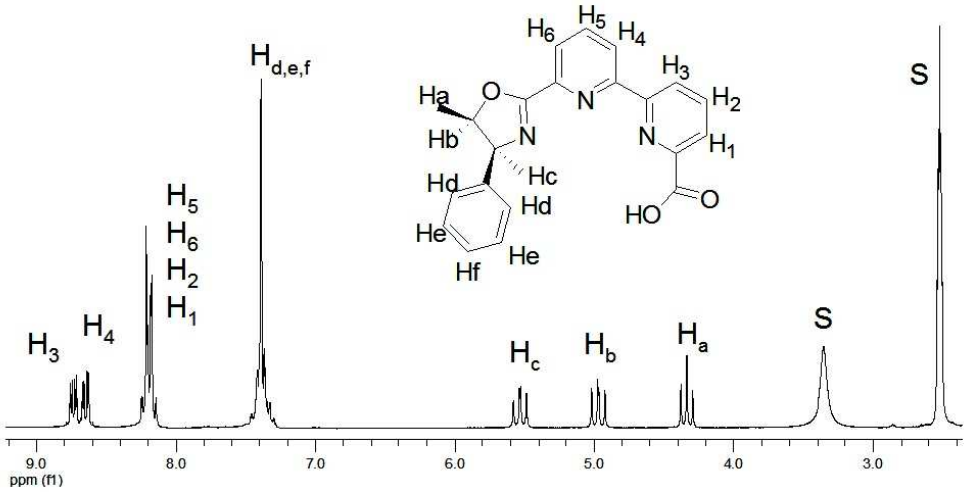

Figure III-17: ^{1}H NMR of the ligand S-Phbipox in DMSO at 298 K

3- Synthesis and characterization of mono/trinuclear complexes

Homoleptic lanthanide complexes [Ln(Phbipox)$_2$]Otf have been prepared by reacting lanthanide triflate with two equivalents of ligand in presence of triethylamine in methanol, as shown in Scheme III-7. The complexes were isolated by slow diffusion of diisopropylether onto methanolic solutions. The isolated complexes have been characterized by single crystal X-Ray diffraction, proton NMR spectroscopy, COSY correlation and NOESY experiments (to assign the peaks completely), circular dichroism, mass spectroscopy and elemental analysis.

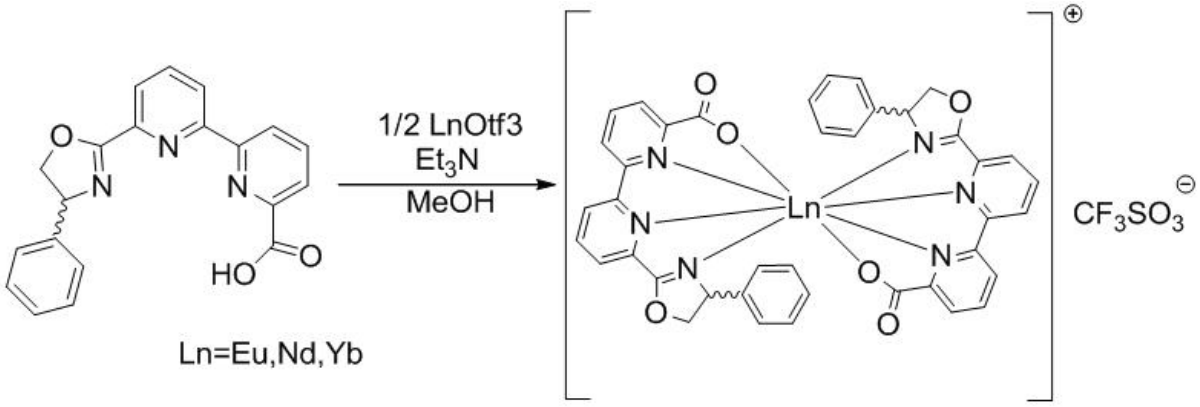

Scheme III-7: Reaction scheme for the synthesis of complexes

3.1- X-Ray Crystallography Studies

3.1.1 {(ΔΔΔ)-[Eu(S-Phbipox)$_2$]$_3$·(Λ)[Eu(S-Phbipox)$_2$]}(Otf)$_4$ (VI) / {(ΛΛΛ)-[Eu(R-Phbipox)$_2$]$_3$·(Δ)[Eu(R-Phbipox)$_2$]}(Otf)$_4$ (VII)

Crystals suitable for X-ray diffraction were obtained by diffusion of diisopropylether in methanol solutions of the complexes. X-ray diffraction analysis revealed the presence of two distinct co-crystallized molecules (trinuclear and mononuclear) in the compounds {(ΔΔΔ)-[Eu(S-Phbipox)$_2$]$_3$·(Λ)[Eu(S-Phbipox)$_2$]}(Otf)$_4$ (**VI**) (Figure III-18) and {(ΛΛΛ)-[Eu(R-Phbipox)$_2$]$_3$·(Δ)[Eu(R-Phbipox)$_2$]}(Otf)$_4$ (**VII**). The complexes obtained by R and S-Phbipox are isostructural with opposite chirality and they crystallize in the chiral orthorhombic space group $P2_12_12_1$. Isomorphous crystals were obtained from a concentrated acetonitrile solution. The details of the (Δ)-[Eu(S-Phbipox)$_2$]$^+$ and (Λ)-[Eu(S-Phbipox)$_2$]$^+$ fragments are shown in Figure III-19.

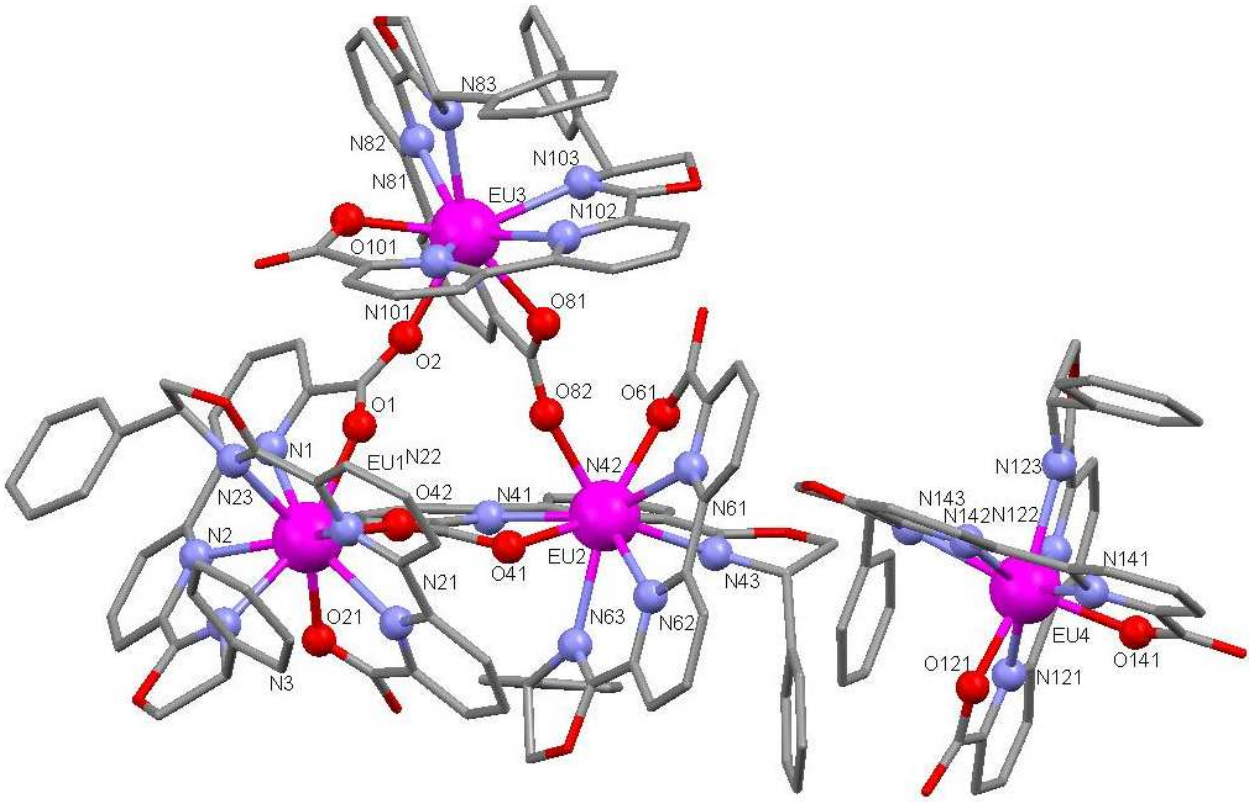

Figure III-18: Mercury diagram of the structure of {(ΔΔΔ)-[Eu(S-Phbipox)$_2$]$_3$·(Λ)[Eu(S-Phbipox)$_2$]}Otf$_4$ (**VI**). (Otf$_4$ has been omitted for clarity)

In the {(ΔΔΔ)-[Eu(S-Phbipox)$_2$]$_3$}$^{3+}$ cation, three crystallographically inequivalent (Δ)-[Eu(S-Phbipox)$_2$]$^+$ complexes are connected through a carboxylate oxygen from one of the S-Phbipox ligands to form a pseudo-equilateral triangle with Eu-Eu distances ranging from 6.685 to 6.780 Å. Each Eu ion is nine coordinated with distorted tricapped trigonal

prism geometry by the six nitrogen and the two oxygen atoms from the two S-Phbipox ligands and by the carboxylate oxygen from a neighbour complex.

In the (Λ)-$[Eu(S\text{-}Phbipox)_2]^+$ cation, the Eu ion is eight-coordinated by the six nitrogen atoms and the two oxygens from the S-Phbipox ligand with a distorted dodecahedron geometry (Figure III-20). The two S ligands wrap around the metal with a Λ stereochemistry. The two ligands mean planes form an angle of about 90°. Strong π-π interactions (see Table A1 Eu4) are found between the oxazoline phenyl rings of each tetradentate ligand and one pyridine ring of the other ligand. The presence of π-π interactions between the two ligands should play an important role in the observed rigidity of complexes in solution. Selected bond distances are given in Table III-1. The mean values of the Eu-N (2.57(2) Å for (ΔΔΔ)-$[Eu(S\text{-}Phbipox)_2]_3^{+3}$ and 2.54(3) Å for (Λ)$[Eu(S\text{-}Phbipox)_2]^+$) and Eu-O distances (2.39(2) Å for (ΔΔΔ)-$[Eu(S\text{-}Phbipox)_2]_3^{+3}$ and 2.30(3) Å for (Λ)$[Eu(S\text{-}Phbipox)_2]^+$) are similar to those found in the eight-coordinate complex $[Eu(terpya)_2]^+$ isolated from methanol in the presence of the dissymmetric terpya ligand (mean Eu-O = 2.31(1) Å and mean Eu-N=2.53(5) Å).

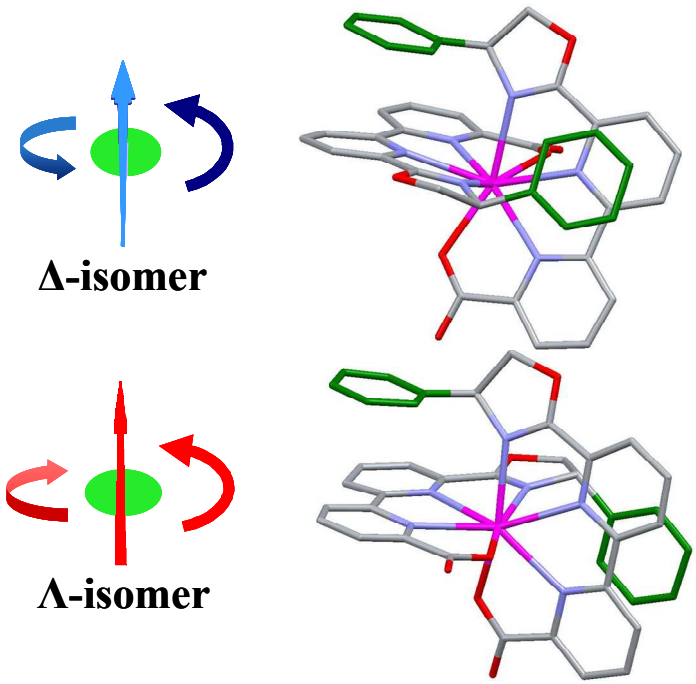

Figure III-19: The structure of the monomeric (Λ)-$[Eu(S\text{-}Phbipox)_2]^+$ and (Δ)-$[Eu(S\text{-}Phbipox)_2]^+$ isomers. The arrow starts from the carboxylic group and ends at the phenyl group (colored as green) of the ligand

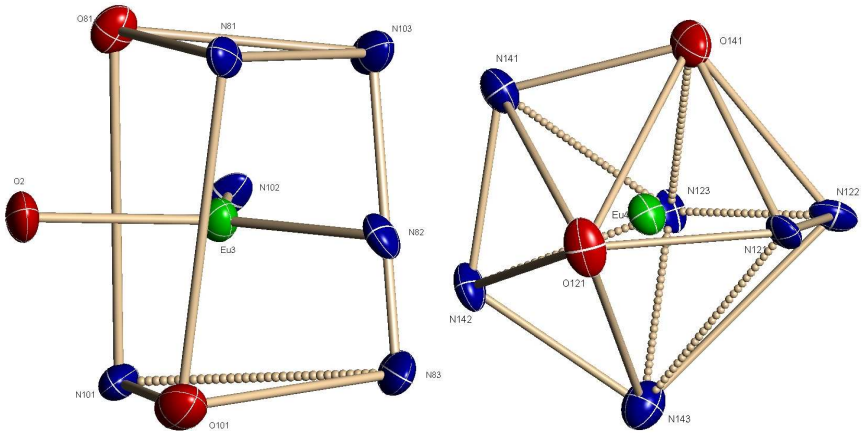

Figure III-20: Coordination polyhedrons of the europium ions in (ΔΔΔ)-$[Eu(S\text{-}Phbipox)_2]_3^{+3}$ and in (Λ)-$[Eu(S\text{-}Phbipox)_2]^+$

In each monomeric unit of the trinuclear complex **VI** the two S-Phbipox ligands wrap around the metal ion with a Δ stereochemistry. The angle between the two ligands mean planes is of ~108°. Strong π-π interactions (see Appdendix Table A1) are found between the oxazoline phenyl rings of each tetradentate ligand and one pyridine ring of the other ligand. The crystal structure shows that the S-Phbipox ligands can wrap around the metal with the two different Δ and Λ stereochemistry. However, only Δ complexes self-assemble to form a homochiral trinuclear structure. The mercury molecular model of a trinuclear structure built from mononuclear (Λ)-$[Eu(S\text{-}Phbipox)_2]^+$ entities (Figure III-21) suggests that important steric constraints resulting from the orientation of the phenyl substituents on the oxazoline ring are present when mononuclear complexes with Λ conformation are brought in close proximity. Similar constraints are observed for ΛΔΔ and ΛΛΔ isomers. Such sterical constraints should play an important role in the diastereoselectivity of the self-assembly process.

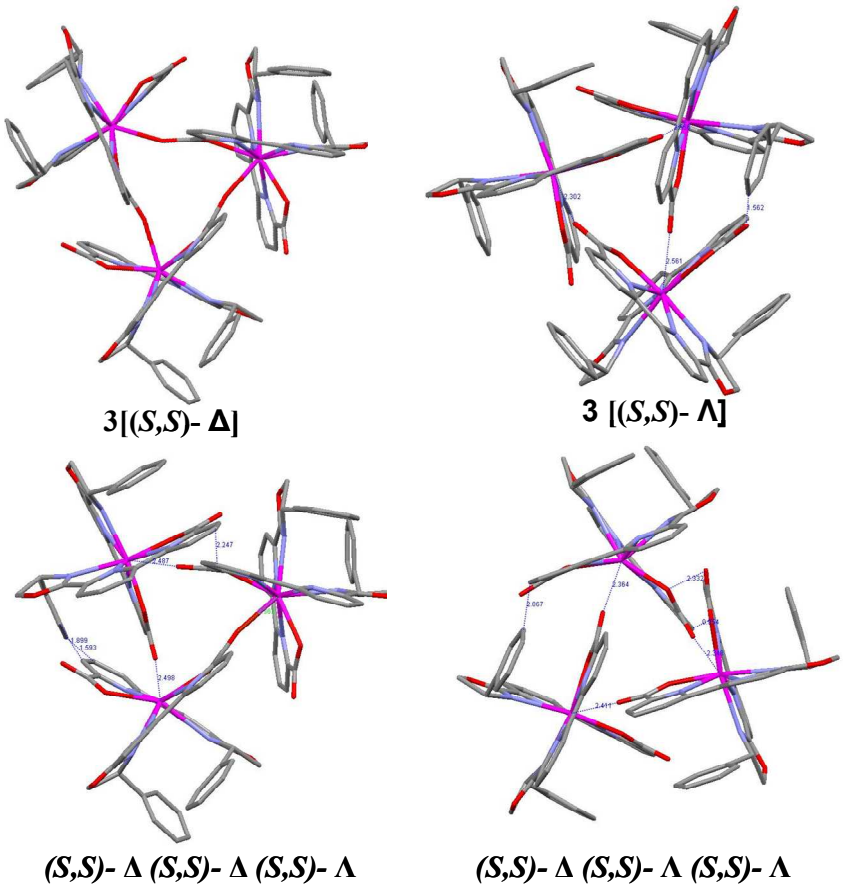

Figure III-21: Mercury molecular models built from the structures of the Δ and Λ in (**VI**) showing the sterical constraints preventing the formation of the (ΛΛΛ)-[Eu(S-Phbipox)$_2$]$_3$ and the heterochiral trinuclear complexes (ΔΔΛ)-[Eu(S-Phbipox)$_2$]$_3$ and (ΛΛΔ)-[Eu(S-Phbipox)$_2$]$_3$

3.1.2 {(ΛΛΛ)-[Nd(R-Phbipox)$_2$]$_3$}I$_3$ (VIII)

Crystals suitable for X-ray diffraction were obtained by slow diffusion of diisopropylether in acetonitrile solutions of the {(ΛΛΛ)-[Nd(R-Phbipox)$_2$]$_3$}I$_3$ (**VIII**) (Figure III-22). The compound crystallizes in the monoclinic space group C2. Many attempts to crystallize the {(ΛΛΛ)-[Nd(R-Phbipox)$_2$]$_3$}(Otf)$_3$ failed (probably due to disorder in the counterion) therefore counterion Otf$^-$ changed with I$^-$ in order to obtain better quality crystals. Proton NMR spectra of the complexes prepared with NdOtf$_3$ and NdI$_3$ are identical, showing no effect of counterion to the complex formation. In the {(ΛΛΛ)-[Nd(R-Phbipox)$_2$]$_3$}$^{3+}$ cation, three crystallographically inequivalent (Λ)-[Nd(R-Phbipox)$_2$]$^+$ complexes are connected through a carboxylate oxygen from one of the R-Phbipox ligands to form an equilateral triangle with Nd-Nd distances ranging from 6.774 to 6.790 Å. Each Nd ion is nine coordinated with distorted tricapped trigonal prism geometry by the six nitrogen and the two oxygen atoms from the two R-Phbipox ligands and by the carboxylate oxygen from a neighbour complex.

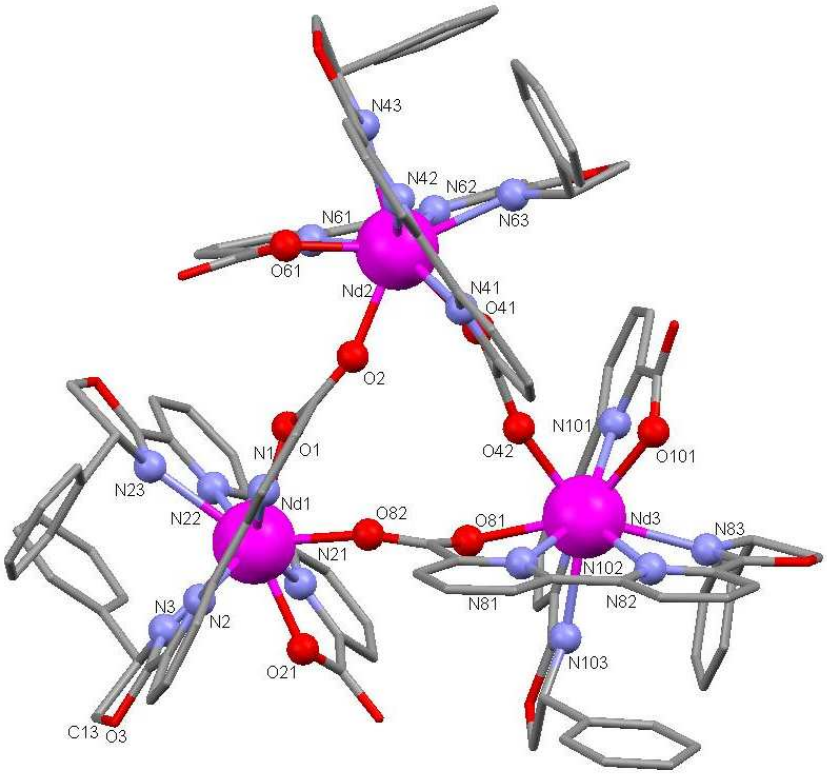

Figure III-22: Mercury diagram of the structure {(ΛΛΛ)-[Nd(R-Phbipox)$_2$]$_3$}$^{+3}$ (**VIII**)

In each monomeric unit of the trinuclear complex the two R-Phbipox ligands wrap around the metal ion with a Λ stereochemistry. The angle between the two ligands mean planes is about 110°. Strong π-π interactions (see Appendix Table A1) are found between the

oxazoline phenyl rings of each tetradentate ligand and one pyridine ring of the other ligand. The crystal structure shows that the R-Phbipox- ligands can wrap around the metal with the two different Δ and Λ stereochemistry. However, as observed with Eu complexes only Λ complexes self-assemble to form a homochiral trinuclear structure. Selected bond distances (Å) for the cation (ΛΛΛ)-$[Nd(R\text{-}Phbipox)_2]_3^{3+}$ are given in Table III-1. The mean values of the Nd-N (2.60 (2) Å), Nd-O distances (2.43 (2) Å) and Nd-$O_{bridging}$ distances (2.390 (7) Å) are similar to those found in Eu triangle (**VII**) (mean Eu-N (2.56 (1) Å), Eu-O distances (2.40 (3) Å) and Eu-$O_{bridging}$ distances (2.36 (3) Å) (Table III-1).

Table III-1: Selected bonds distances (Å) for the cations (ΛΛΛ)-$[Eu(R\text{-}Phbipox)_2]_3^{3+}$(**VII**) and (ΛΛΛ)-$[Nd(R\text{-}Phbipox)_2]_3^{3+}$ (**VIII**)

	Distance Å		Distance Å
Eu(1)-O(1)	2.456(3)	Nd(1)-O(1)	2.448(3)
Eu(1)-O(21)	2.371(3)	Nd(1)-O(21)	2.398(3)
Eu(1)-O(82)	2.350(3)	Nd(1)-O(82)	2.397(3)
Eu(1)-N(1)	2.561(4)	Nd(1)-N(1)	2.581(4)
Eu(1)-N(2)	2.586(4)	Nd(1)-N(2)	2.612(4)
Eu(1)-N(3)	2.589(4)	Nd(1)-N(3)	2.614(4)
Eu(1)-N(21)	2.525(4)	Nd(1)-N(21)	2.560(4)
Eu(1)-N(22)	2.584(4)	Nd(1)-N(22)	2.613(4)
Eu(1)-N(23)	2.612(4)	Nd(1)-N(23)	2.638(4)
Eu(2)-O(41)	2.395(3)	Nd(2)-O(41)	2.457(3)
Eu(2)-O(61)	2.389(3)	Nd(2)-O(61)	2.403(3)
Eu(2)-O(2)	2.407(3)	Nd(2)-O(2)	2.392(4)
Eu(2)-N(41)	2.540(4)	Nd(2)-N(41)	2.583(4)
Eu(2)-N(42)	2.566(4)	Nd(2)-N(42)	2.608(4)
Eu(2)-N(43)	2.552(4)	Nd(2)-N(43)	2.610(4)
Eu(2)-N(61)	2.535(4)	Nd(2)-N(61)	2.547(4)
Eu(2)-N(62)	2.562(4)	Nd(2)-N(62)	2.586(4)
Eu(2)-N(63)	2.600(4)	Nd(2)-N(63)	2.617(4)
Eu(3)-O(81)	2.404(3)	Nd(3)-O(81)	2.452(3)
Eu(3)-O(101)	2.400(3)	Nd(3)-O(101)	2.432(3)
Eu(3)-O(42)	2.347(3)	Nd(3)-O(42)	2.383(4)
Eu(3)-N(81)	2.549(4)	Nd(3)-N(81)	2.607(4)
Eu(3)-N(82)	2.560(4)	Nd(3)-N(82)	2.640(4)
Eu(3)-N(83)	2.582(4)	Nd(3)-N(83)	2.634(4)
Eu(3)-N(101)	2.521(4)	Nd(3)-N(101)	2.564(4)
Eu(3)-N(102)	2.571(4)	Nd(3)-N(102)	2.624(4)
Eu(3)-N(103)	2.561(4)	Nd(3)-N(103)	2.624(4)

3.1.3 (Δ)-[Yb(R-Phbipox)$_2$](Otf) (IX)

The crystal obtained from the acetonitrile solution of the Yb complex is the mononuclear (Δ)-[Yb(R-Phbipox)$_2$]$^+$ diastereomer (Figure III-23) which is the major species in solution (Δ /Λ ~3.3). The Yb^{3+} is clearly not large enough to accommodate additional carboxylate oxygen therefore no polynuclear assembly formation occurs with this ion. The complexes obtained by R and S-Phbipox are isostructural with opposite chirality and they crystallize in the monoclinic space group $P2_1$. The angle between the two ligands mean planes is of about 97°. In comparison to Eu mononuclear complex (Δ)-[Eu(R-Phbipox)$_2$]$^+$ in (**VII**) larger angles are found between the oxazoline phenyl rings of each tetradentate ligand and one pyridine ring of the other ligand (11.92° & 13.73° for Yb **(IX)** and 4.12° & 1.74° for Eu **(VII)** complex) probably due to interligand repulsion as a result of the smaller size of the ion (Table A1). The selected bond distances for the cations (Δ)-[Yb(R-Phbipox)$_2$]$^+$ and (Δ)-[Eu(R-Phbipox)$_2$]$^+$ are given in Table III-2. The mean values of the Yb-N (2.44 (1) Å and 2.45 (1) Å) and Yb-O distances (2.20 (19) Å and 2.21 (16) Å) are smaller than those found in the eight coordinate complex (Δ)-[Eu(R-Phbipox)$_2$]$^+$ in agreement with the difference in ionic radii [5].

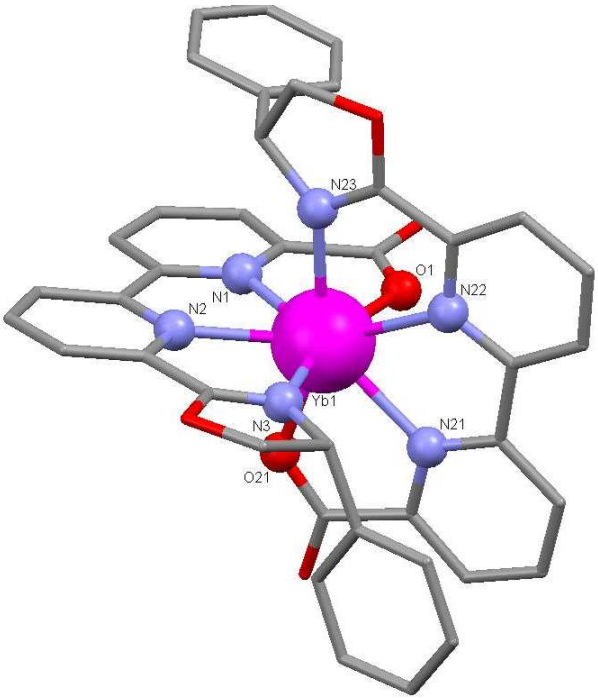

Figure III-23: Mercury diagram of the structure (Δ)-[Yb(R-Phbipox)$_2$]$^+$ (**IX**)

Table III-2: Selected bonds distances (Å) for the cation (Δ)-[Eu(R-Phbipox)$_2$]$^+$ and (Δ)-[Yb(R-Phbipox)$_2$]$^+$

	Distance Å		Distance Å
Eu(4)-O(121)	2.296(3)	Yb(1)-O(1)	2.2099(19)
Eu(4)-O(141)	2.320(3)	Yb(1)-O(21)	2.2168(16)
Eu(4)-N(121)	2.503(4)	Yb(1)-N(1)	2.410(2)
Eu(4)-N(122)	2.546(4)	Yb(1)-N(2)	2.4629(18)
Eu(4)-N(123)	2.530(4)	Yb(1)-N(3)	2.459(2)
Eu(4)-N(141)	2.507(4)	Yb(1)-N(21)	2.415(2)
Eu(4)-N(142)	2.582(4)	Yb(1)-N(22)	2.480(2)
Eu(4)-N(143)	2.542(4)	Yb(1)-N(23)	2.457(2)

3.2- NMR and ESI-MS spectroscopy analysis

3.2.1 Complexation with the enantiopure ligands (S/R)-Phbipox

a) Europium Complexes

Proton NMR studies show that the reaction of Eu(Otf)$_3$ with two equivalents of S-Phbipox or R-Phbipox in anhydrous methanol in the presence of triethylamine affords a mixture of the two diasteroisomeric bis-ligand complexes (Δ)-[Eu(S-Phbipox)$_2$]$^+$ and (Λ)-[Eu(S-Phbipox)$_2$]$^+$ or (Λ)-[Eu(R-Phbipox)$_2$]$^+$ and (Δ)-[Eu(R-Phbipox)$_2$]$^+$ which correspond to the two different helical arrangements (left and right respectively) that the two ligands can adopt when they bind the metal (Scheme III-8). The chirality of the ligand is transferred to the complex resulting Δ diastereomer being the major species when the complex prepared with S ligand while Λ diastereomer is the major species when the complex prepared with R ligand.

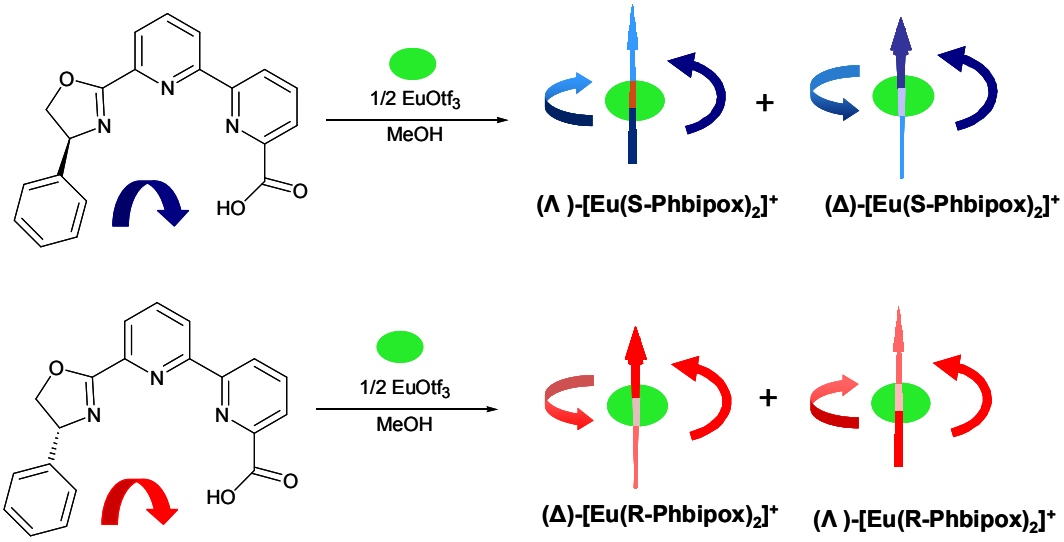

Scheme III-8: Reaction scheme for the synthesis of complexes and helical arrangement of the ligands around Eu ion

Two distinct sets of 12 NMR signals are observed for the 14 protons of the two C_2 symmetric diastereoisomers (Figure III-24). The assignment of the peaks was realised by 2D-COSY, 2D-NOESY and concentration studies. The proton NMR spectrum of the isolated solid is identical to the in situ NMR spectrum. Chiral induction from the S-Phbipox or R-Phbipox ligand occurs during metal coordination leading to a Λ /Δ ratio determined by NMR to be ~1.8 in a 7mM solution of anhydrous methanol at room temperature.

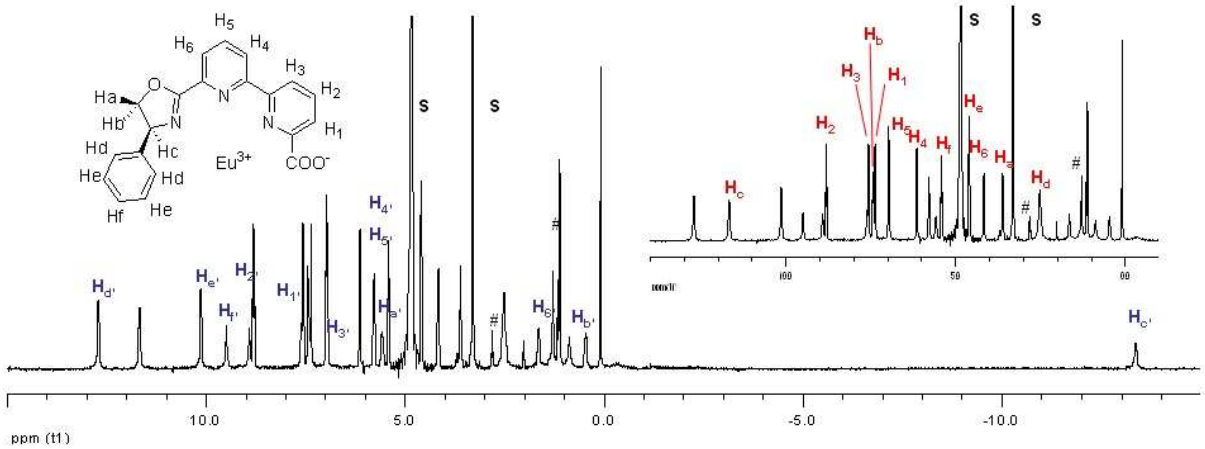

Figure III-24: ^{1}H NMR spectra of (Δ)-[Eu(S-Phbipox)$_2$]$^+$ (H_x') and (Λ)-[Eu(S-Phbipox)$_2$]$^+$ (H_x). (Mercury 400 MHz, 298K, 7 mM, S: CD_3OD, #: triethylamonium)

At higher concentrations (from 14 mM), the NMR spectra show an additional set of 24 signals suggesting the formation of additional species (Figure III-25). These signals were assigned to the trinuclear complex {(ΔΔΔ)-[Eu(S-Phbipox)$_2$]$_3$}$^{+3}$ where the two independent ligands gave rise to two different sets of 12 signals. No signals from heterochiral species were observed, confirming the enantiopurity of the ligand. The addition of small amount of water (<0.03%) does not affect significantly the oligomerization process.

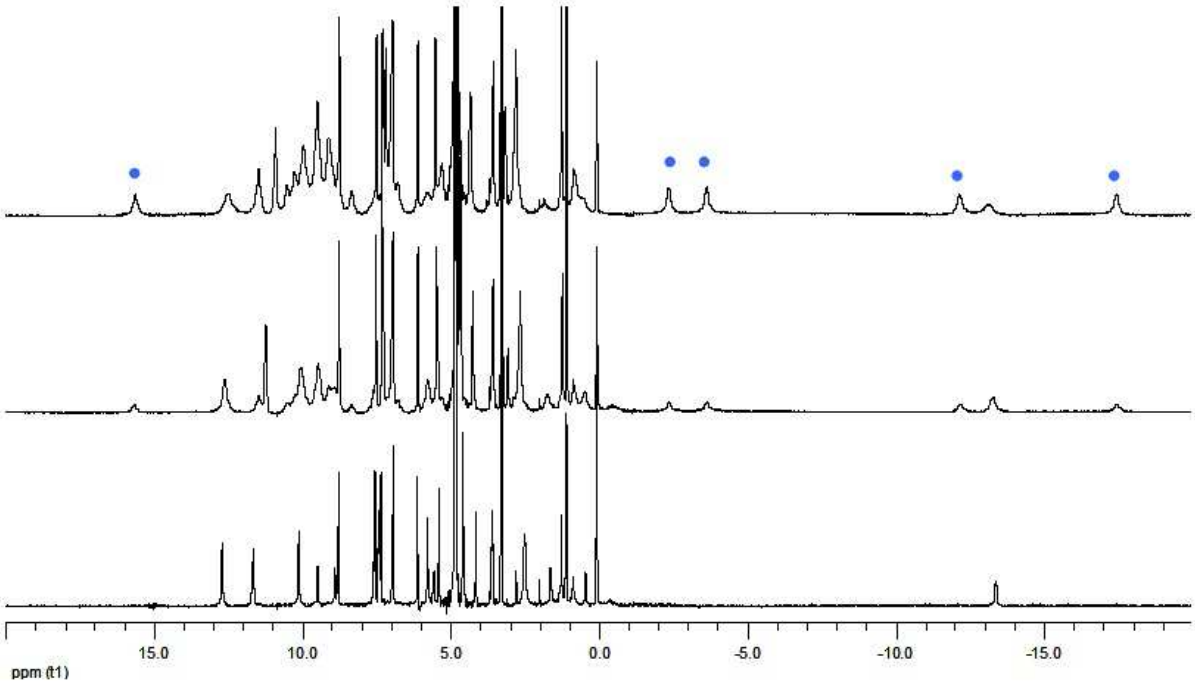

Figure III-25: ^{1}H NMR spectrum of [Eu(S-Phbipox)$_2$] in deuterated methanol at 400 MHz and 298K for three different concentrations (from the bottom 7mM, 14mM, 22mM with Λ/Δ ~1.8 for all) showing the formation of the trinuclear complex (blue dots)

This assignment is in agreement with the solid state crystal structure determined by X-ray diffraction on single crystals of the [Eu(S-Phbipox)$_2$]Otf complex isolated from 24 mM methanol solutions. Notably X-ray diffraction analysis revealed the presence of two distinct co-crystallized molecules in the compound {(ΔΔΔ)-[Eu(S-Phbipox)$_2$]$_3$·(Λ)[Eu(S-Phbipox)$_2$]}Otf$_4$ (Figure III-18). The proton NMR of the bulk isolated complex (Figure III-26) in deuterated acetonitrile shows the presence of trinuclear complex from 6 mM probably as a result of the lower polarity and lower coordinating ability of this solvent.

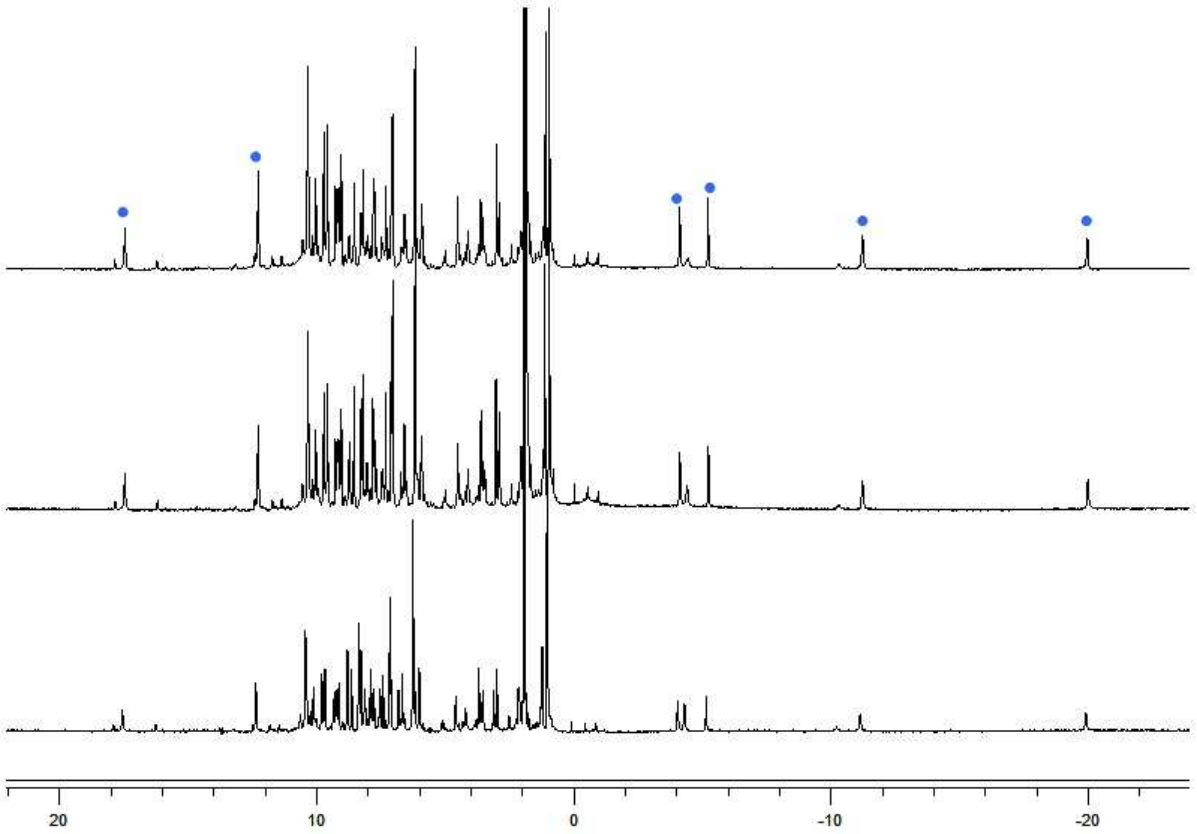

Figure III-26: ^{1}H NMR spectrum of $[Eu(S\text{-}Phbipox)_2]^+$ (isolated from methanol according to experimental description) in deuterated acetonitrile at 400 MHz and 298K for three different concentrations (from the bottom 6, 16 and 24 mM respectively) showing the presence of the trinuclear complex (blue dots) at all concentrations

The intensity of the NMR signals assigned to the trimeric complex increases in methanol and in acetonitrile with increasing concentration (Figure III-25 and III-26). This increase is associated to an intensity decrease of only one of the two set of signals corresponding to the two diastereoisomeric bis-ligand complexes. This shows that only one diastereoisomer, which has been identified as the Δ isomer for S-Phbipox and Λ isomer for R-Phbipox on the basis of the X-ray crystal structure, undergoes the oligomerisation process. Therefore only the presence of the trimeric species and of the residual Λ monomer S-Phbipox can be detected in 30 mM acetonitrile solutions of the $[Eu(S\text{-}Phbipox)_2]^+$ complex (Figure III-27).

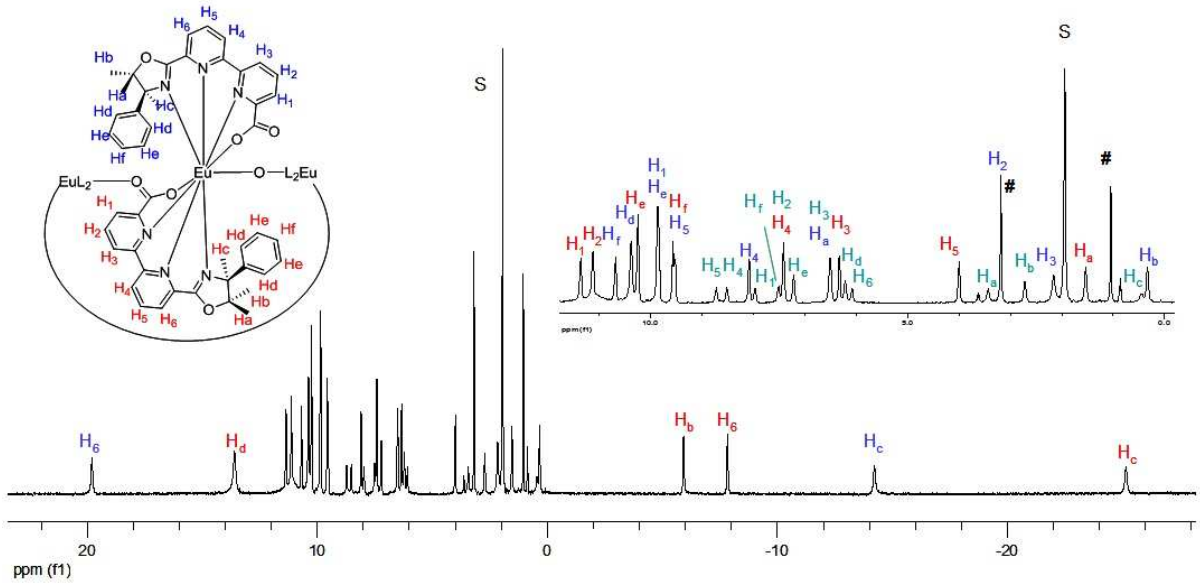

Figure III-27: ^{1}H NMR spectra of (ΔΔΔ)-[Eu(S-Phbipox)$_2$]$_3^{+3}$ (H_x and H_x), (Λ)-[Eu(S-Phbipox)$_2$]$^+$ (H_x). (Bruker 500 MHz, 263K, 30 mM, S: CD_3CN, #: triethylammonium)

These results highlight the diastereoselectivity of the self-assembly process which only involves (Δ)-[Eu(S-Phbipox)$_2$]$^+$ species while the formation of the other possible heterochiral assemblies ΔΔΛ, ΛΛΛ and ΔΛΛ is not observed. This result also suggests that in anhydrous acetonitrile, the ligand S-Phbipox remains bound to the metal ion preventing the rearrangement of the Δ isomer into the Λ one. Table III-3 lists the ratio of Λ/(Δ+ΔΔΔ) and ΔΔΔ/Δ at different concentrations for two solvents. The ratio of lambda over total delta diastereomers does not change with the concentration confirming that there is no interconversion between diastereomers. On the other side, ΔΔΔ/Δ increases by concentration indicating the assembly formation with the increase of concentration. Moreover the NMR spectrum shows a Λ /Δ ratio of ~0.6 in acetonitrile indicating that the crystallization process leads to an increase of the Δ monomer with respect to the Λ complex.

Table III-3: Ratio of the monomeric isomers Λ and Δ and trinuclear ΔΔΔ in anhydrous methanol and acetonitrile at different concentrations, evaluated by integration of ^{1}H NMR signals

Solvent	Concentration/mM	Λ/(Δ+ΔΔΔ)	ΔΔΔ/Δ
CD_3CN	8	0.6	1.54
CD_3CN	30	0.5	4.4
CD_3CN	60	0.6	Δ is not detected
CD_3OD	7	1.8	-
CD_3OD	14	1.9	0.56
CD_3OD	22	1.8	1.56

Pulsed-Field Gradient STimulated Echo (PFGSTE) diffusion NMR was used for measuring the diffusion coefficients (D) of mononuclear and trinuclear complexes in 6 mM acetonitrile and methanol solutions. Diffusion coefficient is a function of the molecular weight (M) and can been conveniently used for discriminating metallosupramolecular architectures in solution [179]. If the species studied could be modelled as a sphere, the relative spherical hydrodynamic radius of the solution species could be estimated by using Stokes-Einstein equation:

$$r_{sph} = \frac{k_B T}{6\pi\eta D} \qquad \text{III-1}$$

where η is the viscosity of the solvent (Pa.s^{-1}) and k_B is the Boltzman constant (m^2.kg.s^{-2}.K^{-1}), T is the absolute temperature (K), D is the diffusion coefficient (m^2.s^{-1}) [180, 181].

Since the trimeric and monomeric complexes have both a globular shape and since similar microscopic densities can be anticipated from their crystal structure, Stokes-Einstein equation could be applied to calculate the spherical hydrodynamic radius of the complexes. In 6 mM methanol solution only the monomeric complexes are present, with diffusion coefficient values of 6.3(4) 10^{-10} and spherical hydrodynamic radius of 6.3 Å (Table III-4). In acetonitrile solutions, two different diffusion coefficients have been found corresponding to the trinuclear and mononuclear species. The values of spherical hydrodynamic radius of the mononuclear complexes in acetonitrile (5.8 Å) and methanol (6.3 Å) are very close to each other, confirming that these species have same nuclearity. Reciprocal cube root dependence of the diffusion coefficient on molecular weight provided us a way to compare the nuclearity of our complexes present in acetonitrile. The values measured in acetonitrile MΔΔΔ/MΔ= (DΔ/DΔΔΔ) ^{3}= 2.8 are in agreement with the presence of one trinuclear complex and two mononuclear species. The calculated values of the 8.2 Å for the trimeric species and 5.8 Å for the monomeric ones in acetonitrile compare very well with the value estimated from the crystal structure (7.7 and 5.1 Å respectively). The fact that no trinuclear species are present in methanol solutions indicates that no assembly formation occurs in protic solvents similar to terpya where only mononuclear complexes are observed in methanol [104].

Table III-4: Diffusion coefficient values of (Δ) / (Λ)-$[Eu(S\text{-}Phbipox)_2]^+$ and (ΔΔΔ)-$[Eu(S\text{-}Phbipox)_2]^{3+}$, and estimated spherical radii

Solvent	Compound	D [$m^2.s^{-1}$]	r_{sph} [Å]$_{exp}$
CD_3OD η=0.5513 mPa.s^{-1} (298K)	(Δ) / (Λ)-$[Eu(S\text{-}Phbipox)_2]^+$	6.3(4) 10^{-10}	6.3
CD_3CN η=0.345 mPa.s^{-1} (298K)	(Δ) / (Λ)-$[Eu(S\text{-}Phbipox)_2]^+$	1.09(7) 10^{-9}	5.8
	(ΔΔΔ)-$[Eu(S\text{-}Phbipox)_2]_3^{+3}$	7.7(4) 10^{-10}	8.2

ESI-MS spectroscopy of the complex in methanolic solution correlates with the NMR spectrum showing only the peak of the mononuclear complex $[Eu(S\text{-}Phbipox)_2]^+$ (m/z = 841.1), no high nuclear species has been observed (Figure III-28). The ES-MS spectrum in acetonitrile indicates the presence of different nuclear species (with intense peak being mononuclear $[Eu(S\text{-}Phbipox)_2]^+$ (m/z= 841.2), and high nuclear species $\{[Eu(S\text{-}Phbipox)_2]_4(Otf)\}^+$ (m/z= 1828) $\{[Eu(S\text{-}Phbipox)_2]_3(Otf)_2\}^+$ (m/z = 1335) (Figure III-29).

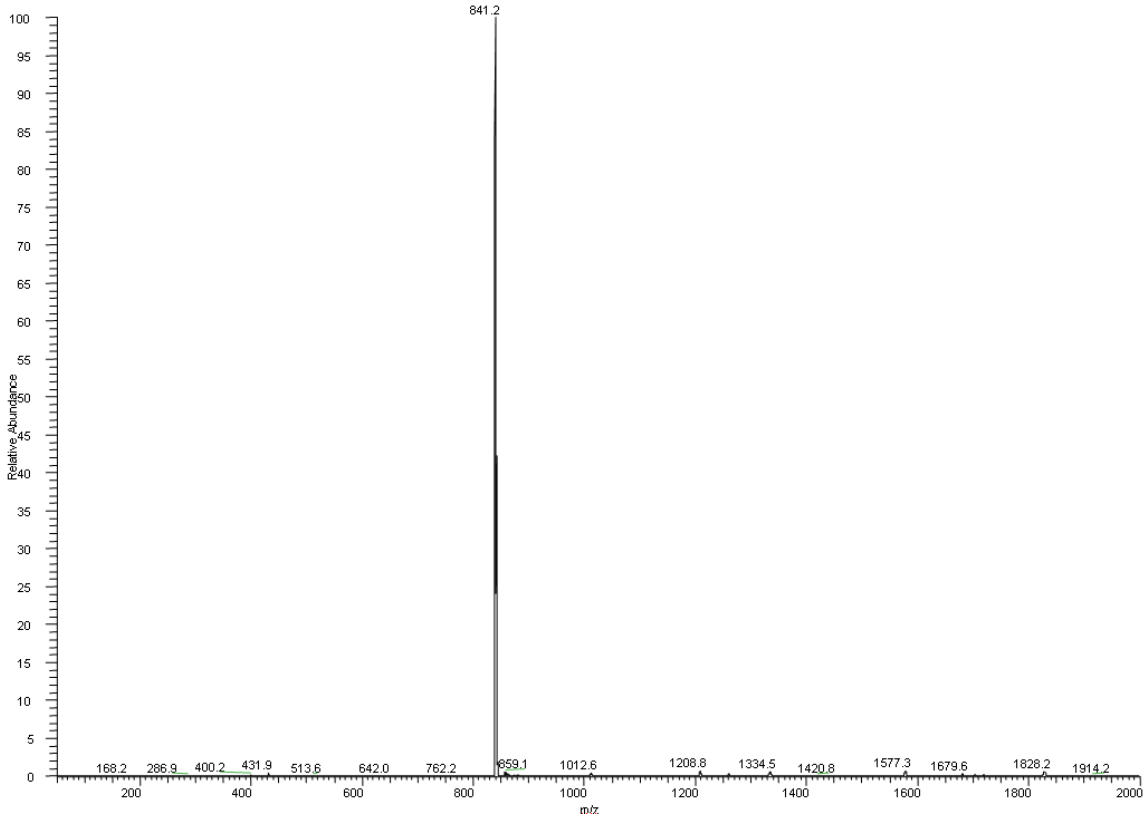

Figure III-28: ESI/MS spectra of a 6 mM methanol solution of $[Eu(S\text{-}Phbipox)_2]^+$ from 150 to 2000 uma showing only the 2:1 complex as major species at m/z 841.2

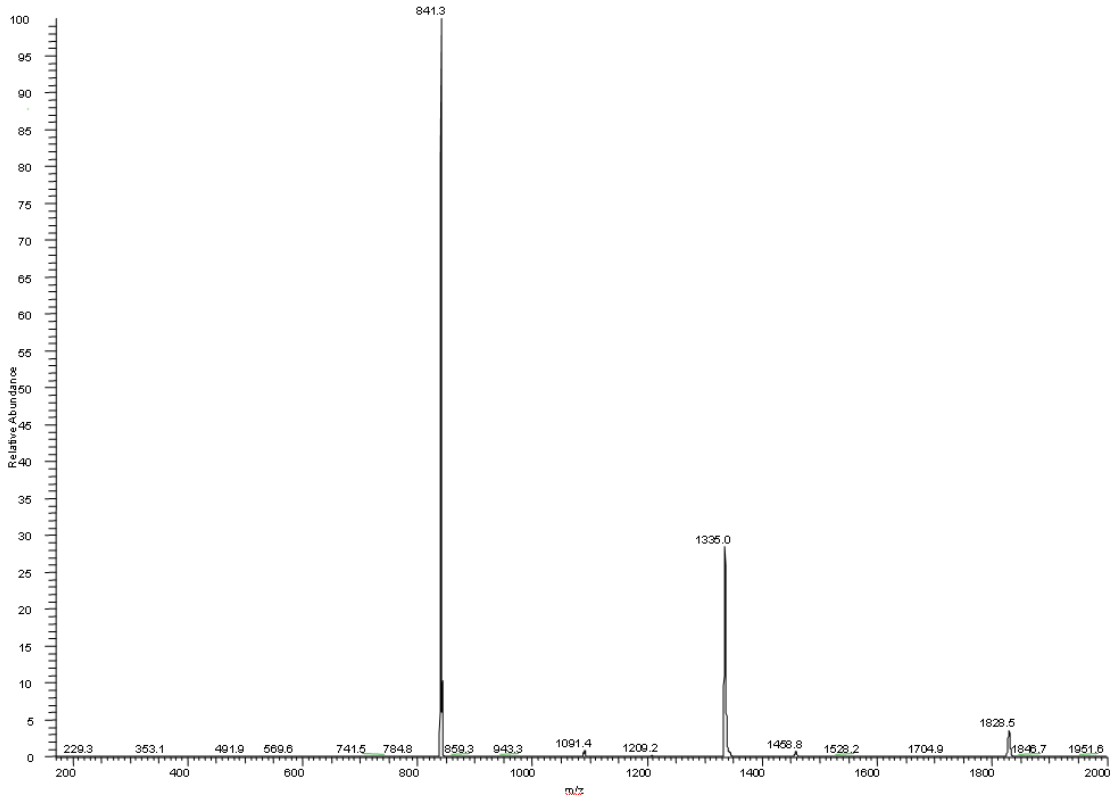

Figure III-29: ESI/MS spectra of a 6 mM acetonitrile solution of $[Eu(S\text{-}Phbipox)_2]^+$ from 200 to 2000 uma showing mononuclear 2:1 complex at m/z 841.2, trinuclear species at m/z 1335

b) Complexation with other Ln (Nd, Yb)

The proton NMR spectrum of methanol solution of the Nd(III) complex (**VIII**) at 3 mM concentration affords a mixture of the two diastereoisomeric bis-ligand complexes (Δ)-$[Nd(R\text{-}Phbipox)_2]^+$ and (Λ)-$[Nd(R\text{-}Phbipox)_2]^+$. Two distinct set of 12 NMR signals are observed for the 14 protons of the two C_2 symmetric diastereoisomers (Figure III-30). The assignment of the peaks were realised by 2D-COSY, 2D-NOESY and concentration studies.

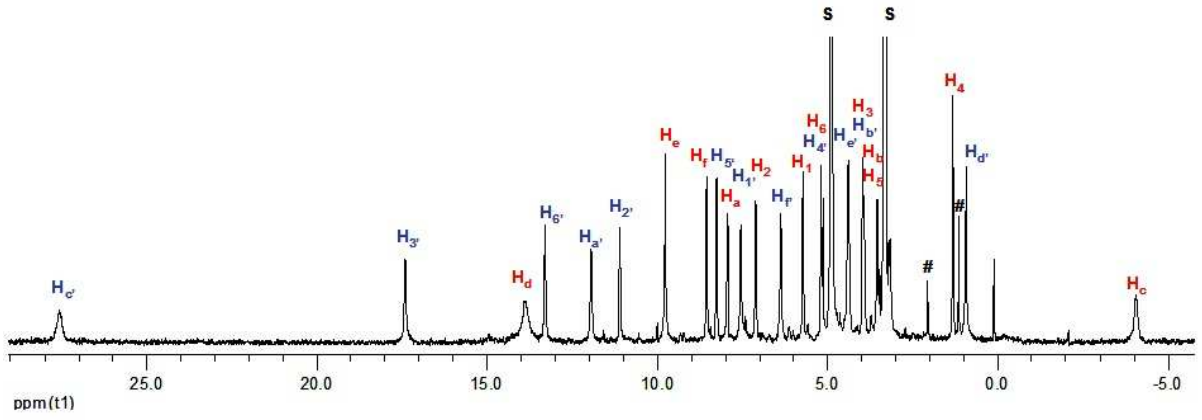

Figure III-30: ^1H NMR spectra of Nd complex (**VIII**) showing diastereomers (Λ)-$[Nd(R\text{-}Phbipox)_2]^+$ (H_x) and (Δ)-$[Nd(R\text{-}Phbipox)_2]^+$ (H_x). (Mercury 400 MHz, 298K, 3 mM, S: CD_3OD, #:triethylamonium)

When the concentration increased to 6 mM, we observed the formation of two new sets of 12 peaks that correspond to the trinuclear species (Figure III-31), while in europium complex (**VII**), at this concentration, no assembly formation was observed. This difference in oligomerization by concentration could result from reduced effect of sterical restrictions due to size of Nd(III) ion being larger than Eu(III) ion. Another effect of cation size shows itself in the chiral selectivity. Δ/Λ ratio determined by NMR is ~1 in a 3 mM solution of Nd complex (**VIII**) in anhydrous methanol at room temperature. This ratio differs from the Eu complex (Δ/Λ ~1.8). Reduced sterical interactions due to larger ion size reduce the preference between two diastereomers. Therefore the latter exist in solution as a 50%-50% mixture.

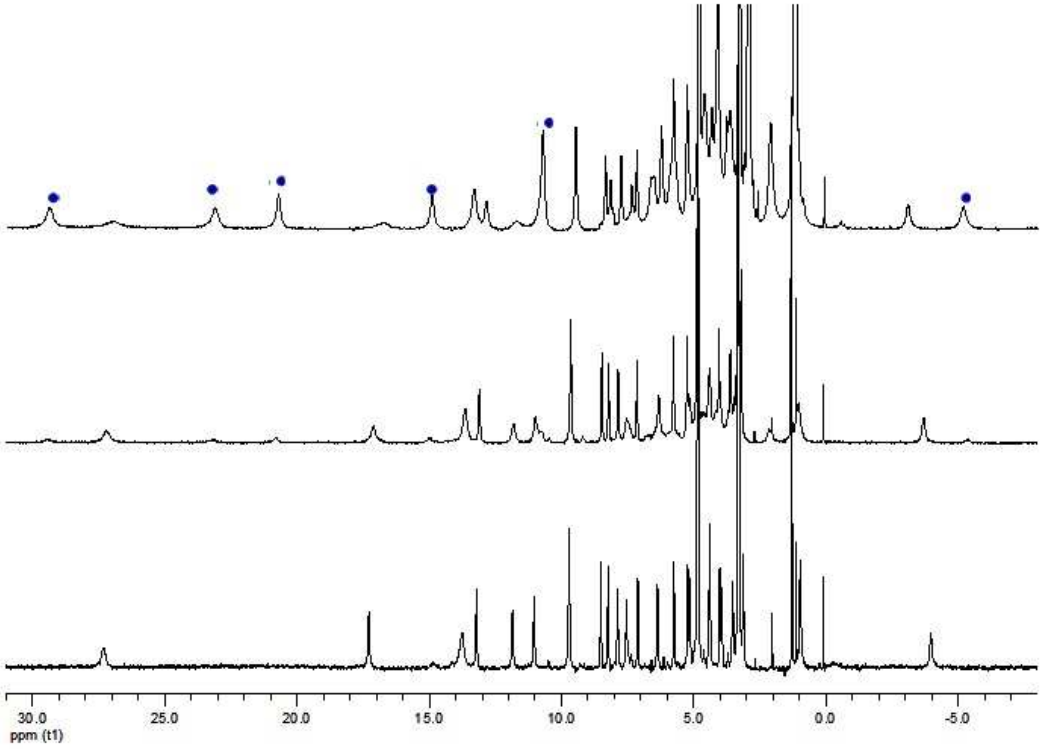

Figure III-31: ^{1}H NMR spectrum of $[Nd(R\text{-}Phbipox)_2]^+$ in deuterated methanol at 400 MHz and 298K for three different concentrations (from the bottom 3mM, 6mM, 14mM with Λ/Δ ~1 for all) showing the formation of the trinuclear complex (blue dots)

In anhydrous acetonitrile, proton NMR spectrum shows only the presence of homochiral trinuclear complexes with two sets of 12 peaks (Figure III-32). No peaks from mononuclear complexes have been observed in anhydrous acetonitrile solution. As a result of steric crowding by the phenyl groups of the ligands, trinuclear species form by the assembly of only one diastereomer which is the (Λ)-$[Nd(R\text{-}Phbipox)_2]^+$ complex. The absence of mononuclear complexes in acetonitrile solution could be explained by the increased lability of the complexes in solution due to large ion size favoring interconversion between diastereomers. The mononuclear (Δ)-$[Nd(R\text{-}Phbipox)_2]^+$ complex could rearrange itself into

(Λ)-$[Nd(R\text{-}Phbipox)_2]^+$ diastereomer which assembles to form trinuclear species. ESI-MS spectroscopy of the complex in methanol and acetonitrile at 6 mM confirms the presence of trinuclear species in both solutions (Figures III-33 and III-34). No higher nuclear species were observed by ESI-MS.

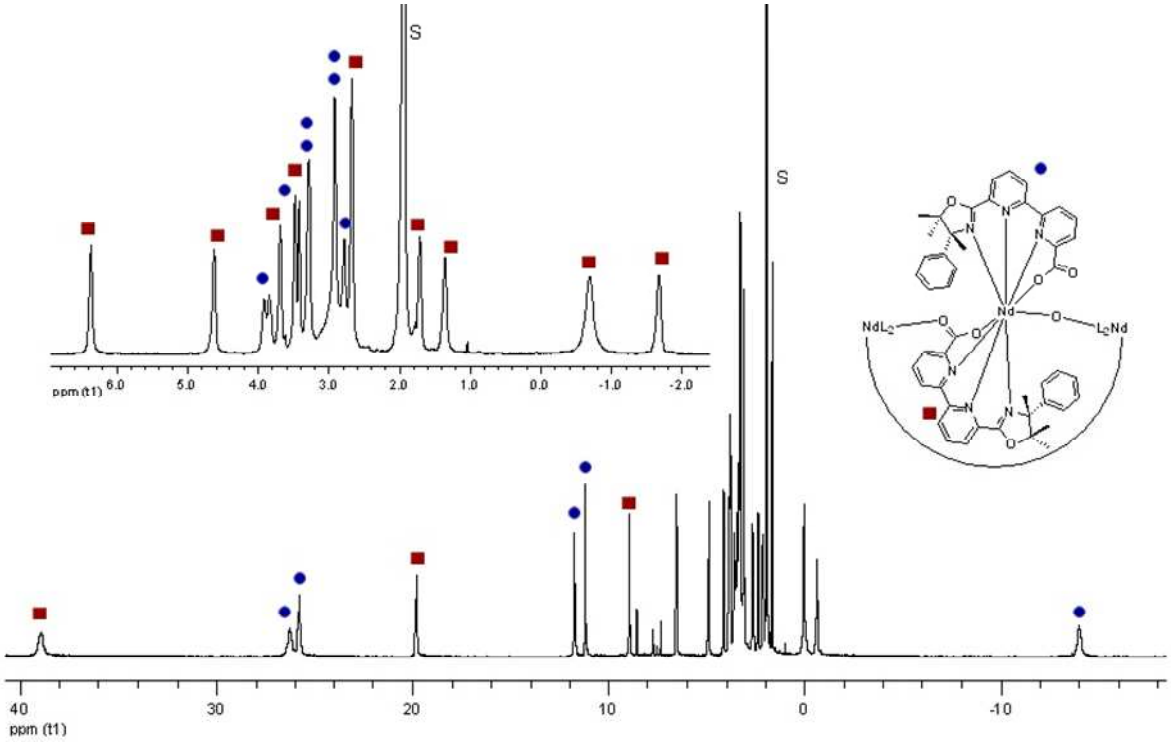

Figure III-32: ^1H NMR spectrum of (ΛΛΛ)-$[Nd(R\text{-}Phbipox)_2]_3^{3+}$. (Bruker 500 MHz, 263K, 30 mM, S: CD_3CN)

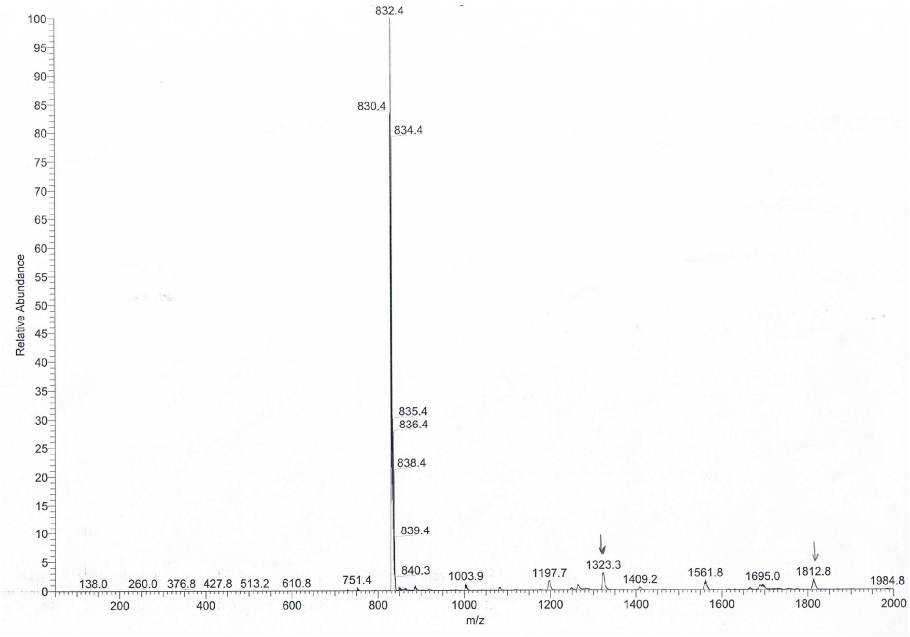

Figure III-33: ESI/MS spectra of a 6 mM methanol solution of $[Nd(R\text{-}Phbipox)_2]^+$ from 150 to 2000 uma showing mononuclear 2:1 complex at m/z 832.4, trinuclear species at m/z 1323.3

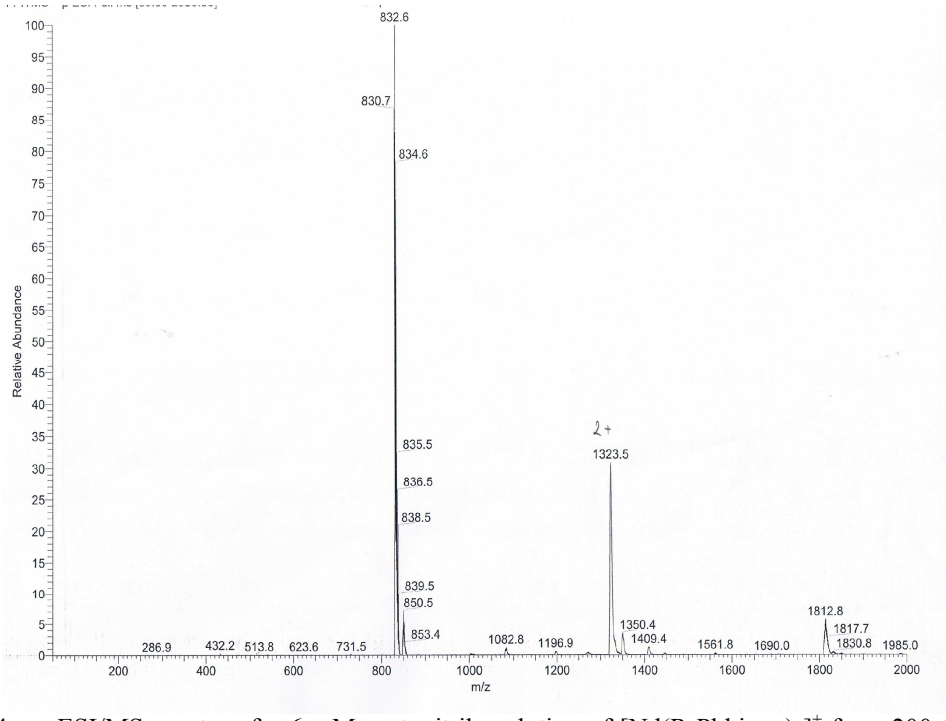

Figure III-34: ESI/MS spectra of a 6 mM acetonitrile solution of $[Nd(R\text{-}Phbipox)_2]^+$ from 200 to 2000 uma showing mononuclear 2:1 complex at m/z 832.6, trinuclear species at m/z 1323.5

Proton NMR spectra of Yb complex (**IX**) in methanol and acetonitrile show two sets of peaks corresponding to Δ and Λ diastereomers with a chiral induction of Δ/Λ~3.3 (Figure III-35) in anhydrous methanol. The phenyl groups are closer to each other for lambda diastereomer compared to delta diastereomer. This could increase the preference of delta diastereomer in solution since Yb ion is quite small. For this system, we observed a strong correlation between chiral induction (Δ/Λ) (Yb >Eu >Nd) and ion size (Yb <Eu <Nd). The biggest lanthanide ion used, Nd(III), shows no preference by having a ratio of Δ/Λ ~1. Eu ion has an increased resolution with Δ/Λ~1.8, finally Yb ion, the smallest among all, show the highest selectivity with Δ/Λ~3.3.

No assembly formation of Yb complex (**IX**) was observed with the increase of concentration. This is due to the absence of free coordination site around the ion and to the increased steric effect around the metal ion as the size of the lanthanide is too small to form carboxylate bridges. ESI-MS spectroscopy of the Yb complex shows only mononuclear species in both solutions at 6 mM concentrations (Figures III-36 and III-37).

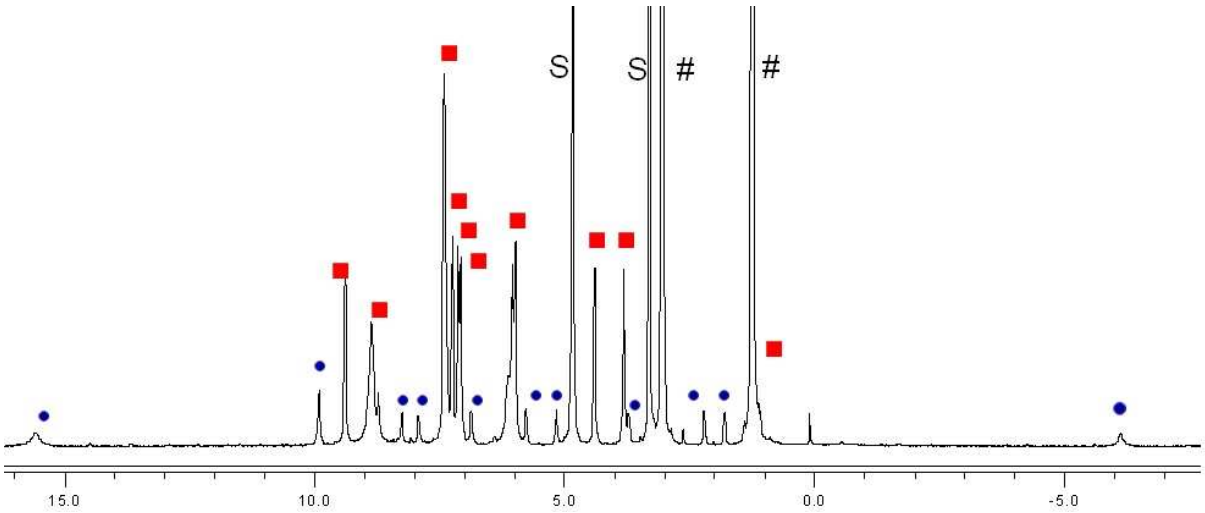

Figure III-35: ^{1}H NMR spectra of Yb complex (**IX**) showing diastereomers (Δ)-[Yb(R-Phbipox)$_2$]$^+$ (■) and (Λ)-[Yb(R-Phbipox)$_2$]$^+$ (●). (Mercury 400MHz, 298K, 6 mM, S: CD_3OD, #:triethylamonium).

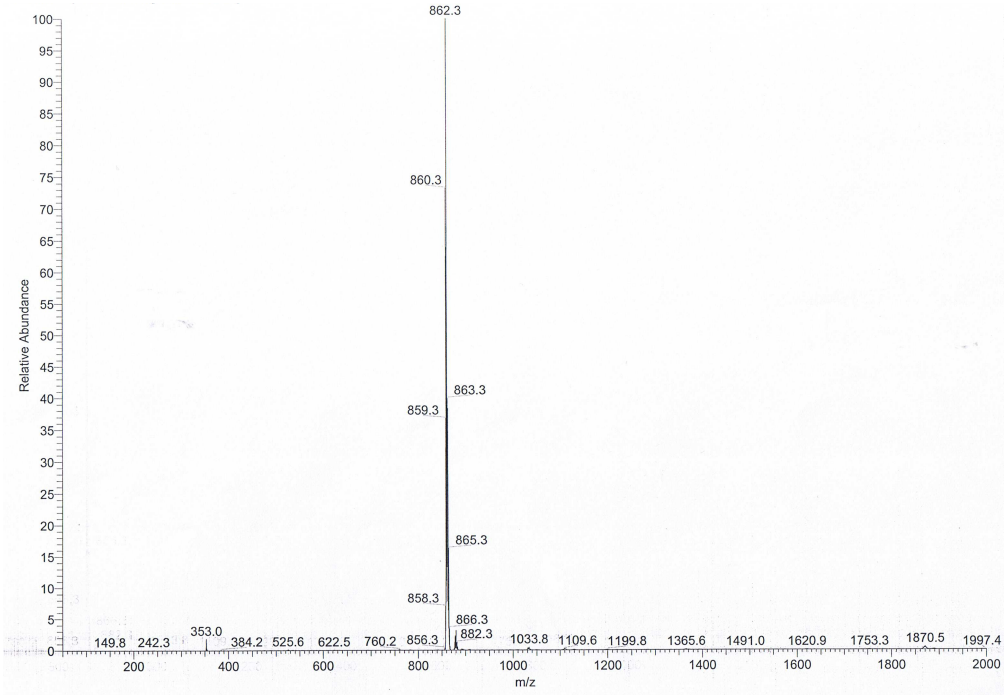

Figure III-36: ESI/MS spectra of a 6 mM methanol solution of [Yb(R-Phbipox)$_2$]$^+$ from 150 to 2000 uma showing only the 2:1 complex species at m/z 862.3

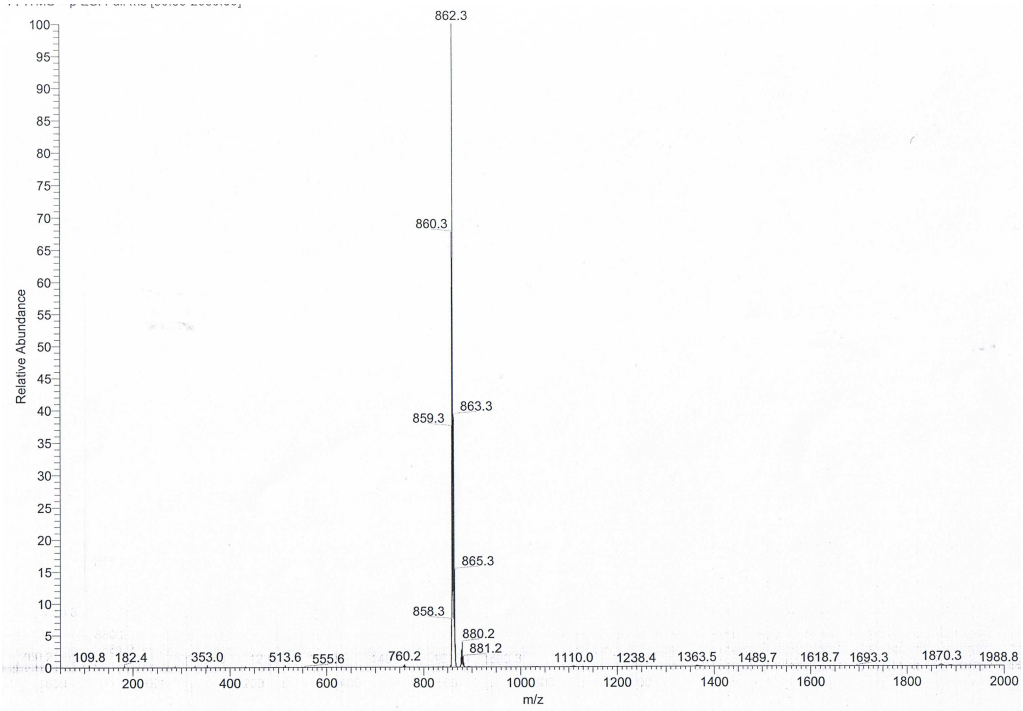

Figure III-37: ESI/MS spectra of a 6 mM acetonitrile solution of $[Yb(R\text{-}Phbipox)_2]^+$ from 100 to 2000 uma showing only the 2:1 complex species at m/z 862.3

3.2.2 Complexation with racemic ligand

In order to study the chiral resolution properties of our system, a racemic Phbipox ligand has been synthesized in our laboratory. ^{1}H NMR spectrum of complexes formed with racemic ligand shows an additional set of peaks that belongs to the heterochiral monomeric complex $[Eu((R,S)\text{-}Phbipox)_2]^+$ (blue dots in Figure III-38). in addition to homochiral $[Eu((S,S)\text{-}or(R,R)\text{-}Phbipox)_2]^+$ complexes ^{1}H NMR integrations reveal that the solution mixture consists of 67% $[Eu((R,S)\text{-}Phbipox)_2]^+$ and 20% $[Eu(\Delta(S,S)/\Lambda(R,R)\text{-}Phbipox)_2]^+$ and 13% $[Eu(\Lambda(S,S)/\Delta(R,R)\text{-}Phbipox)_2]^+$.

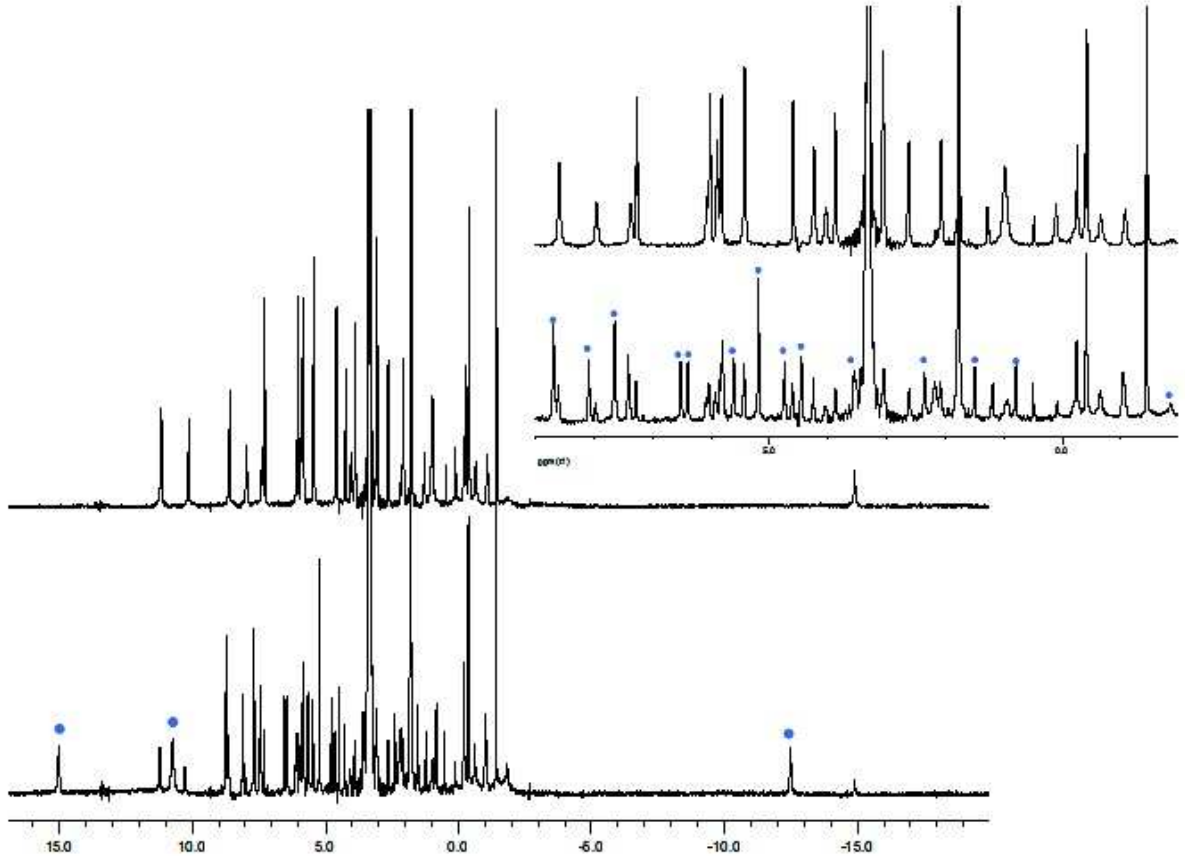

Figure III-38: Comparison of NMR spectra of the complexes $[Eu(S\text{-}Phbipox)_2]^+$ (upper spectra) and Eu(rac-Phbipox)$_2$ (lower spectra) 7 mM (CD_3OD, 400 MHz, 298 K) (blue dots: $[Eu((R,S)\text{-}Phbipox)_2]^+$)

Ion size is known to effect chiral selectivity. The studies with racemic pybox type ligands have shown the preferential formation of diastereomers by different ion size. Aspinall et al. have reported that complexation with rac-Pr^i-pybox ligand with $Eu(Otf)_3$ results in heterochiral [$Eu(Otf)_3$(RR-Pr^i-Pybox)-(SS-Pr^i-Pybox)] complexes, whereas $Yb(Otf)_3$ results in a mixture of mainly homochiral RR- and SS-[$Yb(Otf)_2$(Pr^i-Pybox)$_2$)][Otf], along with a very small amount of heterochiral [$Yb(Otf)_2$(R-Pr^i-Pybox)-(S-Pr^i-Pybox)][Otf] [182].

Similarly in our system the outcome of the reaction varies with the ionic radius of Ln. Figure III-39 shows the proton NMR spectrum of complexes formed with racemic ligand and $Yb(Otf)_3$ generating isomers of 34% $[Yb((R,S)\text{-}Phbipox)_2]^+$, 15% $[Yb(\Delta(S,S)/\Lambda(R,R)\text{-}Phbipox)_2]^+$ and 51% $[Yb(\Lambda(S,S)/\Delta(R,R)\text{-}Phbipox)_2]^+$. The major species in solution for Yb complexes are the homochiral sterically favored $[Yb(\Lambda(S,S)/\Delta(R,R)\text{-}Phbipox)_2]^+$ species. In contrast the major species for Eu complexes were heterochiral $[Eu((R,S)\text{-}Phbipox)_2]^+$ species.

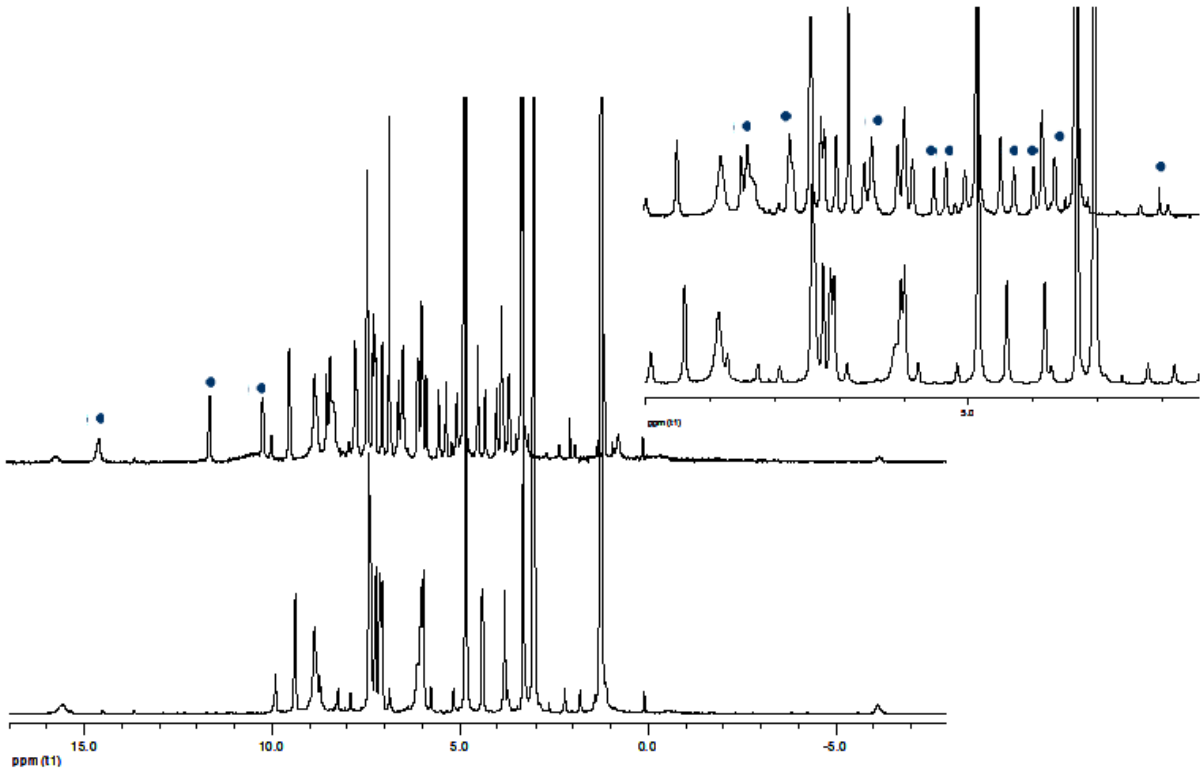

Figure III-39: Comparison of NMR spectra of the complexes $[Yb(S\text{-}Phbipox)_2]^+$ (lower spectra) and Yb(rac-Phbipox)$_2$ (upper spectra) 7 mM (CD_3OD, 400 MHz, 298 K) (blue dots: $[Yb((R,S)\text{-}Phbipox)_2]^+$)

The ^1H NMR spectra of the racemic Eu complex in acetonitrile shows a complex behaviour with broad peaks forming with the increase of concentration (Figure III-40). ESI-MS spectroscopy of the complex in acetonitrile confirms the presence of trinuclear species (Figure III-41) however due to high number of diastereomers in solution NMR spectrum shows a complicated behavior. This should come from the exchange between the several species present in solution as a result of various possibilities to form polynuclear species with combination of different diastereomers in solution. No crystals could be obtained from these solutions. In methanolic solutions above 10 mM precipitation was observed indicating the formation of high nuclear insoluble species.

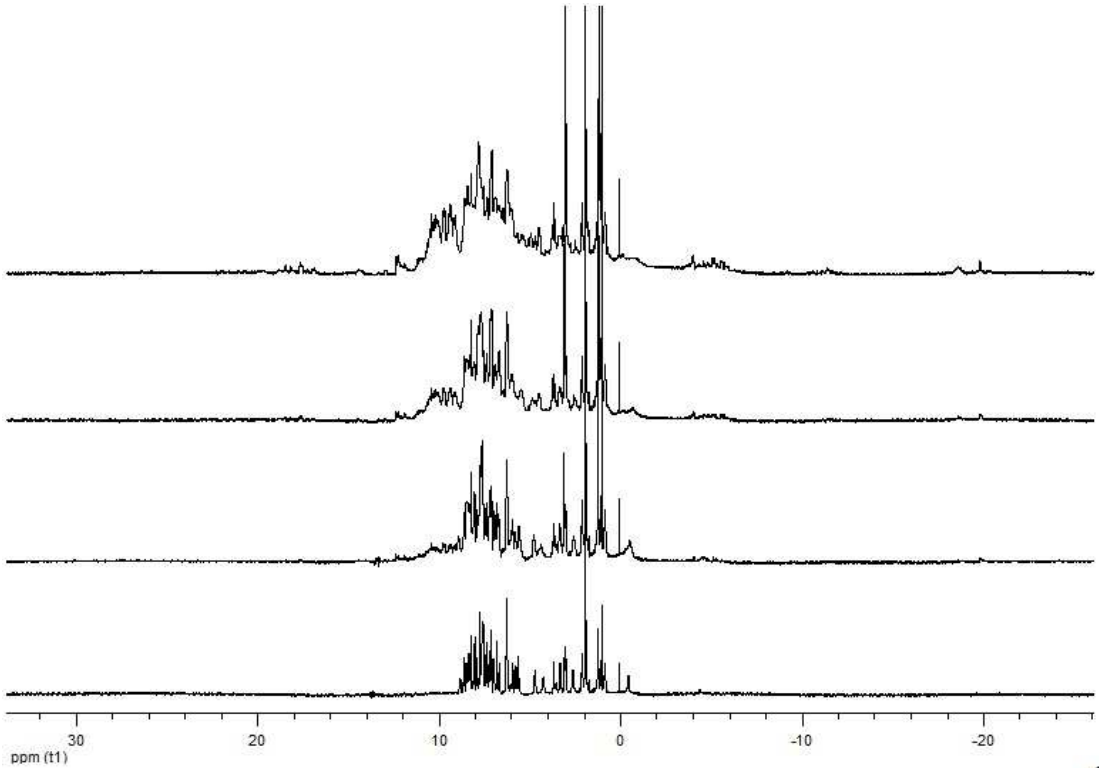

Figure III-40: NMR spectrum of the acetonitrile solutions of the complex $[Eu(rac\text{-}Phbipox)_2]^+$ at different concentrations, from bottom to up 4,12, 20, 28 mM respectively. (400 MHz, 298 K)

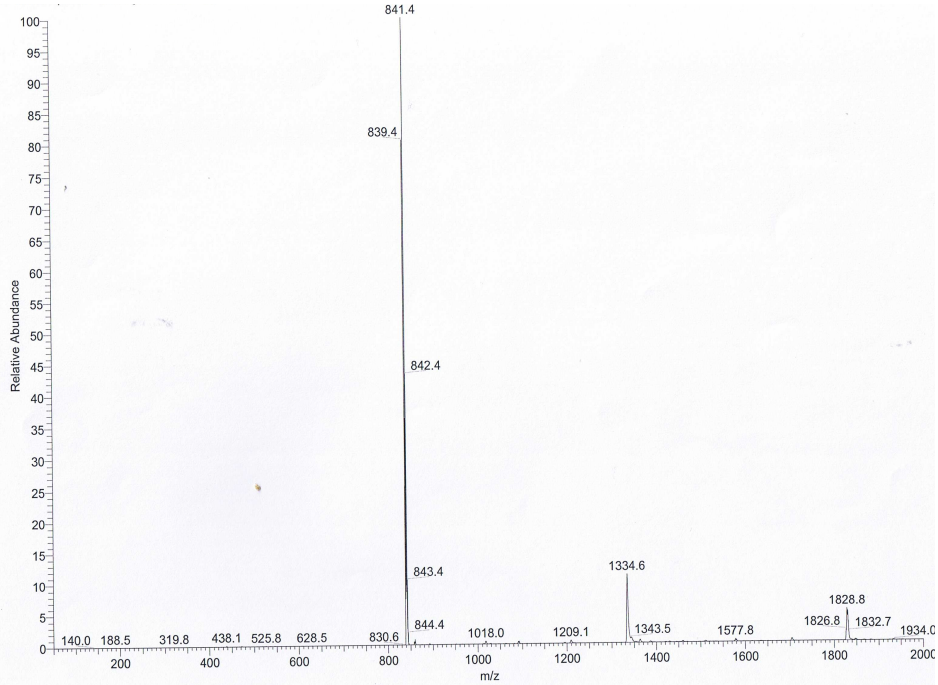

Figure III-41: ESI/MS spectra of a 6 mM acetonitrile solution of $[Eu(rac\text{-}Phbipox)_2]^+$ from 150 to 2000 uma showing mononuclear complex at m/z 841.4, trinuclear species at m/z 1334.6

4- Synthesis and characterization of heptanuclear complexes

In our laboratory, it has been shown that the use of simple asymmetric tetradentate ligand (terpya) leaving some coordination vacancies around the metal ion direct the assembly of large lanthanide clusters [104, 105]. Addition of an excess $Ln(Otf)_3$ to a suspension of mononuclear complexes $[Ln(terpya)_2]^+$ in acetonitrile results in complete dissolution of the complex and isolation of heptanuclear complexes $[Ln\subset(Ln(terpya)_2)_6](Otf)_9$ (Ln = Eu, Tb, Nd, Gd). In order to obtain high nuclearity chiral preprogrammed lanthanide complexes we have adapted this rational approach to the 2:1 complexes prepared with tetradentate chiral Phbipox ligand (Scheme III-9). Moreover direct synthesis of the homo-polymetallic complexes by reaction of Phbipox ligand and lanthanide triflates with a ratio of Ln/L = 7/12 in presence of triethylamine resulted in the same heptanuclear complex.

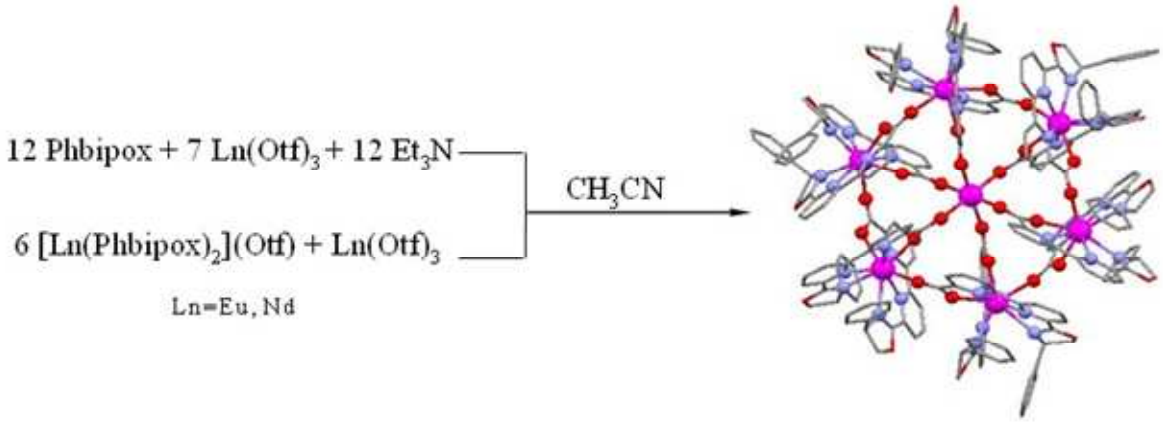

Scheme III-9: Reaction scheme for the synthesis of heptanuclear complexes

4.1- X-Ray Crystallography Studies

Several attempts to crystallize $[Ln\subset(\Lambda\text{-}Ln(Phbipox)_2\Delta\text{-}Ln(Phbipox)_2)_3](Otf)_9$ (Ln = Eu, Nd) resulted in low diffraction quality crystals. Details of several unit cells obtained can be found in the Appendix section. A crystal structure with sufficient quality was obtained by crystals prepared by slow diffusion of hexane into benzonitrile solution of the $[Eu\subset(\Lambda\text{-}Eu(R\text{-}Phbipox)_2\Delta\text{-}Eu(R\text{-}Phbipox)_2)_3](Otf)_9$ (**X**) complexes. The asymmetric unit of the crystal structure consists of two independent hexameric wheels with the same chirality, disordered triflate ions and solvent molecules (Figure III-42). The compound crystallizes in the chiral monoclinic space group C2.

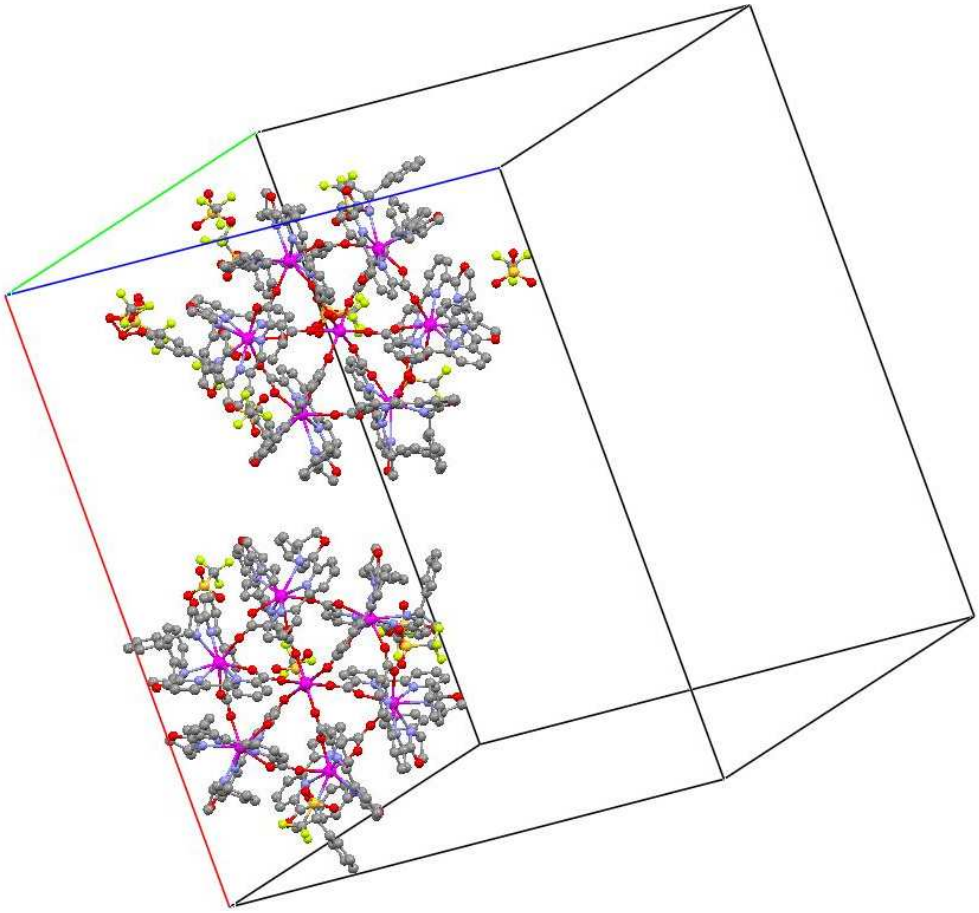

Figure III-42: Asymmetric unit in the unit cell of $[Eu\subset(\Lambda\text{-}Eu(R\text{-}Phbipox)_2\Delta\text{-}Eu(R\text{-}Phbipox)_2)_3](Otf)_9$ **(X)**. The asymmetric unit comprises two independent heptanuclear complex, triflates and solvent molecules.

In the $[Eu\subset(\Lambda\text{-}Eu(R\text{-}Phbipox)_2\Delta\text{-}Eu(R\text{-}Phbipox)_2)_3]^{9+}$ cation three $[\Lambda\text{-}Eu(R\text{-}Phbipox)_2]^{+}$ and three $[\Delta\text{-}Eu(R\text{-}Phbipox)_2]^{+}$ complexes are connected alternatively through a carboxylate oxygen from one of the R-Phbipox ligands to form diastereoselectively the heterochiral cyclic structure. The selectivity of the assembly formation generates from the

steric constraints resulting from the orientation of the phenyl groups on the oxazoline ring (as shown for the trinuclear species in Figure III-21). Therefore no other isomers of the hexameric wheel with different combination of diastereomers (6Δ, 6Λ, 5Δ1Λ, 4Δ2Λ, etc) are observed in solid state and in solution. $[\Lambda\text{-Eu(R-Phbipox)}_2]^+$ complexes are coloured green while $[\Delta\text{-Eu(R-Phbipox)}_2]^+$ complexes coloured orange in Figure III-43. A seventh europium ion is encapsulated in the ring center and has a regular octahedral coordination sphere composed of six carboxylate oxygens from the coordinated Phbipox carboxylate ligands not involved in the ring formation. In the complexes each europium on the cycle is nine coordinated by six nitrogens and two oxygens from the two Phbipox ligands and one oxygen from a bridging Phbipox ligand of the adjacent mononuclear complex. The polyhedron of Eu coordination sphere is best described as a distorted tricapped trigonal prism (Figure III-44).

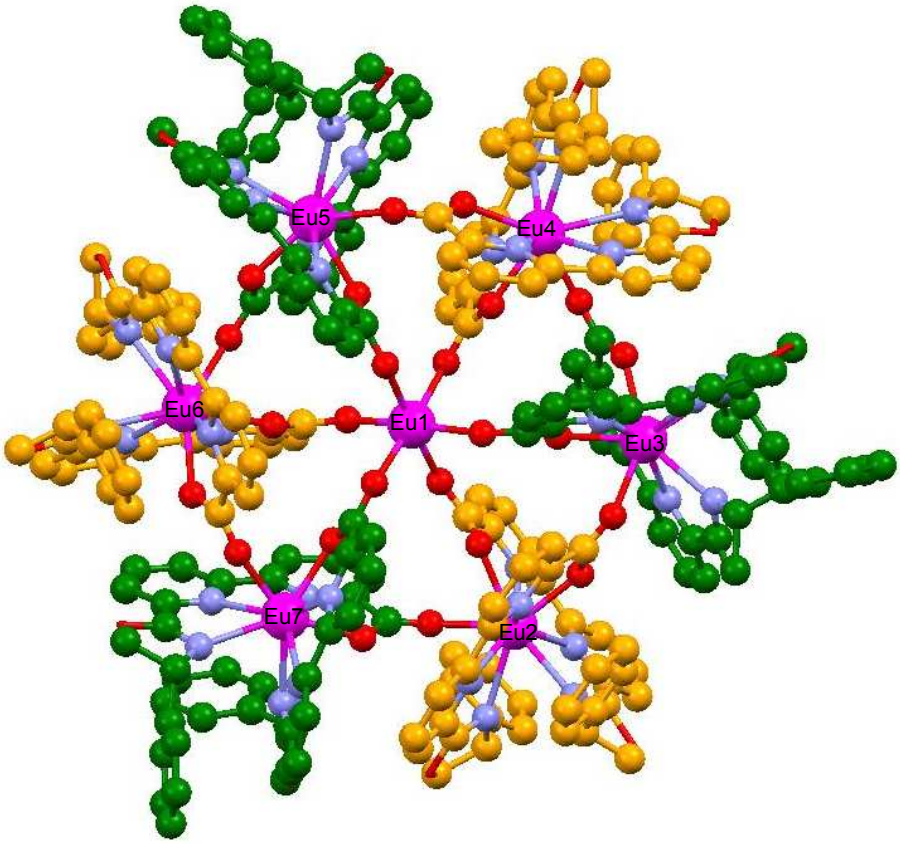

Figure III-43: Crystal structure of the cation $[Eu\subset(\Lambda\text{-Eu(R-Phbipox)}_2\Delta\text{-Eu(R-Phbipox)}_2)_3]^{9+}$. Oxygen: red; europium: pink; carbons of $[\Lambda\text{-Eu(R-Phbipox)}_2]^+$: green; carbons of $[\Delta\text{-Eu(Phbipox)}_2]^+$: orange

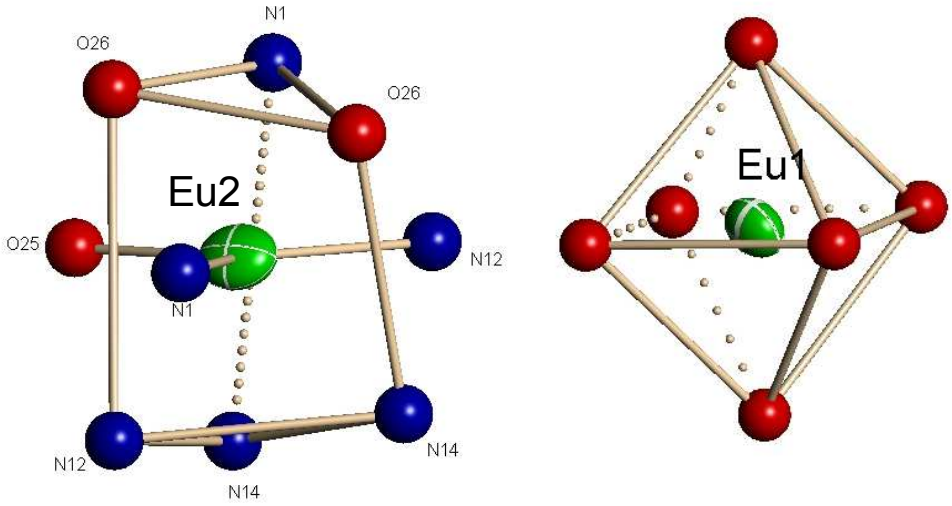

Figure III-44: Coordination polyhedrons of the europium ions in $[Eu_1 \subset (Eu_2(R\text{-}Phbipox)_2)_6](Otf)_9$

The six crystallographically inequivalent lanthanide ions of the noncentrosymmetric cation $[Eu \subset (\Lambda\text{-}Eu(R\text{-}Phbipox)_2\Delta\text{-}Eu(R\text{-}Phbipox)_2)_3]^{9+}$ are located in the corners of a pseudo-hexagon. The diameter of hexagon, defined as the distance of the two opposite europium ions, is 12.6 Å (Figure III-45) similar to the $[Eu \subset (Eu(terpya)_2)_6](Otf)_9$ **(XI)** wheel (12.5 Å) The pseudohexagon deviates only slightly from planarity with three europium (Eu2, Eu4, Eu6) situated above (+0.54 Å) and three europium ions (Eu1, Eu3, Eu5) situated below (-0.40 Å) the mean plane passing through the central Eu1 ion. The six carboxylate atoms are also located in the corners of a pseudohexagon with a smaller deviation from planarity.

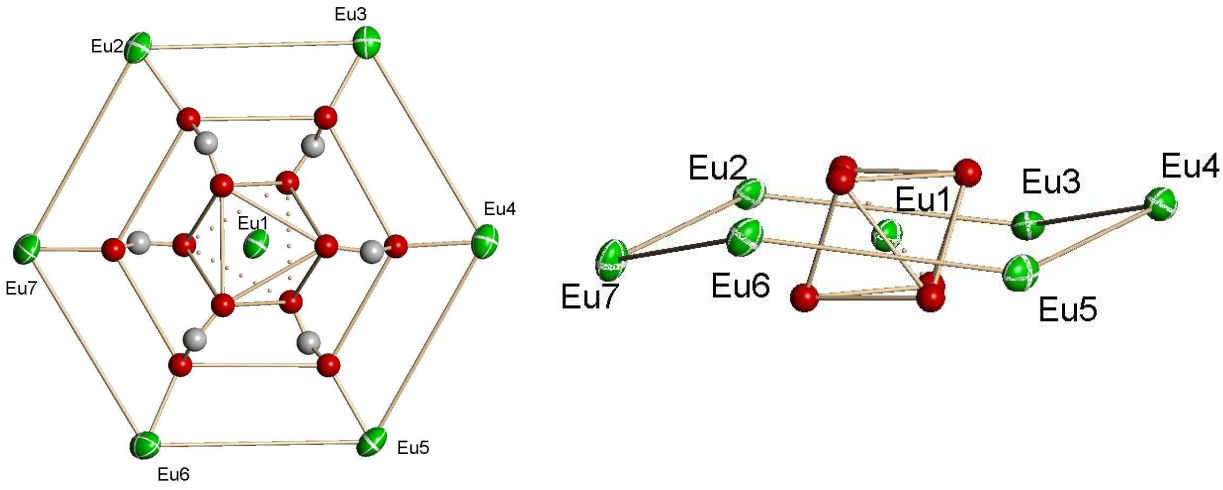

Figure III-45: Top and side view of the coordination polyhedron of Eu1 and of the hexagon formed by the carboxylate oxygens and the six Eu ions.

The angles between the two ligands mean planes are of 74.9(9)° for [Δ-Eu(R-Phbipox)$_2$]$^+$ and 71.1(9)° for [Λ-Eu(R-Phbipox)$_2$]$^+$ in the heptanuclear complex (**X**) which are smaller than the mononuclear [Eu(terpya)$_2$]$^+$ complexes (77.8°) in the **XI**. These angles are also smaller than in the mononuclear [Δ-Eu(R-Phbipox)$_2$]$^+$ (~90°) complex and in the mononuclear [Λ-Eu(R-Phbipox)$_2$]$^+$ (108°) units of the trinuclear {(ΛΛΛ)-[Eu(R-Phbipox)$_2$]$_3$}$^{3+}$ (**VIII**) complexes. Selected bond distances are given in Tables III-6 and III-7. The mean Eu-O distance 2.37(6) Å is smaller than the mean Eu-O distance found in trinuclear complex (2.39(2) Å) of **VIII** and in the **XI** (2.407(12) Å). The mean value of the Eu-N (2.58(6) Å) is similar to the one found in **XI** where Eu-N = 2.57(5) Å. The mean Eu1-O distance for the octahedral coordinated central europium ion in **X** is 2.33(3) Å is similar to the **XI** (2.31(1) Å). The Eu-Eu distances (Eu-Eu1 = 6.29(2) Å and Eu-Eu = 6.34(2) Å) are slightly longer than the ones measured in **XI** (6.24 Å and 6.29 Å). Similar to trinuclear and mononuclear complexes in **VIII** strong π-π interactions are found between the oxazoline phenyl rings of each tetradentate ligand and one pyridine ring of the other ligand (Table A2).

Table III-5: Selected bonds distances (Å) for the central cation in **X**

		Distance Å
Eu(1)-O25-7	(Eu5)	2.29(2)
Eu(1)-O25-3	(Eu4)	2.31(2)
Eu(1)-O25-6	(Eu3)	2.31(2)
Eu(1)-O25-12	(Eu2)	2.34(2)
Eu(1)-O25-1	(Eu7)	2.34(2)
Eu(1)-O25-9	(Eu6)	2.39(2)

Table III-6: Selected bonds distances (Å) for the cations located on the peripheral sites in **X**

	Distance Å		Distance Å
Eu(2)-O2511	2.28(2)	Eu(3)-O263	2.35(2)
Eu(2)-O261	2.42(2)	Eu(3)-O252	2.38(2)
Eu(2)-O262	2.45(2)	Eu(3)-O264	2.41(2)
Eu(2)-N12	2.48(2)	Eu(3)-N123	2.52(2)
Eu(2)-N122	2.56(2)	Eu(3)-N13	2.55(2)
Eu(2)-N121	2.58(2)	Eu(3)-N14	2.53(2)
Eu(2)-N141	2.602(19)	Eu(3)-N124	2.58(2)
Eu(2)-N11	2.60(2)	Eu(3)-N143	2.57(2)
Eu(2)-N142	2.71(2)	Eu(3)-N144	2.59(2)
Eu(4)-O254	2.36(2)	Eu(5)-O255	2.25(2)
Eu(4)-O265	2.39(2)	Eu(5)-O268	2.39(2)
Eu(4)-O266	2.433(19)	Eu(5)-O267	2.41(2)
Eu(4)-N146	2.53(2)	Eu(5)-N18	2.49(2)
Eu(4)-N15	2.55(2)	Eu(5)-N17	2.51(2)
Eu(4)-N16	2.57(2)	Eu(5)-N128	2.54(2)
Eu(4)-N125	2.58(2)	Eu(5)-N127	2.55(2)
Eu(4)-N126	2.65(3)	Eu(5)-N147	2.61(2)
Eu(4)-N145	2.69(3)	Eu(5)-N148	2.65(2)
Eu(6)-O258	2.34(2)	Eu(7)-O2612	2.365(19)
Eu(6)-O2610	2.37(2)	Eu(7)-O2611	2.39(2)
Eu(6)-O269	2.41(2)	Eu(7)-O2510	2.40(2)
Eu(6)-N110	2.57(2)	Eu(7)-N111	2.53(2)
Eu(6)-N19	2.59(2)	Eu(7)-N112	2.54(2)
Eu(6)-N129	2.61(2)	Eu(7)-N1212	2.55(2)
Eu(6)-N1210	2.61(2)	Eu(7)-N1211	2.58(3)
Eu(6)-N149	2.63(2)	Eu(7)-N1412	2.65(2)
Eu(6)-N1410	2.77(2)	Eu(7)-N1411	2.73(3)

4.2- NMR spectroscopy analysis

4.2.1 Assembly of Homopolymetallic Heptanuclear Complexes

The NMR spectrum of the isolated heptanuclear complex [Eu⊂(Λ-Eu(R-Phbipox)$_2$Δ-Eu(R-Phbipox)$_2$)$_3$](Otf)$_9$ (**X**) in anhydrous acetonitrile (Figure III-46) shows the presence of four sets of 12 signals in agreement with the presence of four different R-Phbipox ligands from two different (Δ and Λ) mononuclear complexes present in **X**. In these mononuclear complexes one R-Phbipox ligand coordinates to the neighbouring metal while the other ligand coordinates to the central ion with carboxylate oxygens. No other isomers have been observed in solution indicating the diastereoselective formation of the heptanuclear wheel from three delta and three lambda diastereomers as a result of the steric interactions of the phenyl substituents on the oxazoline ring as discussed in the previous section.

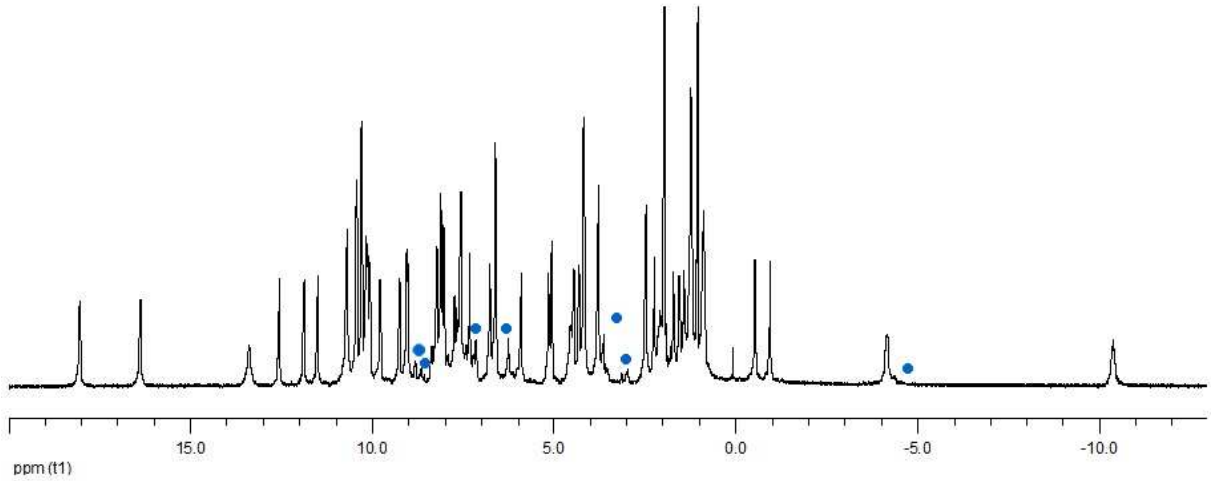

Figure III-46: ^{1}H NMR spectrum of a solution of isolated heptanuclear complex **X** with the minor mononuclear species (blue dots) 1 mM in anhydrous acetonitrile at 298 K and 500 MHz

In addition to the major heptanuclear species we have observed the peaks of minor mononuclear specie (blue dots in Figure III-46) in the NMR spectrum of the isolated complex. The presence of mononuclear species could be explained by the ratio of Δ/Λ = 0.6 being constant in acetonitrile solution at different concentrations (see Table III-3) indicating that no interconversion between the diastereomers occur for europium complexes. Therefore after the formation of wheel (**X**) with equal number of delta and lambda diastereomers, the excess lambda ([Λ-Eu(R-Phbipox)$_2$]$^+$) diastereomer is left in solution and does not interconvert to the lambda diastereomer or self assemble to higher nuclear species.

The overlapping of various signals (38 of the 48 signals) in a small region (0-11ppm) made it difficult to completely assign the protons existing in the heptanuclear complex (**X**). Therefore in order to verify the nuclearity and the presence of **X** in solution, a mixture of trinuclear **VIII** and heptanuclear **X** complexes has been prepared in deuterated acetonitrile. Pulsed-Field Gradient STimulated Echo (PFGSTE) diffusion NMR was used for measuring the diffusion coefficients (D) of the complexes in anhydrous acetonitrile [183]. Diffusion coefficient values are given in Table III-7. Reciprocal cube root dependence of the diffusion coefficient on molecular weight provided us a way to compare the nuclearity of our complexes present in solution. The values measured in acetonitrile are in agreement with the presence of trinuclear and heptanuclear complexes as the ratio of the molecular weights is equal to the reciprocal cube of the ratio of diffusion coefficients measured.

$$\frac{D_A}{D_B} = \sqrt[3]{\frac{M_B}{M_A}}$$

$$\frac{M_{Eu7L12}}{M_{Eu3L6}} = \left(\frac{D_{Eu3L6}}{D_{Eu7L12}} \right)^3 = 2.2$$

Stokes-Einstein equation has been applied to calculate the spherical hydrodynamic radius of the complexes as they have both globular shapes. The calculated values of the 8.0 Å for the trimeric species and 10.3 Å for the hexameric ones in acetonitrile compare very well with the values estimated from the crystal structure (7.7 and 10.1 Å respectively).

Table III-7: Diffusion coefficient values of $[Eu\subset(\Lambda\text{-}Eu(R\text{-}Phbipox)_2\Delta\text{-}Eu(R\text{-}Phbipox)_2)_3]^{9+}$ and $(\Lambda\Lambda\Lambda)\text{-}[Eu(R\text{-}Phbipox)_2]_3^{3+}$, and estimated spherical radii

Solvent	Compound	D [m².s^{-1}]	r_{sph} [Å]$_{exp}$
CD_3CN η=0.345 mPa.s^{-1} (298K)	$(\Lambda\Lambda\Lambda)\text{-}[Eu(R\text{-}Phbipox)_2]_3^{3+}$	7.90(5) 10^{-10}	8.0
	$[Eu\subset(\Lambda\text{-}Eu(R\text{-}Phbipox)_2\Delta\text{-}Eu(R\text{-}Phbipox)_2)_3]^{9+}$	6.08(6) 10^{-10}	10.3

The formation of $[Eu\subset(\Lambda\text{-}Eu(R\text{-}Phbipox)_2\Delta\text{-}Eu(R\text{-}Phbipox)_2)_3](Otf)_9$ has been followed by an NMR titration as given in Figure III-47. The addition of an excess $Eu(Otf)_3$ to a solution of mononuclear $[Eu(R\text{-}Phbipox)_2)](Otf)$ complexes in acetonitrile resulted in large changes in the NMR spectrum. At a Eu/EuL_2 ratio of 1/8 new peaks appeared (red squares) and the intensity of the peaks of trinuclear species (blue dots) decreased indicating the dissociation of these species. At the ratio of 1/6 (Eu/EuL_2) no more trinuclear species were present in solution. Obtained NMR spectrum was identical to the one of the isolated solid (Figure III-46). Addition of further europium triflates (at the ratio of 1/4 (Eu/EuL_2)) did not lead to the formation of additional species suggesting that the heptanuclear wheel is the only thermodynamically favored assembly in solution. In summary the trinuclear species present in solution dissociate with the additional metal ion and the cation assisted re-assembly of the mononuclear species leads to the formation of heptanuclear species.

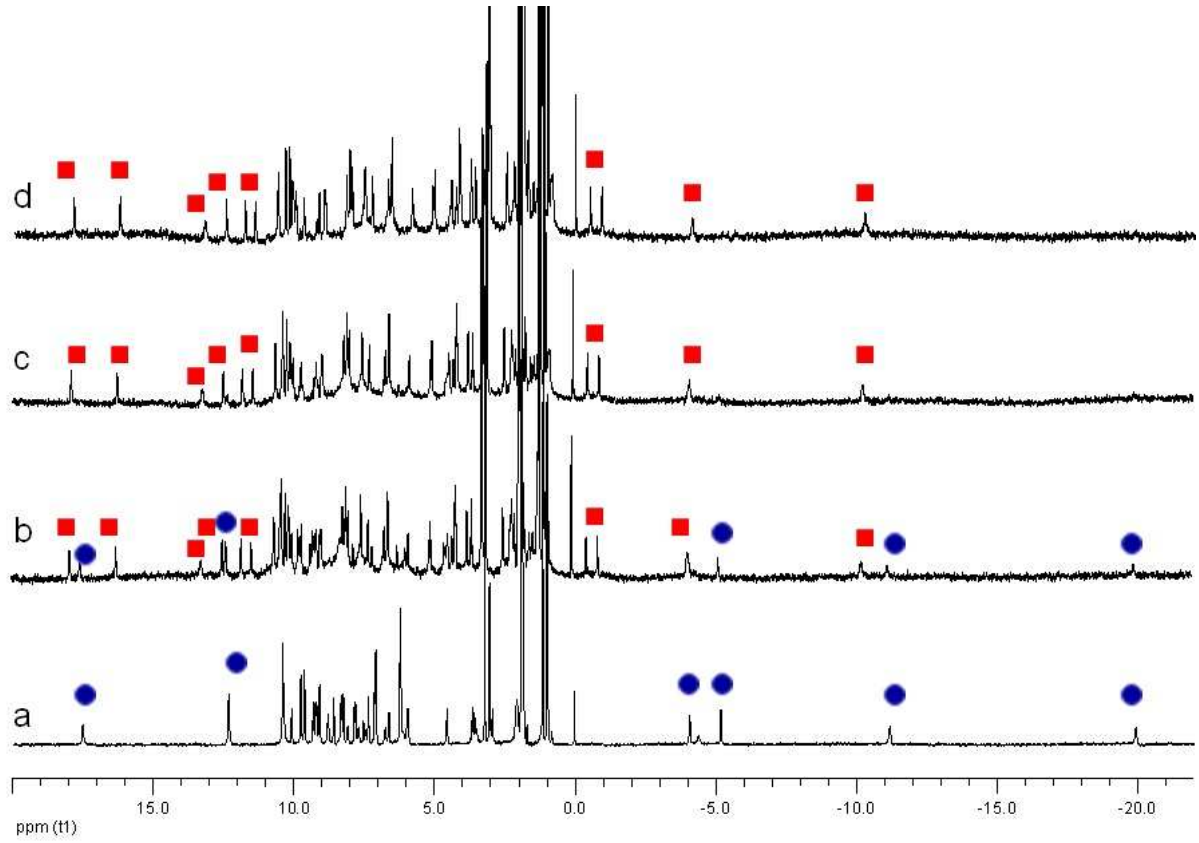

Figure III-47: ^1H NMR titration by addition of excess 1/8 (b), 1/6(c), 1/4(d) equivalent of $Eu(Otf)_3$ to a solution of (a) $[Eu(R\text{-}Phbipox)_2)](Otf)$ in anhydrous acetonitrile at 298 K and 500 MHz. Blue dots: trinuclear (**VIII**) complex and red squares: heptanuclear complex (**X**).

The proton NMR studies show that dissolution of the heptanuclear complex **X** in methanol or pyridine instead of acetonitrile leads to the disruption of the cyclic structure to give the corresponding mononuclear species as indicated by the presence of only 24 signals of two mononuclear species (Figure III-48). The NMR spectrum of the wheel in pyridine at first results in a mixture of mononuclear and wheel species (Figure III-48a). After one day the heptanuclear species dissociated to mononuclear species resulting in identical NMR spectrum to the mononuclear complexes (Figure III-48b). This should result from the coordination of solvent molecules displacing the carboxylate bridges.

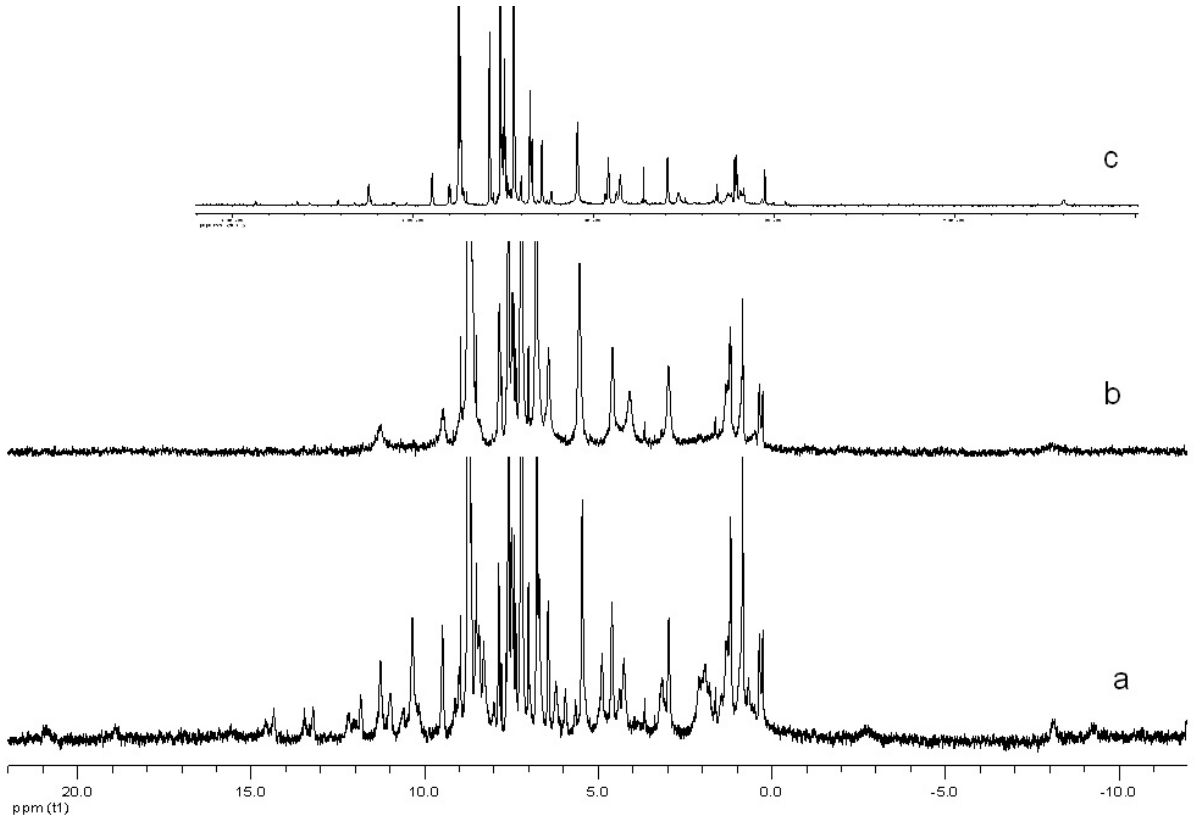

Figure III-48: ^{1}H NMR spectrum of a solution of [Eu⊂(Λ-Eu(R-Phbipox)$_2$Δ-Eu(R-Phbipox)$_2$)$_3$](Otf)$_9$ in a) anhydrous pyridine b) one day after c) mononuclear complex in py-d5 at 298 K and 500 MHz

Similarly addition of excess Nd(III) ion into the [Nd(R-Phbipox)$_2$]$^+$ complex in acetonitrile resulted in the isolation of heptanuclear complex. X-ray diffraction studies of the obtained crystals were not of sufficient quality to obtain a high quality structure, but the unit cell parameters confirmed the isostructural nature of the isolated complex to the Eu wheel. The proton NMR spectrum of the isolated complex shows 48 relatively narrow peaks (4 set of 12 peaks) indicating the presence of heptanuclear complex (Figure III-49). However due to the overlapping of the signals no assignment could be performed but satisfactory elemental analysis was obtained from the isolated crystals.

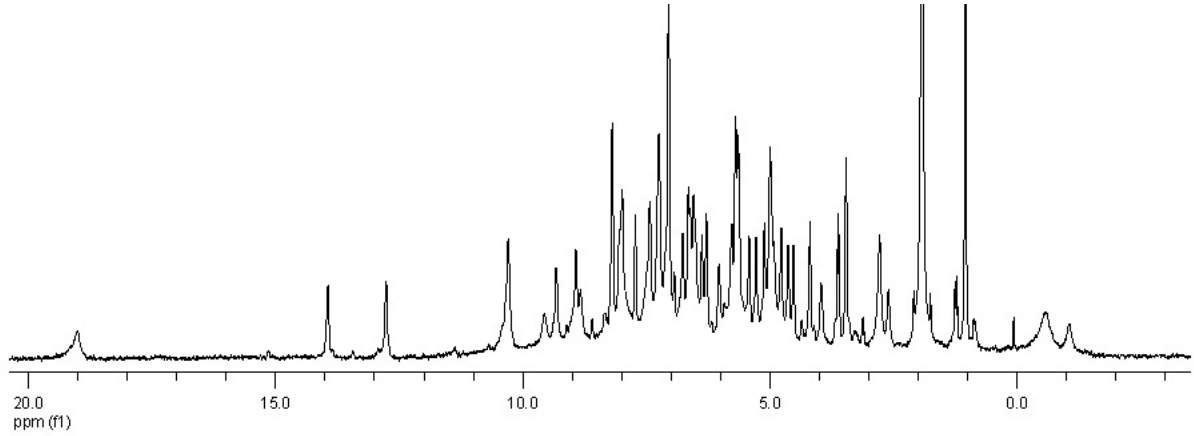

Figure III-49: ^{1}H NMR spectrum of a solution of [Nd⊂(Λ-Nd(R-Phbipox)$_2$Δ-Nd(R-Phbipox)$_2$)$_3$](Otf)$_9$ in anhydrous acetonitrile at 298 K and 500 MHz

In contrast to Eu and Nd wheel, the addition of an excess of Yb(III) ion into the 2:1 Yb complexes did not result in the formation of heptanuclear solution species, but only broad peaks are observed in the NMR spectrum indicating several species present in solution (Figure III-50). The size of the Yb ion is probably too small to allow the formation of the heptanuclear complex similar to **X**.

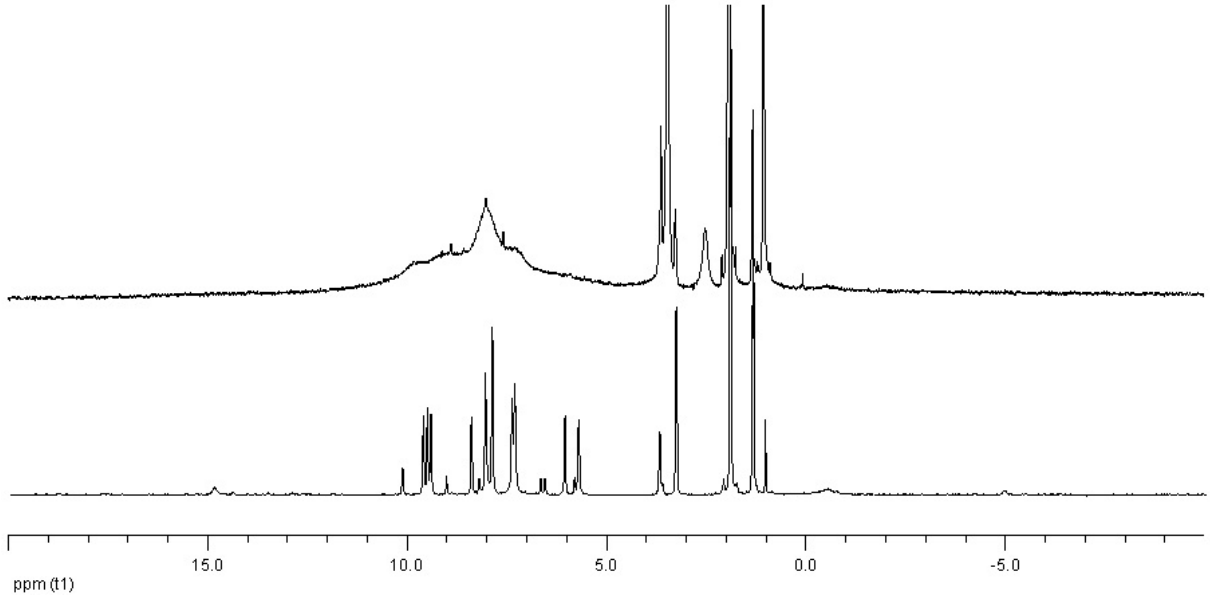

Figure III-50: ^{1}H NMR spectra of [Yb(R-Phbipox)$_2$](Otf) (lower spectrum) and [Yb(R-Phbipox)$_2$](Otf) +1/6 eq. of Yb(Otf)$_3$ (upper spectrum) in anhydrous acetonitrile at 298 K and 500 MHz

In order to check if racemic europium complex would allow a cation controlled chiral selective assembly formation, an NMR titration has been performed by adding 1/8 and 1/6 equivalent of Eu(Otf)$_3$ into racemic 2:1 complexes. Figure III-51 shows that the addition of excess metal ion resulted in broad peaks with several species therefore no selectivity induced

with assembly formation due to large number of diastereomers present in solution. No crystals could be grown from these solutions.

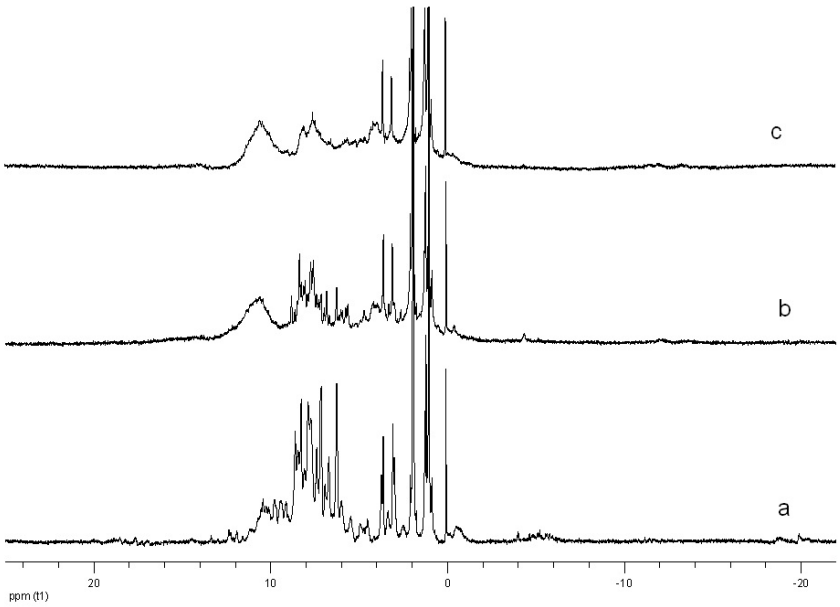

Figure III-51: ^{1}H NMR titration by addition of excess 1/8 (b), 1/6(c) equivalent of $Eu(Otf)_3$ to a solution of (a) $[Eu(rac\text{-}Phbipox)_2)](Otf)$ in anhydrous acetonitrile at 298 K and 500 MHz.

4.2.2 Assembly of Heteropolymetallic Heptanuclear Complexes

The molecular structure of the $[Ln\subset(\Lambda\text{-}Ln(Phbipox)_2\Delta\text{-}Ln(Phbipox)_2)_3](Otf)_9$ complexes presents two very different coordination environments and therefore is well adapted for the assembly of heterobimetallic complexes. The synthetic strategy developed to assemble pure heterobimetallic complexes for terpyacid ligand was applied to our chiral system [105]. We investigated the $[Ln\subset(\Lambda\text{-}Ln(Phbipox)_2\Delta\text{-}Ln(Phbipox)_2)_3](Otf)_9$ complexes with Ln = Lu, Yb and Ln = Eu, Nd. The preliminary NMR studies indicate that the addition of 0.16 equivalent of Yb or Lu ion into the $[Ln(R\text{-}Phbipox)_2](Otf)$ (Ln = Eu, Nd) in anhydrous acetonitrile result in clean in situ NMR spectra (Figures III-52, III-53). The proton NMR spectra of these heterometallic species are highly symmetric with 48 signals for the 4 sets of Phbipox ligands in agreement with the presence of the complex $[Ln\subset(\Lambda\text{-}Ln(Phbipox)_2\Delta\text{-}Ln(Phbipox)_2)_3](Otf)_9$ in which smaller lanthanide ion is located at the center of the cyclic framework.

The NMR spectra of the complexes are very similar suggesting an analogous solution structure for the three europium complexes (Ln = Eu, Lu, Yb and Ln = Eu) (Figure III-52). As already observed with terpya heterometallic wheels, the NMR spectra show differences only in the the chemical shifts of the protons closer to the central metal ion (signals in the

region 10-20 ppm in Figure III-52c). The signals (can be assigned to the pyridine protons next to the carboxylate binding the central atom by 2D NMR spectroscopy) are significantly affected by the replacement of the paramagnetic Eu(III) ion with the diamagnetic Lu(III) ion (Figure (III-52a)) by shifting to the diamagnetic region. When Yb(III) ion is added the signals are spread over a large spectral window due to the high paramagnetic character of the Yb(III) ion (signals in the region 10-40 ppm in Figure III-52b) compared to the Eu(III) or Nd (III) ions (Figure III-52b, III-53).

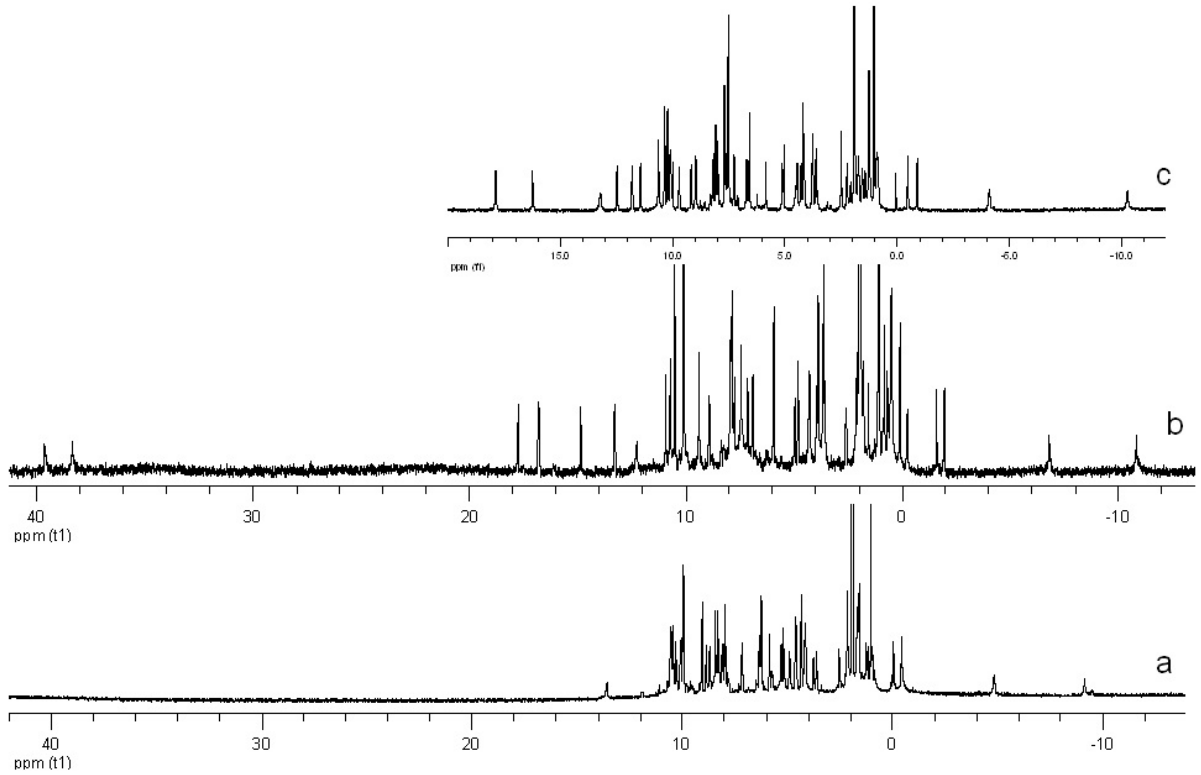

Figure III-52: ^{1}H NMR spectrum of a solution of [Ln⊂(Λ-Eu(Phbipox)$_2$Δ-Eu(Phbipox)$_2$)$_3$](Otf)$_9$ Ln= Lu a), Yb b), Eu c) in anhydrous acetonitrile at 1mM at 298 K and 500 MHz

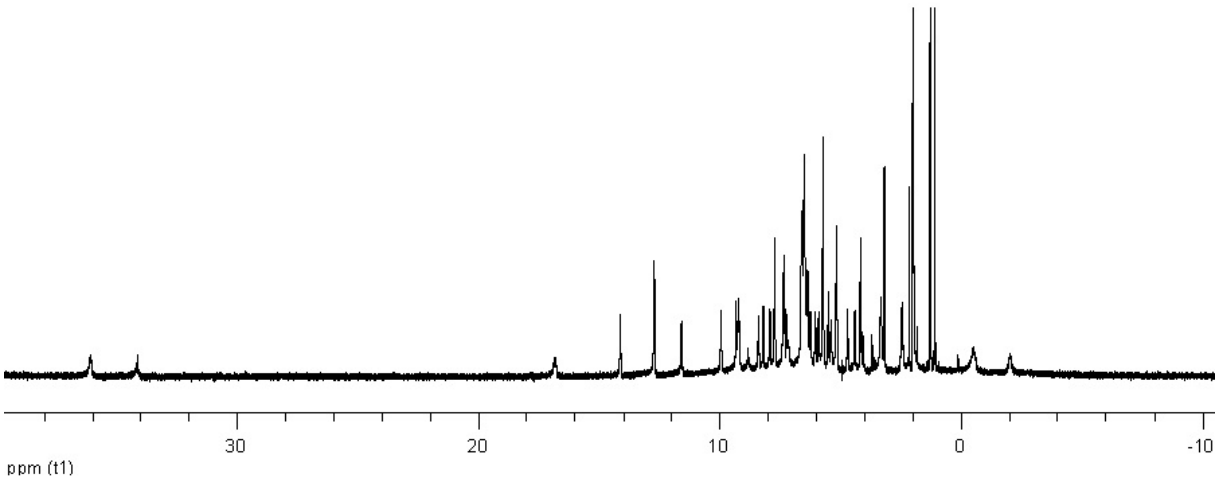

Figure III-53: ^{1}H NMR spectrum of a solution of [Yb⊂(Λ-Nd(Phbipox)$_2$Δ-Nd(Phbipox)$_2$)$_3$](Otf)$_9$ in anhydrous acetonitrile at 298 K and 500 MHz

In contrast the addition of ions larger than the ones in the peripheral sites does not lead to the assembly formation but results in mixture of species. These results show that similar to terpya ligand the heterobimetallic assembly formation with Phbipox ligand is also controlled by the size of the lanthanide ion. The formation of lanthanide wheel requires the smaller ionic size of the central ion compared to the ones in the peripheral sites.

5- Chiroptical Studies

Circular Dichroism (CD) studies were carried out in methanol and acetonitrile solution of the complexes. The Circular Dichroism of a sample is defined as the differential absorption of right and left polarized light ($\Delta\varepsilon = \varepsilon L - \varepsilon R$). CD measurements indicate that the ligand Phbipox and the europium complexes are chiral in solution, without any evidence of epimerization.

The compounds show chiroptical activity in the range 220-350 nm. The CD profiles of the enantiopure complexes S and R obtained with the same metal are expected to be mirror images. Figure III-54 shows the UV absorption and mirror-image CD spectra between the complexes with R and S ligands. The racemic ligand and complexes (green line in Figure III-54) show no CD signal as expected, confirming the 50%-50% racemic (R/S) mixture.

The CD measurements confirm that the Ln complexes retain their chiroptical properties once the ligand is coordinated to the Ln and that the sign of the CD is dependent on the absolute configuration of the chiral center of the ligand (CD sign changes when going from R to S). The spectra are dominated by two bands centered around 270 and 320 nm corresponding to the absorption bands relative to the $n\rightarrow\pi^*$ and $\pi\rightarrow\pi^*$ transitions of the ligand. When the S enantiomer of the ligand is employed, the band at 270 nm assumes a negative sign whereas the band at 320 nm shows a positive Cotton effect. The opposite behaviour observed when the R enantiomer of the ligand is used for complexation. The absorption maximum at ca. 319 nm undergoes a bathochromic shift to ca. 331 nm upon complexation similarly both for UV and CD spectra.

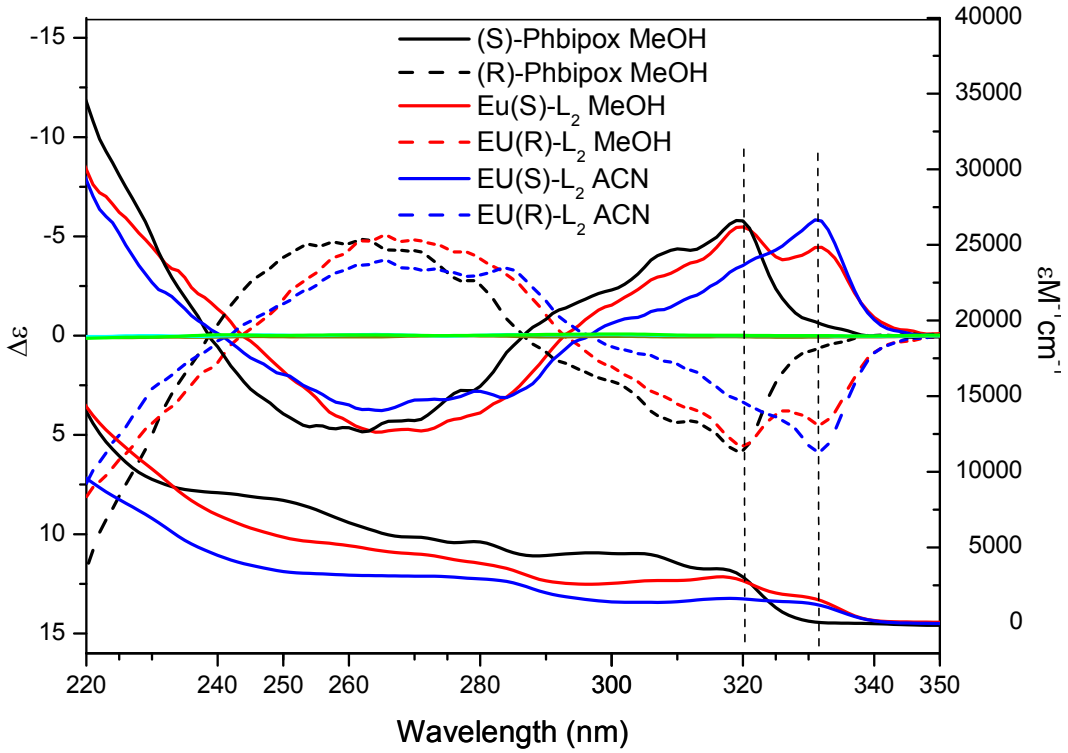

Figure III-54: The UV absorption (lower curves, right axis) and CD spectra (upper curves, left axis) of the deprotonated ligand (black) and the 2:1 complexes in methanol (red) and acetonitrile (blue) at 0.02 mM ligand concentration. Solid lines: S enantiomer, dashed lines R enantiomer, and green line racemic ligand and complexes

The concentration dependence of the assembly formation prevented us from obtaining more specific information from CD on the chirality of the diastereomers (Δ/Λ) observed in NMR at minimum 6 mM concentrations. The CD spectra of the complexes in methanol possess the bands of the free ligand. Similarly the NMR spectrum of Eu complexes in methanol shows the presence of free ligand at the concentration of 0.02 mM due to partial dissociation of the complex. The saturation of organic solvents at high concentration limits the usage of CD for concentration dependent self-assembly studies. Therefore we could not obtain information on the diastereomers or trinuclear species from these CD studies. Although high concentration CD measurements could be performed with a long pathway (10 cm-cuvette), we could not perform that as this would require a large volume of the complex. Another limitation of CD for lanthanide complexes arise from the very low molar extinction coefficients associated with Laporte forbidden f-f transitions. That is the reason why the CPL provide a better picture of the systems of interest (based on the chiroptical properties from the local environment of the Ln ion, whereas the CD measurements are based on the ligand bands).

6- Circularly Polarized Luminescence Studies

The circularly polarized luminescence (CPL) is an emission analogue of CD. CPL measures the difference in the emission intensity of left and right circularly polarized light in order to analyze the excited state chirality. CPL is one of the most sensitive techniques that provide information on the chiral environment of the lanthanide ion with regard to polarized emission bands corresponding to metal centered transitions [184]. The degree of chirality of lanthanide complexes is expressed by luminescence dissymmetry factor (g_{lum}) defined as:

$$g_{lum}(\lambda) = \frac{2\Delta I}{I} = \frac{2(I_L - I_R)}{(I_L + I_R)} \qquad \textbf{III-2}$$

where I_L and I_R refer, respectively to the intensity of left and right circularly polarized emissions [185]. For Eu(III) ion the largest glum factors are obtained in correspondence to transitions $^5D_0 \rightarrow {}^7F_1$ and $^5D_0 \rightarrow {}^7F_2$. The magnetic dipole allowed $^5D_0 \rightarrow {}^7F_1$ transition is more sensitive to the chiral environment therefore displays g_{lum} values slightly higher than the ones obtained from electric dipole allowed $^5D_0 \rightarrow {}^7F_2$ transitions. CPL measurements of our complexes have been performed by Gilles Muller in San José University, USA. Here we will give the preliminary results obtained by these studies.

a) [Eu(S/R-Phbipox)$_2$](Otf)

The CPL and laser excitation measurements were performed on [Eu(S-Phbipox)$_2$](Otf), [Eu(R-Phbipox)$_2$](Otf) in anhydrous 6 mM methanol and 1, 2 and 6 mM acetonitrile. A strong CPL signal was measured for both solvents upon UV excitation. The CPL spectra of the studied $^5D_0 \rightarrow {}^7F_1$ and $^7F_2$ transitions display several peaks corresponding to the crystal-field splitting of electronic levels. As in the case of CD, the complexes ([Eu(S-Phbipox)$_2$](Otf) and [Eu(R-Phbipox)$_2$](Otf)) synthesized from both enantiomers of the ligand give rise to mirror image $^5D_0 \rightarrow {}^7F_1$ transition CPL spectra as expected (Figure III-55). Summary of the CPL results are given in Table III-5.

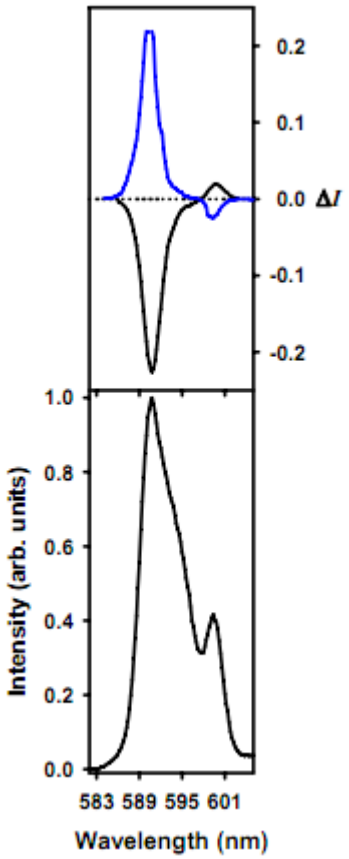

Figure III-55: Circularly Polarized Luminescence (upper curves) and total luminescence (lower curves) spectra of the $^5D_0 \rightarrow {}^7F_1$ transition of [Eu(S-Phbipox)$_2$](Otf) (blue) and [Eu(R-Phbipox)$_2$](Otf) (black) in 6 mM anhydrous CH_3CN solutions at 295 K, upon excitation at 335-338 nm, respectively

The CPL spectra of the complexes in different concentrations were registered and compared with the NMR spectra at these concentrations. The CPL spectra of the complex [Eu(R-Phbipox)$_2$](Otf) in CH_3CN at 1 and 6 mM shows differences in the magnitude, sign, and shape of the signals as shown in Figure III-56. Similarly the dissymmetry factor g_{lum} increases linearly with concentration (Table III-5). Figure III-57 summarizes the concentration dependence of g_{lum} value for S and R complexes. These differences indicate that the chiral structure of the Eu(III) complex is dependent on the concentration. In acetonitrile solution there exist three species: two mononuclear delta and lambda diastereomers and the homochiral trinuclear species. We have seen earlier in NMR spectra (Figure III-26) that the increase of concentration promotes the diastereoselective assembly formation of trinuclear complexes from one of the two diastereomers. The change in the CPL activity at different concentrations correlates with the NMR studies suggesting that the trinuclear species have higher CPL activity compared to mononuclear species. Therefore the increase of trinuclear species or decrease of one mononuclear species due to assembly formation leads to a total

increased CPL activity. Hence, the magnitude of the CPL signal from the 1 mM complex solution in anhydrous CH_3CN is smaller than observed for the 6 mM anhydrous CH_3CN solution. Differences can also be seen in the total luminescence spectra of the Eu(III) complex with different crystal field splitting in 1 and 6 mM anhydrous CH_3CN solutions (Figure III-56 lower curves) due to different species present in solutions.

Table III-8: Dissymmery factors obtained by the CPL measurements of the Eu(III) complexes. at the $^5D_0 \rightarrow {}^7F_1$ (magnetic dipole) and $^5D_0 \rightarrow {}^7F_2$ (electric dipole) transitions

Complex	Electronic transition	Λ [nm]	g_{lum}	Solvent
[Eu(R-Phbipox)$_2$](Otf) (λexc = 331nm)	$^5D_0 \rightarrow {}^7F_1$	592.8	-0.04	1 mM CH_3CN
		597.2	-0.01	
	$^5D_0 \rightarrow {}^7F_2$	613.0	+0.007	
		619.4	+0.04	
[Eu(R-Phbipox)$_2$](Otf) (λexc = 335 nm)	$^5D_0 \rightarrow {}^7F_1$	590.8	**-0.45**	6 mM CH_3CN
		599.8	+0.10	
	$^5D_0 \rightarrow {}^7F_2$	612.4	+0.02	
		620.2	+0.11	
[Eu(R-Phbipox)$_2$](Otf) (λexc = 334 nm)	$^5D_0 \rightarrow {}^7F_1$	588.6	-0.06	6 mM CH_3OH
		598.8	-0.05	
	$^5D_0 \rightarrow {}^7F_2$	612.4	+0.02	
		620.2	+0.11	
[Eu(S-Phbipox)$_2$](Otf) (λexc = 334 nm)	$^5D_0 \rightarrow {}^7F_1$	593.0	+0.06	1 mM CH_3CN
		598.8	-0.02	
	$^5D_0 \rightarrow {}^7F_2$	614.0	-0.003	
		620.8	-0.02	
[Eu(S-Phbipox)$_2$](Otf) (λexc = 335 nm)	$^5D_0 \rightarrow {}^7F_1$	590.6	+0.15	2 mM CH_3CN
		598.8	-0.02	
	$^5D_0 \rightarrow {}^7F_2$	613.8	-0.005	
		620.8	-0.04	
[Eu(S-Phbipox)$_2$](Otf) (λexc = 338 nm)	$^5D_0 \rightarrow {}^7F_1$	590.8	**+0.45**	6 mM CH_3CN
		599.8	-0.10	

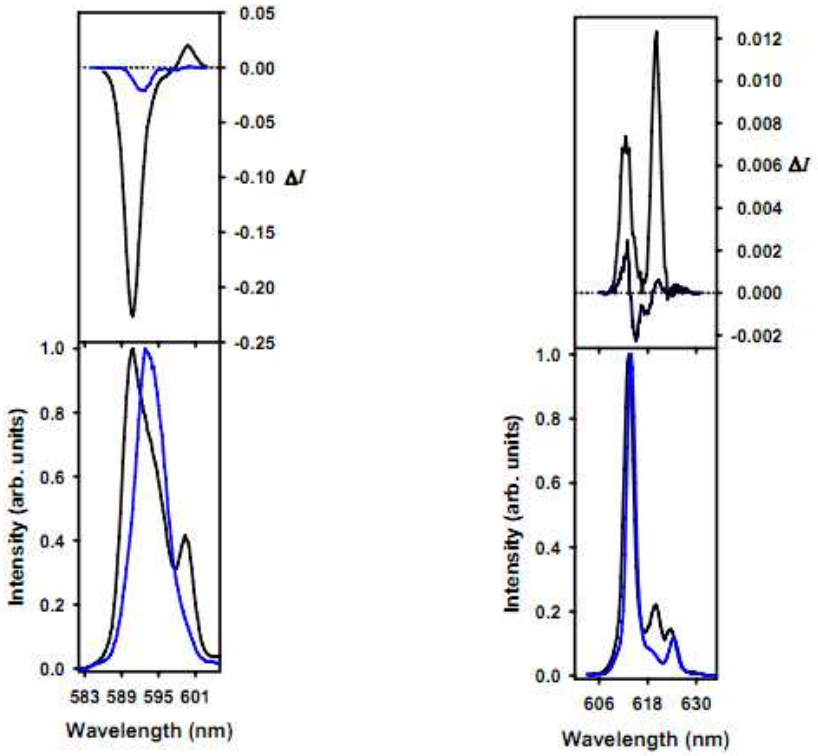

Figure III-56: Circularly Polarized Luminescence (upper curves) and total luminescence (lower curves) spectra of the $^5D_0 \rightarrow {}^7F_1$ (left) and $^5D_0 \rightarrow {}^7F_2$ (right) transitions of the [Eu(R-Phbipox)$_2$](Otf) , in 1 (blue) and 6 (black) mM anhydrous CH_3CN solutions at 295K, upon excitation at 331 and 335 nm, respectively

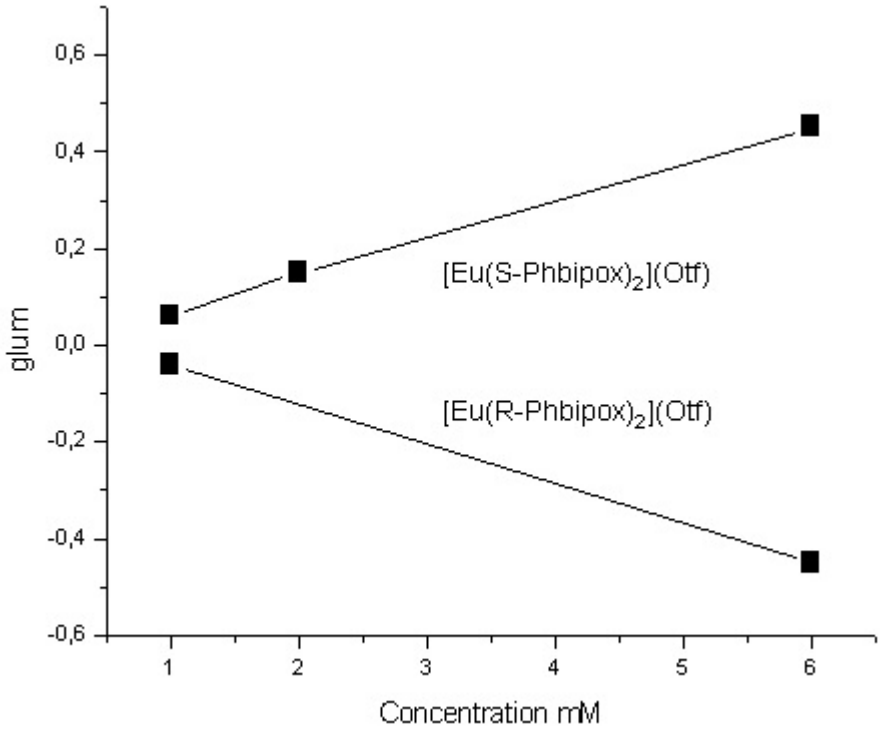

Figure III-57: Concentration dependence of the glum value at $^5D_0 \rightarrow {}^7F_1$ transition for [Eu(S-Phbipox)$_2$](Otf), [Eu(R-Phbipox)$_2$](Otf) at 1, 2 and 6 mM anyhdrous acetonitrile

Similarly the difference in magnitude, sign and shape of the luminescence and CPL signals indicates that the Eu(III) complex does not present the same crystal field structure solution in 6 mM anhydrous acetonitrile and methanol solutions (Figure III-58). Moreover the dissymmetry factor in methanol solution is more than 7 times smaller than the g_{lum} value in acetonitrile. The NMR spectra of complexes at 6 mM solutions of deuterated methanol (Figure III-24) and acetonitrile (Figure III-27) show that in methanol solution only mononuclear complexes exist, while in acetonitrile the presence of trinuclear complexes is observed due to lower polarity and lower coordinating ability of this solvent. We have already seen an increase of CPL activity with increase in concentration in acetonitrile due to the formation of trinuclear species. Similarly the difference in CPL activity in methanol and acetonitrile is due to the absence of trinuclear species in methanol at the concentration of 6 mM. This study is a good example showing that CPL is a good technique to study the self assembly of chiral complexes in solution.

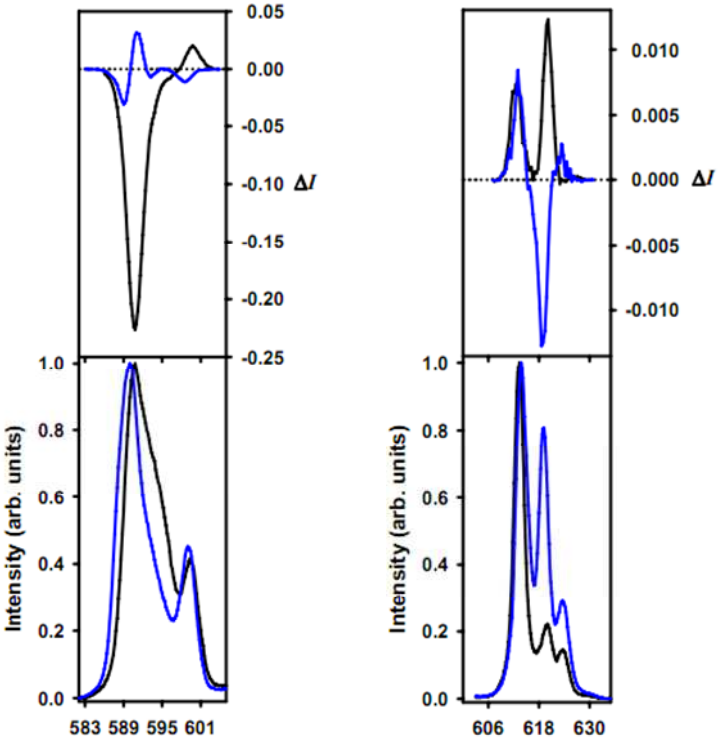

Figure III-58: Circularly Polarized Luminescence (upper curves) and total luminescence (lower curves) spectra of the $^5D_0 \rightarrow {}^7F_1$ (left) and $^5D_0 \rightarrow {}^7F_2$ (right) transitions of the [Eu(R-Phbipox)$_2$](Otf) , in 6 mM anhydrous CH_3CN (black) and anhydrous CH_3OH (blue) solutions at 295 K, upon excitation at 335 and 334 nm, respectively

One very important and interesting result is that Eu(III) complexes exhibit a high CPL activity in 6 mM anhydrous acetonitrile solution with a g_{lum} value of -0.45 [Eu(R-Phbipox)$_2$](Otf) and +0.45 [Eu(S-Phbipox)$_2$](Otf) ({Eu($^5D_0 \rightarrow {}^7F_1$)}) (Table III-5). This should

result from the trinuclear species as the g_{lum} values at lower concentration in acetonitrile or in methanol solutions are less than 0.10. This g_{lum} value is larger than for most of the Eu complexes reported in literature showing strong CPL activities. For example Eu(III) complexes with hydroxyl-2-isophthalamide-, pyridiyl amide-, DOTA based ligand derivates exhibited glum values of +0.29, +0.18, +0.40 respectively [159, 162, 186]. Recently Eu complexes with g_{lum} values of 0.44, and 0.47 has been reported with ternary europium complexes of 3-trifluoroacetyl-d-camphor (D-facam) and 2,20-bis(diphenylphosphoryl)-1,10 binaphthyl or triphenylphosphine oxide ligands respectively [187]. To date the highest CPL activity is reported with a g_{lum} value as high as 1.38 for Eu complexes with a chiral 3-heptafluorobutylryl-(+)-camphorato ligand in chloroform[188]. Other than these mononuclear complexes a few CPL studies have been reported with polynuclear complexes. For example the trinuclear enantiopure europium assembly with bipyridine pinene ligand (Figure III-11) of Mamula et al. [166] have a glum of -0.16, while recently reported enantiopure dimetallic triple stranded helicate [168] have a glum of -0.23 which are lower than the value we have obtained for our trinuclear complex.

These preliminary CPL results are really promising where interesting CPL activity of the characterized species in solution give complementary information to the NMR studies. The [Eu(S-Phbipox)$_2$](Otf) complex in acetonitrile at 6 mM concentration exhibit one of the strongest CPL activities recorded with lanthanide complexes. Therefore we will study further the CPL activity of our Nd and Yb complexes where different speciation and chiral induction have been observed depending on the ion size. These studies are expected to contribute to a better understanding of CPL properties of our complexes in solution.

b) [Eu⊂(Eu(S-Phbipox)$_2$)$_6$](Otf)$_9$

The CPL spectra of the $^5D_0 \rightarrow {}^7F_1$ and $^7F_2$ transitions of [Eu⊂(Eu(S-Phbipox)$_2$)$_6$](Otf)$_9$ were recorded at a concentration of 1 and 2 mM in anhydrous acetonitrile. The preliminary results will be discussed here. Slight changes have been observed in the shape and magnitude of the CPL signal and in the total luminescence spectra as shown in Figure III-59 by 2-fold dilution. Similar luminescence dissymmetry factors (glum) (Table III-9) were obtained at these two different concentrations.

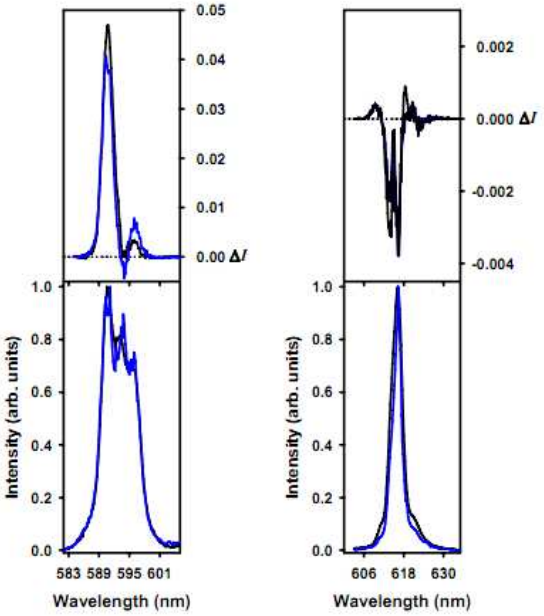

Figure III-59: Circularly Polarized Luminescence (upper curves) and total luminescence (lower curves) spectra of the $^5D_0 \rightarrow {}^7F_1$ (left) and $^5D_0 \rightarrow {}^7F_2$ (right) transitions of $[Eu \subset (Eu(S\text{-}Phbipox)_2)_6](Otf)_9$ in 1 (black) and 2 (blue) mM anhydrous CH_3CN solutions at 295 K, upon excitation at 344 and 348 nm, respectively

The presence of excess mononuclear species in solution has been verified by the $^5D_0 \leftarrow {}^7F_0$ excitation spectra (Figure III-60) of 1 and 2 mM solutions of the $[Eu \subset (Eu(S\text{-}Phbipox)_2)_6](Otf)_9$ complex solutions. In addition to the major heptanuclear wheel species, minor species have been observed since the maximum peak at ~ 581.0 nm is accompanied by shoulders before and after it. The presence of minor mononuclear species has already been shown by NMR spectrum of the isolated complexes (Figure III-46). The base of the maximum peak becomes narrower at 2 mM solutions with a slight decrease of the intensity of the minor species which could be due to the presence of small amount of trinuclear complex.

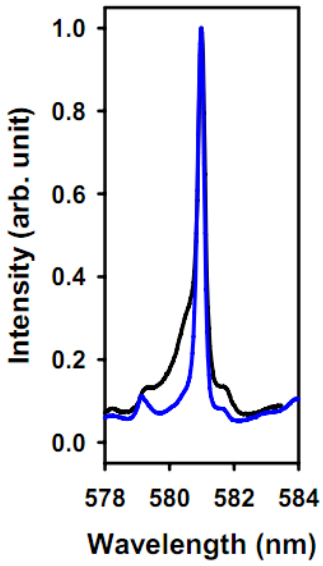

Figure III-60: The $^5D_0 \leftarrow ^7F_0$ excitation spectra of of $[Eu \subset (Eu(S\text{-}Phbipox)_2)_6](Otf)_9$ in 1 (black) and 2 (blue) mM anhydrous CH_3CN solutions at 295 K, upon monitoring at ~615 nm in the spectral range of the $^5D_0 \rightarrow ^7F_2$ emission transition, respectively

No significant increase in the CPL activity was obtained by formation of wheel from mononuclear complexes. The g_{lum} value of around 0.10 (λ = 590.6 nm) was obtained from the heptanuclear wheel $[Eu \subset (Eu(S\text{-}Phbipox)_2)_6](Otf)_9$ while a value of 0.06 was measured for the $[Eu(S\text{-}Phbipox)_2)](Otf)$ in 1 mM acetonitrile (Table III-9). An explanation to this result could be the equal amount of delta and lambda diastereomers in the wheel structure with opposite CPL signal cancelling each other resulting in small CPL effect. The final CPL activity should be coming from the contribution of the minor mononuclear excess delta specie present in solution as the glum values are similar to the ones from the $[Eu(S\text{-}Phbipox)_2)](Otf)$ complex in 1 mM acetonitrile. In addition to Eu wheel, CPL studies with homopolymetallic Nd or heteropolymetallic wheel complexes will be conducted in the future.

Table III-9: Dissymmery factors obtained by the CPL measurements of the heptanuclear Eu(III) wheel at the $^5D_0 \rightarrow {}^7F_1$ (magnetic dipole) and $^5D_0 \rightarrow {}^7F_2$ (electric dipole) transitions

Complex	Electronic transition	λ [nm]	g_{lum}	Solvent
$[Eu \subset (Eu(S\text{-}Phbipox)_2)_6](Otf)_9$ (λexc=344 nm)	$^5D_0 \rightarrow {}^7F_1$	590.6	+0.10	1 mM CH_3CN
		595.6	+0.01	
	$^5D_0 \rightarrow {}^7F_2$	614.0	-0.01	
		616.4	-0.006	
$[Eu \subset (Eu(S\text{-}Phbipox)_2)_6](Otf)_9$ (λexc=348 nm)	$^5D_0 \rightarrow {}^7F_1$	590.6	+0.09	2 mM CH_3CN
		595.6-596.0	+0.02	
	$^5D_0 \rightarrow {}^7F_2$	614.0	-0.01	
		616.4	-0.006	
$[Eu(S\text{-}Phbipox)_2]Otf$ (λexc=334 nm)	$^5D_0 \rightarrow {}^7F_1$	593.0	+0.06	1 mM CH_3CN
		598.8	-0.02	
	$^5D_0 \rightarrow {}^7F_2$	614.0	-0.003	
		620.8	-0.02	
$[Eu(S\text{-}Phbipox)_2]Otf$ (λexc=335 nm)	$^5D_0 \rightarrow {}^7F_1$	590.6	+0.15	2 mM CH_3CN
		598.8	-0.02	
	$^5D_0 \rightarrow {}^7F_2$	613.8	-0.005	
		620.8	-0.04	

7- Photophysical Properties of Lanthanide Complexes

7.1- Metal-Centered Luminescence of the visible emitting lanthanide complexes

The excitation spectra of the europium complexes are presented in Figure III-61 and have been recorded in solid state, methanol and acetonitrile solutions at 295 K monitoring on the Eu($^5D_0 \rightarrow {}^7F_2$) transition. The excitation spectrum of the [Eu(R-Phbipox)$_2$](Otf) complex, in solid state, displays one intense broad band between 30 000 and 26 000 cm^{-1} with a maximum at 28 630 cm^{-1} assigned to ligand $^1\pi\pi^*$ states. In addition, the excitation spectrum displays several features arising from direct excitation onto the Eu(III) excited levels: ^5D_J (J = 2, 3 at 21 505 and 24 096 cm^{-1}, respectively) and $^5L_6$ (25 381 cm^{-1}). In acetonitrile a similar excitation spectrum was obtained with a maximum at 28 674 cm^{-1} and in methanol the broad band is blue shifted *ca.* 300 cm^{-1}. Weaker specific Eu ($^5D_{2,\ 3}$) bands were also observed in methanol and acetonitrile solutions. For the [Eu⊂(Λ-Eu(R-Phbipox)$_2$Δ-Eu(R-Phbipox)$_2$)$_3$](Otf)$_9$ and [Lu⊂(Λ-Eu(R-Phbipox)$_2$Δ-Eu(R-Phbipox)$_2$)$_3$](Otf)$_9$ complexes, essentially identical data were observed with a broad band at high energy and the excitation to the $^5D_2$ and $^5D_3$ was clearly seen.

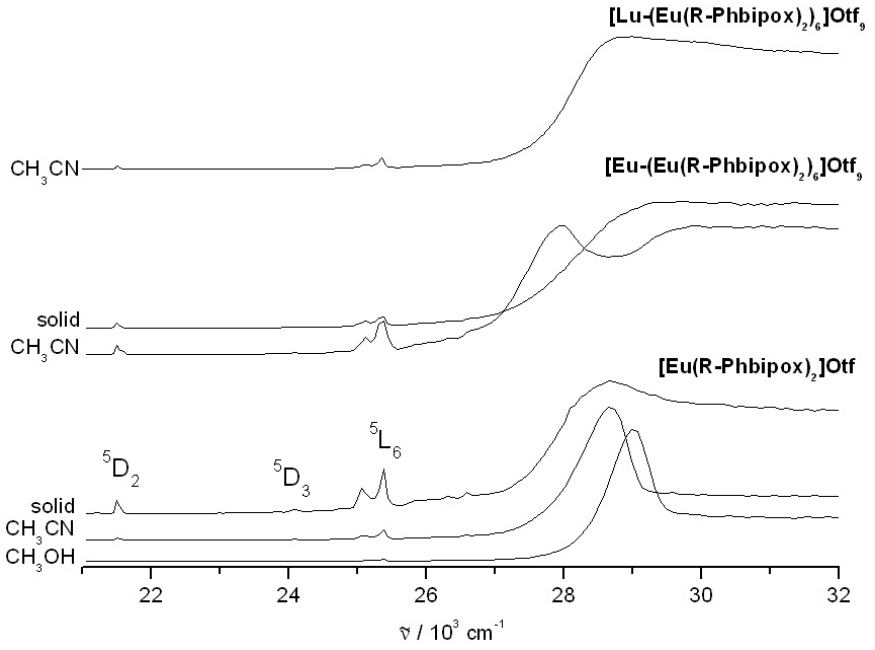

Figure III-61: Normalized excitation spectra of the [Eu(R-Phbipox)$_2$]Otf, [Eu⊂(Λ-Eu(R-Phbipox)$_2$Δ-Eu(R-Phbipox)$_2$)$_3$](Otf)$_9$ and [Lu⊂(Λ-Eu(R-Phbipox)$_2$Δ-Eu(R-Phbipox)$_2$)$_3$](Otf)$_9$ complexes at 295 K upon monitoring the Eu($^5D_0 \rightarrow {}^7F_2$) transition in solid state, 6 mM in methanol and 6 mM inacetonitrile

The emission spectra of the complexes obtained upon excitation through the ligand levels, display the characteristic Eu($^5D_0 \rightarrow {}^7F_J$) transitions ($J$ = 0-4) (Figure III-62, 63). No faint residual ligand centered $^1\pi\pi^*$ emission is detected pointing to a quantitative ligand to Eu(III) energy transfer process. The emission of the Eu(III) is dominated by the transitions to the $^7F_2$ sublevels (the ratio of the integrated emission of the $^5D_0 \rightarrow {}^7F_2$ transition to the integrated total emission from the $^5D_0 \rightarrow {}^7F_J$ transitions (J=0-4), is 0.5-0.6). The resolution is sufficient to interpret the symmetry around the Eu(III) ions and the electronic sub-levels of the ^7F_J (J = 0-4) manifold at 295 K are reported below, in Table III-10, as determined from excitation and emission spectra in solid state, acetonitrile and methanol.

Table III-10: Energy (cm^{-1}) of the identified crystal-field sub-levels of the Eu(^7F_j) manifold (j = 1-4) in [Eu(R-Phbipox)$_2$](Otf), [Eu⊂(Λ-Eu(R-Phbipox)$_2$Δ-Eu(R-Phbipox)$_2$)$_3$](Otf)$_9$ and [Lu⊂(Λ-Eu(R-Phbipox)$_2$Δ-Eu(R-Phbipox)$_2$)$_3$](Otf)$_9$ complexes; $^7F_0$ is taken as the origin. (sh: shoulder, w: weak)

	[Eu(R-Phbipox)$_2$](Otf)			[Eu⊂(EuR-Phbipox$_2$)$_6$](Otf)$_9$		[Lu⊂(EuR-Phbipox$_2$)$_6$](Otf)$_9$
	Solid	CH_3CN	CH_3OH	Solid	CH_3CN	CH_3CN
$\tilde{\nu}_{ex}$ / cm^{-1}	28 720	28 670	29 025	28 985	27 970	28 610
$^7F_0$	17 289	17 289	17 290	17 274	17 273	17 277
$^7F_1$					227	
	311	281sh	269	306	304	305
		317	327	372	353	394
			385	457	463	456
			441			
	555	566	581			
$^7F_2$					872	
	928	923		957	948	961
	972	976	960	1001	1000	1009
	1068	1074	988 sh	1036 sh	1043	1046 sh
	1143	1138	1110	1086	1096	1094
	1198	1208	1222	1149	1151	1148
$^7F_3$	1849	1854	1849	1842	1848	1848
	1950	1968	1980	1920	1904	1917
	2059					
$^7F_4$	2678	2680	2705	2635	2641	2640
	2734	2718		2658	2652	2656
	2818	2818	2831	2705	2712	2713
	2887	2868	2886	2845	2837	2852
	2976	2975	2968	2940	2946	2933
	3060 w	3061 w	3110	3057	3056	3040
	3184 w	3185 w		3142	3148	3162

a) Metal-Centered Luminescence of the [Eu(Phbipox)$_2$](Otf) complexes

At room temperature and upon broad band excitation in solid state, the crystal field splitting of the Eu(R-Phbipox)$_2$](Otf) emission spectra (Figure III-62) can be interpreted in terms of low C_2 symmetry around the Eu(III) ion despite the broadening of the spectra as expected from large contribution from vibronic components. Indeed, the emission of the Eu(III) dominated by the transitions to the $^7F_2$ sublevels indicate a low symmetry as well as the very weak $^5D_0 \rightarrow {}^7F_0$ transition (1% of the intensity of the magnetic dipole transition to $^7F_1$). There are two main transitions to the $^7F_1$ level, corresponding to A→A (16 978 cm^{-1}) and to a A→(split)B level (16 734 cm^{-1}), which are both allowed in C_2 symmetry. The three transitions are not equally spaced and the splitting can not be calculated because of the vibronics. The energy gap between the two A→B transitions reflect a distortion from the idealized C_2. The $^5D_0 \rightarrow {}^7F_2$ transition is comprised of five main bands assigned to the three A→A allowed and two A→B electric dipole transitions in C_2. This analysis is also consistent with the observed $^5D_0 \rightarrow {}^7F_4$ transitions with seven components assigned to the A→A and A→B transitions, despite the broadening of the spectrum hiding two splitted transitions. In acetonitrile solution, the emission spectrum shows the same transitions and splitting, pointing to a very similar structure in solution.

The luminescence emission spectrum of the complex carried out in anhydrous methanol shows the presence of europium species of different symmetry with respect to those found in acetonitrile solution with the appearance of additionnal emission lines in the $^7F_1$ level and a large difference in the $^7F_2$ level. This is in agreement with the different metal environment observed for the trinuclear assembly present in acetonitrile compared with the mononuclear complex (the only species present in 6 mM methanol solution).

The superposition of the emission spectra of the [Eu(S-Phbipox)$_2$](Otf) complex in acetonitrile and methanol solutions and the crystal field splitting reflects a very similar C_2 symmetry. The same maxima can be identified in the $^5D_0 \rightarrow {}^7F_1$, $^5D_0 \rightarrow {}^7F_2$ and $^5D_0 \rightarrow {}^7F_4$ transitions revealing that the Eu(III) complexes of the S-Phbipox and R-Phbipox ligands present in the solutions are similar except the chirality (Figure III-62).

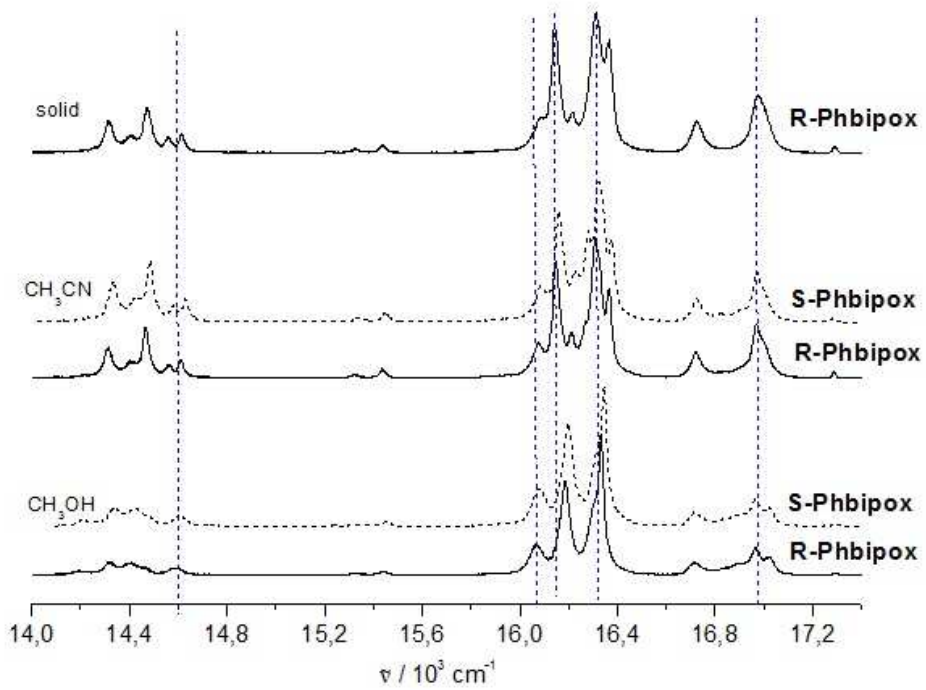

Figure III-62: Normalized emission spectra of [Eu(S-Phbipox$_2$](Otf) and [Eu(R-Phbipox$_2$](Otf) in solid state and at in 6 mM CH_3OH, and CH_3CN

b) Metal-Centered Luminescence of Ln⊂[((Ln(R-Phbipox)$_2$)$_6$](Otf)$_9$ complexes

The emission spectra of the [Eu⊂(Λ-Eu(R-Phbipox)$_2$Δ-Eu(R-Phbipox)$_2$)$_3$](Otf)$_9$ and [Lu⊂(Λ-Eu(R-Phbipox)$_2$Δ-Eu(R-Phbipox)$_2$)$_3$](Otf)$_9$ complexes at room temperature and upon broad band excitation in acetonitrile are given in Figure III-63. The crystal field splitting of the spectra can be interpreted in terms of low C_2 symmetry with three main transitions almost equally spaced to the $^7F_1$ level (1 A→A and 2 A→B levels). The $^5D_0 \rightarrow {}^7F_2$ transition displays five bands close in energy assigned to the A→A and A→B levels and the $^5D_0 \rightarrow {}^7F_4$ transition displays the seven expected bands allowed in C_2 symmetry.

In acetonitrile the [Eu⊂(Λ-Eu(R-Phbipox)$_2$Δ-Eu(R-Phbipox)$_2$)$_3$](Otf)$_9$ and [Lu⊂(Λ-Eu(R-Phbipox)$_2$Δ-Eu(R-Phbipox)$_2$)$_3$](Otf)$_9$ complexes present the same maxima in the $^5D_0 \rightarrow {}^7F_1$, $^5D_0 \rightarrow {}^7F_2$ and $^5D_0 \rightarrow {}^7F_4$ transitions as shown with the dashed lignes in Figure III-63. An additional band in the $^7F_2$ level at 16 406 cm^{-1} has been observed for the [Eu⊂(Λ-Eu(R-Phbipox)$_2$Δ-Eu(R-Phbipox)$_2$)$_3$](Otf)$_9$ complex in acetonitrile which could arise from the central Eu(III) ion in O_h symmetry from the crystal structure. This is in relation with the previous studies on terpya lanthanide wheels [105] where the central Eu(III) ions have

revealed an unexpected emission spectrum dominated by an intense band of the $^5D_0 \rightarrow {}^7F_2$ transition. The absence of this band in the spectrum of [Lu⊂(Λ-Eu(Phbipox)$_2$Δ-Eu(Phbipox)$_2$)$_3$](Otf)$_9$ complex is therefore consistent with the presence of one single site for the Eu(III) ion in this complex. The emission from the central Eu(III) site completely disappears in solid state, probably due to defects in the microcrystals or due to high sensitivity to intramolecular interactions.

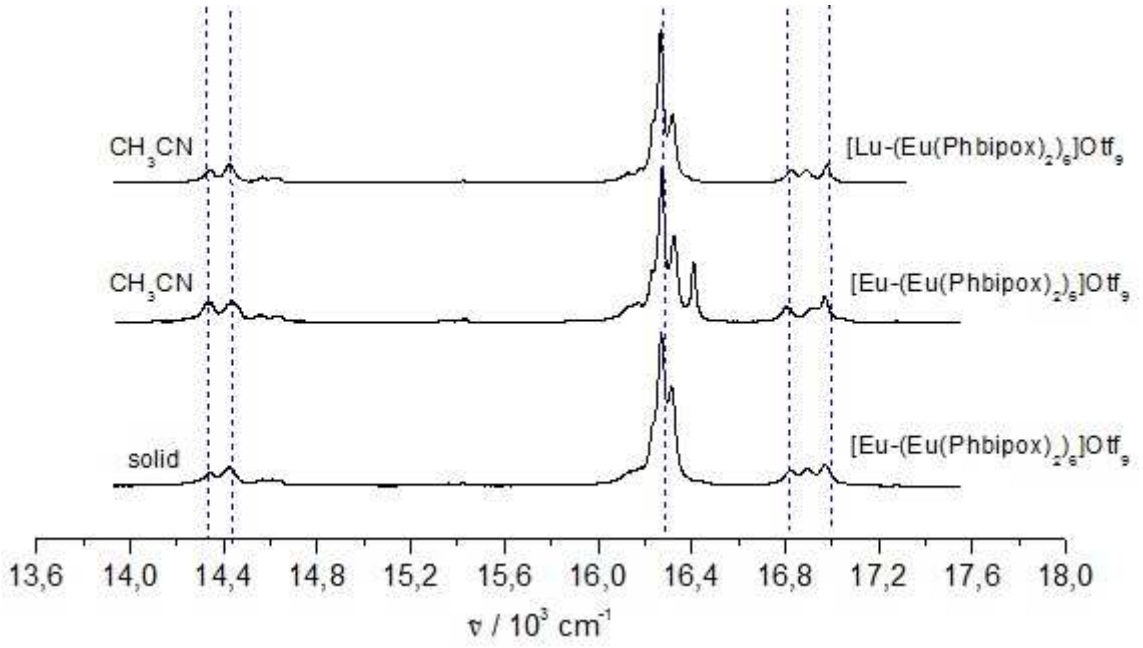

Figure III-63: Normalized emission spectra of [Eu⊂(Λ-Eu(R-Phbipox)$_2$Δ-Eu(R-Phbipox)$_2$)$_3$](Otf)$_9$ in solid state and in CH_3CN at 6 mM; [Lu⊂(Λ-Eu(R-Phbipox)$_2$Δ-Eu(R-Phbipox)$_2$)$_3$](Otf)$_9$ in CH_3CN at 6 mM

c) Lifetime of the Eu ($^5D_0$) level and luminescence quantum yields

The lifetimes of the Eu($^5D_0$) excited state of the mononuclear/trinuclear and heptanuclear complexes measured at 77 K upon direct excitation on the $^5L_6$ level (25 317cm^{-1}) of the Eu(III) ion lie in the range 1.81 to 2.17 and 2.0 to 2.24 ms, respectively, depending on the analyzing energies (Table III-11). They decrease to 1.41-1.87 and 1.75-2.17 ms, respectively at 295 K. These data point to the absence of OH oscillators in the inner coordination sphere of the metal ion, as confirmed by the X-ray structure. The shortening of the lifetime therefore points to an activation of vibrational de-excitation pathways at higher temperature. Excitation through the $^1\pi\pi^*$ ligand state results in similar lifetimes indicating a fast energy transfer from the ligand to the 4f states. All the measured luminescence decays are mono-exponential.

Table III-11: Absolute Quantum Yields and the Lifetimes of the Eu ($^5D_0$) Excited Level (ms) in [Eu(R-Phbipox)$_2$](Otf), [Eu⊂(Eu(R-Phbipox)$_2$)$_6$](Otf)$_9$ and [Lu⊂(Eu(R-Phbipox)$_2$)$_6$](Otf)$_9$ complexes in solid state and acetonitrile solutions at 77K and 298K

complex	$\tilde{\nu}_{ex}$ / (cm^{-1})	Φ_{Eu}^{L} (%)	Φ_{Eu}^{Eu} (%)	τ_{rad} (ms)	η_{sens}	$\tilde{\nu}_{an}$ / (cm^{-1})	τ_{obs} 298 K (ms)	τ_{obs} 77 K (ms)
[Eu(R-Phbipox)$_2$](Otf)								
CH_3CN	29 412	25(1)	31	4.6	81	16 312	1.41(1)	1.81(3)
	25 317						1.32(3)	1.59(2)
CH_3OH	29 412	21(1)	39	4.6	54	16 335	1.78(3)	2.03(5)
	25 317						1.72(2)	1.99(2)
solid	29 412	24(1)	59	3.4	44	16 313	1.87(2)	2.17(10)
	25 317						1.73(2)	1.78(3)
[Eu⊂(EuR-Phbipox)$_2$)$_6$](Otf)$_9$								
CH_3CN	29 412	27(1)	48	3.6	57	16 273	1.75(1)	2.00(1)
	25 317						1.54(1)	1.62(4)
solid	29 412	37(1)	69	3.0	54	16 273	2.05(1)	2.15(4)
	25 317						1.90(1)	2.11(4)
[Lu⊂(EuR-Phbipox$_2$)$_6$](Otf)$_9$								
CH_3CN	29 412	34(1)	60	3.6	57	16 271	2.17(3)	2.24(1)
	25 317						1.97(2)	2.13(1)

The luminescence quantum yields of the [Eu(R-Phbipox)$_2$](Otf) complexes measured in methanol, acetonitrile and in solid state with broad band excitation through the ligand levels at 29 412 cm^{-1} varied between 21 and 25 %. When recording the heptanuclear wheels, we observe an increase of the luminescence quantum yields in the range 27 to 37 %. The rigidity of the complexes influences the metal-centered final lanthanide luminescence step Φ_{Eu}^{Eu} but the overall antenna effect involves a multistep mechanism. The total quantum yield Φ_{Eu}^{L} is thus given by eq III-3 in which η_{ISC} is the $^1\pi\pi^* \rightarrow {}^3\pi\pi^*$ conversion and η_{ET} the energy transfer from the ligand-centered to the metal-centered excited states ($^3\pi\pi^* \rightarrow$ Ln).

$$\Phi_{Eu}^{L} = \eta_{ISC} \cdot \eta_{ET} \cdot \Phi_{Eu}^{Eu} = \eta_{sens} \cdot \Phi_{Eu}^{Eu} \qquad \textbf{III-3}$$

The intrinsic quantum yields of Eu(III) Φ_{Eu}^{Eu} could not be determined experimentally upon direct f-f excitation because of very low absorption intensity. We have thus determined these values for our complexes by assuming that the dipole strength of the magnetic dipole Eu($^5D_0 \rightarrow {}^7F_1$) transition is constant. The radiative lifetime τ_R of the Eu($^5D_0$) level is given by eq III-4 in which n is the refractive index (n = 1.329 for methanol, 1.344 for acetonitrile and 1.5 for solid state complexes), $A_{MD,0}$ = 14.65 s^{-1} is the spontaneous emission probability of the Eu($^5D_0 \rightarrow {}^7F_1$) transition, and I_{MD}/I_{tot} is the ratio of the total integrated intensity of the $^5D_0 \rightarrow {}^7F_J$ transitions (J = 0-6) to the integrated intensity of the magnetic dipole Eu($^5D_0 \rightarrow {}^7F_1$) transition.

$$\tau_R = \frac{1}{A_{MD,0} \cdot n^3} \cdot \left(\frac{I_{MD}}{I_{tot}} \right) \qquad \textbf{III-4}$$

The calculated radiative lifetimes are long in the range 3.0 to 4.6 ms. They are 3.0 and 3.6 ms for the heptanuclear wheels, 3.6 ms for the [Eu(R-Phbipox)$_2$](Otf) complex in methanol and 4.6 in acetonitrile and in solid state where the trinuclear specie is present. Thus, the intrinsic quantum yields of the europium in the complexes estimated from the ratio τ_{obs}/τ_{rad} are included in a wide range, 31 to 69 % indicating a change in the rigidity of the complexes. The sensitization efficiency η_{sens} of the complexes are similar with relatively small variations (average of 55 %) due to their similar coordination environment.

7.2- Metal-Centered Luminescence of the NIR emitting lanthanide complexes

The photophysical properties of the [Ln(R-Phbipox)$_2$](Otf) complexes with Nd(III) and Yb(III) and the [Nd$\subset$(Λ-Nd(Phbipox)$_2\Delta$-Nd(Phbipox)$_2$)$_3$](Otf)$_9$ wheel are reported in Figure III-64. The excitation spectra of complexes in acetonitrile, methanol or in solid state present one broad band between 33 000 and 27 000 cm^{-1} with a maxima between 28 650 and 29 970 cm^{-1} assigned to ligand $^1\pi\pi^*$ states. A sizeable luminescence has been observed at room temperature upon broad band excitation through the ligand levels.

The luminescence spectra of the Nd(III) complexes show three bands in the NIR region, in the spectral range 10 700-11 680, 8 970-9 770 and 7 080-7 750 cm^{-1}. They are assigned to transitions from the $^4F_{3/2}$ level to the $^4I_{9/2}$, $^4I_{11/2}$ and $^4I_{13/2}$ sublevels, respectively. Nevertheless, the crystal field splitting of the spectra can not be interpreted as the spectrum is too broad due to large contribution from vibronic components.

In the same conditions, the Yb(III) complex displays the typical Yb(III) luminescence between 9 390 and 10 690 cm^{-1} assigned to the $^2F_{5/2} \rightarrow {}^2F_{7/2}$ transition as a strong band and a broader vibronic component. The spectra are similar in solution and in solid state. The quantum yields of the complexes are given in Table III-12. A slight increase in the quantum yield is observed for the heptanuclear Nd wheel (0.15 % in acetonitrile and 0.22 % in solid state) compared to the mononuclear Nd complex (0.12 % in acetonitrile and 0.18 in solid state). Even though there is no assembly formation for Yb complex the quantum yield obtained in acetonitrile (0.54%) is higher than the one in methanol (0.44%). The lower quantum yield in methanol could be the result of the quenching from high energy vibrations of the coordinated methanol to the ytterbium center.

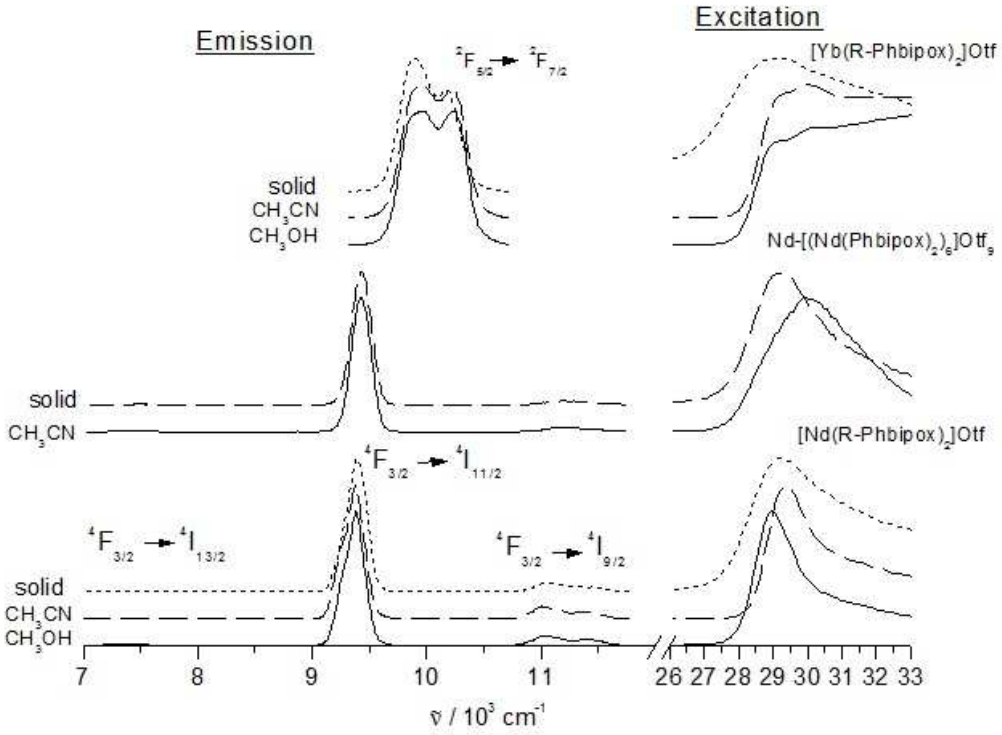

Figure III-64: Normalized emission spectra of [Nd⊂(Λ-Nd(Phbipox)$_2$Δ-Nd(Phbipox)$_2$)$_3$](Otf)$_9$ and [Ln(R-Phbipox)$_2$](Otf) (Ln = Yb and Nd) complexes

Table III-12: Absolute quantum yields (%) of the [Nd(R-Phbipox)$_2$](Otf), [Nd⊂(Nd(R-Phbipox)$_2$)$_6$](Otf)$_9$ and [Yb(R-Phbipox)$_2$](Otf) complexes in solid state, methanol and acetonitrile

	[Nd(R-Phbipox)$_2$](Otf)	[Nd⊂Nd(R-Phbipox)$_2$)$_6$](Otf)$_9$	[Yb(R-Phbipox)$_2$](Otf)
CH_3CN	0.12(1)	0.15(1)	0.54(5)
CH_3OH	0.22(4)	-	0.44(3)
solid	0.18(1)	0.22(2)	0.97(1)

8- Conclusion

The work presented in this chapter focused on the self assembly of chiral luminescent polynuclear lanthanide architectures from mononuclear complexes with a simple dissymmetric tetradentate chiral ligand. The carboxylate-derivatized bipyoxazoline **Phbipox** ligand ((6-(4-phenyloxazolin-2-yl)-2,2-bipyridine-6-carboxylic acid)) has been used for promoting concentration dependent or cation controlled self assembly.

The assembly of a rare homochiral trinuclear complex was observed in acetonitrile or in highly concentrated methanol solutions and followed by NMR studies. The chirality of the ligand is transferred in a concentration dependent formation of the trinuclear assembly to give the enantiopure ΔΔΔ-S or ΛΛΛ-R isomer for europium and neodymium. The formation of

trinuclear assembly is not observed under similar conditions for the smaller size ytterbium ion due to increased sterical interactions. The diastereoselectivity of the assembly formation resides from the sterical interactions from the phenyl groups of the bis-ligand monomeric complexes during the self-assemby process. Moreover strong π-π interactions have been observed in these complexes. Stereoselectivity of the mononuclear complexes was also found in the self-assembly of the two ligands around the europium center to afford the Λ and Δ monomeric isomers and was shown to be linearly changing with the cation size. The CPL studies of europium complex show that the trinuclear species have high CPL activity with a g_{lum} factor of +0.45. Therefore these complexes are promising to further study as luminescent chiral CPL probes. The CPL studies with NIR emitting complexes will be performed in the future.

This system is also particularly well suited for the self-assembly of large polynuclear nano-sized wheel-shaped lanthanide compounds by using template cations as shown with tetradentate terpyridine carboxylate (terpya) ligand. The addition of an excess lanthanide to the 2:1 complexes yields the formation of the largest chiral europium and neodymium architectures up to date. The formation of the heptanuclear complexes is controlled by the cation size. The ytterbium complex did not lead to the formation of heptanuclear complex. The heterochiral hexameric wheel is formed from three delta and three lambda diastereomers connected to each other and to a central cation by carboxylate bridges. Heteropolymetallic complexes have been formed by the rational synthetic strategy developed with terpya ligand requiring different cation size for the two metal sites (central and peripheral) present in the wheel. Moreover, the emission spectrum of the heptanuclear wheel point to the presence of two different emitting sites: one at the center and six at the periphery. According to that $[(Ln(Phbipox)_2)_6]^{9+}$ (Eu, Nd) rings hosting smaller lanthanide ion (Lu, Yb) in the center have been prepared in solutions. The CPL studies show that unexpectedly the wheel (g_{lum} = 0.10) does not have an enhanced CPL activity compared to the mononuclear complexes due to its heterochirality.

The quantum yield of the metal centered luminescence of the heptanuclear complex (27 to 37 %) is slightly higher than the mononuclear complex (21 and 25 %). Suggesting that the cyclic arrangement of six Eu components does not lead to intramolecular quenching effects as observed in the trimetallic helicates [95], despite the shorter distance between neighboring EuL_2 units (6.34 Å) with respect to the intermetallic distance in the trimetallic

helicates (9-9.3Å). Moreover, sizeable NIR emission with the Nd and Yb complexes has been observed at room temperature.

In summary, we have investigated in this part of the thesis work a rare chiral assembly controlled by the ligand geometry, cation size and concentration. The complexes have been fully characterized in solution and solid state. The stereoselectivity of the self-assembly of the mononuclear complexes and the photophysical properties could be tuned by changing the ligand design. That could help to obtain better quality crystals of the wheel as the symmetry of the molecule should increase with the higher stereoselectivity. In addition to that different ligand geometry could provide weaker steric interactions that would allow the formation of higher nuclear assemblies with a wider selection of lanthanides. The heptanuclear species is ideally suited for the study of the intermetallic energy transfer processes but also as potential precursors for the development of lanthanide based optical devices. Obtained trinuclear complexes could also be interesting for magnetic and magnetochiral dichroism studies.

CHAPTER IV Oxidation Chemistry of Divalent Lanthanides

1- Introduction

Lanthanide based nanoclusters have attracted increasing attention in the development of emissive materials with improved photophysical properties for potential applications in optical, electronic and biological devices. The incorporation of lanthanides in polymetallic structures in the nanoscale provides means for combining the advantages of molecular lanthanide complexes (solubility, easy processibility) with the interesting properties of solid state materials (rigidity, high quantum yields due to low phonon environment and absence of high energy vibration modes). Although the research on lanthanide containing clusters focuses mostly on synthetic and structural aspects, several lanthanide clusters with exciting luminescence properties have been reported recently. For example an exceptional Er_{10} cluster [113] (emitting at 1.54 μm) and a Nd_{17} cluster [71] (emitting at 907, 1070, 1357, and 1822 nm) with very high quantum efficiencies of 78% and 35% respectively have been reported by the group of Brennan. This breakthrough substantially increased the interest in such compounds and in the development of efficient pathways to synthesize bright lanthanide clusters.

Even though divalent lanthanides are highly available in solid state and widely studied for spectroscopical studies of doped ceramics for the preparation of optical materials; solution molecular chemistry is limited to a few lanthanide elements. Few interesting examples are given in solution chemistry where divalent molecular precursors are used for preparing cluster like architectures [189-193]. The limited use of divalent molecular complexes for cluster preparation arises from the lack of suitable stable starting materials and from the difficulty in handling these materials. The chemistry of molecular divalent lanthanide complexes in solution is a challenging field where various synthetic strategies have been developed recently [194-198].

In this last chapter, we will first give a brief overview on reductive divalent lanthanide chemistry reported in literature. Afterwards some examples of lanthanide clusters formed by oxidation of divalent precursors will be given. Finally the preliminary results obtained from the synthesis of divalent precursors with the tripodal tris(2-pyridylmethyl)amine (tpa) ligand for the preparation of high nuclearity clusters will be described.

1.2- Reductive Divalent Lanthanide Chemistry

The molecular lanthanide chemistry is dominated by the most stable trivalent oxidation state. The high oxophilicity and reactivity of low valent lanthanide complexes results in high air and moisture sensitivity and prevented the early development of low valent lanthanide chemistry. The general Ln(III)/Ln(II) reduction potentials for lanthanides are given in Table IV-1. Divalent lanthanide species are strong reducing agents and with the unique combination of Lewis acidity properties, they have been widely used in organic chemistry as single electron reductants [199, 200]. The chemistry of divalent europium, ytterbium and samarium has been developed earlier than the other divalent lanthanides as they have more accessible redox potentials as shown in Table IV-1. The stabilization of the divalent state for these ions arise from their electronic configurations reaching the half-filled shell $4f^7$ for Eu(II), the filled shell $4f^{14}$ for Yb(II) and nearly half filled shell $4f^6$ for Sm(II). Recently the chemistry of divalent lanthanides has been expanded to Tm(II), Dy(II), and Nd(II) with the preparation of new molecular species. However, the control of the reactions with these highly reactive ions is highly difficult and rational synthetic efforts are needed to further develop these new systems.

Table IV-1: Ln(III)/Ln(II) reduction potentials (versus NHE) in order of increasing reducing power and the electron configurations of the Ln(II) reductant

Eu	−0.35 V	$[Xe]4f^7$	Ho	−2.9 V	$[Xe]4f^{11}$
Yb	−1.15 V	$[Xe]4f^{14}$	La	−3.1 V	$[Xe]4f^1$
Sm	−1.55 V	$[Xe]4f^6$	Er	−3.1 V	$[Xe]4f^{12}$
Tm	−2.3 V	$[Xe]4f^{13}$	Ce	−3.2 V	$[Xe]4f^2$
Nd	−2.6 V	$[Xe]4f^4$	Tb	−3.7 V	$[Xe]4f^9$
Dy	−2.6 V	$[Xe]4f^{10}$	Gd	−3.9 V	$[Xe]4f^8$
Pr	−2.7 V	$[Xe]4f^3$			

1.2.1 Starting Materials

The divalent lanthanide iodide complexes are the most frequently used starting materials. Many of them were available since the mid 1960s and they have been prepared by a high temperature comproportionation reaction of a mixture of LnI_3 and Ln powder in tantalum crucible under an inert atmosphere (Scheme IV-1(i)) [201]. They can be classified in two groups: the "ionic" salt like compounds of the $[Ln(II)X_2]$ type for Ln = Eu, Yb, Sm, Tm, Dy, Nd and the "metallic" conducting compounds of the $[Ln(III)X_2(e-)]$ type for Ln = La, Ce, Pr, Gd, Ho [202]. The advancement of the reductive chemistry with divalent lanthanides started ever since the divalent diiodide precursors could be made by solution chemistry instead of solid state preparation which requires high temperature and inert atmosphere processing.

The europium(II) and ytterbium(II) iodides have been prepared by reactions of their metallic powders with ammonium iodides in liquid ammonia and led to the preparation of several divalent molecular complexes (Scheme IV-1(ii)). Development of samarium complexes delayed due to the fact that metallic samarium was not soluble in liquid ammonia and it was harder to handle due to its more negative redox potential. In 1980 Kagan et al. have introduced the convenient synthesis of samarium iodide by Grignard like reaction of metal powders with diidoethane in THF at room temperature (Scheme IV-1(iii)) [200]. The easy access to THF soluble starting materials allowed their chemistry to be explored further in detail.

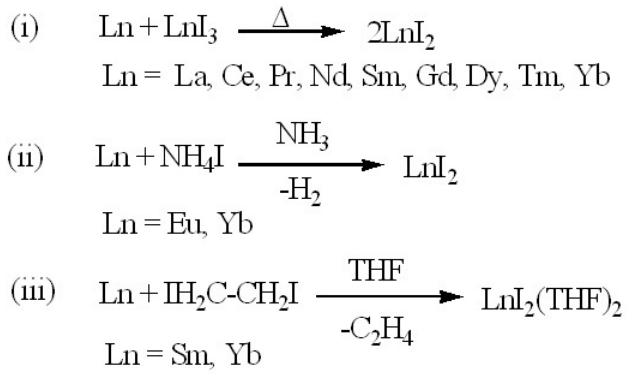

Scheme IV-1: Synthesis of lanthanides (II) iodides complexes

The chemistry of divalent lanthanides was limited to these three elements (Eu, Sm, Yb) for a long time. The next accessible divalent lanthanides after samarium are Tm, Dy and Nd (so called "new" or "non classical" divalent lanthanides) which require special reaction conditions due to their very negative redox potentials and their low thermal stability in organic solvents. In 1997, Evans and Bochkarev reported the first molecular thulium complex $TmI_2(DME)_3$ which was obtained from the reaction of TmI_3 with metallic Tm in refluxing DME [203] (Scheme IV-2(i)). Following the development of a new synthesis for NdI_2 and DyI_2 by a high temperature solid state reaction [204, 205], the first crystallographic data on solvated $DyI_2(DME)_3$ [206] and $NdI_2(THF)_5$ [207] were reported in 2000 and 2001 respectively (Scheme IV-2(ii)). As could be expected from the comparison of the electrode potentials, these compounds are stronger reductants than samarium derivatives so they have provided higher reaction yields in organic chemistry (refs in [195]).

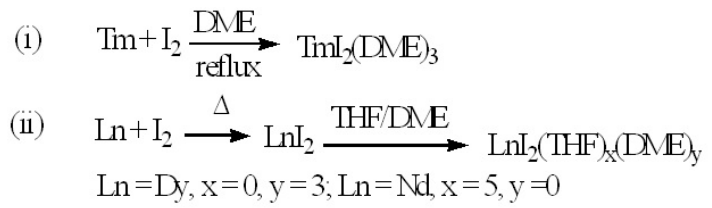

Scheme IV-2: The syntheses of non classical divalent lanthanide diiodides

1.2.2 Molecular Ln(II) Complexes

Divalent lanthanides complexes can be obtained from a divalent precursor, or by reduction of a trivalent derivative. The design of the ligand with sufficient rigidity, steric bulk, thermal and chemical stability is highly important in the stabilization of divalent species. The coordination chemistry of divalent lanthanides is dominated by cyclopentadienyl (Cp) based ligands. Some selected examples are given in Scheme IV-3. The solubility of metallic Eu and Yb in liquid ammonia allowed the synthesis of the cyclopentadienyl (Cp) [208] divalent lanthanide complexes as early as 1964. Solvated cyclopentadienyl divalent samarium complex has been prepared by the reduction of $Sm(C_5H_5)_3$ by potassium in 1969 [209]. Despite the early preparation of these Cp based Ln(II) complexes, the insolubility of these complexes prevented further investigations on their reactivity.

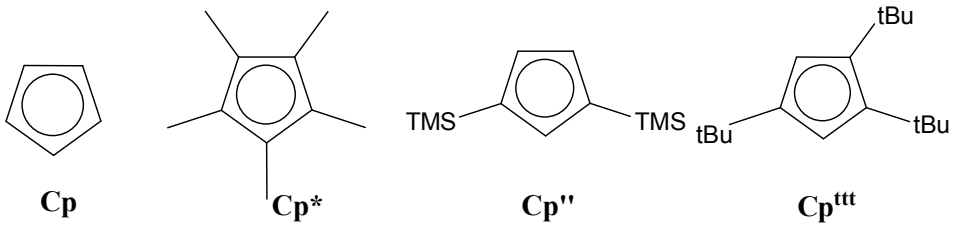

Scheme IV-3: Selected Cp based ligands used for organometallic Ln(II) complexes

In order to provide solubility and increase the steric bulk, Cp ligands have been substituted with variable numbers of methyl, tBu, TMS groups. For example a highly reactive samarium complex with methyl substituted Cp based ligand (C_5Me_5 or Cp*) has been reported by Evans et al. which provided a diverse range of reactivity [210]. For instance, the first dinitrogen complex of an f element [211] has been obtained by reacting this decamethylsamarocene complex with dinitrogen as shown in Scheme IV-4. Resulting complex was also the first example of coplanar coordination of two metals to dinitrogen.

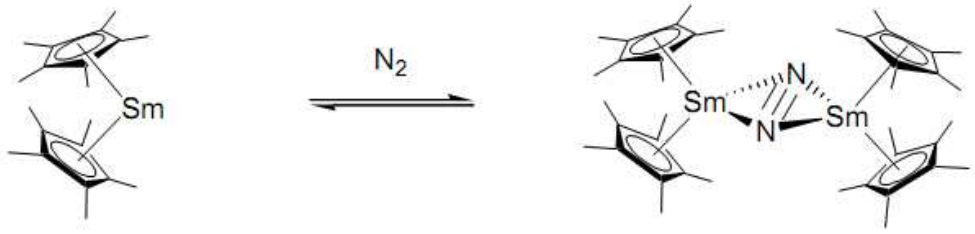

Scheme IV-4: Synthesis of the first dinitrogen complex of an f element from $Sm(Cp^*)_2$

Obtaining stable molecular complexes with non classical divalent lanthanides (Nd, Dy, Tm) is a great challenge due to their high reactivity and low stability in polar organic solvents. As a result of that, their molecular complexes could be obtained almost forty years later than the common divalent lanthanides (Sm, Yb, Eu). The first organometallic complex of Tm(II) is reported in 2002 by Evans et al. synthesized with a substituted Cp ligand in THF and structurally characterized as $(Cp^{ttt})_2Tm(THF)$ [212]. This compound was unstable at room temperature in solution, therefore the phospholyl ligand (phosphacyclopentadienyl ligands: cyclopentadienyl analog with one CH group being replaced by a P atom) were proposed by Nief et al. in view of their weak π donor properties that could stabilise the very electron rich Tm(II) (Scheme IV-5). The complexes $(Dsp)_2Tm(THF)$ and $(Dtp)_2Tm(THF)$ were stable in THF solution at room temperature for a day. Moreover the first unsolvated homoleptic thulium complex $(Dtp)_2Tm$ stable in pentane solution at room temperature has been obtained by using this phospholyl ligand [213].

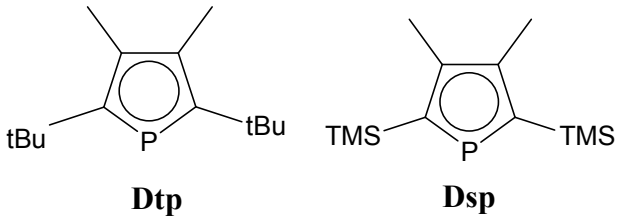

Scheme IV-5: Selected phospholyl ligands used for organometallic Tm(II) complexes

The low stability of DyI_2 and NdI_2 in polar organic solvents prevented organometallic compounds to be obtained by metathesis reactions with organic ligands. Therefore in order to reach stable divalent molecular complexes another synthetic pathway -the reduction of trivalent precursor with an alkali metal - has been adapted. The first molecular compound of Dy(II) were prepared as ate complexes $((Cp^{ttt})_2Dy(\mu\text{-}X)K([18]crown\text{-}6)$ (X = I, Br, BH_4) by the reduction of a suitable trivalent precursor with KC_8 in toluene [214]. Similarly reduction of the trivalent Nd precursor by KC_8 in cyclohexane led to the isolation of the first structurally characterized highly reactive Nd(II) ate complex [215].

Although Ln(II) chemistry is dominated by cyclopentadienyl derivatives there are a vast number of studies on complexes with non-Cp ligands including anionic alkyl, aryl, benzyl, alkynyl, allyl, pentadienyl, cyclooctatetraenyl, aza-allyl, benzamidinato, pyyroyl, pyrazolyl ligands (refs in [216]). Only a few structurally characterized Ln(II) iodide complexes with neutral N donor ligands like N-methylimidazole (N-MeIm) [217] and dimethyl or tert-butyl substituted pyridines [218] are known. All of these studies concentrated on the common divalent lanthanides (Sm, Yb and Eu). Only recently Takats et al. have shown that the bulky tripodal hydro-tris(3-tBu-5-Me-pyrazolyl)borate(Tp^{tBu,Me}) ligand, a second generation Trofimenko "scorpionate", can also be used to prepared stable Tm(II) complexes [219]. The crystal structure of the (Tp^{tBu,Me})Tm[CH(SiMe$_3$)$_2$] is given in Figure IV-1.

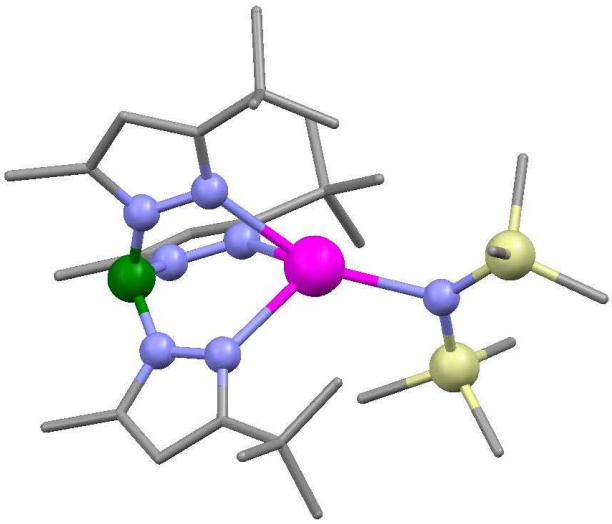

Figure IV-1: Crystal structure of (Tp^{tBu,Me})Tm[CH(SiMe$_3$)$_2$]. Tm: purple, B: green, C: grey, N: blue, Si: yellow

The chemistry of non classical divalent lanthanides is extremely challenging as they have very low stability in most common solvents at room temperature. Most of the complexes have been prepared in THF or DME. Recently Bochkarev et al. found that isopropylamine could be used as a solvent to synthesize Ln(II) complexes thanks to improved stability of the Ln(II) iodides in this solvent. Moreover they could obtain crystals of the TmI$_2$(Pr^{i}NH$_2$)$_4$ and EuI$_2$(Pr^{i}NH$_2$)$_4$ compounds [220].

The non classical divalent lanthanides (Nd, Dy, Tm) react with acetonitrile and pyridine. The dissolution of TmI$_2$, DyI$_2$ and NdI$_2$ in acetonitrile is accompanied by disproportionation leading to the trimerisation of acetonitrile through C-C bond formation into the neutral 1,1,3-bis(iminomethyl)ethylamine, that acts as a ligand in the final LnI$_3$ complex. [221, 222] (Figure IV-2). Another example of C-C bond formation is observed by reacting

TmI_2 in THF with pyridine. Monoelectronic reduction of pyridine results in the Tm(III) coordinated pyridine radical that further dimerises at the 4,4□position [223].

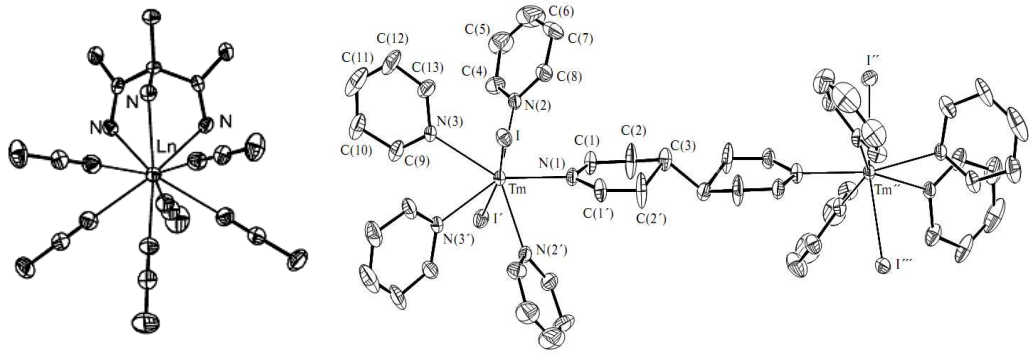

Figure IV-2: Molecular structures of $[HN=CMe)_2C(Me)NH_2]LnI(MeCN)$ resulting from trimerisation of acetonitrile mediated by LnI_2 (Ln=Nd, Dy, Tm) and $[(C_5H_5N)_4TmI_2]_2(\mu\text{-}C_{10}H_{10}N_2)$ resulting from reductive dimerisation of pyridine mediated by TmI_2 [221, 222] [223]

1.2.3 Cluster formation from Ln(II) complexes

There are a few examples in literature where the reduction of ligand or activation of solvent molecules by divalent lanthanides precursors has led to polynuclear lanthanide complexes [189-193]. The rational design of the cluster is highly difficult and most of the clusters are characterized by random self organization. Some selected examples will be given here for the purpose of demonstrating the potential of divalent lanthanides reactivity in the formation of high nuclearity lanthanide complexes.

Several polymetallic organolanthanide structures have been reported with cyclopentadienyl based ligands [224]. Two examples of hexanuclear Cp based clusters formed by oxidation of Sm(II) precursors are given in Figure IV-3 [190, 225]. In these clusters six samarium atoms describe a pseudo-octahedron built around a central μ_6-O and six Cp* ligands encapsulate the cluster core by coordinating each samarium ion.

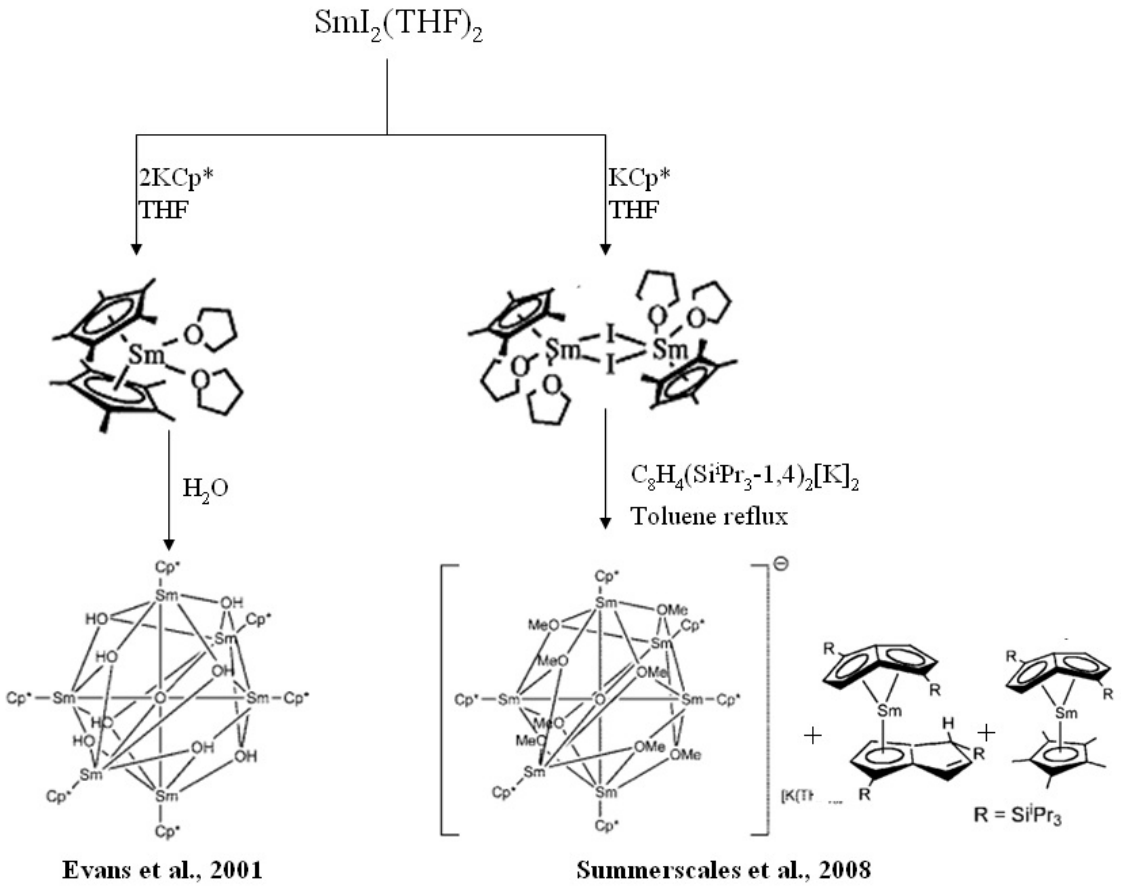

Figure IV-3: Synthetic routes to hexanuclear samarium cluster compounds from samarium diiodide (partial iodides omitted from the cluster on the right for clarity)

The cluster on the left was isolated by Evans et al. from the reaction of water with the Sm(II) organometallic complex $(Cp^*)_2Sm(THF)_2$ that has led to the isolation of the oxo/hydroxo containing hexanuclear cluster $[(Cp^*)Sm]_6(OH)_6(O)_3$ in 40% yield [190]. A similar hexanuclear cluster $[(Cp^*)_6Sm_6(OMe)_8O][K(THF)_6]$ has been obtained as a side product (20% yield) by Summerscales et al. from the reaction of the pentalene salt $C_8H_4\{Si^iPr_3\text{-}1,4\}_2[K]_2$ with $[Sm(Cp^*)(\mu\text{-}I)(THF)_2]_2$ in toluene [225]. The reaction mechanism is complex and the authors suggest that the oxo and methoxy groups in this cluster are derived from Sm(II) based THF cleavage [225].

Another example of cluster formation by C-O bond cleavage of the solvent is given by Bochkarev et al. They have reported the tetranuclear cluster $[Nd_4(\mu_2\text{-}I)_{1.1}(\mu_3\text{-}I)(\mu_2\text{-}OMe)_{4.9}(\mu_4\text{-}O)(MeCN)_{12}]I_3$ which is formed as a side product (17%) by the reaction of NdI_2 with excess methanol in acetonitrile (Scheme IV-6) [226]. The central μ_4-coordinated O^{2-} anion is argued to arise from the partial C-O bond cleavage in the methanol by the strong reducing agent NdI_2.

$$NdI_2 + MeOH \xrightarrow[-H_2]{MeCN} NdI_2(OMe)(MeCN)_3 + Nd_4I_{5.1}(OMe)_{4.9}(O)(MeCN)_{12}$$

Scheme IV-6: The synthesis of $[Nd_4(\mu_2\text{-}I)_{1.1}(\mu_3\text{-}I)(\mu_2\text{-}OMe)_{4.9}(\mu_4\text{-}O)(MeCN)_{12}]I_3$ cluster

Brennan and coworkers have synthesized and characterized a tetranuclear lanthanide cluster from the reduction of elemental sulfur by Yb(II) [227]. The oxidation of YbI_2 in THF with elemental S has led to the formation of a tetranuclear cluster as shown in Figure IV-4. However the isolation of the cluster from the major product YbI_3 was difficult. Therefore another synthetic approach has been developed where $YbI(SPh)_x$ (x = 1, 2) has been used as a starting material and has led to the isolation of the cluster with 40% yield. Similarly series of heterovalent tetranuclear clusters in the form $(DME)_4Ln_4Se(SePh)_8$ Ln = Yb, Sm have been prepared by reduction of elemental selenium by $Ln(SePh)_2$ in DME (5-20 % yield) [189].

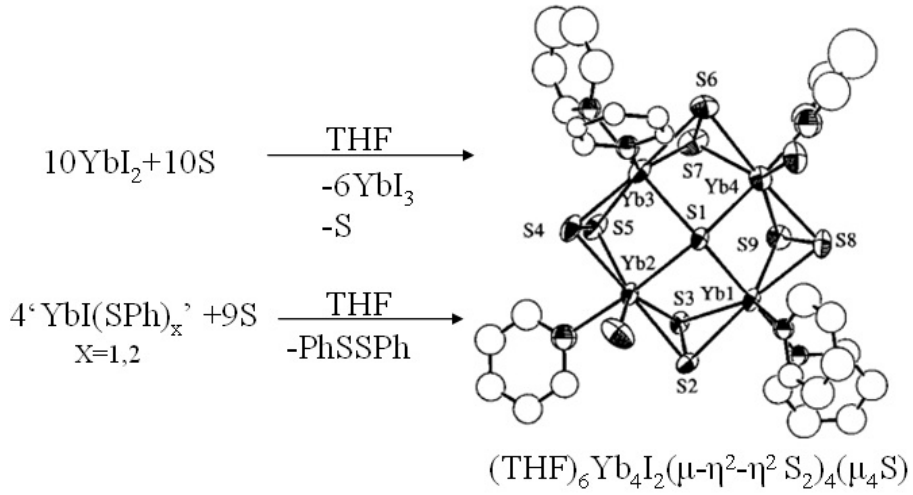

Figure IV-4: Synthesis of tetravalent clusters from the Yb(II) precursors

1.2.4 The Objective of the Study

The short bibliographical overview given in the previous section shows that the reductive chemistry of divalent lanthanides is highly challenging and some significant progress have been recorded showing the potential of molecular divalent precursors in the preparation of lanthanide clusters. The control of reaction conditions and the choice of the ligand is critical to obtain stable compounds.

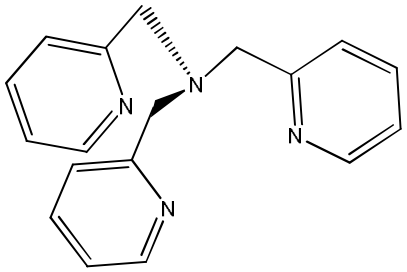

Scheme IV-7: The ligand tris(2-pyridylmethyl)amine (tpa)

In our laboratory, the use of tripodal ligand tris(2-pyridylmethyl)amine (tpa) (Scheme IV-7) has been proven to afford stable mono and bis complexes with the highly reducing U(III) ([U(tpa)I_3(py)] and [U(tpa)$_2$]I_3). The complex [U(tpa)$_2$]I_3 was found to be more reactive towards water than the U(III) complex containing cyclopentadienyl derivatives. The reaction of the complex [U(tpa)$_2$]I_3 with stoichiometric quantities of water in acetonitrile led to the synthesis of trinuclear U(IV) oxo clusters [117]. In this reaction, the presence of a hydroxo

intermediate is proposed and the deprotonation of this hydroxo complex by one of the tpa ligands favours the formation of the trinuclear complex (Figure IV-5). This trinuclear complex has also been prepared in our laboratory by reacting the bis tpa complex with Py-N-Oxide in acetonitrile.

$$[U(tpa)_2]I_3 + H_2O \rightarrow [U(tpa)_2(OH)]I_3 + {}^1/_2H_2 \rightarrow$$

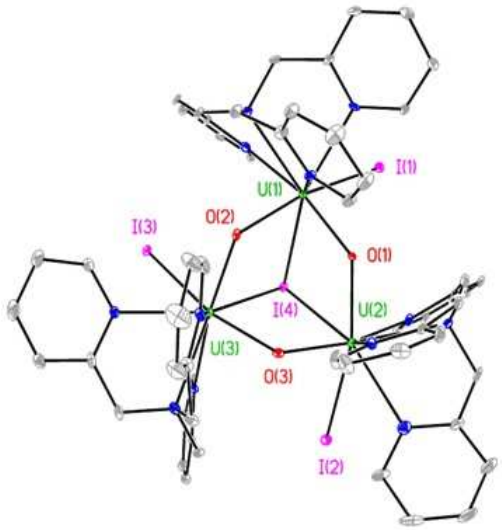

Figure IV-5: Synthesis and crystal structure of $\{[U(tpa)(\mu\text{-}O)I]_3(\mu_3\text{-}I)\}I_2$

Structurally well-defined mononuclear divalent lanthanide complexes are highly desired for the reactivity studies. The Cp based ligands provided a wealth of new complexes and reactivities to the divalent lanthanide chemistry. In this work, we decided to investigate the synthesis of divalent complexes formed with the tripodal tpa ligand, as this neutral N donor ligand have shown to stabilize electron rich U(III).

The aim of this study is to prepare Ln(II) precursors with the tripodal tris(2-pyridylmethyl)amine (tpa) ligand in order to access various luminescent polynuclear lanthanide cluster like complexes by oxidation of divalent complexes. We will present thereafter the preliminary results obtained from the synthesis of mono and bis tpa complexes with divalent lanthanides.

2- Synthesis and characterization of 2:1 divalent lanthanide complexes

Homoleptic divalent lanthanide complexes $[Ln(tpa)_2]I_2$ (Ln = Sm, Yb, Eu) have been prepared by reacting divalent lanthanide iodide salts with two equivalents of tpa in THF at room temperature (Scheme IV-8). The complexes precipitated immediately. The isolated complexes have been characterized by NMR spectroscopy, X-ray crystallography and elemental analysis. Due to the high paramagnetism of $4f^7$ electronic configuration of Eu(II), no informative NMR spectrum could be obtained from the $[Eu(tpa)_2]I_2$ complex.

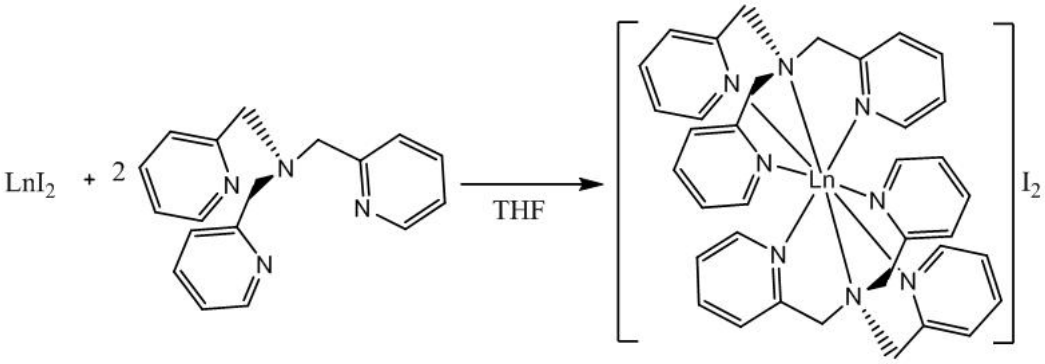

Scheme IV-8: Reaction scheme for the synthesis of $[Ln(tpa)_2]I_2$

2.1- X-ray Crystallography Studies

Crystals suitable for X-ray diffraction were obtained by slow diffusion of ligand into a solution of LnI_2 in THF (for Eu, Sm) or by slow diffusion of diisopropylether into a concentrated solution of the complex in acetonitrile (for Yb). The complexes $[Sm(tpa)_2]I_2$ **(XII)** and $[Eu(tpa)_2]I_2$ **(XIII)** both crystallize in the centrosymmetric $P2_1/c$ space group of the monoclinic system. The complex $[Yb(tpa)_2]I_2$ **(XIV)** crystallizes in the noncentrosymmetric monoclinic Cc space group. The complexes are locally isostructural and only the Mercury diagram of $[Sm(tpa)_2]^{2+}$ is given in Figure IV-6. Selected interatomic angles and distances are given in Table IV-2 and IV-3. In these structures the two tpa ligands are wrapped around the 3-fold axis in such a way that the whole molecular ion has a helical structure like a six bladed propeller (Figure IV-7). The metal ion in these structures achieves eight coordination in a pseudo-S_6 symmetric arrangement.

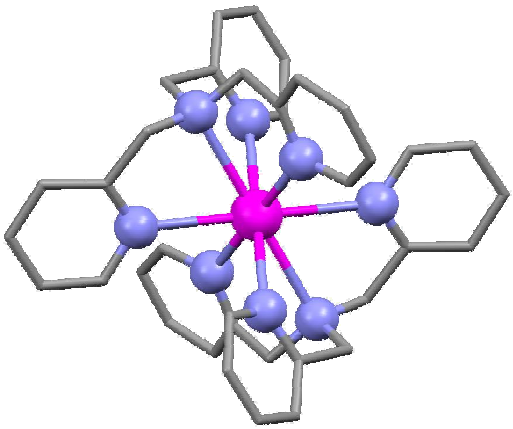

Figure IV-6: Mercury diagram of $[Sm(tpa)_2]^{2+}$.The protons are omitted for clarity

In these complexes the two ligands show the opposite right and left handed helical arrangement for each cation, unlike the Ln(III) and U(III) bis tpa complexes previously prepared in our laboratory (where two ligands have the same right handed helical arrangement) [117, 228]. The difference in the helical arrangement may be the result of an increased ionic size of the metal for the divalent lanthanide complexes compared to the trivalent analogues. In order to investigate the effect of ionic size on ligand helicity a trivalent analogue of the $[Sm(tpa)_2]^{2+}$ complex has been prepared. The complex $[Sm(tpa)_2]I_3$ **(XV)** is isostructural to the previously reported bis tpa complexes with trivalent lanthanides [228] and uranium [117] crystallizing in the chiral noncentrosymmetric space group $P2_12_12_1$. The two ligands show the same right handed helical arrangement resulting in a chiral enantiomer in the crystal. In these complexes, the two tetradentate tpa ligands wrap around the metal ion in a pseudo-D_3 symmetric arrangement (Figure IV-8).

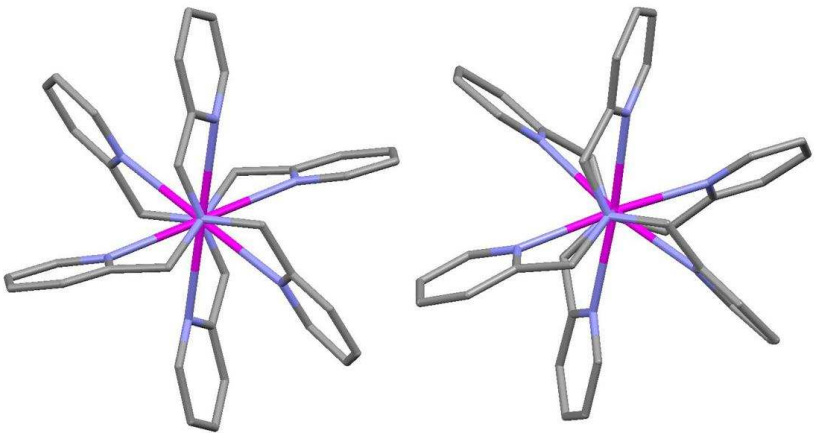

Figure IV-7: Mercury diagram of the structures $[Sm(tpa)_2]I_2$ (left) and $[Sm(tpa)_2]I_3$ (right), S_6 and D_3 symmetric arrangement respectively

The coordination geometries are best described as distorted cubes (Figure IV-8), where N(1), N(2), N(3), N(4)# and N(1)#, N(2)#, N(3)#, N(4) describes the square bases for **XII** and **XIII**, where N(1), N(2), N(23), N(4) and N(21), N(22), N(3), N(24) describes the square bases for **XIV**. The angle between the two square faces is 1.46° for the Yb complex **XIV** while the two faces are perfectly parallel (0°) for Sm **XII** and Eu **XIII** complexes resulting in a less distorted polyhedron for these complexes. The N-N distances defining the edges of the cube are between 2.77 Å and 3.48 Å for **XII**, 2.77 Å and 3.45 Å for **XIII**, 2.65 Å and 3.38 Å for **XIV**, and the angles within the cube described by the eight N atoms lie between 72.67° and 96.19° for **XII**, 73.28° and 96.28° for **XIII**, 75.42° and 97.12° for **XIV**. The N-Ln-N (Ln = Sm, Eu) trans angles are all of 180° as required by the inversion symmetry within **XII** and **XIII**. Metallic ions and the two apical nitrogens of tertiary amines are aligned on a pseudo C_3 axis with the angle 176.9(3)° for **XIV** and 171.2(6)° for **XV**.

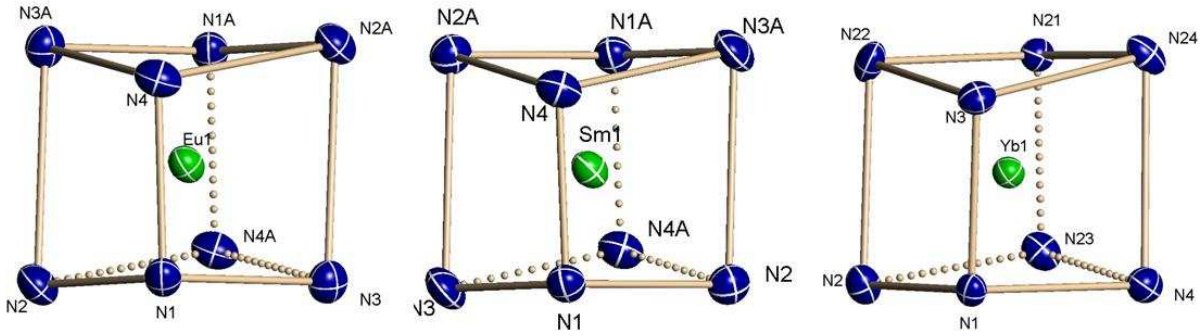

Figure IV-8: Coordination polyhedrons of the Ln(II) ions in $Sm(tpa)_2]I_2$ (XII), $[Eu(tpa)_2]I_2$ (XIII) and $[Yb(tpa)_2]I_2$ (XIV)

The average Ln-N distances found for pyridyl nitrogen are 2.69(2) Å for **XII**, 2.67(2) Å for **XIII**, 2.60(2) Å for **XIV**. Ln-N distances found for the apical tertiary amine nitrogen are 2.730(8) Å for **XII**, 2.727(3) Å for **XIII** and 2.629(7) Å and 2.677(8) Å for **XIV**. For all the complexes, Ln-N_{amine} bond distance is slightly longer than the average Ln-$N_{pyridine}$ bond distance, the difference being 0.06 Å for **XII** and **XIII** and 0.04 Å for **XIV**. Similarly to trivalent analogues, the Ln-N distances show a general linear increase with increasing ionic radius as expected in a purely ionic bonding model for ligands that can adapt well to differently sized metals. The Ln-N distances found in the $[Sm(tpa)_2]I_3$ **XV** (Sm-$N_{pyridine}$= 2.55(3) Å and Sm-N_{amine}=2.581(16) Å - 2.590(17) Å) are shorter than the ones found in $[Sm(tpa)_2]I_2$ **XII** (Sm-$N_{pyridine}$ = 2.69(2) Å and Sm-N_{amine} = 2.730(8) Å) in agreement with the difference in the ionic radius of Sm^{2+} and Sm^{3+} (for CN=8) [5]. Moreover the difference between the Ln-N bond lengths in **XII** and **XV** (0.14 Å) is slightly smaller than the difference between the ionic radius of Sm^{3+} (1.079 Å) and Sm^{2+} (1.27 Å). The reason for this difference

could be the result of the repulsion due to the steric hindrance of the ligand for the Sm(III) complex resulting in longer bond lengths than expected.

Table IV-2: Selected Bond Lengths (Å) and Angles (deg) in the Complexes **XIII** and **XIV**

$[Eu(tpa)_2]I_2$		**$[Yb(tpa)_2]I_2$**	
Eu(1)-N(1)	2.727(3)	Yb(1)-N(1)	2.629(7)
Eu(1)-N(2)	2.679(4)	Yb(1)-N(2)	2.638(9)
Eu(1)-N(3)	2.652(4)	Yb(1)-N(3)	2.596(7)
Eu(1)-N(4)	2.682(4)	Yb(1)-N(4)	2.570(8)
Eu(1)-N(1)#1	2.727(3)	Yb(1)-N(21)	2.677(8)
Eu(1)-N(2)#1	2.679(4)	Yb(1)-N(22)	2.582(8)
Eu(1)-N(3)#1	2.652(4)	Yb(1)-N(23)	2.606(8)
Eu(1)-N(4)#1	2.683(4)	Yb(1)-N(24)	2.585(9)
N(3)-Eu(1)-N(3)#1	180.0	N(4)-Yb(1)-N(22)	179.0(4)
N(3)-Eu(1)-N(2)#1	78.98(12)	N(4)-Yb(1)-N(24)	79.2(3)
N(3)#1-Eu(1)-N(2)#1	101.02(12)	N(22)-Yb(1)-N(24)	101.8(3)
N(3)-Eu(1)-N(2)	101.02(12)	N(4)-Yb(1)-N(3)	101.0(3)
N(3)#1-Eu(1)-N(2)	78.98(12)	N(22)-Yb(1)-N(3)	79.2(3)
N(2)#1-Eu(1)-N(2)	180.0	N(24)-Yb(1)-N(3)	77.2(3)
N(3)-Eu(1)-N(4)	99.94(12)	N(4)-Yb(1)-N(23)	77.9(3)
N(3)#1-Eu(1)-N(4)	80.06(12)	N(22)-Yb(1)-N(23)	102.0(3)
N(2)#1-Eu(1)-N(4)	80.20(12)	N(24)-Yb(1)-N(23)	103.4(3)
N(2)-Eu(1)-N(4)	99.80(12)	N(3)-Yb(1)-N(23)	178.6(4)
N(3)-Eu(1)-N(4)#1	80.06(12)	N(4)-Yb(1)-N(1)	66.1(2)
N(3)#1-Eu(1)-N(4)#1	99.94(12)	N(22)-Yb(1)-N(1)	113.2(3)
N(2)#1-Eu(1)-N(4)#1	99.80(12)	N(24)-Yb(1)-N(1)	119.3(2)
N(2)-Eu(1)-N(4)#1	80.20(12)	N(3)-Yb(1)-N(1)	63.6(3)
N(4)-Eu(1)-N(4)#1	180.0	N(23)-Yb(1)-N(1)	115.0(3)
N(3)-Eu(1)-N(1)#1	117.82(11)	N(4)-Yb(1)-N(2)	104.2(3)
N(3)#1-Eu(1)-N(1)#1	62.18(11)	N(22)-Yb(1)-N(2)	74.8(3)
N(2)#1-Eu(1)-N(1)#1	62.89(12)	N(24)-Yb(1)-N(2)	175.8(3)
N(2)-Eu(1)-N(1)#1	117.11(12)	N(3)-Yb(1)-N(2)	104.3(3)
N(4)-Eu(1)-N(1)#1	117.88(11)	N(23)-Yb(1)-N(2)	75.3(3)
N(4)#1-Eu(1)-N(1)#1	62.12(11)	N(1)-Yb(1)-N(2)	64.7(2)
N(3)-Eu(1)-N(1)	62.18(11)	N(4)-Yb(1)-N(21)	116.1(3)
N(3)#1-Eu(1)-N(1)	117.82(11)	N(22)-Yb(1)-N(21)	64.6(3)
N(2)#1-Eu(1)-N(1)	117.10(12)	N(24)-Yb(1)-N(21)	63.7(2)
N(2)-Eu(1)-N(1)	62.89(12)	N(3)-Yb(1)-N(21)	117.3(3)
N(4)-Eu(1)-N(1)	62.12(11)	N(23)-Yb(1)-N(21)	64.1(3)
N(4)#1-Eu(1)-N(1)	117.88(11)	N(1)-Yb(1)-N(21)	176.9(3)
N(1)#1-Eu(1)-N(1)	180.0	N(2)-Yb(1)-N(21)	112.3(2)

Symmetry transformations used to generate equivalent atoms: #1 = -x+1, -y+1, -z+1

Table IV-3: Selected Bond Lengths (Å) and Angles (deg) in the Complexes **XII** and **XV**

[Smtpa$_2$]I$_2$		**[Smtpa$_2$]I$_3$**	
Sm(1)-N(1)	2.730(8)	Sm(1)-N(1)	2.581(16)
Sm(1)-N(2)	2.672(8)	Sm(1)-N(2)	2.553(16)
Sm(1)-N(3)	2.685(8)	Sm(1)-N(3)	2.548(16)
Sm(1)-N(4)	2.719(9)	Sm(1)-N(4)	2.505(17)
Sm(1)-N(1)#1	2.730(8)	Sm(1)-N(21)	2.590(17)
Sm(1)-N(2)#1	2.672(8)	Sm(1)-N(22)	2.543(18)
Sm(1)-N(3)#1	2.685(8)	Sm(1)-N(23)	2.582(19)
Sm(1)-N(4)#1	2.719(9)	Sm(1)-N(24)	2.580(17)
N(2)-Sm(1)-N(2)#1	180.0	N(4)-Sm(1)-N(22)	175.6(6)
N(2)-Sm(1)-N(3)	100.9(3)	N(4)-Sm(1)-N(3)	105.2(6)
N(2)#1-Sm(1)-N(3)	79.1(3)	N(22)-Sm(1)-N(3)	74.4(6)
N(2)-Sm(1)-N(3)#1	79.1(3)	N(4)-Sm(1)-N(2)	101.2(6)
N(2)#1-Sm(1)-N(3)#1	100.9(3)	N(22)-Sm(1)-N(2)	83.1(6)
N(3)-Sm(1)-N(3)#1	180.0	N(3)-Sm(1)-N(2)	102.4(6)
N(2)-Sm(1)-N(4)	99.5(3)	N(4)-Sm(1)-N(24)	82.1(6)
N(2)#1-Sm(1)-N(4)	80.5(3)	N(22)-Sm(1)-N(24)	98.7(5)
N(3)-Sm(1)-N(4)	99.6(3)	N(3)-Sm(1)-N(24)	171.6(6)
N(3)#1-Sm(1)-N(4)	80.4(3)	N(2)-Sm(1)-N(24)	71.8(5)
N(2)-Sm(1)-N(4)#1	80.5(3)	N(4)-Sm(1)-N(1)	63.0(5)
N(2)#1-Sm(1)-N(4)#1	99.5(3)	N(22)-Sm(1)-N(1)	120.1(5)
N(3)-Sm(1)-N(4)#1	80.4(3)	N(3)-Sm(1)-N(1)	64.9(6)
N(3)#1-Sm(1)-N(4)#1	99.6(3)	N(2)-Sm(1)-N(1)	66.1(6)
N(4)-Sm(1)-N(4)#1	180.0	N(24)-Sm(1)-N(1)	116.4(6)
N(2)-Sm(1)-N(1)	61.8(2)	N(4)-Sm(1)-N(23)	71.4(6)
N(2)#1-Sm(1)-N(1)	118.2(2)	N(22)-Sm(1)-N(23)	104.3(6)
N(3)-Sm(1)-N(1)	62.7(3)	N(3)-Sm(1)-N(23)	77.5(6)
N(3)#1-Sm(1)-N(1)	117.3(3)	N(2)-Sm(1)-N(23)	172.1(6)
N(4)-Sm(1)-N(1)	62.1(3)	N(24)-Sm(1)-N(23)	109.2(6)
N(4)#1-Sm(1)-N(1)	117.9(3)	N(1)-Sm(1)-N(23)	107.2(5)
N(2)-Sm(1)-N(1)#1	118.2(2)	N(4)-Sm(1)-N(21)	109.9(6)
N(2)#1-Sm(1)-N(1)#1	61.8(2)	N(22)-Sm(1)-N(21)	66.7(6)
N(3)-Sm(1)-N(1)#1	117.3(3)	N(3)-Sm(1)-N(21)	114.4(6)
N(3)#1-Sm(1)-N(1)#1	62.7(3)	N(2)-Sm(1)-N(21)	121.9(6)
N(4)-Sm(1)-N(1)#1	117.9(3)	N(24)-Sm(1)-N(21)	65.8(5)
N(4)#1-Sm(1)-N(1)#1	62.1(3)	N(1)-Sm(1)-N(21)	171.2(6)
N(1)-Sm(1)-N(1)#1	180.0	N(23)-Sm(1)-N(21)	64.5(5)

Symmetry transformations used to generate equivalent atoms: #1 = -x+1, -y+1, -z+1

2.2- Structure in Solution

a) $[Sm(tpa)_2]I_2$

The proton NMR spectrum of $[Sm(tpa)_2]I_2$ in CD_3CN (Figure IV-9) shows the presence of one set of signals with four resonances for the pyridine protons and a single resonance for the methylene protons at low temperature (283 K). The spectral features are in agreement with the three-fold symmetry of the solution species in which all chelating arms of the tpa ligand are equivalent. This is in agreement with the averaged D_{3h} solution species where the rapid movement of methylene arms occurs even at low temperature, only single diastereomeric species were observed. The most shifted signal is the H_6 which is closer to the metallic ion due to paramagnetic effect of the metal. The proton NMR spectrum in acetonitrile at room temperature showed a small amount of decomposition products as shown in Figure IV-10a. After one day, the color of the NMR solution turned from blue green to yellow and only decomposition products remains in solution (Figure IV-10c). However no crystals could be grown from this yellow solution in order to analyze the decomposition products.

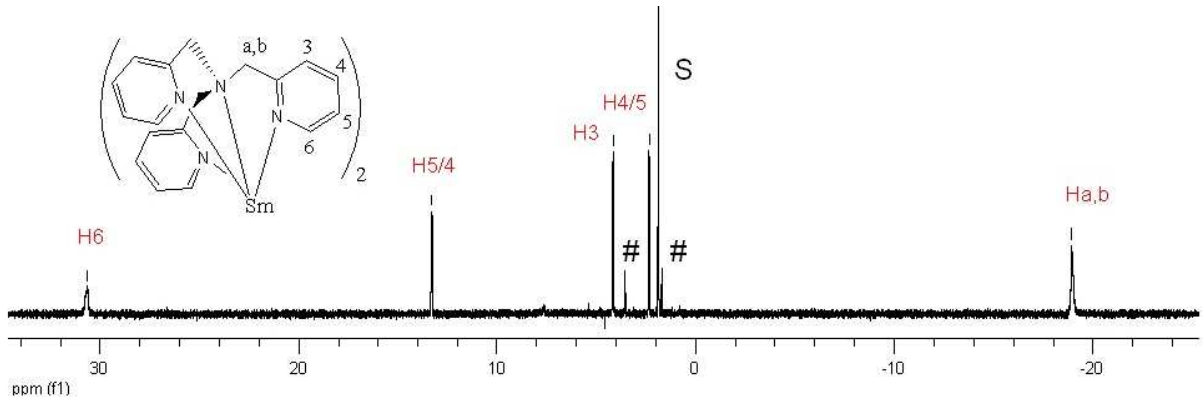

Figure IV-9: ^1H NMR spectrum of $[Sm(tpa)_2]I_2$ in anhydrous acetonitrile (500 MHz, 283K) S: CD_3CN, #: residual THF

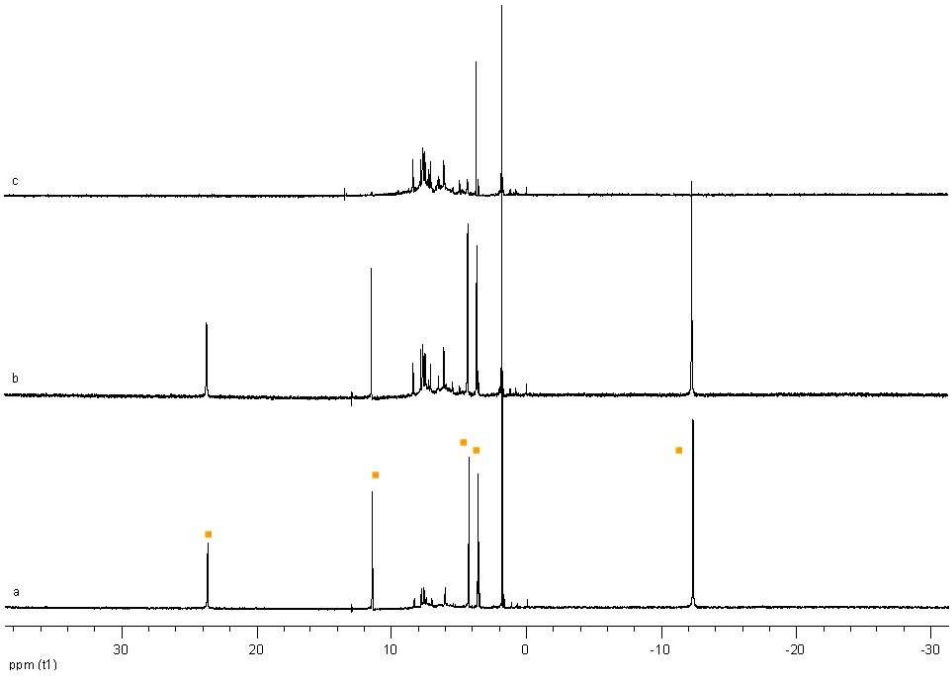

Figure IV-10: ^{1}H NMR spectra of $[Sm(tpa)_2]I_2$ and decomposition products in anhydrous acetonitrile after a) 5 minutes, b) 2 hours, c) 24 hours (CD_3CN, 400 MHz, 298K)

b) $[Yb(tpa)_2]I_2$

The reaction of the YbI_2 salt with two equivalents of tpa in anhydrous THF at room temperature resulted in the immediate precipitation of a green solid. The ^{1}H NMR of this green powder (diamagnetic $[Yb(tpa)_2]I_2$ complex) is given in Figure IV-11. Similar to the Sm analogue only one set of signals corresponding to an averaged D_{3h} symmetry is observed in solution due to the rapid movement of methylene arms. The three fold symmetry of the ligand is conserved in solution resulting in identical chemical shifts for each pyridinyl groups. No decomposition products were observed in acetonitrile solution for a few weeks. This higher stability in solution compared to the Sm(II) analogue is in agreement with the less negative redox potential of the Yb(II) ion.

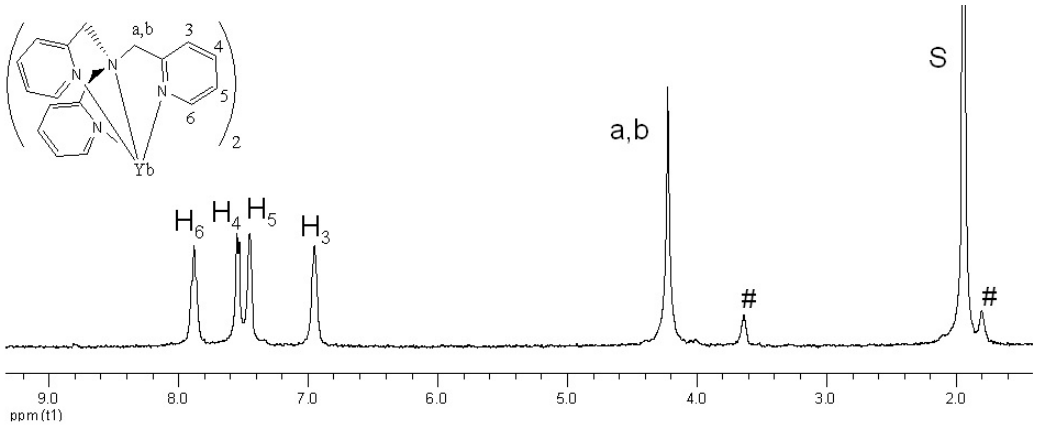

Figure IV-11: ^{1}H NMR spectrum of $[Yb(tpa)_2]I_2$ in anhydrous acetonitrile (400 MHz, 298K) S: CD_3CN, #: residual THF

2.3- Reactivity with oxo donor ligands

In order to investigate the formation of oxo clusters, these bis tpa complexes have been reacted with oxo donor ligands like pyridine-N-oxide in different stoichiometric ratios. The reactions proceeded with a sharp discoloration of the solutions. Due to the insolubility of the bis tpa complexes in THF and DME, the reactions were performed in acetonitrile. Until now, X-ray quality single crystals of $[Ln(tpa)(\mu\text{-}OH)(Py\text{-}N\text{-}Oxide)_2]I_2$ Ln = Sm **(XVI)**, Yb **(XVII)** complexes could be obtained from the the reactions of Yb(II) and Sm(II) bis tpa complexes with 3 eq. of Py-N-oxide in acetonitrile. The resulting complexes are isostructural and both crystallize in $P2_1/n$ space group. The crystal structure shown in Figure IV-12 presents a dimer bridged by two hydroxo groups. The hydrogen is thought to be originated from the relatively acidic proton of acetonitrile. Therefore the reactions were repeated in benzonitrile which does not contain acidic C-H groups; however no crystals could be grown until now. The comparison of the NMR spectra of the compounds prepared by reacting $[Yb(tpa)_2]I_2$ with 3 eq. of Py-N-oxide in acetonitrile (Figure IV-13a) and benzonitrile (Figure IV-13b) show that the reaction in benzonitrile leads to less solution species than the one in acetonitrile. No informative NMR spectra could be obtained from the Sm analogue due to the paramagnetic broadening of the peaks. Isolation of oxo clusters with these complexes using different solvent and oxo donor ligands is under investigation.

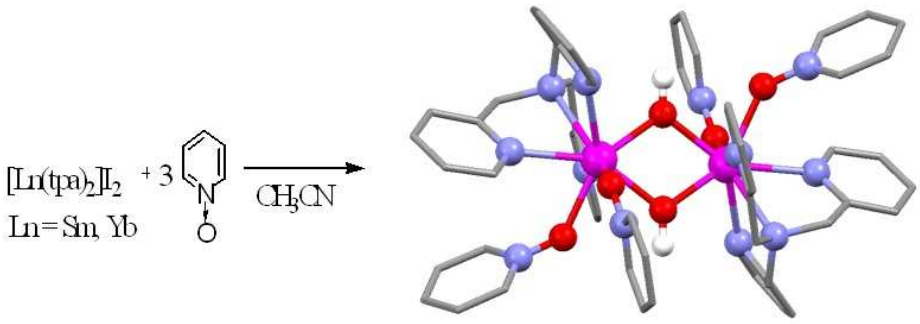

Figure IV-12: Synthesis and crystal structure of $[Ln(tpa)(\mu\text{-}OH)(Py\text{-}N\text{-}Oxide)_2]_2^{2+}$ Ln = Yb, Sm

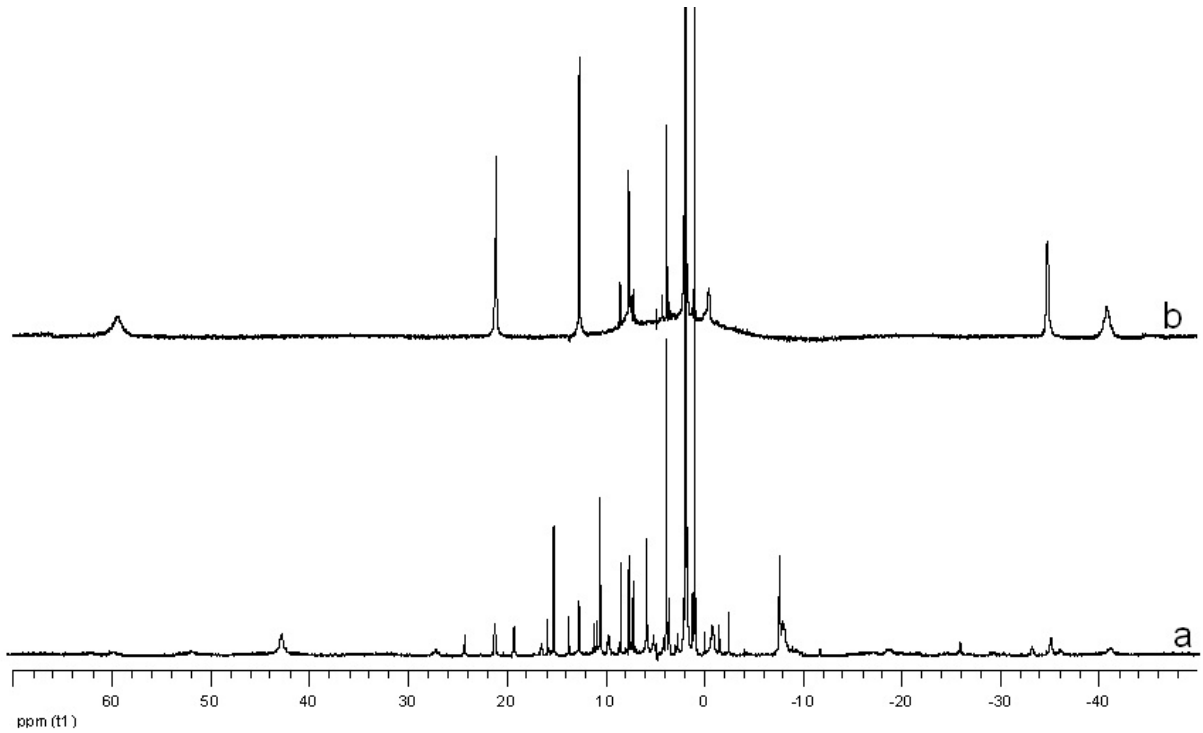

Figure IV-13: The comparison of the ^{1}H NMR spectra (400 MHz, CD_3CN, 298K) of the reactions of $[Yb(tpa)_2]I_2$ with 3 eq. of Py-N-oxide in a) acetonitrile and b) benzonitrile

We have also tested the oxidation of LnI_2 (Sm, Eu, Yb, Dy, Nd, Tm) salts in THF by Py-N-Oxide in order to obtain high nuclearity clusters. All the reactions proceeded with a sharp discoloration of the solutions and the compounds were isolated through precipitation by hexane. Recently, single crystals of a Sm_6 cluster have been obtained by slow diffusion of diisopropylether into the acetonitrile solution of the SmI_2 reacted with Py-N-Oxide. The synthesis and crystal structure is given in Figure IV-14. The low quality of crystal did not allow full structure resolution, however we could identify the Sm_6O_9 cluster core. This result is highly promising and studies are ongoing to prepare this type of oxo clusters.

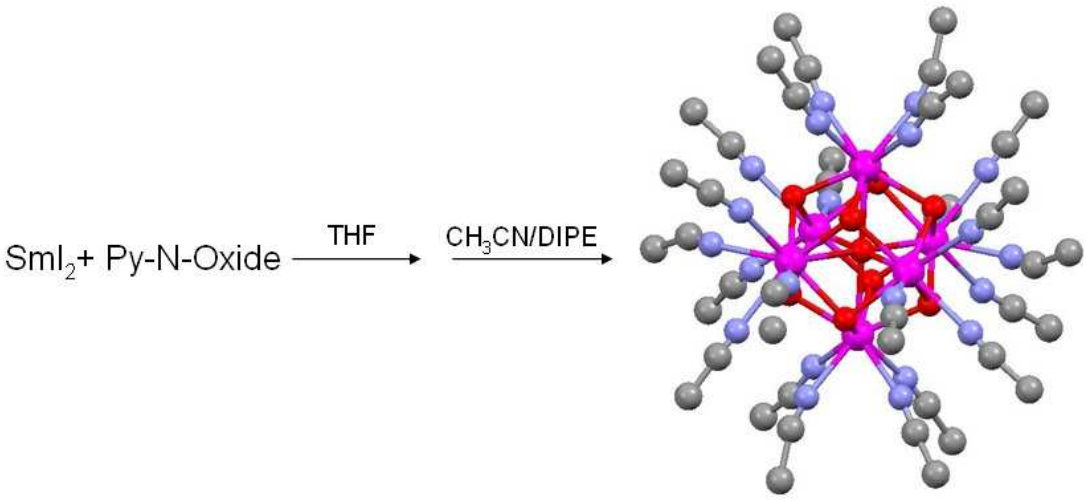

Figure IV-14: Synthesis and X-ray structure of $Sm_6O_9(CH_3CN)_{22}$ cluster

3- Synthesis and characterization of 1:1 divalent lanthanide complexes

Reaction of divalent lanthanide iodide salts (Sm(II), Yb(II), Eu(II)) with one equivalent of tpa in THF resulted in the immediate precipitation of the 1:1 tpa complexes. The crystals suitable for X-ray diffraction were obtained by slow diffusion of diisopropylether into acetonitrile solutions of these precipitated complexes of Yb(II) and Eu(II). The reaction of SmI_2 with one equivalent of tpa led to the isolation of the complex as a red violet powder. Satisfactory elemental analysis could be obtained from this powder indicating the formation of $[Sm(tpa)I_2]$ however no X-ray quality crystals could be obtained from this compound.

a) $[Yb(tpa)I_2(CH_3CN)]$

The proton NMR spectrum in anhydrous deuterated acetonitrile of the blue powder obtained from the reaction of YbI_2 with one equivalent of tpa shows the presence of two sets of peaks corresponding to mono (blue dots) and bis (red dots) tpa complexes (Figure IV-15). Despite the presence of two solution species, we have managed to obtain single crystals of $[Yb(tpa)I_2]$ complex by slow diffusion of diisopropylether into an acetonitrile solution of the isolated compound.

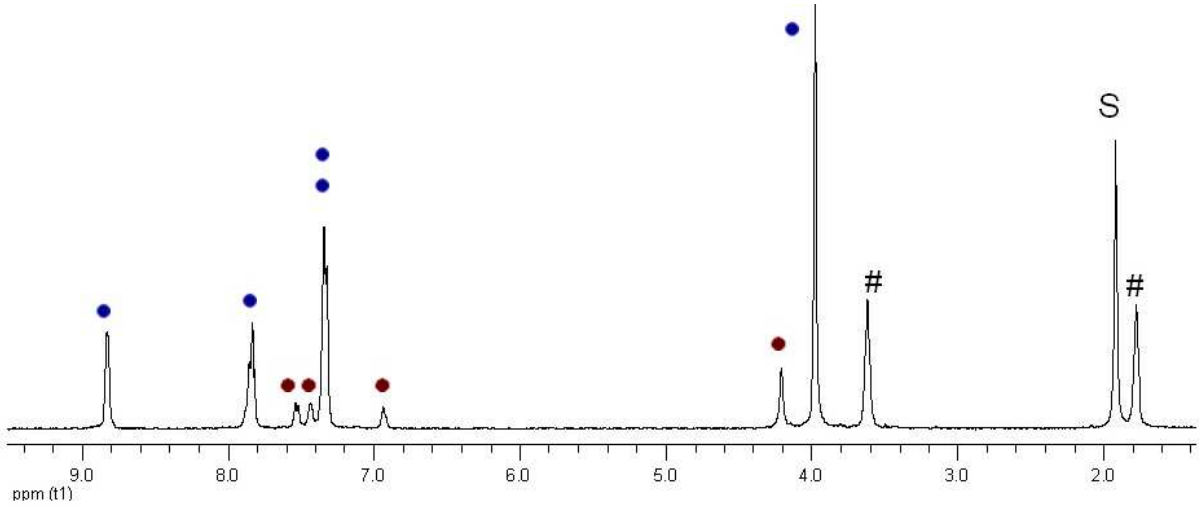

Figure IV-15: ^1H NMR spectrum of the blue powder isolated from the reaction of YbI_2 with one eq. of tpa in THF. (400 MHz, 298K) Red dots: $[Yb(tpa)_2]I_2$ and blue dots: $[Yb(tpa)I_2]$ S: CD_3CN, #: residual THF

The complex $[Yb(tpa)I_2(CH_3CN)]\cdot 0.5CH_3CN$ **(XVIII)** crystallizes in the triclinic space group P-1. Mercury diagram of the complex is given in Figure IV-16, selected interatomic distances and angles are given in Table IV-4. The metal ion is seven coordinated by four nitrogen atoms of tpa, two cis coordinated iodide ions and a nitrogen atom of an

acetonitrile molecule. The coordination of acetonitrile is nearly linear, with an Yb-N(21)-C(21) angle of 172.7(4)°. The coordination geometry can be described as distorted monocapped octahedron (Figure IV-17) with the angles of N(3)-Yb-I(2) 159.38(9)°, N(4)-Yb-I(1) 170.47(9)°, N(2)-Yb-N(21) 172.49(14)° and N(21)-Yb(1)-I(1) 90.15(11)°. The triangular face N(3), N(2), N(4) is capped by N(1) atom. The Yb-N_{amine} bond (2.620(4) Å) is longer than the average Yb-$N_{pyridine}$ bond (2.565(6) Å).

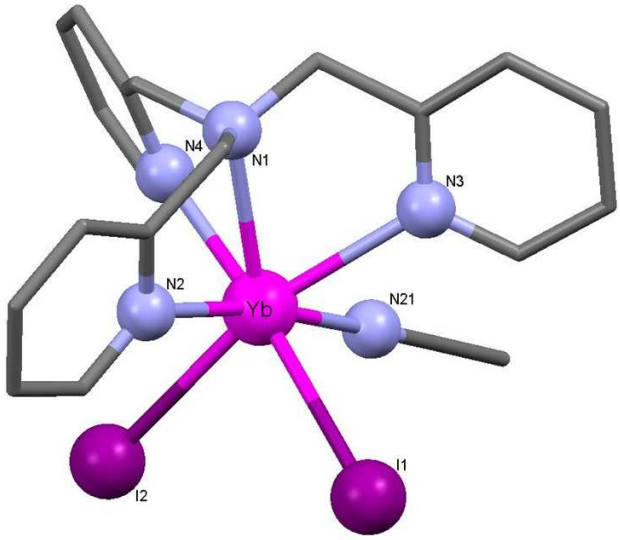

Figure IV-16: Mercury diagram of the complex [Yb(tpa)I_2(CH_3CN)] **(XVIII)**

Table IV-4: Selected Bond Lengths (Å) and Angles (deg) in the Complex **XVIII**

Yb(1)-N(4)	2.559(4)	Yb(1)-I(1)	3.1418(4)
Yb(1)-N(2)	2.567(4)	Yb(1)-I(2)	3.1830(4)
Yb(1)-N(3)	2.571(4)	Yb(1)-N(21)	2.546(5)
Yb(1)-N(1)	2.620(4)		
N(21)-Yb(1)-N(4)	84.48(14)	N(4)-Yb(1)-I(1)	170.47(9)
N(21)-Yb(1)-N(2)	172.49(14)	N(2)-Yb(1)-I(1)	84.07(10)
N(4)-Yb(1)-N(2)	100.56(14)	N(3)-Yb(1)-I(1)	85.80(9)
N(21)-Yb(1)-N(3)	75.38(14)	N(1)-Yb(1)-I(1)	124.31(8)
N(4)-Yb(1)-N(3)	100.38(13)	N(21)-Yb(1)-I(2)	84.73(10)
N(2)-Yb(1)-N(3)	108.85(14)	N(4)-Yb(1)-I(2)	82.78(9)
N(21)-Yb(1)-N(1)	123.01(14)	N(2)-Yb(1)-I(2)	90.36(10)
N(4)-Yb(1)-N(1)	65.16(12)	N(3)-Yb(1)-I(2)	159.38(9)
N(2)-Yb(1)-N(1)	64.43(13)	N(1)-Yb(1)-I(2)	132.68(8)
N(3)-Yb(1)-N(1)	65.26(12)	I(1)-Yb(1)-I(2)	88.902(10)
N(21)-Yb(1)-I(1)	90.15(11)	C(21)-N(21)-Yb(1)	172.7(4)

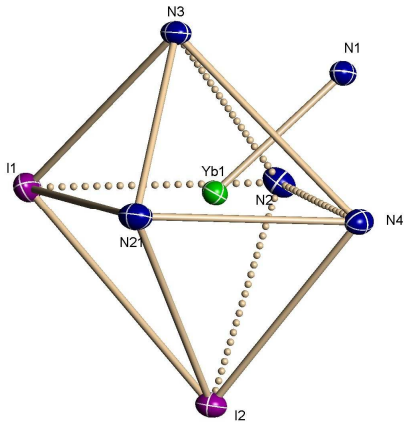

Figure IV-17: Coordination polyhedra of the Yb(II) ion in [Yb(tpa)I_2(CH_3CN)] **(XVIII)**

b) [Eu(tpa)(μ-I)I]$_2$

The complex [Eu(tpa)(μ-I)I]$_2$ **(XIX)** crystallizes as a dimer in orthorhombic Pbca space group. Mercury diagram of the complex is given in Figure IV-18, selected interatomic distances and angles are given in Table IV-5. The europium ion is situated 1.253 Å above the plane defined by the $N_{pyridine}$ atoms, significantly farther than the observed distance for Yb(III) in **XVIII** which is 1.087 Å. This creates a greater access to the metal ion and allows dimerisation. The structure has a C_2 symmetry with a 2 fold axis through the I(1)-I(1)# direction.The europium atoms are seven coordinated with four nitrogen from the tpa ligand, with one terminal and two bridging iodide ligands. The coordination polyhedra around the Eu(II) ion is best described as a distorded mono capped octahedron (Figure IV-19). The average Eu-N distance found for pyridyl nitrogen is 2.565(6) Å and Eu-N_{amine} distance is 2.620(4) Å. The three ligand-Eu-trans ligand angles are 166.51(7)° for N(4)-Eu-I(1)#1 169.57(7)° for N(3)-Eu-I(1), 176.18(6)° for N(2)-Eu-I(2). The angles, which are expected to be 90° in a perfect octahedral, vary from 81.41(6)° to 105.66(10)°. The separation of two europium atoms is 4.9076(1)Å and the I(1)-I(1)# separation is 4.4509(1)Å. The 3.2888(3) Å terminal Eu-I(2) distance is shorter than the bridging distances Eu-I(1) 3.3142(1) Å and Eu-I(1)#1 3.3111(1) Å.

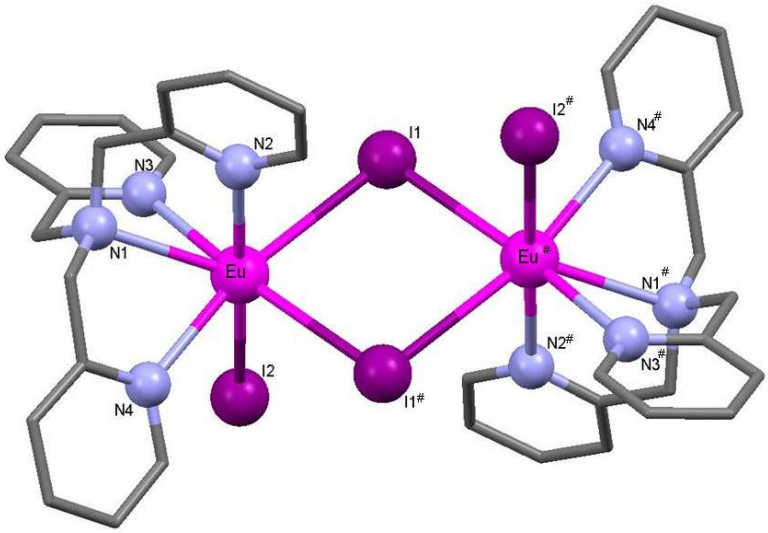

Figure IV-18: Mercury diagram of the complex $[Eu(tpa)(\mu\text{-}I)I]_2$ (**XIX**)

Table IV-5: Selected Bond Lengths (Å) and Angles (deg) in the Complex **XIX**

Eu-N(3)	2.658(3)	Eu-I(2)	3.2888(3)
Eu-N(2)	2.673(3)	Eu-I(1)	3.3111(3)
Eu-N(4)	2.686(3)	Eu-I(1)#1	3.3142(3)
Eu-N(1)	2.748(3)		
N(3)-Eu-N(2)	95.69(10)	N(2)-Eu-I(1)	90.02(6)
N(3)-Eu-N(4)	105.66(10)	N(4)-Eu-I(1)	82.12(7)
N(2)-Eu-N(4)	97.75(10)	N(1)-Eu-I(1)	128.56(6)
N(3)-Eu-N(1)	61.85(9)	I(2)-Eu-I(1)	92.991(7)
N(2)-Eu-N(1)	62.30(8)	N(3)-Eu-I(1)#1	87.81(7)
N(4)-Eu-N(1)	62.03(9)	N(2)-Eu-I(1)#1	81.41(6)
N(3)-Eu-I(2)	80.98(7)	N(4)-Eu-I(1)#1	166.51(7)
N(2)-Eu-I(2)	176.18(6)	N(1)-Eu-I(1)#1	127.59(6)
N(4)-Eu-I(2)	85.01(7)	I(2)-Eu-I(1)#1	96.532(7)
N(1)-Eu-I(2)	117.20(6)	I(1)-Eu-I(1)#1	84.413(6)
N(3)-Eu-I(1)	169.57(7)	Eu-I(1)-Eu#1	95.587(6)

Symmetry transformations used to generate equivalent atoms: #1 -x+1, -y, -z

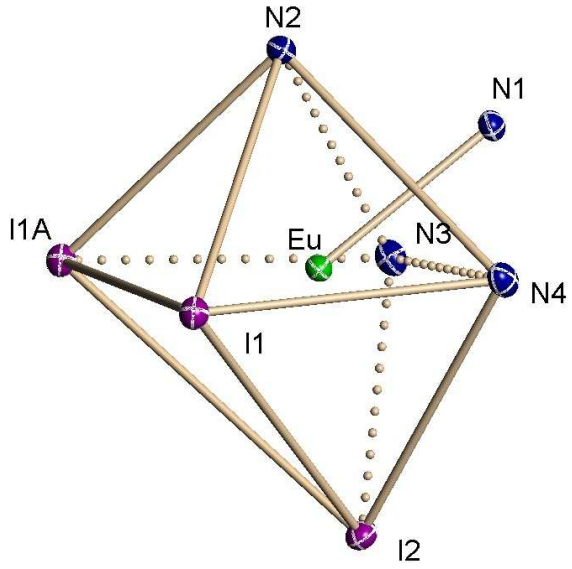

Figure IV-19: Coordination polyhedra of the Eu(II) ion in $[Eu(tpa)(\mu\text{-}I)I]_2$ **(XIX)**

4- Attempts to prepare non-classical divalent lanthanide complexes

The divalent salts of TmI_2, DyI_2 and NdI_2 are highly reactive. The solutions of DyI_2 and NdI_2 in THF are stable below 0 and -20 ºC respectively. Therefore the complexes have been prepared at -40 ºC and they immediately precipitated from the reaction of tpa with LnI_2 as a colored (orange Tm, brown Dy, dark brown Nd) powder as shown in Image IV-1. Satisfactory elemental analysis was obtained from $[Tm(tpa)_2]I_2$. However no NMR study could be performed as Tm(II), Dy(II) complexes oxidized easily in most of the solvents as observed by the sharp color change. Similarly no crystals could be grown from the divalent or the oxidized complexes till now. The insolubility in THF or DME is highly limiting the characterization and further reactivity studies of these complexes. Some interesting results have been obtained from the Nd complex that will be discussed in detail in the next section.

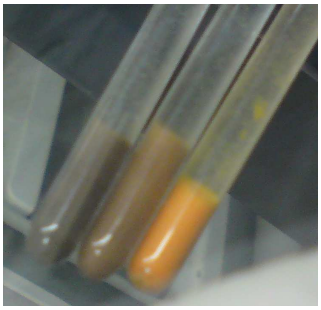

Image IV-1: The reaction tubes of 2 eq. of tpa and $Ln(II)I_2$ (Nd, Dy, Tm respectively) at -40ºC in THF

The reaction of the NdI_2 with two equivalents of tpa in anhydrous THF at -40ºC resulted in an immediate brown precipitate. The ^1H NMR of this brown powder in py-d_5

presents five signals (Figure IV-20), and after a day new chemical shifts appeared, indicating the formation of decomposition products (Figure IV-21). This highly reactive specie is thought to be Nd(II) bis tpa complex, however the attempts to crystallize this compound did not succeed in pyridine at -40 ºC or by slow diffusion of ligand onto NdI_2 solution in THF at -40 ºC. Similarly, the decomposition products formed in pyridine could not be crystallized.

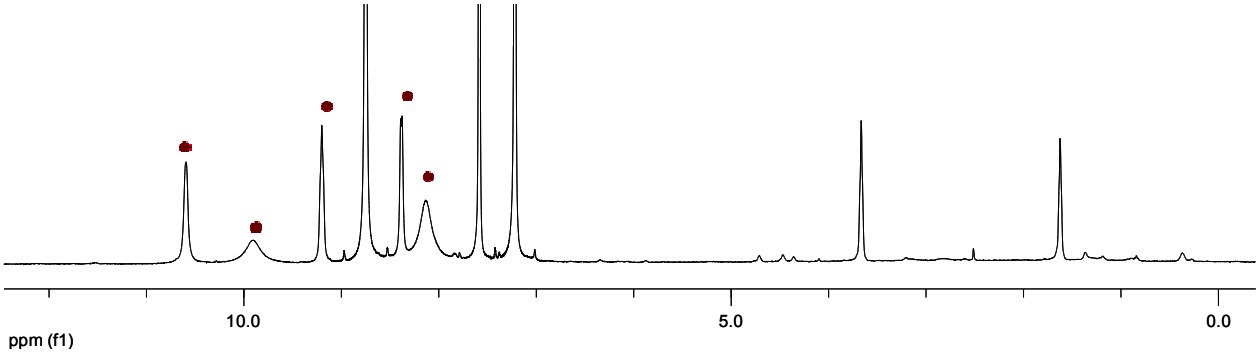

Figure IV-20: ^{1}H NMR of the precipitated dark brown powder from the reaction of NdI_2 with two eq. of tpa in THF. (400 MHz, 298K) S: py-d5, #: residual THF

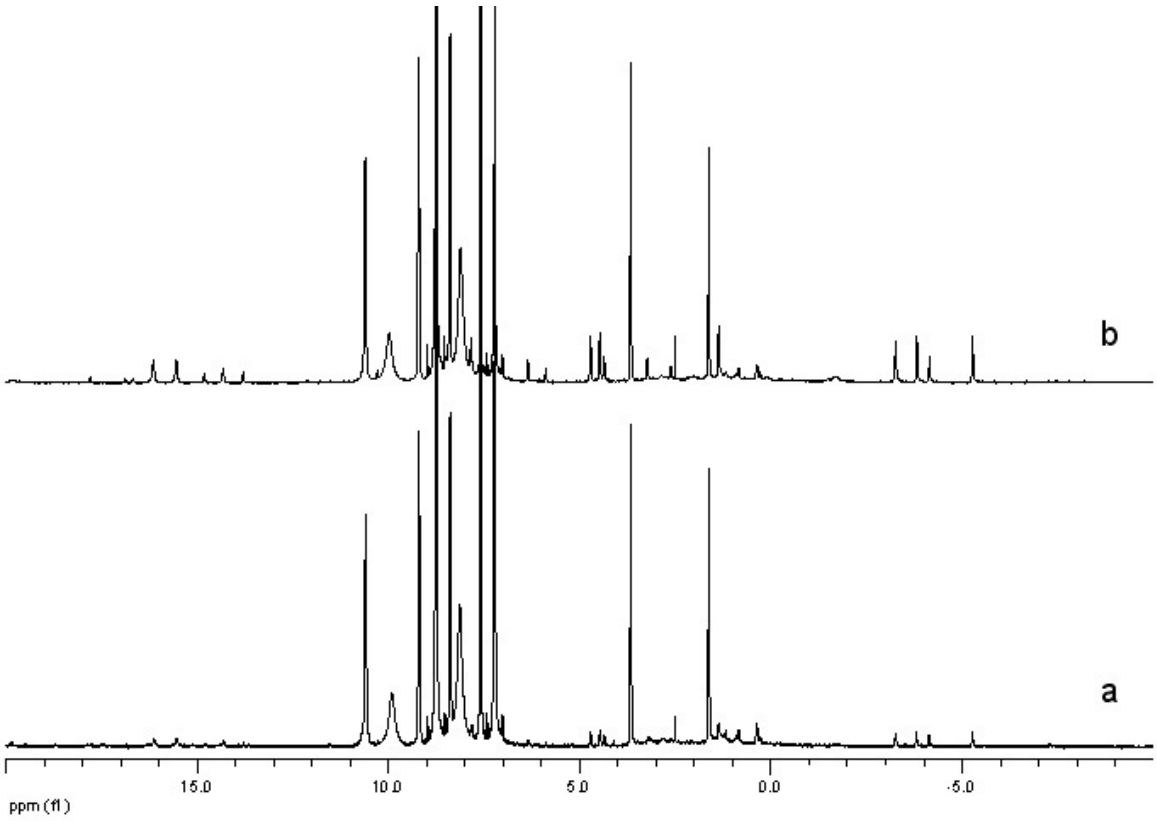

Figure IV-21: ^{1}H NMR of the precipitated dark brown powder after a) 2 hours and b) 24 hours. (400 MHz, 298K) S: py-d5, #: residual THF

Unexpectedly when the reaction was repeated at room temperature, the immediately formed brown precipitate presented an identical proton NMR spectrum to the compound isolated at -40 ºC. Therefore we performed a slow diffusion of 2 eq. of ligand into the deep violet NdI_2 solution in THF at room temperature in order to obtain X-ray quality crystals. After a few days formation of a yellow green powder was observed indicating the oxidation of the compound under these conditions. The proton NMR of this yellow green powder is given in Figure IV-22 in anhydrous acetonitrile. The chemical shifts of the $[Nd(tpa)_2]I_3$ complex (previously reported by our group [228]) could be identified in the spectrum as shown with red dots in Figure 23. Additional unknown species have been identified by the blue dots shown in the spectrum. However no crystals could be grown from this yellow-green powder. Therefore in order to change counterion for obtaining suitable crystals for X-ray diffractometry, the isolated powder is reacted with NaN_3 in pyridine as shown in Scheme IV-9. Single crystals of the Nd_{13} oxo cluster $[Nd_{13}(\mu_4\text{-}O_8)Na_8(\mu_4\text{-}1,1,1,1\text{-}N_3)_6(\mu_3\text{-}1,1,3\text{-}N_3)_{24}(py)_{28}I]\cdot(py)_7$ ({$Nd_{13}Na_8$ cluster} could be obtained from this pyridine solution by slow diffusion of hexane.

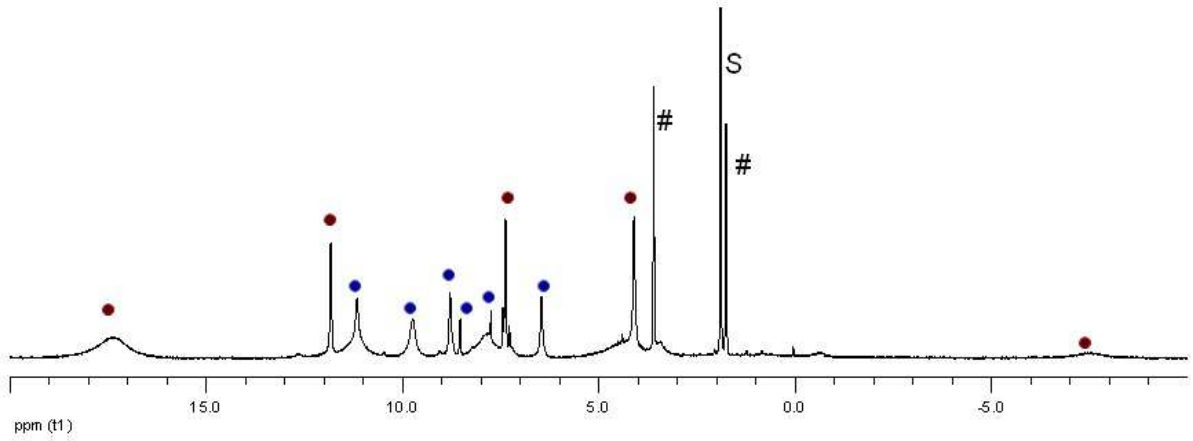

Figure IV-22: ^1H NMR spectrum of the precipitated yellow green powder formed by slow diffusion of ligand (400 MHz, 298K, CD_3CN). S: CD_3CN, #: residual THF, red dots: $[Nd(tpa)_2]I_3$, blue dots: unknown species

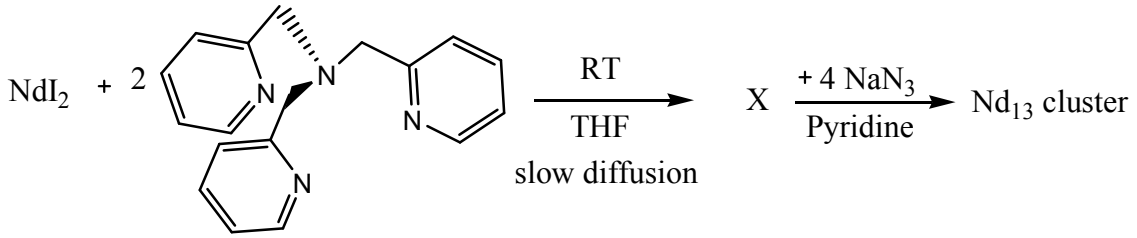

Scheme IV-9: Synthesis of Nd_{13} cluster by slow diffusion of tpa into NdI_2 solution in THF and further reaction in pyridine with NaN_3

4.1- $Nd_{13}Na_8$ cluster

The compound crystallizes in the triclinic space group P-1 with the formula of $[Nd_{13}(\mu_4\text{-}O_8)Na_8(\mu_4\text{-}1,1,1,1\text{-}N_3)_6(\mu_3\text{ -}1,1,3\text{-}N_3)_{24}(py)_{28}\ I]\cdot(py)_7$ ({$Nd_{13}Na_8$ cluster} **(XX)**. The cluster consists of thirteen Nd bridged by eight $\mu_4\text{-}O^{2-}$, 6 end on bridged $\mu_4\text{-}1,1,1,1\text{-}N_3^-$ and 24 end to end bridged μ_3 -1,1,3-N_3 ions, eight Na^+ ions and the final twenty eight coordinated pyridine solvent molecules and one iodide to balance the charge (Figure IV-23). A central Nd ion is eight coordinated by the oxygen atoms defining a cubic coordination polyhedra (Figure IV-24). The 12 neodymium atoms defining the cuboctahedron vertices have a coordination number of nine with two oxygens, four nitrogens of μ_3 -1,1,3-N_3, two nitrogens of μ_4-1,1,1,1-N_3 and one nitrogen of a pyridine. The coordination polyhedra around these neodymium atoms is best described as monocapped square antiprism as shown in Figure IV-24.

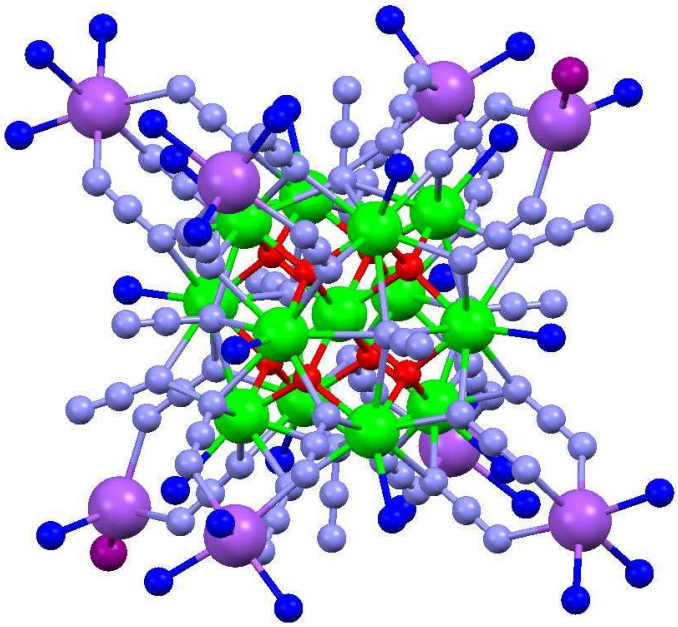

Figure IV-23: $[Nd_{13}(\mu_4\text{-}O_8)Na_8(\mu_4\text{-}1,1,1,1\text{-}N_3)_6(\mu_3\text{-}1,1,3\text{-}N_3)_{24}(py)_{28}I]\cdot(py)_7$ (**XX**) Uncoordinated pyridines and the carbon and hydrogen atoms are removed for clarity. Nd: green, oyxgen: red, azido nitrogens: ligth blue, pyridine nitrogens: dark blue, sodium: lilac, iodide: purple. Both coordinated iodides are shown but only one is occupied for a given molecule

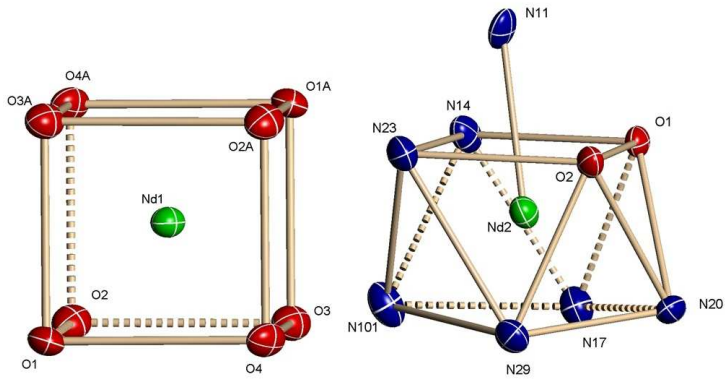

Figure IV-24: Coordination polyhedra for the neodymium atoms in the cluster **XX**

The cuboctahedron is an Archimedean solid consisting of six square faces and eight triangular faces. It posseses twelve identical vertices, each representing the meeting point of two triangles and two squares, and twenty-four identical edges, each separating a triangle from a square [229]. The cluster core is characterized as a Nd^{3+} centered Nd_{12} cuboctahedron (Figure IV- 25) which is stabilized by six sodium atoms bound to azido groups and defining a distorted cube at the cluster shell. Cuboctahedral clusters are rare in lanthanide chemistry. There are no clusters reported in this geometry other than the heterometallic 3d-4f clusters $Cu_{12}Ln_6$ (Ln = Y, Nd, Gd) where six Ln atoms are capping the square faces of the cuboctahedron formed by the twelve Cu atoms [230, 231]. Similar cluster geometry is reported with transition metals by Albano et al. where silver centered cuboctahedron core is stabilized by eight iron atoms forming the $[Ag_{13}Fe_8(CO)_{32}]^{4-}$ cluster [232].

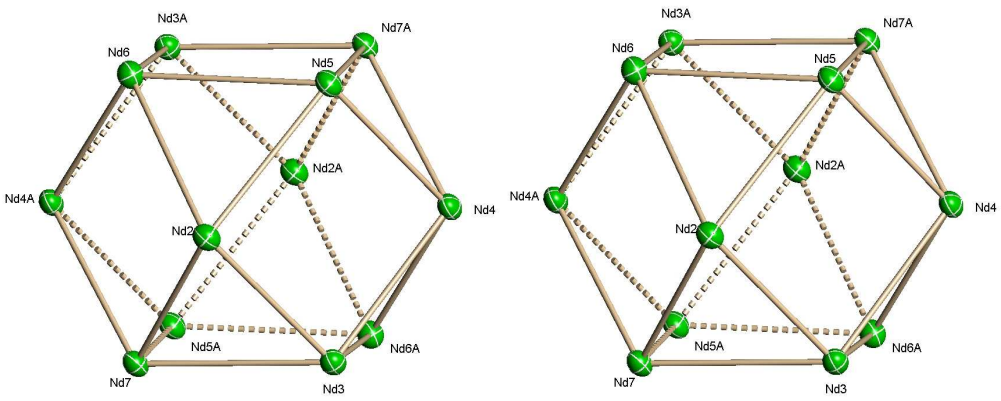

Figure IV-25: The Nd_{12} cuboctahedron without and with the Nd center

The construction of the cluster is summarized in Figure IV-26. The central neodymium ion is bridged to the other twelve neodymium ions by eight μ_4-oxygens (Figure IV-26a). The oxygen ions are located at the center of each tetrahedra formed by three Nd ions defining the triangle faces of the cuboctahedron and the central Nd ion (Figure IV-26b). The square faces of this cuboctahedron cluster core are capped by six azido ligands (Figure IV-26c). The cluster core is further enveloped by twelve azido ligands located in the middle of each triangular edge bridging two neodymium ions. Finally all the triangular faces of the cuboctahedron is capped by eight sodium ions binding the twelve end-to-end bridging azido ligands (Figure IV-26f). Six of these sodium ions complete their coordination sphere with three pyridine molecules and the coordination sphere of the other two Na ions is completed by a half iodine and a pyridine molecule as shown in Figure IV-23.

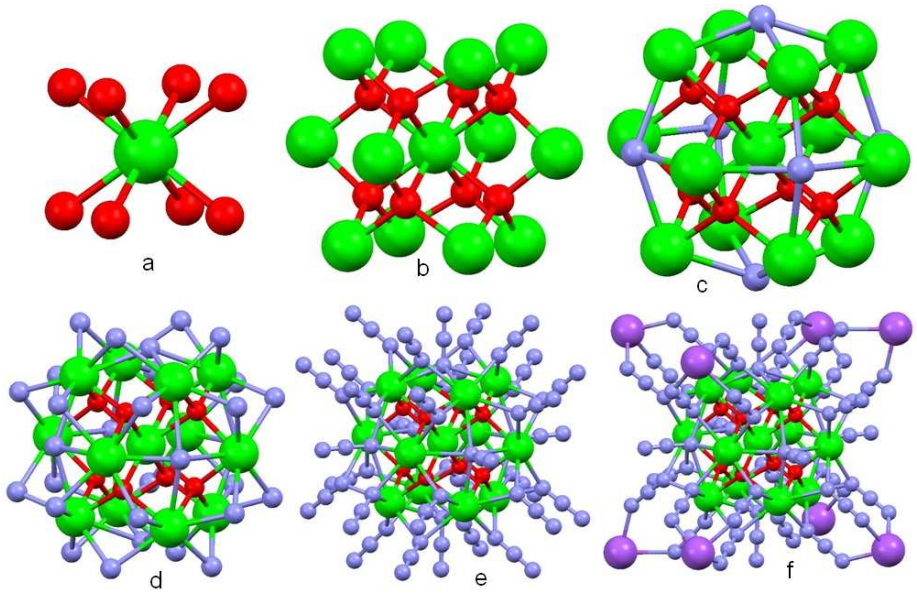

Figure IV-26: Constructing the $Nd_{13}Na_8$ cluster. Nd: green, oyxgen: red, azido nitrogens: ligth blue, sodium: lilac. In c and d only on nitrogen atom of the azido groups are shown for clarity

The $[Nd_{13}(\mu_4\text{-}O_8)Na_8(\mu_4\text{-}1,1,1,1\text{-}N_3)_6(\mu_3\text{-}1,1,3\text{-}N_3)_{24}]^+$ cluster core posseses pseudocubic O_h symmetry, with six 2-fold rotation axes passing through the vertices of the cuboctahedron (py-Nd_{center}-py), four 3-fold rotation axes passing through the triangular faces of the cuboctahedron (Na-Nd_{center}-Na) and three 4-fold rotation axes passing through the square faces of the cuboctahedron (μ_4-N_3-Nd_{center}-μ_4-N_3) as shown in Figure IV-27. In spite of the high symmetry of the cluster core, the crystallographically imposed symmetry is reduced to C_1 as only the inversion center is retained in the crystal due to the distortions imposed by the coordinated iodide and solvent disorder. As a result the Nd-Nd distances (ranging from 3.7645(5) to 3.7811(5) Å) show the deviations from the ideal cuboctahedron O_h (Table IV-6) symmetry. Each pair of sodium atoms capping triangular faces of cuboctahedron defines a distorted cube with Na-Na distances ranging from 9.4992(4) to 10.3318(3) Å (Table IV-7). Selected interatomic distances around each neodymium ion are given in Table IV-8. The mean of Nd-O bond distances for the central neodymium ion is found to be 2.47(1) Å. The mean of the Nd-O bond distances for the 12 Nd ion forming the cuboctahedron core is 2.265(9) Å and the mean of the Nd-N distances is 2.70(9) Å.

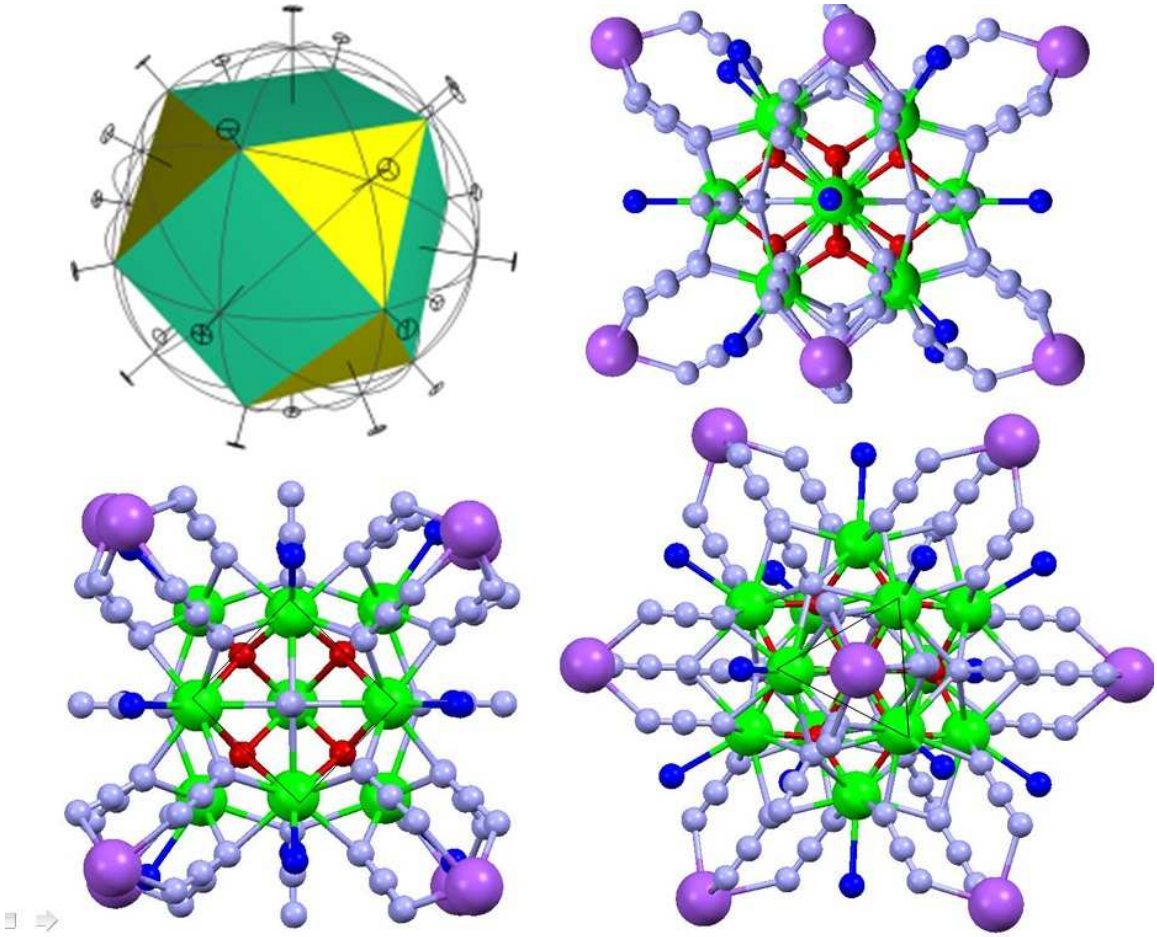

Figure IV-27: The view along the 2-fold (through the vertices), 3-fold (through the center of the triangular faces) and 4-fold (through the center of square faces) axes of symmetry. Nd: green, oyxgen: red, azido nitrogens: ligth blue, sodium: lilac

Table IV-6: Selected interatomic distances in the Nd_{13} cuboctahedron core in **XX**

Nd(1)-Nd(2)#1	3.7698(3)	Nd(2)-Nd(6)	3.7811(5)	Nd(4)-Nd(6)#1	3.7785(4)
Nd(1)-Nd(2)	3.7699(4)	Nd(3)-Nd(6)#1	3.7645(5)	Nd(5)-Nd(7)#1	3.7740(5)
Nd(1)-Nd(3)#1	3.7721(4)	Nd(3)-Nd(7)	3.7746(4)	Nd(6)-Nd(3)#1	3.7645(5)
Nd(1)-Nd(3)	3.7722(4)	Nd(4)-Nd(5)	3.7760(4)	Nd(6)-Nd(4)#1	3.7785(4)
Nd(2)-Nd(7)	3.7774(4)	Nd(4)-Nd(7)#1	3.7781(5)	Nd(7)-Nd(5)#1	3.7740(5)

Symmetry transformations used to generate equivalent atoms: # : -x+1,-y+1,-z+1

Table IV-7: Selected interatomic distances in the distorted cube formed by Na atoms in **XX**

Na(1)-Na(3)	10.2200(3)	Na(5)-Na(3)	10.0012(4)
Na(3)-Na(2)	9.8266(3)	Na(5)-Na(1)	10.3318(3)
Na(2)-Na(5)	9.8914(3)	Na(1)-Na(2)	9.4992(4)
Na(5)-Na(1)	10.3318(3)	Na(1)-Na(3)	10.2200(3)
Na(1)-Na(2)	9.4992(4)	Na(3)-Na(5)	10.0012(4)
Na(2)-Na(5)	9.8914(3)	Na(2)-Na(3)	9.8266(3)

Table IV-8: Selected interatomic distances around each neodymium ion in **XX**

Nd(1)-O(1)	2.486(3)	Nd(2)-O(2)	2.255(3)	Nd(3)-O(3)	2.269(4)	Nd(4)-O(4)	2.266(3)
Nd(1)-O(2)	2.471(4)	Nd(2)-O(1)	2.275(4)	Nd(3)-O(2)	2.284(3)	Nd(4)-O(3)	2.269(3)
Nd(1)-O(3)	2.455(3)	Nd(2)-N(14)	2.608(4)	Nd(3)-N(23)	2.638(5)	Nd(4)-N(41)	2.579(4)
Nd(1)-O(4)	2.478(3)	Nd(2)-N(23)	2.624(5)	Nd(3)-N(35)	2.644(5)	Nd(4)-N(26)	2.633(6)
Nd(1)-O(1)#1	2.486(3)	Nd(2)-N(29)	2.663(4)	Nd(3)-N(50)	2.651(4)	Nd(4)-N(38)	2.656(5)
Nd(1)-O(2)#1	2.471(4)	Nd(2)-N(17)	2.663(5)	Nd(3)-N(26)	2.653(4)	Nd(4)-N(103)	2.686(4)
Nd(1)-O(3)#1	2.455(3)	Nd(2)-N(101)	2.690(5)	Nd(3)-N(102)	2.676(5)	Nd(4)-N(32)	2.694(5)
Nd(1)-O(4)#1	2.478(3)	Nd(2)-N(20)	2.782(4)	Nd(3)-N(11)	2.819(4)	Nd(4)-N(20)#1	2.753(5)
		Nd(2)-N(11)	2.888(4)	Nd(3)-N(44)#1	2.867(4)	Nd(4)-N(11)	2.897(5)

Nd(5)-O(1)	2.253(3)	Nd(6)-O(1)	2.265(3)	Nd(7)-O(4)#1	2.255(4)
Nd(5)-O(4)	2.271(3)	Nd(6)-O(3)#1	2.271(3)	Nd(7)-O(2)	2.256(3)
Nd(5)-N(53)	2.610(5)	Nd(6)-N(50)#1	2.626(5)	Nd(7)-N(32)#1	2.597(4)
Nd(5)-N(47)	2.630(5)	Nd(6)-N(38)#1	2.629(4)	Nd(7)-N(29)	2.646(5)
Nd(5)-N(104)	2.686(4)	Nd(6)-N(17)	2.659(5)	Nd(7)-N(35)	2.647(5)
Nd(5)-N(14)	2.688(5)	Nd(6)-N(105)	2.686(5)	Nd(7)-N(53)#1	2.670(4)
Nd(5)-N(41)	2.720(4)	Nd(6)-N(47)	2.698(4)	Nd(7)-N(106)	2.710(5)
Nd(5)-N(11)	2.730(5)	Nd(6)-N(44)	2.788(5)	Nd(7)-N(44)#1	2.762(5)
Nd(5)-N(44)	2.905(5)	Nd(6)-N(20)	2.880(5)	Nd(7)-N(20)	2.913(5)

Symmetry transformations used to generate equivalent atoms: # : -x+1,-y+1,-z+1

4.2- Bond Valence Sum Calculations

The trivalent oxidation state of the neodymium ions was established by charge considerations and bond valence sum (BVS) calculations. The bond valence for each Nd ion in $\mathbf{Nd_{13}O_8}$ cluster **XX** was calculated using the formula: $s_{ij} = \exp[(r_{ij} - d_{ij})/b)$ (where d_{ij} is the experimental bond length while r_{ij} and b are empirically determined constants for the given *i-j* bond) proposed by Brown [233]. From the parameters published by Brown on the Web [234], we have chosen $r_{ij} = 2.117$ and $b = 0.37$ for calculating the valences of Nd(III)–O bonds, whereas we used $r_{ij} = 2.201$ and $b = 0.37$ for the Nd–N bonds The sum of bond valences for

the **$Nd_{13}O_8$ cluster** are presented in Table 4. The average value of 3.06 is in good agreement with the expected trivalent state of all the neodymium ions in the cluster **XX**.

Table IV-9: Bond valence sum calculations for the Nd atoms of the cluster **XX**

atom	**Nd1**	**Nd2**	**Nd3**	**Nd4**	**Nd5**	**Nd6**	**Nd7**
BVS	3.00	3.12	2.88	3.13	3.09	3.07	3.14

The formation of this Nd_{13} cluster is highly interesting, showing the strong reductive power of NdI_2 and also proving the strong affinity for oxygen abstraction. In order to understand the mechanism of the reaction, several experiments have been performed. THF is the only oxo source in this reaction that had performed at anhydrous conditions therefore the only possible reaction mechanism for the formation of oxo cluster is the THF ring opening by the highly reactive NdI_2. Divalent lanthanides are known for giving decomposition products by scission of C-O bonds of the solvents, leading to the formation of transient products such as LnI_2OR (R=fragments of THF) [204]. Therefore the formation of the Nd_{13} cluster may be the result of the assembly formation of these transient THF opened products like $RONdI_2$. As there is no tpa in the cluster we wanted to check the role of tpa in the cluster formation. We have found that the cluster can only be isolated from the reaction of NdI_2+2tpa with THF but not from the reaction of NdI_2 with THF without tpa. This is probably the result of increased reactivity of NdI_2 in presence of tpa.

The reaction leading to the cluster is highly complex and the yield was quite poor (only a few crystals of the cluster could be obtained). However, isostructural crystals of the cluster could be isolated reproducibly from four different batches. The oxo cluster core forms as a side product along with $[Nd(tpa)_2]I_3$, NaI salts, and probably other unidentified products like $NdI_2OR(THF)_x$ units. In order to optimize the reaction conditions, we have performed the reaction of NdI_2 with 2 tpa at different temperatures and conditions. We have observed that, isolation of single crystals of the cluster is observed only when the reaction of NdI_2 with two equivalents of tpa performed at -70 ºC stirring for over two days or when very slow diffusion of ligand to metal is performed at room temperature. Under these conditions, the color of the resulting precipitate was light yellow-green and identical NMR spectra obtained as shown in Figure IV-23. Even though a complete explanation to these observations is still lacking, these results suggests that the reaction leading to $NdI_2OR(THF)_x$ that assembles to form the oxo

cluster core is slower than the formation of bis tpa complex and the cluster does only form when the reaction is performed slowly.

The cluster XX is a very interesting example of assembly of $NdI_2OR(THF)x$ species formed by the increased reactivity of NdI_2 in presence of tpa. It is clear that unidentified products also formed during our reactions, but only the cluster and the NaI salts have solubility properties that permit isolation from pyridine. The yield of the reaction is very low and further investigation and optimization is still ongoing. We believe that further studies with different oxo donor ligands will lead to the formation of a variety of high nuclear oxo clusters.

5- Conclusion and Perspectives

The work presented in this chapter focused on the preparation of divalent molecular precursors for the isolation of polynuclear lanthanide oxo-clusters. The neutral tripodal N donor ligand tpa has been chosen as it was efficient for stabilizing trivalent uranium complexes. The bis tpa complexes of Eu(II), Sm(II) and Yb(II) could be isolated and fully characterized. The mono tpa complexes presented an equilibrium in solution and only single crystals of Eu and Yb complexes could be analyzed. The non classical divalent lanthanide (Tm(II), Dy(II), Nd(II)) complexes could not be characterized due to their extreme reactivity. A very interesting neodymium oxo cluster has been obtained by cleavage of THF and analyzed crystallographically.

This thematic is in its early stages in the laboratory, and these promising preliminary results demonstrate that the obtained complexes can be useful precursors for the isolation of polymetallic oxo clusters. In close future, in order to maintain the solubility of the final complexes in etheral solvents like THF or DME, the substitution on the tpa ligand with TMS or tBu groups will be performed. More in-depth studies are necessary, especially concerning the reactivity of these complexes with different oxo donor ligands and under different reaction conditions. Reactivity with small molecules like dinitrogen, carbon monoxide and dihydrogen could be tested as an extension of the project. The luminescence studies of the final cluster could not be performed during the limited time of thesis. These studies would provide deeper understanding of the relationship between the structure and properties of this type of large lanthanide clusters.

CHAPTER V Final Conclusions and Perspectives

The aim of this thesis work was related to the development of synthetic strategies to include lanthanide ions in discrete high nuclearity polymetallic architectures by using suitable organic ligands and the study of photophysical properties of the final assemblies to improve optical properties. The fundamental interest in the preprogrammed assembly of polymetallic lanthanide complexes is crucial in the development of luminescent and multifunctional materials (chiral/ luminescent) both in solid state and in solution. This work contributed to a better understanding of the assembly formation through original synthetic methods involving self-assembly directed by small ligands or by reactivity of divalent lanthanide complexes leading to interesting new polynuclear complexes.

In the first part of this work, we have studied the synthesis and photophysical properties of NIR emissive stable complexes obtained with hydroxyquinoline based tridentate dianionic ligands functionalised with carboxylic acid (**H_2hqa**) and tetrazole groups (**H_2hqt**). Only dimeric (stabilized by the strong hydrogen bonds) and polymeric species could be isolated depending on the protonation state as a result of the strength of the base used. These ligands could be used in the future studies for developing new luminescent infinite polymetallic complexes (coordination polymers or extended metal organic frameworks), where dual emission could be obtained by the replacement of the counterion in the networks with different lanthanide ions. Tetrazole unit has been observed to enhance the photophysical properties of these tris complexes. Further improvement could be provided by halogenation of the quinoline units. These ionic complexes provide solubility and stability towards ligand dissociation with respect to neutral compounds. Therefore they could have potential applications in the development of new lanthanide based NIR emissive materials like ionogels and ionic liquids.

In the second part, the carboxylate-derivatized bipyoxazoline **Phbipox** ligand ((6□(4-phenyloxazolin-2-yl)-2,2□bipyridine-6-carboxylic acid)) has been used for promoting a rare diastereoselective self assembly controlled by the ligand geometry, cation size and concentration. The resulting chiral complexes have shown interesting CPL and luminescence properties. For example the assembly of rare homochiral trinuclear complexes of europium has shown to have a very high glum value corresponding to a high CPL activity. The ligand **Phbipox** also led to the synthesis of homo- and hetero-polymetallic assembly of the large polynuclear nano-sized wheel-shaped lanthanide compounds emitting in the visible and NIR

range. The heptanuclear europium complexes have been measured to have slightly higher quantum yields compared to mononuclear complex, suggesting that the cyclic arrangement of six Eu components does not lead to intramolecular quenching effects.

The chiral complexes obtained in this work are highly encouraging to further study their formation and CPL properties. The presence of sterical interactions from the phenyl groups has a great influence in the diastereoselectivity and the selection of lanthanide ion size as smaller lanthanides does not lead to assembly formation. Therefore the stereoselectivity of the self-assembly of the mononuclear complexes and the photophysical properties could be tuned by changing the ligand design. For example the replacement of phenyl group with a chiral methyl group could provide weaker steric interactions that would allow the formation of higher nuclear assemblies with a wider selection of lanthanides. By reducing the sterical interactions homochiral heptanuclear wheel shaped complexes could be obtained providing higher symmetry, better quality of crystals and higher CPL activity. Finally, the CPL studies of the neodymium and ytterbium complexes would provide better understanding of this chiral system as the species present in solution differ from the europium complexes as a result of different cation sizes.

In the last part, we have started to investigate the synthesis of divalent precursors for the preparation of high nuclear clusters by the oxidation of divalent lanthanides. This strategy should lead to oxo or nitride clusters rather than to the classical hydroxo/oxo clusters in which the hydroxo group is deleterious for the photophysical properties. We have managed to prepare and characterize complexes of divalent lanthanides with a neutral tripodal pyridine based ligand (**tpa**). An original neodymium oxo cluster has been obtained by cleavage of THF and analyzed crystallographically. The main limitation of the project was the insolubility of the lanthanide(II) complexes in ethereal solvents like THF or DME. The substitution of the tpa ligand with TMS of tBu groups could be realised in order to provide solubility for further controlled reactivity with different oxo donor ligands in these solvents. We choose to use tpa complexes as a starting materials; however, the reactivity of iodide salt of Sm(II) with an oxo donor ligand resulted also in the isolation of crystals of an octahedral samarium cluster. This result shows that different precursors like iodides, silylamides, and borohydrides could provide different reactivity and cluster architectures. These promising preliminary results demonstrate that the divalent lanthanide complexes can be useful precursors for the isolation of polynuclear oxoclusters. Moreover the use of suitable reagents could provide access to

nitrido clusters. Future studies would be directed to isolate new original lanthanide clusters with interesting optical properties for the development of solid state emissive composite materials.

CHAPTER VI Experimental Part

1- General Information

Solvents and starting materials were obtained from Aldrich, Fluka, Acros, and Alfa and used without further purification unless otherwise stated. Water and H_2O refer to high-purity water with a resistivity value of 18 MΩ·cm, obtained from the Millipore/Milli-Q purification system. All manipulations of the lanthanide complexes with Phbipox and tpa ligands were carried out under an inert argon atmosphere using Schlenk techniques and an MBraun glovebox equipped with a purifier unit (unless otherwise stated). The water and oxygen level were always kept at less than 1 ppm. The solvents were purchased from Aldrich in their anhydrous form conditioned under argon and were vacuum distilled from K/benzophenone (pyridine, diisopropylether, THF, hexane) or CaH_2 (acetonitrile, methanol), triethylamine distilled from potassium hydroxide. $Ln(Otf)_3$ salts were purchased from Aldrich and residual water present in these salts were removed by heating at 120 °C under vacuum (10^{-6} mmHg) for one week. For the studies with hydroxyquinoline based ligands lanthanide triflate salts were titrated for metal content before use, in the presence of EDTA and xylene orange. The ligand 8-hydroxyquinoline-2-carboxylic acid (H_2hqa) was purchased from Fluka and used without further purification. Anhydrous LnI_2 salts were purchased from Aldrich and used as received. The glassware was systematically oven dried at 130°C overnight followed by 3 vacuum/ argon cycles. Elemental analyses were performed either by the Service Central d'Analyses (Vernaison, France) or under argon by Analytische Laboratorien GmbH at Lindlar, Germany.

2- Chromatography

Analytical thin layer chromatography (TLC) was performed on aluminium sheets pre-coated with silica gel or neutral aluminium oxide (Merck Kieselgel 60 F254). Visualization was accomplished by UV light (254 nm). Flash column chromatography were carried out on silica gel (Merck Kieselgel 60, 40-63 μm) or on neutral activated aluminium oxide 90 (Merck, 4.9% water wt, 63-200μm).

3- Nuclear Magnetic Resonance Spectroscopy

^{1}H NMR spectra were recorded on Bruker Advance DMX 200, Varian MERCURY 400 MHz and Bruker 500 MHz spectrometers. NMR chemical shifts are reported in ppm with solvent as internal reference. Abbreviations used for describing multiplicity of the NMR signals are: s (singlet), d (doublet), dd (doublet of doublet), t (triplet), dt (doublet of triplet), q (quadruplet) and m (multiplet) and br (broad).

3.1- Diffusion coefficients measurement

The diffusion NMR experiments were performed using a Pulse-Field Gradient STimulated Echo (PFGSTE) sequence, using bipolar Gradients, at 298 K. No spinning was applied to the NMR tube. The following BPP-LED (Bipolar Pulse Pair-Longitudinal Eddy-current Delay) sequence was applied [235] with δ= 5 ms and τ= 2.9 ms (Figure 6.1).

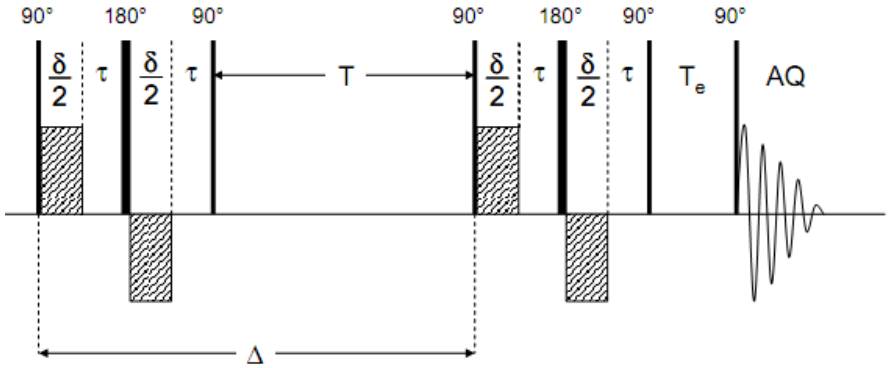

Figure VI-1: BPP-LED pulse sequence for the measurement of diffusion

The diffusion time T was optimized at 50 ms for both complexes in CD_3CN and CD_3OD. The evolution of the pulsed-field gradient during the NMR diffusion experiments was established in 30 steps, applied linearly between 1 and 30 G.cm^{-1}. In the present sequence the intensity of the signal is given by the following equation:

$$I = I(0) \cdot \exp(-D \cdot g^2 \cdot \gamma \cdot \delta \cdot (\Delta - \frac{\delta}{3} - \frac{\tau}{2}))$$

where D: Diffusion coeffcient (m^2.s^{-1}), Δ: Time between two gradient pulse sequences (s)
δ: Bipolar gradient duration (s), τ: Pulse separation delay (s), γ: Magnetogyric ratio of the observed nucleus (s^{-1}.T^{-1}), g: gradient strength (T.m^{-1}).

The diffusion coeffcient can be calculated from the slope of the line obtained potting ln(I/I(0)) against $g^2 \cdot \gamma \cdot \delta \cdot (\Delta - \frac{\delta}{3} - \frac{\tau}{2})$.

The values of the measured coefficient diffusion was used for estimating the solution molecular weight using the following equation [179]:

$$\frac{Da}{Db} = \sqrt[3]{\frac{Mb}{Ma}}$$

The spherical hydrodynamic radius (called Stokes radius) of the molecule was calculated from the Stokes-Einstein equation and compared to the value obtained from the solid state structure and with a similar reference compound in the same solvent:

$$r_{sph} = \frac{k_B T}{6\pi\eta D}$$

where η is the viscosity of the solvent ($Pa.s^{-1}$) and k_B is the Boltzman constant ($m^2.kg.s^{-2}.K^{-1}$), T is the absolute temperature (K), D is the diffusion coefficient ($m^2.s^{-1}$) [180, 181].

4- Mass Spectroscopy

Mass spectra were acquired on a LXQ-linear ion trap (Thermo Scientific, San Jose, CA, USA), equipped with an electrospray source in methanol and acetonitrile which was prepared and filtered on micro porous filters in the glove-box for Phbipox and tpa complexes and under air for Hq complexes and maintained under argon until injection in the spectrometer. Electrospray full scan spectra, in the range of m/z 50 □ 3000 amu, were obtained by infusion through fused silica tubing at 2 □10 μL min□1.

The LXQ calibration (m/z 50-2000) was achieved according to the standard calibration procedure from the manufacturer (mixture of caffeine/MRFA and Ultramark 1621). The LXQ calibration (m/z 2000-4000) was performed with ES tuning mix (Agilent). The temperature of the heated capillary of the LXQ was set to the range of 100 □120 °C, the ion spray voltage was in the range of 3 □5 kV with an injection time of 1-10 ms. The experimental isotopic profile was compared in each case to the theoretical one.

5- Luminescence measurements

Absorption spectra were recorded in 1 cm quartz cells on a Cary 50 Probe UV-vis spectrophotometer. Luminescence measurements (spectra and lifetimes) were recorded by using a modular Fluorolog FL 3-22 spectrometer from Horiba-Jobin Yvon-Spex. It is equipped with a double grating excitation monochromator and a iHR320 imaging spectrometer coupled to a R928P Hamamatsu photomultiplier for visible measurement. For measurements in the NIR spectral range of the Phbipox complexes, the spectrometer was fitted with a second photomultiplier Hamamatsu R5509. The excitation source was a 450W Xe arc lamp and all spectra were corrected for detection and optical spectral response (instrumental functions) of the spectrofluorimeter.

The luminescence measurements of hydroxyquinoline based complexes were performed in the laboratory of Jean-Claude Bünzli in Lausanne. The spectrometer was fitted with a second measuring channel equipped with a FL-1004 single grating monochromator and light intensity was measured by two Jobin-Yvon solid state InGaAs detectors (i) DSS-IGA020L, cooled to 77 K (range 800-1600 nm) and (ii) DSS-IGA020A (range 800-1700 nm) working at room temperature and inserted into a LN2 housing including an elliptical mirror (90° beam path) and coupled to a Jobin Yvon SpectrAcq2 data acquisition system. The equipment and experimental procedures for luminescence measurements in the visible and NIR range have been published previously by Comby et al [101].

Phosphorescence lifetimes were measured in time-resolved mode. They are averages of three independent measurements that were taken by monitoring the decay at the maxima of the emission spectra. The exponential decays were analyzed by using the package Origin 7.0.

The quantum yields of the hydroxyquinoline based complexes in solution at pH 12 and in solid state were determined using a home-modified integrating sphere from Oriel and the previously described procedure [236]. Spectra were corrected for the instrumental function with an absolute method with an integrations sphere.

The quantum yields of the complexes formed with the Phbipox ligand were determined at room temperature through an absolute method [236] using a home-modified

integrating sphere coupled to the modular Fluorolog FL 3-22 spectrofluorimeter. The values reported are the average of three independent determinations for each sample. The absolute quantum yield was calculated using the following expressions:

$$\Phi = \frac{E_c}{L_a - L_c} = \frac{E_c}{L_a \cdot \alpha} \qquad \alpha = \frac{L_a - L_c}{L_a}$$

Where *Ec* is the emission spectra in the emission range of the sample (ex: if the emission maximum is 600 nm, the range of this spectrum will be from 450 to 750 nm), *Lc* is the emission spectra of the excitation wavelength of the sample, *La* is the emission spectra of the excitation wavelength of the reference (quartz capillaries tube 4 mm in diameter filled with the solvent used).

6- Circular Dichroism

The circular dichroism spectra were acquired with an Applied Photophysics Chirascan spectrometer. 2.5 mL of the solutions were prepared in a glove box in a UV cell (1 cm light path). The samples are injected under argon into the UV cell and measurements are performed at 20µM complex and ligand concentration in methanol and acetonitrile.

7- Circularly Polarized Luminescence

Circularly polarized luminescence and total luminescence spectra were recorded on an instrument described previously, [237, 238] operating in a differential photon-counting mode. It is common to report the degree of CPL in terms of the luminescence dissymmetry factor, $g_{lum}(\lambda)$, which is defined as

$$g_{lum} = \frac{\Delta I}{\frac{1}{2}I} = \frac{I_L - I_R}{\frac{1}{2}\left(I_L + I_R\right)}$$

where I_L and I_R refer, respectively to the intensity of left and right circularly polarized emissions. The standard deviation, σ_d, in the measurement of the luminescence dissymmetry factor, g_{lum}, is defined as

$$\sigma_d = \sqrt{\frac{2}{N}}$$

where *N* is the total number of photon-pulses counted. The light source for indirect excitation was a continuous wave 1000 W xenon arc lamp from a Spex FluoroLog-2 spectrofluorometer,

equipped with excitation and emission monochromators with dispersions of 4 nm/mm (SPEX, 1681B). $^5D_0 \leftarrow ^7F_0$ excitation measurements for the Eu(III)-containing compounds were accomplished by using a Coherent-599 tunable dye laser (0.03 nm resolution) with a Coherent Innova Sabre TMS 15 or Innova-70 argon ion laser as a pump source. The laser dye used in all measurements was rhodamine 6G dissolved in ethylene glycol. Calibration of the emission monochromator (and subsequently the dye laser wavelength) was accomplished by passing scattered light from a low power He-Ne laser through the detection system. The error in the dye-laser wavelength is assumed to equal the resolution of the emission monochromator (0.1 nm). The optical detection system consisted of a focusing lens, long pass filter, and 0.22 m monochromator. The emitted light was detected by a cooled EMI-9558B photo-multiplier tube operating in photon-counting mode. All measurements were performed in quartz cuvettes with a path length of 0.4 or 1.0 cm.

8- X-Ray Crystallography

Two different apparatus were used for collecting the crystallographic data. For all the measurements in order to prevent evaporation of co-crystallised solvent molecules the crystals were coated with light hydrocarbon oil and the data were collected at 233 K (Bruker) and 150 K (Oxford). The heptanuclear wheel was collected in ESRF.

The crystals ($[Nd(H_{1/2}hqa)_3]_2(Et_3NH)_3$ **(I)** , $[Nd(hqa)_3]K_3$ **(II)**) were analyzed using a Bruker SMART [239] CCD area detector three-circle diffractometer (Mo-K_α radiation, graphite monochromator, λ= 0.71073 Å). The cell parameters were obtained with intensities detected on three batches of 15 frames with a 10 s (**I),** 30s **(II)** (exposure time). The crystal-detector distance was 5 cm. For three settings of φ narrow data (30s) frames were collected for 0.3° increments in ω. A hemisphere of data was collected. At the end of data collection, the first 50 frames were recollected to establish that crystal decay had not taken place during the collection. Unique intensities with I>10 σ(I) detected on all frames using the SAINT Bruker program [240] were used for refining the values of the cell parameters. The substantial redundancy in data allows empirical absorption corrections to be applied using multiple measurements of equivalent reflection with the SADABS Bruker program [239].

The rest of the crystals were analyzed using an Oxford Diffraction XCalibur S kappa geometry diffractometer (Mo-K_α radiation, graphite monochromator, λ= 0.71073

Å). The cell parameters were obtained with intensities detected on three batches of 5 frames. The crystal-detector distance was 4.5 cm. The number of settings and frames has been established taking in consideration the laue symmetry of the cell by CrysAlisPro Oxford-diffraction software. Unique intensities detected on all frames using the Oxford-diffraction Red program were used for refining the values of the cell parameters. The substantial redundancy in data allows empirical absorption corrections to be applied using multiple measurements of equivalent reflections with the ABSPACK Oxford-diffraction program. For all structures space groups were determined from systematic absences, and they were confirmed by the successful solution of the structure. The structures were solved by direct methods using the SHELXTL 6.14 package [241] and for all atoms, including hydrogen atoms, were found by difference Fourier syntheses.

8.1- Eu⊂[(Λ-Eu(R-Phbipox)$_2$Δ-Eu(R-Phbipox)$_2$)$_3$](Otf)$_9$

Diffraction measurements were done at the Swiss-Norwegian Beam Lines (SNBL) at the European Synchrotron Radiation Facility (ESRF). A crystal of ~150 μm size has been selected and rapidly transferred to a 100 K nitrogen stream. Diffraction data were taken at 100 K using the MAR345 Image Plate detector, at the wavelength 0.70093 Å and the crystal-to-detector distance of 250 mm. 250 frames with Δφ increments of 0.8° and 15 sec exposure time have been collected. All diffraction intensities could be indexed in a C-centered monoclinic lattice. The collected X-ray data were treated by the CrysAlisPro software [242] and were subjected to a 2-cycle 3D integration, followed by the multi-scan absorption correction implemented in the integration software (R_{int} = 0.0477). 63575 diffraction intensities were integrated up to 1.3 Å resolution. Mean $F^2/\sigma(F^2)$ for the data in the outer 1.35-1.30 Å shell equals 5. The data were corrected for Lorentz and polarization effects. Absorption correction and scaling of frames for the decaying intensity of the synchrotron beam were performed using ABSPACK procedure implemented in CrysAlisPro.

The structure was solved by direct methods (SHELXS). Eu atoms and the primary coordination sphere, as well as the majority of the ligands could be partially located in the density maps. One ligand was idealized by applying bond and angle distance restraints and used for fitting onto the other partially resolved ligands using an algorithm implemented in PyMOL [243]. Dictionary restraints were sampled from the CSD database; the benzene rings

were all refined as planar hexagons with C-C bonds of 1.39 Å, and used in the next refinement cycles by conjugate-gradient least-squares method in SHELXL.

Some of the triflate, $CF_3SO_3^-$, anions could be assembled from the difference map peaks and the remaining anions were found by the ligand fitting procedure in COOT [244]. Finally, 14 out of 18 anions were located, with two of them refined at half occupancy. The anions were treated as rigid groups which were allowed to move with and rotate around the sulfur atom, the torsion angles were however restrained in the ideal staggered positions. 2 anions could not be confined to one positions and 2-fold positional disorder was applied to model the diffuse electron density. For the final cycles the structure was refined until the full convergence by full matrix least squares method using 2559 parameters and 2094 restraints for 29668 unique reflections in the 5-1.3 Å resolution range. The complex as well as the located anions fit well into the electron density maps. There are large cavities present in the crystal packing where the remaining 4 anions are thought to reside, although these are not likely to be restrained to a defined position. Only the 14 Eu atoms in the asymmetric unit were refined.

9- Ligand Synthesis

9.1- H_2hqt

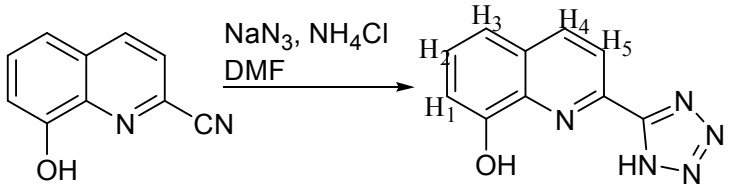

A mixture of 8-hydroxyquinoline-2-carbonitrile (1 g, 5.88 mmol), sodium azide (0.96 g, 14.7 mmol) and ammonium chloride (0.79 g, 14.7 mmol) in anhydrous DMF (10 mL) was stirred under argon at 130ºC for 18 h. After cooling, the inorganic salts were filtrated and the solvent removed under reduced pressure. After addition of dilute HCl (10 mL, 0.1 M), the resulting suspension was stirred for 1h. The precipitate was filtered, washed thoroughly with cold water and dried under vacuum, to yield 1.50 g (90%) of light brown powder.

^{1}H NMR (200 MHz, CD_3OD) δ ppm 8.52 (d, J = 8.58 Hz, 1H, H_1), 8.30 (d, J = 8.57 Hz, 1H, H_2), 7.64-7.46 (m, 2H, H_3, H_4), 7.22 (dd, J = 7.29, 1.39 Hz, 1H, H_5), 1.30 (s, 1H, OH).

^{13}C NMR (200MHz, DMSO) δ ppm 152.89 (C), 140.64 (C), 138.19 (C), 137.21 (CH), 129.38 (CH), 128.73 (C), 118.94 (CH), 117.68 (CH), 111.42 (CH)

Elemental Analysis: calcd. (%) for $H_2hqt{\cdot}H_2O$ $C_{10}H_7N_5O{\cdot}H_2O$ C, 51.95; H, 3.92; N, 30.29 Found: C, 52.00; H, 3.63; N, 30.15

9.2- Phbipox

The enantiomerically pure ligand S/R-Phbipox, and rac-Phbipox has been prepared in 7 steps from commercial dimethylbipyridine in 13% total yield

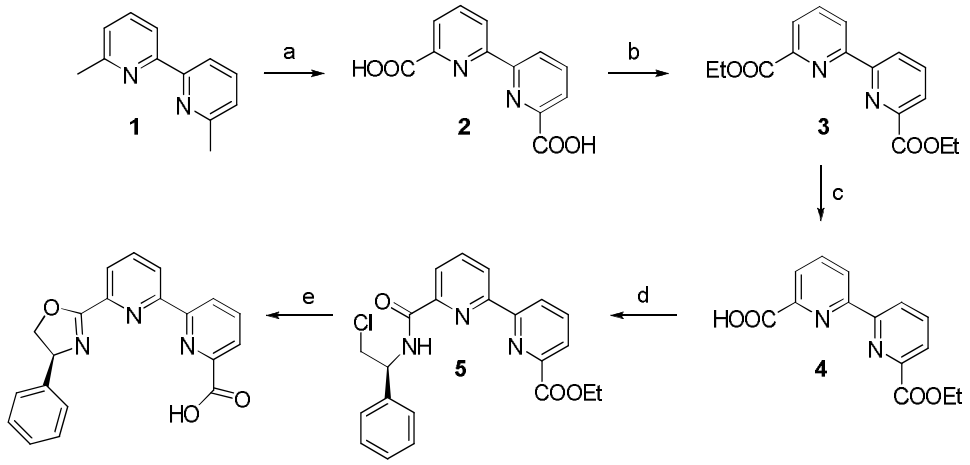

Scheme 1: Reagents and conditions : a) CrO_3, H_2SO_4, 98 %; b) H_2SO_4, EtOH, 83 %; c) NaOH, EtOH/CH_2Cl_2, 38 % ; d) i. $SOCl_2$, DMF cat. ; ii. (S)-2-phenylglycinol, Et_3N, $CHCl_3$; iii. $SOCl_2$, 59 % for S; e) KOH, EtOH/H_2O, 73 % for S

a) 2,2′-bipyridine-6,6′-dicarboxylic acid (2)

Adapted from the procedure described by Cooper and Richard [245].

6,6′-dimethyl-2,2′-bipyridyl **(1)** (5.00 g, 27.1 mmol) was added slowly, with stirring, to concentrated sulphuric acid (100 mL). During the addition, the temperature rose to 35°C. The resulting solution was cooled by an ice-bath and chromium (VI) oxide (16.3 g, 163 mmol) was added in small portions so that the temperature stayed below 40°C. After the addition was complete, the reaction mixture turned rapidly dark green. It was stirred overnight at room temperature and then poured onto crushed ice. The white precipitate formed was filtered off, washed with cold water and dried under vacuum at 40°C overnight to yield the 2,2′-bipyridine-6,6′-dicarboxylic acid **(2)** (6.52 g, 98%).

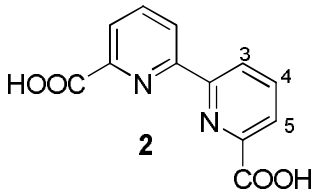

2

^{1}H NMR (400 MHz, DMSO-d6, 298 K) : δ= 8.13 (2H, dd, J= 7.0 , 2.0Hz, H5), 8.19 (2H, t, J= 7.0Hz, H4), 8.75 (2H, dd, J= 7.0 , 2.0Hz, H3)

ES-MS : m/z= 245.5 (MH+).

b) Diethyl-2,2′-bipyridine-6,6′-dicarboxylate (3)

To a suspension of the diacid **(2)** (6.52 g, 26.5 mmol) in ethanol (550 mL) was added dropwise concentrated sulfuric acid (28 mL). The mixture was stirred for 30 minutes at room temperature and was then refluxed overnight under an argon atmosphere. Afterwards the reaction mixture was cooled to 5°C by an ice-bath and was slowly poured to a saturated $NaHCO_3$ solution (1.5 L) to be neutralized (pH=8). After evaporation of ethanol, the mixture was extracted with chloroform (4×550 mL). The combined organic layers were dried over anhydrous Na_2SO_4, filtered, and concentrated under reduced pressure to afford the desired product **3** as a white solid (6.60 g, 83%).

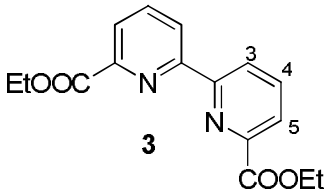

3

^{1}H NMR (400MHz, $CDCl_3$, 298K) : δ= 1.47 (6H, t, J= 7.0Hz, $COOCH_2C\underline{H_3}$), 4.49 (4H, q, J= 7.0Hz, $COOC\underline{H_2}CH_3$), 7.98 (2H, t, J= 7.8Hz, H4), 8.15 (2H, dd, J=7.8, 1.4Hz, H5), 8.77 (2H, dd, J= 7.8, 1.4Hz, H3)

ES-MS : m/z= 301.5 (MH+)

c) 6-ethoxycarbonyl-2,2-bipyridine-6-dicarboxylic acid (4)

The diester **3** (2.60 g, 8.68 mmol) was solubilized in an ethanol/CH_2Cl_2 (2:1) mixture (75 mL) at 50°C. The solution was cooled to room temperature and a solution of NaOH (347 mg, 8.68 mmol) in ethanol (25 mL) was added dropwise under vigorous stirring. After addition was complete (1 hour), the reaction mixture was evaporated to dryness and dissolved in water (50 mL). The insoluble starting product **3** was filtered off (0.60 g, 23%). Further extraction of the aqueous layer by chloroform (3×25 mL) yielded the remaining starting product as well as a very small amount of the desired product. After cooling, a white solid formed in the aqueous solution, which was filtered and dried under vacuum. The operation had to be repeated many times to yield all the desired monoacid **4** (0.89 g, 38%).

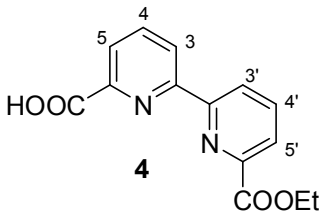

4

^{1}H NMR (400MHz, DMSO-d6, 298K) : δ= 1.38 (3H, t, J= 7.2Hz, $COOCH_2C\underline{H_3}$), 4.41 (2H, q, J= 7.2Hz, $COOC\underline{H_2}CH_3$), 8.19 (4H, m, H4, H4', H5, H5'), 8.62 (1H, dd, J= 7.4, 1.4Hz, H3'), 8.75 (1H, dd, J= 7.4, 1.4Hz, H3)

ES-MS : m/z= 273.5 (MH+)

d) (S)-ethyl-6-(2-chloro-1-phenylethyl)amido)-2,2-bipyridine-6-carboxylate 5

Adapted from the procedure described by Nishiyama et al. [246].

6-ethoxycarbonyl-2,2-bipyridine-6,6-dicarboxylic acid **4** (450 mg, 1.65 mmol) was treated with $SOCl_2$ (4.5 mL) and a catalytic amount of DMF (10µL). The solution was stirred at room temperature for 14h under argon atmosphere. Excess of thionyl chloride was removed under reduced pressure and co-evaporated with dry toluene (3×2mL) to give the corresponding acid chloride. Then to a solution of (S)-2-phenylglycinol (273 mg, 1.98 mmol) and triethylamine (0.75 mL, 5.29 mmol) in chloroform (3.5 mL) at 0°C was added a solution

of the crude acid chloride in chloroform (7 mL). The mixture was stirred for 1 day at room temperature under argon atmosphere and then $SOCl_2$ (0.9 mL) was added. After 3h at room temperature, the mixture was poured into ice-water (60 mL) and extracted with CH_2Cl_2 (5×40 mL). The organic layer was washed with brine (60 mL), dried over anhydrous Na_2SO_4, filtered and concentrated under vacuo to give a pale brown oil which was purified by silica gel flash chromatography (60 mL, CH_2Cl_2/EtOH 98/2) followed by trituration with Et_2O. The corresponding amidochloride **5** was obtained as a white solid (360 mg, 59%).

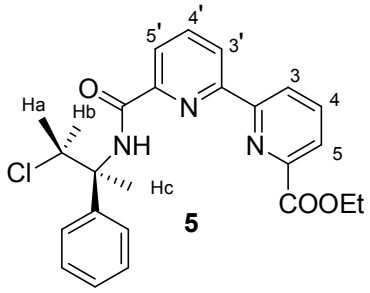

5

^{1}H NMR (400MHz, $CDCl_3$, 298K) : δ= 1.49 (3H, t, J= 7.2Hz, $COOCH_2C\underline{H_3}$), 4.06 (2H, d, J= 5.0Hz, Ha and Hb), 4.51 (2H, q, J= 7.2Hz, $COOC\underline{H_2}CH_3$), 5.61 (1H, t, J=5.0Hz, Hc), 7.41 (5H, m, Ph), 8.02 (1H, t, J= 7.8Hz, H4), 8.04 (1H, t, J= 7.8Hz, H4'), 8.18 (1H, dd, J= 7.8, 1.2Hz, H5), 8.26 (1H, dd, J= 7.8, 1.2Hz, H5'), 8.58 (1H, dd, J= 7.8, 1.2Hz, H3'), 8.76 (1H, dd, J= 7.8, 1.2Hz, H3), 8.85 (1H, d, J= 8.2Hz, NH)

ES-MS : m/z= 410.7 (MH+)

e) 6-(4-phenyloxazolin-2-yl)-2,2'-bipyridine-6-carboxylic acid (S-Phbipox)

To a solution of the amidochloride **5** (360 mg, 0.88 mmol) in ethanol (8.5 mL) was added aqueous KOH (1M, 2.7 mL). The mixture was stirred for 2 days at room temperature and then evaporated under reduced pressure. The residue was dissolved into water (10 mL) and the pH was adjusted to 3 by addition of aqueous 1M HCl. The yellow solid formed was filtered, washed with aqueous 1M HCl and dried under vacuum to yield the desired ligand S-Phbipox (120 mg, 73%).

+

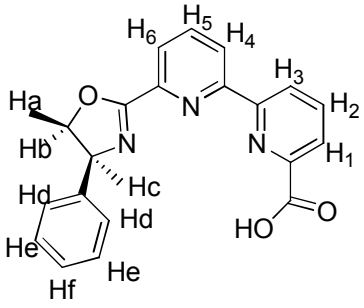

^{1}H NMR (400MHz, DMSO-d6, 308K) : δ= 4.31 (1H, t, J= 7.2Hz, Ha), 4.95 (1H, t, J= 7.2Hz, Hb), 5.51 (1H, t, J= 7.2Hz, Hc), 7.36 (5H, m, Ph), 8.16 (4H, m, H4, H4', H5, H5'), 8.61 (1H, dd, J= 6.4Hz, J= 2.6Hz, H3'), 8.71 (1H, d, J= 6.6Hz, J= 2.4Hz, H3)

^{13}C NMR (400MHz, DMSO-d6, 308K) : δ= 70.0 (CH_2), 75.4 (CHoxa), 123.8 (CHpy), 124.3 (CHpy), 125.4 (CHpy), 125.8 (CHpy), 127.4 (5×CHPh), 127.1 (CHpy), 129.3 (CHpy), 139.2 (CPh), 139.6 (Cpy), 142.99 (Cpy), 146.8 (Cpy), 155.2 (Cpy), 163.6 (Coxa), 166.6 (COOH)

ES-MS : m/z= 346.2 (MH+) and 363.2 (MNa+)

Elemental analysis calculated (%) for:

S-Phbipox: $C_{20}H_{15}N_3O_3$ (345.36 g/mol): C 69.56; H 4.38; N 12.17; Found: C 69.54; H 4.64; N 12.03

R-Phbipox: $C_{20}H_{15}N_3O_3 \cdot 0.01$ HCl (346.29 g/mol): C 69.37; H 4.37; N 12.13; Found: C 69.37; H 4.70; N 12.39

Rac-Phbipox: $C_{20}H_{15}N_3O_3 \cdot 0.35$ HCl (364.08 g/mol): C 65.98; H 4.25; N 11.54; Found: C 65.98; H 4.65; N 11.61.

9.3- tpa (Tris(2-pyridylmethyl)amine)

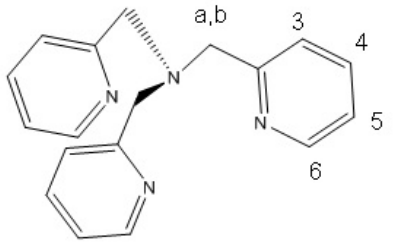

Adapted from the procedure described by White et al. [247]

To a stirring solution of 2-(aminomethyl)pyridine (0.578g, 5.25mmol) and sodium triacetoxyborohydride (3.12g, 14.7mmol) in dichloromethane (75mL) was added 1 mL (10.5mmol) of pyridine-2carboxaldehyde. After stirring 18 h, a saturated aqueous sodium hydrogen carbonate solution was added, and after 15 min of stirring, an extraction of the mixture using ethyl acetate was performed. The organic fraction was dried ($NaSO_4$), and the solvent removed. The residue purified by alumina active III chromatography (6x100 mL, CH_2Cl_2/EtOH 99/1), by Celite No. 545, and followed by crystallization with Et_2O. Obtained white crystals dried under vacuum to yield the desired product (712 mg, 45%).

^{1}H NMR (400MHz, $CDCl_3$, 298K): δ= 8.51 (1H, d, J=8.0 Hz, H6), 7.64 (1H, td, J=8.0 Hz, J=1.7 Hz, H4), 7.56 (1H, d, J=8.0 Hz, H5), 7.12 (1H, t, J=8.0 Hz, H3), 3.86 (2H, s, Ha, Hb).

10- Synthesis of Lanthanide Complexes

10.1- NIR emitting complexes based on hydroxyquinoline based ligands

$[Nd(H_{1/2}hqa)_3]_2(Et_3NH)_3 \cdot Et_3NHOtf$

A solution of $Nd(Otf)_3$ (0.114 mmol) in MeOH (2 mL) was added, under stirring, to a methanolic solution of H_2hqa (0.34 mmol) (2 mL). Deprotonation of the ligand was achieved using Et_3N (95.2 µL, 0.68 mmol). The yellow mixture was refrigerated overnight at 5°C. The insoluble white precipitate formed was removed by filtration and the filtrate was concentrated to a minimum amount of MeOH (~2 mL). Diisopropylether was allowed to slowly diffuse into the resulting solution until some yellow needles of $\{[Nd(H_{1/2}hqa)_3]_2(Et_3NH)_3\} \cdot Et_3NHOtf$ suitable for X-ray diffraction formed. A sufficient amount of the needles were collected to carry out the photoluminescence measurements of the dimeric complex $\{[Nd(H_{1/2}hqa)_3]_2\}^{3-}$

^1H NMR (400 MHz, CD_3OD, 298 K): δ= 6.96 (1H, broad d, H3), 7.59 (1H, broad t, H2), 8.36 (1H, d, J= 7.0 Hz, H1), 9.49 (1H, d, J= 8.0 Hz, H5), 9.84 (1H, d, J= 8.0 Hz, H4).

No correct elemental analysis could be obtained for this neodymium(III) complex. This is probably due to an equilibrium between the complexes presenting different protonation states.

$[Nd(hqa)_3]K_3 \cdot 8MeOH_\infty$

A solution of $Nd(Otf)_3$ (0.092 mmol) in water (1.5 mL) was added, under stirring, to an aqueous solution of 3 mol equivalent of ligand (0.076 mmol) (1.5 mL) at pH 12 adjusted by addition of aqueous KOH (1M). pH of the resulting solution was readjusted to 12 by addition of aqueous KOH (0.1 M). The mixture was evaporated to dryness, the yellow oil obtained was dissolved in a minimum amount of MeOH (~ 2 mL) and the mixture was refrigerated overnight at 5°C. The insoluble white precipitate formed was removed by filtration. Diisopropylether (DIPE) was allowed to slowly diffuse into the resulting filtrate in methanol. The solution was refrigerated until some yellow cubic crystals of $\{[Nd(hqa)_3]K_3\} \cdot 8MeOH_\infty$ suitable for X-ray diffraction formed. The crystals

were separated by filtration and dried under vacuum to yield $[Nd(hqa)_3]K_3$ (62%). The attribution of the signals was performed by 2D- COSY and NOESY experiments at 25°C.

^{1}H NMR (400 MHz, CD_3OD, 298 K): δ = 5.45 (1H, d, J= 8.0 Hz, H5a), 5.95 (1H, d, J= 8.0 Hz, H5b), 6.90 (1H, d, J= 8.0 Hz, H1a), 6.96 (0.4H, d, H3□), 7.30 (1H, d, J= 8.0 Hz, H3a), 7.61 (1H, d, J= 8.0 Hz, H4a), 7.87 (1H, t, J= 8.0 Hz, H2a), 7.97 (0.4H, t, H2□), 7.99 (0.4H, d, H1□), 9.03 (1H, d, J= 8.0 Hz, H4b), 9.17 (1H, d, J= 8.0 Hz, H5c), 9.29 (1H, d, J= 8.0 Hz, H3b), 9.32 (0.4H, d, H5□), 9.40 (0.4H, d, H4□), 9.59 (1H, d, J= 8.0 Hz, H3c), 10.27 (3H, m, H2b, H2c, H4c), 12.16 (1H, d, J= 8.0 Hz, H1b), 12.24 (1H, d, J= 8.0 Hz, H1c)

ES-MS: m/z= 860.0 (100) $\{[Nd(hqa)_3]K_4\}+$

Elemental analysis calcd. (%) for $\{[Nd(hqa)_3]K_3\}\cdot 2.6MeOH + 0.5H_2O$; $C_{30}H_{15}N_3O_9K_3Nd\cdot 2.6\ CH_3OH\ 0.5\ H_2O$ Mw: 915.28: C 42.78; H 2.91; N 4.59; Found C 42.72; H 2.92; N 5.00. (Mw of complex $[Nd(hqa)_3]K_3$: 822.9596)

$[Er(hqa)_3]K_3\cdot 7MeOH\cdot 0.25DIPE_\infty$

The compound was prepared as was described for the corresponding neodymium complex. Full assignment of the ^{1}H NMR spectrum was not possible due to the strong paramagnetic broadening and shift of the peaks.
Yield: 51%.

Elemental analysis calcd. (%) for $\{[Er(hqa)_3]K_3\}\cdot 3.8\ KOtf + 6.2\ H_2O$; $C_{30}H_{15}N_3O_9K_3Er\cdot 3.8\ CF_3SO_3K\ 6.2\ H_2O$ Mw: 1672.81: C, 24.27; H, 1.65; N, 2.51. Found: C, 24.20; H, 1.65; N, 2.33. (Mw of complex $[Er(hqa)_3]K_3$: 846.0596)

$[Yb(hqa)_3]K_3$

The compound was prepared as was described for the corresponding noedymium complex.
Yield: 53%.

Elemental analysis calcd. (%) for {[Yb(hqa)$_3$]K$_3$}. 2.25 KOtf + 3.2 H_2O $C_{30}H_{15}N_3O_9K_3Yb$. 2.25 CF_3SO_3K 3.2 H_2O Mw: 1332.80: C, 29.06; H, 1.62; N, 3.15. Found: C, 29.08; H, 1.63; N, 2.87. (Mw of complex [Yb(hqa)$_3$]K$_3$: 851.7596)

[Nd ($H_{1/2}$hqt)$_3$]$_2$(Et_3NH)$_3$

The compound was prepared as was described for the [Nd ($H_{1/2}$hqa)$_3$]$_2$(Et_3NH)$_3$·Et_3NHOtf complex.

^{1}H NMR (400 MHz, CD_3OD, 298K) δ = 9.81 (1H, s, H_4), 9.64 (1H, s, H_5), 8.06 (1H, s, $H_{3/1}$), 7.27 (2H, br, H_2, $H_{3/1}$).

[Nd(hqt)$_3$]K$_3$

A solution of Nd(Otf)$_3$ (0.16mmol) in water (1.5 mL) was added, under stirring, to an aqueous solution of 3 mol equivalent of ligand (0.48mmol) (1.5 mL) at pH 12 adjusted by addition of aqueous KOH (1M). pH of the resulting solution was readjusted to 12 by addition of aqueous KOH (0.1 M). The mixture was evaporated to dryness, the orange oil obtained was dissolved in a minimum amount of MeOH (~ 2 mL) and the mixture was refrigerated overnight at 5°C. The insoluble white precipitate formed was removed by filtration. Diisopropylether was allowed to slowly diffuse into resulting solution in methanol. The solution was refrigerated until some orange cubic crystals suitable for X-ray diffraction formed. The crystals were separated by filtration and dried under vacuum to yield [Nd(hqt)$_3$]K$_3$ (60%). The attribution of the signals is performed by 2D- COSY and NOESY experiments at 25°C.

^{1}H NMR (500 MHz, CD_3OD, 298K) 1.34 (0.2H, broad d), 4.49 (0.1H, s), 5.56 (0.1H, s), 6.45 (0.1H, s), 6.79 (1H, s, H_1), 7.26 (0.1H, s),8.14(1H, s, H_2), 8.31(1H, s, H_3), 9.70 (0.1H, m), 9.94 (1.10H, s, H_4), 10.25 (1H, s, H_5), 12.49 (0.2H, s), 12.92 (0.1H, d),14.32 (0.2H, s), 14.54 (0.1H, s), 20.45 (0.1H, s), 20.92 (0.1H, s).

Elemental analysis calculated (%) for {[Nd(hqt)$_3$]K$_3$}· MeOH + 3.4 KOtf+ 3 H_2O; $C_{30}H_{15}N_{15}O_3K_3Nd$ CH_3OH + 3.4 Kotf + 3 H_2O Mw: 1620.92; C 25.49; H 1.55; N 12.96; Found C 25.58; H 1.62; N 12.93. (Mw of complex [Nd(hqt)$_3$]K$_3$: 895.046)

$[Er(hqt)_3]K_3$

The compound was prepared as was described for the corresponding neodymium complex. Full assignment of the ^1H NMR spectrum was not possible due to the strong paramagnetic broadening and shift of the peaks.

Yield: 52%.

Elemental analysis calcd. (%) for $\{[Er(hqt)_3]K_3\}\cdot 3.2KOtf + 5H_2O$ $C_{30}H_{15}N_{15}O_3K_3Er\cdot 3.2\ CF_3SO_3K\cdot 5H_2O$ Mw: 1610.38: C, 24.76; H, 1.56; N, 13.05. Found: C, 24.80; H, 1.61; N, 12.95. (Mw of complex $[Er(hqt)_3]K_3$: 918.14)

$[Yb(hqt)_3]K_3$

The compound was prepared as was described for the corresponding neodymium complex.

Yield: 57%.

Elemental analysis calcd. (%) for $\{[Yb(hqt)_3]K_3\}\cdot 4KOtf+ 3H_2O$ $C_{30}H_{15}N_{15}O_3K_3Yb\cdot 4\ CF_3SO_3K\cdot 3H_2O$ Mw: 1730.59: C, 23.60; H, 1.22; N, 12.14. Found: C, 23.78; H, 1.26; N, 12.12. (Mw of complex $[Yb(hqt)_3]K_3$: 923.846)

10.2- Chiral luminescent complexes based on the ligand Phbipox

[Eu(Phbipox)$_2$](Otf)

Triethylamine (20.2 µl) was added to a solution of S/R/rac-Phbipox (50 mg 0.145 mmol) in 2 mL anhydrous methanol. The resulting solution was stirred for 2 hours and a solution of $Eu(Otf)_3$ (0.0725 mmol) in methanol (1mL) was then added. The resulting solution was stirred at room temperature for an hour. Diisopropylether was then added to afford a white microcrystalline solid precipitate that was filtered and dried two weeks at 40 °C under vacuum.

a) [Eu(S-Phbipox)$_2$](Otf)

Yield 54%

Elemental analysis for {[Eu(S-Phbipox)$_2$](Otf)}.1.26Et_3NOtf_3
($C_{49.82}H_{46.9}N_{7.26}O_{12.78}F_{6.78}S_{2.26}Eu$ Mw = 1305.23)
(%) calcd. for C 45.85, H 3.32, N 7.89; found C 45.85, H 3.62, N 7.79.

b) [Eu(R -Phbipox)$_2$](Otf)

Yield 66%

Elemental analysis for [Eu(R-Phbipox)$_2$](Otf) (C_{41} $H_{28}N_6O_9F_3SEu$ Mw = 989.72)
(%) calcd. for C 49.76, H 2.85, N 8.49; found C 49.86, H 2.99, N 8.45.

^{1}H NMR (400MHz, CD_3OD, 298K):

(Λ)-[Eu(S-Phbipox)$_2$]$^+$/ (Δ)-[Eu(R-Phbipox)$_2$]$^+$: δ= 2.45 (4H, broad s, Hd), 3.55 (2H, broad t, Ha), 4.10 (2H, d, J = 7.8Hz, H6), 4.55 (4H, broad s, He), 5.37 (2H, t, J = 6.8Hz, Hf), 6.11 (2H, d, J = 7.8Hz, H4), 6.92 (2H, t, J = 7.8Hz, H5), 7.29 (2H, d, J = 7.8Hz, H1), 7.38 (2H, broad t, Hb), 7.53 (2H, d, J = 7.8Hz, H3), 8.75 (2H, t, J = 7.8Hz, H2), 11.70 (2H, broad t, Hc),

(Δ)-[Eu(S-Phbipox)$_2$]$^+$/ (Λ)-[Eu(R-Phbipox)$_2$]$^+$: δ= -13.38 (0.8H, broad t, Hc□), 0.41 (0.8H, broad t, Hb□), 1.58 (0.8H, broad s, H6□), 5.51 (0.8H, broad t, Ha□), 5.74 (1.6H, s, H4□, H5□), 6.95 (0.8H, m, H3□), 7.58 (0.8H, m, H1□), 8.86 (0.8H, t, J = 7.2Hz, H2□), 9.44 (0.8H, broad t, J = 7.2Hz, Hf□), 10.07 (1.6H, broad t, J = 7.2Hz, He□), 12.64 (1.6H, broad s, Hd□)

1H NMR (500MHz, CD_3CN, 263K) :

(Λ)-[Eu(S-Phbipox)$_2$]$^+$/ (Δ)-[Eu(R-Phbipox)$_2$]$^+$: species: δ= 0.45 (0.4H, broad t, H_c), 3.42 (0.4H, broad t, H_a), 2.71 (0.4H, broad t, H_b), 6.07 (0.4H, broad d, H_6), 6.21 (0.8H, broad s, H_d), 6.50 (0.4H, broad s, H_3), 7.21 (0.8H, broad s, H_e), 7.42 (0.4H, broad d, H_2), 7.50 (0.4H, broad t, H_f), 7.95 (0.4H, broad d, H_1), 8.50 (0.4H, d, J = 5.7Hz, H_4), 8.72 (0.4H, broad t, H_5)

(ΔΔΔ)-[Eu(S-Phbipox)$_2$]$_3^{+3}$/ (ΛΛΛ)-[Eu(R-Phbipox)$_2$]$_3^{+3}$ species:

●δ= -25.18 (1H, broad t, H_c), -7.83 (1H, broad d, H_6), -5.92 (1H, broad t, H_b), 1.53 (1H, broad t, H_a), 3.99 (1H, broad t, H_5), 6.34 (1H, d, J = 6.6Hz, H_3), 7.42 (1H, broad d, H_4), 9.54 (1H, broad t, H_f), 10.24 (2H, broad t, H_e), 11.12 (1H, broad t, H_2), 11.35 (1H, d, J = 6.1Hz, H_2), 13.57 (2H, broad s, H_d)

■ δ= -14.21 (1H, broad t, H_c), 0.33 (1H, broad t, H_b), 2.15 (1H, broad d, H_3), 3.28 (1H, broad t, H_2), 6.50 (1H, broad s H_a), 8.07 (1H, d, J = 7.9Hz, H_4), 9.54 (2H, broad t, H_5), 9.83 (3H, broad t, H_1, H_e), 10.37 (2H, broad s, H_d), 10.68 (1 H, broad t, H_f), 19.78 (1H, broad s, H_6)

ES-MS, CD_3OD: m/z= 841.1 {[Eu(S-Phbipox)$_2$]}$^+$

ES-MS, CD_3CN: m/z= 841.3 {[Eu(S-Phbipox)$_2$]}$^+$ m/z = 1335 [Eu$_3$(S-Phbipox)$_6$](OTf)}$^{2+}$

c) [Eu (rac-Phbipox)$_2$](Otf)

Yield 75%

Elemental analysis for [Eu(rac-Phbipox)$_2$](Otf) (C_{41} $H_{28}N_6O_9F_3SEu$ Mw = 989.72)
(%) calcd. for C 49.76, H 2.85, N 8.49; found C 49.68, H 2.96, N 8.54.

^{1}H NMR (400 MHz, CD_3OD, 298K) :

(Λ)-[Eu(S-Phbipox)$_2$]$^+$/ (Δ)-[Eu(R-Phbipox)$_2$]$^+$: δ= 2.45 (0.4H, broad s, H_d), 3.55 (0.2H, broad t, H_a), 4.10 (0.2H, d, J = 7.8Hz, H_6), 4.55 (0.4H, broad s, H_e), 5.37 (0.2H, t, J=6.8Hz, H_f), 6.11 (0.2H, d, J = 7.8Hz, H_4), 6.92 (0.2H, t, J= 7.8Hz, H_5), 7.29 (0.2H, d, J= 7.8Hz, H_1), 7.38 (0.2H, broad t, H_b), 7.53 (0.2H, d, J = 7.8Hz, H_3), 8.75 (0.2H, t, J = 7.8Hz, H_2), 11.70 (0.2H, broad t, H_c)

(Δ)-[Eu(S-Phbipox)$_2$]$^+$/ (Λ)-[Eu(R-Phbipox)$_2$]$^+$: δ= -13.38 (0.3H, broad t, $H_{c'}$), 0.41 (0.3H, broad t, $H_{b'}$), 1.58 (0.3H, broad s, $H_{6'}$), 5.51 (0.3H, broad t, $H_{a'}$), 5.74 (0.6H, s, $H_{4'}$, $H_{5'}$), 6.95 (0.3H, m, $H_{3'}$), 7.58 (0.3H, m, $H_{1'}$), 8.86 (0.3H, t, J = 7.2Hz, $H_{2'}$), 9.44 (0.3H, broad t, J = 7.2Hz, $H_{f'}$), 10.07 (0.6H, broad t, J = 7.2Hz, $H_{e'}$), 12.64 (0.6H, broad s, $H_{d'}$)

[Eu(S-Phbipox)(R-Phbipox)]$^+$ δ = 15.26-14.58 (1H, m), 10.94-10.47 (1H, m), 8.68 (1H, s), 8.07 (1H, s), 7.64 (1H, t, *J* = 7.41, 7.41 Hz), 6.51 (1H, d, *J* = 7.91 Hz), 6.39 (1H, d, *J* = 8.10 Hz), 5.61 (1H, d, *J* = 7.34 Hz), 5.18 (1H, s), 4.74 (1H, s), 4.45 (1H, d, *J* = 7.89 Hz), 3.54 (1H, s), 2.34 (1H, s), 1.49 (1H, d, *J* = 4.86 Hz), 0.79 (1H, d, *J* = 6.91 Hz), -1.76--2.01 (1H, m), -12.42--12.69 (1H, m)

ES-MS, CD_3CN : m/z= 841.3 {[Eu(rac-Phbipox)$_2$]}$^+$ m/z = 1335 [Eu$_3$(rac-Phbipox)$_6$](OTf)}$^{2+}$

[Nd(R-Phbipox)$_2$](Otf)

The compound was prepared as was described for the corresponding europium complex. Yield 72%

1H NMR (400 MHz, CD_3OD, 298K):

(Δ)-[Nd(R-Phbipox)$_2$]+ species:

δ= 27.56 (1H, m, $H_{c'}$), 17.40 (1H, s, $H_{3'}$), 13.29 (1H, s, $H_{6'}$), 11.93 (1H, s, $H_{a'}$), 11.09 (1H, s, $H_{2'}$), 8.25 (1H, s, $H_{5'}$), 7.56 (1H, s, $H_{1'}$), 6.37 (1H, s, $H_{f'}$), 5.13 (1H, s, $H_{4'}$), 4.39 (1H, s, $H_{e'}$), 3.95 (1H, d, *J* = 16.76 Hz, $H_{b'}$), 0.94 (1H, s, $H_{d'}$)

(Λ)-[Nd(R-Phbipox)$_2$]+ species:

δ= 13.86 (1H, m, H_d), 9.77 (1H, s, H_e), 8.55 (1H, s, H_f), 7.95 (1H, s, H_a), 7.12 (1H, s, H_2), 5.73 (1H, s, H_1), 5.20 (1H, s, H_6), 3.95 (1H, d, *J* = 16.76 Hz, H_3), 3.50 (2H, d, *J* = 32.59 Hz, H_b, H_5), 1.30 (1H, t, *J* = 6.70, 6.70 Hz, H_4), -4.05 (1H, m, H_c)

^{1}H NMR (500 MHz, *CD_3CN,* 263K):

δ= 42.97-42.12 (1H, m, Hox), 28.43 (1H, s, Hox), 27.68 (1H, s, Hpy), 21.31 (1H, s, Hox), 12.45 (1H, s, Hox), 11.45 (1H, s, Hpy), 9.42 (1H, s, Hox), 6.36 (1H, s, Hpy), 4.63 (1H, s, Hpy), 3.88 (1H, m, Hph), 3.69 (1H, s, Hpy), 3.48 (2H, s, Hph), 3.41 (1H, s, Hph), 3.29 (1H, s, Hox), 2.91 (3H, s, Hpyr, Hph), 2.78 (1H, s, Hpy), 2.67 (2H, s, Hph), 1.71 (1H, s, Hpy), 1.36 (1H, s, Hpy), -0.69 (2H, s, Hph), -1.67 (1H, s, Hpy), -16.20 (1H, d, J = 3.77 Hz, Hpy)

Elemental analysis for $\{[Nd(R\text{-}Phbipox)_2]Otf\}\cdot 0.17Et_3NOtf$ ($C_{42.19}H_{30.55}N_{6.17}O_{9.51}F_{3.51}S_{1.17}Nd$ Mw =1024.51) (%) calcd. for C 49.46, H 3.01, N 8.44; found C 49.46, H 3.07, N 8.44.

ES-MS, CD_3OD: m/z= 832.4 $\{[Nd(R\text{-}Phbipox)_2]\}^+$

ES-MS, CD_3CN: m/z= 832.4 $\{[Nd(R\text{-}Phbipox)_2]\}^+$ m/z = 1323.3 $[Nd_3(R\text{-}Phbipox)_6](Otf)\}^{2+}$

[Yb(S/R-Phbipox)$_2$](Otf)

The compound was prepared as was described for the corresponding europium complex. Yield 78%.

^{1}H NMR (500 MHz, CD_3OD, 298K):

(Λ)-$[Yb(S/R\text{-}Phbipox)_2]^+$ species:

δ= 9.47 (1H, s, $H_{1'}$), 8.86 (2H, m, $H_{d'}$), 7.42 (3H, s, $H_{e'}$, $H_{a'}$), 7.25 (1H, s, $H_{b'}$), 7.16 (1H, s, $H_{2'}$), 7.03 (1H, s, $H_{4'}$), 6.34 (1H, m, $H_{c'}$), 6.10 (1H, s, $H_{f'}$), 5.94 (1H, s, $H_{5'}$), 4.40 (1H, s, $H_{3'}$), 3.77 (1H, s, $H_{6'}$)

(Δ)-$[Yb(S/R\text{-}Phbipox)_2]^+$ species:

δ= 15.74 (0.6H, m, H_d), 9.95 (0.3H, m, H_e), 8.76 (0.3H, m, H_f), 8.27 (0.3H, m, H_4), 7.96 (0.3H, m, H_a), 6.82 (0.3H, m, H_1), 5.78 (0.3H, m, H_5), 5.13 (0.3H, m, H_2), 3.67 (0.3H, m, H_b), 2.20 (0.3H, s, H_6), 1.77 (0.3H, s, H_3), -6.26 (0.3H, br m, H_c).

Elemental analysis for $\{[Yb(R\text{-}Phbipox)_2](Otf)\}.1.18Et_3NOtf$ ($C_{49.26}$ $H_{45.7}$ $N_{7.18}$ $O_{12.54}$ $F_{3.51}$ $S_{2.18}$ Yb Mw =1306.7) (%) calcd. for C 45.30, H 3.53, N 7.70; found C 45.30, H 3.52, N 8.06.

ES-MS, CD_3OD: m/z= 862.3 $\{[Yb(R\text{-}Phbipox)_2]\}^+$

ES-MS, CD_3CN : m/z= 862.3 $\{[Yb(R\text{-}Phbipox)_2]\}^+$

[Yb(Rac-Phbipox)$_2$](Otf)

Triethylamine (8µl) was added to a solution of Rac-Phbipox (18.6 mg, 0.051mmol) in 2 mL anhydrous acetonitrile. The resulting solution was stirred for 2 hours and a solution of $Yb(Otf)_3$ (15.8 mg 0.025 mmol) in acetonitrile (1mL) was then added. The resulting solution was stirred at room temperature for an hour. Diisopropylether was then added to afford a white microcrystalline solid precipitate that was filtered and dried two weeks at 40 °C under vacuum (60% yield).

1H NMR (400 MHz, CD_3OD, 298K):

(Δ)-[Yb(R-Phbipox)$_2$]$^+$/ (Λ)-[Yb(S-Phbipox)$_2$]$^+$ species:

δ= 9.47 (1H, s, $H_{1'}$), 8.86 (2H, m, $H_{d'}$), 7.42 (3H, s, $H_{e'}$, $H_{a'}$), 7.25 (1H, s, $H_{b'}$), 7.16 (1H, s, $H_{2'}$), 7.03 (1H, s, $H_{4'}$), 6.34 (1H, m, $H_{c'}$), 6.10 (1H, s, $H_{f'}$), 5.94 (1H, s, $H_{5'}$), 4.40 (1H, s, $H_{3'}$), 3.77 (1H, s, $H_{6'}$).

(Λ)-[Yb(R-Phbipox)$_2$]$^+$/ (Δ)-[Yb(S-Phbipox)$_2$]$^+$ species:

δ= 15.74 (0.6H, m, H_d), 9.95 (0.3H, m, H_e), 8.76 (0.3H, m, H_f), 8.27 (0.3H, m, H_4), 7.96 (0.3H, m, H_a), 6.82 (0.3H, m, H_1), 5.78 (0.3H, m, H_5), 5.13 (0.3H, m, H_2), 3.67 (0.3H, m, H_b), 2.20 (0.3H, s, H_6), 1.77 (0.3H, s, H_3), -6.26 (0.3H, br m, H_c).

[Yb(S-Phbipox)(R-Phbipox)]$^+$:

δ= 13.43-12.78 (0.6H, m), 10.20 (0.6H, s), 8.80 (0.6H, s), 7.09-6.83 (0.6H, m), 6.32 (0.6H, dd, *J* = 15.48, 8.48 Hz), 5.05 (0.6H, dd, *J* = 12.14, 10.05 Hz), 4.09 (0.6H, d, *J* = 2.96 Hz), 3.93 (0.6H, s), 2.86 (0.6H, s), 2.56 (0.6H, d, *J* = 5.65 Hz), 2.24 (0.6H, d, *J* = 5.07 Hz), -0.10 (0.6H, t, *J* = 7.01, 7.01 Hz)

Eu⊂[(Λ-Eu(R-Phbipox)$_2$Δ-Eu(R-Phbipox)$_2$)$_3$](Otf)$_9$

Triethylamine (25µl) was added to a solution of R-Phbipox (55 mg, 0.155 mmol) in 2 mL anhydrous acetonitrile. The resulting solution was stirred for 2 hours and a solution of $Eu(Otf)_3$ (54.6mg 0.090 mmol) in acetonitrile (1 mL) was then added. The resulting solution was stirred at room temperature for an hour. Diisopropylether was then added to afford a white microcrystalline solid precipitate that was filtered and dried two weeks at 40 °C under vacuum (81% yield).

^{1}H NMR (400 MHz, CD_3OD, 298K):

δ= 18.06-17.68 (1H, m), 16.41-16.11 (1H, m), 13.49-13.02 (1H, m), 12.64-12.35 (1H, m), 11.97-11.67 (1H, m), 11.58-11.25 (1H, m), 10.66 (2H, s), 10.40 (2H, d, *J* = 6.99 Hz), 10.25 (2H, s), 10.13 (2H, s), 10.06-9.93 (1H, m), 9.80-9.66 (1H, m), 9.28-9.13 (1H, m), 9.10-8.90 (2H, m), 8.21 (1H, s), 8.10 (2H, s), 8.02 (1H, s), 7.72 (2H, dd, *J* = 24.78, 7.61 Hz), 7.68 (1H, t), 7.54 (4H, t, *J* = 7.54, 7.54 Hz), 7.36-7.25 (1H, m), 6.77-6.68 (1H, m), 6.61 (2H, s), 5.97-5.78 (1H, m), 5.09 (2H, s), 4.67-4.40 (2H, m), 4.40-4.25 (1H, m), 4.21 (3H, s), 3.80 (2H, s), 3.63 (1H, s), 2.52 (2H, s), 2.36-2.20 (1H, m), 2.20-2.05 (1H, m), 1.82-1.65 (2H, m), 1.65-1.52 (1H, m), 1.50-1.40 (1H, m), -0.34--0.54 (1H, m), -0.78--0.92 (1H, m), -3.94--4.18 (1H, m), -10.09--10.42 (1H, m)

ES-MS, CD_3CN: m/z= 1334.5$\{[Eu_6L_{12}]Otf_2\}^{4+}$, 1829 $\{[Eu_6L_{12}]Otf_3\}^{3+}$

Elemental analysis for Eu⊂[(Λ-Eu(R-Phbipox)$_2$Δ-Eu(R-Phbipox)$_2$)$_3$](Otf)$_9$·Et_3NOtf
($C_{256}H_{183}Eu_7F_{30}N_{37}O_{66}S_{10}$ Mw =6787.76)
(%) calcd. for C 45.30, H 2.72, N 7.64; found C 45.10, H 2.71, N 7.84.

Nd⊂[(Λ-Nd(R-Phbipox)$_2$Δ-Nd(R-Phbipox)$_2$)$_3$](Otf)$_9$

Triethylamine (17.5µl) was added to a solution of R-Phbipox (40.4 mg, 0.114 mmol) in 2 mL anhydrous acetonitrile. The resulting solution was stirred for 2 hours and a solution of $Nd(Otf)_3$ (39.7 mg 0.067 mmol) in acetonitrile (1mL) was then added. The resulting solution was stirred at room temperature for an hour. Diisopropylether was then added to afford a white microcrystalline solid precipitate that was filtered and dried two weeks at 40 °C under vacuum (54% yield).

Full assignment of the ^{1}H NMR spectrum was not possible due to the strong paramagnetic broadening, shift and overlapping of the peaks.

ES-MS, CD_3CN : m/z= 1319.5$\{[Nd_6L_{12}]Otf_2\}^{4+}$, 1809 $\{[Nd_6L_{12}]Otf_3\}^{3+}$

Elemental analysis for Nd⊂[(Λ-Nd(R-Phbipox)$_2$Δ-Nd(R-Phbipox)$_2$)$_3$](Otf)$_9$
($C_{249}H_{168}Nd_7F_{27}N_{36}O_{63}S_9$ Mw =6483.13)
(%) calcd. for C 46.13, H 2.61, N 7.78; found C 45.84, H 2.80, N 7.86.

10.3- Divalent Lanthanide Complexes

[Sm(tpa)$_2$]I$_2$

Addition of tpa (50 mg, 0.186 mmol) in THF (2 mL) to a stirring blue solution of SmI_2 (37.7 mg, 0.093 mmol) in THF (2 mL) resulted in a color change to purple-violet and led to the formation of violet blue precipitates of the final complex immediately. After filtration the residue was washed several times with THF and hexane and dried under vacuum to yield $[Sm(tpa)_2]I_2$ as violet blue powder in 76% yield. Dark blue crystals suitable for X-ray diffraction were obtained from slow diffusion of tpa into the SmI_2 solution in THF.

^{1}H NMR (400 MHz, CD_3CN, 298K)
δ= 23.80 (1H, s, H_6), 11.54 (1H, d, *J* = 7.89 Hz, $H_{5/4}$), 4.63-4.24 (1H, m, H_3), 3.88-3.61 (1H, m, $H_{4/5}$), -12.16 (2H, s, $H_{a,b}$)

Elemental analysis for $[Sm(tpa)_2]I_2$ (C_{36} H_{36} I_2 N_8 Sm, Mw =984.89)
(%) calcd. for C 43.90, H 3.68, N 11.38; found C 43.75, H 3.81, N 11.41.

ES-MS, CH_3CN: m/z= 859 $\{[Sm(tpa)_2]I\}^+$, m/z= 569 $\{[Sm(tpa)]I\}^+$

[Sm(tpa)I_2]

Addition of tpa (23.7 mg, 0.081mmol) in THF (1 mL) to a stirring blue solution of SmI_2 (22mg, 0.054mmol) in THF (2 mL) resulted in a color change to red-violet and led to the formation of red-violet precipitates of the final complex immediately. After filtration the residue was washed several times with THF and hexane and dried under vacuum to yield [Sm(tpa)I_2] as violet blue powder in 82% yield.

^{1}H NMR (400 MHz, CD_3CN, 298K)

δ= 8.78 (1H, s, H_6), 7.06 (1H, d, J = 4.91 Hz, $H_{5/4}$), 5.09 (1H, m, $H_{4/5}$), 4.34. (1H, s, H_3), 1.04 (2H, s, $H_{a,b}$)

[Sm(tpa)I_2] 0.2THF ($C_{36.8}$ $H_{37.6}$ I_2 N_8 $O_{0.2}$ Sm, Mw =694.597)
(%) calcd. for C 31.85, H 2.79, N 7.90; found C 31.84, H 3.4, N 7.96.

[Eu(tpa)$_2$]I_2

Addition of tpa (20.9 mg, 0.071 mmol) in THF (1 mL) to a stirring fluorescent solution of EuI_2 (14.6 mg, 0.035 mmol) in THF (1 mL) resulted in a color change to dark red and led to the formation of red precipitates of the final complex immediately. After filtration the residue was washed several times with THF and hexane and dried under vacuum to yield [Eu(tpa)$_2$]I_2 as a red powder in 87% yield. Dark red crystals suitable for X-ray diffraction were obtained from slow diffusion of tpa into the EuI_2 solution THF.

Elemental analysis for [Eu(tpa)$_2$]I_2 (C_{36} H_{36} I_2 N_8 Eu, Mw =986.53)
(%) calcd. for C 43.83, H 3.68, N 11.36; found C 43.53, H 3.85, N 11.44.

ES-MS, CH_3CN: m/z=860 $\{[Eu(tpa)_2]I\}^+$, m/z=570 $\{[Eu(tpa)]I\}^+$

$(Eu(tpa)I(\mu I))_2$

Addition of tpa (20.9 mg, 0.071mmol) in THF (1 mL) to a stirring fluorescent solution of EuI_2 (29.2mg, 0.071 mmol) in THF (1 mL) resulted in a color change to orange and led to the formation of orange precipitates of the final complex immediately. After filtration the residue was washed several times with THF and hexane and dried under vacuum to yield $(Eu(tpa)I(\mu\text{-}I))_2$ as an orange powder in 90% yield. Orange crystals suitable for X-ray diffraction were obtained from an acetonitrile solution of the complex by layering diisopropylether.

$[Yb(tpa)_2]I_2$

Addition of tpa (20 mg, 0.068 mmol) in THF (2 mL) to a stirring yellow solution of YbI_2 (14.7 mg, 0.034 mmol) in THF (1 mL) resulted in a color change to blue-green and led to the formation of green precipitates of the final complex immediately. After filtration the residue was washed several times with THF and hexane and dried under vacuum to yield $[Yb(tpa)_2]I_2$ as a green powder in 65% yield. Dark green crystals suitable for X-ray diffraction were obtained from an acetonitrile solution of the complex by layering diisopropylether.

^{1}H NMR (400 MHz, CD_3CN, 298K)

δ= 7.88 (1H, s, H_6), 7.54 (1H, d, J = 7.11 Hz, $H_{5/4}$), 7.45 (1H, s, $H_{4/5}$), 6.95 (1H, s, H_3), 4.22 (2H, s, $H_{a,b}$)

$[Yb(tpa)I_2]$

Addition of tpa (23.7 mg, 0.081mmol) in THF (2 mL) to a stirring yellow solution of YbI_2 (34.9mg, 0.081mmol) in THF (1 mL) resulted in a color change to violet blue and led to the formation of violet blue precipitates of the final complex immediately. After filtration the residue was washed several times with THF and hexane and dried under vacuum to yield $[Yb(tpa)I_2]$ as a violet blue powder in 70% yield. Dark blue crystals suitable for X-ray diffraction were obtained from an acetonitrile solution of the complex by layering diisopropylether.

^{1}H NMR (400 MHz, CD_3CN, 298K)

δ= 8.83 (1H, s, Hpy), 7.84 (1H, t, J = 7.51, 7.51 Hz, Hpy), 7.33 (2H, d, J = 6.99 Hz, Hpy), 3.98 (2H, s, Ha,b)

$[Tm(tpa)_2]I_2$

Addition of a solution of tpa (50 mg, 0.172 mmol) in THF (2 mL) to an emerald green solution of TmI_2 (36.4 mg, 0.086 mmol) in THF (2 mL) resulted in a color change to orange and led to the formation of orange precipitates of the final complex immediately. After filtration the residue washed several times with THF and hexane and dried under vacuum to yield $[Tm(tpa)_2]I_2$ as an orange powder in 92% yield. The complex is thermally unstable and the color of the powder turned to green in a day.

Elemental analysis for $[Tm(tpa)_2]I_2$ (C_{36} H_{36} I_2 N_8 Tm, Mw = 1003.43)
(%) calcd. for C 43.09, H 3.62, N 11.17; found C 42.95, H 3.73, N 11.32.

$[Dy(tpa)_2]I_2$

Addition of a solution of tpa (16.3 mg, 0.056 mmol) in THF (2 mL) to a dark green solution of DyI_2 (11.7 mg, 0.028 mmol) in THF (2 mL) resulted in a color change to brown and led to the formation of brown precipitates of the final complex immediately. After filtration the residue washed several times with THF and hexane and dried under vacuum to yield $[Dy(tpa)_2]I_2$ as a brown powder in 71% yield. The complex is thermally unstable and the color of the powder turns to cream rapidly in an hour.

10.4- Lanthanide Complexes by the oxidation of divalent precursors

$[Yb(tpa)(\mu\text{-}OH)(Py\text{-}N\text{-}Oxide)_2]I_2$

Addition of Pyridine-N-Oxide (1.8 mg, 0.018 mmol) in acetonitrile (0.5 mL) to a stirring green solution of $[Yb(tpa)_2]I_2$ (4.8 mg, 0.004 mmol) in acetonitrile (1 mL) resulted in an immediate discoloration of the solution. Colorless crystals suitable for X-ray diffraction were obtained from this solution by layering diisopropylether.

$[Sm(tpa)(\mu\text{-}OH)(Py\text{-}N\text{-}Oxide)_2]I_2$

Addition of Pyridine-N-Oxide (6 mg, 0.063 mmol) in acetonitrile (0.5 mL) to a stirring blue solution of $[Sm(tpa)_2]I_2$ (15 mg, 0.015 mmol) in acetonitrile (1 mL) resulted in an immediate color change to yellow. Yellow crystals suitable for X-ray diffraction were obtained from this solution by layering diisopropylether.

$[Nd_{13}(\mu_4\text{-}O_8)Na_8(\mu_4\text{-}1,1,1,1\text{-}N_3)_6(\mu_3\text{-}1,1,3\text{-}N_3)_{24}(py)_{28}I]\cdot(py)_7$

Isostructural crystals of Nd_{13} **XX** cluster have been obtained repetitively from the reactions:

a)

Slow diffusion of tpa (38 mg, 0.130 mmol) in THF (2 mL) into a deep violet solution of NdI_2 (25.1 mg, 0.062 mmol) in THF at room temperature resulted in a light green-yellow precipitate in a few days. (Identical light yellow powder obtained when the diffusion performed at -5ºC and -30ºC). 5.3 mg of this powder was reacted with NaN_3 (3.8 mg, 0.058 mmol) in pyridine at room temperature. After filtration to remove excess NaN_3, colorless rod shape crystals of the cluster **XX** suitable for X-ray diffraction were obtained from this solution by layering hexane.

b)

NdI_2 (35.6 mg, 0.089 mmol) and 2 equivalent of tpa (57.2 mg, 0.196 mmol) placed into a schlenk tube in the glove box and 5 mL of THF condensed onto this mixture at liquid nitrogen temperature. The temperature set to -70ºC and reaction mixture stirred for 2 days. Dark orange precipitates and a black undissolved powder observed at the bottom. Therefore the reaction temperature increased to -40ºC and stirred for 2 more days in order to solubilise undissolved NdI_2. The color of the suspension became light yellow-green. The suspension let stirring at room temperature for 5 hours no color change observed. After filtration (to remove excess tpa in solution) 40.6 mg powder obtained.

The 34.6 mg of this filtered light yellow-green powder reacted at room temperature with NaN_3 (9.2 mg, 0.141 mmol)**.** After filtration to remove excess NaN_3, colorless rod shape crystals of the cluster **XX** suitable for X-ray diffraction were obtained from this solution by layering hexane.

BIBLIOGRAPHY

1. Aspinall, H.C., *Chemistry of the F-Block Elements*. 2001: CRC Press.
2. Cotton, S., *Lanthanides and Actinides*. 1991, London: MacMillan Education.
3. Huang, C.H., *Rare Earth Coordination Chemistry: Fundamentals and Applications*. 2010: John Wiley & Sons.
4. Housecroft, C.E. and A.G. Sharpe, *Inorganic Chemistry*. 2005, Essex England: Pearson.
5. Shannon, R.D., *Revised Effective Ionic Radii and Systematic Studies of Interatomie Distances.* Acta Crystallographica Section A-Crystal Physics, Diffraction, Theoretical and General Crystallography, 1976. **A32**: p. 751-767.
6. Bunzli, J.-C.G. and C. Piguet, *Taking advantage of luminescent lanthanide ions.* Chemical Society Reviews, 2005. **34**(12): p. 1048-1077.
7. Comby, S. and J.-C.G. Bünzli, *Lanthanide Near-Infrared Luminescence in Molecular Probes and Devices*, in *Handbook on the Physics and Chemistry of Rare Earths*, K.A.J. Gschneidner, J.-C.G. Bünzli, and V.K. Pecharsky, Editors. 2007, Elsevier: Amsterdam. p. 217-470.
8. Bunzli, J.-C.G., et al., *New opportunities for lanthanide luminescence.* Journal of Rare Earths, 2007. **25**(3): p. 257-274.
9. Bruce, J.I., M.P. Lowe, and D. Parker, *Photophysical Aspects of Lanthanide(III) Complexes*, in *The Chemistry of Constrast Agents in Medical Magnetic Resonance Imaging*, A.E. Merbach and E. Toth, Editors. 2001, John Willey & Sons. p. 437-460.
10. Werts, M.H.V., *Making sense of lanthanide luminescence.* Science Progress, 2005. **88**: p. 101-131.
11. Weissman, S.I., *Intramolecular Energy Transfer The Fluorescence of Complexes of Europium.* The Journal of Chemical Physics, 1942. **408**: p. 934-944.
12. Bunzli, J.-C.G., *Lanthanide-containing luminescent molecular edifices.* Journal of Alloys and Compounds, 2006. **408**: p. 934-944.
13. de Sa, G.F., et al., *Spectroscopic properties and design of highly luminescent lanthanide coordination complexes.* Coordination Chemistry Reviews, 2000. **196**: p. 165-195.
14. Parker, D., *Luminescent lanthanide sensors for pH, pO_2 and selected anions.* Coordination Chemistry Reviews, 2000. **205**: p. 109-130.
15. Latva, M., et al., *Correlation between the lowest triplet state energy level of the ligand and lanthanide(III) luminescence quantum yield.* Journal of Luminescence, 1997. **75**(2): p. 149-169.
16. Dossing, A., *Luminescence from lanthanide(3+) ions in solution.* European Journal of Inorganic Chemistry, 2005(8): p. 1425-1434.
17. Ronda, C.R., T. Justel, and H. Nikol, *Rare earth phosphors: fundamentals and applications.* Journal of Alloys and Compounds, 1998. **277**: p. 669-676.
18. Justel, T., H. Nikol, and C. Ronda, *New developments in the field of luminescent materials for lighting and displays.* Angewandte Chemie-International Edition, 1998. **37**(22): p. 3085-3103.
19. Feldmann, C., et al., *Inorganic luminescent materials: 100 years of research and application.* Advanced Functional Materials, 2003. **13**(7): p. 511-516.
20. Kuriki, K., Y. Koike, and Y. Okamoto, *Plastic optical fiber lasers and amplifiers containing lanthanide complexes.* Chemical Reviews, 2002. **102**(6): p. 2347-2356.
21. Soini, E. and I. Hemmila, *Fluoroimmunoassay: present status and key problems.* Clin Chem, 1979. **25**(3): p. 353-361.
22. Bunzli, J.-C.G., *Lanthanide Luminescent Bioprobes (LLBs).* Chemistry Letters, 2009. **38**(2): p. 104-109.

23. de Bettencourt-Dias, A., *Lanthanide-based emitting materials in light-emitting diodes.* Dalton Transactions, 2007(22): p. 2229-2241.
24. Kido, J. and Y. Okamoto, *Organo lanthanide metal complexes for electroluminescent materials.* Chemical Reviews, 2002. **102**(6): p. 2357-2368.
25. Kido, J., K. Nagai, and Y. Ohashi, *Electroluminescence in a Terbium Complex.* Chemistry Letters, 1990: p. 657-660.
26. Gillin, W.P. and R.J. Curry, *Erbium (III) tris(8-hydroxyquinoline) (ErQ): A potential material for silicon compatible 1.5 mu m emitters.* Applied Physics Letters, 1999. **74**(6): p. 798-799.
27. Vergeer, P., et al., *Quantum cutting by cooperative energy transfer in Ybx Y1-x P O4 : Tb3+.* Physical Review B, 2005. **71**(1): p. 014119.
28. Liang, X.F., X.Y. Huang, and Q.Y. Zhang, *Gd2(MoO4)3:Er3+ Nanophosphors for an Enhancement of Silicon Solar-Cell Near-Infrared Response* Journal of Fluorescence, 2009. **19**(2): p. 285-289.
29. Eliseevaa, S.V. and J.-C.G. Bunzli, *Rare earths: jewels for functional materials of the future.* New J.Chem., 2011. **35**: p. 1165□1176.
30. Bünzli, J.-C.G., *Europium in the limelight.* Nature Chemistry, 2010. **2**: p. 696.
31. White, K.A., et al., *Near-Infrared Luminescent Lanthanide MOF Barcodes.* J. Am. Chem. Soc, 2009. **131**: p. 18069-18071.
32. Albertsson, J., *Structural Studies on Rare-Earth Carboxylates.10. The Crystal and Molecular Structure of Monoclinic Trisodium Tris(pyridine-2,6-dicarboxylato)ytterbate(III) 13-Hydrate.* Acta Chemica Scandinavica, 1972. **26**(3): p. 985-1004.
33. Brayshaw, P.A., et al., *Synthetic, Structural, and Spectroscopic Studies on Solids Containing Tris(Dipicolinato) Rare-Earth Anions and Transition or Main-Group Metal-Cations.* Inorganic Chemistry, 1995. **34**(8): p. 2068-2076.
34. Aebischer, A., F. Gumy, and J.-C.G. Bunzli, *Intrinsic quantum yields and radiative lifetimes of lanthanide tris(dipicolinates).* Physical Chemistry Chemical Physics, 2009. **11**(9): p. 1346-1353.
35. D'Aleo, A., et al., *Efficient Sensitization of Europium, Ytterbium, and Neodymium Functionalized Tris-Dipicolinate Lanthanide Complexes through Tunable Charge-Transfer Excited States.* Inorganic Chemistry, 2008. **47**(22): p. 10258-10268.
36. Platas-Iglesias, C., et al., *Lanthanide triple-stranded helical complexes with a substituted 2,6-pyridinedicarboxylate.* Journal of the Chemical Society-Dalton Transactions, 2001(20): p. 3084-3091.
37. Nonat, A., et al., *Lanthanide complexes of a picolinate ligand derived from 1,4,7-triazacyclononane with potential application in magnetic resonance imaging and time-resolved luminescence imaging.* Chemistry-a European Journal, 2006. **12**(27): p. 7133-7150.
38. Lis, S. and G.R. Choppin, *Luminescence Study of Europium(Iii) Complexes with Several Dicarboxylic-Acids in Aqueous-Solution.* Journal of Alloys and Compounds, 1995. **225**(1-2): p. 257-260.
39. Gassner, A.L., et al., *Remarkable tuning of the photophysical properties of bifunctional lanthanide tris(dipicolinates) and its consequence on the design of bioprobes.* Inorganic Chemistry, 2008. **47**(17): p. 7802-7812.
40. Chauvin, A.S., et al., *Europium and terbium tris(dipicolinates) as secondary standards for quantum yield determination.* Spectroscopy Letters, 2004. **37**(5): p. 517-532.

41. Chatterton, N., et al., *An efficient design for the rigid assembly of four bidentate chromophores in water-stable highly luminescent lanthanide complexes.* Angewandte Chemie-International Edition, 2005. **44**(46): p. 7595-7598.
42. Marchal, C., et al., *Toward the rational design of lanthanide coordination polymers: A new topological approach.* Inorganic Chemistry, 2007. **46**(16): p. 6242-6244.
43. Marchal, C., et al., *Lanthanide-Based Coordination Polymers Assembled by a Flexible Multidentate Linker: Design, Structure, Photophysical Properties, and Dynamic Solid-State Behavior.* Chemistry - A European Journal 2009. **15**(21): p. 5273-5288.
44. Comby, S., et al., *Influence of Anionic Functions on the Coordination and Photophysical Properties of Lanthanide(III) Complexes with Tridentate Bipyridines.* Inorganic Chemistry, 2004. **43**(23): p. 7369-7379.
45. Kottas, G.S., et al., *Highly luminescent, neutral, nine-coordinate lanthanide(III) complexes.* European Journal of Inorganic Chemistry, 2007(22): p. 3465-3468.
46. Charbonniere, L.J., et al., *Relationship between the ligand structure and the luminescent properties of water-soluble lanthanide complexes containing bis(bipyridine) anionic arms.* Chemistry-a European Journal, 2007. **13**(1): p. 346-358.
47. Charbonniere, L.J., N. Weibel, and R.F. Ziessel, *Synthesis of mono-, bis- and tris-tridentate ligands based on 5'-substituted-2,2'-bipyridine-6-carboxylic acid.* Tetrahedron Letters, 2001. **42**(4): p. 659-662.
48. Alpha, B., J.M. Lehn, and G. Mathis, *Energy-Transfer Luminescence of Europium(III) and Terbium(III) Cryptates of Macrobicyclic Polypyridine Ligands.* . Angewandte Chemie-International Edition, 1987. **26**(3): p. 266-267.
49. Murner, H.R., et al., *Strong enhancement of the lanthanide-centred luminescence in complexes with 4-alkylated 2,2':6',2''-terpyridines.* Journal of the Chemical Society-Dalton Transactions, 2000(16): p. 2809-2816.
50. Petoud, S., et al., *Luminescent properties of lanthanide nitrate complexes with substituted bis(benzimidazolyl)pyridines.* Inorganic Chemistry, 1997. **36**(7): p. 1345-1353.
51. Andreiadis, E.S., et al., *Remarkable Tuning of the Coordination and Photophysical Properties of Lanthanide Ions in a Series of Tetrazole-Based Complexes.* Chemistry-a European Journal, 2009. **15**(37): p. 9458-9476.
52. Giraud, M., et al., *Efficient Sensitization of Lanthanide Luminescence by Tetrazole-Based Polydentate Ligands.* Inorganic Chemistry, 2008. **47**(10): p. 3952-3954.
53. Binnemans, K., *Rare-Earth Beta-Diketonates*, in *Handbook on the Physics and Chemistry of Rare Earths*, K.A.J. Gschneidner, J.-C.G. Bünzli, and V.K. Pecharsky, Editors. 2005. p. 107-272.
54. Frey, S.T., M.L. Gong, and W.D. Horrocks, *Synergistic Coordination in Ternary Complexes of Eu3+ with Aromatic Beta-Diketone Ligands and 1,10-Phenanthroline.* Inorganic Chemistry Communications, 1994. **33**(15): p. 3229-3234.
55. Quici, S., et al., *Visible and near-infrared intense luminescence from water-soluble lanthanide [Tb(III), Eu(III), Sm(III), Dy(III), Pr(III), Ho(III), Yb(III), Nd(III), Er(III)] complexes.* Inorganic Chemistry, 2005. **44**(3): p. 529-537.
56. Quici, S., et al., *Highly Luminescent Eu3+ and Tb3+ Macrocyclic Complexes Bearing an Appended Phenanthroline Chromophore.* Inorganic Chemistry, 2002. **41**(10): p. 2777-2784.
57. Zhang, J., et al., *Sensitization of Near-Infrared-Emitting Lanthanide Cations in Solution by Tropolonate Ligands.* Angew. Chem. Int. Ed. , 2005. **44**: p. 2508-2512.
58. Zhang, J. and S. Petoud, *Azulene-moiety-based ligand for the efficient sensitization of four near-infrared luminescent lanthanide cations: Nd^{3+}, Er^{3+}, Tm^{3+}, and Yb^{3+}.* Chemistry-a European Journal of Inorg Chemistry, 2008. **14**(4): p. 1264-1272.

59. Comby, S., et al., *A novel strategy for the design of 8-hydroxyquinolinate-based lanthanide bioprobes that emit in the near infrared range.* Chemistry-a European Journal, 2007. **13**(3): p. 936-944.
60. Imbert, D., et al., *Lanthanide 8-hydroxyquinoline-based podates with efficient emission in the NIR range.* Chemical Communications, 2005(11): p. 1432-1434.
61. Comby, S., et al., *Stable 8-Hydroxyquinolinate-Based Podates as Efficient Sensitizers of Lanthanide Near-Infrared Luminescence.* Inorganic Chemistry, 2005. **45**(2): p. 732-743.
62. Tallec, G., et al., *Highly stable and soluble bis-aqua Gd, Nd, Yb complexes as potential bimodal MRI/NIR imaging agents.* Dalton Transaction, 2010. **39**: p. 9490-9492.
63. Nonat, A., et al., *Structural and Photophysical Studies of Highly Stable Lanthanide Complexes of Tripodal 8-hydroxyquinolinate Ligands Based on 1,4,7-Triazacyclononane.* Inorganic Chemistry, 2009. **48**: p. 4207-4218.
64. Bunzli, J.C.G., *Benefiting from the unique properties of lanthanide ions.* Accounts of Chemical Research, 2006. **39**(1): p. 53-61.
65. Bunzli, J.-C.G. and C. Piguet, *Lanthanide-containing molecular and supramolecular polymetallic functional assemblies.* Chemical Reviews, 2002. **102**(6): p. 1897-1928.
66. Piguet, C. and J.-C.G. Bunzli, *Mono- and polymetallic lanthanide-containing functional assemblies: a field between tradition and novelty.* Chemical Society Reviews, 1999. **28**(6): p. 347-358.
67. Imbert, D., et al., *Extending lifetimes of lanthanide-based near-infrared emitters (Nd, Yb) in the millisecond range through Cr(III) sensitization in discrete bimetallic edifices.* Journal of the American Chemical Society, 2003. **125**(51): p. 15698-15699.
68. Faulkner, S. and S.J.A. Pope, *Lanthanide-sensitized lanthanide luminescence: Terbium-sensitized ytterbium luminescence in a trinuclear complex.* Journal of the American Chemical Society, 2003. **125**(35): p. 10526-10527.
69. Banerjee, S., et al., *Oxoselenido clusters of the lanthanides: Rational introduction of oxo ligands and near-IR emission from Nd(III).* Journal of the American Chemical Society, 2005. **127**(45): p. 15900-15906.
70. Banerjee, S., et al., *Oxoclusters of the Lanthanides Begin to Resemble Solid-State Materials at Very Small Cluster Sizes: Structure and NIR Emission from Nd(III).* J. Am. Ceram. Soc., 2007. **129** p. 5926 5931.
71. Moore, B.F., et al., *Lanthanide Clusters with Chalcogen Encapsulated Ln: NIR Emission from Nanoscale NdSex.* J. Am. Ceram. Soc. , 2011. **133**: p. 373-378.
72. Hubert-Pfalzgraf, L.G., *Some trends in the design of homo- and heterometallic molecular precursors of high-tech oxides.* Inorganic Chemistry Communications, 2003. **6**: p. 102-120.
73. Bünzli, J.-C.G., et al., *Structural and dynamic properties of calixarene bimetallic complexes : solution versus solid-state structure of dinuclear complexes of Eu(III) and Lu(III) with substituted calix[8]arenes* J. Chem. Soc., Dalton Trans., 1998: p. 497-503.
74. Inoue, M.B., et al., *Binuclear Gd^{3+} complex of a 34-membered macrocycle with six carboxymethyl arms : X-ray structures, formation constants, NMR, EPR, and 1H NMR relaxivities.* Inorg. Chem., 1999. **38**: p. 1596-1602.
75. Matthews, K.D., et al., *The preparation and luminescence decay dynamics of coupled heterolanthanide (III) cations in dinuclear Schiff-base complexes.* J. Chem. Soc., Dalton Trans. , 1993: p. 1719-1723.
76. Guerriero, P., et al., *Synthesis and luminescence study of homo- and hetero- binuclear complexes of lanthanides with a new cyclic compartmental Schiff base.* J. Chem. Soc., Dalton Trans., 1990: p. 647-655.

77. Wang, Z., J. Reibenspies, and A.E. Martell, *Design, synthesis, and x-ray structural characterization of new dinucleating macrocyclic ligands and a novel phenolate-bridged dilanthanum(iii) complex.* Inorg. Chem., 1997. **36**: p. 629-636.
78. Pope, S.J.A., et al., *Synthesis and luminescence properties of dinuclear lanthanide complexes derived from covalently linked macrocyclic ligands.* Dalton Transactions, 2003(19): p. 3780-3784.
79. Newkome, G.R., E. He, and C.N. Moorefield, *Suprasupermolecules with Novel Properties: Metallodendrimers.* Chemical Reviews, 1999. **99**: p. 1689−1746.
80. Kawa, M. and J.M.J. Frechet, *Self-Assembled Lanthanide-Cored Dendrimer Complexes: Enhancement of the Luminescence Properties of Lanthanide Ions through Site-Isolation and Antenna Effects.* Chem. Mater., 1998. **10**: p. 286-296.
81. Cross, J.P., et al., *Polymetallic Lanthanide Complexes with PAMAM-Naphthalimide Dendritic Ligands: Luminescent Lanthanide Complexes Formed in Solution.* J. Am. Ceram. Soc., 2004. **126**: p. 16278 16279.
82. Piguet, C., et al., *Structural and Photophysical Properties of Lanthanide Complexes with Planar Aromatic Tridentate Nitrogen Ligands as Luminescent Building-Blocks for Triple-Helical Structures.* Inorganic Chemistry, 1993. **32**(19): p. 4139-4149.
83. Hamacek, J., G. Bernardinelli, and Y. Filinchuk, *Tetrahedral Assembly with Lanthanides: Toward Discrete Polynuclear Complexes.* Eur. J. Inorg. Chem., 2008: p. 3419□3422.
84. El Aroussi, B., et al., *Rational Design of a Ternary Supramolecular System: Self-Assembly of Pentanuclear Lanthanide Helicates.* J. Am. Ceram. Soc., 2011. **ASAP**.
85. Bretonnière, Y., et al., *Unprecedented Self-Assembly of M3L2 Trinuclear Lanthanide Complexes Assisted by a Tripodal Ligand Containing Terpyridine Binding Units.* Chemical Communication, 2000: p. 1543-1544.
86. Xu, J. and K.N. Raymond, *Lord of ring.* Angewandte Chemie, 2000. **39**: p. 2745-2747.
87. Costes, J.-P., et al., *Homo- (4f, 4f) and Heterodimetallic (4f, 4f') Complexes. The First Structurally Characterized Example of a Heterodimetallic (Yb, La) Complex (1'). Magnetic Properties of 1' and of a Homodinuclear (Gd, Gd) Analogue.* Inorg. Chem., 1998. **37**: p. 153-155.
88. Costes, J.-P. and F. Nicodeme, *Unequivocal Synthetic Pathway to Heterodinuclear (4f,4f') Complexes: Magnetic Study of Relevant (LnIII,GdIII) and (GdIII,LnIII) Complexes.* Chem. Eur. J. , 2002. **8**(15): p. 3442-3447.
89. Piguet, C. and J.-C.G. Bünzli, *Chapter 247 Self-Assembled Lanthanide Helicates: From Basic Thermodynamics to Applications*, in *Handbook on the Physics and Chemistry of Rare Earths*, K.A.J. Gschneidner, J.-C.G. Bünzli, and V.K. Pecharsky, Editors. 2010, Elsevier. p. 301-553.
90. Albrecht, M., *"Let's twist again" - Double-stranded, triple-stranded, and circular helicates.* Chemical Reviews, 2001. **101**(11): p. 3457-3497.
91. Lehn, J.M., et al., *Spontaneous Assembly of Double-Stranded Helicates from Oligobipyridine Ligands and Copper(I) Cations - Structure of an Inorganic Double Helix.* Proc. Natl. Acad. Sci. U. S. A., 1987. **84**: p. 2565-2569.
92. Bernardinelli, G., C. Piguet, and A.F. Williams, *The first self-assembled dinuclear triple-helical lanthanide complex : synthesis and structure* Angew. Chem. Int. Ed., 1992. **31**: p. 1622□1624.
93. Dong, Y.-B., et al., *Coordination-driven nanosized lanthanide "molecular lantern" with tunable luminescent properties.* J. Am. Chem. Soc., 2007. **129**: p. 4872-4873.
94. Senegas, J.-M., S. Koeller, and C. Piguet, *Isolation and characterization of the first circular single-stranded polymetallic lanthanide-containing helicate.* Chem. Commun, 2005: p. 2235-2237.

95. Floquet, S., et al., *The first self-assembled trimetallic lanthanide helicates driven by positive cooperativity.* Chem. Eur. J., 2003. **9**: p. 1860-1875.
96. Zeckert, K., et al., *Predictions, synthetic strategy, and isolation of a linear tetrametallic triple-stranded lanthanide helicate.* Angew. Chem. Int. Ed., 2005. **44**: p. 7954 -7958.
97. André, N., et al., *Discriminating between lanthanide ions : self-assembly of heterodimetallic triple-stranded helicates* Chem. Commun, 2002: p. 214-215.
98. Terazzi, E., et al., *A Simple Chemical Tuning of the Effective Concentration: Selection of Single-, Double-, and Triple-Stranded Binuclear Lanthanide Helicates.* Chemistry-a European Journal, 2009. **15**(46): p. 12719-12732.
99. Albrecht, M., et al., *Highly efficient Near-IR emitting YbNb and Yb/Al helicates.* Journal of the American Chemical Society, 2007. **129**(46): p. 14178-14179.
100. Albrecht, M., et al., *Homo- and Heterodinuclear Helicates of Lanthanide(III), Zinc(II) and Aluminium(III) Based on 8-Hydroxyquinoline Ligands.* Chemistry-a European Journal, 2009. **15**(35): p. 8791-8799.
101. Comby, S., et al., *Dual emission from luminescent nonalanthanide clusters.* Inorganic Chemistry, 2006. **45**: p. 3158-3160.
102. Hou, H., et al., *First Octameric Ellipsoid Lanthanide(III) Complexes: Crystal Structure and Nonlinear Optical Absorptive and Refractive Properties.* Inorganic Chemistry, 2004. **43**(4): p. 1323-1327.
103. Westin, L.G., M. Kritikos, and A. Caneschi, *Self assembly, structure and properties of the decanuclear lanthanide ring complex, Dy-10(OC2H4OCH3)(30).* Chemical Communication, 2003(8): p. 1012-1013.
104. Bretonnière, Y., et al., *Cation-controlled self-assembly of a hexameric europium wheel.* Journal of the American Chemical Society, 2002. **124**(31): p. 9012-9013.
105. Chen, X.Y., et al., *Selective self-assembly of hexameric homo- and heteropolymetallic lanthanide wheels: Synthesis, structure, and photophysical studies.* Inorganic Chemistry, 2007. **46**(3): p. 625-637.
106. Zeng, Z., *Cluster Compounds of Rare-Earth Elements*, in *Handbook on the Physics and Chemistry of Rare Earths*, K.A.J. Gschneidner, J.-C. Bünzli, and V.K. Pecharsky, Editors. 2010, Elsevier: Amsterdam. p. 109-239.
107. Boyle, T.J. and L.A.M. Ottley, *Advances in Structurally Characterized Lanthanide Alkoxide, Aryloxide, and Silyloxide Compounds.* Chemical Reviews, 2008. **108**: p. 1896□1917.
108. Zheng, Z., *Ligand-controlled self-assembly of polynuclear lanthanide-oxo/hydroxo complexes: from synthetic serendipity to rational supramolecular design.* Chemical Communications, 2001(24): p. 2521-2529.
109. Wang, R., D. Song, and S. Wang, *Toward constructing nanoscale hydroxo-lanthanide clusters: syntheses and characterizations of novel tetradecanuclear hydroxo-lanthanide clusters.* Chemical Communications, 2002(4): p. 368-369.
110. Xu, G., et al., *Synthesis and Structural Characterization of Nonanuclear Lanthanide Complexes.* Inorganic Chemistry, 2002. **41**(25): p. 6802-6807.
111. Mudring, A.-V. and A. Babai, *$[Nd_6(\mu_6\text{-}O)(\mu_3\text{-}OH)_8(H_2O)_{24}]I_8\ (H_2O)_{12}$ the First Basic Rare Earth Iodide with an Oxygen-centred M_6X_8 -Cluster Core.* Z. Anorg. Allg. Chem., 2005. **631**: p. 261-263.
112. Mudring, A.-V., T. Timofte, and A. Babai, *Cluster-Type Basic Lanthanide Iodides $[M_6(\mu_6\text{-}O)(\mu_3\text{-}OH)_8(H_2O)_{24}]I_8(H_2O)_8$ (M=Nd, Eu, Tb, Dy).* Inorganic Chemistry 2006. **45**: p. 5162−5166.
113. Kornienko, A., et al., *Lanthanide Clusters with Internal Ln Ions: Highly Emissive Molecules with Solid-State Cores.* J. Am. Ceram. Soc., 2005. **127** p. 3501 3505.

114. Riman, R.E., et al., *Molecular Minerals^{TM}: Lyophillic Colloids for Ceramists.* J. Am. Ceram. Soc., 2006. **89**(6): p. 1809□1815
115. Eliseevaa, S.V. and J.-C.G. Bunzli, *Lanthanide luminescence for functional materials and bio-sciences.* Chemical Society Reviews, 2010. **39**: p. 189□227
116. Evans, W.J., M.A. Greci, and J.W. Ziller, *Reactivity of □Eu(O^{i}Pr)$_2$□ with Phenols: Formation of Linear Eu$_3$, Square Pyramidal Eu$_5$, Cubic Eu$_8$, and Capped Cubic Eu$_9$ Polymetallic Europium Complexes.* Inorg. Chem., 2000. **39**: p. 3213-3220.
117. Karmazin, L., M. Mazzanti, and J. Pecaut, *Oxidation Chemistry of Uranium(III) Complexes of Tpa: Synthesis and Structural Studies of Oxo, Hydroxo, and Alkoxo Complexes of Uranium(IV).* Inorganic Chemistry, 2003. **42**(19): p. 5900-5908.
118. Faulkner, S. and J.L. Matthews, *Comprehensive Coordination Chemistry II*, ed. M.D. Ward. Vol. 9. 2004, Oxford, UK: Elsevier. 913-944.
119. Thompson, J., et al., *Obtaining characteristic 4f-4f luminescence from rare earth organic chelates.* Advanced Functional Materials, 2004. **14**(10): p. 979-984.
120. Faulkner, S., S.J.A. Pope, and B.P. Burton-Pye, *Lanthanide complexes for luminescence imaging applications.* Applied Spectroscopy Reviews, 2005. **40**(1): p. 1-31.
121. Binnemans, K., *Lanthanide-Based Luminescent Hybrid Materials.* Chemical Reviews, 2009. **109**(9): p. 4283-4374.
122. Ward, M.D., *Transition-metal sensitised near-infrared luminescence from lanthanides in d-f heteronuclear arrays.* Coordination Chemistry Reviews, 2007. **251**(13-14): p. 1663-1677.
123. Weissleder, R., *A clearer vision for in vivo imaging.* Nature Biotechnology, 2001. **19**(4): p. 316-317.
124. Marchal, C., *Complexes polymetalliques de lanthanide(III) pour le developpement de nouveaux materiaux luminescents*. 2008, Universite Joseph Fourier: Grenoble
125. Tang, C.W. and S.A. Vanslyke, *Organic Electroluminescent Diodes.* Applied Physics Letters, 1987. **51**(12): p. 913-915.
126. Albrecht, M., M. Fiege, and O. Osetska, *8-Hydroxyquinolines in metallosupramolecular chemistry.* Coordination Chemistry Reviews, 2008. **252**(8-9): p. 812-824.
127. Van Deun, R., et al., *Rare-earth Quinolinates:Infrared-emitting molecular materials with a rich structural chemistry.* Inorganic Chemistry, 2004. **43**: p. 8461-8469.
128. Van Deun, R., et al., *Rare-earth nitroquinolinates: Visible-light-sensitizable near-infrared emitters in aqueous solution.* European Journal of Inorg Chemistry, 2007(2): p. 302-305.
129. Artizzu, F., et al., *Structure and emission properties of Er(3)Q(9) (Q=8-quinolinolate).* Inorganic Chemistry, 2005. **44**(4): p. 840-842.
130. Albrecht, M., O. Osetska, and R. Frohlich, *2- (8-Hydroxyquinolinyl)methylene hydrazinecarboxamide: expanding the coordination sphere of 8-hydroxyquinoline for coordination of rare-earth metal(III) ions.* Dalton Transactions, 2005(23): p. 3757-3762.
131. Albrecht, M., et al., *Enhancement of near-IR emission by bromine substitution in lanthanide complexes with 2-carboxamide-8-hydroxyquinoline.* Chemical Communications, 2007(18): p. 1834-1836.
132. Shavaleev, N.M., et al., *Near-infrared luminescence of nine-coordinate neodymium complexes with benzimidazole-substituted 8-hydroxyquinolines.* Inorganic Chemistry, 2008. **47**(19): p. 9055-9068.

133. Shavaleev, N.M., et al., *Modulating the Near-Infrared Luminescence of Neodymium and Ytterbium Complexes with Tridentate Ligands Based on Benzoxazole-Substituted 8-Hydroxyquinolines.* Inorganic Chemistry, 2009. **48**(7): p. 2908-2918.
134. Parker, D., et al., *Being excited by lanthanide coordination complexes: Aqua species, chirality, excited-state chemistry, and exchange dynamics.* Chemical Reviews, 2002. **102**(6): p. 1977-2010.
135. Okabe, N. and Y. Muranishi, *8-hydroxyquinaldinic acid and its nickel(ii) complex* Acta Cryst., 2002. **C58**: p. 475-477.
136. Nakamura, M., et al., *Crystal structure of 8-hydroxyquinoline-2-carboxylic acid copper(ii) complex.* Analytical sciences, 2005. **21**: p. 115-116.
137. Jeffrey, G.A., *An Introduction to Hydrogen Bonding*. 1997: Oxford University Press.
138. Steiner, T., *The hydrogen bond in the solid state.* Angewandte Chemie-International Edition, 2002. **41**(1): p. 48-76.
139. Lunstroot, K., et al., *Luminescent ionogels based on europium-doped ionic liquids confined within silica-derived networks.* Chemistry of Materials, 2006. **18**(24): p. 5711-5715.
140. Mehdi, H., et al., *Hydrophobic ionic liquids with strongly coordinating anions.* Chemical Communication, 2010. **46**(2): p. 234-236.
141. Binnemans, K., *Lanthanides and actinides in ionic liquids.* Chemical Reviews, 2007. **107**(6): p. 2592-2614.
142. Lunstroot, K., et al., *Lanthanide-doped luminescent ionogels.* Dalton Transaction, 2009(2): p. 298-306.
143. Lunstroot, K., et al., *Visible and Near-Infrared Emission by Samarium(III)-Containing Ionic Liquid Mixtures.* Inorganic Chemistry, 2009. **48**(7): p. 3018-3026.
144. Seeber, G., B.E.F. Tiedemann, and K.N. Raymond, *Supramolecular chirality in coordination chemistry*, in *Supramolecular Chirality*. 2006. p. 147-183.
145. Håkansson, M., et al., *Isolation and Spontaneous Resolution of Eight-Coordinate Stereoisomers.* Angewandte Chemie International Edition, 1999. **38**(15): p. 2199-2201.
146. Gil-Hernandez, B., et al., *Spontaneous resolution upon crystallization of chiral La(iii) and Gd(iii) MOFs from achiral dihydroxymalonate.* Chemical Communications, 2010. **46**(43): p. 8270-8272.
147. Terpin, A.J., et al., *Resolution and Kinetic Stability of a Chiral Supramolecular Assembly Made of Labile Components.* Angew. Chem. Int. Ed., 2001. **40**: p. 157-160.
148. Brayshaw, P.A., et al., *Synthetic, Structural, and Spectroscopic Studies on Solids Containing Tris(dipicolinato) Rare Earth Anions and Transition or Main Group Metal Cations.* Inorganic Chemistry, 1995. **34**(8): p. 2068-2076.
149. Ghosh, I., H. Zeng, and Y. Kishi, *Application of Chiral Lanthanide Shift Reagents for Assignment of Absolute Configuration of Alcohols.* Organic Letters, 2004. **6**(25): p. 4715-4718.
150. Parker, D., *NMR Determination of Enantiomeric Purity* Chemical Reviews, 1991. **91**: p. 1441-1457
151. Bednarski, M., C. Maring, and S. Danishefsky, *Chiral induction in the cyclocondensation of aldehydes with siloxydienes* Tetrahedron Letters, 1983. **24**: p. 3451.
152. Inanaga, J., H. Furuno, and T. Hayano, *Asymmetric Catalysis and Amplification with Chiral Lanthanide Complexes.* Chemical Reviews, 2002. **102**: p. 2211-2225.
153. Shibasaki, M. and N. Yoshikawa, *Lanthanide Complexes in Multifunctional Asymmetric Catalysis.* Chemical Reviews, 2002. **102**: p. 2187-2209.

154. Mikami, K., M. Terada, and H. Matsuzawa, *"Asymmetric" Catalysis by Lanthanide Complexes.* Angew. Chem. Int. Ed., 2002. **41**: p. 3554-3571.
155. Shibasaki, M., H. Sasai, and T. Arai, *Asymmetric Catalysis with Heterobimetallic Compounds.* Angew. Chem. Int. Ed. Engl., 1997. **36**: p. 1236-1256.
156. Yamada, T., S. Shinoda, and H. Tsukube, *Anion sensing with luminescent lanthanide complexes of tris(2-pyridylmethyl)amines: Pronounced effects of lanthanide center and ligand chirality on anion selectivity and sensitivity.* Chemical Communications, 2002(11): p. 1218-1219.
157. Montgomery, C.P., et al., *Enantioselective regulation of a metal complex in reversible binding to serum albumin: dynamic helicity inversion signalled by circularly polarised luminescence.* Chemical Communications, 2008(36): p. 4261-4263.
158. Sasai, H., et al., *The First Heterobimetallic Multifunctional Asymmetric Catalyst.* Journal of the American Chemical Society, 1995. **117**(23): p. 6194-6198.
159. Leonard, J.P., et al., *Self-assembly of chiral luminescent lanthanide coordination bundles.* J. Am. Chem. Soc, 2007. **129**(36): p. 10986-10987.
160. Muller, G., et al., *First diastereoselective formation of lanthanide triple helical complexes with a terdentate chiral C2 symmetric ligand.* Chemical Communications, 2002(14): p. 1522-1523.
161. Seitz, M., et al., *Circularly Polarized Luminescence in Enantiopure Europium and Terbium Complexes with Modular, All-Oxygen Donor Ligands.* Inorganic Chemistry, 2009. **48**(17): p. 8469-8479.
162. Dickins, R.S., et al., *Synthesis, Time-Resolved Luminescence, NMR Spectroscopy, Circular Dichroism and Circularly Polarised Luminescence Studies of Enantiopure Macrocyclic Lanthanide Tetraamide Complexes.* Chemistry □ A European Journal, 1999. **5**(3): p. 1095-1105.
163. Lama, M., et al., *Lanthanide class of a trinuclear enantiopure helical architecture containing chiral ligands: Synthesis, structure, and properties.* Chemistry-a European Journal, 2007. **13**(26): p. 7358-7373.
164. Jeong, K.S., et al., *Lanthanitin: A chiral nanoball encapsulating 18 lanthanum ions by ferritin-like assembly.* Angewandte Chemie-International Edition, 2006. **45**(48): p. 8134-8138.
165. Tang, X.L., et al., *Olive-Shaped Chiral Supramolecules: Simultaneous Self-Assembly of Heptameric Lanthanum Clusters and Carbon Dioxide Fixation.* Angewandte Chemie-International Edition, 2009. **48**(19): p. 3499-3502.
166. Mamula, O., et al., *A trinuclear Eu-III array within a diastereoselectively self-assembled helix formed by chiral bipyridine-carboxylate ligands.* Angewandte Chemie-International Edition, 2005. **44**(17): p. 2527-2531.
167. Mamula, O., et al., *Switchable chiral architectures containing Pr-III ions: An example of solvent-induced adaptive behavior.* Angewandte Chemie-International Edition, 2006. **45**(30): p. 4940-4944.
168. Stomeo, F., et al., *Metal-Directed Synthesis of Enantiomerially Pure Dimetallic Lanthanide Luminescent Triple-Stranded Helicates.* Journal of the American Chemical Society, 2009. **131**(28): p. 9636-9637.
169. Paluch, M., et al., *Enantiopure trinuclear lanthanide(III) complexes: Cooperative formation of $Ln_3(\mu_3\text{-}OH)_2$ core within the macrocycle.* Inorganic Chemistry Communications, 2011. **14**: p. 92-95.
170. Lama, M., et al., *Enantiopure, supramolecular helices containing three-dimensional tetranuclear lanthanide(III) arrays: Synthesis, structure, properties, and solvent-driven Trinuclear/Tetranuclear interconversion.* Inorganic Chemistry, 2008. **47**(18): p. 8000-8015.

171. Mateos-Timoneda, M.A., M. Crego-Calama, and D.N. Reinhoudt, *Supramolecular chirality of self-assembled systems in solution.* Chemical Society Reviews, 2004. **33**(6): p. 363-372.
172. Lessmann, J.J. and W.D. Horrocks, *Supramolecular coordination chemistry in aqueous solution: Lanthanide ion-induced triple helix formation.* Inorganic Chemistry, 2000. **39**(15): p. 3114-3124.
173. Hargaden, G.C. and P.J. Guiry, *Recent Applications of Oxazoline-Containing Ligands in Asymmetric Catalysis.* Chemical Reviews 2009. **109**: p. 2505-2550.
174. Gomez, M., G. Muller, and M. Rocamora, *Coordination chemistry of oxazoline ligands.* Coordination Chemistry Reviews, 1999. **193-195**: p. 769-835.
175. Aspinall, H.C., *Chiral lanthanide complexes: Coordination chemistry and applications.* Chemical Reviews, 2002. **102**(6): p. 1807-1850.
176. de Bettencourt-Dias, A. and P.S. Barber, *An oxazoline derivatized Pybox ligand for Eu(III) and Tb(III) sensitization.* Comptes Rendus Chimie, 2010. **13** p. 691-699.
177. De Bettencourt-Dias, A., S. Viswanathan, and A. Rollett, *Thiophene-derivatized Pybox and its highly luminescent lanthanide ion complexes.* Journal of the American Chemical Society, 2007. **129**(50): p. 15436-15437.
178. Provent, C., et al., *Diastereoselectivity of Octahedral Cobalt(II) Pybox Complexes.* European Journal of Inorganic Chemistry, 2001. **2001**(8): p. 1963-1967.
179. Allouche, L., A. Marquis, and J.-M. Lehn, *Discrimination of Metallosupramolecular Architectures in Solution by Using Diffusion Ordered Spectroscopy (DOSY) Experiments: Double-Stranded Helicates of Different Lengths.* Chemistry-a European Journal, 2006(12): p. 7520 □7525.
180. Waldeck, A.R., et al., *NMR diffusion measurements to characterise membrane transport and solute binding.* Progress in Nuclear Magnetic Resonance Spectroscopy, 1997. **30**(1-2): p. 39-68.
181. Johnson, C.S., *Diffusion ordered nuclear magnetic resonance spectroscopy: principles and applications.* Progress in Nuclear Magnetic Resonance Spectroscopy, 1999. **34**(3-4): p. 203-256.
182. Aspinall, H.C. and N. Greeves, *Defining effective chiral binding sites at lanthanides--highly enantioselective reagents and catalysts from binaphtholate and pybox ligands.* Journal of Organometallic Chemistry, 2002. **647**(1-2): p. 151-157.
183. Edward, J.T.J., Chem. Ed. , 1970. **47**: p. 261-269.
184. Riehl, J.P. and G. Muller, *Circularly Polarized Luminescence Spectroscopy from Lanthanide Systems*, in *Handbook on the Physics and Chemistry of Rare Earths*, K.A.J. Gschneidner, J.-C.G. Bünzli, and V.K. Pecharsky, Editors. 2005, North-Holland Publishing Company: Amsterdam. p. 289-357.
185. Muller, G., *Luminescent Chiral Lanthanide(III) Complexes as Potential Molecular Probes.* Dalton Transaction, 2009: p. 9692-9707
186. Petoud, S., et al., *Brilliant Sm, Eu, Tb, and Dy Chiral Lanthanide Complexes with Strong Circularly Polarized Luminescence.* J. AM. CHEM. SOC., 2007. **129**: p. 77-83.
187. Harada, T., et al., *Circularly Polarized Luminescence of Eu(III) Complexes with Point- and Axis-Chiral Ligands Dependent on Coordination Structures.* inorganic Chemistry, 2009. **48**(23): p. 11242-11250.
188. Lunkley, J.L., et al., *Extraordinary Circularly Polarized Luminescence Activity Exhibited by Cesium Tetrakis(3-heptafluoro-butylryl-( )-camphorato) Eu(III) Complexes in EtOH and CHCl3 Solutions.* J. Am. Chem. Soc, 2008. **130**: p. 13814-13815.

189. Freedman, D., et al., *Heterovalent Clusters: $Ln_4Se(SePh)_8$ (Ln_4 Sm_4,Yb_4,Sm_2Yb_2,Nd_2Yb_2)*. J. Am. Chem. Soc. , 1999. **121**: p. 11713-11719.
190. Evans, W.J., et al., *Hydrolytic Reactivity of a Samarium(II) Organometallic Complex: Synthesis and Structure of a Hexametallic Organosamarium Oxide Hydroxide, $[(C_5Me_5)Sm]_6O_9H_6$.* Organometallics 2001. **20**: p. 2936-2937.
191. Dube, T., S. Gambarotta, and G. Yap, *Preparation and Reactivity of a Compartmental Schiff-Base Samarium Dinuclear Complex.* Organometallics, 1998. **17**: p. 3967-3973.
192. Dube, T., et al., *Tetrametallic Reduction of Dinitrogen: Formation of a Tetranuclear Samarium Dinitrogen Complex.* Angew. Chem. Int. Ed. , 1999. **38**(24): p. 3657-3659.
193. O'Connor, P.E., B. Twamley, and D.J. Berg, *Lanthanide complexes of a cross-bridged cyclam ligand: Isolation and structural characterization of unusual trinuclear μ^3-imido Yb(III) cluster cations and a mixed valence Yb(II/III) salt containing an Yb(II) anion.* Inorganica Chimica Acta, 2006. **359**: p. 2870-2878.
194. Evans, W.J., *Perspectives in reductive lanthanide chemistry.* Coordination Chemistry Reviews, 2000. **206-207**: p. 263-283.
195. Evans, W.J., *The Importance of Questioning Scientific Assumptions: Some Lessons from f Element Chemistry*□ Inorganic Chemistry, 2007. **46**(9): p. 3435-3449.
196. Bochkarev, M.N., *Molecular compounds of* □*new*□ *divalent lanthanides.* Coordination Chemistry Reviews, 2004. **248**: p. 835□851.
197. Nief, F., *Non-classical divalent lanthanide complexes.* Dalton Transactions, 2010. **39**(29): p. 6589-6598.
198. Nief, F., *Molecular chemistry of the rare earth elements in uncommon low-valent states*, in *Handbook on the Physics and Chemistry of Rare Earths* K.A.J. Gschneidner, J.-C.G. Bünzli, and V.K. Pecharsky, Editors. 2010. p. 241-300.
199. Kagan, H.B., *Twenty-five years of organic chemistry with diiodosamarium: an overview.* Tetrahedron, 2003. **59** p. 10351-10372.
200. Girard, P., J.L. Namy, and H.B. Kagan, *Divalent lanthanide derivatives in organic synthesis. 1. Mild preparation of samarium iodide and ytterbium iodide and their use as reducing or coupling agents.* J. Am. Chem. Soc., 1980. **102**(8): p. 2693-2698.
201. Meyer, G., *Reduced halides of the rare-earth elements.* Chemical Reviews, 1988. **88**(1): p. 93□107.
202. Meyer, G., N. Gerlitzki, and S. Hammerich, *Rare-earth diiodides and derivatives.* Journal of Alloys and Compounds, 2004. **380**(1-2): p. 71-78.
203. Bochkarev, M.N., et al., *Synthesis and Structure of the First Molecular Thulium(II) Complex: [TmI2(MeOCH2CH2OMe)3].* Angewandte Chemie International Edition in English, 1997. **36**(1-2): p. 133-135.
204. Bochkarev, M.N. and A.A. Fagin, *A New Route to Neodymium(II) and Dysprosium(II) Iodides.* Chem. Eur. J. , 1999. **5**(10): p. 2990-2992.
205. Evans, W.J., et al., *Large Scale Synthesis of Dysprosium and Neodymium Diiodides.* Inorganic Chemistry, 2003. **42**(9): p. 3097-3099.
206. Evans, W.J., N.T. Allen, and J.W. Ziller, *The Availability of Dysprosium Diiodide as a Powerful Reducing Agent in Organic Synthesis: Reactivity Studies and Structural Analysis of $DyI_2(DME)_3$ and Its Naphthalene Reduction Product.* J. Am. Chem. Soc., 2000. **122**: p. 11749-11750.
207. Bochkarev, M.N., et al., *$[NdI_2(thf)_5]$, the First Crystallographically Authenticated Neodymium(II) Complex.* Angew. Chem. Int. Ed. , 2001. **40**(17): p. 3176-3178.
208. Fischer, E.O. and H. Fischer, *Dicyclopentadienyleuropium.* Angewandte Chemie International Edition in English, 1964. **3**(2): p. 132-133.

209. Watt, G.W. and E.W. Gillow, *Samarium(II) dicyclopentadienide 1-tetrahydrofuranate.* Journal of the American Chemical Society, 1969. **91**(3): p. 775-776.
210. Evans, W.J., L.A. Hughes, and T.P. Hanusa, *Synthesis and crystallographic characterization of an unsolvated, monomeric samarium bis(pentamethylcyclopentadienyl) organolanthanide complex, (C5Me5)2Sm.* Journal of the American Chemical Society, 1984. **106**(15): p. 4270-4272.
211. Evans, W.J., T.A. Ulibarri, and J.W. Ziller, *Isolation and x-ray crystal structure of the first dinitrogen complex of an f-element metal, $[(C_5Me_5)_2Sm]_2N_2$.* Journal of the American Chemical Society, 1988. **110**(20): p. 6877-6879.
212. Evans, W.J., N.T. Allen, and J.W. Ziller, *Expanding Divalent Organolanthanide Chemistry: The First Organothulium(II) Complex and the In Situ Organodysprosium(II) Reduction of Dinitrogen.* Angew. Chem. Int. Ed. , 2002. **41**(2): p. 359-361.
213. Turcitu, D., F. Nief, and L. Ricard, *Structure and Reactivity of Homoleptic Samarium(II) and Thulium(II) Phospholyl Complexes.* Chem. Eur. J. , 2003. **9**: p. 4916 - 4923.
214. Jaroschik, F., F. Nief , and X.-F. Le Goff, *Sterically hindered cyclopentadienyl and phospholyl ligands in dysprosium chemistry.* Polyhedron 2009. **28**: p. 2744-2748.
215. Jaroschik, F., et al., *Dinitrogen Reduction and C-H Activation by the Divalent Organoneodymium Complex $[(C_5H_2tBu_3)_2Nd(\mu\text{-}I)K([18]crown\text{-}6)]$.* Angew. Chem. Int. Ed. , 2009. **48**: p. 1117 -1121.
216. Edelmann, F.T., D.M.M. Freckmann, and H. Schumann, *Synthesis and Structural Chemistry of Non-Cyclopentadienyl Organolanthanide Complexes.* Chem. Rev. , 2002. **102**: p. 1851−1896.
217. Evans, W.J., G.W. Rabe, and J.W. Ziller, *Utility of N-Metbylimidazole in Isolating Crystalline Lanthanide Iodide and Hydroxide Complexes: Crystallographic Characterization of Octasolvated $[Sm(N\text{-}MeIm)_8]I_3$ and Polymetallic $[SmI(\mu\text{-}I)(N\text{-}MeIm)_3]_2$, $[(N\text{-}MeIm)_5Sm(\mu\text{-}OH)]_2I_4$ and $\{[(N\text{-}MeIm)_4Sm(\mu\text{-}OH)]_3(\mu_3{-}OH)_2\}I_4$.* Inorg. Chem., 1994. **33**: p. 3072-3078
218. Maunder, G.H. and A. Sella, *Simple adducts of samarium and ytterbium diiodide: synthesis and molecular structures of $LnI_2(3,5\text{-}lutidine)_4$ (Ln=Sm,Yb) and $YbI_2(4\text{-}t\text{-}butylpyridine)_4$.* Polyhedron, 1998. **17**(1): p. 63-68.
219. Cheng, J., et al., *Heteroleptic Tm(II) Complexes: One More Success for Trofimenko's Scorpionates.* J. Am. Chem. Soc, 2008. **130**(5): p. 1544-1545.
220. Bochkarev , M.N., et al., *Synthesis and characterization of isopropylamine complexes of lanthanide(II) diiodides: Molecular structure of $TmI_2(Pr^iNH_2)_4$ and $EuI_2(Pr^iNH_2)_4$.* Inorganica Chimica Acta 2006. **359**: p. 3315-3320.
221. Bochkarev, M.N., et al., *A Novel Bis(imino)amine Ligand as a Result of Acetonitrile Coupling with the Diiodides of Dy(II) and Tm(II).* J. AM. CHEM. SOC., 2003. **125**: p. 2894 2895.
222. Fagin, A.A., et al., *Reduction of acetonitrile by neodymium diiodide: Molecular structure of $[\{(HN{=}CMe)_2MeCNH_2\}NdI(MeCN)_5]I_2$ and $[\{(HN{=}CMe)_2MeCNH_2\}Nd(MeCN)_6]I_3$.* Inorganica Chimica Acta, 2007. **360**: p. 2923-2928.
223. Fedushkin, I.L., et al., *Reduction of 2,5-di-tert-butylcyclopentadienone and pyridine with thulium diiodide. Structures of the complexes $TmI_2(THF)_2[\eta^5\text{-}Bu^{t2}C_5H_2O]TmI_2(THF)_3$ and $[TmI_2(C_5H_5N)_4]_2(\mu_2\text{-}N_2C_{10}H_{10})$.* Russ.Chem.Bull., Int.Ed., 2003. **52**(1): p. 154-159.

224. Anwander, R., *"Self-Assembly" in Organolanthanide Chemistry: Formation of Rings and Clusters.* Angew. Chem. Int. Ed., 1998. **37**(5): p. 599-602.
225. Summerscales, O.T., et al., *Samarium(III) Pentalene Sandwich Compounds [Sm(η^8-C_8H_4{Si^{i}Pr$_3$-1,4}$_2$)(Cp*)] and [Sm(η^8-C_8H_4{Si^{i}Pr$_3$-1,4}$_2$)(η^5-C_8H_5{Si^{i}Pr$_3$-1,4}$_2$)] and a Mixed-Valence Hexasamarium Cluster Derived from Sm(II)-Based Solvent Activation.* Organometallics, 2008. **27**(21): p. 5612-5618.
226. Kuzyaev, D.M., et al., *Reaction of neodymium diiodide with methanol in acetonitrile. Structure of the cluster $[Nd_4(\mu_2\text{-}I)_{1.1}(\mu_3\text{-}I)(\mu_2\text{-}OMe)_{4.9}(\mu_4\text{-}O)(MeCN)_{12}]I_3$.* Russ.Chem.Bull., Int.Ed., 2007. **56**(10): p. 1960-1963.
227. Melman, J.H., et al., *Chalcogen-Rich Lanthanide Clusters from Lanthanide Halide Starting Materials: A New Approach to the Low-Temperature Synthesis of LnSx Solids from Molecular Precursors.* J. Am. Chem. Soc. , 1999. **121**: p. 10247-10248.
228. Natrajan, L., et al., *Controlled Hydrolysis of Lanthanide Complexes of the N-donor Tripod Tris(2-pyridylmethyl)amine versus Bis-ligand Complex Formation.* Inorganic Chemistry, 2005. **44**: p. 4756-4765.
229. Lampropoulos, C., et al., *Synthesis, Magnetism, and High-Frequency EPR Spectroscopy of a Family of Mixed-Valent Cuboctahedral Mn13 Complexes with 1,8-Naphthalenedicarboxylate Ligands.* Inorganic Chemistry, 2008. **47**(23): p. 11180-11190.
230. Chen, X.-M., et al., *Novel octadecanuclear copper(II)-lanthanoid(III) clusters. Synthesis and structures of $[Cu_{12}Ln_6(\mu_3\text{-}OH)_{24}(O_2CCH_2CH_2NC_5H_5)_{12}(H_2O)_{16}([\mu_{12}\text{-}ClO_4)][ClO_4]_{17}\cdot 16H_2O$ (Ln= Gd or Sm).* Journal of the Chemical Society, Dalton Transactions, 1996(12): p. 2443-2448.
231. Yanga, Y.-Y., et al., *A New Octadecanuclear Copper(II)-Lanthanide(III) Cluster Complex:Synthesis and Structural Characterization of $[Cu_{12}Nd_6(OH)_{24}(betaine)_{16}(NO_3)_3(H_2O)_{10}](NO_3)[PF_6]_{14}\cdot 5H_2O$.* Z. Anorg. Allg. Chem. , 2004. **630**: p. 286-290.
232. Albano, V.G., et al., *Synthesis and Characterization of the Paramagnetic $[Ag_{13}Fe_8(CO)_{32}]^{4-}$ Tetraanion: A Cuboctahedral Ag_{13} Cluster Stabilized by $Fe(CO)_4$ Groups Behaving as Four-Electron*

Donors J. Am. Chem. Soc., 1992. **114**: p. 5108-5113
233. Brown, I.D. and D. Altermatt, Acta crystallographica Section B, 1985. **B41**: p. 244-247.
234. Brown, I.D. 2006; Available from: http://www.ccp14.ac.uk/ccp/web-mirrors/i_d_brown/bond_valence_param/.
235. Wu, D., A. Chen, and C.S.J. Johnson, *An improved diffusion-ordered spectroscopy experiment incorporating bipolar-gradient pulse.* J. Magn. Reson, 1995. **115**: p. 260-264.
236. deMello, J.C., H.F. Wittmann, and R.H. Friend, *An improved experimental determination of external photoluminescence quantum efficiency.* Advanced Materials, 1997. **9**(3): p. 230-&.
237. Bonsall, S.D., et al., Chem. Commun., 2007: p. 3676.
238. Do, K., F.C. Muller, and G. Muller, J. Phys. Chem. A 2008. **112,**: p. 6789.
239. *SADABS, An Empirical Absorption Correction Program*. 1995, Bruker AXS: Madison, WI.
240. *SAINT, Bruker Molecular Analysis Research Tool*. 2002, Bruker AXS: Madison, WI.
241. Sheldrick, G.M., *SHELXS97 and SHELXL97*. 1997: University of Göttingen, Germany.
242. Oxford, *CrysAlisPro Software Package*. 2010: Oxfordshire, UK.

243. DeLano, W.L., *The PyMOL Molecular Graphics System* 2002, DeLano Scientific: San Carlos, CA, USA.
244. Emsley, P. and K. Cowtan, Acta Cryst., 2004. **D60**: p. 2126-2132.
245. Cooper, G.H. and R.L. Richard, Synthesis, 1971. **31**.
246. Nishiyama, H., et al., *New chiral bis(oxazolinyl)bipyridine ligand (bipymox) : enantioselection in the asymmetric hydrosilylation of ketones.* Tetrahedron : asymmetry, 1993. **4**(1): p. 143-150.
247. Britovsek, G.J.P., J. England, and A.J.P. White, *Non-heme Iron(II) Complexes Containing Tripodal Tetradentate Nitrogen Ligands and Their Application in Alkane Oxidation Catalysis.* Inorganic Chemistry, 2005. **44**(22): p. 8125-8134.

APPENDIX

A) π-π Interactions in Chiral Complexes VII, VIII, IX, X

Table A1: Distances and angles between rings centroids showing π-π interactions in **VII**, **VIII**, **IX**

	Pyridine	Phenyl	Distance	Angle
Eu1	N102 C107 C108 C109 C110 C111	C95 C96 C97 C98 C99 C100	3.511	7.93
Eu1	N82 C87 C88 C89 C90 C91	C115 C116 C117 C118 C119 C120	3.584	12.59
Eu2	N42 C47 C48 C49 C50 C51	C75 C76 C77 C78 C79 C80	3.595	6.82
Eu2	N62 C67 C68 C69 C70 C71	C55 C56 C57 C58 C59 C60	4.272	23.85
Eu 3	N2 C7 C8 C9 C10 C11	C35 C36 C37 C38 C39 C40	3.633	4.85
Eu 3	N22 C27 C28 C29 C30 C31	C15 C16 C17 C18 C19 C20	3.681	8.06
Eu4	N121 C122 C123 C124 C125 C126	C155 C156 C157 C158 C159 C160	3.562	4.12
Eu4	N141 C142 C143 C144 C145 C146	C135 C136 C137 C138 C139 C140	3.715	1.74
Nd1	N42 C47 C48 C49 C50 C51	C75 C76 C77 C78 C79 C80	3.606	11.15
Nd1	N62 C67 C68 C69 C70 C71	C55 C56 C57 C58 C59 C60	3.593	8.26
Nd2	N102 C107 C108 C109 C110 C111	C95 C96 C97 C98 C99 C100	3.565	3.47
Nd2	N82 C87 C88 C89 C90 C91	C115 C116 C117 C118 C119 C120	3.647	7.18
Nd 3	N22 C27 C28 C29 C30 C31	C15 C16 C17 C18 C19 C20	3.565	6.01
Nd 3	N2 C7 C8 C9 C10 C11	C35 C36 C37 C38 C39 C40	3.723	16.69
Yb	N1 C2 C3 C4 C5 C6	C35 C36 C37 C38 C39 C40	3.576	11.92
Yb	N21 C22 C23 C24 C25 C26	C15 C16 C17 C18 C19 C20	3.563	13.73

Table A2: Distances and angles between rings centroids showing π-π interactions in **X**

	Pyridine	Phenyl	Distance	Angle
Eu2	N1_2 C2_2 C3_2 C4_2 C5_2 C6_2	C18_1C19_1C20_1C21_1C22_1C23_1	3.557	6.04
Eu2	C7_1 C8_1 C9_1 C10_1 C11_1 N12_1	C18_2C19_2C20_2C21_2C22_2C23_2	3.761	1.49
Eu3	C7_4 C8_4 C9_4 C10_4 C11_4 N12_4	C18_3C19_3C20_3C21_3C22_3C23_3	3.690	6.07
Eu3	C7_3 C8_3 C9_3 C10_3 C11_3 N12_3	C18_4C19_4C20_4C21_4C22_4 C23_4	3.947	3.78
Eu4	C7_6 C8_6 C9_6 C10_6 C11_6 N12_6	C18_5C19_5C20_5C21_5C22_5C23_5	3.851	1.27
Eu4	N1_5 C2_5 C3_5 C4_5 C5_5 C6_5	C18_6C19_6C20_6C21_6C22_6C23_6	3.520	4.07
Eu5	C7_7 C8_7 C9_7 C10_7 C11_7 N12_7	C18_8C19_8C20_8C21_8C22_8C23_8	3.881	11.59
Eu5	N1_8 C2_8 C3_8 C4_8 C5_8 C6_8	C18_7C19_7C20_7C21_7C22_7C23_7	3.931	8.79
Eu6	C7_9 C8_9 C9_9 C10_9 C11_9 N12_9	C18_10C19_10C20_10C21_10C22_10C23_10	3.728	9.03
Eu6	N1_10C2_10C3_10C4_10C5_10C6_10	C18_9C19_9C20_9C21_9C22_9C23_9	3.476	4.11
Eu7	C7_11C8_11C9_11C10_11C11_11N12_11	C18_12C19_12C20_12C21_12C22_12C23_12	3.737	6.58
Eu7	C7_12C8_12C9_12C10_12C11_12N12_12	C18_11C19_11C20_11C21_11C22_11C23_11	3.905	12.08

B) Crystallization trials of $Ln\subset[(\Lambda\text{-}Ln(Phbipox)_2\Delta\text{-}Ln(Phbipox)_2)_3](Otf)_9$ complexes

Obtaining suitable crystals of supramolecular complexes is the main challenge in this field of chemistry. Several attempts to crystallize $Ln\subset[(\Lambda\text{-}Ln(Phbipox)_2\Delta\text{-}Ln(Phbipox)_2)_3]^{9+}$ resulted in low diffraction quality crystals. Layering diisopropylether on a solution of heptanuclear europium or neodymium complexes in acetonitrile resulted in the formation of colourless crystals (Table A3a, d), however due to obtained large unit cell dimensions (c = 72 Å for Eu, c = 74 Å for Nd) the structure could not be solved (detector crystal distance = 120 mm). Crystallization from benzonitrile/ hexane resulted in a crystal structure with two wheels in the unit cell (Table A3b). Even though the unit cell axis were smaller, it was not possible to solve the structure completely.

In order to improve the crystal quality it is thought to use different lanthanide salts to decrease the number of atoms in counter ions. Therefore instead of using triflates we have tried chlorides and iodides. Europium chloride did not lead to formation of hexameric wheel. Similarly trials with the neodymium iodide ended at trinuclear species. Addition of excess neodymium iodide resulted in a suspension that after filtration we recovered trinuclear complexes. Strong coordination of halides to the lanthanide ion prevented carboxylate bridging to yield to the assembly. Trials with $Eu(ClO_4)_3$ resulted in isolation of crystals (Table A3c) in which unit cell consists of two wheel, however the resolution was quite low. The unit cells of all the trials are given in Table 5.

Table A3: Unit cell data obtained from several crystallization trials with heptanuclear complexes

	$[Eu_7(L)_{12}](Otf)_9$ ACN/DIPE **a**	$[Eu_7(L)_{12}](Otf)_9$ PhCN/Hexane **B**	$[Eu_7(L)_{12}](ClO_4)_9$ ACN/DIPE **c**	$[Nd_7(L)_{12}](Otf)_9$ ACN/DIPE **d**
Space group	P 2_1 2_1 2	C2	P 2_1	not found
a/ Å	17.90(2)	46.014 (16)	23.9904(3)	17.47(3)
b/ Å	22.44(4)	31.1849(11)	57.8494(8)	22.547(7)
c/ Å	71.67 (9)	45.7418 (13)	24.0248(5)	74.22(11)
α /deg	90.50 (14)	90.00	90.00	90.27(8)
β/deg	91.32 (11)	92.834(3)	118.570(2)	89.96(13)
γ/deg	90.81 (4)	90.00	90.00	90.07(9)
V / $Å^3$	29290(2)	65556.6(4)	29282.4(9)	29429(7)

Low resolution (to 1.4Å) and large unit cell dimensions of our crystals required the use of Synchrotron radiation. Crystals prepared by slow diffusion of hexane on benzonitrile solution of the complexes have given to ESRF. Synchrotron radiation X-ray diffraction provides good spatial resolution for crystals with large unit cells and permits collection of usable data from very small, weekly diffracting crystals. However no better quality data obtained due to large voids existing in the structure, and the disorder of solvent molecules filling these voids. Eu atoms and the primary coordination sphere, as well as the majority of the ligands could be partially located in the electronic density maps by solving the structure with direct methods. In order to solve the structure completely one ligand was idealized by applying bond and angle distance restraints and used for fitting onto the other partially resolved ligands using an algorithm implemented in PyMOL. Some of the triflate, $CF_3SO_3^-$, anions 14 out of 18 anions were located, with two of them refined at half occupancy. The packing of the large supramolecular entities is not dense so there are large cavities present in the crystal packing where the remaining 4 anions are thought to reside, although these are not likely to be restrained to a defined position. Only the 14 Eu atoms in the asymmetric unit were refined anisotropically, lighter atoms - isotropically, and hydrogens - in the riding mode.

C) Crystallographic Tables

Table A4: Crystal data and structure refinement for $[Nd(H_{1/2}hqa)_3]_2(Et_3NH)_3{\cdot}Et_3NHOtf$ (**I**)

Empirical formula	C85 H97 F3 N10 Nd2 O21 S	
Formula weight	1972.27	
Temperature	223(2) K	
Wavelength	0.71073 Å	
Crystal system	Monoclinic	
Space group	C2/c	
Unit cell dimensions	a = 24.988(4) Å	alpha = 90 deg.
	b = 16.929(3) Å	beta = 90.610(3) deg.
	c = 20.689(3) Å	gamma = 90 deg.
Volume, Z	8751(2) Å^3, 4	
Density (calculated)	1.497 Mg/m^3	
Absorption coefficient	1.280 mm^-1	
F(000)	4032	
Crystal size	0.40 x 0.20 x 0.20 mm	
Theta range for data collection	1.76 to 28.30 deg.	
Limiting indices	-29<=h<=32, -20<=k<=22, -27<=l<=13	
Reflections collected	23874	
Independent reflections	10356 [R(int) = 0.0200]	
Absorption correction	None	
Refinement method	Full-matrix least-squares on F^2	
Data / restraints / parameters	10356 / 13 / 718	
Goodness-of-fit on F^2	1.059	
Final R indices [I>2sigma(I)]	R1 = 0.0409, wR2 = 0.1055	
R indices (all data)	R1 = 0.0590, wR2 = 0.1180	
Largest diff. peak and hole	1.681 and -0.722 e. Å^-3	

Table A5: Crystal data and structure refinement for $[Nd(hqa)_3]K_3 \cdot 8CH_3OH_\infty$ **(III)**

Empirical formula	C38 H47 K3 N3 Nd O17	
Formula weight	1079.33	
Temperature	223(2) K	
Wavelength	0.71073 Å	
Crystal system	Monoclinic	
Space group	P2(1)/n	
Unit cell dimensions	a = 14.3830(19) Å b = 20.469(3) Å c = 16.184(2) Å	alpha = 90 deg. beta = 100.312(2) deg. gamma = 90 deg.
Volume, Z	4687.8(11) Å^3, 4	
Density (calculated)	1.529 Mg/m^3	
Absorption coefficient	1.444 mm^-1	
F(000)	2196	
Crystal size	0.30 x 0.20 x 0.20 mm	
Theta range for data collection	1.99 to 28.30 deg.	
Limiting indices	-19<=h<=16, -27<=k<=26, -21<=l<=20	
Reflections collected	30021	
Independent reflections	11194 [R(int) = 0.0179]	
Absorption correction	None	
Max. and min. transmission	0.7610 and 0.6711	
Refinement method	Full-matrix least-squares on F^2	
Data / restraints / parameters	11194 / 0 / 747	
Goodness-of-fit on F^2	1.038	
Final R indices [I>2sigma(I)]	R1 = 0.0241, wR2 = 0.0575	
R indices (all data)	R1 = 0.0308, wR2 = 0.0603	
Largest diff. peak and hole	0.776 and -0.397 e.Å^-3	

Table A6: Crystal data and structure refinement for$[Er(hqa)_3]K_3 \cdot 7CH_3OH \cdot 0.25DIPE_\infty$ **(IV)**

Empirical formula	C38.75 H46.50 Er K3 N3 O16.25	
Formula weight	1098.85	
Temperature	150(2) K	
Wavelength	0.71073 Å	
Crystal system	Monoclinic	
Space group	C 1 2/c 1	
Unit cell dimensions	a = 28.8105(12) Å b = 15.6426(4) Å c = 23.5338(8) Å	alpha = 90 deg. beta = 118.865(5) deg. gamma = 90 deg.
Volume, Z	9288.3(5) Å^3, 8	
Density (calculated)	1.572 Mg/m^3	
Absorption coefficient	2.146 mm^-1	
F(000)	4440	
Crystal size	0.2 x 0.1 x 0.05 mm	
Theta range for data collection	3.06 to 26.37 deg.	
Limiting indices	-36<=h<=32, -19<=k<=16, -29<=l<=27	
Reflections collected	17247	
Independent reflections	9137 [R(int) = 0.0330]	
Absorption correction	Semi-empirical from equivalents	
Max. and min. transmission	1.00000 and 0.97568	
Refinement method	Full-matrix least-squares on F^2	
Data / restraints / parameters	9137 / 0 / 660	
Goodness-of-fit on F^2	0.791	
Final R indices [I>2sigma(I)]	R1 = 0.0304, wR2 = 0.0531	
R indices (all data)	R1 = 0.0627, wR2 = 0.0556	
Largest diff. peak and hole	0.959 and -0.652 e.Å^-3	

Table A7: Crystal data and structure refinement for $[Nd(hqt)_3]K_3 \cdot 6CH_3OH_\infty$ **(V)**

Empirical formula	C149 H176 K12 N60 Nd4 O41	
Formula weight	4509.66	
Temperature	150(2) K	
Wavelength	0.71073 Å	
Crystal system	Triclinic	
Space group	P -1	
Unit cell dimensions	a = 12.4042(5) Å b = 18.9257(7) Å c = 21.6698(8) Å	alpha = 67.155(3) deg. beta = 86.944(3) deg. gamma = 84.896(3) deg.
Volume, Z	4668.5(3) Å^3, 1	
Density (calculated)	1.604 Mg/m^3	
Absorption coefficient	1.451 mm^-1	
F(000)	2286	
Theta range for data collection	3.05 to 24.71 deg.	
Limiting indices	-13<=h<=14, -22<=k<=22, -25<=l<=23	
Reflections collected	31098	
Independent reflections	15288 [R(int) = 0.0449]	
Absorption correction	Semi-empirical from equivalents	
Max. and min. transmission	1.00000 and 0.97099	
Refinement method	Full-matrix least-squares on F^2	
Data / restraints / parameters	15288 / 0 / 1214	
Goodness-of-fit on F^2	0.830	
Final R indices [I>2sigma(I)]	R1 = 0.0459, wR2 = 0.0867	
R indices (all data)	R1 = 0.1055, wR2 = 0.0937	
Largest diff. peak and hole	0.818 and -0.704 e.Å^-3	

Table A8: Crystal data and structure refinement for {(ΔΔΔ)-[Eu(S-Phbipox)$_2$]$_3$·(Λ)[Eu(S-Phbipox)$_2$]}(Otf)$_4$ **(VI)**

Empirical formula	C172.50 H148 Eu4 F12 N24 O45.50 S4	
Formula weight	4249.23	
Temperature	150(2) K	
Wavelength	0.71073 Å	
Crystal system	Orthorhombic	
Space group	P 21 21 21	
Unit cell dimensions	a = 17.3481(10) Å b = 32.1765(15) Å c = 32.4386(12) Å	alpha = 90 deg. beta = 90 deg. gamma = 90 deg.
Volume, Z	18107.3(15) Å ^3, 4	
Density (calculated)	1.559 Mg/m^3	
Absorption coefficient	1.510 mm^-1	
F(000)	8556	
Crystal size	0.20 x 0.15 x 0.15 mm	
Theta range for data collection	3.02 to 23.25 deg.	
Limiting indices	-12<=h<=19, -32<=k<=35, -23<=l<=36	
Reflections collected	42715	
Independent reflections	25589 [R(int) = 0.0459]	
Absorption correction	Semi-empirical from equivalents	
Max. and min. transmission	0.8051 and 0.7521	
Refinement method	Full-matrix-block least-squares on F^2	
Data / restraints / parameters	25589 / 56 / 2282	
Goodness-of-fit on F^2	0.892	
Final R indices [I>2sigma(I)]	R1 = 0.0503, wR2 = 0.1001	
R indices (all data)	R1 = 0.0806, wR2 = 0.1058	
Absolute structure parameter	-0.024(9)	
Largest diff. peak and hole	1.515 and -0.820 e.Å^-3	

Table A9: Crystal data and structure refinement for {(ΛΛΛ)-[Eu(R-Phbipox)$_2$]$_3$·(Δ)[Eu(R-Phbipox)$_2$]}(Otf)$_4$ **(VII)**

Empirical formula	C42.88 H35.50 Eu F3 N6 O10.88 S	
Formula weight	1049.79	
Temperature	150(2) K	
Wavelength	0.71073 Å	
Crystal system	Orthorhombic	
Space group	P 21 21 21	
Unit cell dimensions	a = 17.3261(2) Å b = 32.2069(3) Å c = 32.3667(3) Å	alpha = 90 deg. beta = 90 deg. gamma = 90 deg.
Volume, Z	18061.2(3) Å^3, 16	
Density (calculated)	1.544 g/cm^3	
Absorption coefficient	1.512 mm^-1	
F(000)	8444	
Crystal size	0.26 x 0.18 x 0.13 mm	
Theta range for data collection	3.36 to 30.51 deg.	
Limiting indices	-22<=h<=24, -46<=k<=43, -46<=l<=43	
Reflections collected	146014	
Independent reflections	54983 [R(int) = 0.0695]	
Absorption correction	Semi-empirical from equivalents	
Max. and min. transmission	0.8288 and 0.6936	
Refinement method	Full-matrix-block least-squares on F^2	
Data / restraints / parameters	54983 / 41 / 2377	
Goodness-of-fit on F^2	0.777	
Final R indices [I>2sigma(I)]	R1 = 0.0439, wR2 = 0.0765	
R indices (all data)	R1 = 0.0968, wR2 = 0.0830	
Absolute structure parameter	-0.019(5)	
Largest diff. peak and hole	1.472 and -1.026 e.Å^-3	

Table A10: Crystal data and structure refinement for {(ΛΛΛ)-[Nd(R-Phbipox)$_2$]$_3$}I$_3$ **(VIII)**

Empirical formula	C136 H108 I3 N26 Nd3 O18	
Formula weight	3207.90	
Temperature	150(2) K	
Wavelength	0.71073 Å	
Crystal system	Monoclinic	
Space group	C 1 2 1	
Unit cell dimensions	a = 29.3540(7) Å b = 16.8787(4) Å c = 26.7603(6) Å	alpha = 90 deg. beta = 96.684(2) deg. gamma = 90 deg.
Volume, Z	13168.5(5) Å^3, 4	
Density (calculated)	1.618 g/cm^3	
Absorption coefficient	1.945 mm^-1	
F(000)	6356	
Crystal size	0.28 x 0.17 x 0.05 mm	
Theta range for data collection	3.29 to 28.28 deg.	
Limiting indices	-39<=h<=39, -22<=k<=22, -32<=l<=35	
Reflections collected	63412	
Independent reflections	32663 [R(int) = 0.0615]	
Absorption correction	Semi-empirical from equivalents	
Max. and min. transmission	0.9159 and 0.6159	
Refinement method	Full-matrix-block least-squares on F^2	
Data / restraints / parameters	32663 / 22 / 1680	
Goodness-of-fit on F^2	0.821	
Final R indices [I>2sigma(I)]	R1 = 0.0454, wR2 = 0.0825	
R indices (all data)	R1 = 0.0711, wR2 = 0.0864	
Absolute structure parameter	-0.050(8)	
Largest diff. peak and hole	1.150 and -0.683 e.Å^-3	

Table A11: Crystal data and structure refinement for (Δ)-[Yb(R-Phbipox)$_2$](Otf) **(IX)**

Empirical formula	C43 H36 F3 N6 O11 S Yb	
Formula weight	1074.88	
Temperature	150(2) K	
Wavelength	0.71073 Å	
Crystal system	Monoclinic	
Space group	P 1 21 1	
Unit cell dimensions	a = 9.4039(4) Å b = 14.7596(4) Å c = 15.2074(5) Å	alpha = 90 deg. beta = 99.186(3) deg. gamma = 90 deg.
Volume, Z	2083.68(12) Å^3, 2	
Density (calculated)	1.713 g/cm^3	
Absorption coefficient	2.378 mm^-1	
F(000)	1074	
Crystal size	0.57 x 0.06 x 0.06 mm	
Theta range for data collection	3.49 to 26.37 deg.	
Limiting indices	-10<=h<=11, -18<=k<=18, -19<=l<=18	
Reflections collected	17416	
Independent reflections	8513 [R(int) = 0.0464]	
Absorption correction	Semi-empirical from equivalents	
Max. and min. transmission	0.8724 and 0.3437	
Refinement method	Full-matrix least-squares on F^2	
Data / restraints / parameters	8513 / 116 / 663	
Goodness-of-fit on F^2	1.080	
Final R indices [I>2sigma(I)]	R1 = 0.0408, wR2 = 0.0877	
R indices (all data)	R1 = 0.0487, wR2 = 0.0927	
Absolute structure parameter	-0.020(9)	
Largest diff. peak and hole	1.763 and -0.950 e. Å^-3	

Table A12: Crystal data and structure refinement for [Eu⊂(Λ-Eu(R-Phbipox)$_2$Δ-Eu(R-Phbipox)$_2$)$_3$](Otf)$_9$ (**X**)

Empirical formula	C246.25 H168 Eu7 F18.75 N36 O54.75 S6.25	
Formula weight	6127.51	
Temperature	100(1) K	
Wavelength	0.70093 Å	
Crystal system	Monoclinic	
Space group	C 2	
Unit cell dimensions	a = 45.7446(11) Å b = 31.0966(5) Å c = 45.7325(11) Å	alpha = 90 deg. beta = 92.945(2) deg. gamma = 90 deg.
Volume, Z	64969(2) Å^3, 8	
Density (calculated)	1.253 g/cm^3	
Absorption coefficient	1.447 mm^-1	
F(000)	24362	
Crystal size	~150 μm	
Theta range for data collection	4.02 to 15.65 deg.	
Limiting indices	-35<=h<=35, -23<=k<=23, -35<=l<=35	
Reflections collected	62696	
Independent reflections	29668 [R(int) = 0.0477]	
Absorption correction	Semi-empirical from equivalents	
Max. and min. transmission	1.00000 and 0.55453	
Refinement method	Full-matrix least-squares on F^2	
Data / restraints / parameters	29668 / 2094 / 2559	
Goodness-of-fit on F^2	1.013	
Final R indices [I>2sigma(I)]	R1 = 0.0975, wR2 = 0.2698	
R indices (all data)	R1 = 0.1119, wR2 = 0.2913	
Absolute structure parameter	0.050(18)	
Largest diff. peak and hole	1.126 and -0.795 e.Å^-3	

Table A13: Crystal data and structure refinement for $[Sm(tpa)_2]I_2$ **(XII)**

Empirical formula	C36 H36 I2 N8 Sm	
Formula weight	984.88	
Temperature	300(2) K	
Wavelength	0.71073 Å	
Crystal system	Monoclinic	
Space group	P21/c	
Unit cell dimensions	a = 9.7886(11) Å b = 10.8139(12) Å c = 18.363(2) Å	alpha = 90 deg. beta = 104.764(12) deg. gamma = 90 deg.
Volume, Z	1879.6(4) Å ^3, 2	
Density (calculated)	1.740 Mg/m^3	
Absorption coefficient	3.240 mm^-1	
F(000)	952	
Crystal size	0.37 x 0.18 x 0.08 mm	
Theta range for data collection	3.28 to 26.37 deg.	
Limiting indices	-12<=h<=10, -13<=k<=13, -22<=l<=22	
Reflections collected	8052	
Independent reflections	3795 [R(int) = 0.0396]	
Max. and min. transmission	0.7770 and 0.3794	
Refinement method	Full-matrix least-squares on F^2	
Data / restraints / parameters	3795 / 0 / 214	
Goodness-of-fit on F^2	1.073	
Final R indices [I>2sigma(I)]	R1 = 0.0631, wR2 = 0.1637	
R indices (all data)	R1 = 0.0922, wR2 = 0.1711	
Largest diff. peak and hole	2.082 and -1.039 e. Å^-3	

Table A14: Crystal data and structure refinement for $[Eu(tpa)_2]I_2$ **(XIII)**

Empirical formula	C36 H36 Eu I2 N8	
Formula weight	986.49	
Temperature	303(2) K	
Wavelength	0.71073 Å	
Crystal system	Monoclinic	
Space group	P 21/c	
Unit cell dimensions	a = 9.7342(15) Å b = 10.7319(14) Å c = 18.243(4) Å	alpha = 90 deg. beta = 104.684(19) deg. gamma = 90 deg.
Volume, Z	1843.5(6) Å^3, 2	
Density (calculated)	1.777 Mg/m^3	
Absorption coefficient	3.412 mm^-1	
F(000)	954	
Crystal size	0.19 x 0.14 x 0.09 mm	
Theta range for data collection	3.33 to 32.55 deg.	
Limiting indices	-14<=h<=14, -15<=k<=13, -26<=l<=26	
Reflections collected	11263	
Independent reflections	5929 [R(int) = 0.0427]	
Absorption correction	Semi-empirical from equivalents	
Max. and min. transmission	0.7510 and 0.5603	
Refinement method	Full-matrix least-squares on F^2	
Data / restraints / parameters	5929 / 0 / 214	
Goodness-of-fit on F^2	0.703	
Final R indices [I>2sigma(I)]	R1 = 0.0394, wR2 = 0.0708	
R indices (all data)	R1 = 0.0992, wR2 = 0.0788	
Largest diff. peak and hole	1.006 and -0.880 e. Å^-3	

Table A15: Crystal data and structure refinement for [Ybtpa$_2$]I$_2$ **(XIV)**

Empirical formula	C42 H45 I2 N11 Yb	
Formula weight	1130.73	
Temperature	150(2) K	
Wavelength	0.71073 Å	
Crystal system	Monoclinic	
Space group	C c	
Unit cell dimensions	a = 20.9808(4) Å b = 17.9897(3) Å c = 11.8325(2) Å	alpha = 90 deg. beta = 93.1003(16) deg. gamma = 90 deg.
Volume, Z	4459.54(13) Å^3, 4	
Density (calculated)	1.684 g/cm^3	
Absorption coefficient	3.524 mm^-1	
F(000)	2200	
Crystal size	0.24 x 0.10 x 0.03 mm	
Theta range for data collection	3.39 to 28.28 deg.	
Limiting indices	-26<=h<=27, -23<=k<=23, -15<=l<=15	
Reflections collected	24007	
Independent reflections	10194 [R(int) = 0.0351]	
Absorption correction	Semi-empirical from equivalents	
Max. and min. transmission	0.9171 and 0.4876	
Refinement method	Full-matrix least-squares on F^2	
Data / restraints / parameters	10194 / 3 / 537	
Goodness-of-fit on F^2	0.858	
Final R indices [I>2sigma(I)]	R1 = 0.0420, wR2 = 0.0882	
R indices (all data)	R1 = 0.0572, wR2 = 0.0910	
Absolute structure parameter	0.00	
Largest diff. peak and hole	1.544 and -0.509 e.Å^-3	

Table A16: Crystal data and structure refinement for $[Sm(tpa)_2]I_3$ **(XV)**

Empirical formula	C42 H45 I3 N11 Sm	
Formula weight	1234.94	
Temperature	150(2) K	
Wavelength	0.71073 Å	
Crystal system	Orthorhombic	
Space group	P 21 21 21	
Unit cell dimensions	a = 11.8320(15) Å b = 17.840(3) Å c = 22.175(4) Å	alpha = 90 deg. beta = 90 deg. gamma = 90 deg.
Volume, Z	4680.7(12) Å ^3, 4	
Density (calculated)	1.752 g/cm^3	
Absorption coefficient	3.274 mm^-1	
F(000)	2380	
Crystal size	0.12 x 0.09 x 0.07 mm	
Theta range for data collection	3.40 to 24.71 deg.	
Limiting indices	-13<=h<=13, -8<=k<=20, -17<=l<=26	
Reflections collected	15281	
Independent reflections	7901 [R(int) = 0.1138]	
Absorption correction	Semi-empirical from equivalents	
Max. and min. transmission	0.8056 and 0.6966	
Refinement method	Full-matrix least-squares on F^2	
Data / restraints / parameters	7901 / 24 / 517	
Goodness-of-fit on F^2	1.019	
Final R indices [I>2sigma(I)]	R1 = 0.0875, wR2 = 0.1820	
R indices (all data)	R1 = 0.1303, wR2 = 0.2168	
Absolute structure parameter	-0.08(4)	
Largest diff. peak and hole	2.793 and -1.710 e.Å^-3	

Table A17: Crystal data and structure refinement for $[Sm(tpa)(\mu\text{-}OH)(Py\text{-}N\text{-}Oxide)_2]I_2$ **(XVI)**

Empirical formula	C68 H76 I4 N18 O6 Sm2	
Formula weight	2049.79	
Temperature	150(2) K	
Wavelength	0.71073 Å	
Crystal system	Monoclinic	
Space group	P 1 21/n 1	
Unit cell dimensions	a = 16.1919(10) Å b = 14.4828(7) Å c = 18.7847(12) Å	alpha = 90 deg. beta = 112.578(8) deg. gamma = 90 deg.
Volume, Z	4067.5(4) Å^3, 4	
Density (calculated)	1.674 Mg/m^3	
Absorption coefficient	3.004 mm^-1	
F(000)	1988	
Crystal size	0.10 x 0.10 x 0.10 mm	
Theta range for data collection	3.07 to 23.26 deg.	
Limiting indices	-12<=h<=17, -16<=k<=11, -20<=l<=20	
Reflections collected	10688	
Independent reflections	5444 [R(int) = 0.0450]	
Absorption correction	Semi-empirical from equivalents	
Max. and min. transmission	0.7532 and 0.7532	
Refinement method	Full-matrix least-squares on F^2	
Data / restraints / parameters	5444 / 0 / 445	
Goodness-of-fit on F^2	0.935	
Final R indices [I>2sigma(I)]	R1 = 0.0523, wR2 = 0.1169	
R indices (all data)	R1 = 0.0934, wR2 = 0.1248	
Largest diff. peak and hole	1.538 and -0.649 e.Å^-3	

Table A18: Crystal data and structure refinement for $[Yb(tpa)(\mu\text{-}OH)(Py\text{-}N\text{-}Oxide)_2]I_2$ **(XVII)**

Empirical formula	C60 H64 I4 N14 O6 Yb2	
Formula weight	1930.93	
Temperature	150(2) K	
Wavelength	0.71073 Å	
Crystal system	Monoclinic	
Space group	P 1 21/c 1	
Unit cell dimensions	a = 13.4359(3) Å b = 11.8449(3) Å c = 21.3171(6) Å	alpha = 90 deg. beta = 93.834(2) deg. gamma = 90 deg.
Volume, Z	3384.97(15) Å^3, 2	
Density (calculated)	1.893 g/cm^3	
Absorption coefficient	4.627 mm^-1	
F(000)	1840	
Crystal size	0.15 x 0.08 x 0.04 mm	
Theta range for data collection	3.35 to 28.28 deg.	
Limiting indices	-16<=h<=17, -15<=k<=6, -18<=l<=28	
Reflections collected	15313	
Independent reflections	8354 [R(int) = 0.0365]	
Absorption correction	Semi-empirical from equivalents	
Max. and min. transmission	0.8258 and 0.5417	
Refinement method	Full-matrix least-squares on F^2	
Data / restraints / parameters	8354 / 0 / 389	
Goodness-of-fit on F^2	1.013	
Final R indices [I>2sigma(I)]	R1 = 0.0476, wR2 = 0.0862	
R indices (all data)	R1 = 0.0752, wR2 = 0.0968	
Largest diff. peak and hole	1.728 and -1.023 e. Å^-3	

Table A19: Crystal data and structure refinement for $[Yb(tpa)I_2(CH_3CN)]\cdot 0.5CH_3CN$ **(XVIII)**

Empirical formula	C21 H22.50 I2 N5.50 Yb	
Formula weight	778.78	
Temperature	293(2) K	
Wavelength	0.71073 Å	
Crystal system	Triclinic	
Space group	P -1	
Unit cell dimensions	a = 9.7066(4) Å b = 11.8441(5) Å c = 13.2726(5) Å	alpha = 81.086(3) deg. beta = 67.813(4)deg. gamma = 66.875(4)deg.
Volume, Z	1299.35(9) Å^3, 2	
Density (calculated)	1.991 g/cm^3	
Absorption coefficient	5.991 mm^-1	
F(000)	726	
Crystal size	0.68 x 0.44 x 0.27 mm	
Theta range for data collection	3.36 to 30.51 deg.	
Limiting indices	-13<=h<=13, -16<=k<=16, -18<=l<=17	
Reflections collected	11849	
Independent reflections	7790 [R(int) = 0.0243]	
Absorption correction	Semi-empirical from equivalents	
Max. and min. transmission	0.2966 and 0.1067	
Refinement method	Full-matrix least-squares on F^2	
Data / restraints / parameters	7790 / 42 / 311	
Goodness-of-fit on F^2	1.021	
Final R indices [I>2sigma(I)]	R1 = 0.0361, wR2 = 0.0836	
R indices (all data)	R1 = 0.0456, wR2 = 0.0893	
Largest diff. peak and hole	1.708 and -0.998 e. Å^-3	

Table A20: Crystal data and structure refinement for $[Eu(tpa)(\mu\text{-}I)I]_2$ **(XIX)**

Empirical formula	C36 H36 Eu2 I4 N8	
Formula weight	1392.25	
Temperature	150(2) K	
Wavelength	0.71073 Å	
Crystal system	Orthorhombic	
Space group	P c a b	
Unit cell dimensions	a = 18.7333(5) Å b = 9.8963(2) Å c = 23.0485(8) Å	alpha = 90 deg. beta = 90 deg. gamma = 90 deg.
Volume, Z	4273.0(2) Å^3, 4	
Density (calculated)	2.164 g/cm^3	
Absorption coefficient	5.833 mm^-1	
F(000)	2584	
Crystal size	0.26 x 0.07 x 0.06 mm	
Theta range for data collection	3.48 to 40.24 deg.	
Limiting indices	-34<=h<=30, -17<=k<=15, -37<=l<=41	
Reflections collected	42811	
Independent reflections	13402 [R(int) = 0.0665]	
Absorption correction	Semi-empirical from equivalents	
Max. and min. transmission	0.7137 and 0.3145	
Refinement method	Full-matrix least-squares on F^2	
Data / restraints / parameters	13402 / 0 / 298	
Goodness-of-fit on F^2	1.002	
Final R indices [I>2sigma(I)]	R1 = 0.0411, wR2 = 0.0699	
R indices (all data)	R1 = 0.0660, wR2 = 0.0794	
Largest diff. peak and hole	1.827 and -1.360 e. Å^-3	

Table A 21: Crystal data and structure refinement for $[Nd_{13}(\mu_4\text{-}O_8)Na_8(\mu_4\text{-}1,1,1,1\text{-}N_3)_6(\mu_3\text{-}1,1,3\text{-}N_3)_{24}(py)_{28}I]\cdot(py)_7$ **(XX)**

Empirical formula	C175 H175 I N125 Na8 Nd13 O8	
Formula weight	6343.34	
Temperature	150(2) K	
Wavelength	0.71073 Å	
Crystal system	Triclinic	
Space group	P -1	
Unit cell dimensions	a = 18.9134(5) Å b = 20.1171(5) Å c = 20.1581(6) Å	alpha = 71.441(3) deg. beta = 63.285(3) deg. gamma = 65.880(3) deg.
Volume, Z	6167.2(3) Å^3, 1	
Density (calculated)	1.708 g/cm^3	
Absorption coefficient	2.896 mm^-1	
F(000)	3085	
Crystal size	0.21 x 0.11 x 0.09 mm	
Theta range for data collection	3.28 to 28.28 deg.	
Limiting indices	-25<=h<=23, -26<=k<=26, -26<=l<=24	
Reflections collected	60346	
Independent reflections	30554 [R(int) = 0.0505]	
Absorption correction	Semi-empirical from equivalents	
Max. and min. transmission	0.7867 and 0.5775	
Refinement method	Full-matrix-block least-squares on F^2	
Data / restraints / parameters	30554 / 409 / 1593	
Goodness-of-fit on F^2	0.807	
Final R indices [I>2sigma(I)]	R1 = 0.0490, wR2 = 0.1183	
R indices (all data)	R1 = 0.1247, wR2 = 0.1319	
Largest diff. peak and hole	1.867 and -1.031 e.Å^-3	

PUBLICATIONS

DOI: 10.1002/chem.201000572

Diastereoselective Self-Assembly of a Homochiral Europium Triangle from a Bipyoxazoline–Carboxylate Ligand

Gülay Bozoklu, Claire Marchal, Christelle Gateau, Jacques Pécaut, Daniel Imbert, and Marinella Mazzanti*[a]

Self-assembly plays a crucial role in the formation of many chiral structures in nature. The control of the chirality of self-assembled architectures is very important for the application of these systems in catalysis, molecular recognition and sensing of biological substrates.[1,2] Lanthanide-based chiral supramolecular architectures are particularly attractive because of the spectroscopic and catalytic properties of these ions.[3–5] However, their kinetic lability and weak stereochemical preferences cause the design of enantiopure molecular and supramolecular architectures to be particularly difficult. A few mononuclear complexes of lanthanides with chiral pre-determination have been obtained by using enantiopure ligands and have been used as chiral luminescent probes or chiral catalysts.[1,4–10] Fewer examples of chiral polynuclear assemblies have been described for lanthanides.[3,11–16] Some original examples of chiral assemblies were obtained from the controlled hydrolysis[11–13] or CO_2 fixation reactions[15,16] of lanthanide salts in the presence of chiral ligands. In these synthetic methods the hydroxo and the carbonate groups play an important role in the formation of the heteroleptic assemblies causing the rational design of the final assembly to be difficult. Dimetallic triple-stranded helicates are to date the only reported example of pre-programmed,[17,18] enantiomerically pure polynuclear lanthanide assemblies.[3,16] We have previously demonstrated that large polynuclear wheel-shaped lanthanide compounds can be selectively assembled by using a metal-directed synthesis in the presence of a dissymmetric terpyridine–carboxylate ligand.[19] This ligand promotes the assembly of oligonuclear lanthanide complexes rather then polymeric structures through the formation of carboxylate bridges. This work has now been successfully extended to the synthesis of a chiral polynuclear assembly through a careful ligand design. Here we describe the use of the chiral carboxylate-derivatised bipyoxazoline ligand (*S*)-Phbipox (6′-(4-phenyloxazolin-2-yl)-2,2′-bipyridine-6-carboxylic acid; Figure 1) to promote the diastereoselective self-assembly of the novel homochiral trinuclear europium complex $(\Delta\Delta\Delta)$-[Eu((*S*)-Phbipox)$_2$]$_3^{+3}$ (**1**).

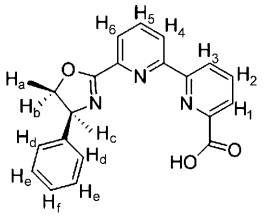

Figure 1. Structure and numbering scheme for NMR spectral assignments of the ligand (*S*)-PhbipoxH.

We demonstrate that the chirality of the ligand is transferred in a concentration-dependent formation of the trinuclear assembly to give the enantiopure $\Delta\Delta\Delta$ isomer. At low concentration the diastereomeric complexes (Δ)-[Eu((*S*)-Phbipox)$_2$]$^+$ (**2**) and (Λ)-[Eu((*S*)-Phbipox)$_2$]$^+$ (**3**) form with partial stereoselectivity (Λ/Δ ratio of $\approx$1.8). At higher concentration the homochiral trinuclear complex **1** self-assembles selectively in solution from the mononuclear bis-ligand **2** complex through the formation of carboxylate bridges.

The enantiomerically pure ligand (*S*)-Phbipox has been prepared in seven steps from commercial dimethylbipyridine in 13% total yield. The synthetic procedure is outlined in Scheme S1 in the Supporting Information and involves the reaction of the ethyl 6′-(chlorocarbonyl)-2,2′-bipyridine-6-carboxylic acid with (*S*)-2-phenylglycinol followed by the simultaneous intramolecular ring closure and saponification in an aqueous ethanolic potassium hydroxide solution to afford the desired (*S*)-Phbipox product.

Proton NMR studies show that the reaction of Eu(OTf)$_3$ with two equivalents of (*S*)-Phbipox in anhydrous methanol in the presence of triethylamine affords a mixture of the two diastereoisomeric bis-ligand complexes **2** and **3**, which

[a] G. Bozoklu, Dr. C. Marchal, Dr. C. Gateau, J. Pécaut, Dr. D. Imbert, Dr. M. Mazzanti
Laboratoire de Reconnaissance Ionique et Chimie de Coordination
Service de Chimie Inorganique et Biologique
(UMR E-3 CEA/UJF, FRE3200 CNRS), CEA-Grenoble
INAC, 17 rue des Martyrs 38054 Grenoble Cedex 9 (France)
Fax: (+33) 0438785090
E-mail: marinella.mazzanti@cea.fr

Supporting information for this article is available on the WWW under http://dx.doi.org/10.1002/chem.201000572.

correspond to the two different helical arrangements (left and right, respectively) that the two ligands can adopt when they bind the metal. Chiral induction from the (*S*)-Phbipox ligand occurs during metal coordination leading to a Λ/Δ ratio determined by NMR spectroscopy to be approximately 1.8 in a 7 mM solution of anhydrous methanol at room temperature. Two distinct sets of 12 NMR signals are observed for the 14 protons of the two C_2 symmetric diastereoisomers (Figure 2). The 2D EXSY (exchange spectroscopy) NMR

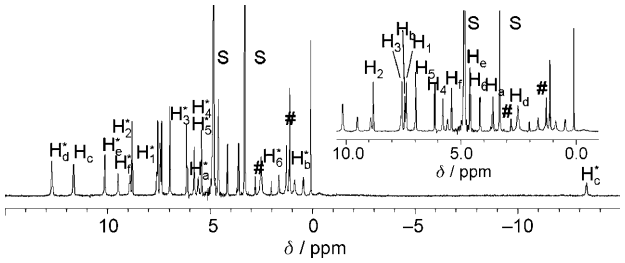

Figure 2. ^{1}H NMR spectra of (Δ)-[Eu((*S*)-Phbipox$_2$)]$^+$ (H$_x^*$) and (Λ)-[Eu((*S*)-Phbipox$_2$)]$^+$ (H$_x$; Mercury 400 MHz, 298 K, 7 mM). S = CD_3OD, # = triethylammonium.

study shows the presence of a slow exchange between the two complexes in solution. At higher concentrations (from 14 mM) the NMR spectra show an additional set of 24 signals suggesting the formation of an additional species (Figure S1 in the Supporting Information). These signals were assigned to the trinuclear complex [(ΔΔΔ)-{Eu((*S*)-Phbipox$_2$}$_3$]$^{+3}$ in which the two independent ligands give rise to two different sets of 12 signals. No signals from heterochiral species were observed. The addition of a small amount of water (< 0.03 %) does not significantly affect the oligomerisation process.

This assignment is in agreement with the solid-state crystal structure determined by X-ray diffraction on single crystals of the [Eu((*S*)-Phbipox$_2$]OTf complex isolated from 24 mM methanol solutions. Notably, X-ray diffraction analysis revealed the presence of two distinct co-crystallised molecules in the compound [(ΔΔΔ)-{Eu((*S*)-Phbipox$_2$}$_3$·(Λ)-{Eu((*S*)-Phbipox$_2$}]OTf$_4$ (**4**). The proton NMR spectra of the bulk isolated complex (see the Experimental Section and Figure S2 in the Supporting Information) in deuterated acetonitrile shows the presence of the trinuclear complex from 6 mM, probably as a result of the lower polarity and lower coordinating ability of this solvent. Moreover, the NMR spectrum shows a Λ/Δ ratio of approximately 0.6 indicating that the crystallisation process leads to an increase of the Δ monomer with respect to the Λ complex. Pulsed-field gradient stimulated echo (PFGSTE) diffusion NMR spectroscopy was used to measure the diffusion coefficient (*D*) of **1**, **2** and **3** in 6 mM acetonitrile and methanol solutions.[20] The diffusion coefficient is a function of the molecular weight (*M*) and can been conveniently used to discriminate metallosupramolecular architectures in solution.[21] Because the trimeric and monomeric complexes have both globular shape and similar microscopic densities, which can be anticipated from their crystal structure, the Stokes–Einstein equation can be used to estimate the relative molecular size of the solution species.[21] The values measured in acetonitrile [$M\Delta\Delta\Delta/M\Delta = (D\Delta/D\Delta\Delta\Delta)^3 = 2.8(6)$] are in agreement with the presence of one trinuclear complex and two mononuclear species. In 6 mM methanol solution only the monomeric complexes are present. The calculated values of the spherecal hydrodynamic radius (8.2 Å for the trimeric species and 5.8 Å for the monomeric ones) compare very well with the value estimated from the crystal structure (7.7 and 5.1 Å, respectively). The intensity of the NMR signals assigned to the trimeric complex increases in methanol and acetonitrile with increasing concentration. This increase is associated with an intensity decrease of only one of the two set of signals corresponding to the two diastereoisomeric bis-ligand complexes. This shows that only one diastereoisomer, which has been identified as the Δ isomer on the basis of the X-ray crystal structure, undergoes the oligomerisation process. Only the presence of the trimeric species and of the residual Λ monomer can be detected in 30 mM acetonitrile solutions of the [Eu((*S*)-Phbipox$_2$]$^+$ complex (Figure 3).

These results highlight the diastereoselectivity of the self-assembly process, which only involves (Δ)-[Eu((*S*)-Phbipox$_2$] species whereas the formation of the other possible chiral assemblies ΔΔΛ, ΛΛΛ and ΔΛΛ is not observed.

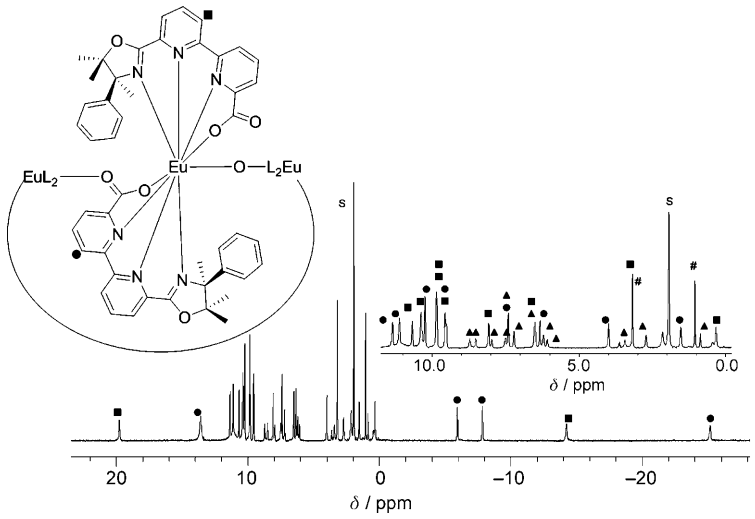

Figure 3. 1H NMR spectra of (ΔΔΔ)-[Eu((*S*)-Phbipox$_2$]$_3$$^{+3}$ (■ and ●) and (Λ)-[Eu((*S*)-Phbipox$_2$]$^+$ (▲; Bruker 500 MHz, 263 K, 30 mM). S: = CD_3CN, # = triethylammonium.

This result also suggests that in anhydrous acetonitrile the ligand (*S*)-Phbipox$^-$ remains bound to the metal ion preventing the rearrangement of the Δ isomer into the Λ one.

Compound **4** crystallises in the chiral orthorhombic space group $P2_12_12_1$. Isomorphous crystals were obtained from a concentrated acetonitrile solution. The structure of the monomeric (Λ)-[Eu((*S*)-Phbipox)$_2$]$^+$ cation in **4** is shown in Figure 4. The structure of the trinuclear cation [(ΔΔΔ)-{Eu((*S*)-Phbipox)$_2$}$_3$]$^{3+}$ in **4** is presented in Figure 5 whereas detail of the (Δ)-[Eu((*S*)-Phbipox)$_2$]$^+$ fragments is shown in Figure 4.

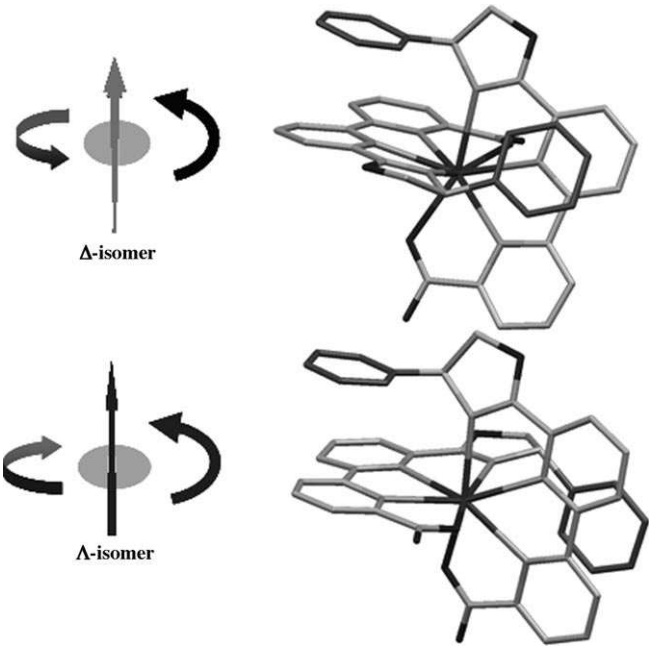

Figure 4. The structure of the monomeric (Λ)-[EuL$_2$]$^+$ and (Δ)-[EuL$_2$]$^+$ isomers. The arrow starts from the carboxylic group and ends at the phenyl group of the ligand.

In the (Λ)-[Eu((*S*)-Phbipox)$_2$]$^+$ cation the Eu ion is eight-coordinated by the six nitrogen atoms and the two oxygen atoms from the (*S*)-Phbipox$^-$ ligand with a distorted dodecahedron geometry (Figure S6 in the Supporting Information). The two S ligands wrap around the metal with a Λ stereochemistry. The two ligand mean planes form an angle of approximately 90°. Strong π–π interactions (see Table S3 in the Supporting Information) are found between the oxazoline phenyl rings of each tetradentate ligand and one pyridine ring of the other ligand. The presence of π–π interactions between the two ligands should play an important role in the observed rigidity of complexes **2** and **3** in acetonitrile solution. The mean values of the Eu–N (2.57 Å (2) and 2.54 Å (3)) and Eu–O bond lengths (2.39 Å (2) and 2.30 Å (3)) are similar to those found in the eight-coordinate complex [Eu(L)$_2$] isolated from methanol in the presence of the dissymmetric ligand 2,2′:6′,2″-terpyridine-2-carboxylic acid (mean Eu–O = 2.31(1) and Eu–N = 2.53(5) Å).

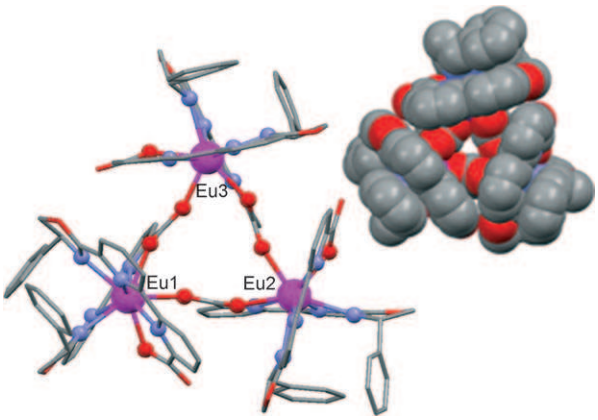

Figure 5. Diagram of the structure [(ΔΔΔ)-{Eu((*S*)-Phbipox)$_2$}$_3$]$^{+3}$ in **4** and the spacefill diagram (created by using the MERCURY 2.2 program).

In the [(ΔΔΔ)-{Eu((*S*)-Phbipox)$_2$}$_3$]$^{3+}$ cation three crystallographically inequivalent (Δ)-[Eu((*S*)-Phbipox)$_2$]$^+$ complexes are connected through a carboxylate oxygen from one of the (*S*)-Phbipox$^-$ ligands to form an equilateral triangle with the Eu–Eu distances ranging from 6.685 to 6.780 Å. Each Eu ion is nine-coordinate with distorted tricapped trigonal prism geometry by the six nitrogen and the two oxygen atoms from the two (*S*)-Phbipox$^-$ ligands and by the carboxylate oxygen from a neighbour complex.

In each monomeric unit of the trinuclear complex the two (*S*)-Phbipox$^-$ ligands wrap around the metal ion with a Δ stereochemistry. The angle between the two ligand mean planes is approximately 107°. Strong π–π interactions (see Table S3 in the Supporting Information) are found between the oxazoline phenyl rings of each tetradentate ligand and one pyridine ring of the other ligand. The crystal structure of **4** shows that the (*S*)-Phbipox$^-$ ligands can wrap around the metal with the two different Δ and Λ stereochemistries. However, only the Δ complexes self-assemble to form a homochiral trinuclear structure. The molecular model (made by using the MERCURY 2.2 program)[22] of a trinuclear structure built from mononuclear (Λ)-[Eu((*S*)-Phbipox)$_2$]$^+$ entities (Figure 6) suggests that important steric constraints resulting from the orientation of the phenyl substituents on the oxazoline ring are present when mononuclear complexes with Λ conformation are brought in close proximity. Similar constraints are observed for ΛΔΔ and ΛΛΔ isomers (see Figure S7 in the Supporting Information). Such sterical constraints should play an important role in the diastereoselectivity of the self-assembly process.

The luminescence emission spectrum of the [Eu((*S*)-Phbipox)$_2$]$^+$ complex carried out in anhydrous methanol (7 mM) also show the presence of europium species of different symmetry with respect to those found in acetonitrile solutions (7–26 mM). This is in agreement with the different metal environment observed for the trinuclear assembly (present in acetonitrile) compared with the mononuclear complex (the only species present in 7 mM methanol solution, Figure 7). The luminescence quantum yield measured

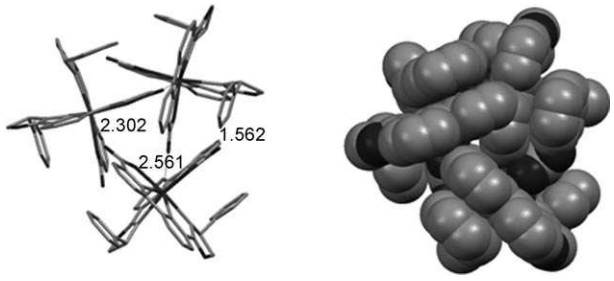

Figure 6. Molecular models built from the structures of the Δ and Λ in **4** showing the sterical constraints preventing the formation of the heterochiral trinuclear complexes $[(\Lambda\Lambda\Lambda)\text{-}\{Eu((S)\text{-Phbipox})_2\}_3]^{+3}$ (created by using the MERCURY 2.2 program).

in methanol with excitation at 279 and 340 nm varied between 20(2) and 28(1)% depending of the concentration used (6–7 mM). Circularly polarised luminescence studies

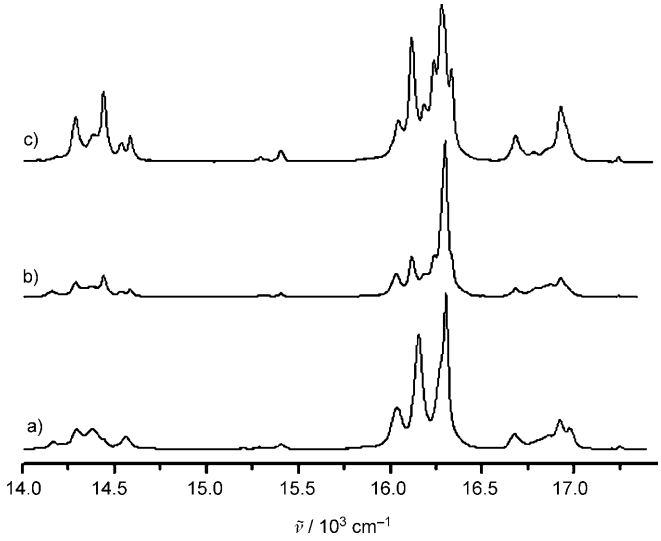

Figure 7. Normalised emission spectra of $[Eu((S)\text{-Phbipox})_2]OTf$ at a) 7 mM in CD_3OD, b) 7 mM in CH_3CN, c) 26 mM in CH_3CN.

will be carried out in future work to investigate the influence of the concentration and of chirality on the photophysical properties.[23]

In summary, we have reported a rare enantiopure trinuclear europium complex obtained in a novel concentration-dependent self-assembly process promoted by a new (*S*)-Phbipox$^-$ ligand. We have shown that selective homochiral recognition occurs, probably as a result of sterical interaction, during the self-assembly of the bis-ligand monomeric complexes to yield the final trinuclear species. Some selectivity was also found in the self-assembly of the two ligands around the europium centre to afford the Λ and Δ monomeric isomers.

Future studies will be directed to tune the ligand bulk and cation size with the objective of increasing the stereoselectivity of the self-assembly of the monomeric complex. This system is also particularly well suited for the self-assembly of larger cluster structures by using template cations,[19] and work in this direction is in progress.

Experimental Section

Synthesis of $[Eu((S)\text{-Phbipox})_2]OTf$: Triethylamine (20.2 μL) was added to a solution of (*S*)-Phbipox (50 mg 0.145 mmol) in anhydrous methanol (2 mL). The resulting solution was stirred for 2 h and a solution of $Eu(OTf)_3$ (0.0725 mmol) in methanol (1 mL) was then added. The resulting solution was stirred at room temperature for an hour. Diisopropylether was then added to afford a white microcrystalline solid precipitate that was filtered and dried for two weeks at 40 °C under vacuum (87% yield). ^{1}H NMR for the (Λ)-$[Eu((S)\text{-Phbipox})_2]^+$ species (500 MHz, CD_3CN, −10 °C): $\delta = 0.45$ (0.4H, brt; H_c), 3.42 (0.4H, brt; H_a), 2.71(0.4H, brt; H_b), 6.07 (0.4H, brd; H_6), 6.21(0.8H, brs; H_d), 6.50 (0.4H, brs; H_3), 7.21 (0.8H, brs; H_e), 7.42 (0.4H, brd; H_2), 7.50 (0.4H, brt; H_f), 7.95 (0.4H, brd; H_1), 8.72 (0.4H, brt; H_5), 8.50 (0.4H, d, $J = 5.7$ Hz; H_4); ^{1}H NMR for the (ΔΔΔ)-$[Eu((S)\text{-Phbipox})_2]_3^{+3}$ species (500 MHz, CD_3CN, −10 °C): ●: −25.18 (1H, brt; H_c), −7.83 (1H, brd; H_6), −5.92 (1H, brt; H_b), 1.53 (1H, brt; H_a), 3.99 (1H, brt; H_5), 6.34 (1H, d, $J = 6.6$ Hz; H_3), 7.42 (1H, brd; H_4), 9.54 (1H, brt; H_f), 10.24 (2H, brt; H_e), 11.12 (1H, brt; H_2), 11.35 (1H, d, $J = 6.1$ Hz; H_2), 13.57 (2H, brs; H_d); ■:−14.21 (1H, brt; H_c), 0.33 (1H, brt; H_b), 2.15 (1H, brd; H_3), 3.28 (1H, brt; H_2), 6.50(1H, brs; H_a), 8.07 (1H, d, $J = 7.9$ Hz; H_4), 89.54 (2H, brt; H_5), 9.83 (3H, brt, H1; H_e), 10.37 (2H, brs; H_d), 10.68 (1H, brt; H_f), 19.78 (1H, brs; H_6); MS (ES$^+$) CD_3OD: $m/z = 841.1$ $[Eu((S)\text{-Phbipox})_2]^+$; MS (ES$^+$) CD_3CN: $m/z = 841.3$ $[Eu((S)\text{-Phbipox})_2]^+$, 335 $[\{Eu_3((S)\text{-Phbipox})_6\}(OTf)]^{2+}$; elemental analysis calcd (%) for $[Eu((S)\text{-Phbipox})_2]OTf{\cdot}1.26Et_3NOTf_3$ ($C_{49.82}H_{46.9}N_{7.26}O_{12.78}F_{6.78}S_{2.26}Eu$, $M_w = 1305.23$): C 45.85, H 3.32, N 7.89; found: C 45.85, H 3.62, N 7.79;

Crystal data for 4: $C_{172.50}H_{148}Eu_4F_{12}N_{24}O_{45.50}S_4$; $M_r = 4249.23$; crystal size = $0.20 \times 0.15 \times 0.15$ mm^3; orthorhombic; space group $P2_12_12_1$; $a = 17.3481(10)$, $b = 32.1765(15)$, $c = 32.4386(12)$ Å; $\alpha = \beta = \gamma = 90°$; $V = 18107.3(15)$ Å^3; $Z = 4$; $\rho_{calcd} = 1.559$ mg m^{-3}; $\mu = 1.510$ mm^{-1}; $\lambda = 0.71073$ Å; $T = 150$ (2) K; $3.02° < 2\theta\max < 23.25°$; 42715 reflections collected; 25589 unique reflections ($R_{int} = 0.0459$); $R_1 = 0.05031$, $wR_2 = 0.1001$ [$I > 2\sigma(I)$]; $R_1 = 0.0806$, $wR_2 = 0.1058$ (all data); residual electron density = 1.515 e A^{-3}.

CCDC-763804 contains the supplementary crystallographic data for this paper. These data can be obtained free of charge from The Cambridge Crystallographic Data Centre via www.ccdc.cam.ac.uk/data_request/cif.

The figure graphics were generated by using the MERCURY 2.2 program supplied with the Cambridge Structural Database.[22] Further experimental details, including ligand synthesis, X-ray crystallography and mass spectroscopy are given in the Supporting Information.

Acknowledgements

This research was carried out in the frame of the EC COST Action D-38 "Metal-Based Systems for Molecular Imaging Applications". We thank Lydia Ouadah for ligand synthesis, Colette Lebrun and Pierre A. Bayle for their help with the spectroscopic characterisations.

Keywords: chirality · cluster compounds · lanthanides · luminescence · N,O ligands · self-assembly

[1] J. Crassous, *Chem. Soc. Rev.* **2009**, *38*, 830–845.
[2] S. Faulkner, J. L. Matthews, *Comprehensive Coordination Chemistry II, Vol. 9*, Elsevier, Oxford, **2004**.

[3] M. Cantuel, G. Bernardinelli, G. Muller, J. P. Riehl, C. Piguet, *Inorg. Chem.* **2004**, *43*, 1840–1849.
[4] H. C. Aspinall, *Chem. Rev.* **2002**, *102*, 1807–1850; H. C. Aspinall, N. Greeves, *J. Organomet. Chem.* **2002**, *647*, 151–157; H. Tsukube, S. Shinoda, *Chem. Rev.* **2002**, *102*, 2389–2403.
[5] D. Parker, R. S. Dickins, H. Puschmann, C. Crossland, J. A. K. Howard, *Chem. Rev.* **2002**, *102*, 1977–2010.
[6] H. Tsukube, S. Shinoda, *Chem. Rev.* **2002**, *102*, 2389–2403.
[7] R. S. Dickins, J. A. K. Howard, C. W. Lehmann, J. Moloney, D. Parker, R. D. Peacock, *Angew. Chem.* **1997**, *109*, 541–543; *Angew. Chem. Int. Ed. Engl.* **1997**, *36*, 521–523; J. I. Bruce, R. S. Dickins, L. J. Govenlock, T. Gunnlaugsson, S. Lopinski, M. P. Lowe, D. Parker, R. D. Peacock, J. J. B. Perry, S. Aime, M. Botta, *J. Am. Chem. Soc.* **2000**, *122*, 9674–9684.
[8] J. P. Leonard, P. Jensen, T. McCabe, J. E. O'Brien, R. D. Peacock, P. E. Kruger, T. Gunnlaugsson, *J. Am. Chem. Soc.* **2007**, *129*, 10986–10987.
[9] M. Seitz, E. G. Moore, A. J. Ingrarn, G. Muller, K. N. Raymond, *J. Am. Chem. Soc.* **2007**, *129*, 15468–15470.
[10] S. D. Bonsall, M. Houcheime, D. A. Straus, G. Muller, *Chem. Commun.* **2007**, 3676–3678.
[11] M. Lama, O. Mamula, G. S. Kottas, F. Rizzo, L. De Cola, A. Nakamura, R. Kuroda, H. Stoeckli-Evans, *Chem. Eur. J.* **2007**, *13*, 7358–7373.
[12] O. Mamula, M. Lama, H. Stoeckli-Evans, S. Shova, *Angew. Chem.* **2006**, *118*, 5062–5066; *Angew. Chem. Int. Ed.* **2006**, *45*, 4940–4944.
[13] O. Mamula, M. Lama, S. G. Telfer, A. Nakamura, R. Kuroda, H. Stoeckli-Evans, R. Scopelitti, *Angew. Chem.* **2005**, *117*, 2583–2587; *Angew. Chem. Int. Ed.* **2005**, *44*, 2527–2531.
[14] K. S. Jeong, Y. S. Kim, Y. J. Kim, E. Lee, J. H. Yoon, W. H. Park, Y. W. Park, S. J. Jeon, Z. H. Kim, J. Kim, N. Jeong, *Angew. Chem.* **2006**, *118*, 8314–8318; *Angew. Chem. Int. Ed.* **2006**, *45*, 8134–8138.
[15] X. L. Tang, W. H. Wang, W. Dou, J. Jiang, W. S. Liu, W. W. Qin, G. L. Zhang, H. R. Zhang, K. B. Yu, L. M. Zheng, *Angew. Chem.* **2009**, *121*, 3551–3554; *Angew. Chem. Int. Ed.* **2009**, *48*, 3499–3502.
[16] F. Stomeo, C. Lincheneau, J. P. Leonard, J. E. O'Brien, R. D. Peacock, C. P. McCoy, T. Gunnlaugsson, *J. Am. Chem. Soc.* **2009**, *131*, 9636–9637.
[17] S. Floquet, N. Ouali, B. Bocquet, G. Bernardinelli, D. Imbert, J. C. G. Bunzli, G. Hopfgartner, C. Piguet, *Chem. Eur. J.* **2003**, *9*, 1860–1875.
[18] K. Zeckert, J. Hamacek, J. M. Senegas, N. Dalla-Favera, S. Floquet, G. Bernardinelli, C. Piguet, *Angew. Chem.* **2005**, *117*, 8168–8172; *Angew. Chem. Int. Ed.* **2005**, *44*, 7954–7958.
[19] Y. Bretonnière, M. Mazzanti, J. Pécaut, M. M. Olmstead, *J. Am. Chem. Soc.* **2002**, *124*, 9012–9013; X. Y. Chen, Y. Bretonniere, J. Pecaut, D. Imbert, J. C. Bunzli, M. Mazzanti, *Inorg. Chem.* **2007**, *46*, 625–637.
[20] J. T. J. Edward, *Chem. Educ.* **1970**, *47*, 261–269.
[21] L. Allouche, A. Marquis, J.-M. Lehn, *Chem. Eur. J.* **2006**, *12*, 7520–7525; G. Bellachioma, G. Ciancaleoni, C. Zuccaccia, D. Zuccaccia, A. Macchioni, *Coord. Chem. Rev.* **2008**, *252*, 2224–2238.
[22] MERCURY 2.2, CCDC, Cambridge (UK), **2004**.
[23] J. L. Lunkley, D. Shirotani, K. Yamanari, S. Kaizaki, G. Muller, *J. Am. Chem. Soc.* **2008**, *130*, 13814–13815; J. Gregolinski, P. Starynowicz, K. T. Hua, J. L. Lunkley, G. Muller, J. Lisowski, *J. Am. Chem. Soc.* **2008**, *130*, 17761–17773.

Received: March 4, 2010
Published online: April 26, 2010

Structural and photophysical properties of trianionic nine-coordinated near-IR emitting 8-hydroxyquinoline-based complexes†

Gülay Bozoklu, Claire Marchal, Jacques Pécaut, Daniel Imbert and Marinella Mazzanti*

Received 30th March 2010, Accepted 11th July 2010
DOI: 10.1039/c0dt00225a

Two building blocks, 2-(1H-tetrazol-5-yl)quinoline-8-ol (8-hydroxyquinoline-2-tetrazole) (H_2hqt) and 8-hydroxyquinoline-2-carboxylic acid (H_2hqa) provide convenient dianionic tridentate O,N,N- and O,N,O-chelating units containing the 8-hydroxyquinoline chromophore. These ligands form tris-chelate tris-anionic complexes $[Ln(hqa)_3]K_3$ and $[Ln(hqt)_3]K_3$ in water at pH = 12. At lower pH partially protonated species are formed. The Nd(III), Yb(III) and Er(III) complexes of hqa, and hqt and the partially protonated complex $[Nd(H_{1/2}hqa)_3]_2(Et_3NH)_3.Et_3NHOTf$ have been crystallised from methanol solution. The X-ray crystal structure ($[Nd(hqa)_3]K_3.7MeOH_\infty\cdot MeOH$, $[Er(hqa)_3]K_3.4MeOH_\infty\cdot 3MeOH$ and $[Nd(hqt)_3]K_3.5MeOH_\infty\cdot MeOH$) show a helical arrangement of both ligands with an "*anti*" geometry for hqa and a "*syn*" geometry for hqt. Only tris-chelate complexes are formed in water and 0.04 M methanol solutions for both ligands. A "*syn*" geometry is found for the partially protonated dimeric complexes which is preserved in methanol solution. A statistical distribution of "*anti*" and "*syn*" species is found for $[Ln(hqa)_3]K_3$ complexes in solution while the major solution geometry of $[Ln(hqt)_3]K_3$ complexes is "*syn*". Sizable near-IR emission quantum yields were measured for the $[Ln(hqa)_3]K_3$ complexes in solid state (0.06%, 0.18%, 0.0051% for Nd(III), Yb(III) and Er(III) respectively) and in methanol (0.063%, 0.28%, 0.0019% for Nd(III), Yb(III) and Er(III) respectively). All the values of quantum yields obtained for the hqt complexes are 5–17% higher than those measured for the hqa complexes. The trianionic complexes present a high solubility in organic and aqueous solvents and a good resistance to ligand dissociation compared to neutral tris 8-hydroxyquinoline complexes.

Introduction

There is currently high interest for the design of lanthanide complexes displaying metal-centered luminescence emission in the near-infrared (NIR) region because of the wide variety of applications in material science, lighting and telecommunication technology and in bioanalysis.[1–12] The emission of Nd^{III}, Yb^{III} or Er^{III} ions is particularly attractive because it falls in the transparent window of biological tissues and silica.[13,14] Thanks to its low energy triplet state (17 100 cm^{-1}, 500–600 nm) and its visible absorption the 8-hydroxyquinoline unit (8-hq) is a choice chromophore for the sensitisation of these lanthanide NIR emitters. The first reports of the use of 8-hydroxyquinolinate complexes of Nd^{III}, Yb^{III} and Er^{III} in the fabrication of NIR emitting organic light-emitting diodes (OLED's) have led to numerous coordination chemistry studies directed to elucidate the structure of these complexes and/or to optimise the photophysical properties.[15–18] These studies showed that species differing for their nuclearity and stoichiometry form in the reaction of lanthanide ions with bidentate 8-hydroxyquinolines. Some characterised species also present coordinated water molecules which are deleterious for the efficiency of near-IR luminescence emission. Moreover these complexes are sensitive to moisture, which leads to ligand dissociation reducing the devices stability and efficiency. In order to gain a better control of the structural properties and the photophysical properties of the final complexes several groups have included hydroxyquinolate groups in polydentate ligands predisposed for the formation of dinuclear helicates[19,20] or water soluble mononuclear podate[21–24] which display a high water stability and should provide suitable probes for bioanalysis.

In a more simple approach the groups of Albrecht and Bünzli have reproducibly prepared mononuclear neutral tris-ligand complexes of lanthanides using monoanionic tridentate N,N,O ligands obtained by substitution of the hydroxyquinoline group with neutral carboxamide, benzimidazole and benzoxazole groups.[25–27] Halogenation of some of these expanded hydroxyquinoline ligands afforded complexes with very strong near-IR emission and enhanced quantum yields.[28]

However, we considered that dianionic ligands could afford a better control of the coordination sphere and of the solubility and should afford ionic complexes with potential application in the design of lanthanide-based ionogels and ionic liquids.[29,30] Dianionic expanded ligands can be prepared by substitution of 8-hydroxyquinoline with well chosen lanthanide binding groups such as carboxylate and tetrazolate. Carboxylate have been widely used in lanthanide chemistry to yield water stable complexes.[31] Recently we have shown that tetrazolate groups are convenient analogues of carboxylates which can be used to tune the photophysical properties of lanthanides in podates or self-assembled

CEA, INAC, Service de Chimie Inorganique et Biologique (UMR-E 3 CEA-UJF, FR 3200 CNRS), Laboratoire de Reconnaissance Ionique et Chimie de Coordination, CEA-Grenoble, 38054, GRENOBLE, Cedex 09, France. E-mail: marinella.mazzanti@cea.fr

† Electronic supplementary information (ESI) available: ^{1}H NMR spectra of $[Nd(H1/2hqt)_3]_2(Et_3NH)_3$ and complexes of Yb. See DOI: 10.1039/c0dt00225a

complexes.[32,33] Here we report the first example of water soluble hydroxyquinoline-based tris-anionic tris-ligand complexes prepared using dianionic hydroxyquinoline ligands substituted with carboxylate (H_2hqa) and tetrazolate (H_2hqt) binding groups (Scheme 1).

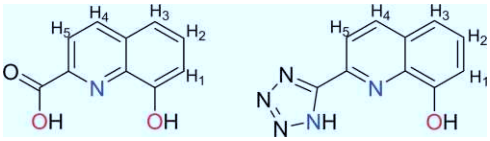

Scheme 1 H_2hqa and H_2hqt ligands.

Tris-anionic tris-ligand complexes were synthesised for both ligands with Nd(III), Yb(III) and Er(III) ions and the structural and photophysical properties of the complexes were elucidated in the solid and solution states. The isolated complexes present a high solubility in polar solvents and a high resistance to hydrolysis.

Results and discussion

Synthesis and solution structure

H_2hqa is commercially available. H_2hqt was conveniently prepared from commercial 8-hydroxyquinoline-2-carbonitrile in a one-step synthesis with 90% yield. The easy access to both ligands renders them very attractive for potential applications. The homoleptic complexes $[Ln(hqa)_3]K_3$ and $[Ln(hqt)_3]K_3$ were prepared by reacting a solution of $Ln(OTf)_3$ (H_2hqa; Ln = Nd, **1** Er, **2** Yb, **3**; H_2hqt; Ln = Nd, **4** Er, **5** Yb, **6**) in water with 3 equivalents of ligand (H_2hqa/H_2hqt) at pH 12 adjusted by addition of aqueous KOH (1 M). Crystallisation from a mixture of methanol/diisopropylether afforded the complexes in ~60% yield. The analytical results are in agreement with the presence of tris-ligand complexes. In the crystal structure of the $[Ln(hqa)_3]K_3$ complexes only the *anti* arrangement of the ligands was observed, while in the $[Ln(hqt)_3]K_3$ complexes only the *syn* arrangement was observed probably as a result of the coordination of the potassium counterion to the tetrazole nitrogen atoms of the three ligands. However in solution a statistical 1 : 3 distribution of the *syn* : *anti* species is expected.

The ^{1}H NMR spectrum of $[Nd(hqa)_3]K_3$ in CD_3OD shows two well defined sets of signals which were assigned to the two geometric isomers *syn* (12%) and *anti* present in solution (Fig. 1).

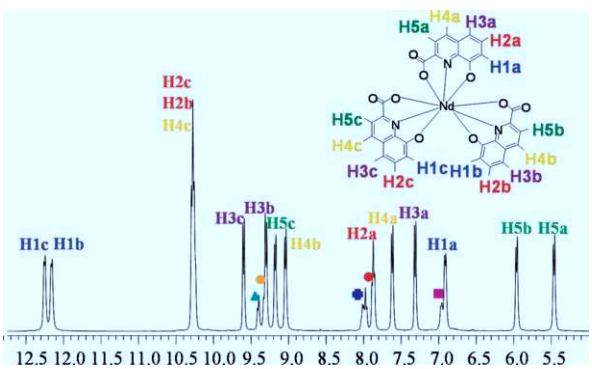

Fig. 1 ^{1}H NMR spectrum of $[Nd(hqa)_3]^{-3}$ (CD_3OD, 400 MHz, 298 K) [0.04 M].

The major set of 13 signals was assigned to the 15 protons of an unsymmetrical *anti* species in which the three hqa^{-2} ligands are arranged in an "up, up, down" geometry. The second set of 5 signals was assigned to the 15 protons of the C_3 symmetric *syn* species in which the three hqa^{-2} adopt an "up, up, up" arrangement. The observed *anti*/*syn* ratio is only slightly higher of the expected statistical 75% ratio observed in other tridentate unsymmetrical substituted hydroxyquinoline ligands.[28] A very similar proton NMR spectrum was found for the $[Nd(hqa)_3]K_3$ complex in water at pD 12. At 298 K the ^{1}H NMR signals are relatively large suggesting an exchange between *anti* and *syn* isomers. At 278 K the ^{1}H NMR spectrum of the $[Nd(hqa)_3]K_3$ complex in water at pD 12 is well resolved (Fig. 2). These results show that the $[Nd(hqa)_3]K_3$ complex does not dissociate in basic 0.04 M aqueous solution and confirms the strong resistance of these anionic complexes to hydrolysis.

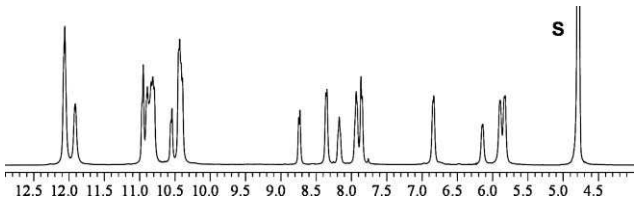

Fig. 2 ^{1}H NMR (400 MHz, 278 K) spectrum of $[Nd(hqa)_3]^{-3}$ in D_2O (0.04 M at pH = 12).

The ^{1}H NMR spectrum of $[Nd(hqt)_3]K_3$ in CD_3OD also shows two sets of signals which were assigned to the two geometric isomers *syn* and *anti* (Fig. 3). However in this complex the *syn*/*anti* ratio is inverted (*syn*: 65%) with respect to the expected statistical distribution. This result suggests that the solid state structure is retained in solution probably due to the coordination of potassium by the tetrazole binding units. ^{1}H NMR spectrum of $[Ln(hqt)_3]K_3$ complexes in water at pD 12 at 25 °C gives similar signals as in methanol revealing the stability of complexes in aqueous media.

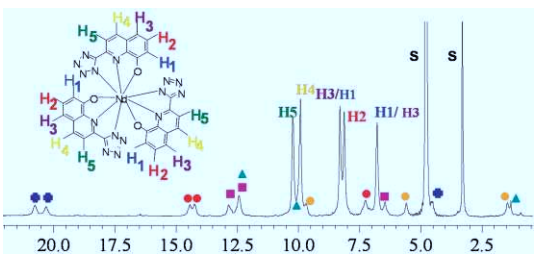

Fig. 3 ^{1}H NMR spectrum of $[Nd(hqt)_3]^{-3}$ (CD_3OD, 400 MHz, 298 K) [0.04 M].

The ^{1}H NMR spectra of 1 : 3 Nd/ligand (H_2hqa or H_2hqt) solutions in methanol after addition of triethylamine (6 equivalents) shows only the presence of one set of 5 signals in agreement with the presence of C_3 symmetric species in solution (Fig. 4 for hqa and Fig. S1, ESI, for hqt†). Crystallisation of the dimeric complex $[Nd(H_{1/2}hqa)_3]_2(Et_3NH)_3.Et_3NHOTf$, **7**, by diffusion of diisopropylether in the methanolic solution showed the presence of partially protonated species. Dimerisation occurs through hydrogen bond formation between two partially protonated *syn* complexes. X-Ray diffraction of crystals isolated in similar conditions for the neodymium complex of hqt^{2-} suggests the presence

of a similar species although the crystal data are not of quality sufficient for publication.

The formation of lanthanide complexes containing partially protonated ligands is observed (presence of C_3 symmetric species in proton NMR) in water at pH lower than 12 or in methanol solution in the presence of weak bases and is compatible with the high pK_a value of the hydroxyl group of the 8-hydroxyquinoline moiety (pK_a = 9.8 in 8-hydroxyquinoline). Similar species have been already observed for 8-hydroxyquinoline based podating ligands.[21,24] The high solution symmetry of the partially protonated species suggests that the strong hydrogen bonds observed in the solid state structure are maintained in solution.

Solid-state structure

$[Nd(H_{1/2}hqa)_3]_2(Et_3NH)_3.Et_3NHOTf$ (7). The X-ray diffraction study of **7** reveals the presence of a centrosymmetric dimer in the $C2/c$ space group with the formula $[Nd(H_{1/2}hqa)_3]_2(Et_3NH)_3.Et_3NHOTf$. An ORTEP view of the $\{[Nd(H_{1/2}hqa)_3]_2\}^{3-}$ anion is presented in Fig. 5 and selected distances are given in Table 1. The structure consists of nine-coordinated neodymium ions with a slightly distorted tricapped trigonal prism geometry. The metal ion is coordinated by three non-symmetry related hqa ligands which act as tridentate ligands, binding to neodymium through

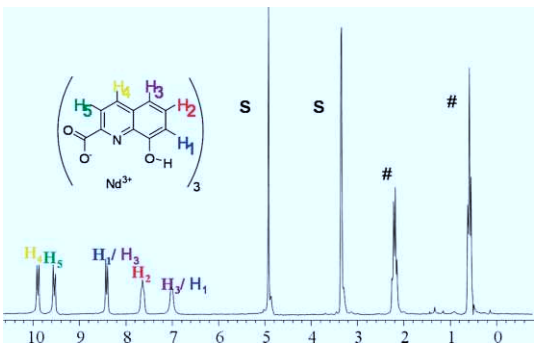

Fig. 4 ^{1}H NMR spectra of a 1 : 3 Nd : H_2hqa solution after addition of 6 equivalents of triethylamine. Symbols # and S indicate the signals of triethylammonium and solvents, respectively (0.03 M in ligand CD_3OD, 400 MHz, 298 K).

Table 2 Hydrogen bonds (Å) and angles (°) in complex $\{[Nd(H_{1/2}hqa)_3]_2(Et_3NH)_3\}$ (**7**): A (acceptor), D (donor)

D–H···A	d(D–H)	d(H···A)	d(D···A)	<(DHA)
O(3)–H(3O)···O(3A)	1.224(14)	1.224(14)	2.421(2)	163(9)
O(23)–H(23O)···O(13A)	0.93(7)	1.57(7)	2.492(4)	173(7)
O(23A)–H(23P)···O(13)	0.93(7)	1.57(7)	2.492(4)	173(7)

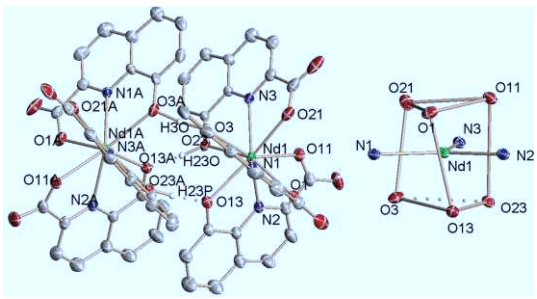

Fig. 5 ORTEP view of the anion $[Nd(H_{1/2}hqa)_3]_2^{3-}$ and coordination polyhedron. Atoms labelled A and P are C_2-symmetry related. The ellipsoids are shown at the 30% probability level.

the pyridine nitrogen and the hydroxo and carboxylate oxygen atoms. The three ligand strands bind the metal ion in a helical fashion with a *syn* arrangement. The three hydrogen atoms of the partially deprotonated hqa ligand are shared between the six phenol oxygen atoms. The resulting strong H-bonds connect two neodymium complexes in a dimeric structure with a Nd–Nd separation of 5.795 Å. The geometries of the H-bonds are reported in Table 2. Such dimerisation has already been observed for a partially deprotonated hydroxyquinoline based tripodal ligand.[24]

According to the Jeffrey's classification[34,35] these hydrogen bonds have energies close to covalent bonds. Because of the strong hydrogen bonds the presence of dimeric structures could also be anticipated in solution and is probably at the origin of the observed high symmetry of the protonated solution species. The mean value of the distances between the metal center and carboxylate oxygen atoms 2.47(2) Å are shorter than Nd–O phenol distances 2.53(5) Å, in agreement with the presence of partially protonated phenol oxygen atoms.

Table 1 Selected bond lengths (Å) for the complexes

$[Nd(H1/2hqa)_3]_2(Et_3NH)_3$		$[Nd(hqa)_3](K_3)$		$[Er(hqa)_3](K_3)$		$[Nd(hqt)_3](K_3)$	
$Ln–O_{carboxyl}$		$Ln–O_{carboxyl}$		$Ln–O_{carboxyl}$		$Ln–O_{carboxyl}$	
Nd(1)–O(1)	2.488(3)	Nd–O(1)	2.546(14)	Er–O(1)	2.431(3)	Nd(1)–O(1)	2.396(5)
Nd(1)–O(11)	2.478(3)	Nd–O(11)	2.470(14)	Er–O(11)	2.411(2)	Nd(1)–O(2)	2.436(4)
Nd(1)–O(21)	2.453(3)	Nd–O(21)	2.492(13)	Er–O(21)	2.447(2)	Nd(1)–O(3)	2.425(4)
Nd–O av	2.47(2)	Nd–O av	2.50 (4)	Er–O av	2.43(2)	Nd–O av	2.42(2)
$Ln–N_{py}$		$Ln–N_{py}$		$Ln–N_{py}$		$Ln–N_{py}$	
Nd(1)–N(1)	2.605(4)	Nd–N(1)	2.609(16)	Er–N(1)	2.466(4)	Nd(1)–N(5)	2.608(6)
Nd(1)–N(2)	2.574(4)	Nd–N(2)	2.563(16)	Er–N(11)	2.458(3)	Nd(1)–N(15)	2.604(6)
Nd(1)–N(3)	2.589(3)	Nd–N(3)	2.574(15)	Er–N(21)	2.435(3)	Nd(1)–N(25)	2.625(5)
Nd–N av	2.59(2)	Nd–N av	2.58 (2)	Er–N av	2.45(2)	Nd–N av	2.61(1)
$Ln–O_{phenol}$		$Ln–O_{phenol}$		$Ln–O_{phenol}$		$Ln–N_{tetrazole}$	
Nd(1)–O(3)	2.505(3)	Nd–O(3)	2.509(13)	Er–O(3)	2.417(3)	Nd(1)–N(1)	2.672(5)
Nd(1)–O(13)	2.501(3)	Nd–O(13)	2.478(14)	Er–O(13)	2.426(3)	Nd(1)–N(11)	2.681(6)
Nd(1)–O(23)	2.595(2)	Nd–O(23)	2.482(14)	Er–O(23)	2.368(2)	Nd(1)–N(21)	2.650(5)
Nd–O av	2.53(5)	Nd–O av	2.49(2)	Er–O av	2.40(3)	Nd–N av	2.67(2)

Finally the use of Et_3N as a base results in a very different solid state structure with respect to the complexes prepared in the presence of KOH. The weaker basicity of Et_3N results in the presence of partially protonated ligands yielding a dimeric structure. Moreover the associated counterion Et_3NH^+ acts as non-coordinating cation in the resulting discrete structure of 7. In contrast the use of KOH as a base results in polymeric structures because of the coordination of potassium to hqa oxygen atoms or to hqt nitrogen atoms of adjacent complexes.

$[Nd(hqa)_3]K_3$ (1) and $[Er(hqa)_3]K_3$ (2). X-Ray diffraction studies on crystals of **1** and of **2** revealed respectively the formation of a centrosymmetric structure crystallising in the $P2_1/n$ space group with the formula $[Nd(hqa)_3]K_3.7MeOH_\infty \cdot MeOH$ and of a structure crystallising in the $C2/c$ space group with the formula $[Er(hqa)_3]K_3 \cdot 4MeOH.0.25DIPE_\infty \cdot 3MeOH$ (DIPE = diisopropylether). ORTEP views of the structure of **1** are represented in Fig. 6 and selected bond distances of **1** and **2** are given in Table 1.

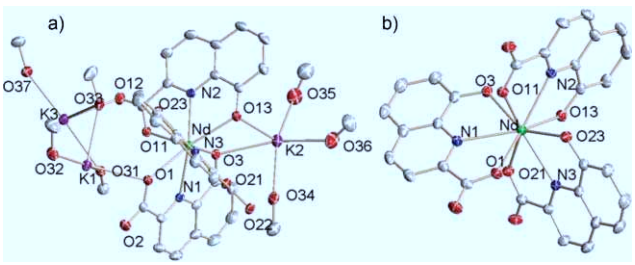

Fig. 6 ORTEP views of $[Nd(hqa)_3]K_3 \cdot 7MeOH$ (**1**) (asymmetric unit) (a) and of the $[Nd(hqa)_3]^{3-}$ anion (b). The ellipsoids are shown at the 30% probability level.

In **1** and **2** three deprotonated hqa^{2-} ligands bind the metal ion in a tridentate fashion through the 8-hydroxyquinolato units and the carboxylate oxygen atoms, yielding a nine-coordinated complex with a slightly distorted tricapped trigonal prism geometry (Fig. 7). The three ligands adopt a helical arrangement with an *anti* conformation "up, up, down" ((O(23), O(21) and N(3)) is the down ligand). A very similar coordination environment was also found from X-ray studies for the ytterbium complex **3** although the quality of the resulting crystal structure is not sufficient for publication due to the quality of the isolated crystals.

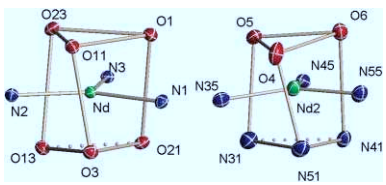

Fig. 7 Coordination polyhedron in $[Nd(hqa)_3]^{-3}$ (left) and $[Nd(hqt)_3]^{-3}$ (right) respectively.

The mean values of the Nd–O distances (Nd–O phenol 2.49(2) Å and Nd–O carboxyl 2.50(4) Å) in **1** are very similar to those found in the dimeric (Nd–O phenol 2.53(5) Å and Nd–O carboxyl 2.48(2) Å) partially protonated complex, indicating that the partial protonation of the ligand is not affecting significantly the Nd–O bond strength.

The influence of protonation on the Nd–L distances of the hqa complex is smaller than that observed in a neutral trishydroxyquinoline based podate.[24] On the other end smaller values of the Er–O phenol (2.40(3) Å) and Er–O carboxyl (2.43(2) Å) distances are found in **2** with respect to the Nd(III) complex **1** which is in agreement with the decrease of ionic radii along the lanthanide series.[36]

The complete deprotonation of the three hqa^{2-} ligands in **1** and **2** leads to the presence of three potassium counter-ions in the structures which coordinate the phenol and carboxylate oxygen atoms as shown in Scheme 2. The potassium ions also bind seven methanol molecules which act as bridging ligands between adjacent neodymium complexes leading to a 2D polymeric network. For the erbium complex **2** the methanol molecules do not act as bridging ligands, but the potassium ions bind directly to the carboxylate oxygen atoms of the adjacent complex yielding a 2D network (Fig. 8). Therefore the Er–Er distances are significantly shorter in **2** (9.964 Å) than the Nd–Nd (12.728 Å) distances in **1**.

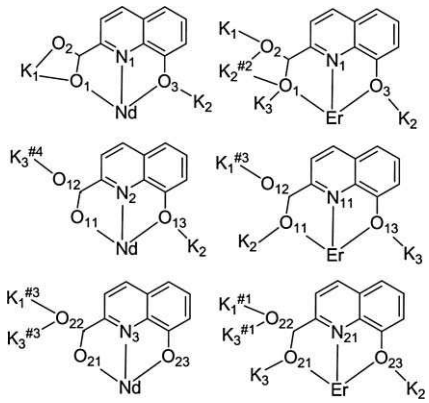

Scheme 2 Coordination mode of the three hqa^{2-} ligands in $[Nd(hqa)_3]K_3$ and $[Er(hqa)_3]K_3$. Symmetry transformations used to generate equivalent atoms in ($[Nd(hqa)_3]K_3$): #3 $x - 1/2, -y + 3/2, z - 1/2$; and in ($[Er(hqa)_3]K_3$) #4 $-x + 2, -y + 2, -z + 2$; #1 $-x + 1/2, -y + 1/2, -z + 1$; #2 $-x + 1/2, y - 1/2, -z + 1/2$; #3 $-x + 1/2, y + 1/2, -z + 1/2$.

$[Nd(hqt)_3]K_3.5MeOH_\infty \cdot MeOH$ (4). X-Ray diffraction studies on single crystals of **4** revealed the formation of a centrosymmetric structure crystallising in the $P\bar{1}$ space group with the formula $[Nd(hqt)_3]K_3.5MeOH_\infty \cdot MeOH$. ORTEP views of the structure are represented in Fig. 9.

The three deprotonated hqt^{2-} ligands bind in a tridentate O,N,N fashion through the quinolato units and the tetrazole nitrogen atoms, affording a nine-coordinated Nd(III) complex with a slightly distorted tricapped trigonal prism geometry (Fig. 7). As a major feature of the complex the helical arrangement of the three ligands present a *syn* conformation. A similar arrangement is also suggested by X-ray studies for the Er complex $[Er(hqt)_3]K_3$ although the crystal structure is not of quality sufficient for publication.

Complete deprotonation of the three hqt^{2-} ligands leads to the presence of three potassium ions as counter-ions. The mean value of the distances between the metal center and carboxylate oxygen atoms 2.42(2) Å are shorter than Nd–N tetrazole distances 2.67(2) Å. Two crystallographically independent complexes are found in the structure. They differ for the potassium coordination (see Scheme 3). Each complex is bound to six potassium ions connecting different complexes to yield a 2D network which

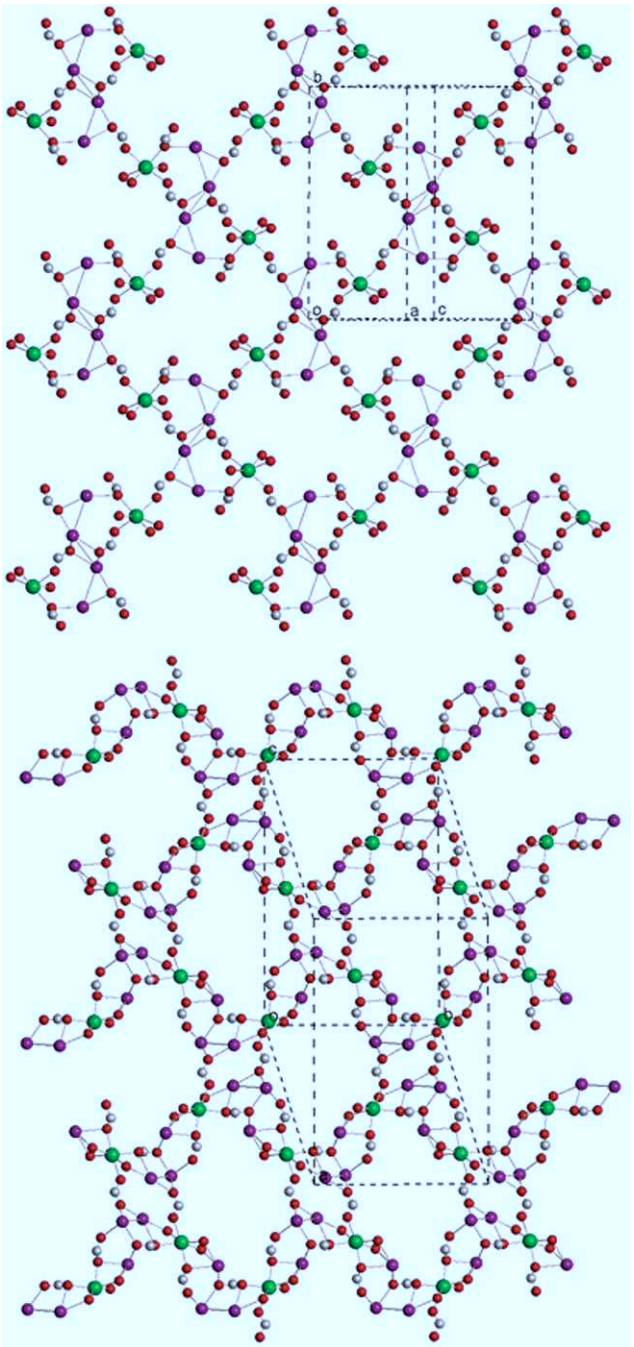

Fig. 8 ORTEP diagram of the polymeric 2D network in $[Nd(hqa)_3]K_3.7MeOH_\infty \cdot MeOH$ along *c*–*a* axis (*a* + *c*, *b* plane) and $[Er(hqa)_3]K_3.4MeOH.0.25DIPE_\infty \cdot 3MeOH$ (b,c plane). K: purple, O: red, Ln: green.

propagates along the *a*,*b* plane. The potassium ions bound to the three hydroxyquinoline oxygen atoms are connected trough methanol molecules yielding a 3D network (Fig. 10).

Sensitisation of lanthanide-centered NIR emission by hqt and hqa

In methanol, the absorption spectrum of the hqa and hqt ligands features three main bands located around 250, 305, 344 and 264, 317, 349 nm, respectively (Fig. 11) with absorption extending up to 400 nm. They are assigned to $\pi \rightarrow \pi^*$ and $n \rightarrow \pi^*$ transitions. In

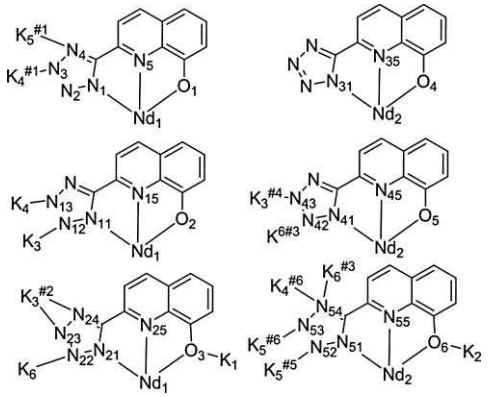

Scheme 3 Coordination mode of the three hqt^{2-} ligands in complex $[Nd(hqt)_3]K_3$. Symmetry transformations used to generate equivalent atoms: #1 $-x, -y, -z + 1$; #2 $-x + 1, -y, -z + 1$; #3 $x, y, z - 1$; #4 $-x + 1, -y, -z$; #5 $x, y + 1, z - 1$; #6 $-x, -y, -z$.

the Ln(III) complexes of both ligands, the more energetic bands are blue-shifted and a characteristic band appears at 411 and 402 nm for the hqa and hqt ligands, respectively with absorption extending up to 500 nm.

Photophysical studies were carried out on all complexes in the solid state and in methanol. The measurements were effectuated in air without particular precaution to prevent the presence of oxygen. All the isolated complexes of hqt and hqa with the Nd(III), Yb(III) and Er(III) ions including the dimeric partially protonated complex ($[Nd(H_{1/2}Hqa)_3]_2^{3-}$) display sizable metal-centered NIR luminescence in solid state and in methanolic solution. In addition, at 295 K, the ligand-centered emission contributes only faintly to the luminescence with UV excitation in the $\pi \rightarrow \pi^*$ and $n \rightarrow \pi^*$ absorption bands of the ligand resulting in a very faint emission (<5% compared with the free ligand) through fluorescence from the $^1\pi\pi^*$ state ligand emission spectra. It indicates an efficient energy transfer process to the acceptor levels of the metal ions. Sensitisation of the NIR luminescence by the ligands is ascertained by the excitation spectra of the Nd(III), Yb(III) and Er(III) complexes and clearly demonstrate the antenna effect of the ligand with components matching the absorption bands of the electronic spectra (Fig. 12, left). At room temperature and upon broad band excitation through both ligand levels at 371, 344 and 483 nm all complexes show identical luminescence spectra in solid state or dissolved in methanol and display peaks corresponding to the expected f–f NIR transitions.

The Yb(III) complexes are characterised by a band in the 905–1095 nm range, assigned to the $^2F_{5/2} \rightarrow {}^2F_{7/2}$ transition, with a sharp main component at 981 nm and broader components at longer wavelengths due, in part, to vibronic transitions. The Nd(III) complexes display three bands in the 835–1420 nm range, the main band occurring between 1005 and 1145 nm ($^4F_{3/2} \rightarrow {}^4I_{11/2}$), with a maximum at 1060 nm; two other bands are visible between 835–950 ($^4F_{3/2} \rightarrow {}^4I_{9/2}$) and 1285–1420 nm ($^4F_{3/2} \rightarrow {}^4I_{13/2}$). Finally the Er(III) complexes emit a band centered at 1551 nm, assigned to the $^4I_{13/2} \rightarrow {}^4I_{15/2}$ transition.

The luminescence decays obtained upon excitation through both hqa and hqt ligands electronic levels are single-exponential functions of time, indicating a fast energy transfer from the ligand to the metal ion and also the presence of efficient non-radiative deactivation processes, since they are much shorter than the

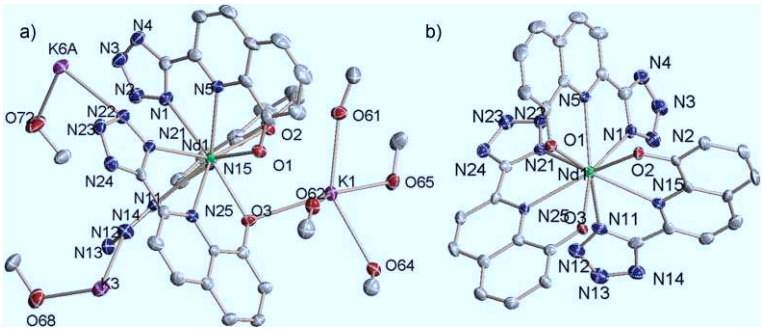

Fig. 9 ORTEP views of (a) $[Nd(hqt)_3]K_3$ showing the potassium bridged tetrazoles and (b) of the $[Nd(hqt)_3]^{3-}$ anion. The ellipsoids are shown at the 30% probability level.

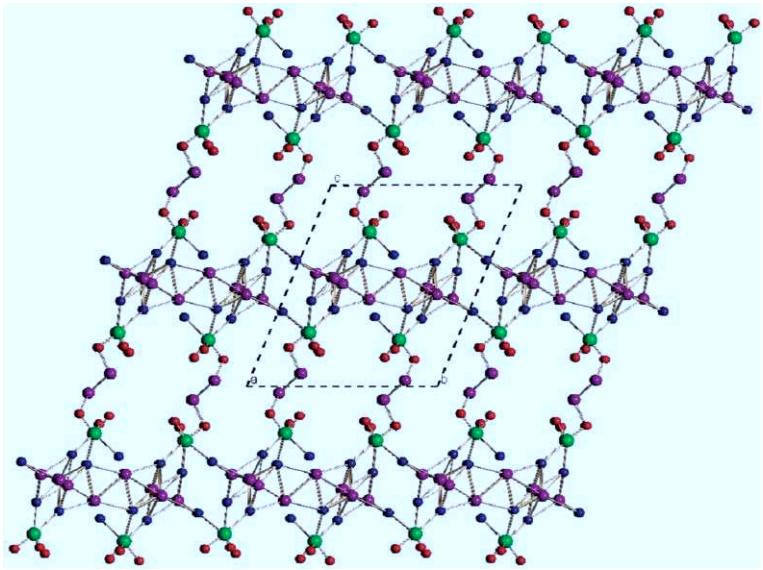

Fig. 10 ORTEP diagram of the polymeric 2D network in $[Nd(hqt)_3]K_3.5MeOH_\infty \cdot MeOH$ along the *a* axis. K: purple, O: red, Nd: green, N: blue.

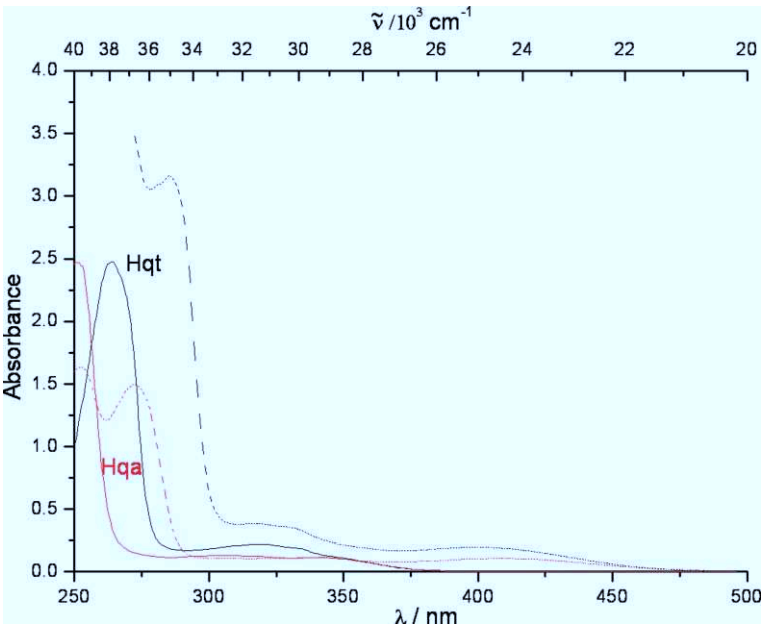

Fig. 11 Absorption spectra of the hqa (red line) and hqt (black line) ligands and their respective Nd^{III} complexes (dotted lines) in MeOH at 16 μM.

Table 3 Crystallographic data for the structures

	$[Nd(H_{1/2}hqa)_3]_2(Et_3NH)_3.Et_3NHOTf$ (**7**)	$[Nd(hqa)_3]K_3.7MeOH_{89}\cdot MeOH$ (**1**)	$[Er(hqa)_3]K_3.4MeOH.0.25DIPE\cdot 3MeOH$ (**2**)	$[Nd(hqt)_3]K_3.5MeOH_\infty\cdot MeOH$ (**4**)
Formula	$C_{85}H_{97}F_3N_{10}Nd_2O_{21}S$	$C_{38}H_{47}K_3N_3NdO_{17}$	$C_{38.75}H_{46.50}ErK_3N_3O_{16.25}$	$C_{149}H176K_{12}N_{60}Nd_4O_{41}$
Mw	1972.27	1079.33	1098.85	4509.66
Crystal system	Monoclinic	Monoclinic	Monoclinic	Triclinic
Space group	$C2/c$	$P2_1/n$	$C2/c$	$P\bar{1}$
a/Å	24.967(6) A	14.3830(19)	28.8105(12)	12.4042(5)
b/Å	17.066(4) A	20.469(3)	15.6426(4)	18.9257 (7)
c/Å	20.643(5) A	16.184(2)	23.5338(8)	21.6698(8)
α/°	90	90	90	67.155(3)
β/°	90.550(4)	100.312(2)	118.865(5)	86.944(3)
γ/°	90	90	90	84.896(3)
V/Å^3	8796(4)	4687.8(11)	9288.3(5)	4668.5(3)
Z	4	4	8	1
$D_c$alc/Mg m^{-3}	1.489	1.529	1.572	1.604
μ(Mo-Kα)/mm^{-1}	1.274	1.444	2.146	1.451
T/K	293(2)	223(2)	150(2)	150(2)
R_1, wR_2 [$I > 2\sigma(I)$]	0.0469, 0.1222	0.0241, 0.0575	0.0304, 0.0531	0.0459, 0.0867
Reflections collected	24 427	30 021	17 247	31 098
Independent reflections, *R*int	8949, 0.0427	11 194, 0.0179	9137, 0.033	15 288, 0.0449

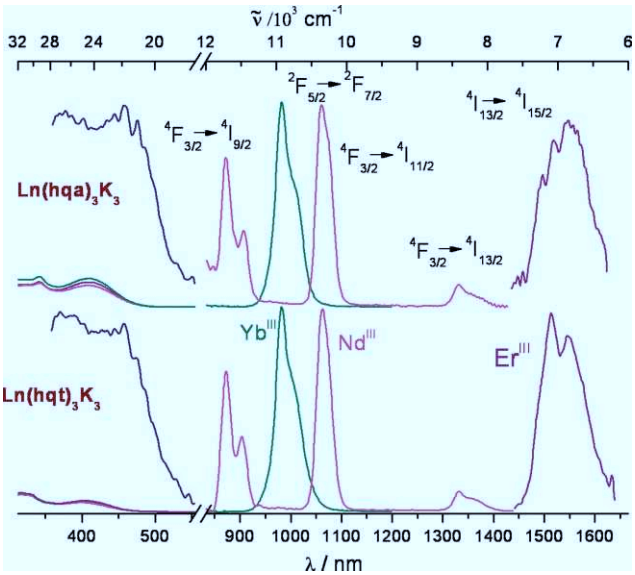

Fig. 12 Left: Normalised absorption and excitation spectra (λ_{an} = 1540 (Er), 1063 (Nd), and 976 nm (Yb)). Right: Emission spectra in the NIR region (λ_{ex} = 371 nm) of the hqa and hqt complexes of Er^{III}, Nd^{III}, and Yb^{III}.

radiative lifetimes. The corresponding lifetimes of the Nd($^4F_{3/2}$), Yb($^2F_{5/2}$) and Er($^4I_{13/2}$) excited states are reported in Table 4 and indicate that both ligands provide an adequate protective coordination environment around the metal ion.

In the solid state, the lifetimes are smaller than in methanol solution as often observed for lanthanide complexes. The lifetimes of the monomeric ($Ln(hqa)_3K_3$, $Ln(hqt)_3K_3$) Nd(III) and Yb(III) complexes in the solid state are 0.240, 0.225, 2.99 and 3.15 µs, and compare well to those measured in methanol (0.322, 0.367, 3.89 and 5.15 µs respectively). The situation is different for the Er(III) complexes of both ligands where the luminescence decays increases significantly in the solid state compared to the methanol solutions.

To quantify the ability of the chromophoric subunits to sensitise the NIR-emitting lanthanides, the absolute quantum yields of the

Table 4 Metal-ion-centered lifetimes and absolute quantum yields for Nd($^4F_{3/2}$), Er ($^4I1_{3/2}$), and Yb($^2F_{5/2}$) in the hqa and hqt Ln^{III} complexes (Ln = Nd, Er, Yb) in MeOH in solution and in solid state

Compound		τ/µs	Q^L_{Ln} (%)
$Nd(hqa)_3K_3$	Solid	0.240(1)	0.060(1)
	MeOH	0.322(1)	0.063(2)
	H_2O	0.127(1)	$<2\times10^{-4}$
$[Nd(H_{1/2}hqa)_3]_2^{3-}$	Solid	0.356(1)	0.059(4)
	MeOH	0.296(1)	0.035(1)
$Nd(hqt)_3K_3$	Solid	0.225(1)	0.067(1)
	MeOH	0.367(1)	0.068(1)
$Yb(hqa)_3K_3$	Solid	2.99(1)	0.18(1)
	MeOH	3.89(1)	0.28(1)
$Yb(hqt)_3K_3$	Solid	3.15(1)	0.21(1)
	MeOH	5.15(1)	0.31(1)
$Er(hqa)_3K_3$	Solid	0.479(1)	0.0051(1)
	MeOH	0.375(1)	0.0019(1)
$Er(hqt)_3K_3$	Solid	0.623(1)	0.0059(2)
	MeOH	0.471(1)	0.0020(1)

Ln(III) complexes (Ln = Nd, Er, Yb) in solid state and methanol solution have been determined upon ligand excitation. The quantum yields are sizeable for the $Nd(hqa)_3K_3$ (0.06%) and $Yb(hqa)_3K_3$ (0.18%) complexes in the solid state, and 0.063% and 0.28%, respectively, in methanol solution. The NIR luminescence of the $Er(hqa)_3K_3$ chelate is sufficiently intense at room temperature for allowing the calculation of quantum yields which are smaller in methanol (0.0019%) compare to 0.0051% obtained in solid state. The NIR luminescence of the $Nd(hqa)_3K_3$ complex in water is detectable but not sufficiently intense at room temperature for allowing the calculation of the quantum yield.

However, the luminescence lifetime values measured in methanol (0.367(1) and 0.322(1) µs, for $Nd(hqt)_3K_3$ and $Nd(hqa)_3K_3$, respectively and the one obtained for complex $Nd(hqa)_3K_3$ in water (0.127(1) µs) are very similar to the values found for water stable Nd podates in water (0.13(1)–0,25(3) µs).[23] This result suggests that deprotonated complexes remain mainly associated even in low concentration aqueous solutions. According to the good values observed for the overall quantum yields, the efficiencies of the sensitising process are important

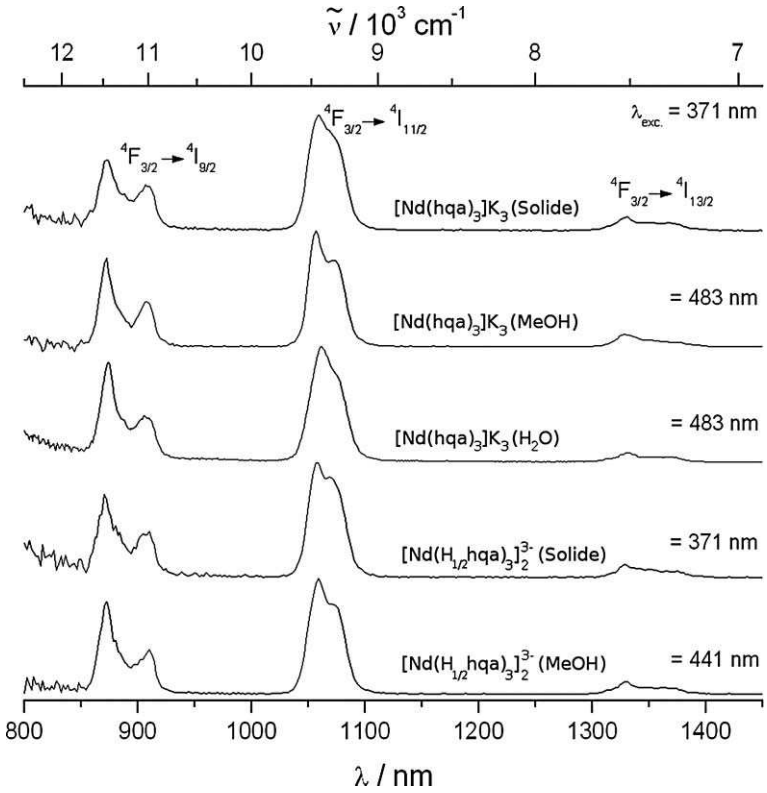

Fig. 13 Normalised emission spectra (λ_{ex} = 371 nm) of the Nd^{III} complexes of hqa and hqt in solution and in the solid state at 295 K.

and the de-activation processes are essentially due to vibrational oscillators located outside the first coordination sphere. Finally in order to study the influence of the protonation state of the hydroxyquinoline unit on the spectroscopic properties of the Nd(III) ion, luminescence measurements were carried out also on the dimeric ($[Nd(H_{1/2}hqa)_3]_2^{3-}$) complex in the solid state as well as in solution. Excitation and emission spectra of the complexes in solution and in the solid state are almost identical (Fig. 13). The luminescence decay of the Nd($^4F_{3/2}$) excited state measured at room temperature is mono-exponential. Corresponding luminescence lifetimes and absolute quantum yields are listed in Table 4. They are very similar for both protonated and deprotonated Nd^{III} complexes in the solid state and in solution in MeOH. The presence of the O–H oscillators close to the metal ion has apparently no influence on the Nd(III) luminescence, probably because of the implication of these O–H groups in very strong H-bonds; deactivation of the Nd^{III} luminescence is therefore limited.

All the values of quantum yields obtained for the hqt complexes are 5–17% higher than those measured for the hqa complexes. This is consistent with the general trend observed for the lifetimes (except for the Nd complexes in the solid state) where a general increase is observed for the hqt complexes with respect to the hqa ones. The percentages are not totally correlated because the lanthanide ions emitting in the near infrared present different time scales with the erbium ion being more sensitive to de-excitation processes. The quantum yields are lower than those found for halogenated expanded 8-hydroxyquinoline ligands (up to 0.4% in the solid state for a neutral Nd^{III} tris 8-hydroxyquinoline complex)[27,28] but comparable to the best photophysical properties reported in the literature for lanthanide complexes of non-halogenated 8-hydroxyquinolines in solutions (between 0.01 and 0.07% for the Nd^{III} and from 0.14 to 0.53% for Yb^{III}).[12]

Conclusions

Two new ligands (commercial or of versatile synthesis) have been identified for the sensitisation of near-infrared luminescence of the Nd(III), Yb(III) and Er(III) ions. In these ligands the combination of the 8-hydroxyquinoline chromophore with an additional anionic binding group (carboxylate or tetrazolate) yields luminescent trianionic complexes. The emission quantum yields could be further optimised by halogenation of the quinoline units. These complexes show a significantly increased solubility and stability towards ligand dissociation with respect to neutral compounds providing robust systems for potential applications. Moreover the trianionic nature of these complexes allows the tuning of solubility by suitable choice of counterions and should prove very useful in the development of new lanthanide based materials.[37–39]

Experimental

Solvents and starting materials were obtained from Aldrich, Fluka, Acros, and Alfa and used without further purification unless otherwise stated. Water and H_2O refer to high-purity water with a resistivity value of 18 MΩ cm, obtained from the Millipore/Milli-Q purification system. ^{1}H-NMR spectra were recorded on Bruker 200 MHz, Varian Mercury 400 MHz spectrometer. Chemical shifts are reported in ppm with a solvent as the internal reference. Elemental analyses were performed by the Service Central d'Analyses (Vernaison, France).

X-Ray crystallography

The crystals (**7**, **1**) were analysed using a Bruker SMART[40] CCD area detector three-circle diffractometer (Mo-Kα radiation, graphite monochromator, $\lambda = 0.71073$ Å). The cell parameters were obtained with intensities detected on three batches of 15 frames with a 30 s (**7** and **1**), (exposure time). The crystal-detector distance was 5 cm. For three settings of φ narrow data (30 s) frames were collected for 0.3° increments in ω. A hemisphere of data was collected. At the end of data collection, the first 50 frames were recollected to establish that crystal decay had not taken place during the collection. Unique intensities with $I > 10\ \sigma(I)$ detected on all frames using the SAINT Bruker program[41] were used to refine the values of the cell parameters. The substantial redundancy in data allows empirical absorption corrections to be applied using multiple measurements of equivalent reflection with the SADABS Bruker program[42]

The crystals (**2**, **4**) were analysed using an Oxford Diffraction XCalibur diffractometer (Mo-Kα radiation, graphite monochromator, $\lambda = 0.71073$ Å). The cell parameters were obtained with intensities detected on three batches of 5 frames with a 5 s (**4**), 10 s (**2**) (exposure time). The crystal-detector distance was 4.5 cm. 409 (**4**), 219 (**2**) narrow data (60 s (**4**), 90 s (**2**)) frames were collected for 1° increments in ω. Unique intensities detected on all frames using the Oxford-Diffraction Crysalis Red program were used to refine the values of the cell parameters. The substantial redundancy in data allows empirical absorption corrections to be applied using multiple measurements of equivalent reflections with the ABSPACK Oxford-Diffraction program.

Space groups were determined from systematic absences, and they were confirmed by the successful solution of the structure (Table 3). They were solved by direct methods using the SHELXTL 6.14 package[43] and for all structures, all atoms were found by difference Fourier syntheses. All non-hydrogen atoms were anisotropically refined on F^2. Hydrogen atoms of **1** and **4** were fixed on ideal positions and refined isotropically with a riding model. Hydrogen atoms of **2** were fixed in ideal positions and refined with a riding model except for four hydroxyl hydrogens of the coordinating methanol. Hydrogen atoms of the ligand of **7** were fixed in ideal position except for H13o and H23o which were refined with isotropic thermal coefficients, hydrogen atoms of the counterions have been introduced in ideal position. H23o is located on the twofold symmetry axis of the structure. The Et_3NH counterion in **7** is fully disordered over two positions (corresponding to the two helical configuration of the nitrogen) with occupation factors of 0.68 and 0.32 respectively. All the hydrogen atoms were refined using a riding model. The triflate ($OTf^- = CF_3SO_3^-$) anion in **7** is disordered around the symmetry center. The distances were constraint around their usual values (S–O = 1.42 Å, O–O = 2.40 Å, C–F = 1.30 Å, F–F = 2.10 Å).

In **4** potassium atom K6 is disordered over two positions K6a and K6b with occupation factor of 0.39 and 0.61 respectively. Also in **4** the methanol molecule C83–O83 is disordered over two positions with an occupation factor of 0.5. It is coordinated either to one complex or to its symmetric adjacent complex. C83 is localised on a symmetry center of the space group $P\bar{1}$.

Luminescence measurements

Low-resolution luminescence measurements (spectra and lifetimes) were recorded on a Fluorolog FL 3–22 spectrometer from Spex-Jobin-Yvon-Horiba with double grating emission and excitation monochromators, and a R928P photomultiplier. For measurements in the NIR spectral range, the spectrometer was fitted with a second measuring channel equipped with a FL-1004 single grating monochromator and light intensity was measured by two Jobin-Yvon solid state InGaAs detectors (i) DSS-IGA020L, cooled to 77 K (range 800–1600 nm) and (ii) DSS-IGA020A (range 800–1700 nm) working at room temperature and inserted into a LN2 housing including an elliptical mirror (90° beam path) and coupled to a Jobin Yvon SpectrAcq2 data acquisition system. The equipment and experimental procedures for luminescence measurements in the visible and NIR range have been published previously by Comby *et al.*[23] All spectra were corrected for the instrumental functions. Lifetimes were measured in time-resolved mode and are averages of three independent measurements, which were made by monitoring the decay at the maxima of the emission spectra. The mono-exponential decays were analysed with Origin 7.0®. Quantum yields of the complexes in solution at pH 12 and in solid state were determined using a home-modified integrating sphere from Oriel and the previously described procedure.[44] Spectra were corrected for the instrumental function.

Ligand synthesis

The ligand 8-hydroxyquinoline-2-carboxylic acid (H_2hqa) was purchased from Fluka and used without further purification.

Synthesis of the ligand H_2hqt

A mixture of 8-hydroxyquinoline-2-carbonitrile (1 g, 5.88 mmol), sodium azide (0.96 g, 14.7 mmol) and ammonium chloride (0.79 g, 14.7 mmol) in anhydrous DMF (10 mL) was stirred under argon at 130 °C for 18 h. After cooling, the inorganic salts were filtrated and the solvent removed under reduced pressure. After addition of dilute HCl (10 mL, 0.1 M), the resulting suspension was stirred for 1 h. The precipitate was filtered, washed thoroughly with cold water and dried under vacuum, to yield 1.50 g (90%) of light brown powder.

^{1}H NMR (200 MHz, CD_3OD) δ ppm 8.52 (d, $J = 8.58$ Hz, 1H, H_1), 8.30 (d, $J = 8.57$ Hz, 1H, H_2), 7.64–7.46 (m, 2H, H_3, H_4), 7.22 (dd, $J = 7.29$, 1.39 Hz, 1H, H_5), 1.30 (s, 1H, OH).

^{13}C NMR (200 MHz, DMSO) δ ppm 152.89 (C), 140.64 (C), 138.19 (C), 137.21 (CH), 129.38 (CH), 128.73 (C), 118.94 (CH), 117.68 (CH), 111.42 (CH).

Elemental analysis: calcd. (%) for $H_2hqt{\cdot}H_2O$ $C_{10}H_7N_5O{\cdot}H_2O$ C, 51.95; H, 3.92; N, 30.29 Found: C, 52.00; H, 3.63; N, 30.15.

Synthesis of the lanthanide complexes

$[Nd(H_{1/2}hqa)_3]_2(Et_3NH)_3.Et_3NHOTf$. A solution of $Nd(OTf)_3$ (0.114 mmol) in MeOH (2 mL) was added, under stirring, to a methanolic solution of H_2hqa (0.34 mmol) (2 mL). Deprotonation of the ligand was achieved using Et_3N (95.2 µL, 0.68 mmol). The yellow mixture was refrigerated overnight at 5 °C. The insoluble white precipitate formed was removed by filtration and the filtrate was concentrated to a minimum amount

of MeOH (~2 mL). Diisopropylether was allowed to slowly diffuse into the resulting solution until some yellow needles of $\{[Nd(H_{1/2}hqa)_3]_2(Et_3NH)_3\}.Et_3NHOTf$ (**7**) suitable for X-ray diffraction formed. A sufficient amount of the needles were collected to carry out the photoluminescence measurements of the dimeric complex $\{[Nd(H_{1/2}hqa)_3]_2\}^{3-}$.

^{1}H NMR (400 MHz, CD_3OD, 298 K): δ = 0.65 (27H, t, J = 7.0 Hz, HN–CH_2CH_3), 2.22 (18H, q, J = 7.0 Hz, HN–CH_2CH_3), 6.96 (6H, broad d, H3), 7.59 (6H, broad t, H2), 8.36 (6H, d, J = 7.0 Hz, H1), 9.49 (6H, d, J = 8.0 Hz, H5), 9.84 (6H, d, J = 8.0 Hz, H4).

ES-MS: m/z = 706.6 $[Nd_2(H_{1/2}hqa)_4(hqa)_2]^{2-}$.

No correct elemental analyses could be obtained for this neodymium(III) complex. This is probably due to an equilibrium between the complexes presenting different protonation states.

$[Nd(hqa)_3]K_3.7MeOH_\infty$·MeOH. A solution of $Nd(OTf)_3$ (0.092 mmol) in water (1.5 mL) was added, under stirring, to an aqueous solution of 3 mol equivalent of ligand (0.076 mmol) (1.5 mL) at pH 12 adjusted by addition of aqueous KOH (1 M). pH of the resulting solution was readjusted to 12 by addition of aqueous KOH (0.1 M). The mixture was evaporated to dryness, the yellow oil obtained was dissolved in a minimum amount of MeOH (~2 mL) and the mixture was refrigerated overnight at 5 °C. The insoluble white precipitate formed was removed by filtration. Diisopropylether (DIPE) was allowed to slowly diffuse into the resulting filtrate in methanol. The solution was refrigerated until some yellow cubic crystals of $\{[Nd(hqa)_3]K_3\}.7MeOH_\infty$·MeOH (**1**) suitable for X-ray diffraction formed. The crystals were separated by filtration and dried under vacuum to yield $[Nd(hqa)_3]K_3$ (62%). The attribution of the signals was performed by 2D-COSY and NOESY experiments at 25 °C.

^{1}H NMR (400 MHz, CD_3OD, 298 K): δ = 5.45 (1H, d, J = 8.0 Hz, H5a), 5.95 (1H, d, J = 8.0 Hz, H5b), 6.90 (1H, d, J = 8.0 Hz, H1a), 6.96 (0.4H, d, H3′), 7.30 (1H, d, J = 8.0 Hz, H3a), 7.61 (1H, d, J = 8.0 Hz, H4a), 7.87 (1H, t, J = 8.0 Hz, H2a), 7.97 (0.4H, t, H2′), 7.99 (0.4H, d, H1′), 9.03 (1H, d, J = 8.0 Hz, H4b), 9.17 (1H, d, J = 8.0 Hz, H5c), 9.29 (1H, d, J = 8.0 Hz, H3b), 9.32 (0.4H, d, H5′), 9.40 (0.4H, d, H4′), 9.59 (1H, d, J = 8.0 Hz, H3c), 10.27 (3H, m, H2b, H2c, H4c), 12.16 (1H, d, J = 8.0 Hz, H1b), 12.24 (1H, d, J = 8.0 Hz, H1c).

ES-MS: m/z = 860.0 $\{[Nd(hqa)_3]K_4\}^+$.

Elemental analysis calcd. (%) for $\{[Nd(hqa)_3]K_3\}$·2.6MeOH + 0.5H_2O; $C_{30}H_{15}N_3O_9K_3Nd$. 2.6 CH_3OH 0.5 H_2O Mw: 915.28: C 42.78; H 2.91; N 4.59; Found C 42.72; H 2.92; N 5.00. (Mw of complex $[Nd(hqa)_3]K_3$:822.96.)

Crystal data $[Nd(hqa)_3]K_3.7MeOH_\infty$·MeOH: $C_{38}H_{47}K_3N_3Nd_1O_{17}$, M = 1079.33, Monoclinic, space group $P2_1/n$, a = 14.3830(19) Å, b = 20.469(3) Å, c = 16.184(2) Å, α = 90°, β = 100.312(2)°, γ = 90°, V = 4687.8 (11) Å^3, Z = 4, ρ_c = 1.529 Mg m^{-3}, μ = 1.444 mm^{-1}, T = 223 K. Of the 30 021 reflections collected, 11 194 were unique (R_{int} = 0.0179). Refinement on all data converged at R_1 = 0.0308, wR_2 = 0.0603. Max/min residual density 0.776 and –0.397 e Å^{-3}.

$[Er(hqa)_3]K_3.4MeOH.0.25DIPE_\infty$·3MeOH. The compound was prepared as was described for the corresponding neodymium complex. Full assignment of the ^{1}H NMR spectrum was not possible due to the strong paramagnetic broadening and shift of the peaks.

Yield: 51%.

Elemental analysis calcd. (%) for $\{[Er(hqa)_3]K_3\}$.3.8 KOTf + 6.2 H_2O; $C_{30}H_{15}N_3O_9K_3Er$. 3.8 CF_3SO_3K 6.2 H_2O Mw: 1672.81: C, 24.27; H, 1.65; N, 2.51. Found: C, 24.20; H, 1.65; N, 2.33. (Mw of complex $[Er(hqa)_3]K_3$: 846.06.)

Crystal data. $[Er(hqa)_3]K_3.7MeOH.0.25DIPE_\infty$·3MeOH: $C_{38.75}H_{46.50}ErK_3N_3O_{16.25}$, M = 1098.85, monoclinic, space group $C12/c1$, a = 28.8105(12) Å, b = 15.6426(4) Å, c = 23.5338(8) Å, α = 90°, β = 118.865(5)°, γ = 90°, volume = 9288.3(5) A^3, Z = 8, ρ_c = 1.572 Mg m^{-3}, μ = 2.146 mm^{-1}, T = 150(2) K. Of the 17 247 reflections collected, 9137 were unique (R_{int} = 0.0330). Refinement on all data converged at R_1 = 0.0627, wR_2 = 0.0556. Max/min residual density 0.959 and –0.652 e A^{-3}.

$[Yb(hqa)_3]K_3$. The compound was prepared as was described for the corresponding neodymium complex.

Yield: 53%.

Elemental analysis calcd. (%) for $\{[Yb(hqa)_3]K_3\}$.2.25 KOTf + 3.2 H_2O $C_{30}H_{15}N_3O_9K_3Yb$. 2.25 CF_3SO_3K 3.2 H_2O Mw: 1332.80: C, 29.06; H, 1.62; N, 3.15. Found: C, 29.08; H, 1.63; N, 2.87. (Mw of complex $[Yb(hqa)_3]K_3$: 851.76.)

$[Nd(H_{1/2}hqt)_3]_2(Et_3NH)_3$. The compound was prepared as was described for the $[Nd(H_{1/2}hqa)_3]_2(Et_3NH)_3.Et_3NHOTf$ complex.

^{1}H NMR (400 MHz, CD_3OD, 298 K) 9.81 (1H, s, H_4), 9.64 (1H, s, H_5), 8.06 (1H, s, $H_{3/1}$), 7.27 (1H, s, H_2, $H_{3/1}$).

$[Nd(hqt)_3]K_3.5MeOH_\infty$·MeOH. A solution of $Nd(OTf)_3$ (0.16 mmol) in water (1.5 mL) was added, under stirring, to an aqueous solution of 3 mol equivalent of ligand (0.48 mmol) (1.5 mL) at pH 12 adjusted by addition of aqueous KOH (1 M). pH of the resulting solution was readjusted to 12 by addition of aqueous KOH (0.1 M). The mixture was evaporated to dryness, the orange oil obtained was dissolved in a minimum amount of MeOH (~ 2 mL) and the mixture was refrigerated overnight at 5 °C. The insoluble white precipitate formed was removed by filtration. Diisopropylether was allowed to slowly diffuse into resulting solution in methanol. The solution was refrigerated until some orange cubic crystals suitable for X-ray diffraction formed. The crystals were separated by filtration and dried under vacuum to yield $[Nd(hqt)_3]K_3.5MeOH_\infty$·MeOH (60%). The attribution of the signals is performed by 2D-COSY and NOESY experiments at 25 °C.

^{1}H NMR (500 MHz, CD_3OD, 298 K) 1.34 (0.2H, broad d), 4.49 (0.1H, s), 5.56 (0.1H, s), 6.45 (0.1H, s), 6.79 (1H, s, H_1), 7.26 (0.1H, s),8.14(1H, s, H_2), 8.31(1H, s, H_3), 9.70 (0.1H, m), 9.94 (1.10H, s, H_4), 10.25 (1H, s, H_5),12.49 (0.2H, s), 12.92 (0.1H, d),14.32 (0.2H, s), 14.54 (0.1H, s), 20.45 (0.1H, s), 20.92 (0.1H, s).

Elemental analysis calculated (%) for $\{[Nd(hqt)_3]K_3\}$. MeOH + 3.4KOTf + 3H_2O; $C_{30}H_{15}N_{15}O_3K_3Nd.CH_3OH$ + 3.4$KOTf_3$ + 3H_2O. Mw: 1620.92; C 25.49; H 1.55; N 12.96; Found C 25.58; H 1.62; N 12.93. (Mw of complex $[Nd(hqt)_3]K_3$: 895.046.)

The complex was recrystallised from methanol by diffusion of diisopropylether after removal of the white precipitate (KOTf). The obtained crystals were filtered and washed several times with cold diisopropylether to remove the remaining salts.

Elemental analysis of the recrystallised compound calculated (%) for $\{[Nd(hqt)_3]K_3\}$.0.5MeOH + 2.2H_2O; $C_{30}H_{15}N_{15}O_3K_3Nd.0.5CH_3OH$ + 2.2H_2O. Mw: 950.70; C 38.53; H

2.27; N 22.10; Found C 38.51; H 2.63; N 22.12. (Mw of complex $[Nd(hqt)_3]K_3$: 895.046.)

$[Er(hqt)_3]K_3$. The compound was prepared as was described for the corresponding neodymium complex. Full assignment of the ^1H NMR spectrum was not possible due to the strong paramagnetic broadening and shift of the peaks.

Yield: 52%.

Elemental analysis calcd. (%) for $\{[Er(hqt)_3]K_3\}.3.2KOTf + 5H_2O$ $C_{30}H_{15}N_{15}O_3K_3Er.3.2CF_3SO_3K.5H_2O$ Mw: 1610.38: C, 24.76; H, 1.56; N, 13.05. Found: C, 24.80; H, 1.61; N, 12.95. (Mw of complex $[Er(hqt)_3]K_3$: 918.146.)

$[Yb(hqt)_3]K_3$. The compound was prepared as was described for the corresponding neodymium complex.

Yield: 57%.

Elemental analysis calcd. (%) for $\{[Yb(hqt)_3]K_3\}.4KOTf + 3H_2O$ $C_{30}H_{15}N_{15}O_3K_3Yb.4CF_3SO_3K.3H_2O$. Mw: 1730.59: C, 23.60; H, 1.22; N, 12.14. Found: C, 23.78; H, 1.26; N, 12.12. (Mw of complex $[Yb(hqt)_3]K_3$: 923.846.)

Acknowledgements

This research was carried out in the frame of the EC COST Action D-38 "Metal-Based Systems for Molecular Imaging Applications". We thank, Pierre A. Bayle for his help with the NMR experiments and Prof. J.-C. Bünzli for hosting D. Imbert in his laboratory for photophysical studies.

Notes and references

1 K. Kuriki, Y. Koike and Y. Okamoto, *Chem. Rev.*, 2002, **102**, 2347–2356.
2 S. Faulkner and J. L. Matthews, *Comp. Coord. Chem. II*, Elsevier, Oxford, UK, 2004.
3 J. Thompson, R. I. R. Blyth, G. Gigli and R. Cingolani, *Adv. Funct. Mater.*, 2004, **14**, 979–984.
4 S. Faulkner, S. J. A. Pope and B. P. Burton-Pye, *Appl. Spectrosc. Rev.*, 2005, **40**, 1–31.
5 J. C. G. Bunzli and C. Piguet, *Chem. Soc. Rev.*, 2005, **34**, 1048–1077.
6 K. Binnemans, *Chem. Rev.*, 2009, **109**, 4283–4374.
7 M. D. Ward, *Coord. Chem. Rev.*, 2007, **251**, 1663–1677.
8 S. Comby and G. J.-C. Bünzli, *Handbook on the Physics and Chemistry of Rare Earths*, Elsevier, Amsterdam, 2007.
9 J. C. G. Bunzli, *Acc. Chem. Res.*, 2006, **39**, 53–61.
10 J. C. G. Bunzli, S. Comby, A. S. Chauvin and C. D. B. Vandevyver, *J. Rare Earths*, 2007, **25**, 257–274.
11 A. de Bettencourt-Dias, *Dalton Trans.*, 2007, 2229–2241.
12 S. V. Eliseeva and J. C. G. Bunzli, *Chem. Soc. Rev.*, 2010, **39**, 189–227; D. T. de Lill, A. de Bettencourt-Dias and C. L. Cahill, *Inorg. Chem.*, 2007, **46**, 3960–3965.
13 R. Weissleder, *Nat. Biotechnol.*, 2001, **19**, 316–317.
14 W. P. Gillin and R. J. Curry, *Appl. Phys. Lett.*, 1999, **74**, 798–799.
15 M. Albrecht, M. Fiege and O. Osetska, *Coord. Chem. Rev.*, 2008, **252**, 812–824.
16 R. Van Deun, P. Fias, P. Nockemann, A. Schepers, T. N. Parac-Vogt, K. Van Hecke, L. Van Meervelt and K. Binnemans, *Inorg. Chem.*, 2004, **43**, 8461–8469.
17 R. Van Deun, P. Fias, P. Nockemann, K. Van Hecke, L. Van Meervelt and K. Binnemans, *Eur. J. Inorg. Chem.*, 2007, 302–305.
18 F. Artizzu, P. Deplano, L. Marchio, M. L. Mercuri, L. Pilia, A. Serpe, F. Quochi, R. Orru, F. Cordella, F. Meinardi, R. Tubino, A. Mura and G. Bongiovanni, *Inorg. Chem.*, 2005, **44**, 840–842.
19 E. Terazzi, L. Gunenee, B. Bocquet, J. F. Lemonnier, N. D. Favera and C. Piguet, *Chem.–Eur. J.*, 2009, **15**, 12719–12732.
20 M. Albrecht, O. Osetska, R. Frohlich, J. C. G. Bunzli, A. Aebischer, F. Gumy and J. Hamacek, *J. Am. Chem. Soc.*, 2007, **129**, 14178–14179.
21 S. Comby, D. Imbert, C. Vandevyver and J. C. G. Bunzli, *Chem.–Eur. J.*, 2007, **13**, 936–944.
22 D. Imbert, S. Comby, A. S. Chauvin and J. C. G. Bunzli, *Chem. Commun.*, 2005, 1432–1434.
23 S. Comby, D. Imbert, A. S. Chauvin and J. C. G. Bunzli, *Inorg. Chem.*, 2006, **45**, 732–743.
24 A. Nonat, D. Imbert, J. Pecaut, M. Giraud and M. Mazzanti, *Inorg. Chem.*, 2009, **48**, 4207–4218.
25 M. Albrecht, O. Osetska and R. Frohlich, *Dalton Trans.*, 2005, 3757–3762.
26 N. M. Shavaleev, R. Scopelliti, F. Gumy and J. C. G. Bunzli, *Inorg. Chem.*, 2008, **47**, 9055–9068.
27 N. M. Shavaleev, R. Scopelliti, F. Gumy and J. C. G. Bunzli, *Inorg. Chem.*, 2009, **48**, 2908–2918.
28 M. Albrecht, O. Osetska, J. Klankermayer, R. Frohlich, F. Gumy and J. C. G. Bunzli, *Chem. Commun.*, 2007, 1834–1836.
29 K. Lunstroot, K. Driesen, P. Nockemann, K. Van Hecke, L. Van Meervelt, C. Gorller-Walrand, K. Binnemans, S. Bellayer, L. Viau, J. Le Bideau and A. Vioux, *Dalton Trans.*, 2009, 298–306.
30 K. Lunstroot, P. Nockemann, K. Van Hecke, L. Van Meervelt, C. Gorller-Walrand, K. Binnemans and K. Driesen, *Inorg. Chem.*, 2009, **48**, 3018–3026.
31 D. Parker, R. S. Dickins, H. Puschmann, C. Crossland and J. A. K. Howard, *Chem. Rev.*, 2002, **102**, 1977–2010.
32 E. S. Andreiadis, R. Demadrille, D. Imbert, J. Pecaut and M. Mazzanti, *Chem.–Eur. J.*, 2009, **15**, 9458–9476.
33 M. Giraud, E. S. Andreiadis, A. S. Fisyuk, R. Demadrille, J. Pecaut, D. Imbert and M. Mazzanti, *Inorg. Chem.*, 2008, **47**, 3952–3954.
34 G. A. Jeffrey, *An Introduction to Hydrogen Bonding*, Oxford University Press, 1997.
35 T. Steiner, *Angew. Chem., Int. Ed.*, 2002, **41**, 48–76.
36 R. D. Shannon, *Acta Crystallogr., Sect. A: Cryst. Phys., Diffr., Theor. Gen. Crystallogr.*, 1976, **32**, 751–767.
37 K. Lunstroot, K. Driesen, P. Nockemann, C. Gorller-Walrand, K. Binnemans, S. Bellayer, J. Le Bideau and A. Vioux, *Chem. Mater.*, 2006, **18**, 5711–5715.
38 H. Mehdi, K. Binnemans, K. Van Hecke, L. Van Meervelt and P. Nockemann, *Chem. Commun.*, 2010, **46**, 234–236.
39 K. Binnemans, *Chem. Rev.*, 2007, **107**, 2592–2614.
40 *SMART v. 5.628*, Bruker Molecular Analysis Research Tool, Bruker AXS, Madison, WI, 2002.
41 *SAINT v. 6.22*, Bruker Molecular Analysis Research Tool, Bruker AXS, Madison, WI, 2002.
42 *SADABS v. 2.01*, An Empirical Absorption Correction Program, Bruker AXS: Madison, WI, 1995.
43 *SHELXTL v. 6.14*, Structure Determination Software Suite, Bruker AXS, Madison, WI, 2006.
44 J. C. deMello, H. F. Wittmann and R. H. Friend, *Adv. Mater.*, 1997, **9**, 230.